Halogen and Hydrogen Bonding Host Structures for Anion Recognition and Ternary Complexes for Modulating Luminescent Output

Alexander Edward Hess

St. Hugh's College, University of Oxford



A thesis submitted for the degree of Doctor of Philosophy

Inorganic Chemistry Laboratory

University of Oxford

Trinity Term 2016

Hydrogen and Halogen Bonding Host Structures for Anion Recognition and Ternary Complexes for Switchable Luminescent Output

Alexander Edward Hess, St. Hugh's College, University of Oxford

Abstract of thesis submitted for the degree of:

Doctor of Philosophy, Trinity Term 2016

This thesis describes the synthesis and anion recognition properties of a series of halogen and hydrogen bonding acyclic and interlocked host receptors and the use of the inclusion supramolecular chemistry of cucurbit[n]uril derivatives in switchable luminescent output.

Chapter 1 introduces the field of anion supramolecular chemistry and the properties of cucurbit[n]uril macrocycles which pertain to the research detailed in subsequent chapters.

Chapter 2 describes the synthesis and anion recognition properties of a new class of chelating, halogen and hydrogen bonding host molecules. The halogen bonding enhanced selectivity for the Br^- anion is demonstrated.

Chapter 3 probes the anion recognition characteristics of a series of novel halogen and hydrogen bonding motifs. Evidence for intramolecular hydrogen bond enhanced halogen bonding recognition of halides is presented and the selective recognition of the anion $H_2PO_4^-$ by a [3]rotaxane host is displayed.

Chapter 4 discusses the redox-mediated modulation of the luminescent output of a series of visible and near-infrared emitting lanthanide complexes within cucurbit[8]uril based ternary complexes.

Chapter 5 describes the experimental procedures and characterisation of the compounds presented in Chapters 2-4.

Chapter 6 summarises the conclusions of this thesis.

Acknowledgements

It was readily apparent from the start of writing this hefty tome that I have a number of people who have contributed immensely to this task. First of all, the supervisor himself, Professor Paul D. Beer, deserves a large amount of gratitude for accepting me into his group way back in 2012 and conferring upon me the generous ERC funding my stay here in Oxford. His expertise and encouragement during the lab years was critical and his patience in coping with my somewhat lyrical prose during the editing of the thesis is much appreciated.

My fellow 4th year DPhil comrades Stuart Cornes, Timothy Barendt and Sean Robinson have helped me soldier through the daily trials and tribulations that are all part of doing a DPhil, from having a good humoured approach to life in the lab, providing level headed advice and more recently patiently reading chapters. We made it! Not to forget other current members like Dr. Asha Brown for synthetic advice beyond reproach, tackling the HPLC bugbears head-on, reading my eclectic introduction chapter and generally being an indispensable pillar of the S7 lab. Thanks also to Jason Lim for reading my chapter 3 and helping me get to the bottom of a number of interesting chemical phenomena. Past Beer group members like Dr. Rich Knighton and the visiting Dr. Mike Chudzinski are people I have thoroughly enjoyed the company of. Also especially, one Anna Spearing-Ewyn who, despite betraying us for the Weller group, has continued to be my constantly dancing 'rock' inside and outside of the lab.

Credit is due to my long-time colleague and friend Dr. Gearóid Ó Máille, from the early years being my acerbic undergraduate lab supervisor in Trinity College Dublin to being a well spring of advice on all things photophysical as a postdoc with the Faulkner group, all the while bringing me up to be a critically-thinking scientist.

My ERC project collaborators were immensely helpful for the work described in Chapter 4, especially my persistent Part II student Andrew Baxter who was exceedingly tolerant of my ever-present optimism in suggesting "one more thing to try" and of course Matthew Cunningham for giving up his time and lending his expertise with the multitude of ternary complex experiments under the auspices of Professors Jason J. Davis and Stephen Faulkner. In addition, Dr. Manuel Tropiano and Dr. Octavia Blackburn have been instrumental in helping me use the fluorolog and introducing me to the delights of lanthanide luminescence.

I would like to thank St. Hugh's College MCR for providing my first point of contact for many great, brainy friends who will last me a lifetime. The unique privilege of living within the college for so long and getting the chance to contribute as an MCR committee member to this rich collegiate community has been brilliant. My friends Sam Griffiths and Tim Flight over in faraway Magdalen College have been a great source of fun and escape from stress, engaged with the plumbing the depths of the B-movie catalogue, making hilarious memories at several metal music festivals and just being good sports.

And last but not least, I must thank my parents Louis Hess and Patricia Anderson – for your unwavering faith in me, given that I was not the easiest child to raise. I hope you know now that all the work that you put in was worth it! Indeed, my whole extended family deserves a big thank you for the constant well-wishing and especially all the prayers from my grandmother Maureen being a big part of that.

This thesis is dedicated to the memory of another dear grandma:

Betty Lou Hess (July 30th, 1926 – January 21st, 2014)

Table of Contents

1. Introduction 1

1.1. Supramolecular Chemistry 2

1.1.1. Non-covalent interactions 3

1.1.2. Principles of host-guest chemistry 7

1.1.3. Host-guest complementarity 7

1.1.4. Preorganisation, the chelate effect and the macrocyclic effect 8

1.2. Anion Supramolecular Chemistry 10

1.2.1. The importance of anions 10

1.2.2. The challenge of anion coordination 11

1.2.3. Synthetic anion receptor design 13

1.2.3.1. Positively charged anion receptors 14

1.2.3.2. Neutral anion receptors 19

1.2.3.3. Anion receptors exploiting the hydrophobic effect 23

1.2.3.4. Lewis acidic main group and metal based receptors 24

1.2.4. Anion sensors 25

1.2.4.1. Luminescent anion sensors 25

1.2.4.2. Electrochemical anion sensors 28

1.3. Mechanically Interlocked Host Systems 30

1.3.1. Strategies for the synthesis of interlocked host systems 31

1.3.2. Templation strategies 32

1.3.2.1. Cationic templates 33

1.3.2.2. Neutral templates 38

1.3.2.3. Anionic templates 39

1.3.3. Alternative applications of interlocked structures 45

1.4. Water Soluble Macrocyclic Inclusion Complexes 49

1.4.1. The cucurbit[n]uril family 49

1.4.2. Synthesis of CB[n] derivatives 50

1.4.3. Host-guest chemistry of CB[n] derivatives 51

1.4.4. Applications of CB[n] derivatives 52

1.5. Project Outline 55

1.6. References for Chapter 1 56

2. Halogen and Hydrogen Bonding Pyridyl Triazole Axle Containing Rotaxanes For Halide Recognition 65

2.1. Introduction 66

2.1.1. Halogen bonding anion recognition 66

2.1.2. Chelating anion host systems 67

2.1.3. Chapter aims 68

2.2. A Chelating Acyclic Pyridinium-triazole Receptor 69

2.2.1. Receptor synthesis 69

2.2.2. Preliminary anion binding investigations with chloride 71

2.3. Synthesis of Pyridinium Halogen/Hydrogen Bonding Axle Containing [2]rotaxanes 73

2.3.1. [2]Rotaxane synthetic strategy 73

2.3.2. Synthesis of axle precursor and macrocycle components 74

2.3.3. Halogen bonding/hydrogen bonding [2]rotaxane synthesis 77

2.3.4. ^{1}H NMR anion binding investigations 85

2.4. Dicationic Pyridinium-Triazolium [2]Rotaxanes 89

2.4.1. Synthesis of dicationic pyridinium-triazolium [2]rotaxanes 89

2.4.2. ^{1}H NMR anion binding investigations 92

2.4.3. Summary 96

2.5. Towards a Halogen Bonding Rhenium(I) Anion Sensor 97

2.5.1. The 4-4'-bis-triazole ligand system 97

2.5.2. [2]Rotaxane design 98

2.5.3. Synthesis of triazole-alkyne stoppering component 99

2.5.4. Synthesis of a rhenium(I)-bta axle containing [2]rotaxane 101

2.5.5. Summary 106

2.6. Towards Neutral Halogen Bonding Rhenium(I) Anion Sensors 107

2.6.1. Design of an acyclic chelating halogen bonding receptor 107

2.6.2. Receptor synthesis 107

2.6.3. ^{1}H NMR anion binding studies 110

2.6.4. Summary 114

2.7. Conclusion and Future Work 114

2.8. References for Chapter 2 116

3. Halogen and Hydrogen Bonding Amide-Triazole Motifs for Anion Recognition 118

3.1 Introduction 119

3.1.1. Amide-triazole based anion receptors 119

3.1.2. Intramolecular hydrogen bonding: preorganisation 119

3.2. Amide-iodotriazole and amide-triazole receptors for anion recognition 121
3.2.1. Receptor design 121
3.2.2. Chapter aims 122
3.2.3. Synthesis of acyclic halogen and hydrogen bonding bis-triazole-amide receptors 122
3.2.4. Synthesis of isomeric halogen and hydrogen bonding bis-amide-triazole receptors 126
3.2.5. Anion binding studies 131
3.2.6. Synthesis and anion binding studies of isomeric amide-triazolium and amide-iodotriazolium receptors 134
3.2.7. Summary 139
3.3. Synthesis of halogen bonding macrocycles 140
3.3.1. Chloride anion templated synthesis of interlocked structures 140
3.3.2. Chloride anion templated synthesis of halogen bonding macrocycles 141
3.3.3. Pseudorotaxane studies 147
3.3.4. Summary 149
3.4. Synthesis of a [3]Rotaxane Anion Host System 149
3.4.1. Higher order [3]rotaxane structures for anion recognition 149
3.4.2. [3]rotaxane design 150
3.4.3. Pseudorotaxane studies 151
3.4.4. [3]Rotaxane synthesis 153
3.4.5. Anion binding studies 158
3.4.6. Summary 162
3.5 Conclusions and Future Work 162
3.6 References for Chapter 3 164

4. Luminescent Cucurbit[n]uril Host-Guest Systems: Towards Redox Switchable Output 167
4.1. Introduction 168
4.1.1. Donor-acceptor ternary complexes of CB[8] 168
4.1.2. Lanthanide luminescence: the antenna effect 170
4.2. Towards a Redox Switchable Luminescent Ternary Complex Switch 172
4.2.1. Design of naphthalene-appended lanthanide complexes 172
4.2.2. Design of the ferrocene-viologen component 172
4.2.3. CB[8] ternary complex assembly design 173
4.2.4. Chapter aims 174
4.2.5. Synthesis of the lanthanide containing component 175
4.2.6. Ternary complex studies 180
4.2.6.1. UV-Vis properties 180

4.2.6.2. Luminescence properties 181
4.2.6.3. Towards redox switching of optical output 183
4.2.7. Summary 186
4.3. Towards Redox Switchable NIR Lanthanide Luminescence 186
4.3.1. Introduction 186
4.3.2. Design of NIR emitting heteroternary complexes 187
4.3.3. Ternary complex studies 189
4.3.3.1. Luminescence properties 190
4.3.4. Summary 192
4.4. Towards a Ferrocene Containing Heteroternary Complex Featuring Redox Switchable Luminescent Output 193
4.4.1. Synthesis of ferrocene-viologen component 193
4.4.2. Ternary complex studies 196
4.4.3. Summary 198
4.5. Conclusions 199
4.6. References for Chapter 4 200

5. Experimental 202
5.1. General Considerations 203
5.1.1. Solvents and reagents 203
5.1.2. Instrumental methods 203
5.1.2.1. NMR spectroscopy and other characterisation methods 203
5.1.2.2. Absorption and luminescence spectroscopy 203
5.1.3. ^{1}H titration protocol 204
5.1.4. Ternary complexation protocol 204
5.1.5. General procedure for acid chloride synthesis 205
5.2. Synthesis of Compounds from Chapter 2 205
5.3. Synthesis of Compounds from Chapter 3 235
5.4. Synthesis of Compounds from Chapter 4 262
5.5. References for Chapter 5 272

6. Conclusions 274

7. Appendix A1
7.1. Excitation Spectra A1
7.2. Europium(III) Luminescence Lifetime Experiment Methodology A1

Abbreviations

υ	frequency
δ	chemical shift
λ	wavelength
μ	micro
Δ	change in (a measurement)
Φ_X	quantum yield of process 'X'
^{0}C	degrees Celsius
*	excited state
A^-	anion
Å	Ångström
AcO$^-$	acetate
aq.	aqueous
ANS	1-anilino-8-naphthalenesulfonate
Ar	aromatic
ATP	adenosine triphosphate
a.u.	arbitrary units
$[BAr^F{}_4]^-$	tetrakis[3,5-bis(trifluoromethyl)phenyl]borate
BET	back energy transfer
Boc	di-*tert*-butyl dicarbonate
BODIPY	boron-dipyrromethene
bs	broad singlet
bta	4-4'-bis-triazole
Bu	butyl
ca.	*circa*, approximately
cat.	catalytic
CB[n]	cucurbit[n]uril
cyclen	1,4,7,10-tetraazacyclododecane
CDPR	cyclodextrin based polypseudorotaxanes
conc.	concentrated
CT	charge transfer
CuAAC	copper(I)-catalysed azide–alkyne cycloaddition
d	doublet
DBU	1,8-diazabicycloundec-7-ene
DCC	*N*,*N'*-dicyclohexylcarbodiimide
DCM	dichloromethane
dd	doublet of doublets
DHN	2,6-dihydroxynaphthalene
DIPEA	*N*,*N'*-di-*iso*-propylethylamine
DMAP	4-Dimethylaminopyridine
DMF	*N*,*N'*-dimethylformamide
DMSO	dimethyl sulfoxide
DO3A	1,4,7,10-tetraazacyclododecane-1,4,7-triacetic acid
DOTA	1,4,7,10-tetraazacyclododecane-1,4,7,10-tetraacetic acid
DNA	deoxyribonucleic acid
DRAM	dynamic random access memory

EDC.HCl	*N*-(3-dimethylaminopropyl)-*N*′-ethylcarbodiimide hydrochloride
em	emission
eq., equiv.	equivalent
ESI	electrospray ionisation
ET	energy transfer
Et	ethyl
et al.	*et alia*
ex	excitation
g	gram
Grubbs' II	Grubbs' second generation catalyst
h	Planck's constant
HOBt	hydroxybenzotriazole
HOPfP	pentafluorophenol
HQ	hydroquinone
hr	hour
HRMS	high resolution mass spectrometry
Hz	hertz
IHB	intramolecular hydrogen bond
i.e.	*id est*
ISC	intersystem crossing
J	Joule
J	coupling constant
k	kilo
K	Kelvin
K_A	association constant
l	litre
Ln	Lanthanide metal
M	mega, molecular ion, moles per litre
m	milli, multiplet, metre
m	*meta*
m/z	mass-to-charge ratio
max	maximum
Me	methyl
MeCN	acetonitrile
Mes	1,3,5-trimethylbenzene
min	minute
MLCT	metal-to-ligand charge transfer
mol	mole
MS	mass spectrometry
MV^{2+}	methyl viologen dication, 1,1′-dimethyl-4,4′-bipyridinium
$MV^{\bullet+}$	methyl viologen radical monocation
n	nano
o	*ortho*
NIR	near-infrared
NMR	nuclear magnetic resonance
p	pentet (quintet)
p	*para*
PEG	polyethylene glycol

PET	photoinduced electron transfer
Ph	phenyl
PFP	pentafluorophenyl
pH	$-\log_{10}[H^+]$
pK_a	$-\log_{10}[K_a]$
PMT	photomultiplier
ppm	parts per million
Pyr	pyridinium
pyta	pyridine-triazole
q	quartet
quant%	quantitative yield/conversion
R	chemical substituent
RCM	ring closing metathesis
ROESY	rotating frame nuclear Overhauser effect correlation spectroscopy
rt	room temperature
s	second, singlet
S_n	singlet photophysical state 'n'
SAM	self-assembled monolayer
sat.	saturated
SBP	sulphate binding protein
sept.	septet
t	triplet
T_n	triplet photophysical state 'n'
t, tert	tertiary
TBA	tetrabutylammonium
TBTA	tris[(1-benzyl-1*H*-1,2,3-triazol-4-yl)methyl]amine
TFA	trifluoroacetic acid
THF	tetrahydrofuran
TLC	thin layer chromatography
TM	transition metal
TMS	trimethylsilyl
Ts, tosyl	*para*-toluenesulfonyl chloride
TTF	tetrathiafulvalene
UV	ultraviolet
V	volt
vis.	visible
vs.	*versus*
v/v	volume/volume ratio
W	watt
wt.	weight
X^-	halide

CHAPTER 1

Introduction

1.1. Supramolecular Chemistry

Supramolecular chemistry, championed by the 1987 Nobel Prize winner Jean-Marie Lehn as "*the chemistry of molecular assemblies and the intermolecular bond",* uses the Latin prefix 'supra-' to simply communicate the concept of "*chemistry beyond the molecule*" as it is more colloquially defined.[1] Seminal contributions from Cram[2] and Pedersen[3], the other winners of the 1987 prize, gave the field its pre-eminence seen today with the ever growing volume of contributions globally. In contrast to 'molecular' chemistry which can be thought of as dealing only with strong covalent bonds between the atoms of molecules, supramolecular chemistry investigates the wide breadth of *non-covalent* interactions between molecules that take place in an infinite variety of dynamic natural and artificial molecular assemblies.

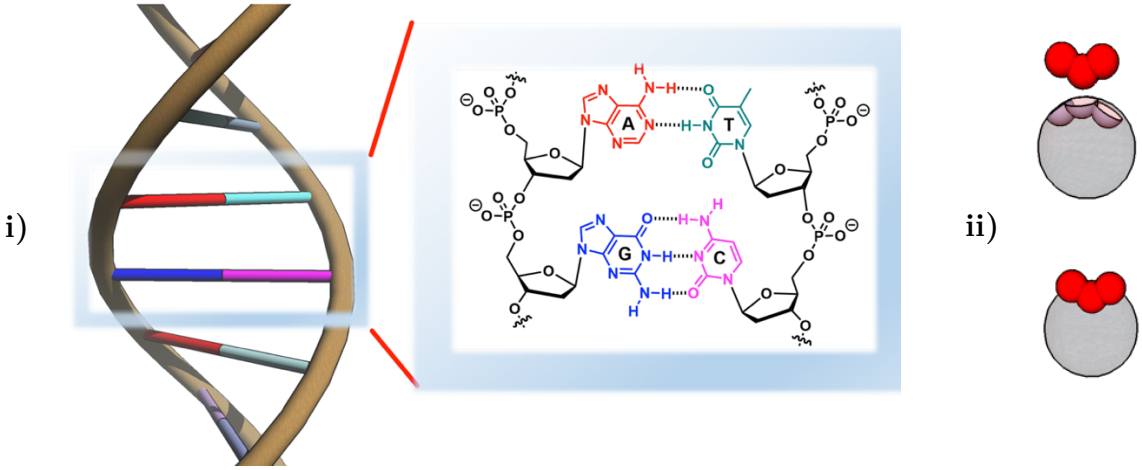


Figure 1.1 – Schematics illustrating i) the hydrogen bond directed self-assembly of DNA base pairs and ii) the prototypical "lock and key" host-guest binding model of enzymatic substrate (red) to an enzyme (grey).

Conceptually, supramolecular chemistry can be broadly split into two categories: i) *self-assembly* and ii) *host-guest* chemistry. The former can be readily demonstrated in the quintessential self-assembly of DNA strands (**Figure 1.1-i**) and the even more complex tertiary structure of proteins arising from precise polypeptide sequences, made possible by the non-covalent intermolecular interactions of base

pairs or amino acids along their length. The latter, *host-guest* chemistry, can trace its origins back to Hermann Emil Fischer's observation of the marked selectivity of yeast enzymes in the digestion of particular stereoisomers of glucose. In 1894 he hypothesised that this selectivity arose from a high degree of complementarity of the shape of the active site of the enzyme (the host or 'lock') for the substrate (the guest or 'key') (**Figure 1.1-ii**).[4] It is evident that this early analogy underlies one of the most important aspects of supramolecular chemistry: the closeness of fit between the structures of host and guest molecules.

1.1.1. Non-covalent interactions

Whilst individual non-covalent bonding interactions are weak (<~50 kJ mol^{-1}) in comparison to typically stronger covalent bonds (300-500 kJ mol^{-1}), in concert these interactions have proven to be powerful tools in the construction and function of a huge array of self-assembled supramolecular systems.

Electrostatic interactions

Electrostatic interactions are ordered by the strength of association; they can occur through either i) ion-ion, ii) ion-dipole or iii) dipole-dipole interactions (**Figure 1.2**). In all cases, they involve a net positive charge or localised dipole moment on a given molecule interacting with a similarly net negative charge or dipole moment.[5]



Figure 1.2 – Schematic representations of i) ion-ion, ii) dipole-ion and iii) dipole-dipole interactions.

Hydrogen bonding

Although technically a subtype of dipole-dipole/ion-dipole interactions, hydrogen bonds can be considered to inhabit a separate category of non-covalent interaction. A hydrogen bond is defined specifically as "an attractive interaction between a hydrogen atom from a molecule or a molecular fragment X–H in which X is more electronegative than hydrogen, and an atom or a group of atoms in the same or a different molecule".[6] Hydrogen bonds exhibit directionality, with observed linear or near-linear interatomic interactions. These prove to be very strong in some cases, notably in the HF_2^- anion, possessing a bond enthalpy of 161.5 kJ mol^{-1}.[7] There are many examples of both *intra-* and *inter-molecular* hydrogen bonds, instances of the former include the hydrogen bonding regime that stabilises the enol tautomer of acetylacetone (**Figure 1.3-i**)[8]. *Inter-molecular* hydrogen bonds stabilise the intricate hexagonal structural ordering of the ice polymorph known as 'Ih' (**Figure 1.3-ii**), which exhibits an anomalous lower density in comparison to liquid water as a result of its more 'open' supramolecular structure.[9]

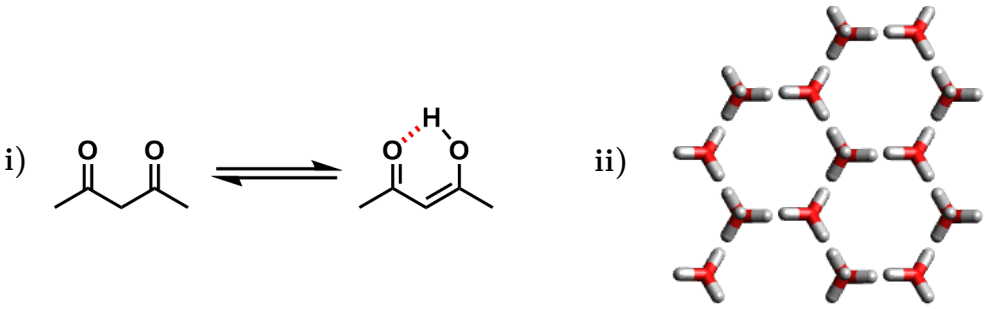


Figure 1.3 – i) The equilibrium between keto (left) and the hydrogen bonded enol form (right) of acetylacetone and ii) the hexagonal ordered hydrogen bonded network of water ice polymorph Ih.

Halogen bonding

A relatively overlooked intermolecular interaction since it was first observed in the unanticipated isolation of an adduct of ammonia and molecular iodine in the laboratory of Frederick Guthrie in 1863[10], the resurgence of halogen bonding as a

tool of the supramolecular chemist and the crystal engineer in recent times has been dramatic.[11–13] Often considered to be analogous to hydrogen bonding, a IUPAC recommendation in 2013 defines the phenomenon as, "*a net attractive interaction between an electrophilic region associated with a halogen atom in a molecular entity and a nucleophilic region in another, or the same, molecular entity*".[14] This interaction is generated by an electron withdrawing group 'R' attached to the donor halogen atom 'X', which gives rise to an anisotropic distribution of electron density, notably an area of net positive potential located at the terminus of the halogen atom commonly known as the 'sigma hole' (**Figure 1.4-i**)[15] that interacts with a Lewis basic halogen bond acceptor 'A'. This theorised anisotropy lent credence to the frequently observed 180° angle about the R-X…A axis observed in crystal structure surveys of halogen bonding arrays (**Figure 1.4-ii and iii**).[16] The strength of the halogen bond varies widely from the weak Cl^{-}-Cl_2 halogen bond (5 kJ mol^{-1}) to approximately 180 kJ mol^{-1} for the strong I^{-}-I_2 halogen bond observed in the I_3^{-} anion.[17] In most cases the more polarisable the halogen donor atom, the stronger the observed halogen bond, as evidenced by the potency of iodo-substituted halogen bond donors in comparison to chloro- or bromo-substituted analogues.[18,19]

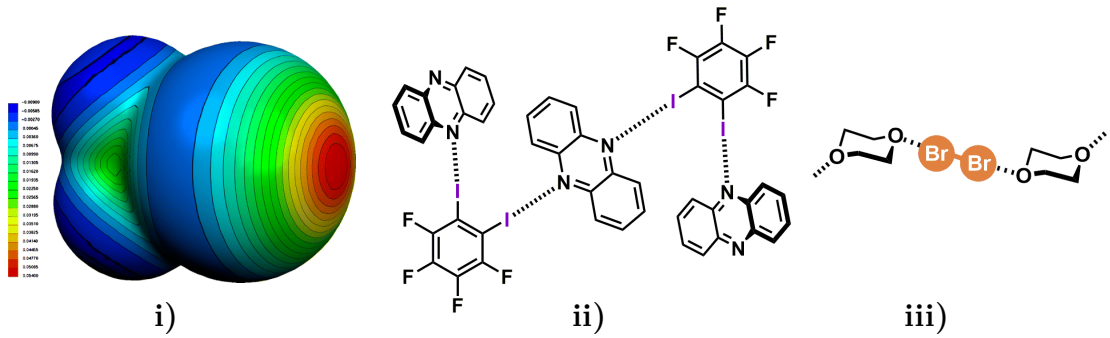


Figure 1.4 – i) Electron density map of CF_3I, showing the electron deficient 'sigma-hole'[20]; schematic examples of halogen bonding seen in the adducts of ii) 1,2 tetrafluoroiodobenzene and phenazine[21] and iii) the adduct of Br_2 and 1,4-dioxane seen in the seminal first crystallographic evidence of the halogen bond.[22]

Aromatic π-π donor-acceptor interactions

Aromatic molecules uniquely possess quadrupolar electronic topologies with an electron π cloud above and below the plane of the ring(s) and polarised ring edges. Through subtle substitution of these ring systems, the polarity of these quadrupolar regions can be tuned[23] to give rise to an array of favoured intermolecular geometries.[24] The more commonly seen geometrical homologues such as face to face and edge to face interactions result from a fine balance of the alignment of these positive or negative aromatic quadrupolar moments, solvation effects[25] and the weak dispersive forces displayed by these molecules (**Figure 1.5**).

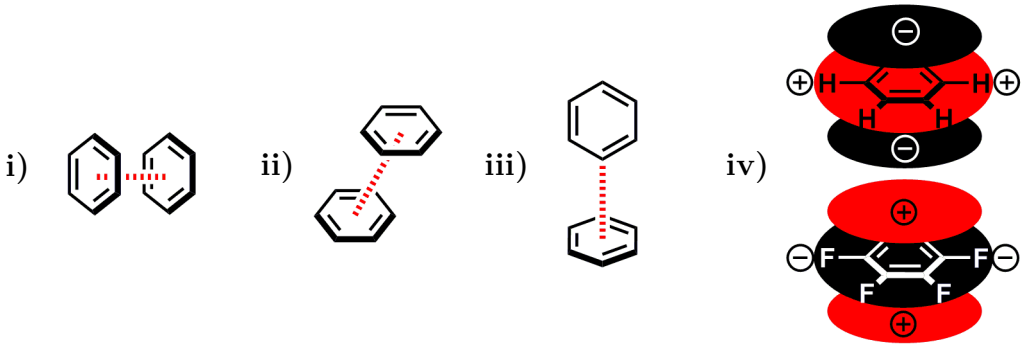


Figure 1.5 – Schematic of the general subtypes of aromatic interactions: i) face to face sandwich, ii) face to face parallel offset, iii) edge to face and iv) a schematic of the quadrupolar electronic distibutions of *π-basic* benzene (top) and *π-acidic* hexafluorobenzene (bottom).

The delocalised electronic structure of these molecules readily interacts with non-aromatic species. The two main examples observed are the interaction of electron rich or *π-basic* aromatic molecules interacting with cations, *cation-π interactions* (**Figure 1.6-i)** and electron-deficient or *π-acidic* aromatics interacting with anionic species, *anion-π interactions* (**Figure 1.6-ii)**. The prevalence of cation-π interactions is well known for its importance in protein tertiary structure[26,27] and abiotic[28] regimes, with anion-π interactions being relatively less studied but gaining significant momentum in the areas of anion transport[29,30] and recognition.[31]

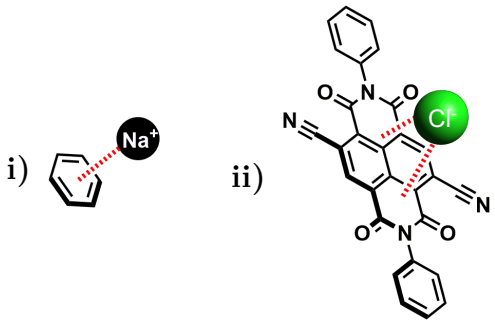


Figure 1.6 – Illustrative examples of i) cation-π interactions between a Na^+ cation and π-basic benzene[32] and ii) anion-π interactions between a Cl^- anion and π-acidic dicyano-naphthalenediimide.[29]

Solvophobic Forces

Although not explicitly a non-covalent bonding interaction, phenomena relating to solvent effects are often ingeniously exploited by Nature and are underestimated in artificial receptor design. The solvation of both host and guest are important thermodynamically, from the finely balanced entropic and enthalpic compensations arising from the displacement of energetic water molecules from a hydrophobic protein cavity driving strong protein-ligand interactions[33] to the solvent dependent structure of foldamers.[34]

1.1.2. Principles of host-guest chemistry

Alongside the consideration of non-covalent forces in the design of synthetic supramolecular architectures and host-guest systems, the use of powerful organisational tools such as complementarity, the chelate/macrocyclic effect and preorganisation stand out in numerous examples in both synthetic and natural supramolecular architectures.

1.1.3. Host-guest complementarity

The arrangement of the non-covalent interactions mentioned in **Section 1.1.1** in such a way as to maximise favourable, complementary host-guest interactions is

often necessary to achieve strong and selective host-guest recognition. Invoking Fischer's lock and key concept (**Section 1.1**), Lehn's variation of the length of the polyether chains in the macrobicyclic cryptands gives rise to size-constrained three dimensional cavity volumes selective for Na^+ and K^+ in methanol solutions. It was reported that a higher association constant for Na^+ was found with the cryptand 2.2.1 and correspondingly the larger volume 2.2.2 cryptand bound the larger diameter ion K^+ selectively, correlating to a size match between the respective cations for the correctly sized host (**Figure 1.7-i**).[35] This principle can be extended to include more complex guests; Hamilton's macrocyclic host, incorporating four hydrogen bond donors and two hydrogen bond acceptors, binds the complementary barbital guest with a high association constant of ($K_A = 1.37 \times 10^6$ M^{-1}) in chloroform (**Figure 1.7-ii**).[36]

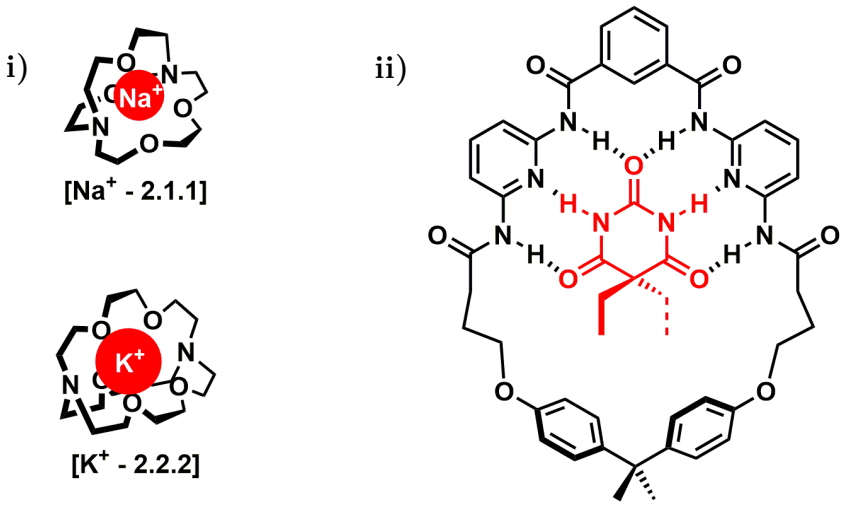


Figure 1.7 – i) Size selective binding of alkali metal cations in Lehn's macrobicyclic cryptands, ii) Hamilton's receptor utilising six convergent hydrogen bonds in recognition of the barbital guest.

1.1.4. Preorganisation, the chelate effect and the macrocyclic effect

Host systems that satisfy the requirements of complementarity may still need to overcome thermodynamic barriers to guest binding, such as thermodynamically disfavoured host geometry, by exploiting the concept of preorganisation. The Nobel laureate Donald J. Cram, whom defined the concept, stated, *"the more highly host*

and guest are organized for binding and low solvation prior to their complexation, the more stable will be their complexes."[2] A subtle but powerful structurally preorganising element is the chelate effect and its extension: the macrocyclic effect. These effects arise from the increased affinity of chelating ligand hosts for guests over homologous monodentate ligand donors, demonstrated by the increasing stability constants for the Pb(II) ion concurrent with the increasing linkages between a four nitrogen donor coordination sphere (**Figure 1.8**).

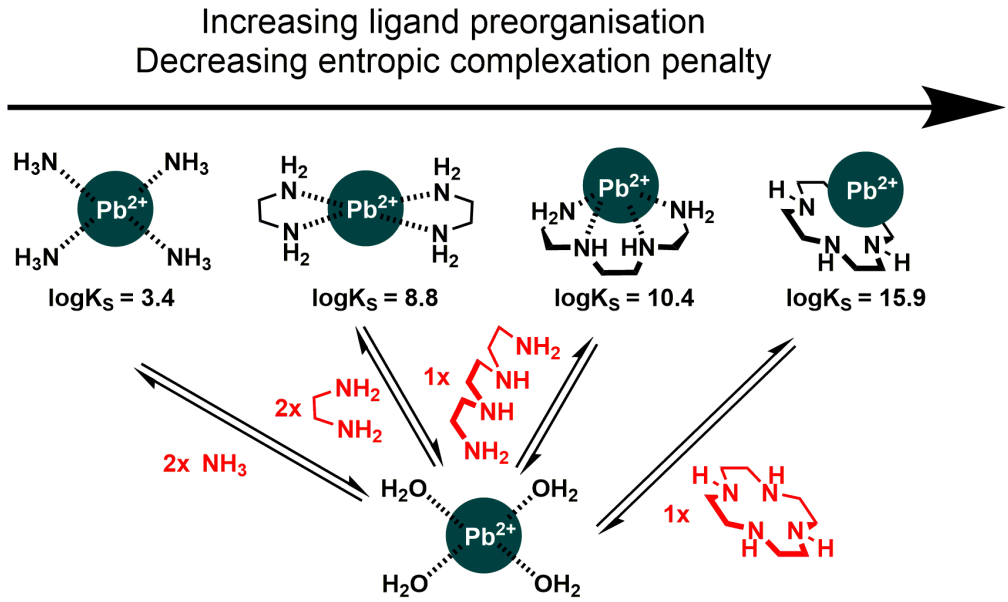


Figure 1.8 – A selection of amine derived complexes demonstrating the chelate and macrocyclic effects on the enhancement of the association of Pb(II).

The observed enhanced binding affinity is the product of the favourable entropic gain upon the substitution of multiple water molecules for multidentate ligand species, which possess fewer degrees of freedom. The watershed macrocyclic effect enhancement is the result of not only an entropic effect but also an enthalpically favoured minimal conformational rearrangement upon guest binding due to the 'enforced' cyclic structure of the macrocycle. Additionally, the slow kinetics of guest dissociation inherent to the highly preorganised macrocycle structure also plays a role.[37,38] Preorganisation can also manifest itself in examples such as the Pt(II)-

induced rigidification of a bipyridine containing acyclic receptor; where the neutral, metal containing host exhibits a two orders of magnitude enhancement in binding of $H_2PO_4^-$ in DMSO/water mixtures in contrast to the un-metallated host (**Figure 1.9**).[39]

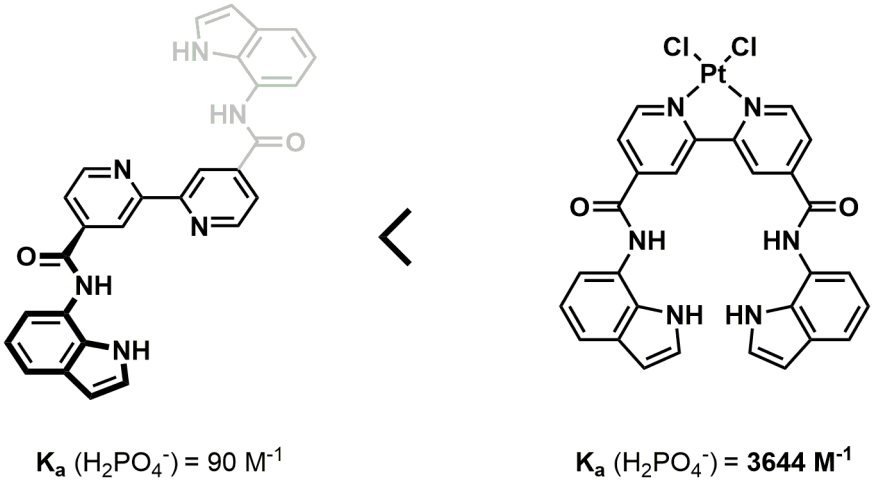


Figure 1.9 – Metal induced host preorganisation leads to enhanced binding of $H_2PO_4^-$ in DMSO/H_2O mixtures.

1.2. Anion Supramolecular Chemistry

Anion supramolecular chemistry is an increasingly complex and interdisciplinary field; it brings together not only the supramolecular concepts utilised extensively in cation binding but also design and function principles from biology, medicine, catalysis, materials science and nanotechnology. The theme of this thesis is to establish the importance of anions and the reasons for their study, their unique physical properties, anion receptor design and the role of anions as templates in the assembly of complex supramolecular architectures employed in the recognition of anions will be explored.

1.2.1. The importance of anions

Anions, as an entity of interest to supramolecular chemists, occupy an important place alongside their cation counterparts in an infinite variety of natural and

artificial processes. The energy currency of life, adenosine triphosphate (ATP), which the human body consumes its own weight of in quantity daily,[40] is a polyanion, as are many of the key intermediates in the metabolic Krebs cycle such as citrate, malonate, fumarate and succinate.[41] Anions such as chlorite and hypochlorite generated in textile production and dichromate from the manufacture of raw materials for the chemical industry have all been reported as major contaminants in environmentally damaging waste runoff. From the drinking water crises in the Ganges Delta caused by high levels of arsenate[42] to the currently ongoing Flint, Michigan water crisis that implicates toxic concentrations of chloride in treated drinking water[43,44], it is clear that anions must be carefully monitored for the good of public health. Anions play important roles in many technologies: in automobile airbags the explosive azide anion is harnessed to react with heat activated oxidants to rapidly generate nitrogen gas to inflate the airbag in the event of a violent collision.[45] An example of the use of anions in the field of homogenous catalysis would be the ubiquitous non-coordinating $[BAr^{F}{}_{4}]^{-}$ anion, which crucially stabilises cationic coordinately unsaturated polymerisation catalysts such as the bimetallic rhodium 'Xantphos' complexes[46], enabling high turnover rates. What is sought to be communicated here is that the understanding of the reactivity and coordination chemistry of anions is worthy of study and of high importance in the design and function of any application involving these species.

1.2.2. The challenge of anion coordination

The design of anion selective coordinating hosts presents a meticulous challenge. Unlike cations, they are in possession of filled valence orbitals - thus rendering them in most cases incapable of strong covalent bonds to ligands or hosts. Anions have small charge:radius ratios and often exhibit demanding geometries, particularly in the polyatomic anions such as linear (SCN^{-}, N_3^{-}), trigonal planar (NO_3^{-}, CO_3^{-}), square

planar ($PtCl_4^{2-}$, $AuCl_4^-$), tetrahedral (SO_4^{2-}, $H_2PO_4^-$) and octahedral (PF_6^-, $[Fe(CN)_6]^{4-}$) (**Figure 1.10**).

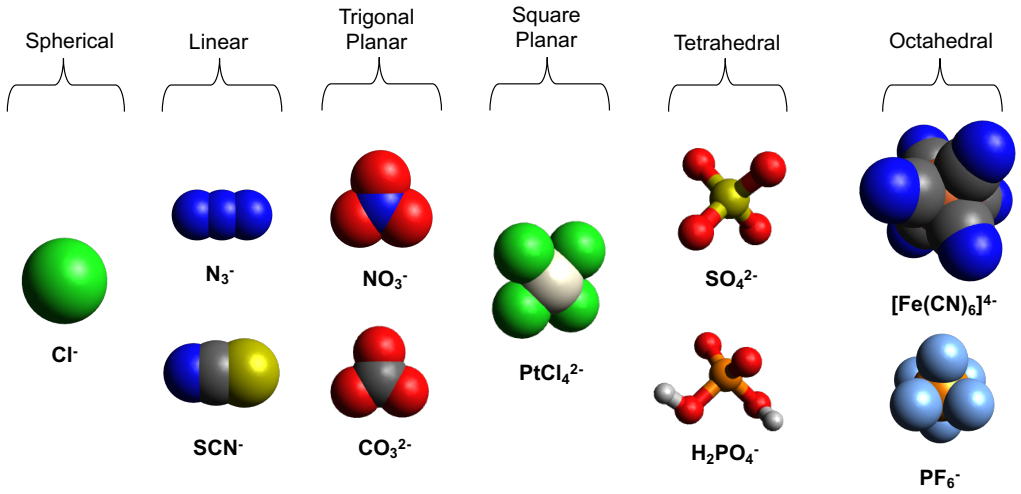


Figure 1.10 – The geometries of some commonly studied anions.

Considering factors apart from structure, it is worth considering that certain anions can only exist within the confines of a pH window, for example the basic AcO^- anion can only exist above pH 5.5.[47] Anions experience a higher degree of solvation in comparison to similarly sized cations, they are favourably solvated in protic media such as alcoholic solvents and water due to their ability to accept hydrogen bonds (in their capacity as Lewis bases).[48] A useful measure of an anion's relative hydrophilicity/hydrophobicity in this context is the Hofmeister series, a scale originally conceived to explain the dependence of protein salts to dissolve or precipitate in aqueous solution conditional on the counterion present (**Figure 1.11**).[49] Historically, the Hofmeister effect has been thought to result from the attenuation of the ordering of water molecules encapsulating the anion, kosmotropic or "salting-out" anions such as SO_4^{2-} and HPO_4^{2-} interacting constructively with aqueous solvation structure and therefore strongly hydrated, whereas chaotropic anions or "salting-in" such as ClO_4^- and I^- interact disruptively and are weakly hydrated.

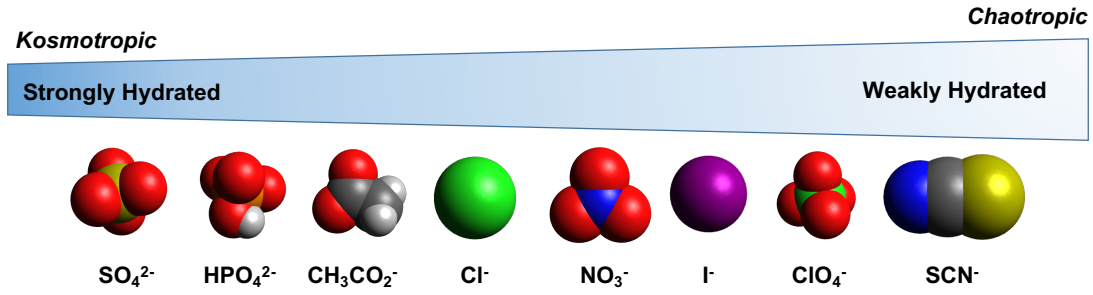


Figure 1.11 – The Hofmeister series of anions.

Natural examples elegantly overcome these aformentioned challenges and provide ongoing inspiration for synthetic receptor design. Anion binding proteins such as sulphate binding protein (SBP) offer geometrically complementary binding pockets shielded from competing solvent, in this case the highly pre-organised arrangement of hydrogen bond donating tryptophan and glycine peptide residues to accommodate the tetrahedral and highly hydrated SO_4^{2-} remarkably enables aqueous bacterial anion transport (**Figure 1.12**).[50]

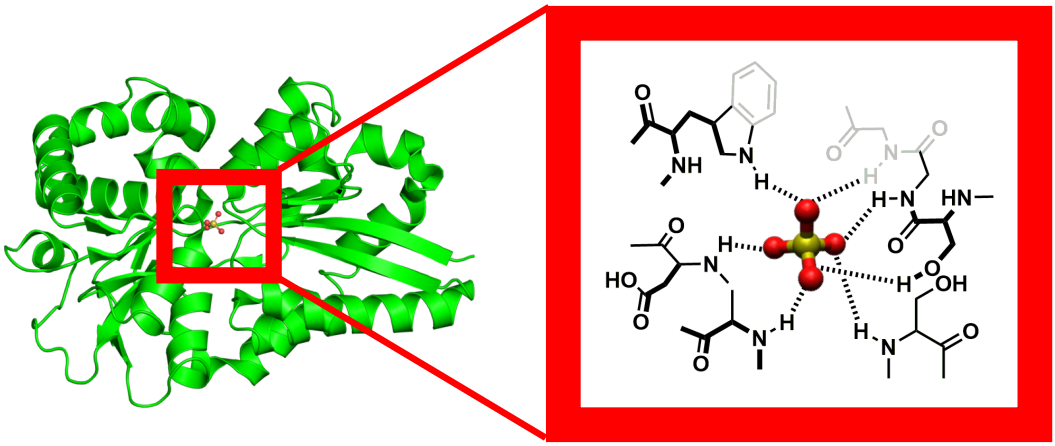


Figure 1.12 – The structure of the SO_4^{2-} binding cleft of SBP (inset) showing the complementary seven convergent hydrogen bonds to the tetrahedral dianion.

1.2.3. Synthetic anion receptor design

Most synthetic anion receptors and the enlightening natural examples that inspire them have common factors that arbitrate their effectiveness in the strength and selectivity of their recognition of anionic guests. Often numerous, preorganised

dipole-anion interacting species such as hydrogen or halogen bond donors are applied in tandem with i) cationic organic functional groups, ii) highly polarised neutral species or iii) main group/metallic Lewis acids to provide electrostatic assistance in attracting negatively charged guests.

1.2.3.1. Positively charged anion receptors

Ammonium based anion receptors

The genesis of anion binding supramolecular chemistry began with Park and Simmons in 1968, who synthesised a family of polyammonium macrobicycles that bound halide anions in acidic water *via* a combination of favourable electrostatic interactions and hydrogen bonding, the very first known example of anion encapsulation by an organic ligand (**Figure 1.13**).[51]

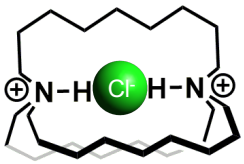


Figure 1.13 – Park & Simmons halide binding ammonium cryptand.

Almost a decade later, in 1976, Lehn and co-workers capitalised on their knowledge of cryptand synthesis to create spherical halide cryptates (**Figure 1.14-i**)[52] and in 1978 an oval-shaped polyammonium cryptand (**Figure 1.14-ii**) which selectively bound the complementarily shaped linear N_3^- anion.[53] Recently, polyammonium cryptand hosts have been revisited by Amendola and co-workers to selectively bind the radioactive anionic pollutant pertechnetate in pure water (**Figure 1.14-iii**).[54]

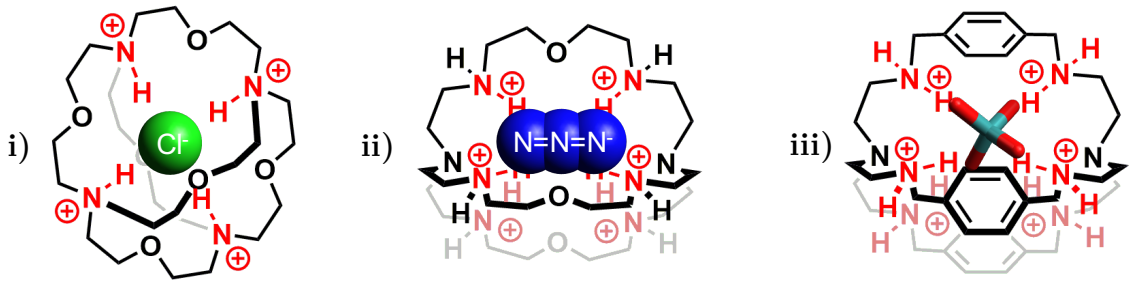


Figure 1.14 – Lehn's i) macrotricyclic Cl^- and ii) macrobicyclic N_3^- cryptates; iii) Amendola's phenyl substituted TcO_4^- cryptate.

Polyammonium hosts are fundamentally constrained to function only within the low pH window in which the ammonium groups remain protonated. To overcome this limitation, Schmidtchen used quaternary ammonium cages that relied almost exclusively on point electrostatic interactions to bind anions in water. By varying the length of the vertices of the polygonal receptors, the smaller receptor (R = R^1; cavity radii = 1.95 Å) showed a stronger affinity for the smaller halides Cl^- and Br^- whereas the larger receptors (R = R^2, R^3; cavity radii = 2.3 Å, 3.8 Å respectively) bound I^- strongly at the expense of Cl^- (**Figure 1.15**).[55] Second generation zwitterionic hosts incorporating anionic carboxylate[56] and carboranyl[57] moieties to negate any competing counterion effects were later shown to exhibit greatly enhanced binding of halides whilst still maintaining selectivity trends.

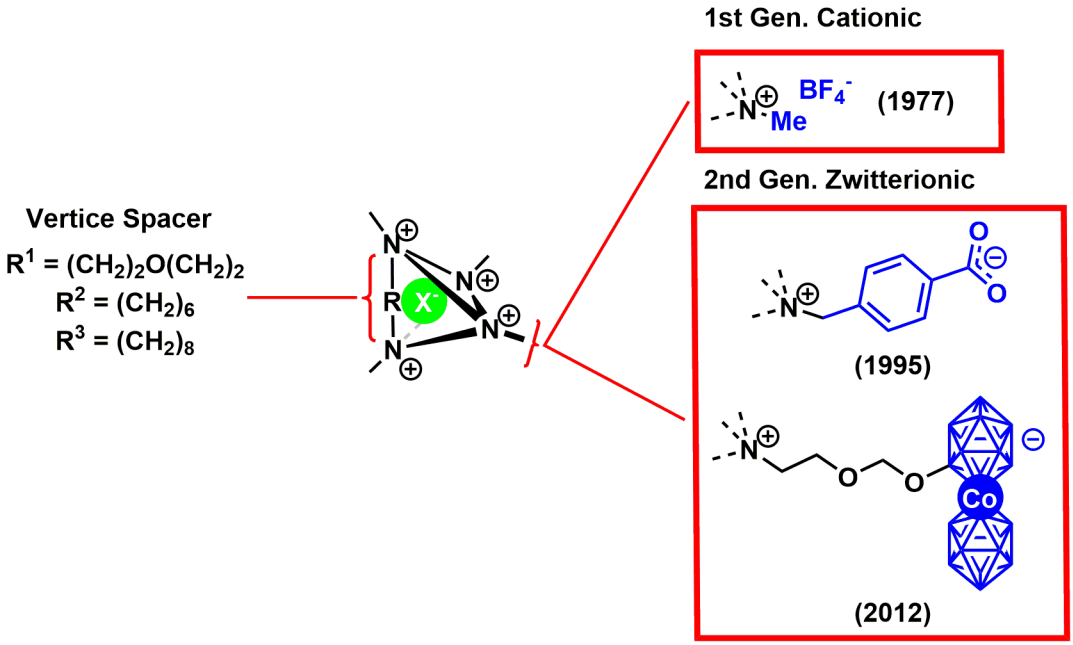


Figure 1.15 – Schematic of Schmidtchen's quaternary ammonium cage design, showing vertex lengths used (left red box) and ammonium functionalisation (right red boxes) for the 1st (1977) and 2nd generation (1995 and 2012) cages.

Taking inspiration from Nature's extensive use of the cationic side chain of the arginine amino acid residue in anion binding[58], the advantages of the guanidinium cation are numerous, the conjugate base guanidine's basicity (up to $pK_a = 13.5$) ensures the protonated form exists across a very wide pH range. The organocation's unique Y-shape complements the carboxylate anion through strong hydrogen bonding. Its appropriation into synthetic receptors has been pervasive[59]; from uses in sequence specific peptide binding in combinatorial chemistry (**Figure 1.16-i**)[60] to highly specific and enantioselective citrate receptors such as Anslyn's tripodal receptor in water (**Figure 1.16-ii**).[61]

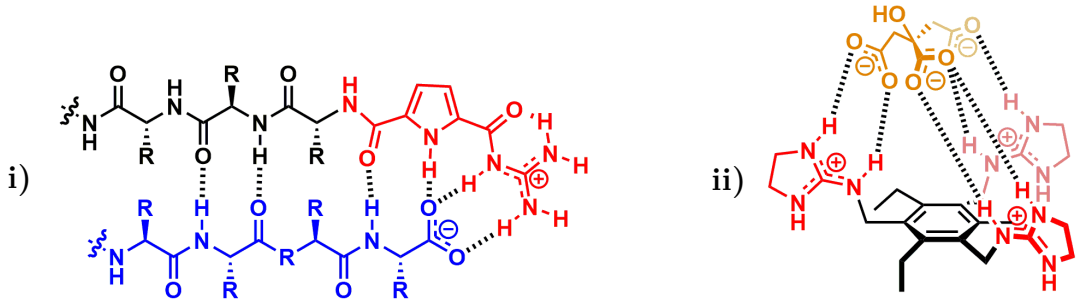


Figure 1.16 – i) Wich's peptide sequence specific guanidiniocarbonyl pyrrole receptor; ii) Anslyn's citrate selective triguanidinium tripod.

Cationic heterocyclic receptors

Imidazolium and triazolium receptors have received sustained interest due to their relative ease of synthesis and incorporation into a wide variety of acyclic, cyclic and interlocked hosts. This class of receptor exploits tandem cationic electrostatic attraction and directional C-H hydrogen bonding akin to the guanidinium receptors but importantly the cationic heterocyclic motif does not rely on protonation to introduce positive charge. Imidazolium donors were effectively brought together in a tripodal convergent anion binding site preorganised by distal Fe(II) tris-complexation. The resulting Fe(II) host system displayed selectivity for the linear N_3^- anion ($K_A(N_3^-)$ = 5.0 x 10^5 M^{-1}) versus Cl^- ($K_A(Cl^-)$ = 6.3 x 10^3 M^{-1}) in MeCN-H_2O (4:1 v/v) (**Figure 1.17-i**).[62] Kim and co-workers recently reported a series of macrocyclic calix[n]imidazolium derivatives where the tetrameric homologue bound even strongly hydrated F^- with remarkable selectivity in water (**Figure 1.17-ii**).[63] The triazolium motif is readily accessible *via* the ubiquitous copper(I)-catalysed cycloaddition of azides and alkynes (CuAAC). Beer and co-workers constructed a tetratriazolium macrocycle that bound SO_4^{2-} selectively in the competitive 1:1 DMSO/H_2O solvent mixture (**Figure 1.17-iii**).[64]

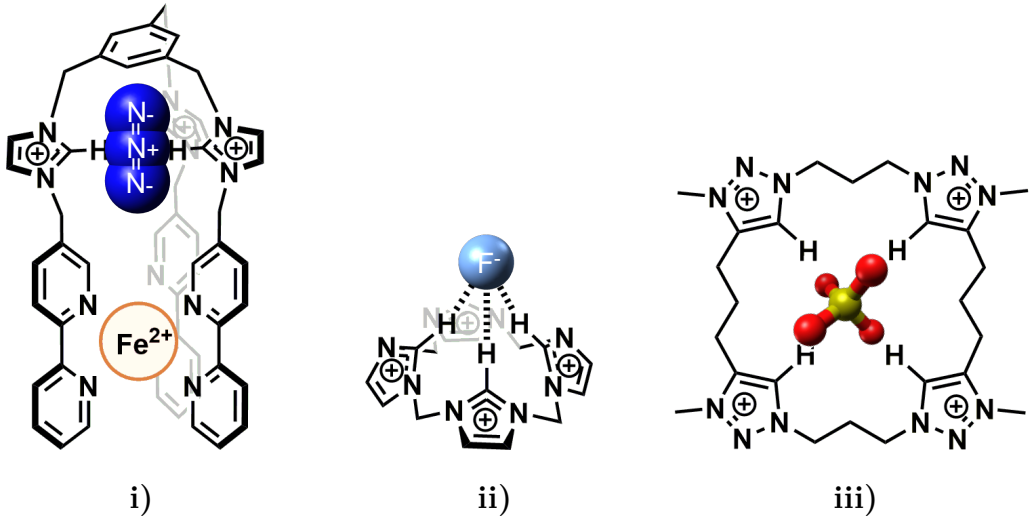


Figure 1.17 – i) Fabbrizzi's ditopic Fe(II) triimidazolium cage; ii) Kim's calix[4]imidazolium F^- selective macrocycle; iii) Beer's tetratriazolium macrocycle binding SO_4^{2-}.

Cationic anion-π receptors do not utilise hydrogen bonds as directional recognition vectors but instead utilise the rarely observed interaction of an anion with an aromatic π-acid. Recently, Stoddart and coworker's hexacationic "BlueCage" cyclophane shows the unusual encapsulation of the non-coordinating PF_6^- anion through convergent anion-π interactions sandwiched between two π-acidic tripyridinium-triazine panels in the solid state (**Figure 1.18**).[65]

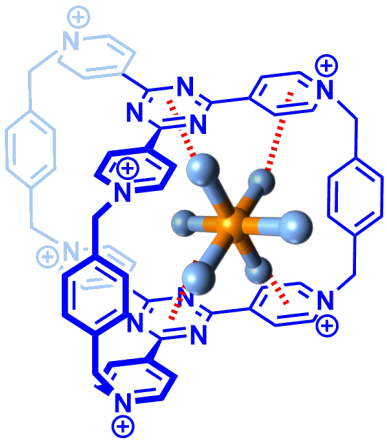


Figure 1.18 – Stoddart's "BlueCage" binding a PF_6^- anion.

1.2.3.2. Neutral anion receptors

In contrast to their charge assisted analogues, neutral anion receptors often rely solely on weaker ion-dipole interactions such as hydrogen bonding. Nonetheless, to overcome competitive solvent effects, this class of receptor often exhibits a high degree of preorganisation to provide convergent, strong anion binding interactions.

Amide functionalised receptors

The amide motif, utilising a polarised N-H hydrogen bond donor, is considered the prototypical neutral anion binding moiety. Ever since Crabtree demonstrated in 1997 the halide anion binding capability of a simple isophthalamide anion binding cleft in DCM (**Figure 1.19-i**)[66], there has been a burgeoning interest in amide functionalised anion receptors. Template driven dynamic combinatorial chemistry was used to develop Sander's ferrocenyl $H_2PO_4^-$ receptor (**Figure 1.19-ii**). The synergy of reversible hydrazone formation and cooperative $H_2PO_4^-$ templation spontaneously forms a ditopic receptor that binds two anions *via* amide and hydrazone hydrogen bonds, a structure that reflects the optimisation of the interactions between host and guest.[67]

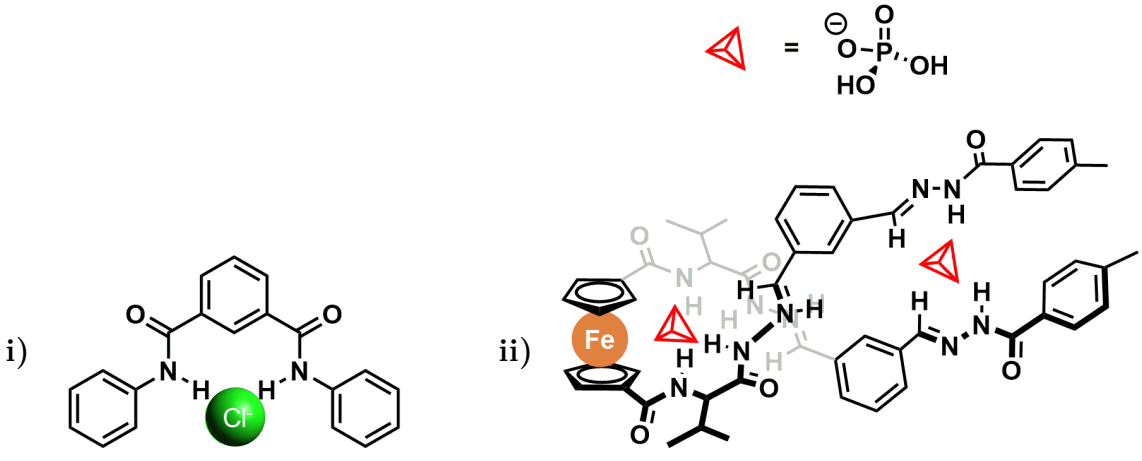
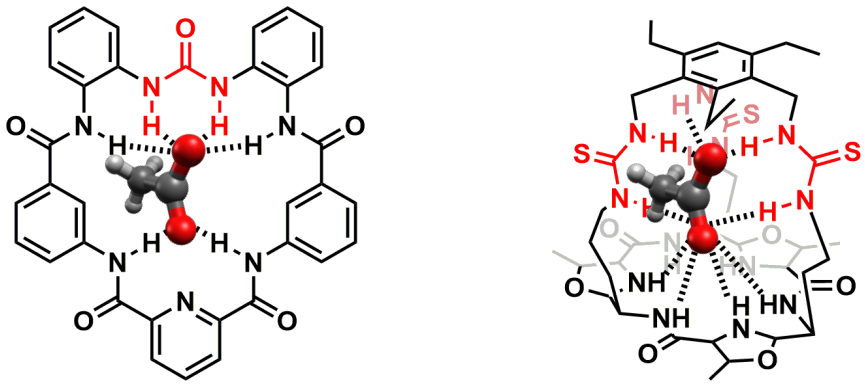


Figure 1.19 – i) Crabtree's isopthalamide receptor; ii) Sander's dynamically assembled helical linear $H_2PO_4^-$ receptor.

Urea and thiourea functionalised receptors

Urea and thiourea based hosts employ multiple hydrogen bonds in the recognition of often complementary oxoanion guests such as trigonal NO_3^- and AcO^- ions. Gale's macrocyclic host utilises the strongly polarised N,N′-diphenylurea moiety in cooperation with four amide hydrogen bond donors to bind AcO^- selectively over halides and other oxoanions in DMSO-water mixtures (**Figure 1.20-i**).[68] Adding a degree of dimensional complexity, Jolliffe and co-worker's tetra-cyclic thiourea cryptand selectively bound AcO^- in 0.5% D_2O/DMSO with an association constant remarkably three orders of magnitude greater than the other halides and oxoanions studied (**Figure 1.20-ii**).[69]



i) ii)

Figure 1.20 – Acetate binding in i) Gale's amidourea macrocycle; ii) Jolliffe's tetracyclic peptide-thiourea cryptand.

Neutral C-H hydrogen bonding receptors

Neutral C-H hydrogen bonding receptors have been relatively overlooked because of weak C-H bond polarisation in the absence of positive charge. The influence of preorganisation overcame these limitations in the exemplary series of Flood and co-worker's highly preorganised triazolophane systems.[70] The correlation of the increasing strength of association for Cl^- in DCM with increasing preorganisation of the triazolophane host confirms that the macrocyclic effect and structural

rigidification of these receptors is crucial in anion recognition (**Figure 1.21-i**).[71] Taking into account this understanding of triazolophane structure, the binding of the linear HF_2^- anion was optimised in the computer-aided design of a triazolophane scaffold to enable co-planar binding geometry between the anion and macrocycle to enhance binding association of this exotic anion in DCM (**Figure 1.21-ii**).[72]

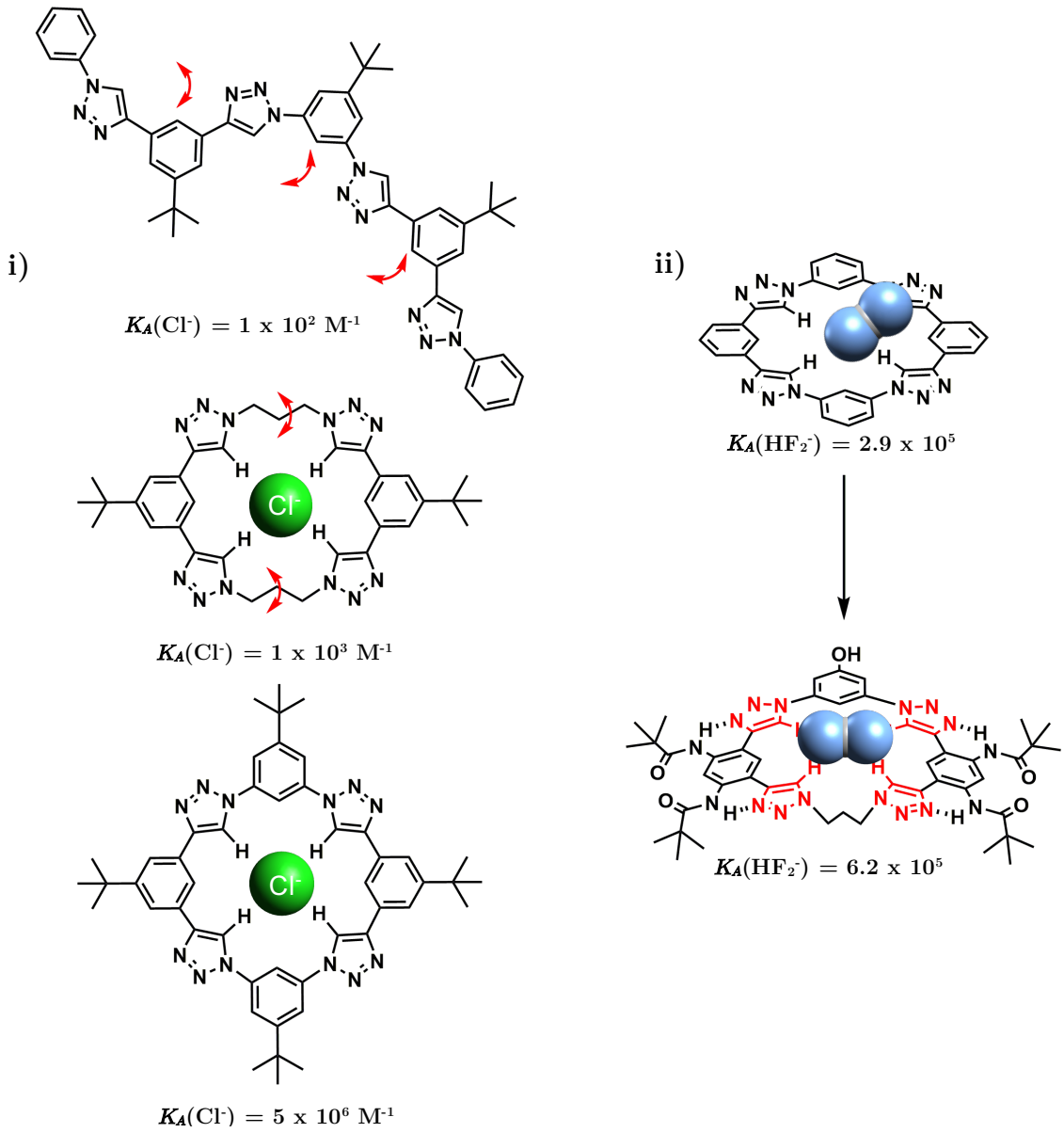


Figure 1.21 – i) Flood's demonstration of increasing macrocycle preorganisation leading to higher binding constants for Cl^- in DCM; ii) the computer optimised design of Flood's HF_2^- receptor to allow coplanar binding by the macrocycle.

Halogen bonding anion receptors

Although relatively well known in crystal engineering applications for its desirable linear mode of binding[73,74], halogen bonding is much less exploited in the solution phase binding of anions and other Lewis bases. Superficially, this interaction in the context of anion recognition is similar to hydrogen bonding but when integrated into anion receptors often displays contrasting selectivity trends and anion affinities.[11,75] A notable early example is Taylor's convergent tripodal tetrafluoroiodobenzene receptor, which was shown by ^{19}F NMR to be Cl^- selective in acetone over a series of other halides and oxoanions.[76] In another example of a tripodal tetrafluoroiodobenzene receptor, halogen bonding contributes 7.5 kJ mol^{-1} to the free energy of association of Resnati's ditopic ion-pair receptor to NaI in $CDCl_3$ (**Figure 1.22-ii).**[77]

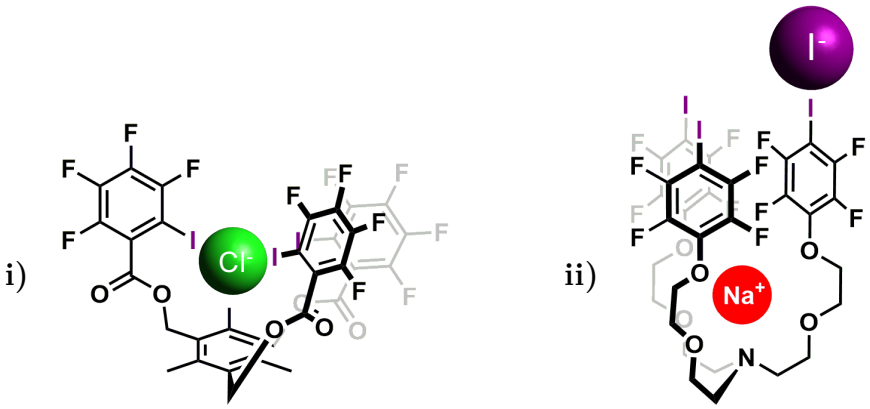


Figure 1.22 – i) Taylor's tripodal convergent tetrafluoroiodobenzene receptor, ii) Resnati's ion pair halogen bonding receptor.

Via adaptation of the preorganisational approach to the design of Flood's receptors, Schubert has utilised intramolecular hydrogen bonds to orient polarised iodotriazole halogen bond donors into a convergent binding cleft which led to an order of magnitude enhancement in the binding of both Cl^- and Br^- in THF in comparison to the un-preorganised receptor (**Figure 1.23**).[78]

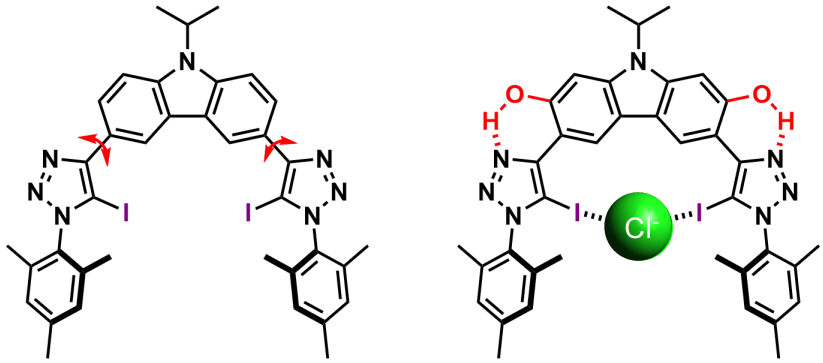


Figure 1.23 – Schubert's hydrogen bonding preorganised (right) convergent halogen bonding receptor.

1.2.3.3. Anion receptors exploiting the hydrophobic effect

As previously discussed in section 1.2.2, Hofmeister effects can be very important factors in dictating the strength and selectivity patterns of anion receptors. In recent years, this has led to increasing numbers of receptors using predominantly hydrophobic effects in the recognition of anions in aqueous solvent media. The remarkable dimerisation of Kubik's peptidic macrocycle in 1:1 MeOH/H_2O which encapsulates the strongly hydrated kosmotrope SO_4^{2-}, exhibited a positive entropic contribution to the binding, implicating the hydrophobic effect in the displacement of ordered water molecules solvating the anion as a strong thermodynamic driving force for the binding event (**Figure 1.24-i**).[79] More recently, Gibb's anionic octa-carboxylate cavitand demonstrates that anion binding competition in hydrophobic receptors is dictated by the Hofmeister series (**Figure 1.24-ii**).[80] In water, the chaotropic ClO_4^- is the most strongly bound within the hydrophobic cavity of the receptor in the presence of kosmotropic co-salts such as NaCl and weakest in the presence of chaotropic salt NaSCN that competes with ClO_4^- for binding within the cavitand.

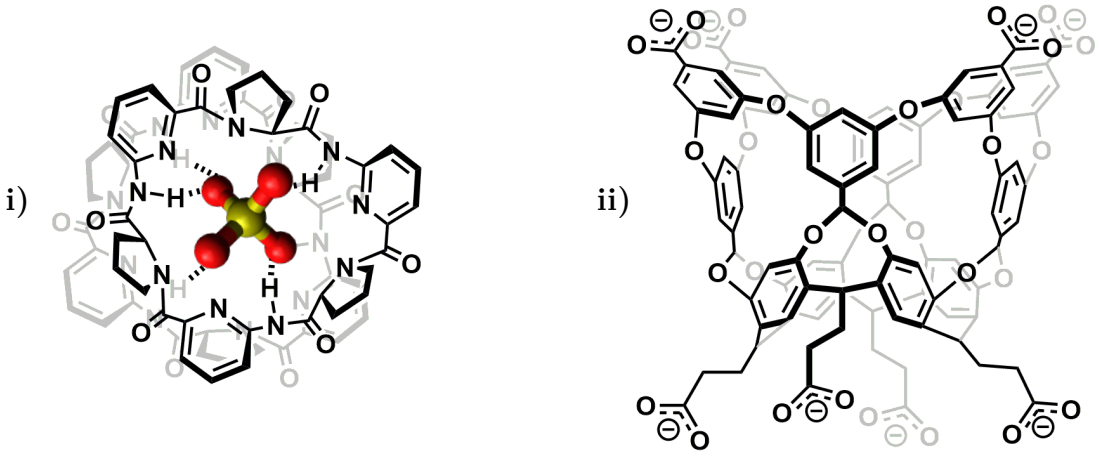


Figure 1.24 – i) Kubik's peptidic macrocycle dimer with SO_4^{2-}; ii) Gibb's octa-acid water soluble cavitand.

1.2.3.4. Lewis acidic main group and metal based receptors

The use of electron deficient main group Lewis acids such as boron, silicon and antimony are attractive motifs in anion receptor design, where anion coordination is driven by the formation of a dative bond to the Lewis acidic centre. This predominantly manifests itself in the filled orbitals of an anion donating to an empty acceptor orbital, such as the halide binding in MeOH seen in Gabbaï's unique dual binding site receptor consisting of an electron deficient chalcogen atom with an empty σ^*-orbital and a Lewis acidic boron centre possessing an empty p-orbital (**Figure 1.25-i**).[81] Anions are able to coordinate strongly to transition metals, such as apical binding to coordinatively unsaturated polyhedral metal centres such as those found in Murase's bimetallic Cu(II) octa-aza macrocycle that can chelate N_3^- in H_2O ($K_A(N_3^-) = 1.25 \times 10^4$) (**Figure 1.25-ii**).[82]

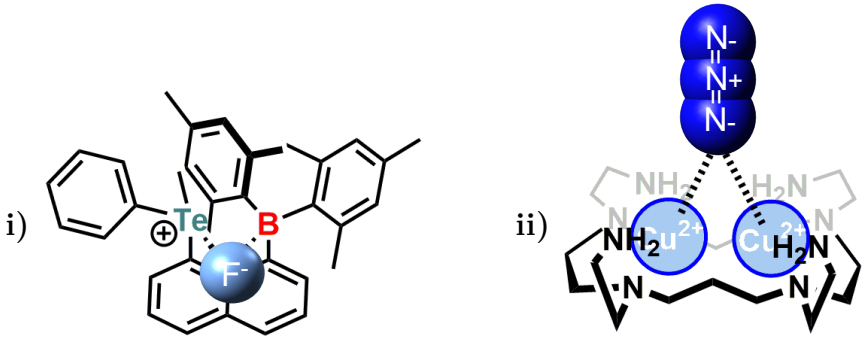


Figure 1.25 – i) Gabbaï's dual binding site telluronium/trimesityl boron receptor; ii) Murase's bidentate anion binding Cu(II) octa-aza macrocycle.

1.2.4. Anion sensors

Anion recognition events that produce a measurable, macroscopic optical or electrochemical response is a desired trait in anion sensor design. This active field has produced many examples of receptors that sense anions *via* fluorescent, colourimetric and electrochemical responses. Considerable changes in the bound and unbound states are a requirement, commonly achieved *via* the integration of optical or electrochemical reporter groups proximal to the anion recognition site.

1.2.4.1. Luminescent anion sensors

The sensing of anions *via* changes in the emission profile (*via* luminescence lifetime, wavelength or intensity) of a metal centre or organic chromophore has been explored extensively in the past several decades.[83–85] Examples that utilise the anion-induced activation or deactivation of photo-induced electron transfer (PET) fluorescence quenching processes to sense anions include Czarnik's HPO_4^{2-} sensor where the anthracene-centred fluorescence is switched from "off" to "on" *via* the protonation of the PET quenching tertiary amine group (**Figure 1.26-i**).[86] "On" to "off" is possible in the case of Ravikanth's colourimetric BODIPY F^- receptor. The deprotonation and formation of HF_2^- in MeCN upon the addition of two equivalents

of F^- initiates a disruption to the coplanarity of the benzimidazole and BODIPY groups, leading to the PET quenching of the chromophore and loss of the pink fluorescence in favour of a weak blue luminescence (**Figure 1.26-ii**).[87] This regime can also be replicated harnessing the PET sensitive fluorescence of quantum dots, Li and co-worker's CdSe quantum dots stabilised by anion binding urea appended thiols demonstrated PET deactivation and quantum dot centered fluorescence upon the addition of carbonate in $CHCl_3$/EtOH 4:1 (**Figure 1.26-iii**).[88]

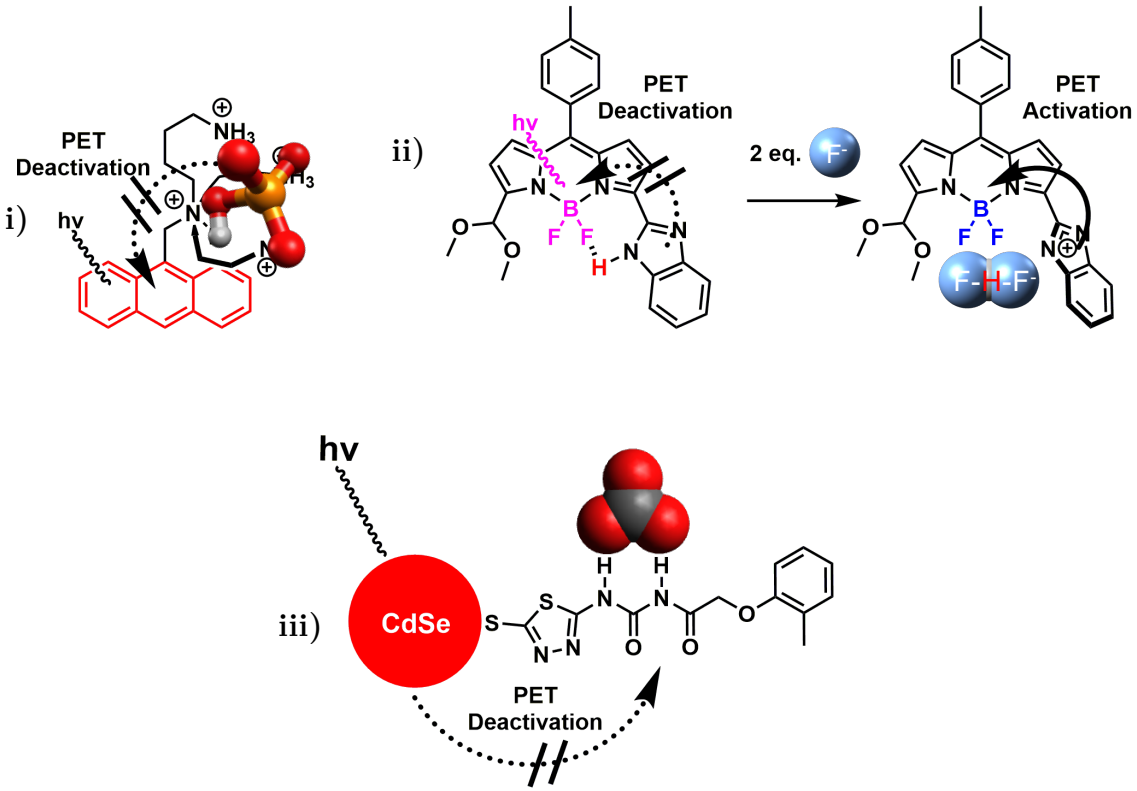


Figure 1.26 – i) Czarnik's HPO_4^{2-} receptor showing the cessation of PET quenching of anthracene fluorescence upon protonation; ii) Ravikanth's BODIPY F^- receptor exhibiting PET quenching upon deprotonation; iii) Li's CdSe nanoparticle centred luminescence upon carbonate binding.

Gunnlaugsson's urea-functionalised tris-bipyridine ruthenium complex exhibits ^{3}MLCT enhancement upon the binding of $H_2PO_4^-$ and quenching with $P_2O_7^{4-}$ in MeCN (**Figure 1.27-i**).[89] Yam and co-worker's calixarene-preorganised bis-alkynylplatinum(II) terpyridine complexes exhibited an enhanced degree of spectral changes in the emission and absorbtion spectra compared to the mononuclear

analogues particularly upon the addition of F^- and AcO^- in DMSO. This structural dependence was attributed to cooperative anion binding in the dipodal receptor and the lack thereof in the monopod (**Figure 1.27-ii**).[90]

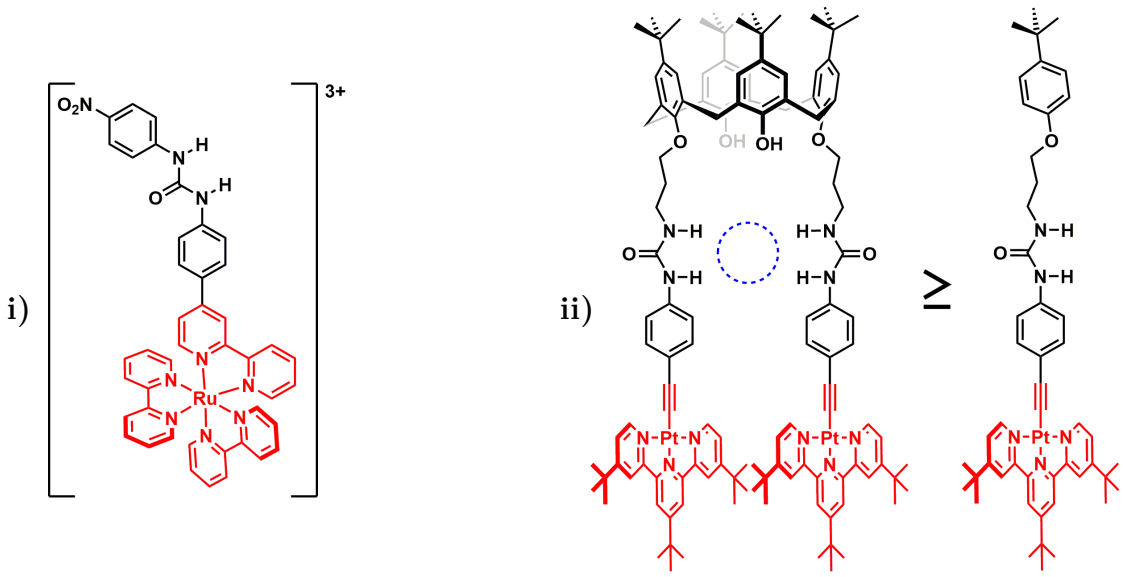


Figure 1.27 – i) Gunnlaugsson's ruthenium tris-bipyridyl urea $H_2PO_4^-/P_2O_7^{4-}$ receptor; ii) Yam's cooperative alkynylplatinium(II) dipodal F^- and AcO^- receptor.

Lanthanide based anion receptors

Lanthanide based receptors represent a unique class of receptors, one that principally utilises phosphorescence as the signalling mode of an anion binding event. Considerable interest has been dedicated to this class of anion sensor due to their long lived luminescence lifetimes, which deems them useful in biological regimes where background autofluorescence can be detrimental to the use of traditional fluorescent probes.[91] Direct apical coordination of anions such as carboxylates to Lewis acidic lanthanide centres leads to a luminescence enhancement as a result of the displacement of coordinated water which, as an O-H vibronic oscillator, is a known quencher of lanthanide luminescence[92]. Impressive anion selectivities can be achieved in this recognition mode in water; as exemplified by Parker's Eu(III) and

Tb(III) carbonate selective mitochondrial imaging probes (**Figure 1.28-i**)[93] and citrate selective Eu(III) receptors (**Figure 1.28-ii**).[94]

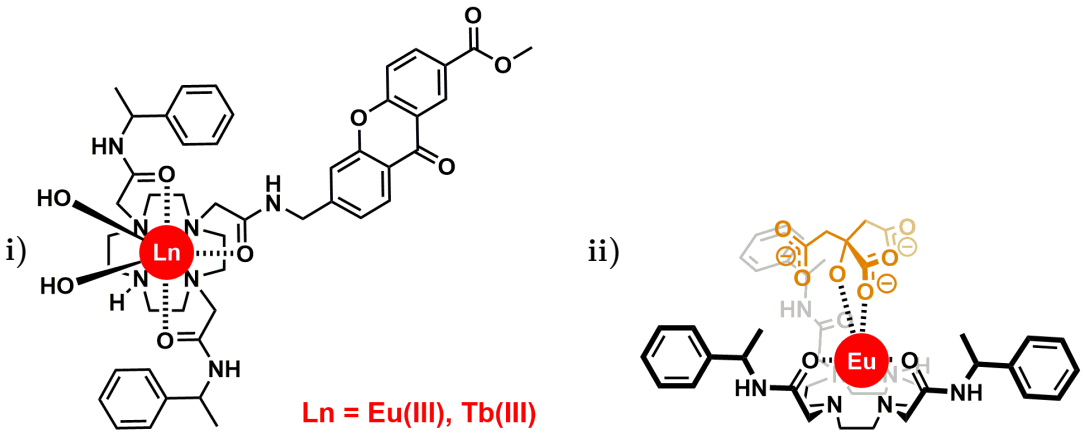


Figure 1.28 – Parker's i) carbonate selective mitochondrial imaging probes and ii) citrate selective Eu(III) complex (citrate anion shown in orange).

1.2.4.2. Electrochemical anion sensors

The observation of changes in a redox couple potential upon anion binding of well-known electrochemically active species is an attractive approach to sensing anions, possessing innate sensitivity and the prospect of incorporation into devices. Among the most commonly utilised in this manner are metallocene redox couples, where the addition of anions to these systems stabilize the positively charged metallocenium redox state. The cobaltocenium/cobaltocene redox couple was first used in this way by Beer's series of cobaltocenium macrocycles to sense Br^- *via* cathodic shifts of the redox couple of up to 45 mV (**Figure 1.29-i**).[95] The ferrocenium/ferrocene redox couple has been analogously applied; large cathodic shifts upon the binding of CN^- (560 mV in MeCN) were observed in Aldridge's Lewis acidic ferrocene triaryl boron receptor (**Figure 1.29-ii**).[96] Sensing of oxoanions was demonstrated in Astruc's ferrocenyl dendrimers where the assistance of dendritic effects saw up to a 315 mV cathodic shift in DCM upon the addition of one equivalent of $H_2PO_4^-$ (**Figure 1.29-iii**).[97] Very recently, Beer's series of exotic

halogen bonding ferrocenyl bis-iodotriazolium receptors showed superior recognition of halides in competitive MeCN/H_2O solvent mixtures with significantly larger cathodic shifts observed upon the addition of halides in comparison to hydrogen bonding homologues (**Figure 1.29-iv**).[98]

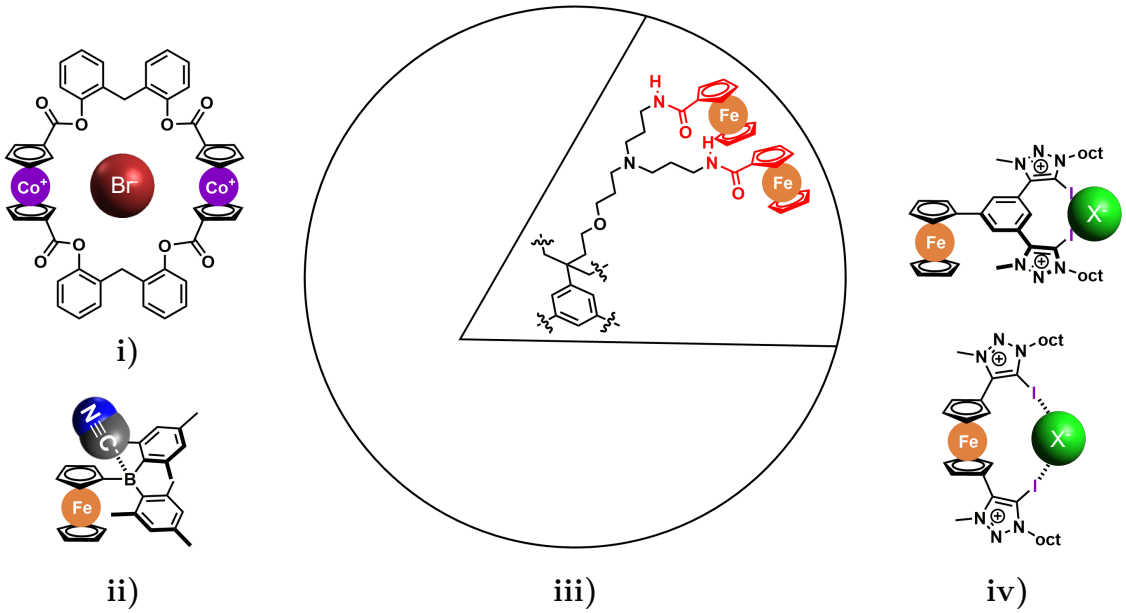


Figure 1.29 – i) Beer's macrocyclic bis-cobaltocenium Br^- sensor; ii) Aldridge's ferrocene derivatised Lewis acidic triaryl-boron CN^- receptor; iii) a cross section of Astruc's oxoanion sensing ferrocene dendrimer; iv) Beer's ferrocenyl bis-iodotriazolium halide sensing halogen bonding receptors.

Tetrathiafulvalene (TTF) is another multi-state redox reporter group used in electrochemical anion sensing applications. It undergoes sequential oxidation processes to the monocationic $TTF^{\cdot+}$ and dicationic TTF^{2+} species.[99] Zhu's dual optical/electrochemical TTF-based sensor electrochemically senses the selective binding of $H_2PO_4^-$ in DCM with a strong cathodic shift of 172 mV of the first TTF/$TTF^{\cdot+}$ oxidation potential (**Figure 1.30-i**).[100] Strongly electron donating 1,3-dithiol-2-ylidene subunits present in TTF form part Sessler's Zn(II) porphyrins; which upon the coordination of Cl^- at the Zn metal centre, induces a 130 mV cathodic shift of the oxidation potential of the Zn(II) TTF-porphyrin, favouring a

thermal electron transfer to the electron acceptor $Li^+@C_{60}$ endofullerene in DCM (**Figure 1.30-ii**).[101]

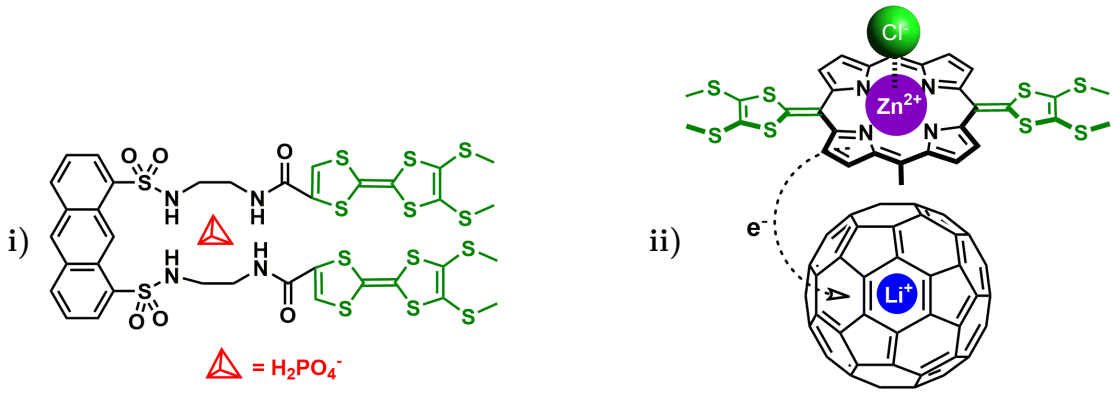


Figure 1.30 – i) Zhu's multisignalling TTF functionalised $H_2PO_4^-$ receptor; ii) Sessler's TTF-Zn(II) porphyrin sensing Cl^- *via* electrochemical activation of thermal electron transfer to $Li^+@C_{60}$.

1.3. Mechanically Interlocked Host Systems

The simplest definition for a mechanically interlocked molecule is a molecule that is connected by virtue of only its topology. Initially the subject of academic curiosity when sparing amounts of the first isolated catenane was synthesised in a "bathtub" scale high dilution reaction in 1961 by Wasserman and co-workers[102], the advent of supramolecular chemistry and increasing knowledge of strong self-assembly processes between molecules drove a reassessment of how these structures could be constructed beyond purely statistical reactions.[103–107] The interlocked architectures that have been prepared by using various templating methods are multitude; [n]catenanes[108], [n]rotaxanes[109], more complex knot-like compounds such as Borromean rings[110], Solomon links[111] and other molecular knot topologies[112] have been synthesised. '[n]' simply denotes the number of discrete molecular components that comprise the interlocked structure. The main classes considered in this thesis are rotaxanes which consist of a macrocyclic ring mechanically bonded around a linear axle component with stoppering motifs to prevent the disassociation of the ring component (**Figure 1.31-i**), and catenanes, which are simply two or more

interlocked rings mechanically bonded together (**Figure 1.31-ii**). The term "pseudo-rotaxane" denotes an interpenetrated structure much like a rotaxane but with no stoppering components, purely held together by either reversible intermolecular forces or coordinate bonds to a central guest (**Figure 1.31-iii**). Often these are precursors to the synthesis of catenanes and rotaxanes.

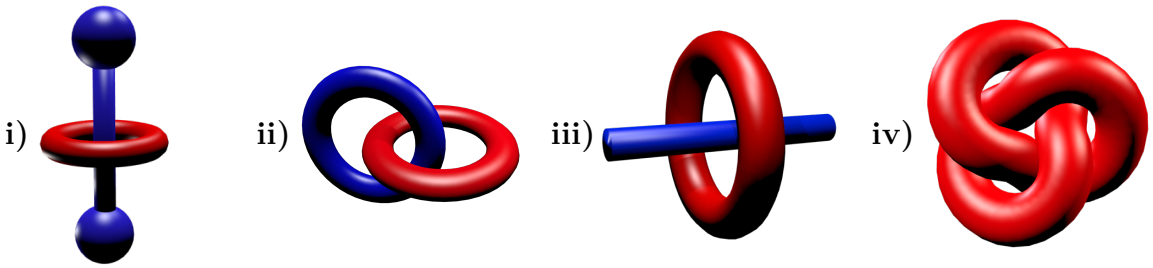


Figure 1.31 – Commonly encountered interlocked architectures: i) rotaxane, ii) catenane, iii) pseudorotaxane and iv) trefoil knot, an example of molecular knot.

In the context of this thesis, by appropriate design, rotaxanes and catenanes can provide unique, three dimensional host cavities for anion recognition and sensing that can exclude competitive solvent binding for the anion recognition sites that plague other classes of receptor and can be 'tailor made' to greatly enhance selectivity for particular anions of interest.

1.3.1. Strategies for the synthesis of interlocked host systems

Numerous synthetic strategies for mechanical bond formation have been reported to date. Chiefly, [n]catenanes are formed *via* the so called 'clipping' methodology, either 'singly clipping' a macrocyle precursor around an extant macrocycle (**Figure 1.32-i**) or 'double clipping' which entails clipping two macrocycle precursors simultaneously to form catenated structures (**Figure 1.32-ii**). Clipping is also a feasible method for introducing the macrocyclic component of [n]rotaxanes (**Figure 1.32-iii**). [n]Rotaxanes are often synthesised *via* entrapment of a pseudorotaxane

intermediate by the use of efficient covalent bond forming reactions to attach bulky groups to an axle component, a method known as 'stoppering' (**Figure 1.32-iv**). A less conventional procedure for the formation of [n]rotaxanes, particularly when the interior annulus of the macrocycle is large enough, is 'ring slippage' over a preformed stoppered axle (**Figure 1.32-v**). This can occur when high temperatures can allow the macrocyclic component to traverse the potential energy barriers to the formation of the mechanical bond caused by the presence of preinstalled bulky stoppers.

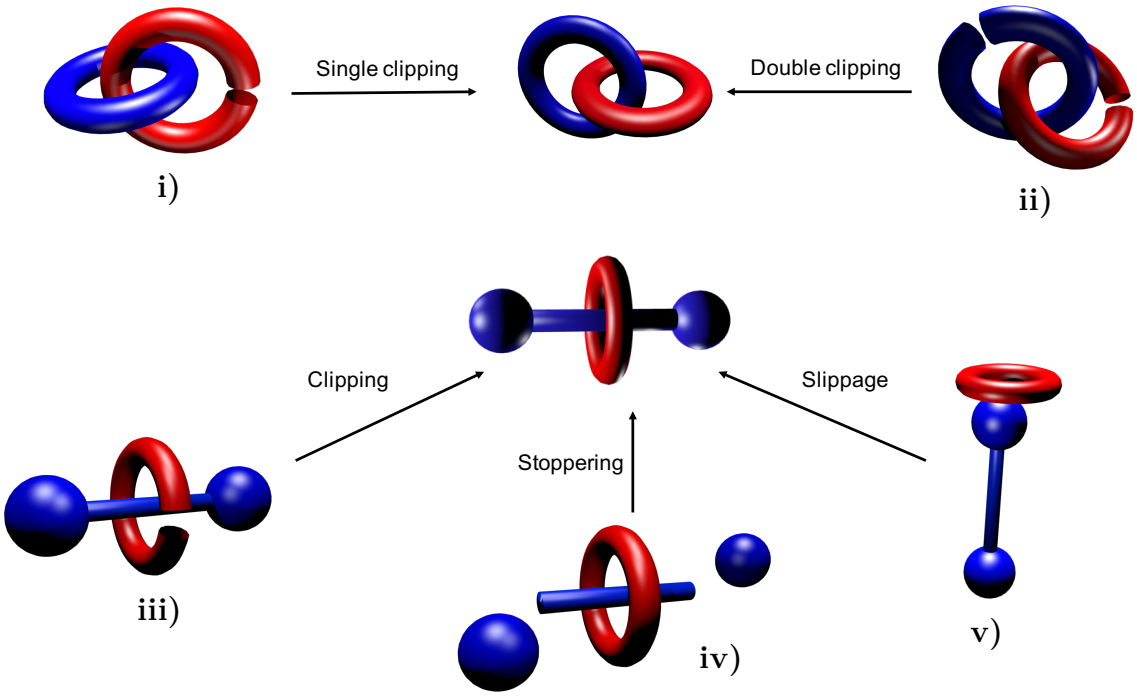


Figure 1.32 – Schematic representations of synthetic strategies for catenanes: i) single clipping, ii) double clipping and strategies for rotaxanes: iii) clipping, iv) stoppering, v) slippage.

1.3.2. Templation strategies

Following Wasserman's aforementioned first contributions using statistical methods to form a [2]catenane in a miniscule isolated yield of 1% (**Figure 1.33-i**)[102], Harrison and co-workers in 1967 sought a higher yielding synthesis by treating a resin bound macrocycle with reactive pre-axle components (**Figure 1.33-ii**).[113] After 70 laborious

treatments of the resin and hydrolysis of the reaction products, the [2]rotaxane was isolated in a marginally improved yield of 6%.

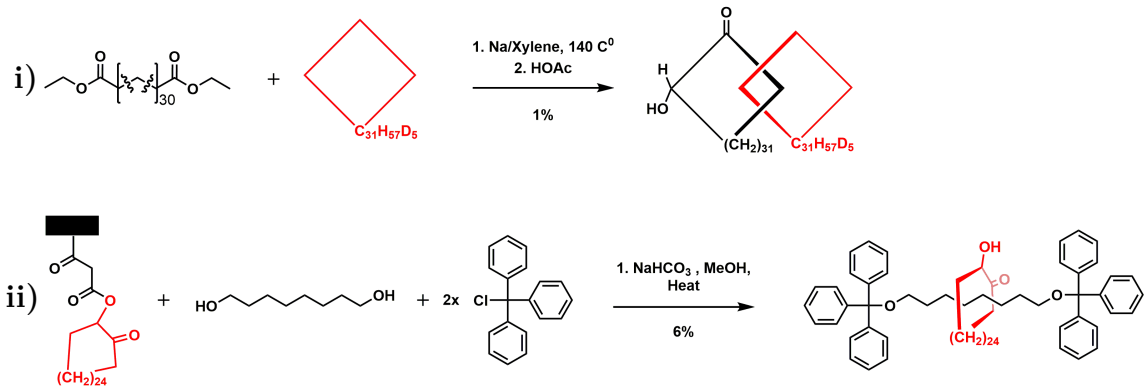


Figure 1.33 – i) Wasserman's [2]catenane; ii) Harrison's resin synthesised [2]rotaxane.

Busch and co-workers pioneered the use of Ni(II) in the transition metal templated formation of a macrocycle *via* reaction of α,α'-dibromo-*o*-xylene with a Ni(II) containing tetradentate Schiff base (**Figure 1.34**).[114] This work led to the conceptualisation of a chemical template as an entity that "*organises an assembly of atoms, with respect to one or more geometric loci, in order to achieve a particular linking of atoms.*"[115] This approach to the high-yielding synthesis of macrocycles was readily adopted by the supramolecular community in the wake of the onerous synthetic conditions of the earliest interlocked structures.

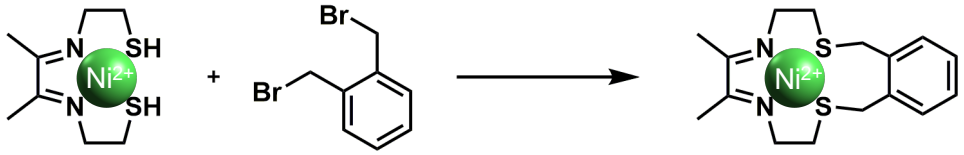


Figure 1.34 – Busch's Ni(II) templated synthesis of a Schiff base macrocycle.

1.3.2.1. Cationic templates

Building upon the work of Busch *et al.*, Sauvage and co-workers in 1983 made use of the tetrahedral coordination preferences of Cu(I) to orthogonally pre-associate two phenanthroline diols which, upon treatment with di-tosylate polyether chains

of sufficient length in the presence of Cs_2CO_3, a 'double clipping' synthesis of an interlocked metallocatenane was achieved in a good yield of 42%. This represented a watershed improvement on previous methods used to form interlocked structures (**Figure 1.35**).[116]

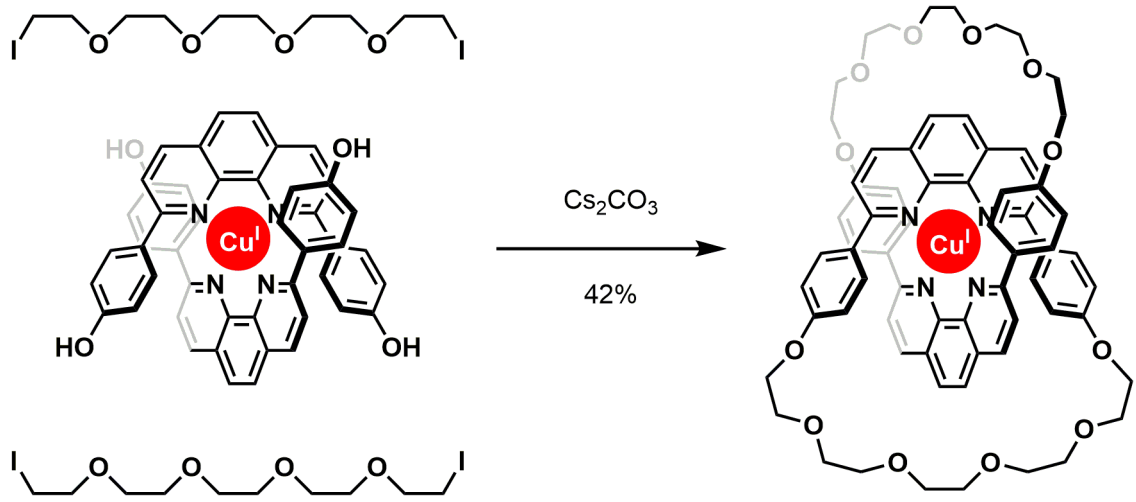


Figure 1.35 – Sauvage's Cu(I) templated synthesis of the first known metallocatenane.

The supramolecular research community took inspiration from this example, with further contributions adapting this metal template approach to many different metal-ligand complexes with varying geometries, as well as more complex multi-metallic interlocked assemblies. Contributions from Leigh and co-workers took advantage of the geometrical preferences of a large array of transition metals to template pyridine ligand-based rotaxanes and catenanes: the square-planar coordination of Pd(II) in a [2]catenane (**Figure 1.36-i**)[117], the octahedral coordination of Fe(II), Mn(II) and Co(III) in a series of Schiff base stoppered [2]rotaxanes (**Figure 1.36-ii**)[118], the linear coordination of Au(I) in a [2]rotaxane (**Figure 1.36-iii**)[119] and impressively the nonacoordinate lanthanide coordination sphere in a recent Lu(III) templated chiral molecular trefoil knot (**Figure 1.36-iv**).[120]

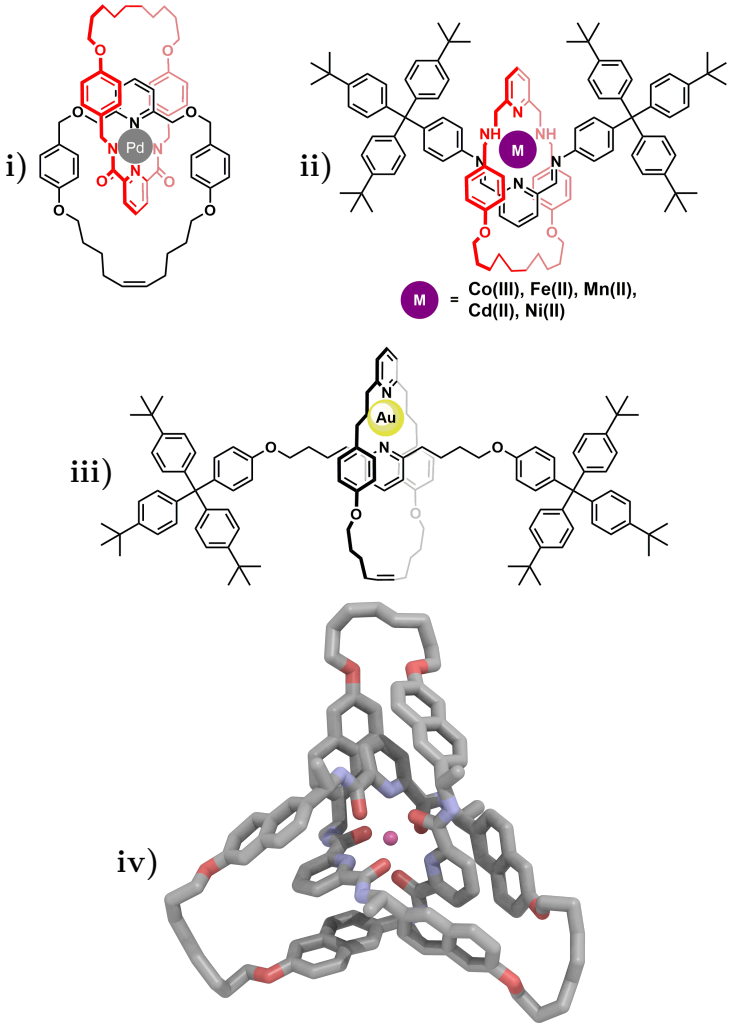


Figure 1.36 – Leigh's i) Pd(II) templated [2]catenane, ii) octahedral metal templated Schiff base stoppered series of [2]rotaxanes, iii) Au(I) templated [2]rotaxane and iv) the crystal structure of a Lu(III) templated chiral trefoil knot[120] (hydrogen atoms omitted for clarity).

Even the challenge of using alkali metal templates such as Na^+, which do not possess stringent geometric coordination preferences, has been overcome with Chiu's [2]rotaxane templated *via* cooperative endotopic binding of Na^+ and hydrogen bonding by a urea-containing axle component within a polyether macrocycle (**Figure 1.37**).[121]

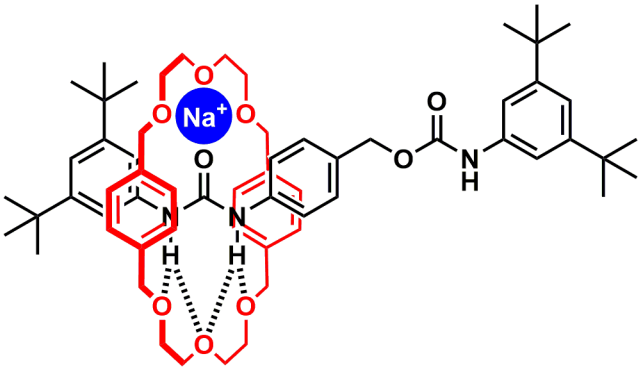


Figure 1.37 – Chiu's Na^+ templated urea-containing [2]rotaxane.

The use of multiple metals can be used to template complex interlocked knot topologies; Sauvage's seminal revisiting of the phenanthroline/Cu(I) templation motif was used to synthesise the elegant trefoil knot structure centred around two Cu(I) ions (**Figure 1.38-i**)[122] and aesthetically pleasing examples such as Leigh's "Star of David" catenane was based on the association of multiple linked bipyridine ligands and Fe(II) ions (**Figure 1.38-ii**).

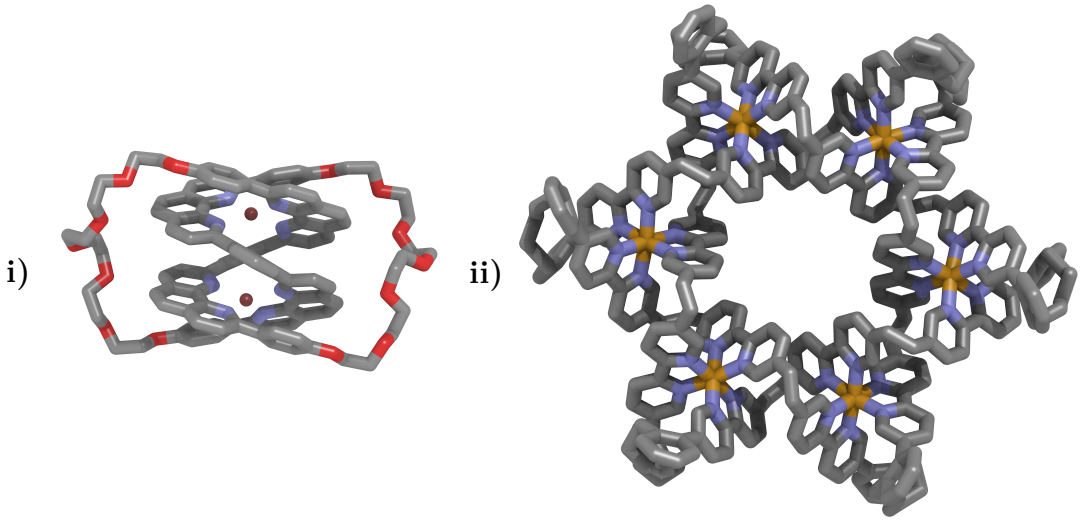


Figure 1.38 – Crystal structures of i) Sauvage's Cu(I) templated trefoil knot[122]; ii) Leigh's Fe(II) templated "Star of David" molecular knot.[123] (Hydrogen atoms omitted for clarity.)

Metals can be used to template interlocked structures *passively* as seen in previous examples but can also participate in the covalent bond forming chemistry required

to create the interlocked structures. Leigh and co-workers have pioneered the use of *active* metal templation[105] in this way *via* the identification of a key intermediate of the CuACC reaction, which involves the co-coordination of the component azide and alkyne to the Cu(I) catalyst. The development of a macrocycle functionalised with an *endo* Cu(I) ligating group enabled the reaction of a stoppered azide and alkyne to be directed through the annulus of the macrocycle, leading to the formation of a [2][124] and even [3]rotaxane[125] under suitable conditions (**Figure 1.38-i**). [n]Catenanes are also possible using a similar macrocycle and a linear macrocycle precursor with azide and alkyne functionalised end groups (**Figure 1.38-ii**)[126], as are trefoil knot structures.[127] This principle has been applied to other metal catalysed bond forming reactions such as Goldberg Cu(I) coupling of amides to aromatic iodides[128] and Pd(II) oxidative homocoupling of alkynes (**Figure 1.38-iii**).[129]

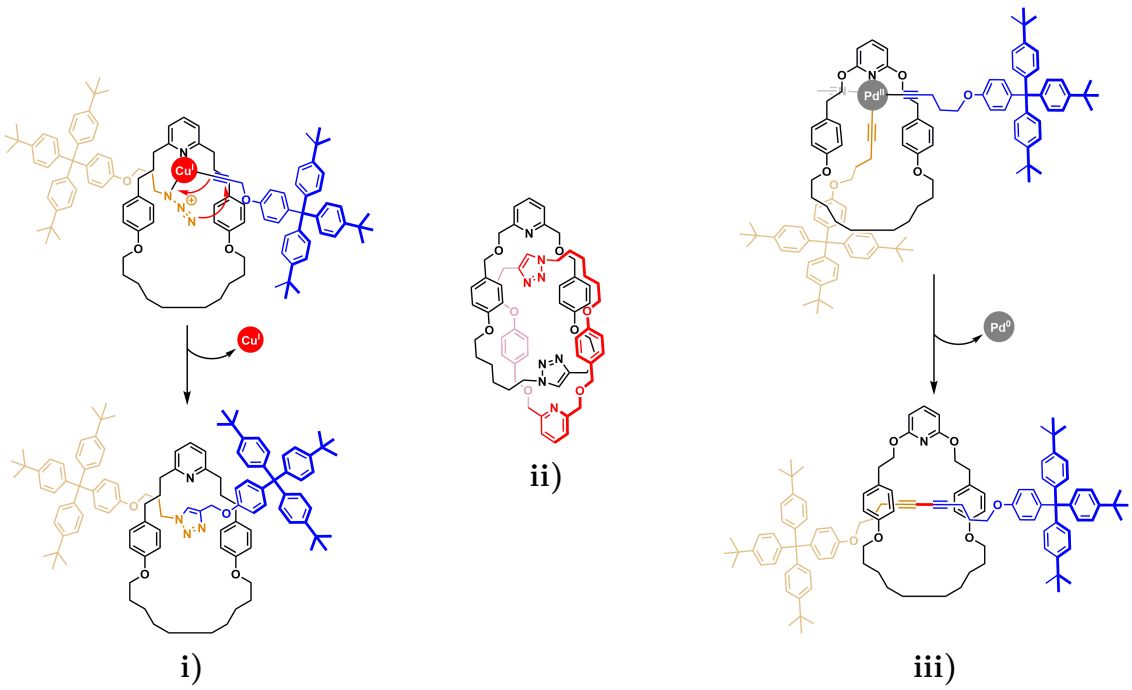


Figure 1.38 – Leigh's Cu(I)-mediated active metal templation of i) a [2]rotaxane, ii) [2]homocatenane; iii) Pd(II)-mediated active metal templation of a [2]rotaxane.

Organic cations can also participate in the construction of interlocked molecules; as elegantly exemplified by the π-acidic 4,4'-bipyridinium-type employed by Stoddart

to interact *via* repeating donor-acceptor interactions with electron rich naphthalene motifs to form the [5]catenane "olympiadane"[130] and numerous other higher order structures (**Figure 1.39-i**).[131] Secondary ammonium cations can act as templates through a combination of electrostatics and hydrogen bonding, seen in the efficient clipping of a pyridine bis-aldehyde that undergoes ammonium stabilised imine formation with an amine macrocycle precursor to give a [2]rotaxane as the thermodynamic product in a 70% yield (**Figure 1.39-ii**).[132]

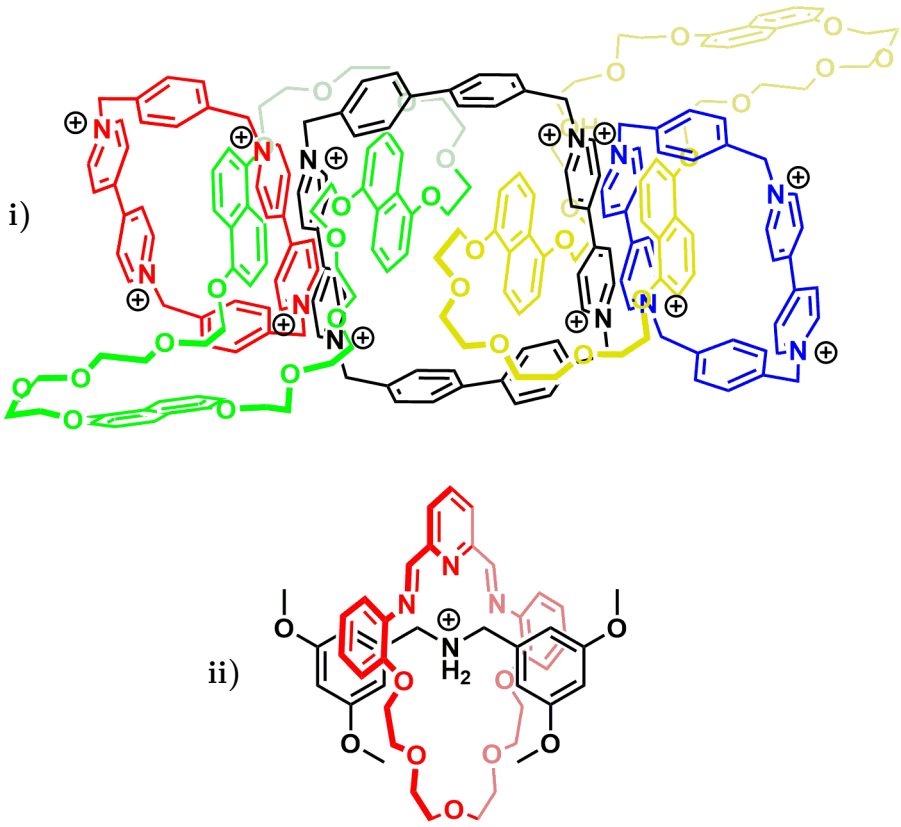


Figure 1.39 – Stoddart's i) cationic π donor-acceptor [5]catenane "olimpiadane" and ii) ammonium cation templated imine [2]rotaxane.

1.3.2.2. Neutral templates

Neutral templates, although comparatively rare, still see utility in the formation of interlocked molecules.[133] Sander's neutral benzenediimide [2]catenane takes advantage of strong interfacial π-donor-acceptor self-assembly to form the interlocked structure, trapped by Glaser coupling methods (**Figure 1.40-i**).[134]

Strong hydrogen bonding arrays like that seen between barbiturate-type guests and complementary hosts (**Section 1.1.2.1.**) have been utilised in McClenaghan's barbiturate axle component photocaptured [2]rotaxane (**Figure 1.40-ii**).[135] The strong association of the hydrophobic cavity of cyclodextrin derivatives for hydrophobic organic molecules as a templating interaction has been demonstrated by Anderson's highly fluorescent, water soluble stilbene/α-cyclodextrin [2]rotaxane (**Figure 1.40-iii**).[136]

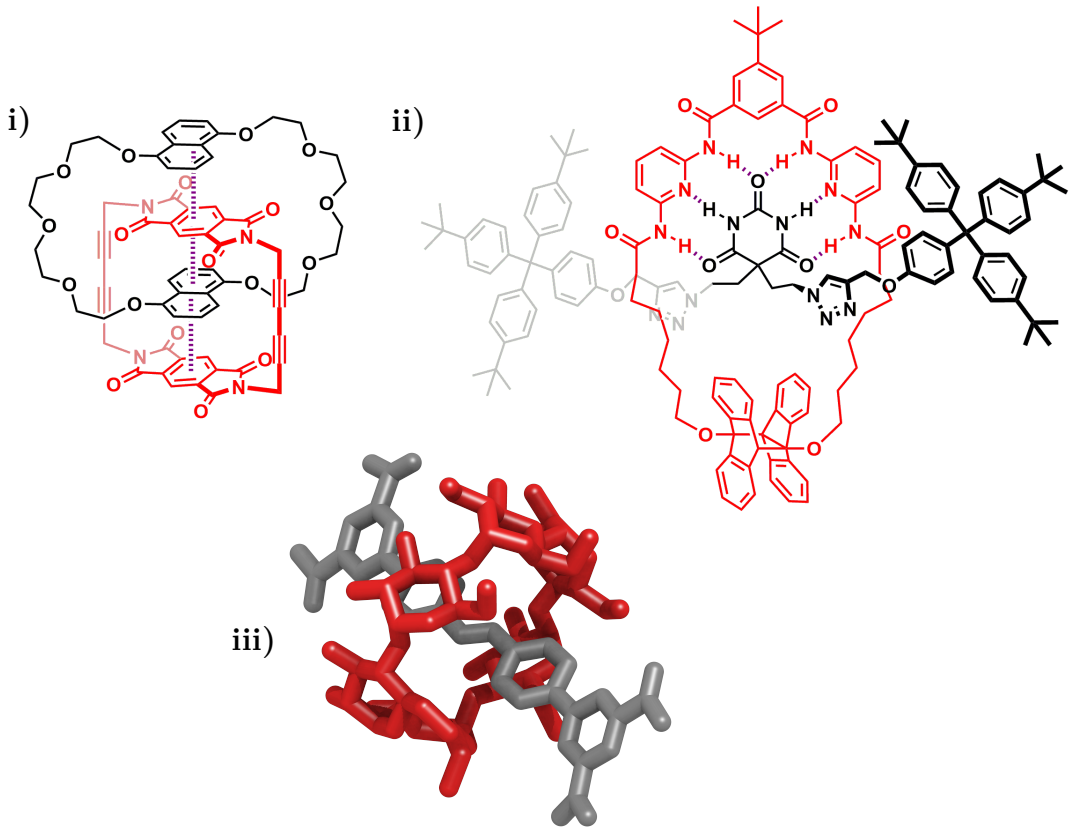


Figure 1.40 – i) Sanders' Glaser-clipping π-donor-acceptor [2]catenane; ii) McClenaghan's barbiturate templated photocaptured [2]rotaxane; iii) crystal structure of Anderson's cyclodextrin (shown in red) stilbene threaded [2]rotaxane (non-polar hydrogen atoms omitted for clarity).[136]

1.3.2.3. Anionic templates

Despite the inherent difficulties of coordinating anions in comparison to cations, the use of anions in templating interlocked architectures is steadily growing. This class of interlocked structures are broadly synthesised *via* either: i) mechanical bond formation around an anionic templating motif which is covalently integrated into

one of the molecular precursor components or ii) mechanical bond formation around discrete anionic guest templates. The former approach was illustrated by Vögtle's tetralactam macrocycle endotopically directing a bulky phenoxide anion *via* hydrogen bonds followed by an S_N2 reaction with another bulky alkyl bromide stopper, templating the formation of a [2]rotaxane in an impressive 95% yield (**Figure 1.41-i**).[137] More recently, Flood's cyanostar C-H hydrogen bonding macrocycles thread an anionic dialkyl phosphate axle component to form a [3]rotaxane *via* a CuACC stoppering methodology (**Figure 1.41-ii**).[138]

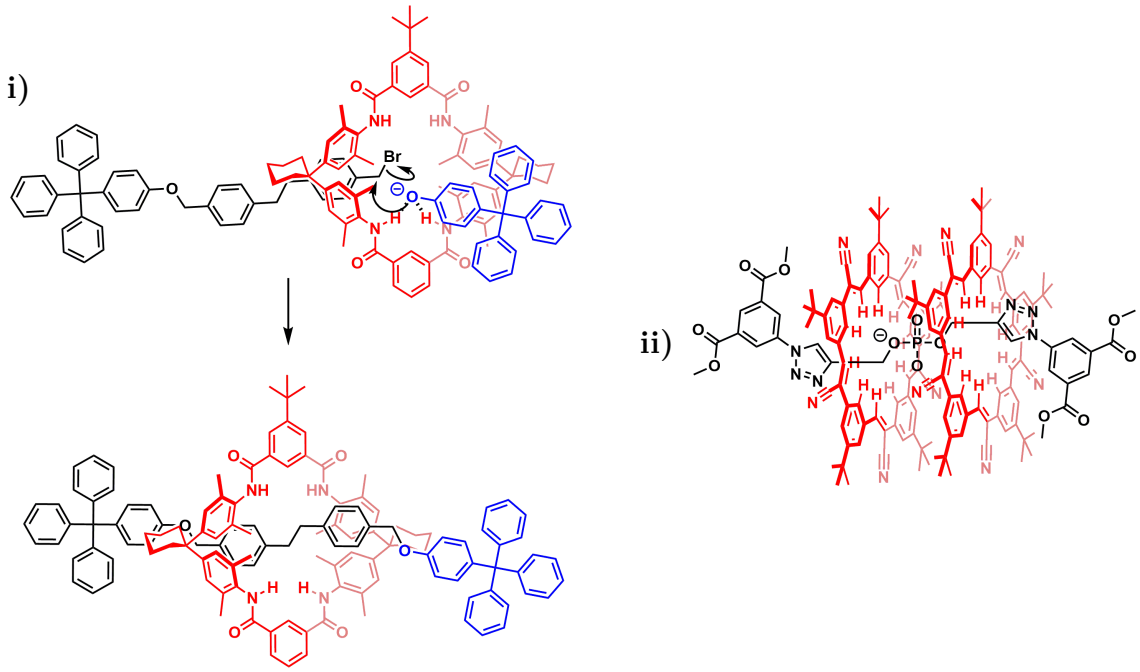


Figure 1.41 – i) The formation of Vögtle's phenoxide anion templated [2]rotaxane; ii) Flood's cyanostar [3]rotaxane.

The use of discrete anions as templates for the synthesis of mechanically bonded molecules was pioneered by Beer's insightful conceptualisation that anions could act as the centrepiece of an orthogonal arrangement of ligands, akin to Sauvage's seminal Cu(I) templated phenanthroline catenane. This was realised by the assembly of a pseudorotaxane comprising an isophthalamide macrocycle and a simple pyridinium bis-amide acyclic anion recognition motif, directed primarily by

strong hydrogen bonds to a discrete chloride anion template and assisted by favourable donor acceptor interactions between the electron poor pyridinium and electron rich hydroquinone moieties contained within the macrocycle (**Figure 1.42**).[139]

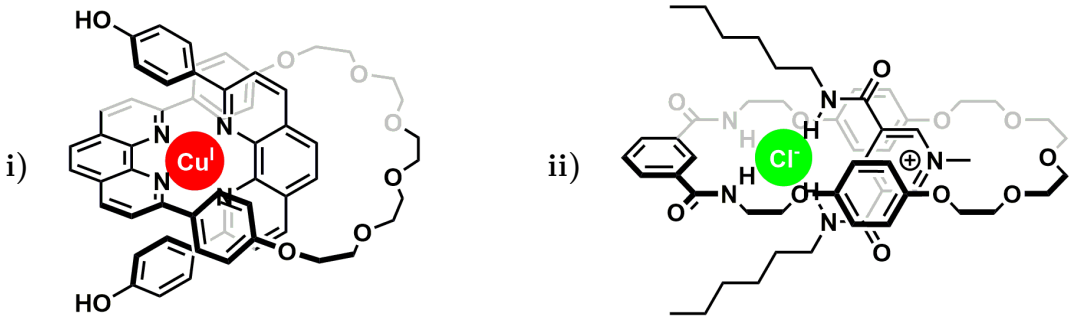


Figure 1.42 – Comparison of the orthogonal association of i) Sauvage's Cu(I) complex and ii) Beer's Cl^- templated pseudorotaxane.

This strategic chloride anion templation was subsequently extended to the synthesis of an interlocked [2]rotaxane by employing a Grubbs' ring-closing metathesis clipping protocol to cyclise an isophthalamide bis-alkene functionalised macrocycle precursor around a pyridinium chloride bis-amide stoppered axle component (**Figure 1.43**).[139]

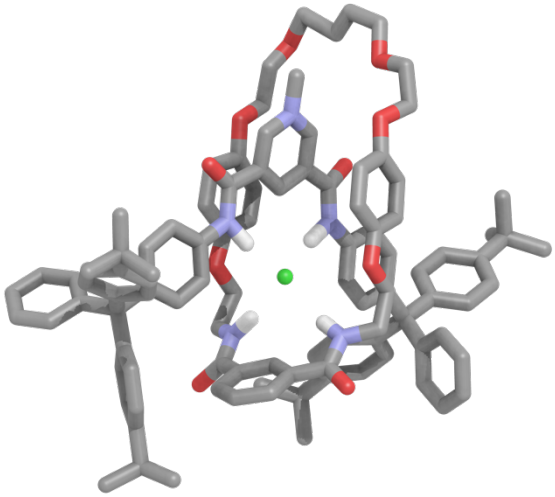


Figure 1.43 – Crystal structure of Beer's Cl^- templated [2]rotaxane (non-polar hydrogens are omitted for clarity).[139]

After the formation of the [2]rotaxane, the Cl^- template could be easily removed *via* anion exchange for the non-coordinating anion PF_6^- to give a highly preorganised, three dimensional binding pocket for the anionic guest, shielded from bulk solvent. It was found that the unique anion recognition site profoundly changed the anion binding selectivity in comparison to the non-interlocked pyridinium axle in 1:1 $CD_3OD/CDCl_3$; the axle showed a pronounced selectivity for the highly basic AcO^- (K_{11} = 22000 M^{-1}) over Cl^- (K_A = 125 M^{-1}) (**Figure 1.44-i**), whilst the [2]rotaxane exhibited very weak AcO^- recognition (K_A = 100 M^{-1}), the Cl^- binding (K_A = 1130 M^{-1}) was considerably enhanced by an order of magnitude in comparison to the axle alone (**Figure 1.44-ii**). This size constrained interlocked binding site was clearly able to exclude the larger AcO^- anion and preferentially bind smaller halides.

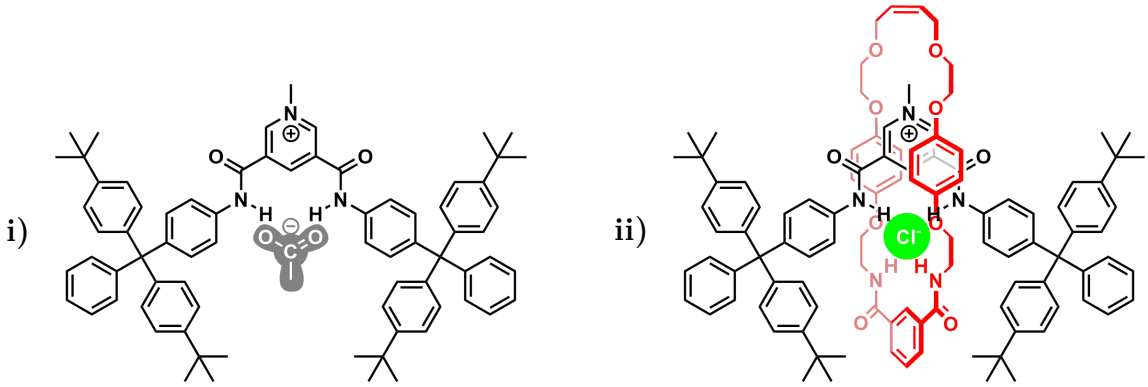


Figure 1.44 – i) Rotaxane axle component that exhibits selectivity for AcO^- over Cl^-; ii) [2]rotaxane that is Cl^- selective at the expense of AcO^-.

This approach was expanded to synthesise other interlocked architectures such as [3]rotaxanes for the sensing of SO_4^{2-} (**Figure 1.45-i**)[140,141], charge neutral catenanes (**Figure 1.45-ii**)[142] and even topologically complex structures such as Janus [2]rotaxanes[143] and handcuff catenanes (**Figure 1.45-iii**).[144]

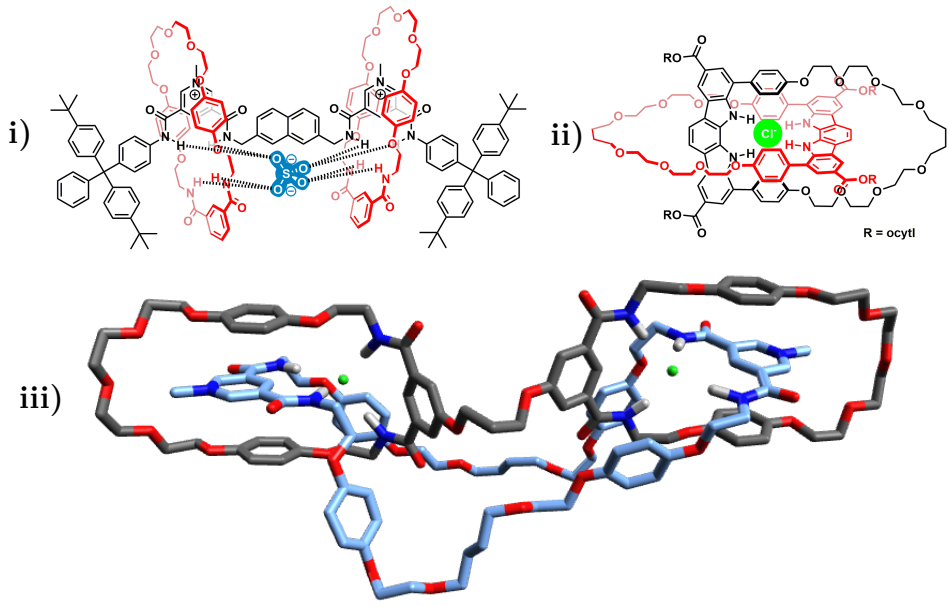


Figure 1.45 – i) Beer's Cl^- templated SO_4^{2-} selective [3]rotaxane; ii) Jeong's indolocarbazole [2]homocatenane; iii) crystal structure of Beer's Cl^- templated, doubly interlocked "handcuff" catenane (non-hydrogen bonding hydrogens are omitted for clarity).[144]

These interlocked systems have proven to be useful anion recognition scaffolds in which to incorporate reporting groups. Beer and co-workers reported a series of

ferrocene appended rotaxanes (**Figure 1.46-i**)[145,146] that can electrochemically sense Cl^- in a variety of solvents. Optical sensing of Cl^- in Smith's squaraine-based [2]rotaxane shuttle exhibits a deep red emission upon Cl^- induced translocation of the macrocyclic component to either of the triazole stations (**Figure 1.46-ii**).[147]

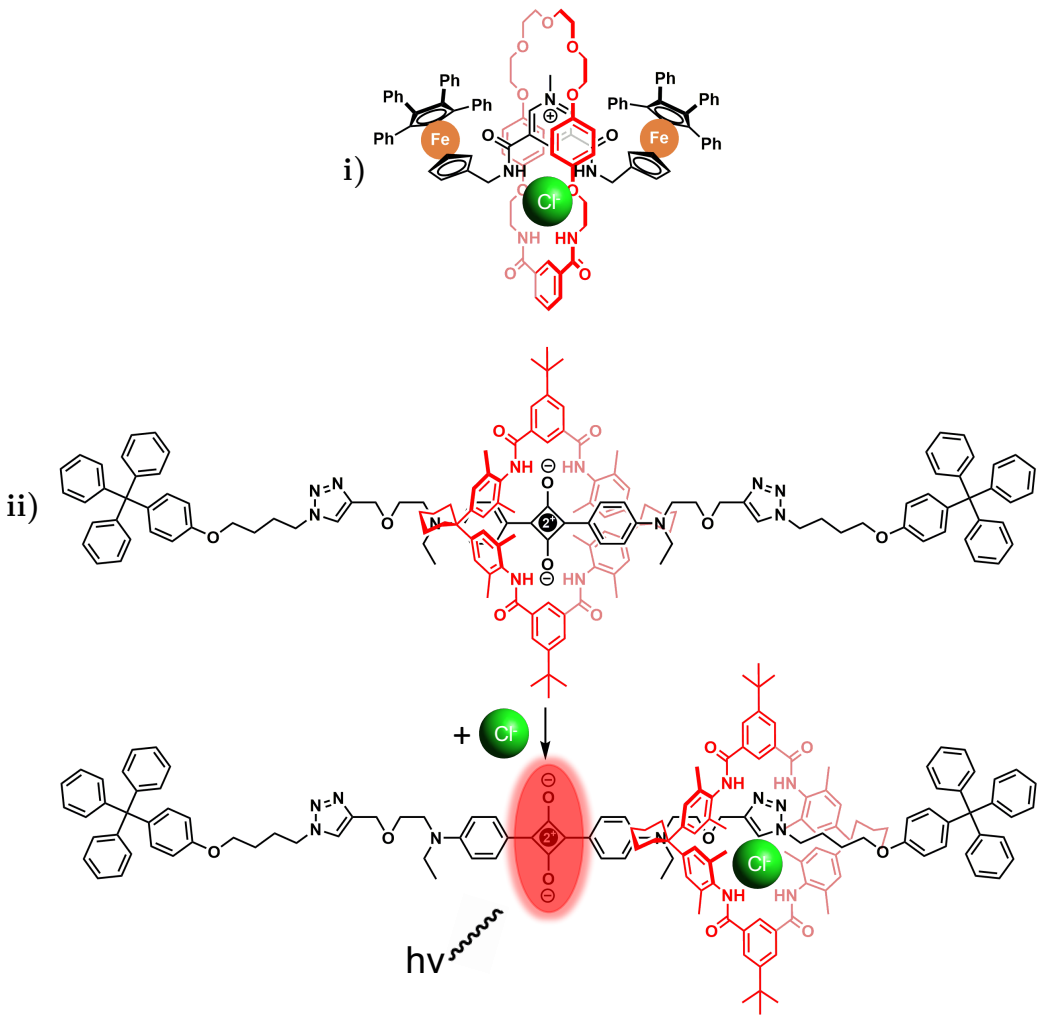


Figure 1.46 – i) Beer's pentaphenylferrocene stoppered [2]rotaxane for electrochemical Cl^- sensing; ii) Smith's squaraine dye based [2]rotaxane optical sensor for Cl-.

The use of other templating anions has been particularly successful for creating interlocked anion receptors with unique geometries and selectivities, such as Beer's NO_3^- (**Figure 1.47-i**)[148] and NO_2^- (**Figure 1.47-ii**)[149] templated [2]rotaxanes and SO_4^{2-} templated [2]homocatenane (**Figure 1.47-iii**).[150]

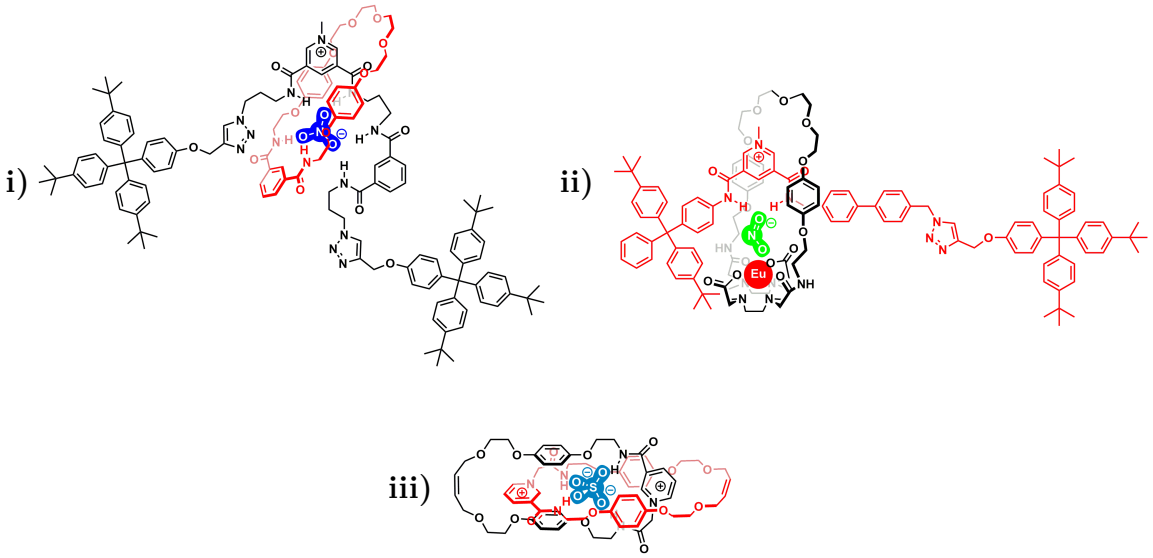


Figure 1.47 – Examples of interlocked structures templated by i) NO_3^-, ii) NO_2^- and iii) SO_4^{2-}.

1.3.3. Alternative applications of interlocked structures

The complex three-dimensional topologies that mechanically interlocked structures exhibit have led to their application as host systems for cations, ion-pairs and neutral species in addition to anion host systems discussed in the previous section. With the increasing practicality of the synthesis of interlocked structures, there has been a commensurate increase in their application in nanotechnology[151,152], medicine[153–155], catalysis[156,157] and sensing[158]; exploiting the unique set of dynamic properties such as stimuli sensitive molecular motion and strong guest. In a visionary effort to increase storage memory density within nanoscale dynamic random access memory (DRAM) circuits, Stoddart synthesised a bi-stable [2]rotaxane that consisted of a hydrophilic stopper component for attachment to silicon nanowire electrodes. The TTF station with a paraquat macrocycle positioned proximally in its un-oxidised state would serve as the low conductance or '0' state. When oxidised to $TTF^{+\cdot}$, the station would electrostatically repulse the cationic macrocycle, causing shuttling from the TTF station to the naphthalene station, resulting in a high conductance or '1' state (**Figure 1.48**)[159]. Despite not fulfilling the necessary

robustness of switch cycling needed for a practical device, a functional 160,000 bit memory cell was created which is less than 3% the size of the smallest DRAM circuit available.

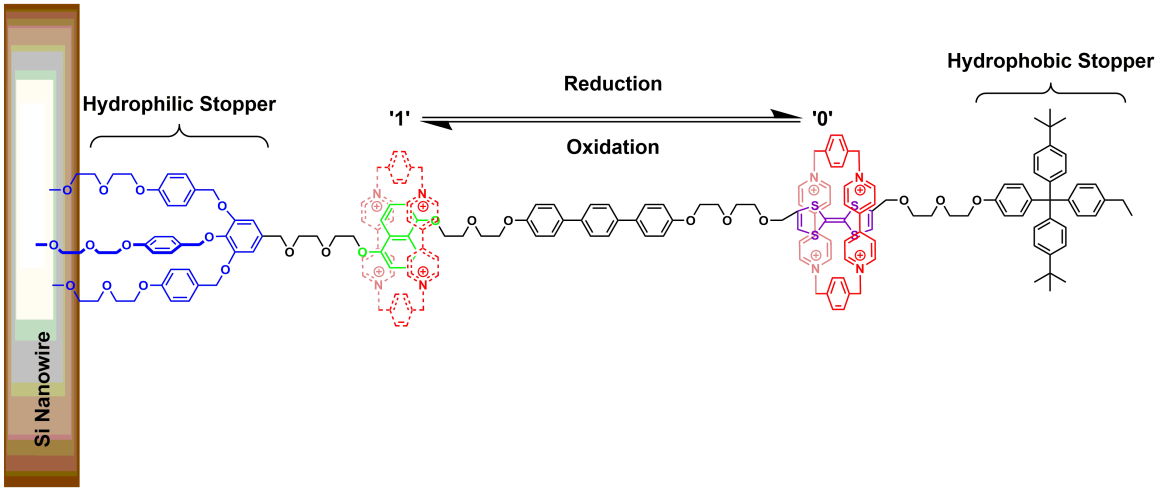


Figure 1.48 – Stoddart's silicon nanowire bound [2]rotaxane transistor, showing the TTF-mediated redox switching between the '0' state where the macrocycle resides over the naphthalene station and the '1' state where the macrocycle resides over the TTF station.

Rotaxanes have also seen application in biomedical drug delivery, a class of polymeric materials known as cyclodextrin based polypseudorotaxanes (CDPRs) have been shown to increase biocompatibility of drug molecules, introducing favourable solubility parameters and enhanced membrane translocation.[160] An illustrative example is Yang's CDPR delivery system, where the cancer chemotherapy drug Doxorubicin is conjugated to an α-cyclodextrin threaded by a simple PEG chain and stoppered by biodegradable tyrosine peptide stoppers (**Figure 1.49**)[161]. Upon entering the cell, cleavage of the peptidic stoppers by enzymes such as papain and α-chymotrypsin leads to the targeted release of the drug molecules from the interlocked structure into the cytoplasm or other cellular domains.

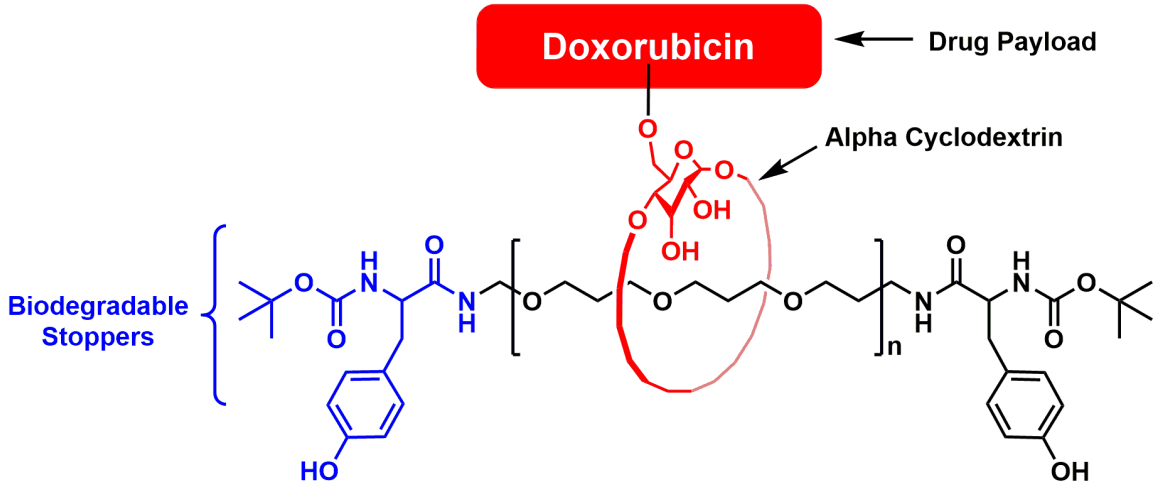


Figure 1.49 – Generalised structure of Yang's CDPR polyrotaxane doxorubicin delivery system.

Rotaxanes have been used for fluorescent cellular imaging using a similar approach to biocompatibility functionalisation. Smith's deep red fluorescent imaging reagent is based on a highly luminescent squaraine rotaxane core appended with dendritic iminodiacetate groups which possess a strong affinity for Ca^{2+} ions that form part of the structure of bone tissue, thus acting as "bone-seeking" functional structures (**Figure 1.50**).[162] It was found that the tetra iminodiacetate rotaxane was shown to localise in the same skeletal regions of living mice as the commercially available bone imaging reagent OsteoSense 750 and had the added advantage of higher chemical stability and narrower emission wavelength band, enabling its potential use in multiplex imaging protocols involving the simultaneous use of other fluorescent imaging probes.

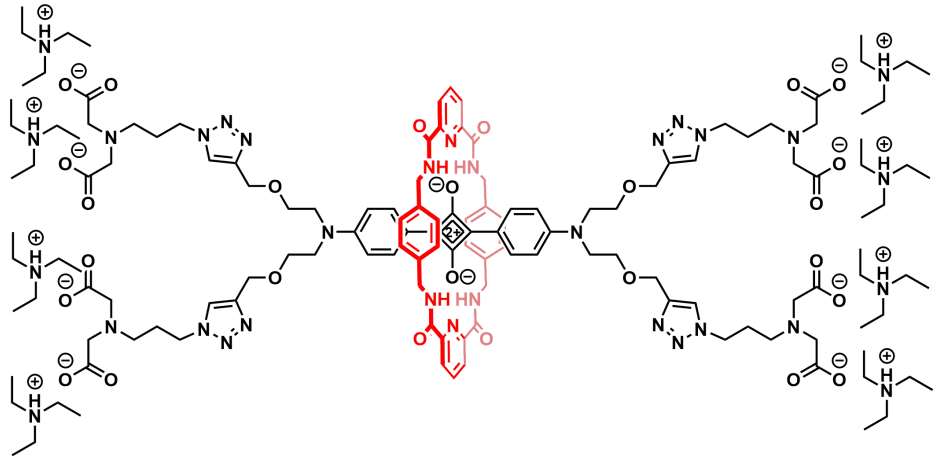


Figure 1.50 – Smith's bone imaging squairaine-dye-based [2]rotaxane with biocompatible iminodiacetate dendrimer stoppers.

The study of the activity of catalytic metals contained within mechanically bonded scaffolds is a current topic of interest. The sterically hindered environment in Leigh's [2]rotaxane containing a chiral di-amino macrocycle component strongly influenced the activity of the Ni(II)-catalysed Michael addition of diethyl malonate and trans-β-nitrostyrene (**Figure 1.51-i**).[128] Despite slower reaction times, there was a significant increase in enantioselectivity from 68:32 *S:R* for the acyclic chiral diamine co-catalyst to up to *93:7 S:R* in the interlocked catalyst host. Recently, a stimuli-responsive interlocked Au(I) catalyst synthesised by Goldup (**Figure 1.51-ii**)[157] showed that the complexation of guests such as $[Cu(MeCN)_4PF_6]$ could enhance or in the case of $Cd(OTf)_2$, diminish the enantioselctivity of the Au(I) promoted Ohe–Uemura cyclopropanation by varying the degree to which the Au(I) was bound by the macrocyclic component, thus creating a catalyst with an "on and off" switch mediated by guest binding.

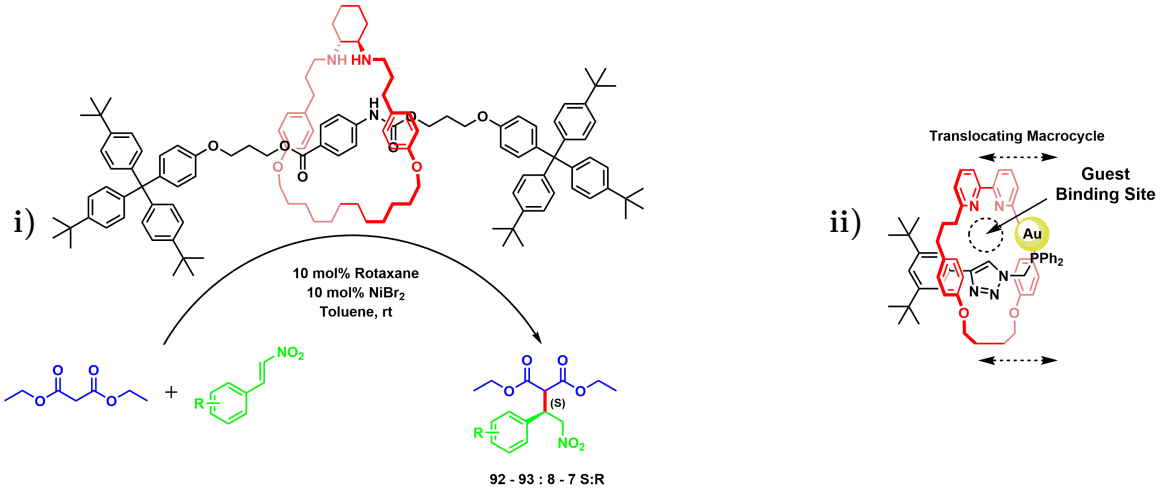


Figure 1.51 – i) Leigh's Cu(I) Goldberg active metal templated [2]rotaxane capable of enantioselective Ni(II)-catalysed Michael additions; ii) Goldup's guest-switchable Au(I) [2]rotaxane catalyst for Ohe–Uemura cyclopropanations.

1.4. Water Soluble Macrocyclic Inclusion Complexes

Since the advent of the macrocycle in supramolecular chemistry with Cram's spherands[2], Pedersen's crown ethers[3] and Lehn's cryptands[163], the prevalence and diversity of macrocyclic host molecules is manifold. Particularly, the host-guest chemistry of large, water soluble macrocycles such as cyclodextrins and cucurbiturils has received considerable attention given their strong association between lipophilic organic guest molecules and their hydrophobic internal cavities, leading to various applications in inclusion complex driven self-assembly of relevant biocompatible materials, technological processes, food preservatives and advanced supramolecular molecular machines and switches.

1.4.1. The cucurbit[n]uril family

Cucurbit[n]urils (CBs or CB[n]s) are a homologous family of methylene bridged macrocyclic oligomers composed of repeating glycouril subunits. The uriedo-carbonyl groups that line the edges of the macrocycle pitch inward, giving it an appearance akin to a pumpkin – a member of the *cucurbitaceae* family of plants.

The most commonly studied homologues are CB[5], CB[6], CB[7] and CB[8], some larger variants are possible such as the CB[10], isolated as an inclusion complex containing another CB[5] within its larger cavity.[164] Possessing a common depth of 9.1 Å, the annular and ring diameters of CB[n]s increase with increasing [n] value whilst the pitch of the carbonyl motifs encircling the portals cause them to be on average 2 Å narrower than the central cavity (**Figure 1.52**).

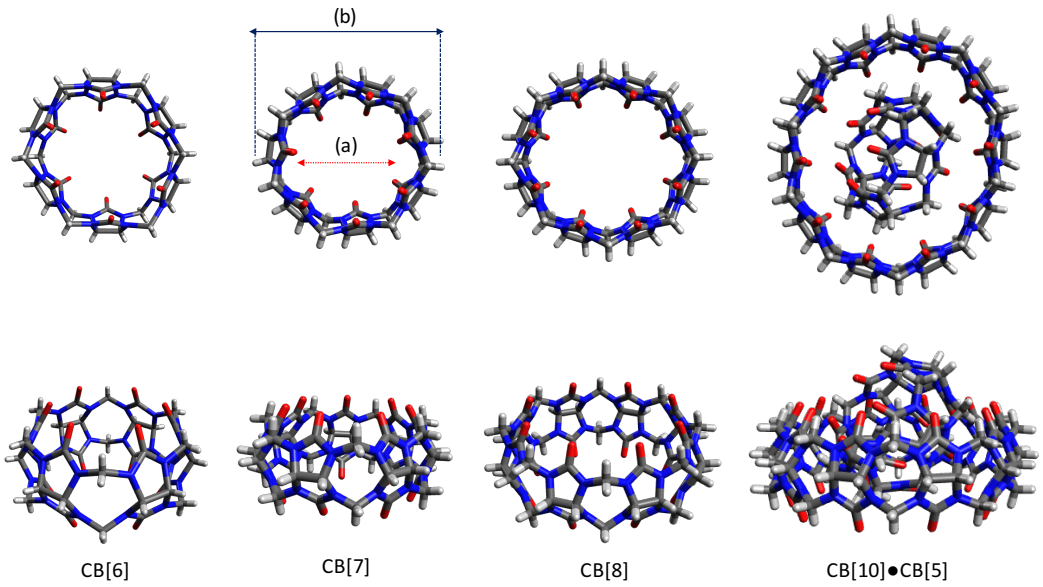


Figure 1.52 – Topside and side views of the crystal structures of CB[6][165], CB[7][166], CB[8][166] and CB[10] • CB[5].[164] Legend: (a) = annular diameter, (b) = ring diameter.

1.4.2. Synthesis of CB[n] derivatives

The potential of Behrend's poorly soluble polymeric substance that recrystallised from the condensation of glycouril and formaldehyde under acidic conditions in 1905[167] went unrealised for almost eighty years. In 1981, Mock and co-workers revisited the synthesis and determined that the substance was in fact a macrocycle, CB[6].[165] Behrend's earlier observations on the ability of this "polymer" to form co-crystals with metal compounds such as $NaAuCl_4$, $KMnO_4$ and organic dyes like congo red were thus explained as the net result of favourable host-guest interactions. Later the combined efforts of the Kim and Day research groups optimised the

conditions for the synthesis of CB[n] derivatives, the use of milder reaction conditions furnished CBs [5] through to [10] *via* kinetic control (**Figure 1.53**).[166,168]

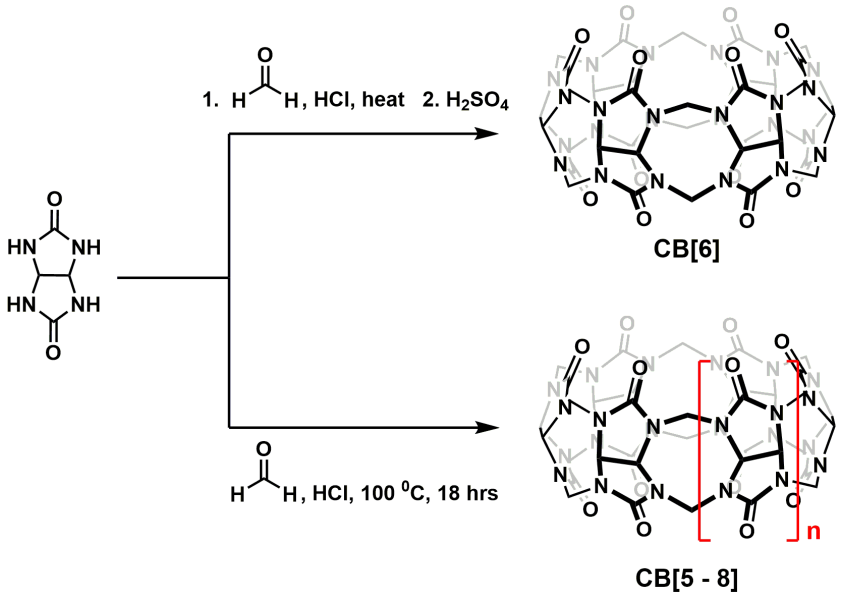


Figure 1.53 Cucurbit[n]uril synthetic conditions.

1.4.3. Host-guest chemistry of CB[n] derivatives

From their inception, CB[n] derivatives were recognised for their remarkable host-guest properties. The presence of the unique, negatively polarised portal carbonyls consequentially makes the inclusion of cationic guests favourable. Smaller CB[5] derivatives are too small to include guests with the exception of gas molecules (**Figure 1.54-i**)[169] whilst the exterior complexation *via* the portal carbonyl groups of metals, ammonium cations and protons are more commonplace (**Figure 1.54-ii**).[170,171] CB[6] derivatives are sufficiently large enough to bind 1-anilino-8-naphthalenesulfonate (ANS) dyes (**Figure 1.54-iii**)[172], and thread the axle component of rotaxanes such as Nakamura's polyammonium axle [2]rotaxane (**Figure 1.54-iv**).[173] CB[7] and CB[8] derivatives see the widest application in host-guest inclusion; CB[7] can bind a wide range of aromatic guests including metallocenes (**Figure 1.54-v**)[174,175] and viologen compounds (**Figure 1.54-vi**)[176] whilst CB[8] exhibits the ability to not only complex guests of larger size such as

cyclen macrocycles (**Figure 1.54-vii**)[177] but can uniquely bind more than one guest simultaneously in strong, three component ternary complexes[178]. An example of this phenomenon include the inclusion dimer of two phenylphosphonic acid molecules (**Figure 1.54-viii**).[179]

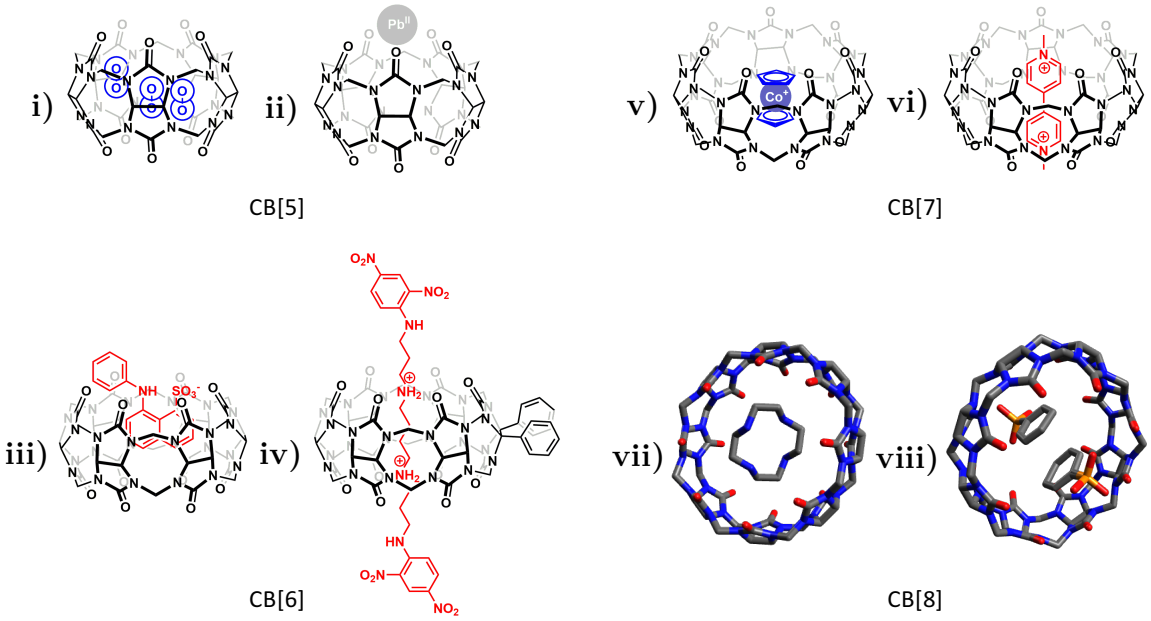


Figure 1.54 – Cucurbituril host-guest complexes: i) CB[5]-dioxygen gas inclusion complex, ii) CB[5]-Pb(II) *exo*-complex, iii) CB[6]-ANS dye inclusion complex, iv) Nakamura's polyammonium axle [2]rotaxane, v) CB[7]-cobaltocene inclusion complex, vi) CB[7]-paraquat inclusion complex, vii) crystal structure of CB[8]-cyclen inclusion complex (hydrogens omitted for clarity)[177], viii) crystal structure of CB[8]-di-phenylphosphonic acid ternary complex (hydrogens omitted for clarity).[179]

1.4.4. Applications of CB[n] derivatives

CB[n] derivatives are able to fulfil an impressive number of roles in molecular machines, directed synthesis of nanostructures, interlocked structures[180] and catalysts. Winter and co-workers utilised the strong guest association of a diradical diviologen derivative inside two CB[7] hosts in a reversible diamagnetic/ paramagnetic switch (**Figure 1.55**).[181] The lone diradical diviologen is diamagnetic as a result of spin pairing whereas upon the addition of two equivalents of CB[7], the proximity reliant spin pairing is disrupted and the system becomes paramagnetic

upon CB[7] inclusion. The switch could be cycled by additions of the strongly associating trimethylammonium ferrocene to displace the diradical.

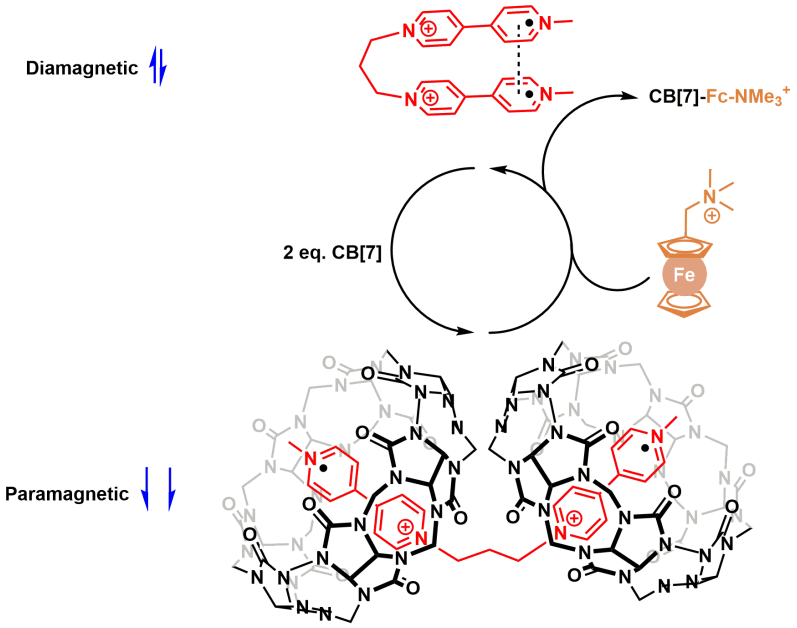


Figure 1.55 – CB[7] inclusion mediated paramagnetic/diamagnetic switch.

The formation and stabilisation of metal nanoparticles, particularly gold nanoparticles, is a pressing challenge in the quest for monodisperse mixtures of these entities that can interact with small molecules.[182] Conventional methods for synthesis of gold nanoparticles normally make use of reducing agents such as $NaBH_4$ and strongly coordinating ligands. The use of cucurbit[n]urils provides a "ligandless" approach to stabilising gold nanoparticles and dynamic aggregates as shown by Scherman's use of CB[5] capped at one carbonyl portal by Na^+ cations.[183] Peréz-Prieto and co-workers synthesised uncapped CB[7]-stabilised nanoparticles with a vacant carbonyl portals that were capable of electrochemical reduction of dissolved oxygen, which was reportedly due to the available nanoparticle surface inside the CB[7] cavity (**Figure 1.56**).[184]

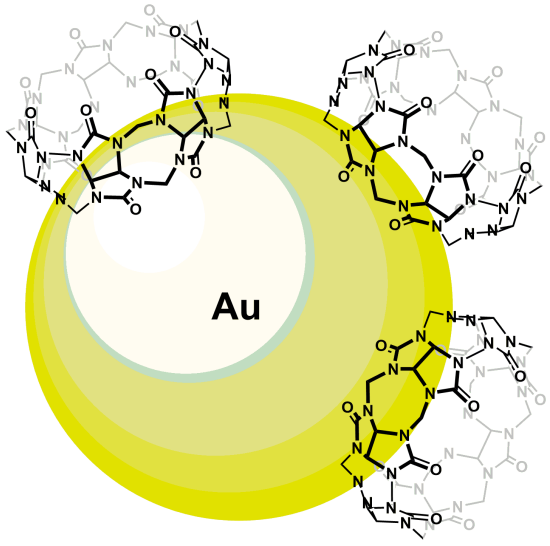


Figure 1.56 – Schematic showing CB[7] stabilisation of a gold nanoparticle.

The remarkable catalytic properties of CB[n] can be attributed to their ability to use host-guest chemistry to fulfil one of the key requirements of catalysis: the kinetically favourable proximity of the reacting species. Even before the advent of CuACC "click" chemistry, CB[6] was shown to enforce regioselective triazole formation *via* the strong guest binding of ammonium groups grafted onto the azide and alkyne reactants enabling the normally kinetically unfavourable dipolar cycloaddition to take place 5 orders of magnitude faster than in the absence of CB[6] and no regioselectivity (**Figure 1.57**).[185]

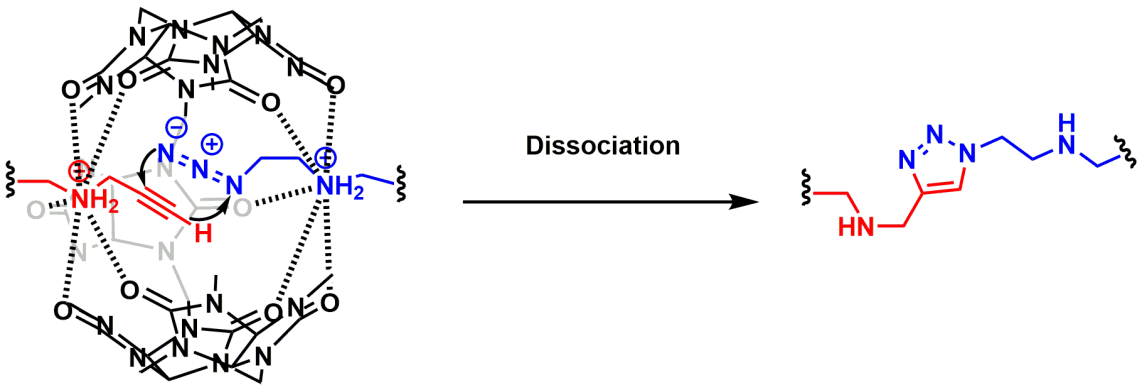


Figure 1.57 – Conjectured cycloaddition mechanism between an azide and alkyne within CB[6].

1.5. Project Outline

This project chiefly concerns two areas: i) the synthesis of hydrogen and halogen bonding acyclic, macrocyclic and higher order interlocked structures synthesised *via* anion templation for anion recognition and sensing and ii) the synthesis of luminescent f-metal appended molecular probes for sensing and ternary complex switching within cucurbit[n]uril macrocyclic hosts in water.

Chapter Two describes the anion templated formation of a series of hybrid hydrogen bonding/halogen bonding pyridinium [2]rotaxanes and explores the influence on selectivity of additional halogen bonding 5-iodo-1,2,3-triazole and cationic iodotriazolium motifs in these systems. The synthesis of structurally homologous transition metal appended hydrogen bonding/halogen bonding acyclic pyridine *N*-oxide and interlocked pyridinium receptors are also investigated.

Chapter Three is concerned with the incorporation of hydrogen bonding amide-triazole and halogen bonding amide-iodotriazole motifs into acyclic, macrocyclic and higher-order rotaxane hosts. Investigation of anion recognition trends, the influence of structural isomerism and anion binding geometries in the receptors is discussed.

Chapter Four details the synthesis of luminescent visible and NIR emitting napthyl-appended lanthanide complexes for use as a ternary partners in electrochemically switchable viologen/cucurbit[8]uril scaffolds.

1.6. References for Chapter 1

(1) Steed, J. W.; Atwood, J. L. *Supramolecular chemistry*; John Wiley & Sons, 2013.

(2) Cram, D. J. *Angew. Chem. Int. Ed. Engl.* **1988**, *27* (8), 1009–1020.

(3) Pedersen, C. J. *Angew. Chem. Int. Ed. Engl.* **1988**, *27* (8), 1021–1027.

(4) Fischer, E. *Berichte Dtsch. Chem. Ges.* **1894**, *27* (3), 2985–2993.

(5) Fèvre, R. J. W. L. *Dipole moments: their measurement and application in chemistry*; Methuen, 1953.

(6) Arunan, E.; Desiraju, G. R.; Klein, R. A.; Sadlej, J.; Scheiner, S.; Alkorta, I.; Clary, D. C.; Crabtree, R. H.; Dannenberg, J. J.; Hobza, P.; Kjaergaard, H. G.; Legon, A. C.; Mennucci, B.; Nesbitt, D. J. *Pure Appl. Chem.* **2011**, *83* (8), 1637–1641.

(7) Emsley, J. *Chem. Soc. Rev.* **1980**, *9* (1), 91–124.

(8) Yoshida, Z.; Ogoshi, H.; Tokumitsu, T. *Tetrahedron* **1970**, *26* (24), 5691–5697.

(9) Petrenko, V. F.; Whitworth, R. W. *Physics of ice*; Oxford University Press: Oxford; New York, 1999.

(10) Guthrie, F. *J. Chem. Soc.* **1863**, *16* (0), 239–244.

(11) Gilday, L. C.; Robinson, S. W.; Barendt, T. A.; Langton, M. J.; Mullaney, B. R.; Beer, P. D. *Chem. Rev.* **2015**, *115* (15), 7118–7195.

(12) Erdélyi, M. *Chem. Soc. Rev.* **2012**, *41* (9), 3547–3557.

(13) Mukherjee, A.; Tothadi, S.; Desiraju, G. R. *Acc. Chem. Res.* **2014**, *47* (8), 2514–2524.

(14) Desiraju, G. R.; Ho, P. S.; Kloo, L.; Legon, A. C.; Marquardt, R.; Metrangolo, P.; Politzer, P.; Resnati, G.; Rissanen, K. *Pure Appl. Chem.* **2013**, *85* (8), 1711–1713.

(15) Politzer, P.; Murray, J. S.; Clark, T. *Phys. Chem. Chem. Phys. PCCP* **2013**, *15* (27), 11178–11189.

(16) Pedireddi, V. R.; Reddy, D. S.; Goud, B. S.; Craig, D. C.; Rae, A. D.; Desiraju, G. R. *J. Chem. Soc. Perkin Trans. 2* **1994**, No. 11, 2353–2360.

(17) Metrangolo, P.; Neukirch, H.; Pilati, T.; Resnati, G. *Acc. Chem. Res.* **2005**, *38* (5), 386–395.

(18) Legon, A. C. *Phys. Chem. Chem. Phys.* **2010**, *12* (28), 7736–7747.

(19) Sarwar, M. G.; Dragisić, B.; Dimitrijević, E.; Taylor, M. S. *Chem. – Eur. J.* **2013**, *19* (6), 2050–2058.

(20) Clark, T.; Hennemann, M.; Murray, J. S.; Politzer, P. *J. Mol. Model.* **2006**, *13* (2), 291–296.

(21) Cinčić, D.; Friščić, T.; Jones, W. *CrystEngComm* **2011**, *13* (9), 3224–3231.

(22) Hassel, O.; Hvoslef, J.; Vihovde, E. H.; Sörensen, N. A. *Acta Chem. Scand.* **1954**, *8*, 873–873.

(23) Fukui, K.; Yonezawa, T.; Nagata, C.; Shingu, H. *J. Chem. Phys.* **1954**, *22* (8), 1433–1442.
(24) Hunter, C. A.; Sanders, J. K. M. *J. Am. Chem. Soc.* **1990**, *112* (14), 5525–5534.
(25) Yang, L.; Brazier, J. B.; Hubbard, T. A.; Rogers, D. M.; Cockroft, S. L. *Angew. Chem.* **2016**, *128* (3), 924–928.
(26) Mecozzi, S.; West, A. P.; Dougherty, D. A. *Proc. Natl. Acad. Sci. U. S. A.* **1996**, *93* (20), 10566–10571.
(27) Ma, J. C.; Dougherty, D. A. *Chem. Rev.* **1997**, *97* (5), 1303–1324.
(28) Kearney, P. C.; Mizoue, L. S.; Kumpf, R. A.; Forman, J. E.; McCurdy, A.; Dougherty, D. A. *J. Am. Chem. Soc.* **1993**, *115* (22), 9907–9919.
(29) Davis, J. T. *Nat. Chem.* **2010**, *2* (7), 516–517.
(30) Dawson, R. E.; Hennig, A.; Weimann, D. P.; Emery, D.; Ravikumar, V.; Montenegro, J.; Takeuchi, T.; Gabutti, S.; Mayor, M.; Mareda, J.; Schalley, C. A.; Matile, S. *Nat. Chem.* **2010**, *2* (7), 533–538.
(31) Rosokha, Y. S.; Lindeman, S. V.; Rosokha, S. V.; Kochi, J. K. *Angew. Chem. Int. Ed.* **2004**, *43* (35), 4650–4652.
(32) Mecozzi, S.; West, A. P.; Dougherty, D. A. *J. Am. Chem. Soc.* **1996**, *118* (9), 2307–2308.
(33) Breiten, B.; Lockett, M. R.; Sherman, W.; Fujita, S.; Al-Sayah, M.; Lange, H.; Bowers, C. M.; Heroux, A.; Krilov, G.; Whitesides, G. M. *J. Am. Chem. Soc.* **2013**, *135* (41), 15579–15584.
(34) Zhao, Y.; Zhong, Z.; Ryu, E.-H. *J. Am. Chem. Soc.* **2007**, *129* (1), 218–225.
(35) Lehn, J. M. *Acc. Chem. Res.* **1978**, *11* (2), 49–57.
(36) Chang, S. K.; Hamilton, A. D. *J. Am. Chem. Soc.* **1988**, *110* (4), 1318–1319.
(37) Hancock, R. D.; Martell, A. E. *Comments Inorg. Chem.* **1988**, *6* (5–6), 237–284.
(38) Martell, A. E.; Hancock, R. D.; Motekaitis, R. J. *Coord. Chem. Rev.* **1994**, *133*, 39–65.
(39) Caltagirone, C.; Mulas, A.; Isaia, F.; Lippolis, V.; Gale, P. A.; Light, M. E. *Chem. Commun.* **2009**, No. 41, 6279–6281.
(40) Karp, G. *Cell and Molecular Biology: Concepts and Experiments*; John Wiley & Sons, 2009.
(41) *Krebs' Citric Acid Cycle - Half a Century and Still Turning*; Kay, J., Weitzman, P. D. J., Eds.; The Biochemical Society: London, 1987.
(42) Acharyya, S. K.; Chakraborty, P.; Lahiri, S.; Raymahashay, B. C.; Guha, S.; Bhowmik, A. *Nature* **1999**, *401* (6753), 545–545.
(43) Roy, S. [Complete Dataset] Lead results from Tap Water Sampling in Flint, MI. *Flint Water Study Updates*, 2015.
(44) Kaushal, S. S. *Environ. Sci. Technol.* **2016**, *50* (6), 2765–2766.

(45) Ramaswamy, C. P.; Souriraja, F. Gas generating composition for air bags. US5089069 A, February 18, 1992.
(46) Johnson, H. C.; Weller, A. S. *Angew. Chem. Int. Ed.* **2015**, *54* (35), 10173–10177.
(47) Zumdahl, S. S.; Zumdahl, S. A. *Chemistry*, 9 edition.; Brooks Cole: Belmont, CA, 2013.
(48) Hormadaly, J.; Marcus, Y. *J. Phys. Chem.* **1979**, *83* (22), 2843–2848.
(49) Hofmeister, F. *Arch. Für Exp. Pathol. Pharmakol.* **1888**, *24* (4–5), 247–260.
(50) He, J. J.; Quiocho, F. A. *Science* **1991**, *251* (5000), 1479–1481.
(51) Park, C. H.; Simmons, H. E. *J. Am. Chem. Soc.* **1968**, *90* (9), 2431–2432.
(52) Graf, E.; Lehn, J. M. *J. Am. Chem. Soc.* **1976**, *98* (20), 6403–6405.
(53) Lehn, J. M.; Sonveaux, E.; Willard, A. K. *J. Am. Chem. Soc.* **1978**, *100* (15), 4914–4916.
(54) Alberto, R.; Bergamaschi, G.; Braband, H.; Fox, T.; Amendola, V. *Angew. Chem.* **2012**, *124* (39), 9910–9914.
(55) Schmidtchen, F. P. *Angew. Chem. Int. Ed. Engl.* **1977**, *16* (10), 720–721.
(56) Worm, K.; Schmidtchen, F. P. *Angew. Chem. Int. Ed. Engl.* **1995**, *34* (1), 65–66.
(57) Ursu, A.; Schmidtchen, F. P. *Angew. Chem. Int. Ed.* **2012**, *51* (1), 242–246.
(58) Riordan, J. F. *Mol. Cell. Biochem.* **1979**, *26* (2), 71–92.
(59) Blondeau, P.; Segura, M.; Pérez-Fernández, R.; Mendoza, J. de. *Chem. Soc. Rev.* **2007**, *36* (2), 198–210.
(60) Schmuck, C.; Wich, P. *Angew. Chem. Int. Ed.* **2006**, *45* (26), 4277–4281.
(61) Metzger, A.; Lynch, V. M.; Anslyn, E. V. *Angew. Chem. Int. Ed. Engl.* **1997**, *36* (8), 862–865.
(62) Amendola, V.; Boiocchi, M.; Colasson, B.; Fabbrizzi, L.; Rodriguez Douton, M.-J.; Ugozzoli, F. *Angew. Chem. Int. Ed.* **2006**, *45* (41), 6920–6924.
(63) Chun, Y.; Jiten Singh, N.; Hwang, I.-C.; Woo Lee, J.; Yu, S. U.; Kim, K. S. *Nat. Commun.* **2013**, *4*, 1797.
(64) White, N. G.; Carvalho, S.; Félix, V.; Beer, P. D. *Org. Biomol. Chem.* **2012**, *10* (34), 6951–6959.
(65) Hafezi, N.; Holcroft, J. M.; Hartlieb, K. J.; Dale, E. J.; Vermeulen, N. A.; Stern, C. L.; Sarjeant, A. A.; Stoddart, J. F. *Angew. Chem. Int. Ed.* **2015**, *54* (2), 456–461.
(66) Kavallieratos, K.; de Gala, S. R.; Austin, D. J.; Crabtree, R. H. *J. Am. Chem. Soc.* **1997**, *119* (9), 2325–2326.
(67) Beeren, S. R.; Sanders, J. K. M. *J. Am. Chem. Soc.* **2011**, *133* (11), 3804–3807.
(68) Brooks, S. J.; Gale, P. A.; Light, M. E. *Chem. Commun.* **2006**, No. 41, 4344–4346.

(69) Young, P. G.; Clegg, J. K.; Bhadbhade, M.; Jolliffe, K. A. *Chem. Commun.* **2010**, *47* (1), 463–465.
(70) Hua, Y.; Flood, A. H. *Chem. Soc. Rev.* **2010**, *39* (4), 1262–1271.
(71) Hua, Y.; Ramabhadran, R. O.; Karty, J. A.; Raghavachari, K.; Flood, A. H. *Chem. Commun.* **2011**, *47* (21), 5979–5981.
(72) Ramabhadran, R. O.; Liu, Y.; Hua, Y.; Ciardi, M.; Flood, A. H.; Raghavachari, K. *J. Am. Chem. Soc.* **2014**, *136* (13), 5078–5089.
(73) Walsh, R. B.; Padgett, C. W.; Metrangolo, P.; Resnati, G.; Hanks, T. W.; Pennington, W. T. *Cryst. Growth Des.* **2001**, *1* (2), 165–175.
(74) Nguyen, H. L.; Horton, P. N.; Hursthouse, M. B.; Legon, A. C.; Bruce, D. W. *J. Am. Chem. Soc.* **2004**, *126* (1), 16–17.
(75) Cavallo, G.; Metrangolo, P.; Pilati, T.; Resnati, G.; Sansotera, M.; Terraneo, G. *Chem. Soc. Rev.* **2010**, *39* (10), 3772–3783.
(76) Sarwar, M. G.; Dragisic, B.; Sagoo, S.; Taylor, M. S. *Angew. Chem. Int. Ed.* **2010**, *49* (9), 1674–1677.
(77) Mele, A.; Metrangolo, P.; Neukirch, H.; Pilati, T.; Resnati, G. *J. Am. Chem. Soc.* **2005**, *127* (43), 14972–14973.
(78) Tepper, R.; Schulze, B.; Görls, H.; Bellstedt, P.; Jäger, M.; Schubert, U. S. *Org. Lett.* **2015**, *17* (23), 5740–5743.
(79) Kubik, S.; Goddard, R. *Proc. Natl. Acad. Sci.* **2002**, *99* (8), 5127–5132.
(80) Carnegie, R. S.; Gibb, C. L. D.; Gibb, B. C. *Angew. Chem. Int. Ed.* **2014**, *53* (43), 11498–11500.
(81) Zhao, H.; Gabbaï, F. P. *Nat. Chem.* **2010**, *2* (11), 984–990.
(82) Murase, I.; Mikuriya, M.; Sonoda, H.; Fukuda, Y.; Kida, S. *J. Chem. Soc. Dalton Trans.* **1986**, No. 5, 953–959.
(83) Gunnlaugsson, T.; Glynn, M.; Tocci (née Hussey), G. M.; Kruger, P. E.; Pfeffer, F. M. *Coord. Chem. Rev.* **2006**, *250* (23–24), 3094–3117.
(84) Callan, J. F.; de Silva, A. P.; Magri, D. C. *Tetrahedron* **2005**, *61* (36), 8551–8588.
(85) Silva, A. P. de; Moody, T. S.; Wright, G. D. *Analyst* **2009**, *134* (12), 2385–2393.
(86) Huston, M. E.; Akkaya, E. U.; Czarnik, A. W. *J. Am. Chem. Soc.* **1989**, *111* (23), 8735–8737.
(87) Madhu, S.; Ravikanth, M. *Inorg. Chem.* **2014**, *53* (3), 1646–1653.
(88) Han, C.; Cui, Z.; Zou, Z.; Sabahaiti; Tian, D.; Li, H. *Photochem. Photobiol. Sci.* **2010**, *9* (9), 1269–1273.
(89) Kitchen, J. A.; Boyle, E. M.; Gunnlaugsson, T. *Inorganica Chim. Acta* **2012**, *381*, 236–242.
(90) Hau, F. K.-W.; Lo, H.-S.; Yam, V. W.-W. *Chem. – Eur. J.* **2016**, *22* (11), 3738–3749.

(91) Butler, S. J.; Parker, D. *Chem. Soc. Rev.* **2013**, *42* (4), 1652–1666.
(92) Meshkova, S. B.; Topilova, Z. M.; Lozinskii, M. O.; Bol'shoi, D. V. *J. Appl. Spectrosc.* **1997**, *64* (2), 229–233.
(93) Bruce, J. I.; Dickins, R. S.; Govenlock, L. J.; Gunnlaugsson, T.; Lopinski, S.; Lowe, M. P.; Parker, D.; Peacock, R. D.; Perry, J. J. B.; Aime, S.; Botta, M. *J. Am. Chem. Soc.* **2000**, *122* (40), 9674–9684.
(94) Pal, R.; Parker, D.; Costello, L. C. *Org. Biomol. Chem.* **2009**, *7* (8), 1525–1528.
(95) Beer, P. D.; Keefe, A. D. *J. Organomet. Chem.* **1989**, *375* (1), C40–C42.
(96) Broomsgrove, A. E. J.; Addy, D. A.; Bresner, C.; Fallis, I. A.; Thompson, A. L.; Aldridge, S. *Chem. – Eur. J.* **2008**, *14* (25), 7525–7529.
(97) Valério, C.; Fillaut, J.-L.; Ruiz, J.; Guittard, J.; Blais, J.-C.; Astruc, D. *J. Am. Chem. Soc.* **1997**, *119* (10), 2588–2589.
(98) Lim, J. Y. C.; Cunningham, M. J.; Davis, J. J.; Beer, P. D. *Chem. Commun.* **2015**, *51* (78), 14640–14643.
(99) Canevet, D.; Sallé, M.; Zhang, G.; Zhang, D.; Zhu, D. *Chem. Commun.* **2009**, No. 17, 2245–2269.
(100) Lu, H.; Xu, W.; Zhang, D.; Chen, C.; Zhu, D. *Org. Lett.* **2005**, *7* (21), 4629–4632.
(101) Bill, N. L.; Ishida, M.; Bähring, S.; Lim, J. M.; Lee, S.; Davis, C. M.; Lynch, V. M.; Nielsen, K. A.; Jeppesen, J. O.; Ohkubo, K.; Fukuzumi, S.; Kim, D.; Sessler, J. L. *J. Am. Chem. Soc.* **2013**, *135* (29), 10852–10862.
(102) Frisch, H. L.; Wasserman, E. *J. Am. Chem. Soc.* **1961**, *83* (18), 3789–3795.
(103) Vickers, M. S.; Beer, P. D. *Chem. Soc. Rev.* **2007**, *36* (2), 211–225.
(104) Amabilino, D. B.; Stoddart, J. F. *Chem. Rev.* **1995**, *95* (8), 2725–2828.
(105) Crowley, J. D.; Goldup, S. M.; Lee, A.-L.; Leigh, D. A.; McBurney, R. T. *Chem. Soc. Rev.* **2009**, *38* (6), 1530–1541.
(106) Hubin, T. J.; Busch, D. H. *Coord. Chem. Rev.* **2000**, *200–202*, 5–52.
(107) Breault, G. A.; Hunter, C. A.; Mayers, P. C. *Tetrahedron* **1999**, *55* (17), 5265–5293.
(108) Gil-Ramírez, G.; Leigh, D. A.; Stephens, A. J. *Angew. Chem. Int. Ed.* **2015**, *54* (21), 6110–6150.
(109) Xue, M.; Yang, Y.; Chi, X.; Yan, X.; Huang, F. *Chem. Rev.* **2015**, *115* (15), 7398–7501.
(110) Chichak, K. S.; Cantrill, S. J.; Pease, A. R.; Chiu, S.-H.; Cave, G. W. V.; Atwood, J. L.; Stoddart, J. F. *Science* **2004**, *304* (5675), 1308–1312.
(111) Pentecost, C. D.; Chichak, K. S.; Peters, A. J.; Cave, G. W. V.; Cantrill, S. J.; Stoddart, J. F. *Angew. Chem. Int. Ed.* **2007**, *46* (1–2), 218–222.
(112) Ayme, J.-F.; Beves, J. E.; Campbell, C. J.; Leigh, D. A. *Chem. Soc. Rev.* **2013**, *42* (4), 1700–1712.

(113) Harrison, I. T.; Harrison, S. *J. Am. Chem. Soc.* **1967**, *89* (22), 5723–5724.
(114) Thompson, M. C.; Busch, D. H. *J. Am. Chem. Soc.* **1962**, *84* (9), 1762–1763.
(115) Busch, D. H. *J. Incl. Phenom. Mol. Recognit. Chem.* **1992**, *12* (1–4), 389–395.
(116) Dietrich-Buchecker, C. O.; Sauvage, J. P.; Kintzinger, J. P. *Tetrahedron Lett.* **1983**, *24* (46), 5095–5098.
(117) Fuller, A.-M. L.; Leigh, D. A.; Lusby, P. J.; Slawin, A. M. Z.; Walker, D. B. *J. Am. Chem. Soc.* **2005**, *127* (36), 12612–12619.
(118) Hogg, L.; Leigh, D. A.; Lusby, P. J.; Morelli, A.; Parsons, S.; Wong, J. K. Y. *Angew. Chem. Int. Ed.* **2004**, *43* (10), 1218–1221.
(119) Goldup, S. M.; Leigh, D. A.; Lusby, P. J.; McBurney, R. T.; Slawin, A. M. Z. *Angew. Chem. Int. Ed.* **2008**, *47* (37), 6999–7003.
(120) Zhang, G.; Gil-Ramírez, G.; Markevicius, A.; Browne, C.; Vitorica-Yrezabal, I. J.; Leigh, D. A. *J. Am. Chem. Soc.* **2015**, *137* (32), 10437–10442.
(121) Lin, Y.-H.; Lai, C.-C.; Liu, Y.-H.; Peng, S.-M.; Chiu, S.-H. *Angew. Chem. Int. Ed.* **2013**, *52* (39), 10231–10236.
(122) Dietrich-Buchecker, C. O.; Sauvage, J.-P. *Angew. Chem. Int. Ed. Engl.* **1989**, *28* (2), 189–192.
(123) Leigh, D. A.; Pritchard, R. G.; Stephens, A. J. *Nat. Chem.* **2014**, *6* (11), 978–982.
(124) Aucagne, V.; Hänni, K. D.; Leigh, D. A.; Lusby, P. J.; Walker, D. B. *J. Am. Chem. Soc.* **2006**, *128* (7), 2186–2187.
(125) Aucagne, V.; Berná, J.; Crowley, J. D.; Goldup, S. M.; Hänni, K. D.; Leigh, D. A.; Lusby, P. J.; Ronaldson, V. E.; Slawin, A. M. Z.; Viterisi, A.; Walker, D. B. *J. Am. Chem. Soc.* **2007**, *129* (39), 11950–11963.
(126) Goldup, S. M.; Leigh, D. A.; Long, T.; McGonigal, P. R.; Symes, M. D.; Wu, J. *J. Am. Chem. Soc.* **2009**, *131* (43), 15924–15929.
(127) Barran, P. E.; Cole, H. L.; Goldup, S. M.; Leigh, D. A.; McGonigal, P. R.; Symes, M. D.; Wu, J.; Zengerle, M. *Angew. Chem. Int. Ed.* **2011**, *50* (51), 12280–12284.
(128) Hoekman, S.; Kitching, M. O.; Leigh, D. A.; Papmeyer, M.; Roke, D. *J. Am. Chem. Soc.* **2015**, *137* (24), 7656–7659.
(129) Berná, J.; Crowley, J. D.; Goldup, S. M.; Hänni, K. D.; Lee, A.-L.; Leigh, D. A. *Angew. Chem. Int. Ed.* **2007**, *46* (30), 5709–5713.
(130) Amabilino, D. B.; Ashton, P. R.; Reder, A. S.; Spencer, N.; Stoddart, J. F. *Angew. Chem. Int. Ed. Engl.* **1994**, *33* (12), 1286–1290.
(131) Fang, L.; Olson, M. A.; Benítez, D.; Tkatchouk, E.; Iii, W. A. G.; Stoddart, J. F. *Chem. Soc. Rev.* **2009**, *39* (1), 17–29.
(132) Glink, P. T.; Oliva, A. I.; Stoddart, J. F.; White, A. J. P.; Williams, D. J. *Angew. Chem. Int. Ed.* **2001**, *40* (10), 1870–1875.

(133) Barin, G.; Coskun, A.; Fouda, M. M. G.; Stoddart, J. F. *ChemPlusChem* **2012**, *77* (3), 159–185.
(134) Hamilton, D. G.; Prodi, L.; Feeder, N.; Sanders, J. K. M. *J. Chem. Soc. [Perkin 1]* **1999**, No. 8, 1057–1066.
(135) Tron, A.; Thornton, P. J.; Lincheneau, C.; Desvergne, J.-P.; Spencer, N.; Tucker, J. H. R.; McClenaghan, N. D. *J. Org. Chem.* **2015**, *80* (2), 988–996.
(136) Stanier, C. A.; O'Connell, M. J.; Clegg, W.; Anderson, H. L. *Chem. Commun.* **2001**, No. 5, 493–494.
(137) Hübner, G. M.; Gläser, J.; Seel, C.; Vögtle, F. *Angew. Chem. Int. Ed.* **1999**, *38* (3), 383–386.
(138) Lee, S.; Chen, C.-H.; Flood, A. H. *Nat. Chem.* **2013**, *5* (8), 704–710.
(139) Wisner, J. A.; Beer, P. D.; Drew, M. G. B.; Sambrook, M. R. *J. Am. Chem. Soc.* **2002**, *124* (42), 12469–12476.
(140) Evans, N. H.; Serpell, C. J.; Beer, P. D. *Chem. Commun.* **2011**, *47* (31), 8775–8777.
(141) Langton, M. J.; Beer, P. D. *Chem. – Eur. J.* **2012**, *18* (45), 14406–14412.
(142) Chae, M. K.; Suk, J.; Jeong, K.-S. *Tetrahedron Lett.* **2010**, *51* (32), 4240–4242.
(143) Evans, N. H.; Beer, P. D. *Chem. – Eur. J.* **2011**, *17* (38), 10542–10546.
(144) Evans, N. H.; Serpell, C. J.; Beer, P. D. *Angew. Chem. Int. Ed.* **2011**, *50* (11), 2507–2510.
(145) Evans, N. H.; Beer, P. D. *Org. Biomol. Chem.* **2010**, *9* (1), 92–100.
(146) Evans, N. H.; Serpell, C. J.; White, N. G.; Beer, P. D. *Chem. – Eur. J.* **2011**, *17* (44), 12347–12354.
(147) Gassensmith, J. J.; Matthys, S.; Lee, J.-J.; Wojcik, A.; Kamat, P. V.; Smith, B. D. *Chem. – Eur. J.* **2010**, *16* (9), 2916–2921.
(148) Langton, M. J.; Duckworth, L. C.; Beer, P. D. *Chem. Commun.* **2013**, *49* (77), 8608–8610.
(149) Langton, M. J.; Blackburn, O. A.; Lang, T.; Faulkner, S.; Beer, P. D. *Angew. Chem. Int. Ed.* **2014**, *53* (43), 11463–11466.
(150) Huang, B.; Santos, S. M.; Felix, V.; Beer, P. D. *Chem. Commun.* **2008**, No. 38, 4610–4612.
(151) Browne, W. R.; Feringa, B. L. *Nat. Nanotechnol.* **2006**, *1* (1), 25–35.
(152) Balzani, V.; Credi, A.; Raymo, F. M.; Stoddart, J. F. *Angew. Chem. Int. Ed.* **2000**, *39* (19), 3348–3391.
(153) Higashi, T.; Motoyama, K.; Arima, H. *J. Drug Deliv. Sci. Technol.* **2013**, *23* (6), 523–529.
(154) White, A. G.; Fu, N.; Leevy, W. M.; Lee, J.-J.; Blasco, M. A.; Smith, B. D. *Bioconjug. Chem.* **2010**, *21* (7), 1297–1304.

(155) Lee, J.-J.; Baumes, J. M.; Connell, R. D.; Oliver, A. G.; Smith, B. D. *Chem. Commun.* **2011**, *47* (25), 7188–7190.
(156) Thordarson, P.; Bijsterveld, E. J. A.; Rowan, A. E.; Nolte, R. J. M. *Nature* **2003**, *424* (6951), 915–918.
(157) Galli, M.; Lewis, J. E. M.; Goldup, S. M. *Angew. Chem. Int. Ed.* **2015**, *54* (46), 13545–13549.
(158) Langton, M. J.; Beer, P. D. *Acc. Chem. Res.* **2014**, *47* (7), 1935–1949.
(159) Green, J. E.; Wook Choi, J.; Boukai, A.; Bunimovich, Y.; Johnston-Halperin, E.; DeIonno, E.; Luo, Y.; Sheriff, B. A.; Xu, K.; Shik Shin, Y.; Tseng, H.-R.; Stoddart, J. F.; Heath, J. R. *Nature* **2007**, *445* (7126), 414–417.
(160) Zhang, J.; Ma, P. X. *Adv. Drug Deliv. Rev.* **2013**, *65* (9), 1215–1233.
(161) Moon, C.; Kwon, Y. M.; Lee, W. K.; Park, Y. J.; Yang, V. C. *J. Controlled Release* **2007**, *124* (1–2), 43–50.
(162) Harmatys, K. M.; Cole, E. L.; Smith, B. D. *Mol. Pharm.* **2013**, *10* (11), 4263–4271.
(163) Lehn, J.-M. *Angew. Chem. Int. Ed. Engl.* **1988**, *27* (1), 89–112.
(164) Day, A. I.; Blanch, R. J.; Arnold, A. P.; Lorenzo, S.; Lewis, G. R.; Dance, I. *Angew. Chem. Int. Ed.* **2002**, *41* (2), 275–277.
(165) Freeman, W. A.; Mock, W. L.; Shih, N. Y. *J. Am. Chem. Soc.* **1981**, *103* (24), 7367–7368.
(166) Kim, J.; Jung, I.-S.; Kim, S.-Y.; Lee, E.; Kang, J.-K.; Sakamoto, S.; Yamaguchi, K.; Kim, K. *J. Am. Chem. Soc.* **2000**, *122* (3), 540–541.
(167) Behrend, R.; Meyer, E.; Rusche, F. *Justus Liebigs Ann. Chem.* **1905**, *339* (1), 1–37.
(168) Day, A.; Arnold, A. P.; Blanch, R. J.; Snushall, B. *J. Org. Chem.* **2001**, *66* (24), 8094–8100.
(169) Rudkevich, D. M. *Angew. Chem.* **2004**, *116* (5), 568–581.
(170) Jansen, K.; Buschmann, H.-J.; Wego, A.; Döpp, D.; Mayer, C.; Drexler, H.-J.; Holdt, H.-J.; Schollmeyer, E. *J. Incl. Phenom. Macrocycl. Chem.* **2001**, *39* (3–4), 357–363.
(171) Buschmann, H.-J.; Cleve, E.; Jansen, K.; Schollmeyer, E. *Anal. Chim. Acta* **2001**, *437* (1), 157–163.
(172) Wagner, B. D.; MacRae, A. I. *J. Phys. Chem. B* **1999**, *103* (46), 10114–10119.
(173) Isobe, H.; Sato, S.; Nakamura, E. *Org. Lett.* **2002**, *4* (8), 1287–1289.
(174) Ong, W.; Kaifer, A. E. *Organometallics* **2003**, *22* (21), 4181–4183.
(175) Lee, J. W.; Samal, S.; Selvapalam, N.; Kim, H.-J.; Kim, K. *Acc. Chem. Res.* **2003**, *36* (8), 621–630.
(176) Kim, H.-J.; Jeon, W. S.; Ko, Y. H.; Kim, K. *Proc. Natl. Acad. Sci.* **2002**, *99* (8), 5007–5011.
(177) Wu, X.; Hu, K.; Meng, X.; Cheng, G. *New J. Chem.* **2010**, *34* (1), 17–20.

(178) Assaf, K. I.; Nau, W. M. *Chem. Soc. Rev.* **2014**, *44* (2), 394–418.
(179) Chubarova, E. V.; Samsonenko, D. G.; Sokolov, M. N.; Gerasko, O. A.; Fedin, V. P.; Platas, J. G. *J. Incl. Phenom. Macrocycl. Chem.* **2004**, *48* (1–2), 31–35.
(180) Kim, K. *Chem. Soc. Rev.* **2002**, *31* (2), 96–107.
(181) Buck, A. T.; Paletta, J. T.; Khindurangala, S. A.; Beck, C. L.; Winter, A. H. *J. Am. Chem. Soc.* **2013**, *135* (29), 10594–10597.
(182) Zhao, P.; Li, N.; Astruc, D. *Coord. Chem. Rev.* **2013**, *257* (3–4), 638–665.
(183) Lee, T.-C.; Scherman, O. A. *Chem. – Eur. J.* **2012**, *18* (6), 1628–1633.
(184) Lanterna, A.; Pino, E.; Doménech-Carbó, A.; González-Béjar, M.; Pérez-Prieto, J. *Nanoscale* **2014**, *6* (16), 9550–9553.
(185) Mock, W. L.; Irra, T. A.; Wepsiec, J. P.; Adhya, M. *J. Org. Chem.* **1989**, *54* (22), 5302–5308.

CHAPTER 2

Halogen and Hydrogen Bonding Pyridyl Triazole Axle Containing Rotaxanes for Halide Recognition.

2.1. Introduction

2.1.1. Halogen bonding anion recognition

As discussed in Chapter 1, the use of halogen bonding interactions in solution-state anion recognition is a comparatively novel phenomenon; receptors utilising this unique dipolar interaction have only appeared in the last decade.[1–3] The development of convergent acyclic anion receptors featuring halogen bond donors has been relatively slow. Recent examples include Taylor's use of highly polarised neutral iodoperfluorophenyl species incorporated into a urea-scaffold which is selective for Cl^- in acetone (**Figure 2.1-i**)[4] and Ghosh's charge-assisted iodoimidazolium tripodal receptor which is selective for Br^- in MeCN (**Figure 2.1-i**).[5]

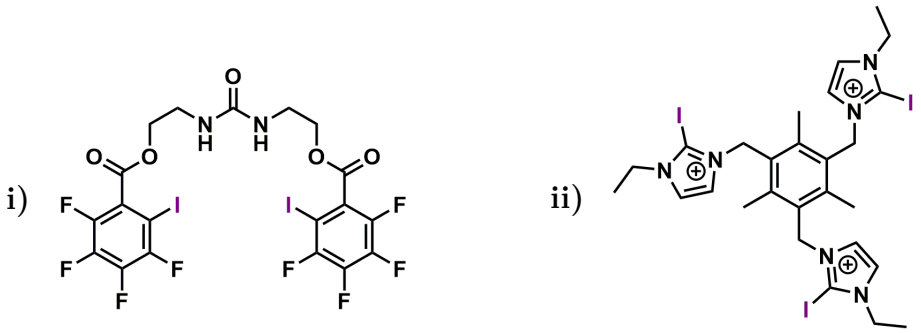


Figure 2.1 – i) Taylor's urea bis-iodoperfluorobenzene Cl^- receptor; ii) Ghosh's tripodal Br^- selective tris-iodoimidazolium receptor.

The incorporation of halogen bonding motifs into interlocked structures however, are rare. Beer's pioneering chloride templated iodotriazolium [2]rotaxane[6] paved the way for the incorporation of halogen bond donors into mechanically interlocked hosts such as a pyridinium bis-iodotriazole [2]catenane (**Figure 2.2-i)**[7] and a water soluble permethylated β-cyclodextrin stoppered [2]rotaxane (**Figure 2.2-ii).**[8] The anion recognition properties of these receptors are impressive in comparison to their all-hydrogen bonding counterparts; the [2]catenane displayed selectivity for the heavier halides such as Br^- and I^- ($K_A(Br^-)$, $K_A(I^-) = >10^4\ M^{-1}$) in 45:45:10

$CDCl_3/CD_3OD/D_2O$ whilst the cyclodextrin axle containing [2]rotaxane was selective for iodide ($K_A(I^-) = 2.2 \times 10^3\ M^{-1}$) in pure water.

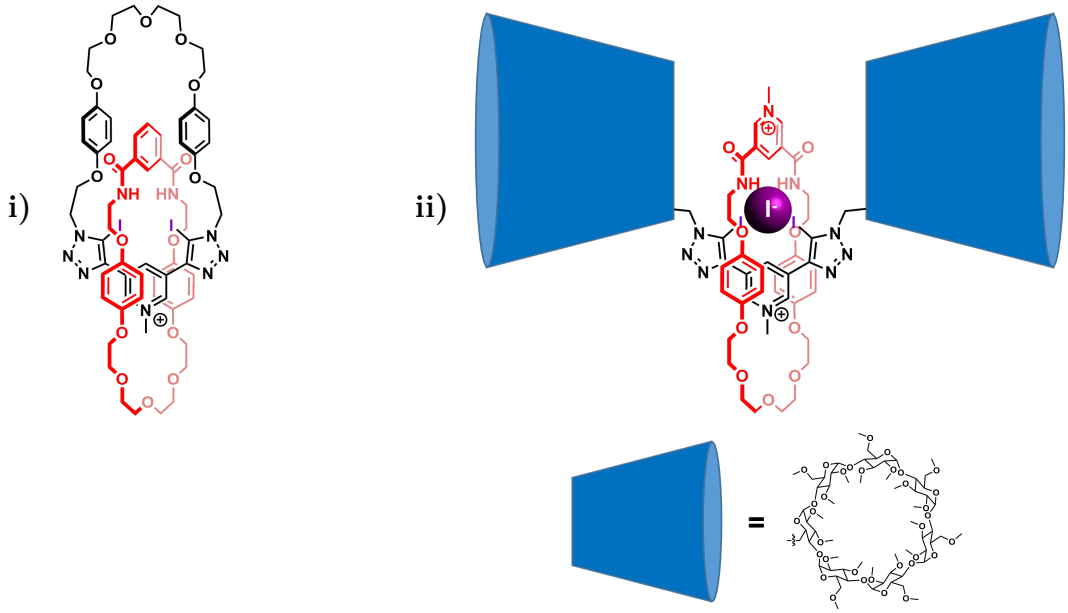


Figure 2.2 – Beer's i) halide selective halogen bonding pyridinium bis-iodotriazole [2]catenane; ii) halogen bonding water soluble permethylated β-cyclodextrin stoppered [2]rotaxane selective for I^- in water.

2.1.2. Chelating anion host systems

The use of acyclic anion receptor systems with more than one binding site, designed to undergo significant anion-induced conformational change, is a unique approach to anion recognition. Beer and co-workers developed dual binding site acyclic anion receptors that contain either a pyridine, pyridine *N*-oxide or pyridinium bis-amide binding site covalently attached *via* a flexible propyl spacer to a cationic imidazolium group.[9] Prior to anion chelation, the bis-amide motif adopts a syn-anti-conformation to minimize the overall dipole moment, resulting in an 'open' conformation (**Figure 2.3**).

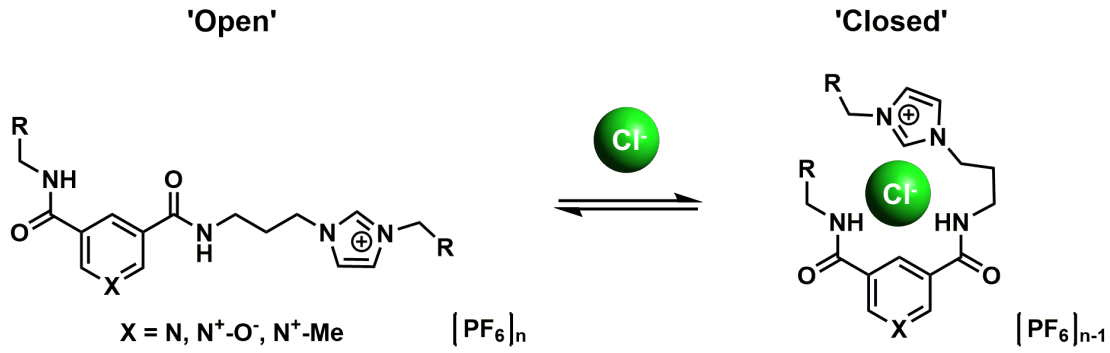


Figure 2.3 – Beer's flexible pyridyl-imidazolium receptor system exploiting anion chelation induced conformational change.

^{1}H NMR titration experiments conducted in 1:1 CD_2Cl_2/acetone-d_6 revealed evidence for the cooperative chelation of Cl^- by both pyridyl bis-amide and imidazolium groups, as indicated by the simultaneous downfield shifts of the binding site protons present in both motifs. Additionally, increases in the excimer emission when R = pyrene were observed, resulting from the receptor adopting a 'closed' conformation that brings the pyrene arms in close enough proximity to form an emissive exciplex.

2.1.3. Chapter aims

The objective of this Chapter is to further exploit the chelating anion binding mode exhibited in the acyclic receptor example (**Figure 2.3**) *via* the integration of pyridinium-triazole and -iodotriazole bidentate chelating motifs into the axle component of target halogen and hydrogen bonding rotaxanes (**Figure 2.4-i**). Initially, an acyclic pyridinium triazole receptor was prepared in order to establish the synthetic protocol required for the preparation of the axle component (**Figure 2.4-ii**). Following this, benchmarking Cl^- binding studies were conducted to assess the binding mode of the acyclic pyridinium triazole receptor. Finally, assessment of the effect upon the anion recognition properties of this chelating axle structural

motif incorporated within a series of isostructural halogen and hydrogen bonding [2]rotaxanes anion host structures was conducted with a series of anions.

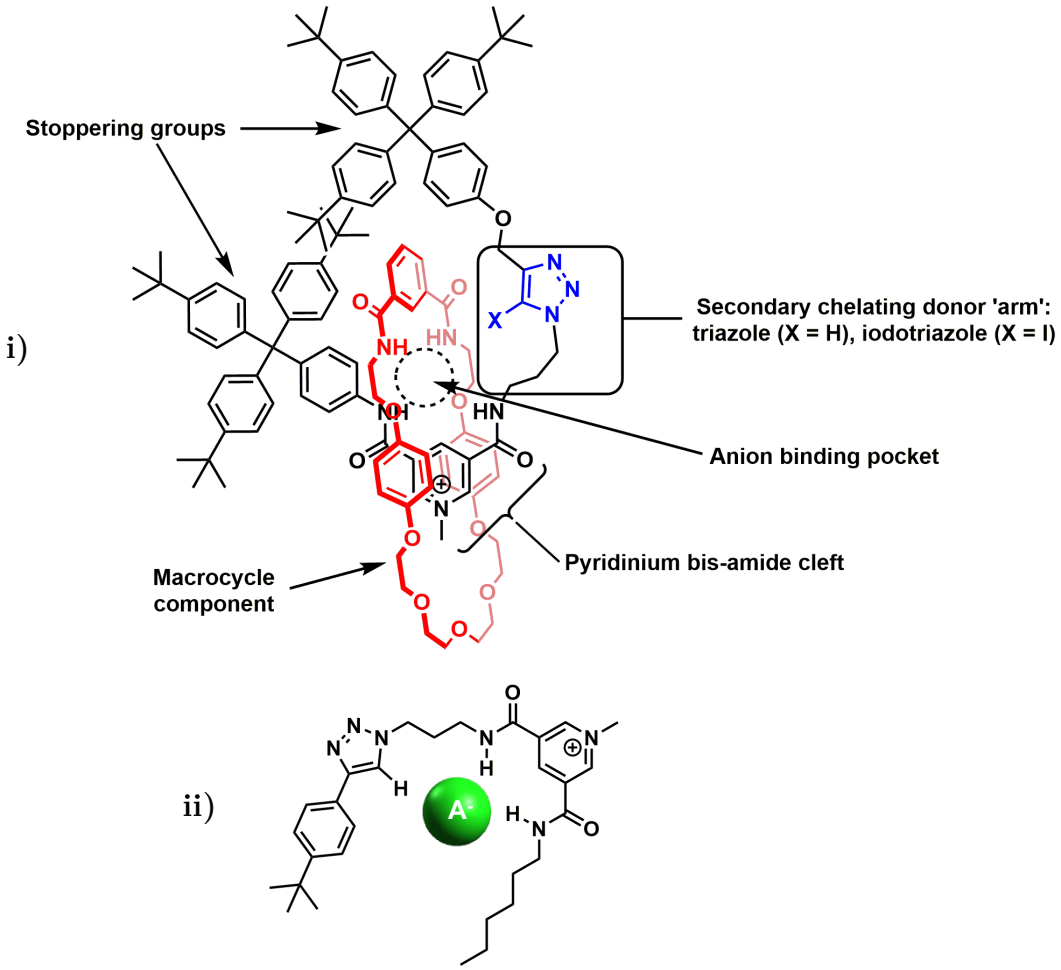


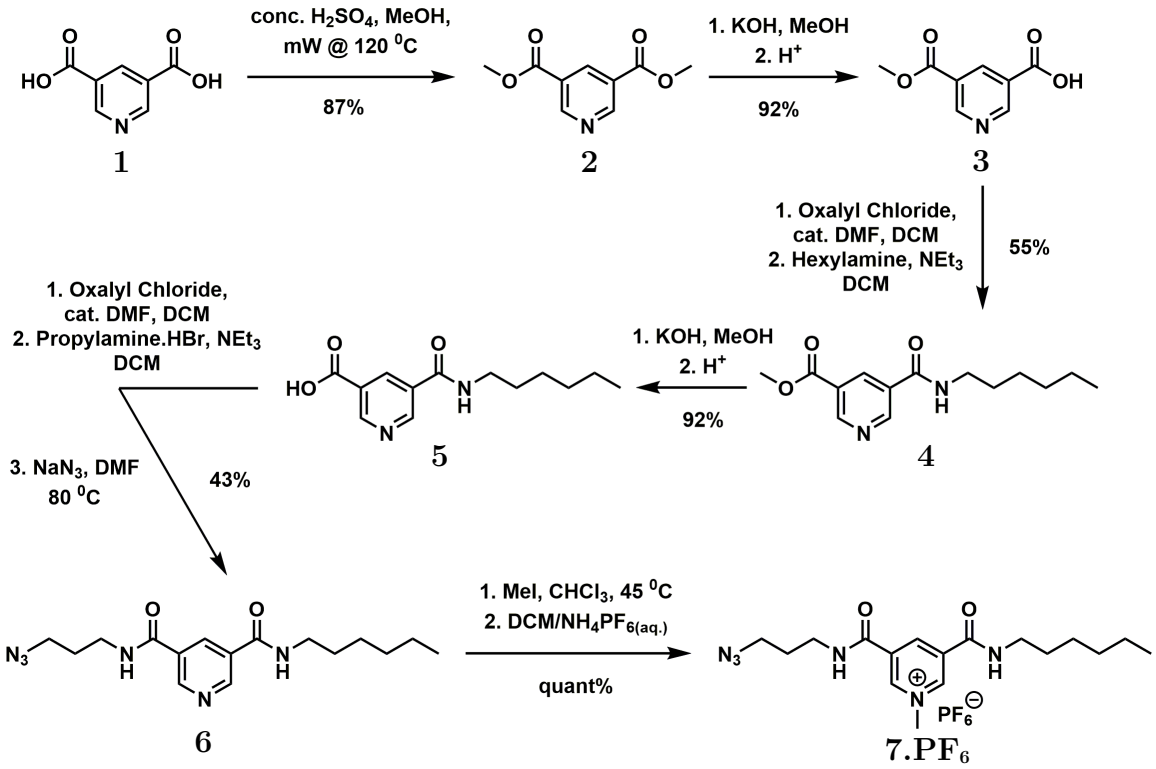
Figure 2.4 – i) Structural design of target halogen (X = I) and hydrogen bonding (X = H) pyridinium-triazole [2]rotaxanes; ii) structure and proposed anion binding mode of target acyclic pyridinium triazole receptor.

2.2. A Chelating Acyclic Pyridinium-triazole Receptor

2.2.1. Receptor synthesis

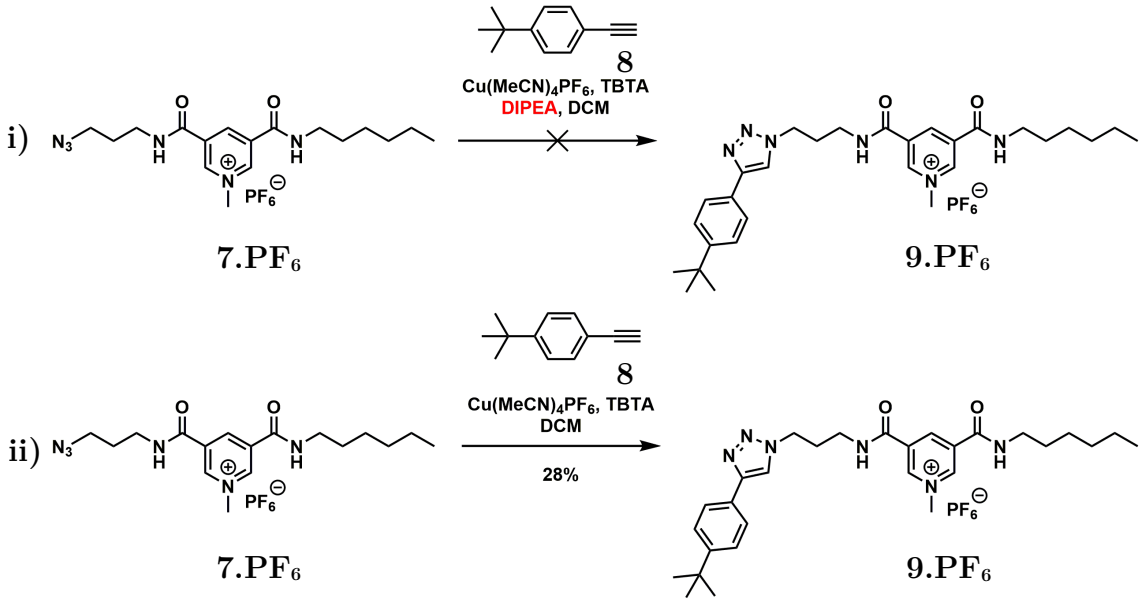
Exploiting the same propyl spacing between the pyridyl and imidazolium motifs of the receptor depicted in **Figure 2.3**, the substitution of a triazole hydrogen bonding motif for the imidazolium group was sought. This was devised through a CuAAC 'click' dipolar cycloaddition of an azide-terminated pyridinium bis-amide core with an alkyne to form the triazole in the desired position within the receptor. The

asymmetric synthesis of the pyridine core precursor motif is described in **Scheme 2.1**. Firstly, heating commercially available pyridine-3,5 dicarboxylic acid **1** in the presence of MeOH and concentrated H_2SO_4 under microwave irradiation gave bis-methyl ester **2**[10] in an 87% yield. Mono-saponification was achieved in a 92% yield using a slight excess of KOH in MeOH to give mono-methyl ester **3**[10]. This was reacted with oxalyl chloride and subsequent acid chloride amine condensation with hexylamine afforded amide-ester compound **4**[11] in a 55% yield. The ester group was hydrolysed with KOH in MeOH to give carboxylic acid **5**[11] in a 77% yield which upon acid chloride formation was reacted with propylamine bromide hydrobromide in the presence of excess triethylamine. Without further purification the bromide intermediate was reacted with sodium azide in DMF to give mono-azide **6** in an overall yield of 43%. Reaction of **6** with a large excess of MeI in DCM, followed by counter-ion exchange to the non-coordinating PF_6^- salt gave pyridinium derivative **7.PF$_6^-$** in quantitative yield.



Scheme 2.1 – Synthesis of pyridine core motif.

Commerically available 1-(*tert*-butyl)-4-ethynylbenzene **8** was reacted with **7.PF$_6$** in the presence of Cu((MeCN)$_4$PF$_6$), DIPEA and TBTA in an attempt to afford the CuAAC 'click' product pyridinium-triazole **9.PF$_6$**. However, only pyridinium decomposition products were detected, possibly resulting from the presence of base (**Scheme 2.2-i**).[12] DIPEA was henceforth excluded and triazole **9.PF$_6$** was isolated in a 28% yield (**Scheme 2.2-ii**).



Scheme 2.2: i) Attempted CuACC "click" reaction in the presence of DIPEA of **7.PF$_6$** and alkyne **8** to give **9.PF$_6$**. ii) Successful CuACC "click" reaction without DIPEA of **7.PF$_6$** and alkyne **8** to give **9.PF$_6$**.

2.2.2. Preliminary anion binding investigations with chloride

Upon titrating **9.PF$_6$** with one equivalent of TBACl in acetone-d_6, downfield shifts of pyridinium proton **c** ($\Delta\delta$(ppm) = 1.23), amides **NH** ($\Delta\delta$(ppm) = 1.53) and pendant triazole proton **d** ($\Delta\delta$(ppm) = 0.56) were observed, indicating strong hydrogen bonding of the halide in a chelating manner (**Figure 2.6-i**). WinEQNMR2[13] analysis of the titration data indicated that the strength of binding was too strong to be quantified (K_A(Cl$^-$) = >10^4 M^{-1}). An analogous titration was undertaken in a more competitive solvent mixture of 1:1 CD$_3$OD:CDCl$_3$ and a 1:1 stoichiometric association constant was determined (K_A(Cl$^-$) = 415 M^{-1}), *via*

WinEQNMR2 analysis of the titration data monitoring the downfield shifts of internal pyridinium proton **c** (**Figure 2.5-ii**). A similar association constant value was also determined ($K_A(Cl^-)$ = 438 M^{-1}) monitoring the downfield movement of triazole proton **d** (**Figure 2.5-ii**).

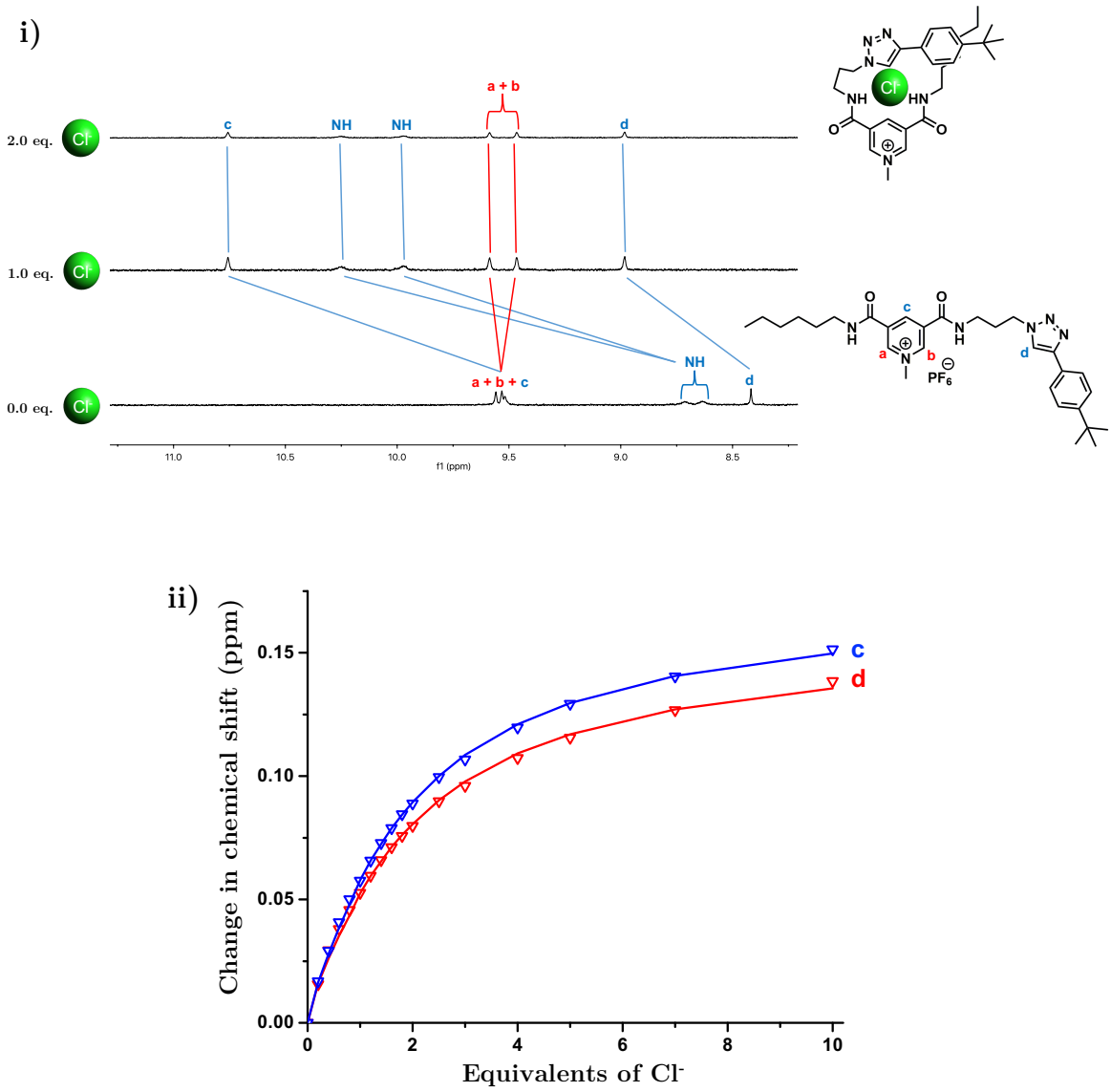
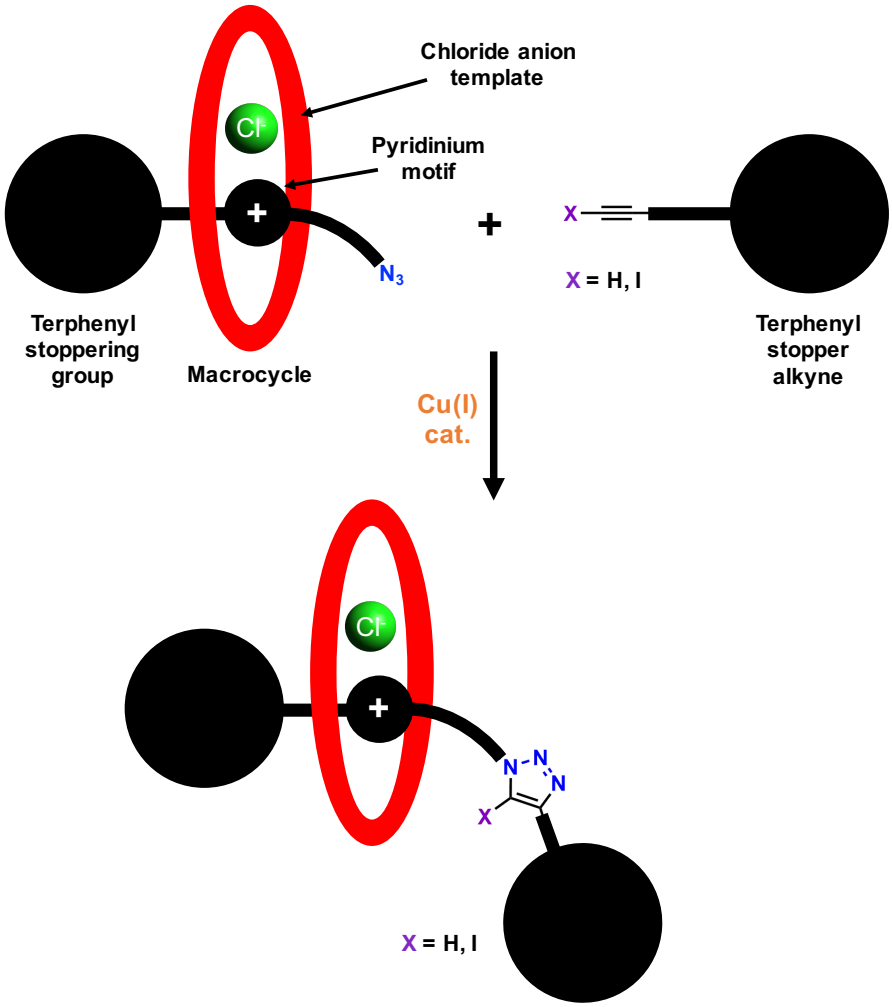


Figure 2.5 – i) Changes in the ^{1}H NMR spectra of **9.PF$_6$** with additions of increasing equivalents of TBACl, binding site protons shown in blue (acetone-d_6, 500 MHz, 298 K). ii) Titration plots of the change in ppm shift vs. equivalents of Cl^- monitoring internal pyridinium proton **c** and triazole proton **d** (1:1 $CDCl_3/CD_3OD$, 500 MHz, 298 K). Experimental data points shown as hollow triangles and calculated fit as a solid line.

2.3. Synthesis of Pyridinium Halogen/Hydrogen Bonding Axle Containing [2]rotaxanes

2.3.1. [2]Rotaxane synthetic strategy

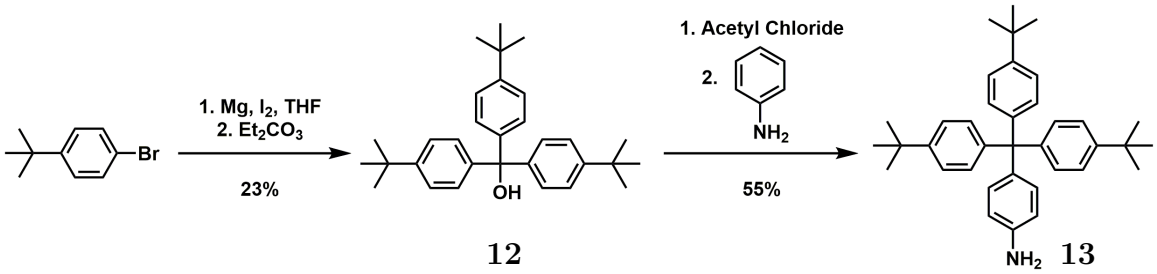
Having demonstrated the cooperative participation of the triazole hydrogen bond donor for binding Cl^- in the simple acyclic receptor **9.PF$_6$**, the synthesis of [2]rotaxanes containing bis-amide pyridinium triazole hydrogen and halogen bonding axle components was undertaken. A chloride templated, CuAAC mediated monostoppering rotaxane synthesis was proposed between an azide functionalised pyridinium bis-amide axle precursor, a macrocycle and a terphenyl stoppering group functionalised with either an alkyne or iodo-alkyne (**Scheme 2.3**).



Scheme 2.3 – The proposed Cu(I)-catalysed, chloride templated monostoppering synthesis of target hydrogen bonding (X = H) and halogen bonding (X = I) [2]rotaxanes.

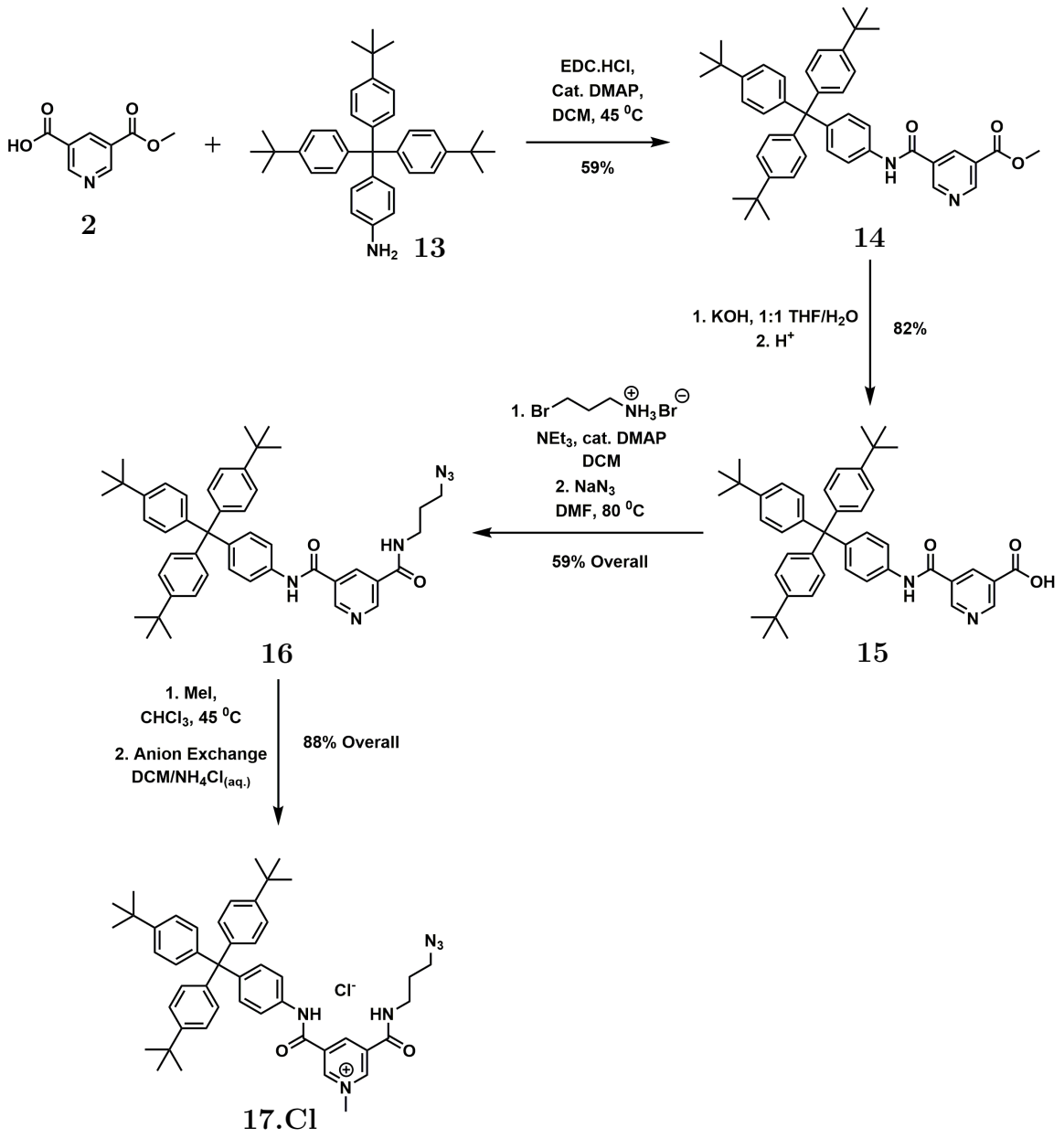
2.3.2. Synthesis of axle precursor and macrocycle components

The strategy outlined in **Scheme 2.3** first required the multi-step synthesis of azide functionalised axle precursor **17.Cl**. The terphenyl amine functionalised stoppering group **13**[14] was synthesised *via* the initial reaction of the Grignard intermediate of 4-*tert*-butyl bromobenzene with diethyl carbonate to form trityl stopper precursor **12**[15] followed by activation with acetyl chloride to facilitate an electrophilic aromatic substitution of aniline to give stopper amine **13** in a 55% yield (**Scheme 2.4**).



Scheme 2.4 – Stopper amine **13** synthesis.

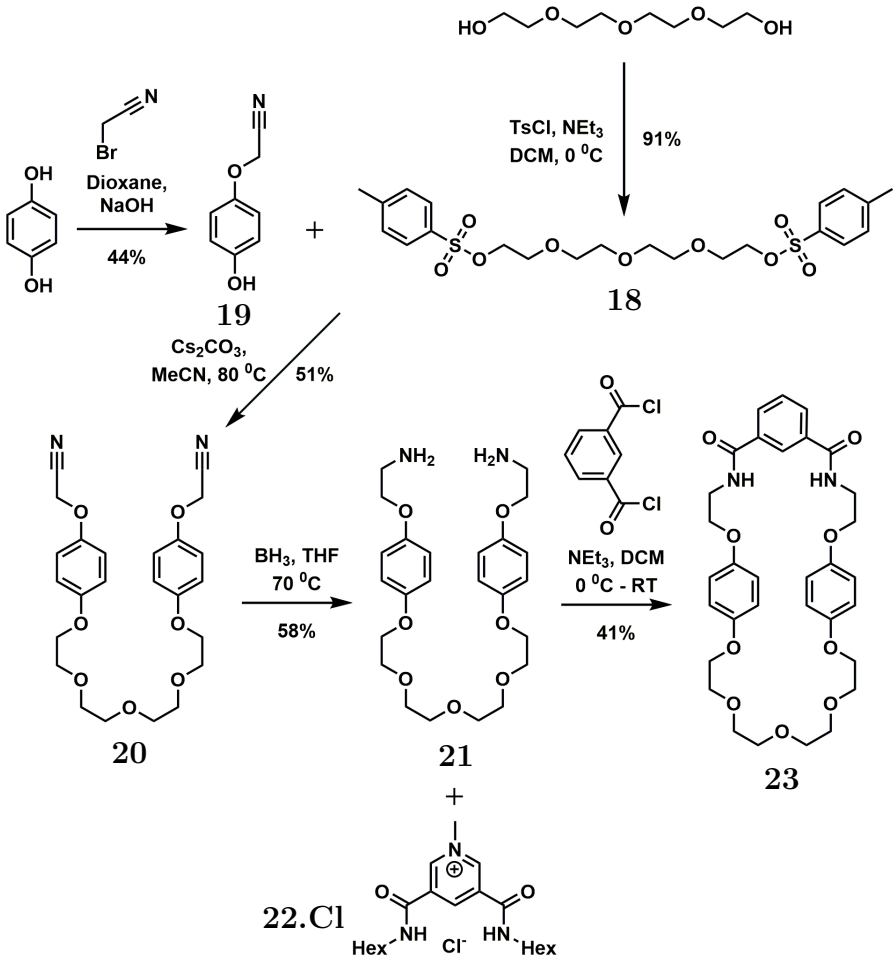
The multi-step approach used to prepare azide axle precursor **17.Cl** is shown in **Scheme 2.5**. The EDC.HCl mediated amide coupling of pyridine mono-methyl ester **2** with terphenyl amine **13** in refluxing DCM in the presence of a catalytic amount of DMAP gave terphenyl mono-amide **14** in a 59% yield. Basic ester hydrolysis to produce acid **15** followed by EDC.HCl-mediated amide coupling with propylamine bromide hydrobromide and subsequent reaction with NaN_3 in DMF, afforded azide **16** in an overall yield of 59%. Methylation of **16** using a large excess of MeI in refluxing $CHCl_3$ and anion exchange with 1M $NH_4Cl_{(aq.)}$ gave axle precursor **17.Cl** in an 88% yield.



Scheme 2.5 – Synthesis of axle precursor **17.Cl**.

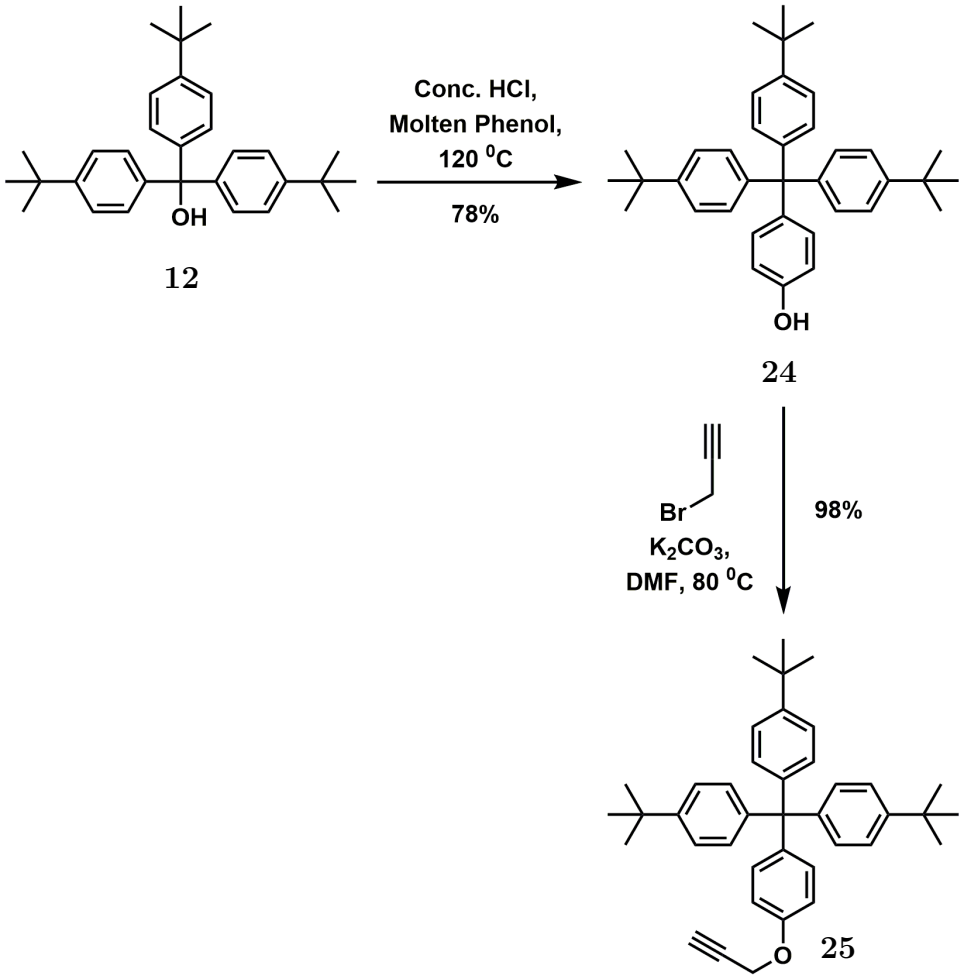
The isophthalamide macrocyclic component **23** was synthesized *via* modification of a literature procedure (**Scheme 2.6**).[16] Tetraethylene glycol bis-tosylate **18**[17] was synthesised by reaction of tosyl chloride with tetraethylene glycol in DCM and triethylamine in a 91% yield. Mono-substituted nitrile-hydroquinone **19**[18] was obtained in a 44% yield *via* statistical reaction of hydroquinone and bromoacetonitrile in MeCN under basic conditions. This was subsequently reacted with bis-tosylate **18** using Cs_2CO_3 in MeCN to give bis-nitrile **20**[18] in a 51% yield.

Reduction of **20** with borane to bis-amine macrocycle precursor **21**[18] was achieved in a 58% yield. The chloride anion templated synthesis of macrocycle **23** was undertaken with equimolar amounts of pyridinium template **22.Cl**[16] (kindly donated by Dr. Richard Knighton), bis-amine **21** and isophthaloyl dichloride in dry DCM and NEt_3 to produce the macrocycle **23** in an isolated yield of 41% following recrystallization from MeOH.



Scheme 2.6 – Isophthalamide macrocycle **23** synthesis.

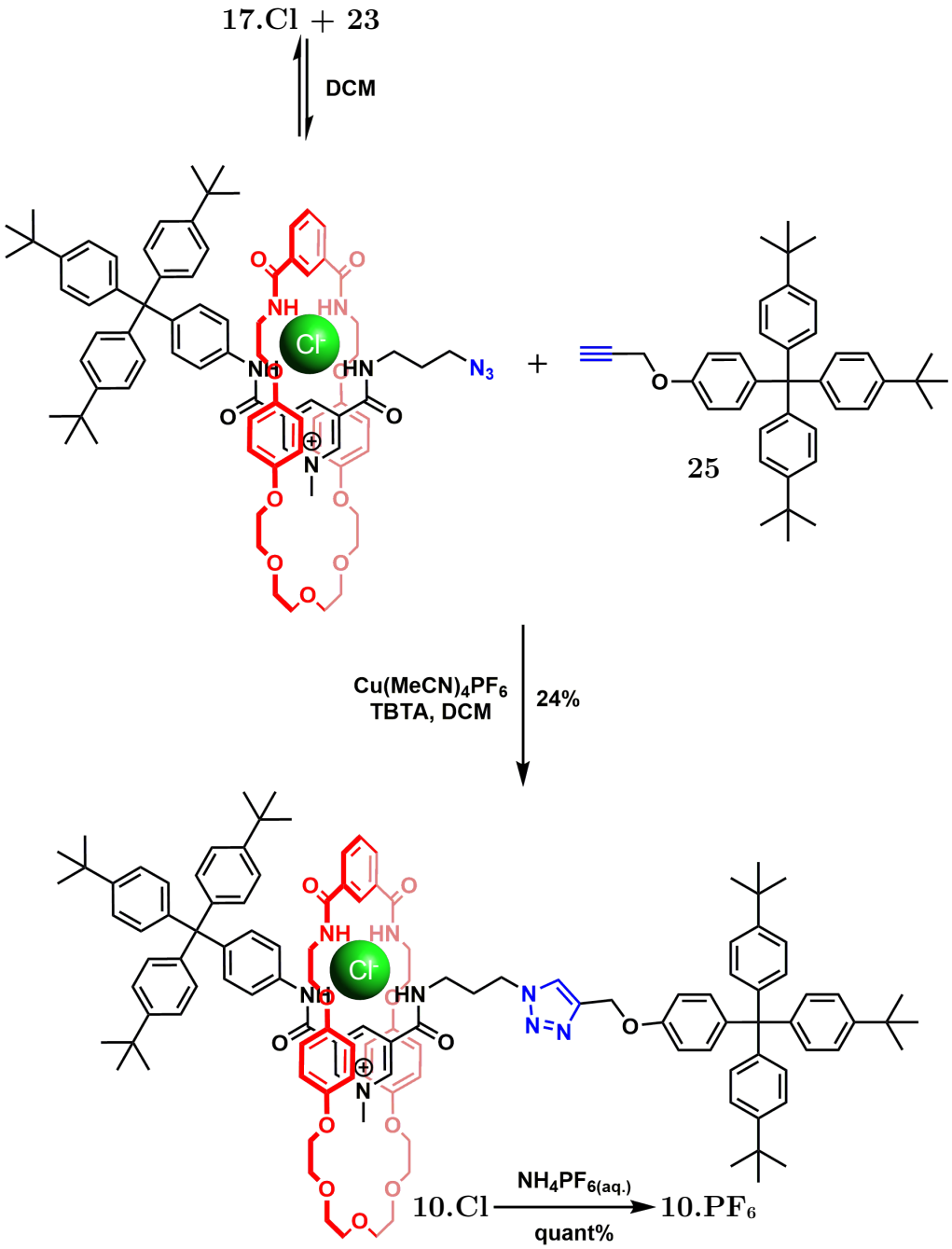
Alkyne functionalised terphenyl derivative **25**[19] was synthesised according to **Scheme 2.7**. Trityl alcohol **12** was reacted in an acidified phenol melt to form terphenyl alcohol **24**[15] in a 78% yield. The target alkyne **25** was obtained in near quantitative yield upon reaction with propargyl bromide in dry DMF and K_2CO_3.



Scheme 2.7 – Synthesis of target stopper alkyne **25**.

2.3.3. Halogen bonding/hydrogen bonding [2]rotaxane synthesis

A CuAAC-mediated monostoppering rotaxanation synthetic strategy was devised to synthesise the target pyridinium proto- and iodotriazole axle containing rotaxanes. The hydrogen bonding rotaxane **10.Cl** was prepared initially according to **Scheme 2.8**. Axle precursor **17.Cl** was stirred with 1.5 equivalents of macrocycle **23** and 1.2 equivalents of stopper alkyne **25** under CuAAC conditions in DCM for 24 hours. A combination of preparative TLC followed by size exclusion chromatography was used to remove free macrocycle and TBTA, allowing rotaxane **10.Cl** to be isolated in a 24% yield.



Scheme 2.8 – Synthesis of triazole-containing rotaxane **10.Cl**.

The novel rotaxane was characterised by ^{1}H NMR, ^{13}C NMR and ESI-HRMS. The ^{1}H NMR spectrum of rotaxane **10.Cl** displays distinct features attributed to the molecule's unique interlocked nature when compared to ^{1}H NMR spectra of macrocycle **23** and axle precursor **17.Cl** (**Figure 2.6**). A downfield shift of internal

macrocycle proton 1 and upfield shifts of pyridinium axle protons **a**, **b** and **c** indicate hydrogen bonding interactions to the Cl^- template. Secondly, the macrocycle component's hydroquinone proton resonances (**HQ**) are also characteristically split and shifted upfield, diagnostic of aromatic donor-acceptor interactions to the pyridinium axle motif.

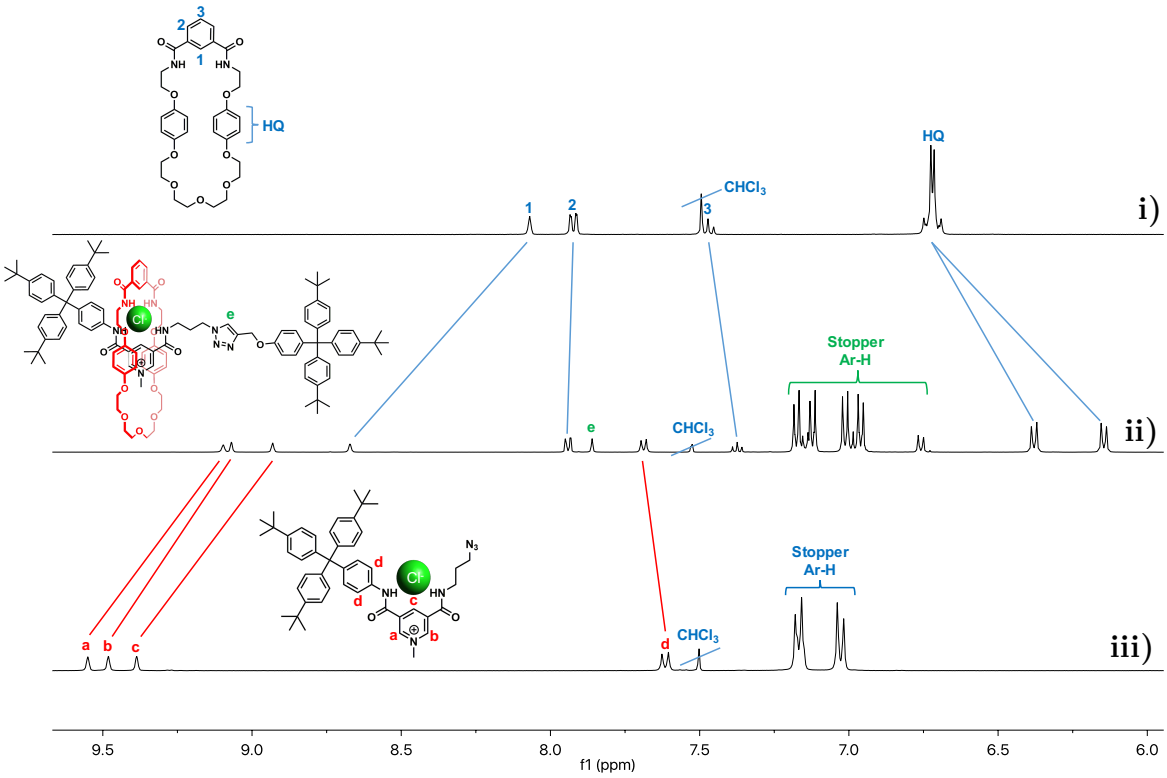


Figure 2.6 – Assigned ^{1}H NMR spectra (1:1 $CDCl_3/CD_3OD$, 400 MHz, 298 K) of i) Macrocycle **23**, ii) rotaxane **10.Cl** and iii) axle precursor azide **17.Cl**.

Further confirmation of the mechanically interlocked nature of the rotaxane **10.Cl** was obtained *via* a ^{1}H-^{1}H-ROESY NMR experiment. Proximal through-space correlations between the proton environments **a**, **b**, **c**, **d** and **e** of the axle component and proton 1 and hydroquinone proton environments (**HQ**) of the macrocyclic component are observed (**Figure 2.7**).

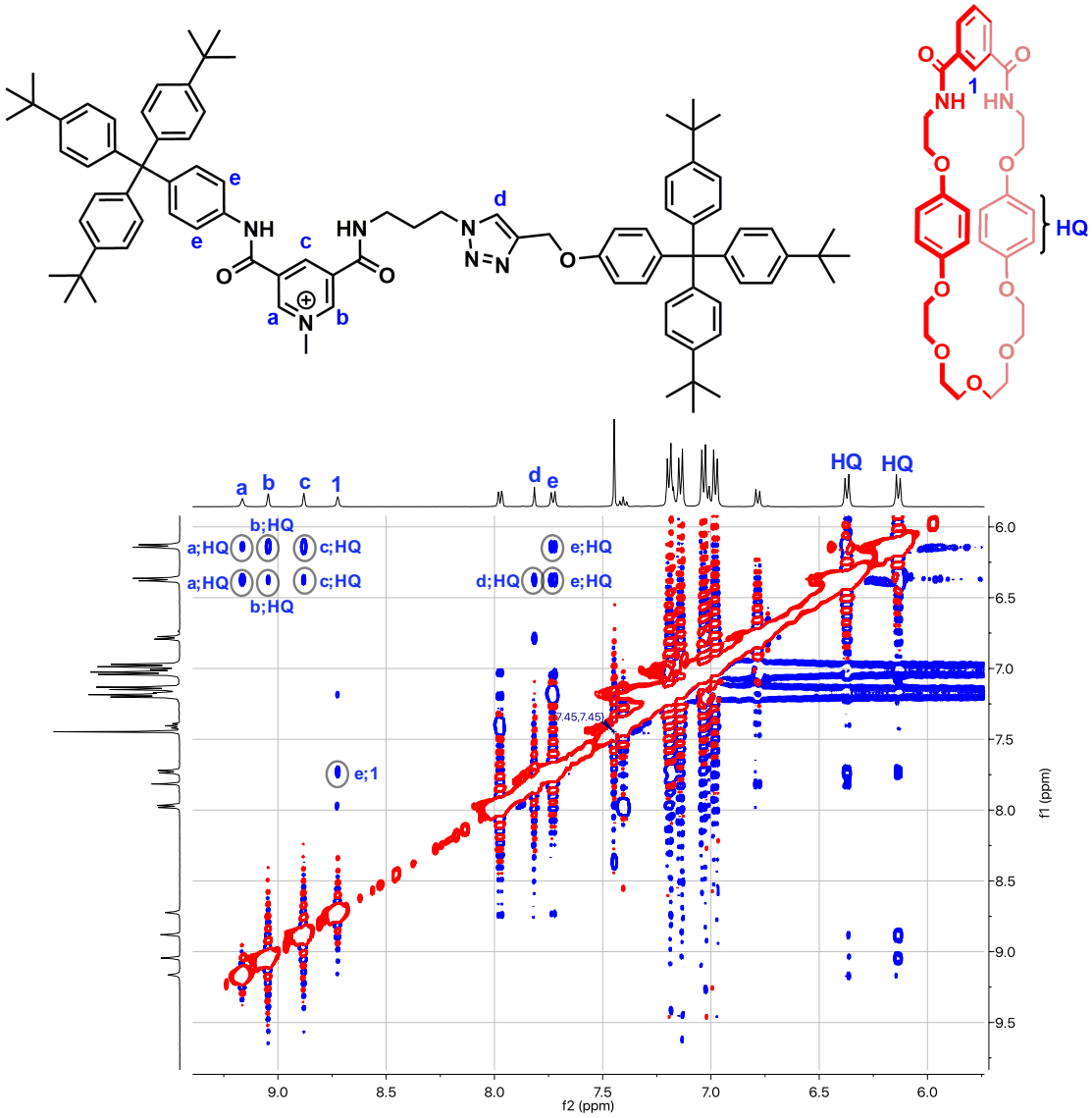
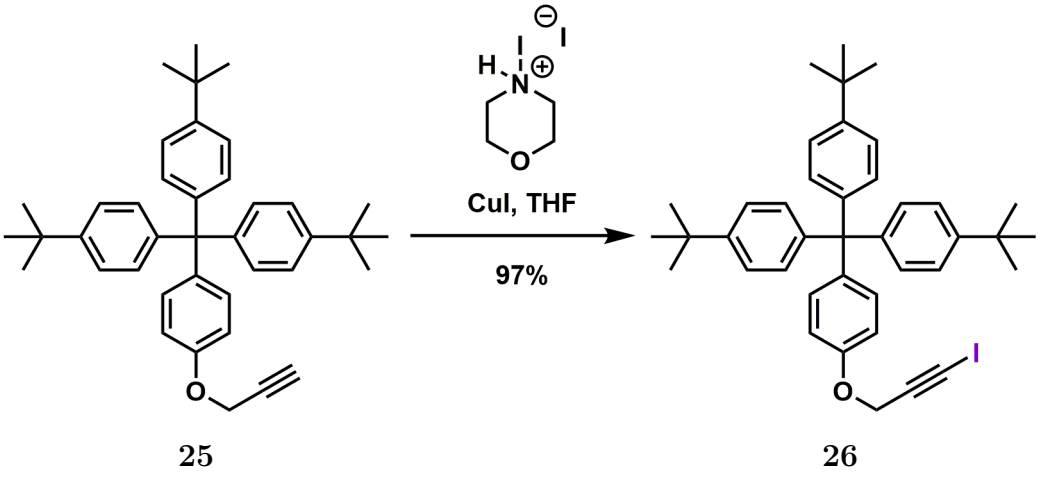


Figure 2.7 – Truncated ^{1}H NMR ROESY spectrum of rotaxane **10.Cl**, in which through-space proton-proton correlations between axle and macrocyclic components are indicated by grey circles (1:1 $CDCl_3/CD_3OD$, 500 MHz, 298 K).

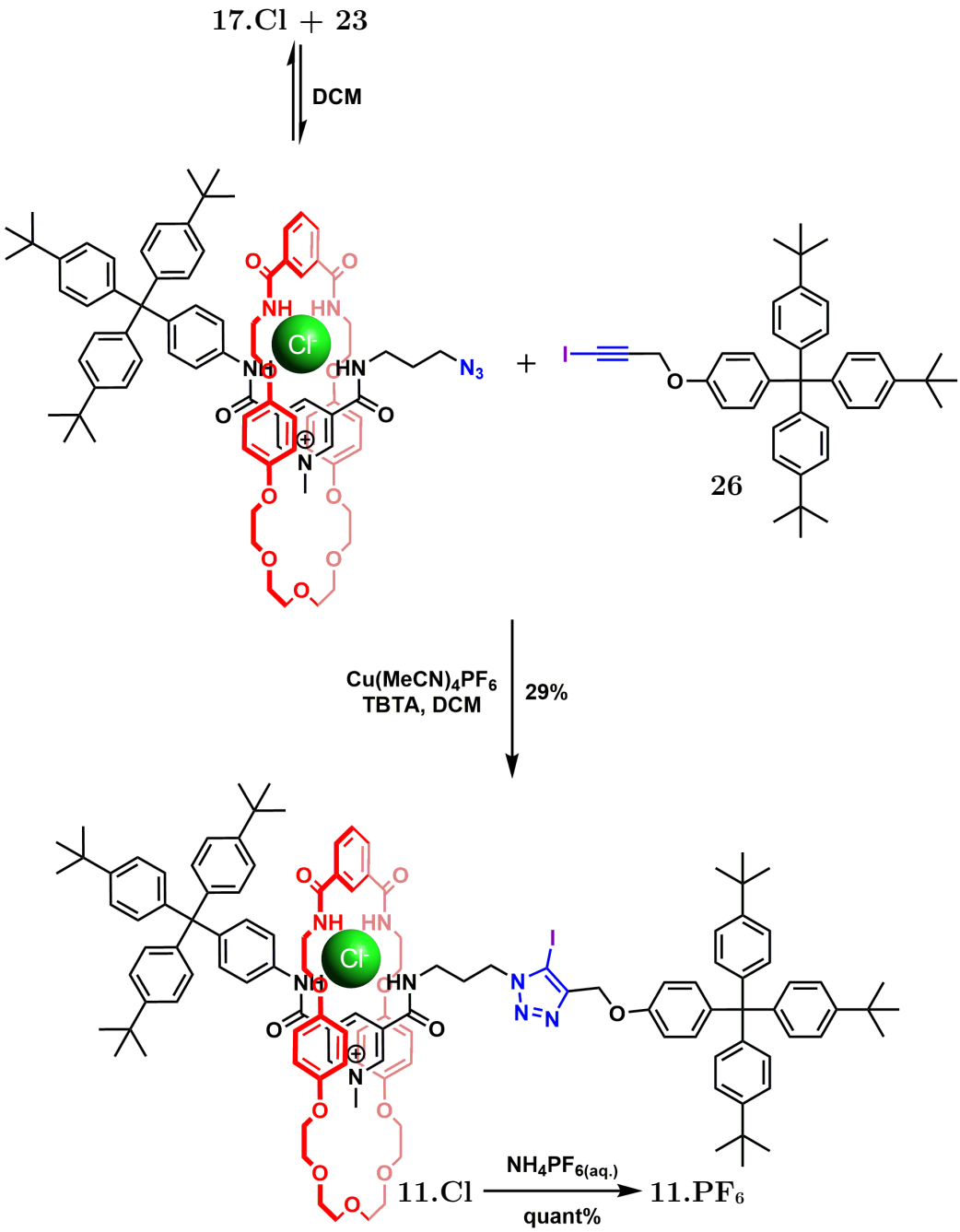
To synthesise the halogen bonding pyridinium iodotriazole axle containing rotaxane **11.Cl**, the iodoalkyne functionalised terphenyl derivative **26** was prepared (**Scheme 2.9**). Stopper alkyne **25** was converted to its corresponding iodo-alkyne **26** *via* a modified literature procedure[6] using *N*-iodomorpholine hydroiodide and catalytic CuI in THF in an excellent yield of 97%.



25 **26**

Scheme 2.9 – Synthesis of iodo-alkyne stopper **26**.

An analogous CuAAC-mediated monostoppering rotaxanation synthetic procedure was used to prepare the halogen bonding rotaxane **11.Cl** (**Scheme 2.10**). The halogen bonding rotaxane **11.Cl** was isolated in a yield of 29% after preparative TLC purification and characterised by ^{1}H NMR, ^{13}C NMR and ESI-HRMS.



Scheme 2.10 – Synthesis of iodotriazole-containing rotaxane **11.Cl**.

The expected mass for the iodinated product in ESI-HRMS analysis was observed at m/z = 2011.9659 ($[M]^+$). Comparison of the ^{1}H NMR spectra of macrocycle **23** and axle precursor **17.Cl** in 1:1 $CDCl_3/CD_3OD$ showed that akin to hydrogen bonding rotaxane **10.Cl**, halogen bonding rotaxane **11.Cl** also exhibited the Cl^- induced shifts characteristic of an interlocked structure of this type: a downfield

shift of macrocycle proton 1, upfield shifts of the pyridinium resonances **a**, **b** and **c** and upfield shifts and splitting of the hydroquinone proton signals (**HQ**) (**Figure 2.8**).

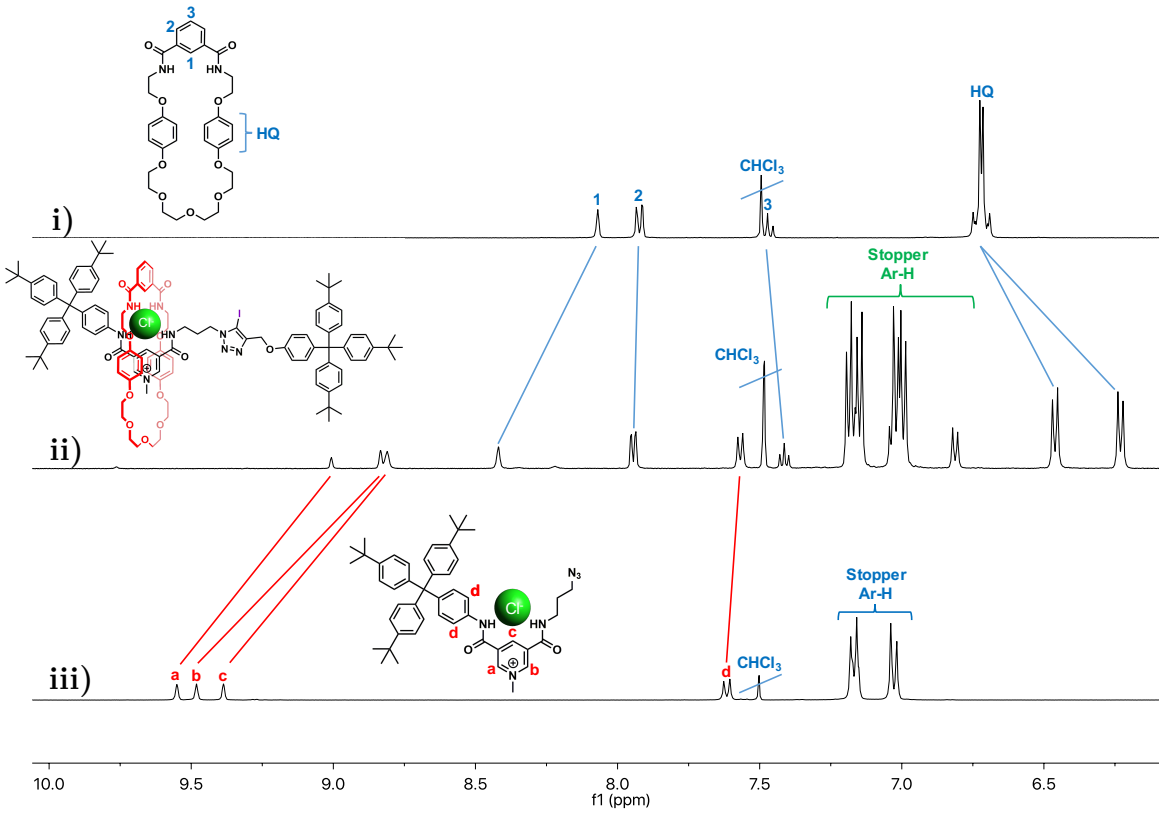


Figure 2.8 – Assigned ^{1}H NMR spectra (1:1 $CDCl_3/CD_3OD$, 400 MHz, 298 K) of i) Macrocycle **23**, ii) rotaxane **11.Cl** and iii) axle precurosor azide **17.Cl**.

A ^{1}H-^{1}H ROESY NMR spectrum of **11.Cl** exhibited analogous through-space correlations to rotaxane **10.Cl**; interactions were observed between proton environments **a**, **b**, **c** and **e**; internal macrocycle proton 1 and the hydroquinone proton environments (**HQ**) of the macrocyclic component (**Figure 2.9**).

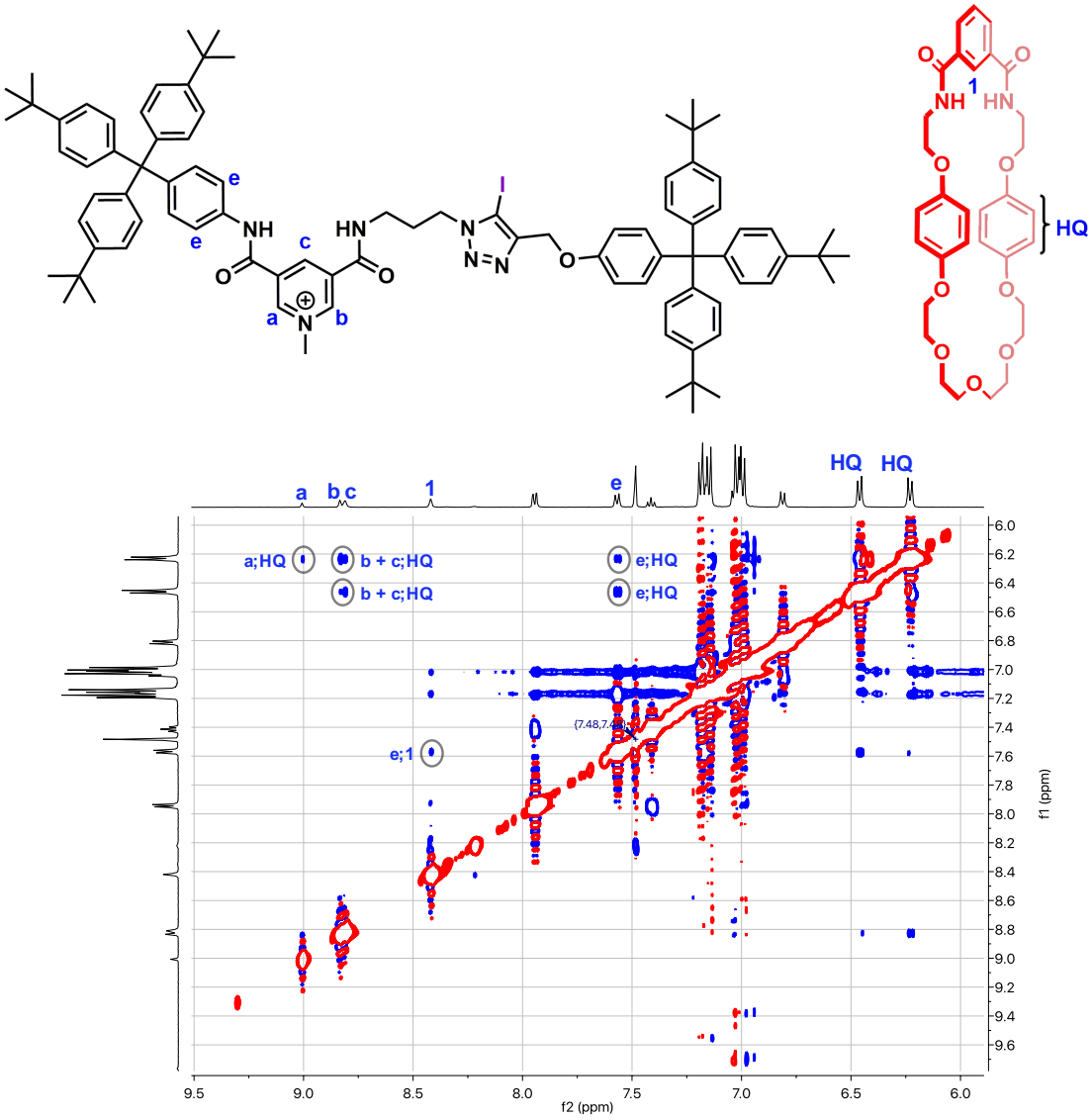


Figure 2.9 – Truncated ^{1}H NMR ROESY spectrum of rotaxane **11.Cl**, through-space proton-proton correlations between axle and macrocyclic components indicated by grey circles (1:1 $CDCl_3/CD_3OD$, 500 MHz, 298 K).

Removal of the chloride anion template from the interlocked rotaxane cavities of **10.Cl** and **11.Cl** was achieved *via* anion exchange to the corresponding PF_6^- salts *via* dissolution in $CHCl_3$ and repeated washing with $NH_4PF_{6(aq.)}$ (**Schemes 2.8** and **2.10**). It was confirmed that both rotaxanes **10.PF$_6$** and **11.PF$_6$** remained interlocked by ^{1}H NMR and ESI-MS analysis.

2.3.4. ^{1}H NMR anion binding investigations

Comparative ^{1}H NMR anion binding titrations were carried out in the competitive aqueous solvent mixture of 45:45:10 $CDCl_3/CD_3OD/D_2O$. Preliminary studies were conducted with the halides Cl^-, Br^- and I^-. Upon addition of increasing equivalents of TBACl, hydrogen bonding rotaxane **10.PF$_6$** exhibited significant downfield shifts of internal macrocycle proton 1, axle internal pyridinium proton **c** and aryl stopper protons **d** indicating strong binding of the Cl^- anion within the interlocked rotaxane cavity (**Figure 2.10**). Surprisingly, axle triazole proton **e** was not perturbed (< 0.01 ppm), which suggests it does not hydrogen bond to Cl^- which is in contrast to acyclic receptor **9.PF$_6$** (**Section 2.2.1**). This may be attributed to the aqueous solvent mixture, where competitive solvation of the triazole disfavours its participation in multidentate anion chelation.

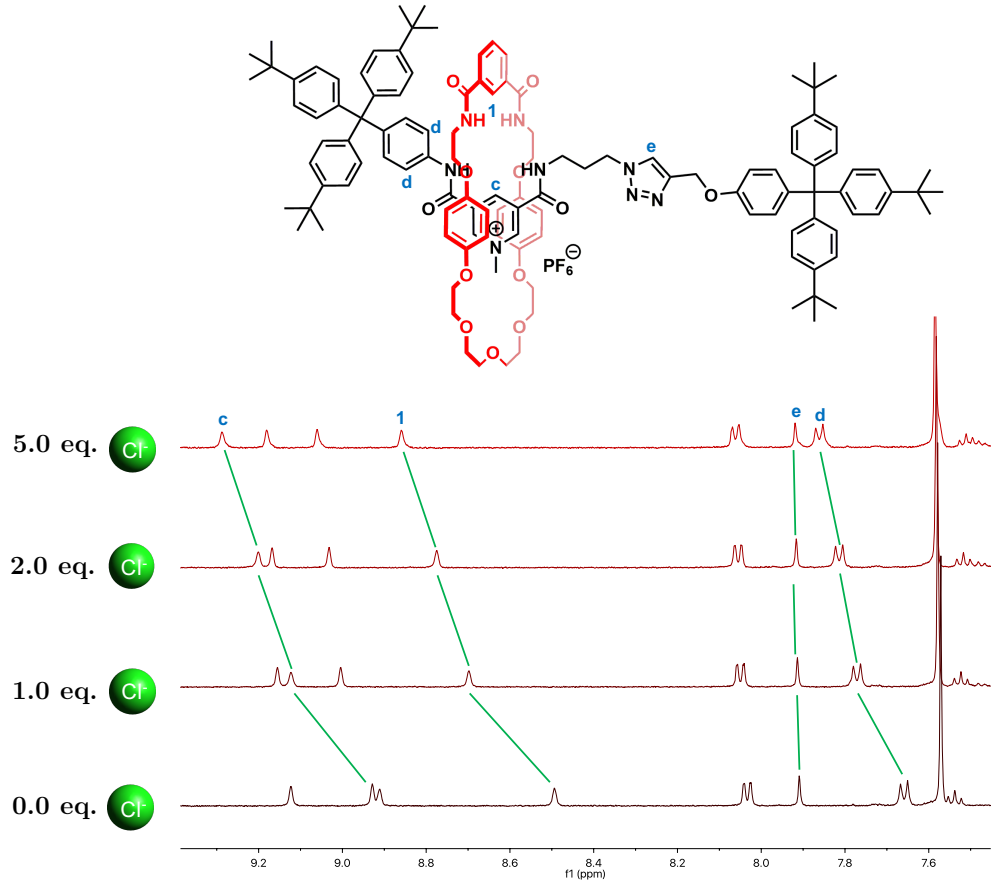


Figure 2.10 – Changes in the ^{1}H NMR spectrum with addition of increasing equivalents of TBACl to rotaxane **10.PF$_6$** (45:45:10 $CDCl_3/CD_3OD/D_2O$, 500 MHz, 298 K).

Analogous ^{1}H NMR titration experiments with Br^- and I^- exhibited similar shifts of rotaxane cavity protons of a relatively lower magnitude, indicating halide binding. Cl^- and Br^- titrations with halogen bonding iodotriazole axle containing rotaxane **11.PF$_6$** exhibited precipitation during the course of the titration experiments; prior to addition of one equivalent of Cl^- extensive precipitation occurred, to a lesser extent with Br^- after approximately five equivalents of anion had been added. Upon titration of I^-, minimal perturbations ($\Delta\delta$ (ppm) = < 0.01) of the internal macrocycle proton 1 in comparison to internal pyridinium axle cavity proton **c** inferred that the larger halide anion was binding to the pyridinium bis amide cleft, perched outside of the interlocked cavity of halogen bonding rotaxane **11.PF$_6$** (**Figure 2.11**). Similar behaviour was observed in the titration of I^- with the hydrogen bonding rotaxane **10.PF$_6$**.

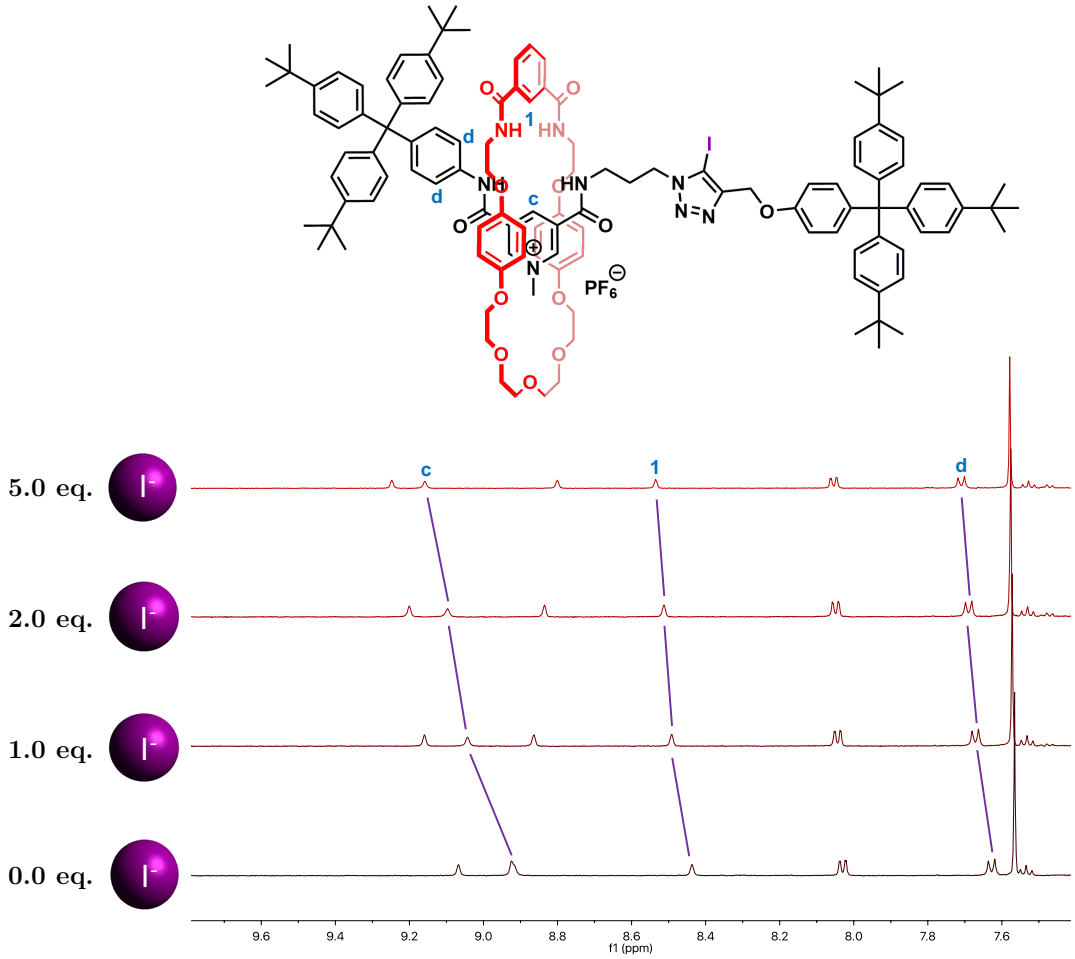


Figure 2.11 – Changes in the ^{1}H NMR spectrum upon the addition of increasing equivalents of TBAI to rotaxane **11.PF$_6$** (45:45:10 $CDCl_3$/CD_3OD/D_2O, 500 MHz, 298 K).

WinEQNMR2[13] analysis of the halide titration data of both rotaxanes monitoring the internal axle pyridinium proton **c** (**Figure 2.12**) determined 1:1 stoichiometric association constants, shown in **Table 2.1**.

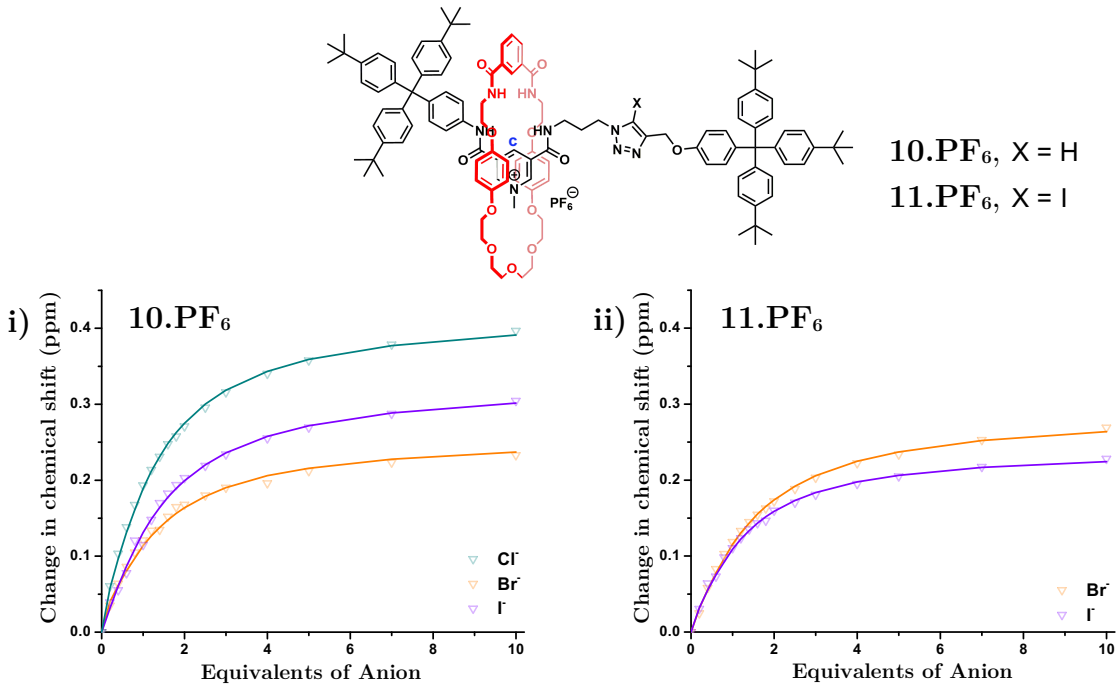


Figure 2.12 – Plots of change in chemical shift (ppm) against equivalents of anion added for i) **10.PF$_6$** and ii) **11.PF$_6$** (45:45:10 $CDCl_3/CD_3OD/D_2O$, 298 K). Observed data (hollow triangles) and fitted isotherms (solid lines) are shown, monitoring internal pyridinium axle proton **c**.

Table 2.1 – Anion association constants for rotaxanes **10.PF$_6$** and **11.PF$_6$** (45:45:10 $CDCl_3/CD_3OD/D_2O$, 298 K).

(a) Anions added as their respective tetrabutylammonium (TBA) salts at 298 K. (b) Anion association constants calculated using WinEQNMR2 using chemical shift data of internal binding site pyridinium axle proton ***c*** (**Figure 2.14**). ± *errors in parentheses. (c) Partial precipitation occurred, estimated association constant shown.*

Anion[(a)]	**10.PF$_6$** $K_a[M^{-1}]$[(b)]	**11.PF$_6$** $K_a[M^{-1}]$[(b)]
Cl$^-$	850(55)	Precipitation
Br$^-$	723(24)	883(70)[(c)]
I$^-$	702(68)	668(43)

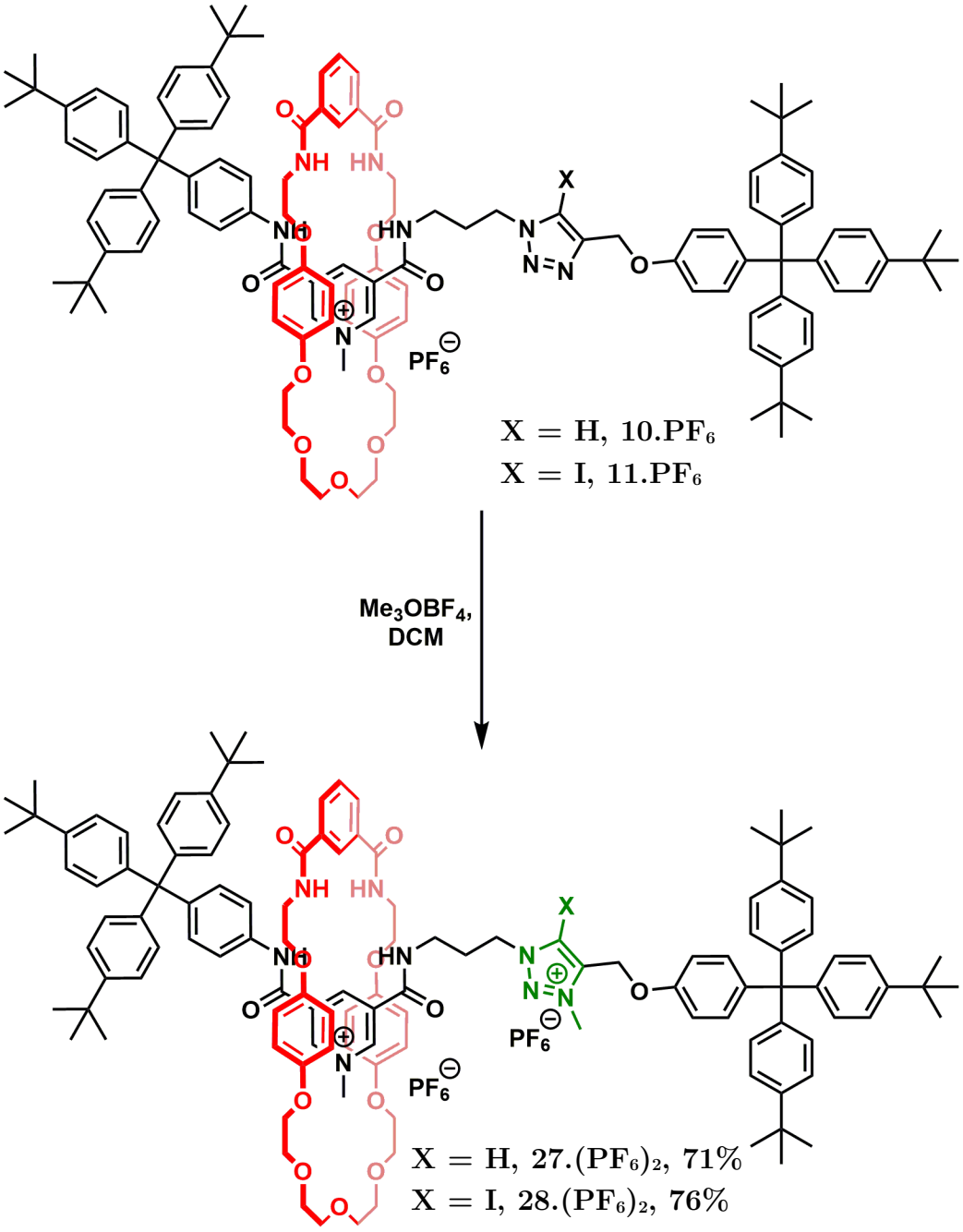
All the halides are bound strongly by both rotaxanes, however no significant selectivity was observed. In comparison to the hydrogen bonding rotaxane **10.PF$_6$**, a modest increase in the association constant value of Br$^-$ was found with halogen

bonding rotaxane **11.PF$_6$**, which may be attributed to weak halogen bonding bestowing a bias towards heavier halides, as noted in previous examples of halogen bonding receptors.[3,20]

2.4. Dicationic Pyridinium-Triazolium [2]Rotaxanes

2.4.1. Synthesis of dicationic pyridinium-triazolium [2]rotaxanes

Charge assisted halogen bond donors such as iodotriazolium and iodoimidazolium, when integrated into acyclic and macrocyclic receptor frameworks, have demonstrated high affinity recognition of halides.[6,21,22] In an effort to increase the halide binding potency of the monocationic rotaxanes, the corresponding dicationic rotaxanes **27.(PF$_6$)$_2$** and **28.(PF$_6$)$_2$** were prepared *via* post-rotaxanation alkylation of the triazole motifs of rotaxanes **10.PF$_6$** and **11.PF$_6$**. This was achieved using methylating agent trimethyloxonium tetrafluoroborate (Meerwein's salt) in DCM followed by anion exchange with aqueous NH_4PF_6 affording dicationic pyridinium-triazolium containing rotaxane **27.(PF$_6$)$_2$** and pyridinium-iodotriazolium containing rotaxane **28.(PF$_6$)$_2$** in 71% and 76% yields respectively (**Scheme 2.11**).



Scheme 2.11 – Conversion of rotaxanes **10.PF$_6$** and **11.PF$_6$** *via* methylation to yield di-cationic rotaxanes **27.(PF$_6$)$_2$** and **28.(PF$_6$)$_2$**

Characterization data of the di-cationic rotaxanes **27.(PF$_6$)$_2$** and **28.(PF$_6$)$_2$** was consistent with methylation at the triazole position in both cases, the products exhibiting the predicted masses corresponding to $[M]^{2+}$ fragments in HRMS-ESI for each; m/z = 950.5442 for **27.(PF$_6$)$_2$** and m/z = 1013.4925 for **28.(PF$_6$)$_2$**. The ^{1}H

NMR spectra agreed with the proposed triazolium and iodotriazolium axle containing structures by the appearance of an additional methyl peak **e** in both cases (**Figures 2.13 + 2.14**).

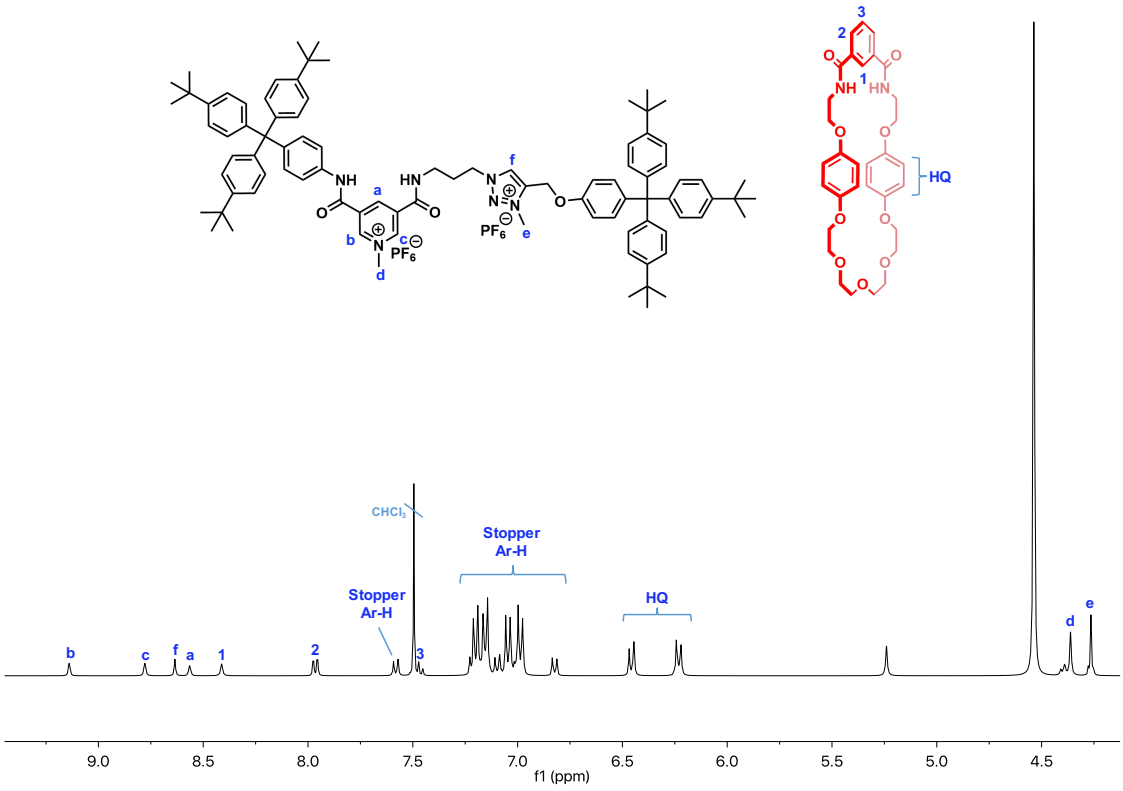


Figure 2.13 – Truncated ^{1}H NMR spectrum of rotaxane **27.(PF$_6$)$_2$** (1:1 $CDCl_3$/CD_3OD, 500 MHz, 298 K).

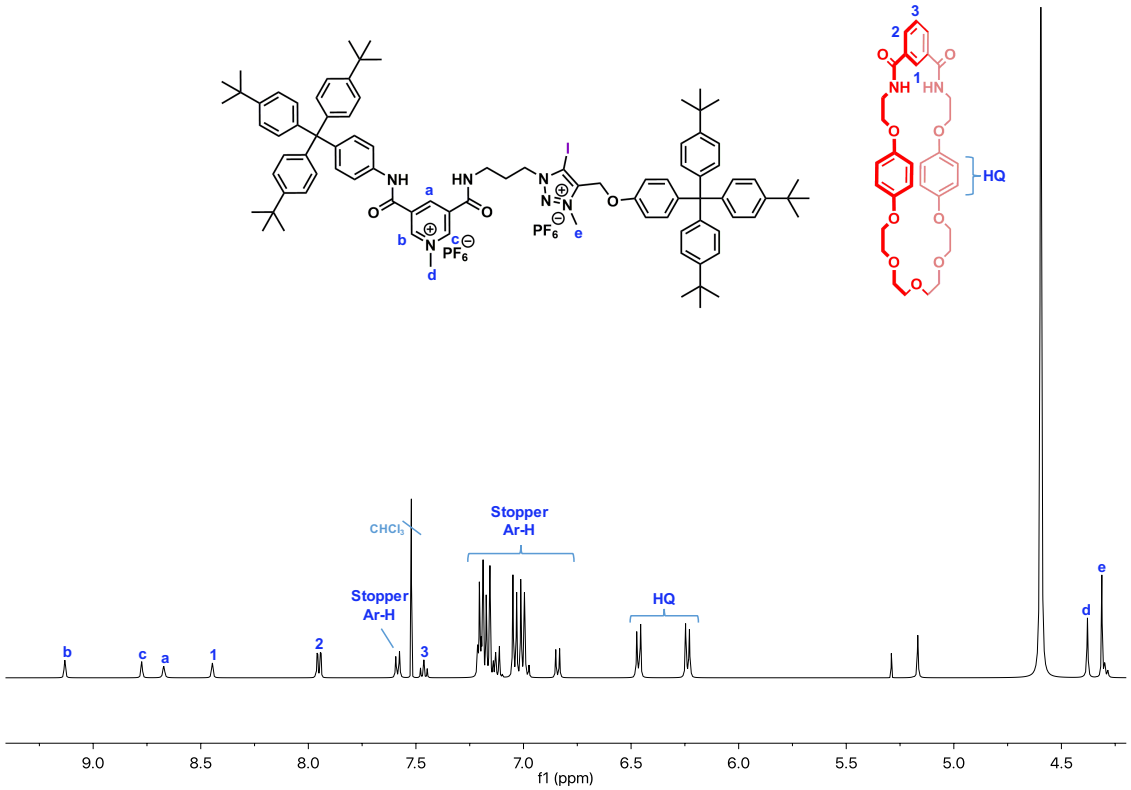


Figure 2.14 – Truncated ^{1}H NMR spectrum of rotaxane **28.(PF$_6$)$_2$** (1:1 $CDCl_3/CD_3OD$, 500 MHz, 298 K).

2.4.2. ^{1}H NMR anion binding investigations

Analogous ^{1}H NMR titrations were undertaken with the di-cationic rotaxanes **27.(PF$_6$)$_2$** and **28.(PF$_6$)$_2$** using the same titration protocol as described with the monocationic rotaxanes **10.PF$_6$** and **11.PF$_6$** (**Section 2.3.1**). Upon titration with TBACl and TBABr in competitive aqueous 45:45:10 $CDCl_3/CD_3OD/D_2O$, rotaxane **27.(PF$_6$)$_2$** exhibited concurrent shifts of internal macrocycle proton 1 and internal pyridinium proton **a**, suggesting the encapsulation of Cl^- and Br^- within the rotaxane cavity in a similar way to monocationic rotaxane **10.PF$_6$** (**Figure 2.10**). Unfortunately, due to deuterium exchange with the solvent, the acidic triazolium C-H proton could not be directly observed, however *N*-triazolium methyl proton environment **e** was observed to shift downfield, suggesting the participation of the triazolium moiety in the chelation of the halide anions in cooperation with the primary binding site located within the rotaxane cavity (**Figure 2.15**). The addition

of I^- and oxoanions NO_3^- and $H_2PO_4^-$ caused negligible shifts of internal macrocycle proton 1, modest upfield shifts of internal pyridinium proton **a** and no apparent association with the axle triazolium group inferred by the lack of chemical shift change observed in triazolium methyl proton environment **e**.

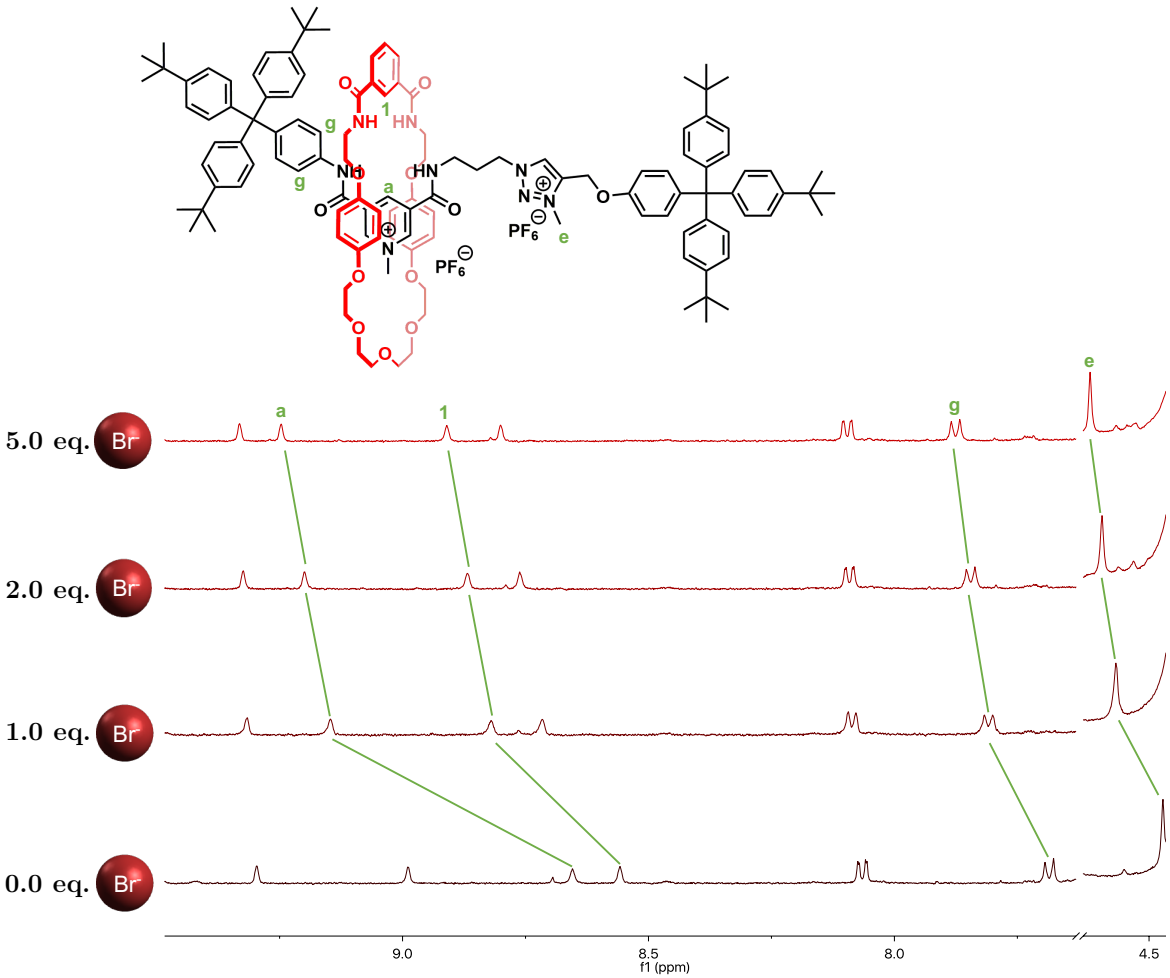


Figure 2.15 – Changes in the ^{1}H NMR spectrum upon the addition of increasing equivalents of TBABr to rotaxane **27.(PF$_6$)$_2$** (45:45:10 $CDCl_3/CD_3OD/D_2O$, 500 MHz, 298 K).

Upon addition of TBACl and TBABr, iodotriazolium axle containing rotaxane **28.(PF$_6$)$_2$** exhibited significant downfield shifts of interlocked cavity protons **a**, **g**, 1 and evidence for the participation of the iodotriazolium motif was observed with downfield shifts of triazolium methyl proton **e** (**Figure 2.16**). Small shifts of macrocycle proton 1 and upfield shifts of cavity proton **a** were observed on addition of I^-, NO_3^- and $H_2PO_4^-$.

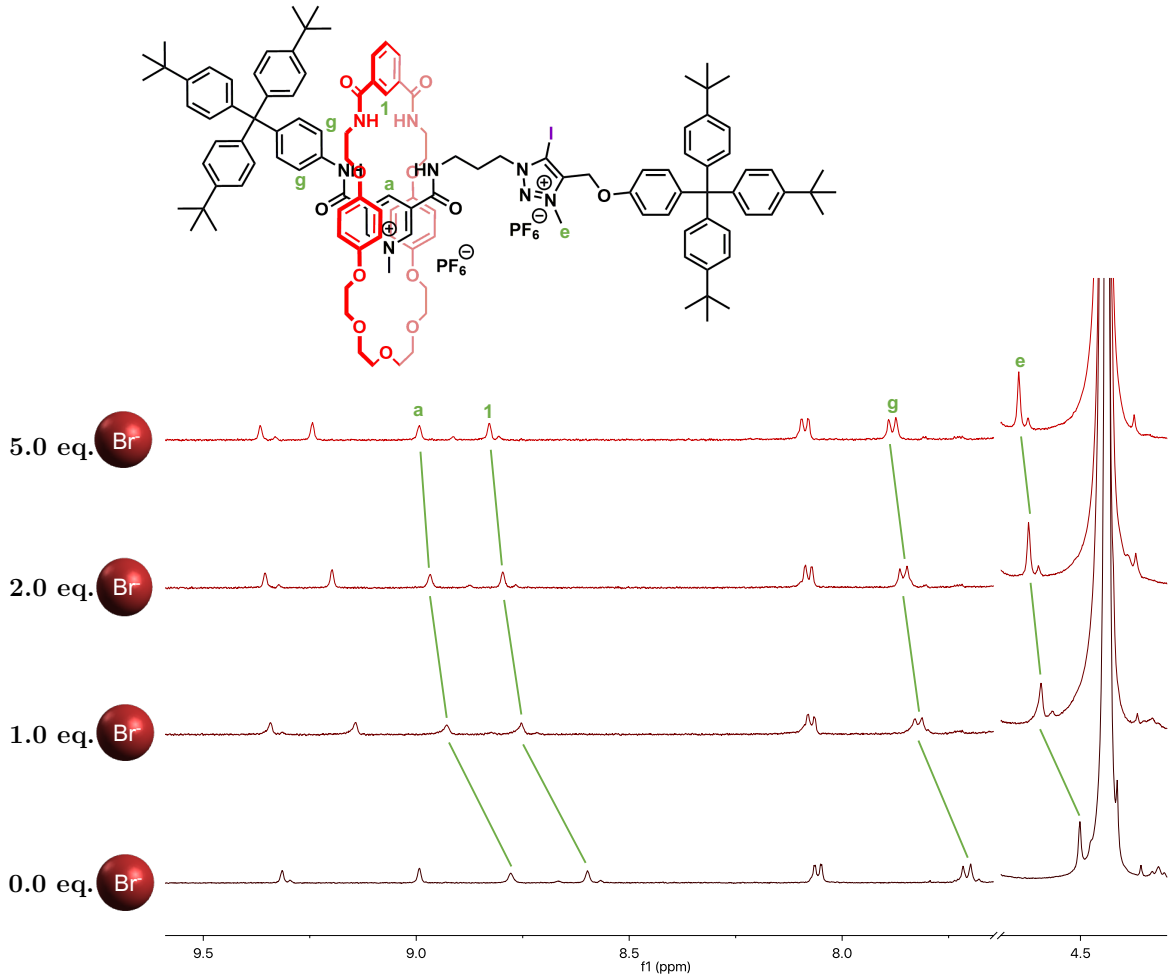


Figure 2.16 – Changes in the ^{1}H NMR spectrum upon addition of increasing equivalents of TBABr to rotaxane **27.(PF$_6$)$_2$** (45:45:10 $CDCl_3$/CD_3OD/D_2O, 500 MHz, 298 K).

The anion induced shifts upon addition of Cl^-, Br^-, I^-, NO_3^- and $H_2PO_4^-$ of internal pyridinium proton **a** in both rotaxanes were plotted against equivalents of anion (**Figure 2.17**). The 1:1 stoichiometric association constants obtained from the titration data for rotaxanes **27.(PF$_6$)$_2$** and **28.(PF$_6$)$_2$** *via* WinEQNMR2[13] analysis are summarised in **Table 2.2**.

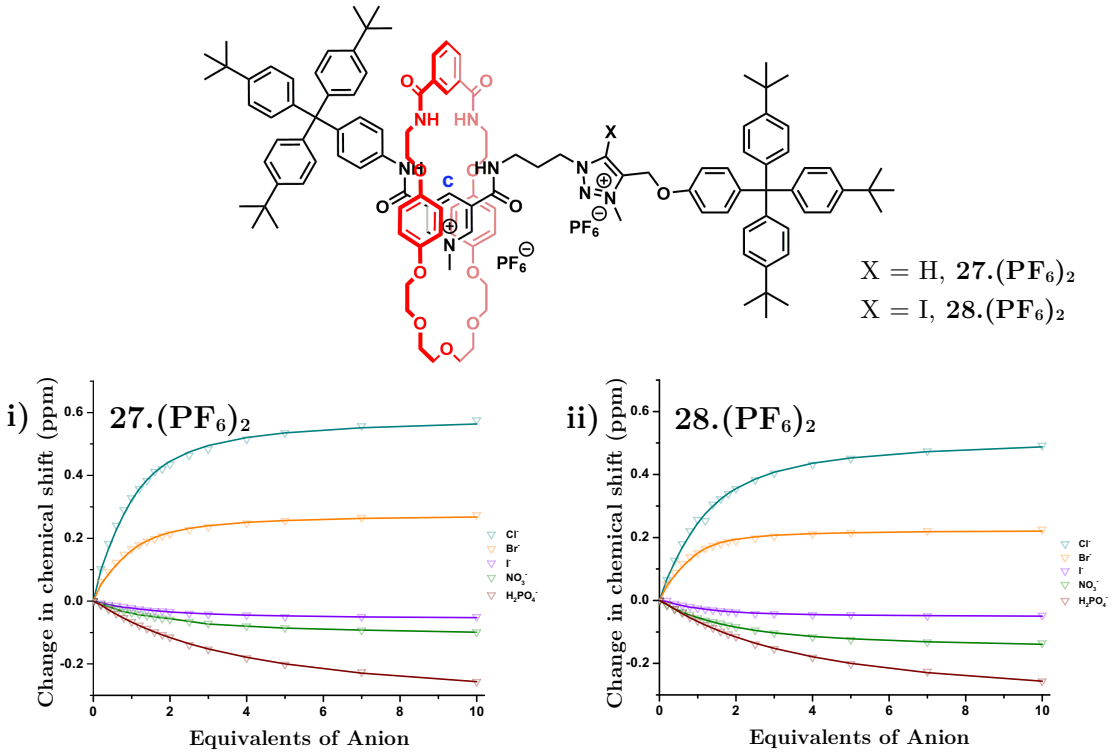


Figure 2.17 – Plots of change in chemical shift (ppm) against equivalents of anion added for i) **27.(PF$_6$)$_2$** and ii) **28.(PF$_6$)$_2$** (45:45:10 $CDCl_3/CD_3OD/D_2O$, 298 K). Observed data (hollow triangles) and fitted isotherms (solid lines) are shown, monitoring internal pyridinium axle proton **c** in both receptors.

Table 2.2 – Anion association constants for rotaxanes **27.(PF$_6$)$_2$**, **28.(PF$_6$)$_2$**, **10.PF$_6$** and **11.PF$_6$** (45:45:10 $CDCl_3/CD_3OD/D_2O$, 298 K)

(a) Anions added as their respective tetrabutylammonium (TBA) salts at 298K. (b) Anion association constants calculated using WinEQNMR2 using chemical shift data of internal binding site pyridinium axle proton ***c*** in all cases. ± *errors in parentheses.*

Anion[(a)]	**27.(PF$_6$)$_2$** K_a[M^{-1}][(b)]	**28.(PF$_6$)$_2$** K_a[M^{-1}][(b)]	**10.PF$_6$** K_a[M^{-1}][(b)]	**11.PF$_6$** K_a[M^{-1}][(b)]
Cl$^-$	1545(33)	1041(84)	850(55)	-
Br$^-$	1825(24)	3447(436)	723(24)	883(70)
I$^-$	686(10)	1393(14)	702(68)	668(43)
NO$_3^-$	454(25)	510(6)	-	-
H$_2$PO$_4^-$	195(8)	263(7)	-	-

Overall, both dicationic rotaxanes **27.(PF$_6$)$_2$** and **28.(PF$_6$)$_2$** display considerable increases in the strength of association of the halide anion guests in comparison to monocationic rotaxanes **10.PF$_6$** and **11.PF$_6$**, attributable to increased electrostatic attraction. Size discrimination of the halide anions was observed in both rotaxanes, where for hydrogen bonding rotaxane **27.(PF$_6$)$_2$** the halides followed the trend Br^- >Cl^->I^-, whereas the selectivity trend Br^->I^->Cl^- was adopted by halogen bonding rotaxane **28.(PF$_6$)$_2$**. This halide selectivity difference suggests significant participation of the hydrogen bonding triazolium and halogen bonding iodotriazolium axle motifs in the overall anion recognition process.

Considerable enhancement in the selectivity for Br^- was observed in halogen bonding rotaxane **28.(PF$_6$)$_2$** in comparison to hydrogen bonding rotaxane **27.(PF$_6$)$_2$**, implicating strong halogen bond enhanced chelation of this anion. Additionally, rotaxane **28.(PF$_6$)$_2$** displayed an increased association constant value for I^- in comparison to rotaxane **27.(PF$_6$)$_2$**, likely due to interaction with the axle iodotriazolium moiety on the periphery of the rotaxane cavity.

The relatively low association constants determined for oxoanions NO_3^- and $H_2PO_4^-$ infer that the three dimensional interlocked cavities of rotaxanes **27.(PF$_6$)$_2$** and **28.(PF$_6$)$_2$** are not complementary to the geometry and size of these anions.

2.4.3. Summary

It was shown that *via* chloride anion templated, CuAAC-mediated mono-stoppering of an azide functionalised pyridinium axle component with either alkyne or iodoalkyne stoppering components that positively charged hydrogen and halogen bonding pyridinium-triazole axle containing rotaxane anion hosts **10.PF$_6$** and **11.PF$_6$** could be synthesised. ^{1}H NMR halide binding titration experiments conducted with both rotaxanes revealed no evidence of the cooperation between the axle pyridinium and triazole/iodotriazole motifs to bind anions in a chelating

manner, as reflected in the lack of selectivity differences of halide binding in the hydrogen bonding rotaxane **10.PF$_6$** and halogen bonding rotaxane **11.PF$_6$**.

By contrast, the dicationic rotaxanes exhibited enhanced strength of halide binding due to increased electrostatic attraction and notably selectivity for Br^- was attributed to halogen bond halide chelation of the iodo-triazolium axle containing rotaxane **28.(PF$_6$)$_2$** in comparison to the all hydrogen bonding counterpart **27.(PF$_6$)$_2$**.

2.5. Towards a Halogen Bonding Rhenium(I) Anion Sensor

2.5.1. The 4-4'-bis-triazole ligand system

Symmetrical 4-4'-bis-triazole (bta) ligand systems have attracted attention for their ease of synthesis and their ability to form stable complexes with a variety of transition metals (**Figure 2.18-i**).[23,24] The homologous 4-4'-bis-iodotriazole motif has been recently incorporated within the macrocyclic component of Beer's neutral halogen bonding [2]rotaxane, synthesised *via* Cu(I) active metal templation. Post-rotaxane synthesis, the ligating macrocyclic component was functionalised with a rhenium(I) coordination complex and shown to sense halide anions in $CHCl_3$ *via* UV-Vis spectroscopy (**Figure 2.18-ii**).[25]

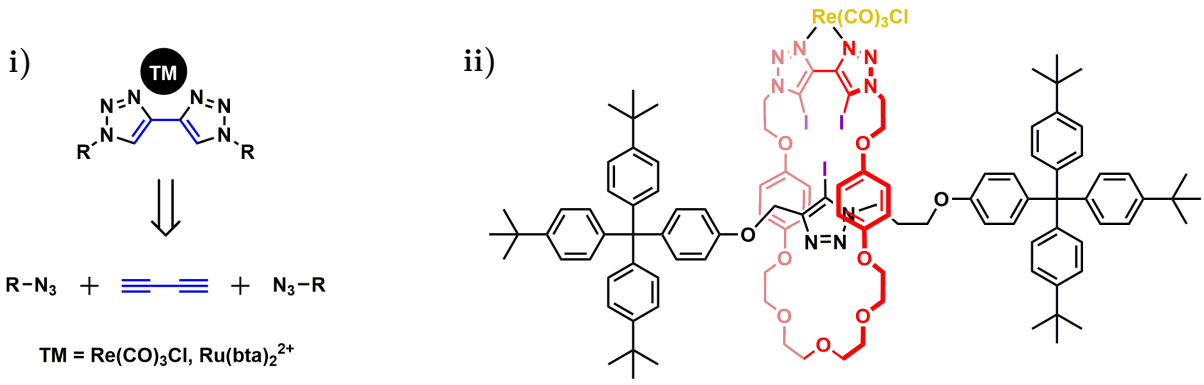
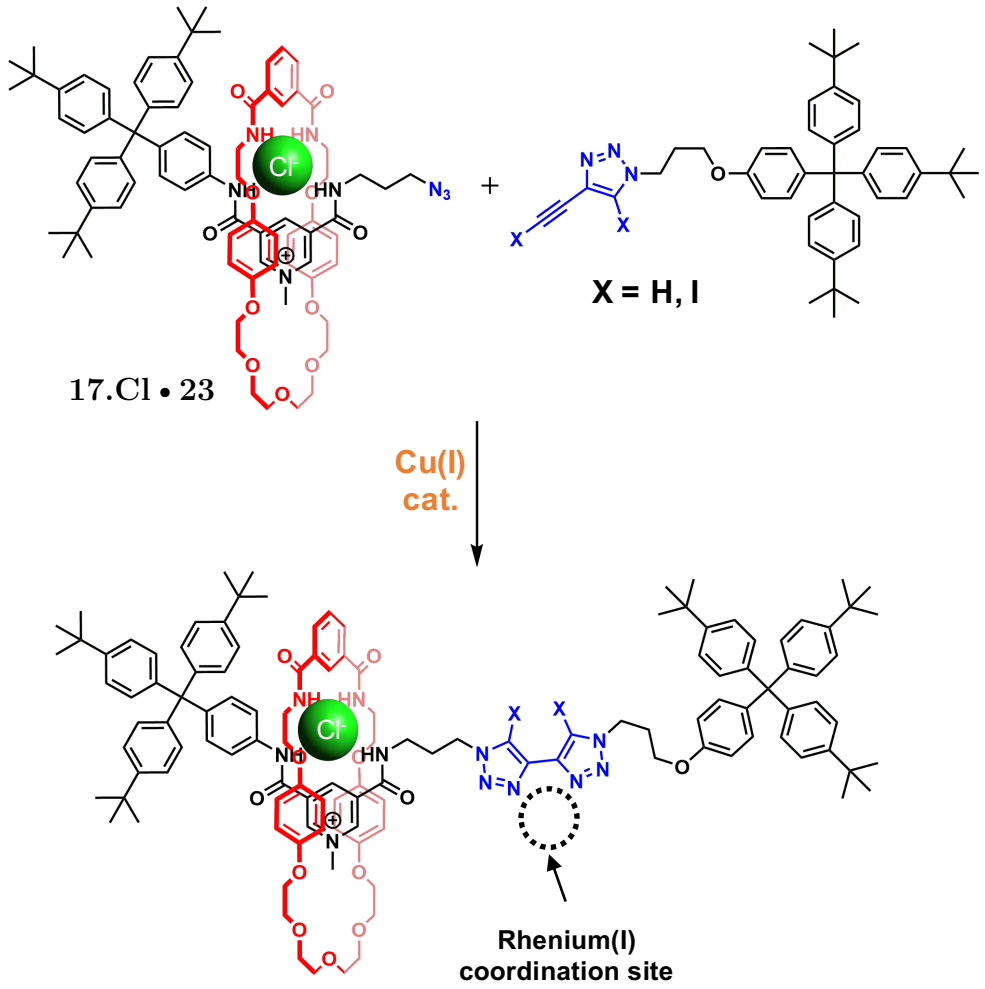


Figure 2.18 – i) The 4-4'-bis-triazole (bta) ligand system, showing retrosynthetic route to azide and bis-alkyne starting materials; ii) Beer's all halogen bonding bta ligand based rhenium(I) containing halide sensor.

2.5.2. [2]Rotaxane design

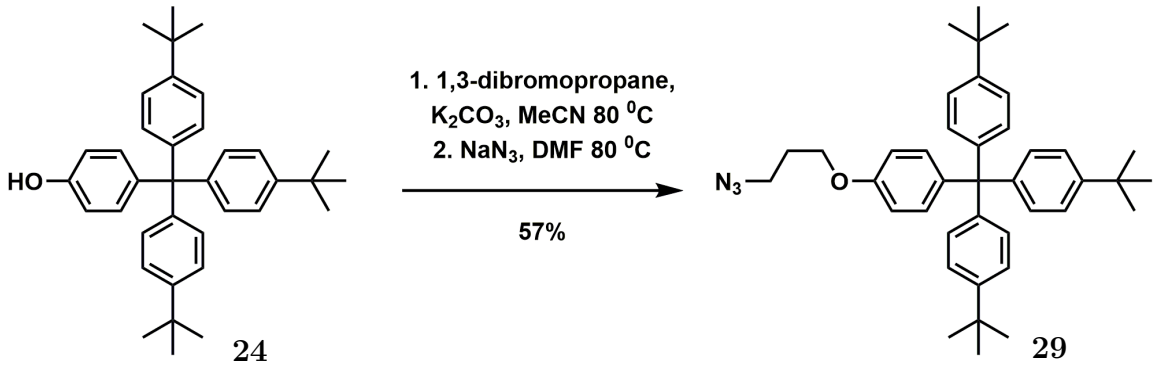
It was envisioned that the integration of the bta ligand motif into the axle component of a rotaxane could be achieved *via* adapting the monostoppering rotaxane synthesis decribed in **Section 2.3** to prepare analogous hydrogen and halogen bonding cationic pyridinium rotaxanes (**Scheme 2.12**). Subsequent metal complexation would produce the target rhenium(I) axle containing halogen and hydrogen bonding rotaxanes with the potential to sense anions.



Scheme 2.12 – Proposed CuAAC mono-stoppering synthesis of target hydrogen (X = H) and halogen bonding (X = I) pyridinium-bta axle containing rotaxanes from reaction of **17.Cl • 23** with terphenyl triazole alkynes.

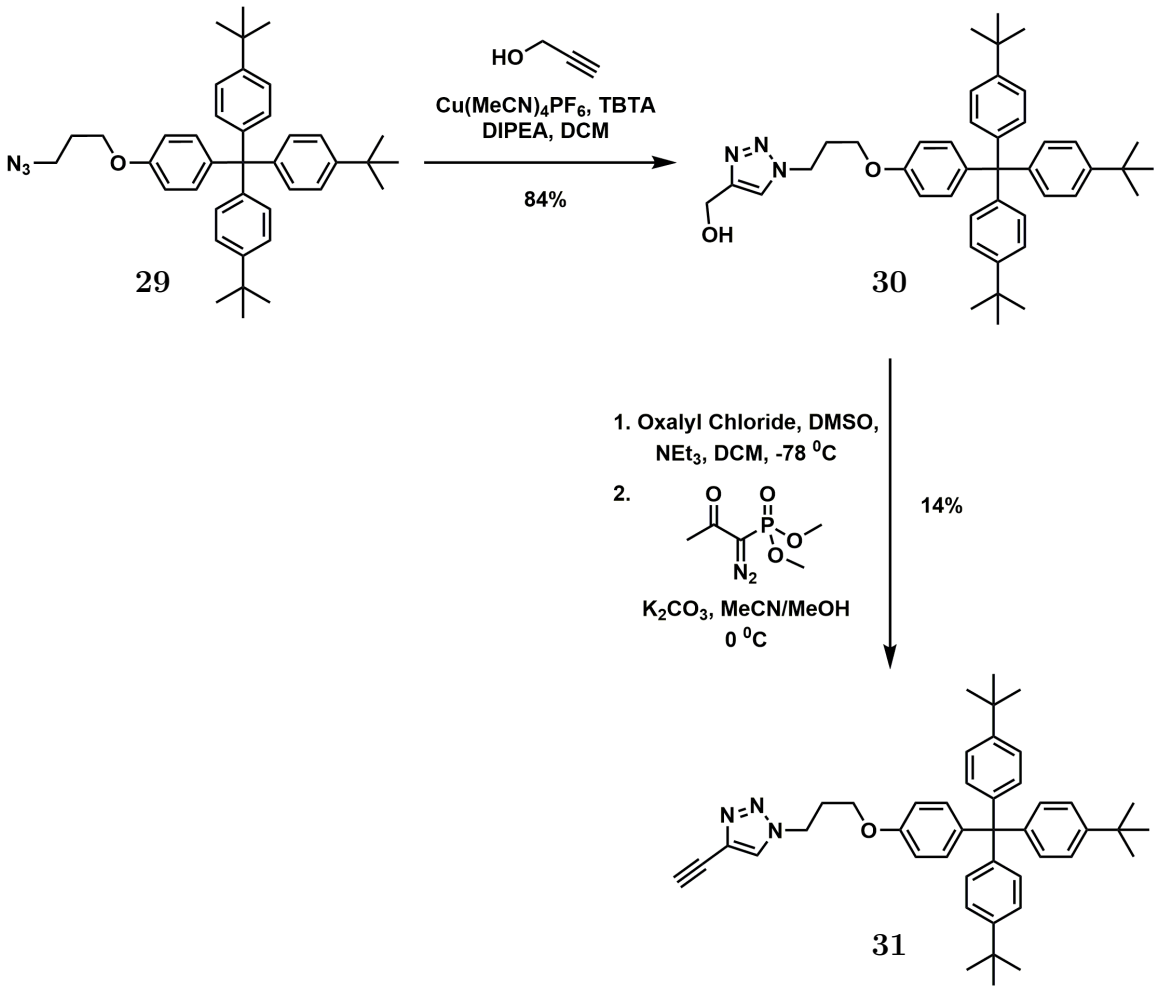
2.5.3. Synthesis of triazole-alkyne stoppering component

Firstly, the synthesis of terphenyl triazole alkyne stoppering component **35** for the synthesis of the hydrogen bonding bta axle containing rotaxane was undertaken. This was attempted *via* the initial preparation of triazole alcohol **30** for the two step Swern oxidation to the aldehyde then subsequent conversion to triazole alkyne **31** *via* the Bestmann-Ohira modification[26] of the Seyferth-Gilbert homolgation. This involves the synthesis of alkynes from aldehydes *via* a Wittig-like cycloelimination enacted by a diazo-phosphonate followed by loss of N_2 to yield the alkyne. Reaction of terphenyl alcohol **24** with an excess of 1,3-dibromopropane in refluxing MeCN and subsequent treatment with NaN_3 in DMF gave azide **29**[27] in a 57% yield (**Scheme 2.13**).



Scheme 2.13 – Synthesis of stopper azide **29**.

Terphenyl azide **29** was converted to terphenyl triazole alcohol **30** using CuAAC conditions with propargyl alcohol in an 84% yield. Swern oxidation of alcohol **30** in DCM generated the corresponding aldehyde *in-situ*, which was used immediately in the next step. Adapting a literature procedure[26], the subsequent Bestmann-Ohira step was intiated by treatment of the aldehyde with commercially available dimethyl 1-diazo-2-oxopropylphosphonate in the presence of K_2CO_3 in 1:1 MeCN/MeOH mixture to produce the terphenyl triazole **31** in an isolated yield of 14% (**Scheme 2.14**).

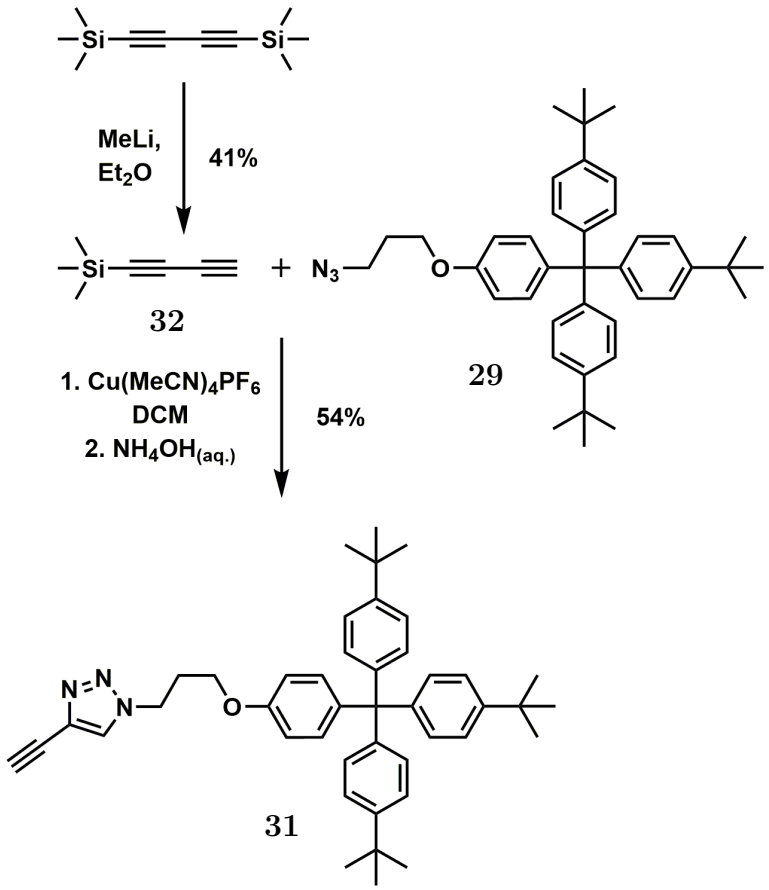


Scheme 2.14 – Sequential Swern oxidation/Bestmann-Ohira homologation route to stoppering component terphenyl triazole alkyne **31**.

The disappointing yield was attributed to the poor solubility of terphenyl triazole alcohol **30** in DCM, likely preventing the Swern oxidation step from proceeding to completion. The alcohol **30** is readily soluble in DMSO, but the use of this solvent has been shown to inhibit the Bestmann-Ohira reaction in literature examples.[28]
To overcome solubility issues, an alternative synthesis for triazole alkyne **31** was devised. The use of mono(trimethylsilyl)butadiyne is a known synthetic precursor in the synthesis of triazole alkynes.[29]

Mono(trimethylsilyl)butadiyne **32**[29] was obtained in a 41% yield after statistical mono-desilylation of commercially available 1,4-bis-(trimethylsilyl)-butadiyne in the presence of MeLi in Et_2O. Compound **32** was then reacted with

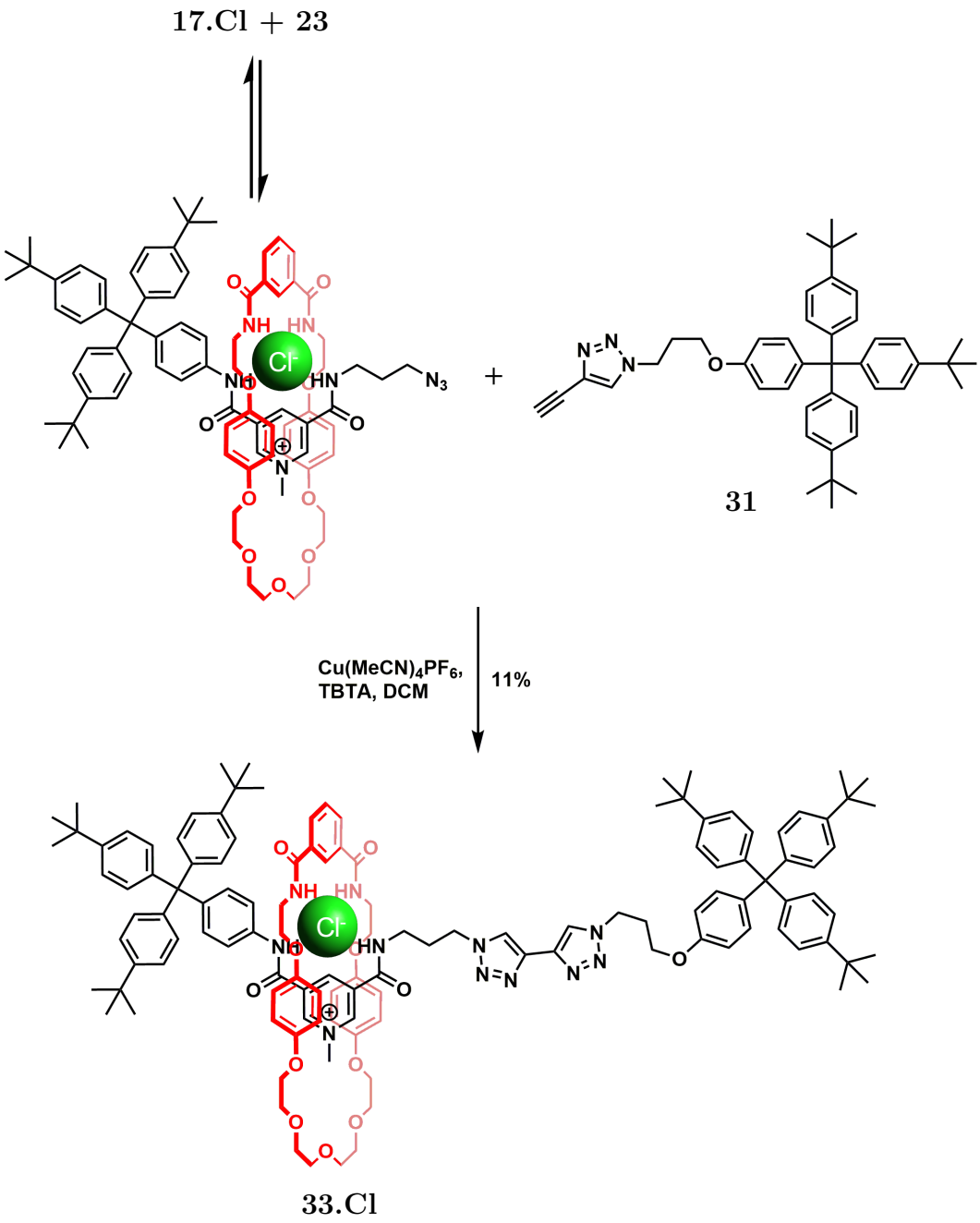
stopper azide **29** using CuAAC conditions in DCM followed by basic work-up to remove the TMS protecting group to produce stopper triazole alkyne **31** in an improved yield of 54% (**Scheme 2.15**).



Scheme 2.15 – Mono-TMS butadiyne CuACC route to stopper triazole alkyne **31**.

2.5.4. Synthesis of a rhenium(I)-bta axle containing [2]rotaxane

To synthesise the hydrogen bonding bta-axle containing rotaxane, axle precursor **17.Cl** was stirred in DCM in the presence of isophthalamide macrocycle **23** and stopper triazole alkyne **31** under CuAAC conditions to afford bta axle containing rotaxane **33.Cl** in 11% yield after purification by preparative TLC (**Scheme 2.16**).



Scheme 2.16 – CuACC monostoppering synthesis of bta-containing rotaxane **33.Cl**.

The novel rotaxane was characterised by ^{1}H NMR, ^{13}C NMR and ESI-HRMS. The ^{1}H NMR spectrum of **33.Cl** in 1:1 $CDCl_3/CD_3OD$ is shown in comparison to **17.Cl** and macrocycle **23** (**Figure 2.19**).

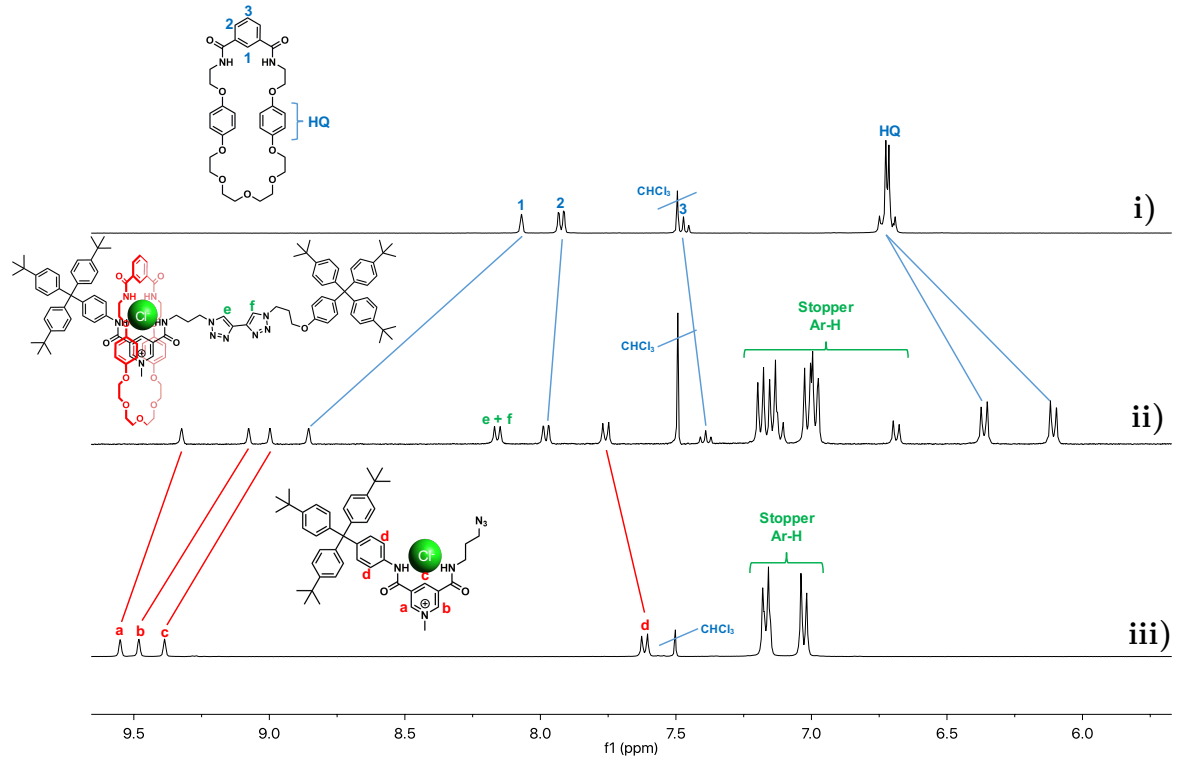
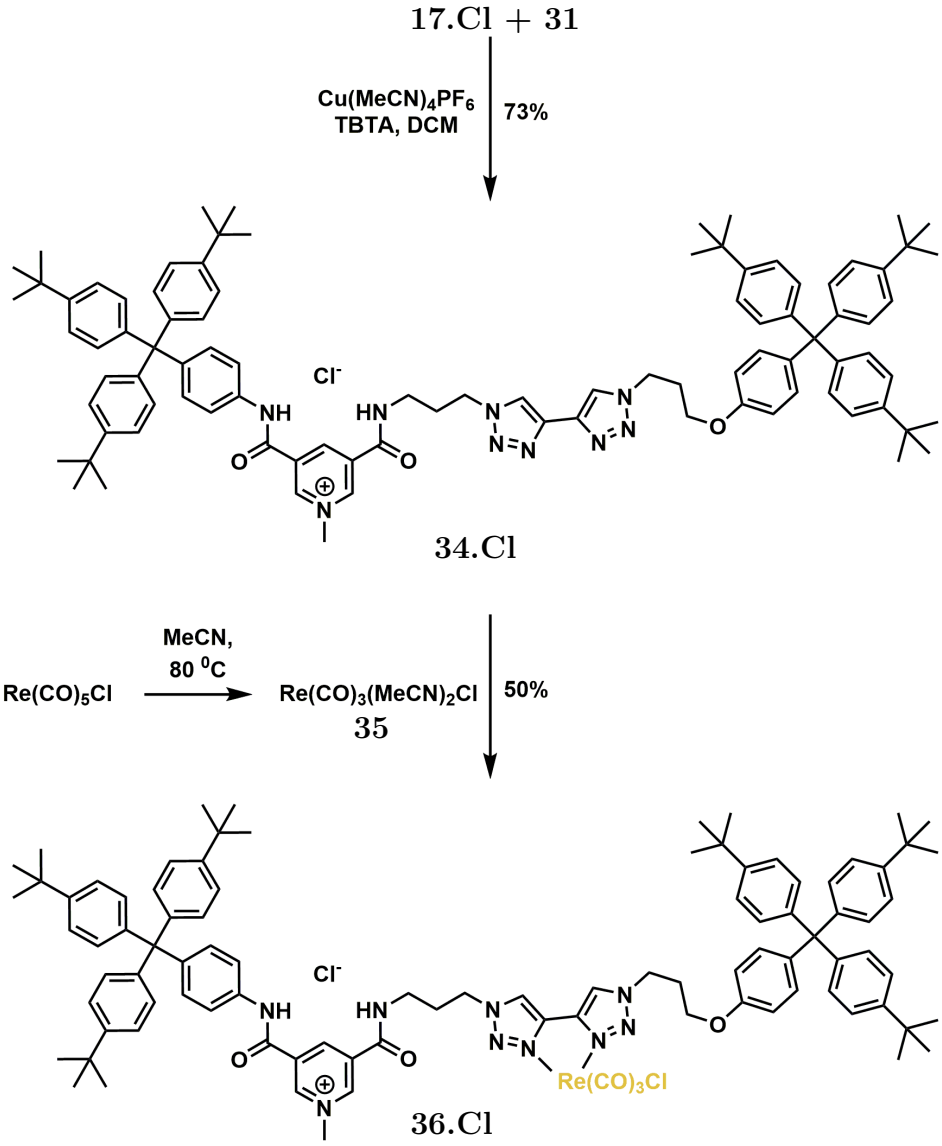


Figure 2.19 – Assigned ^{1}H NMR spectra (1:1 $CDCl_3/CD_3OD$, 400 MHz, 298 K) of i) macrocycle **23**, ii) rotaxane **33.Cl** and iii) axle precursor azide **17.Cl**.

Upfield shifts of axle protons **a**, **b** and **c**, downfield shifts of macrocycle proton 1 and upfield and split macrocycle hydroquinone resonances (**HQ**) indicated the interlocked nature of **33.Cl** and hydrogen bonding to the Cl^- template. Analysis of the ^{1}H-^{1}H ROESY NMR spectrum of **33.Cl** showed a total of ten intercomponent through-space interactions between the bta-containing axle and the macrocycle component.

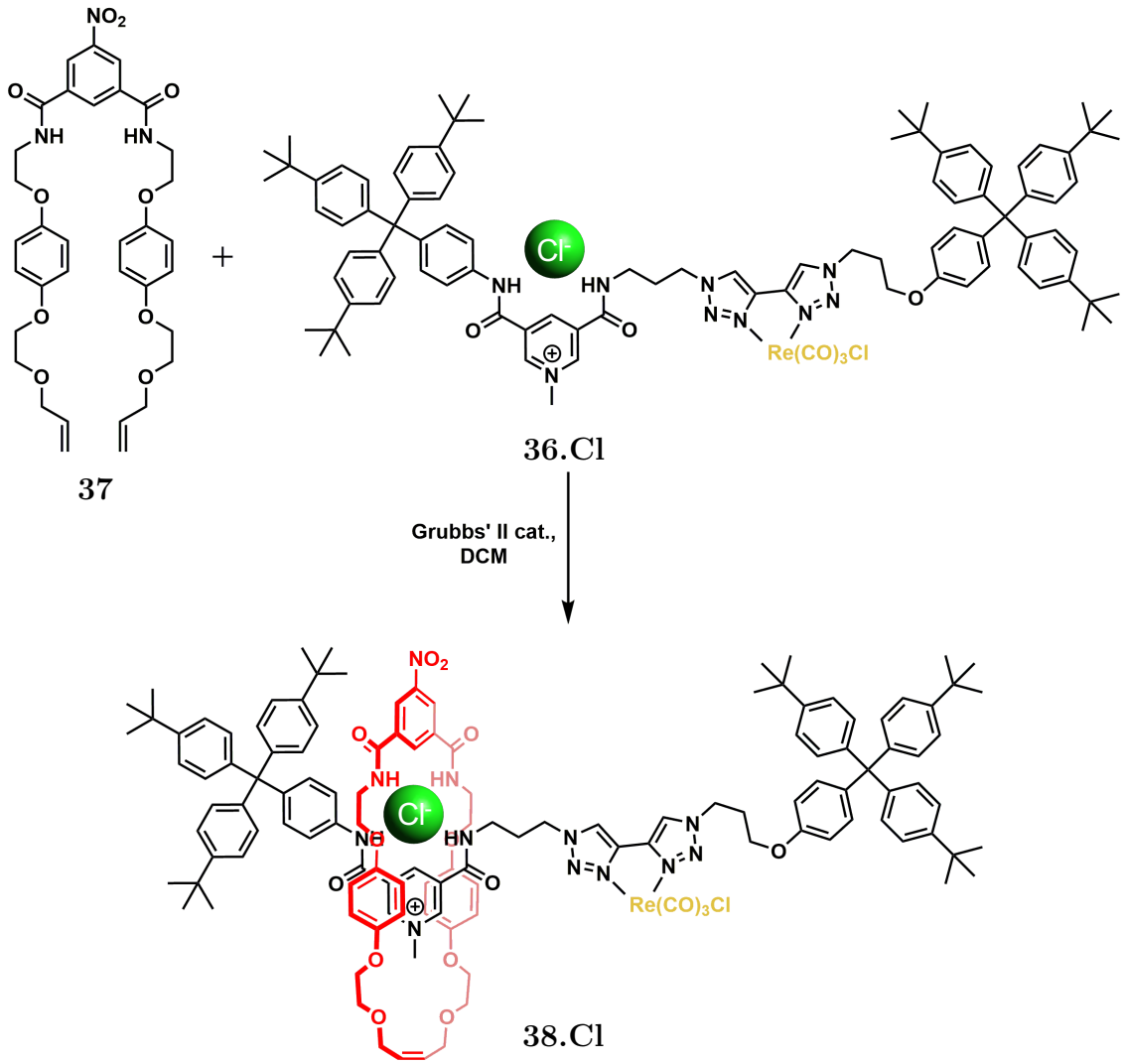
In an effort to improve the yield of rotaxane, an alternative clipping synthetic procedure was undertaken using a rhenium(I) coordinated bta containing axle. The synthesis of the rhenium(I)-bta pyridinium axle **36.Cl** is detailed in **Scheme 2.17**. Azide **17.Cl** was reacted with stopper triazole alkyne **31** under CuAAC conditions to give pyridinium-bta axle component **34.Cl** in a 73% yield. For rhenium(I) coordination, $Re(CO)_5Cl$ was activated by stirring in refluxing MeCN for three hours

to produce $Re(CO)_3Cl(MeCN)_2$ complex **35**[30] which was added to a DCM solution of **34.Cl** to give **36.Cl** in a 50% yield.



Scheme 2.17 – Synthesis of rhenium(I) appended bta axle component **36.Cl**.

Rotaxane synthesis was attempted with bis-vinyl appended nitro-isophthalamide macrocycle precursor **37**[31] (kindly donated by Dr. Richard Knighton) and rhenium(I)- bta axle component **36.Cl** in the presence of Grubbs' 2nd generation RCM catalyst (**Scheme 2.18**).



Scheme 2.18 – Synthesis of rhenium(I) appended bta rotaxane **38.Cl**.

After repeated purification attempts by preparative TLC and size exclusion chromatography, the purity of the target rotaxane **38.Cl** still could not be ascertained. The rotaxane's ^{1}H NMR spectrum in 1:1 $CDCl_3/CD_3OD$ of rotaxane **38.Cl** reveals two sets of broad resonances in the expected hydroquinone region of the spectrum (**HQ**) and multiple broad resonances corresponding to pyridinium and bta protons (**Figure 2.20**).

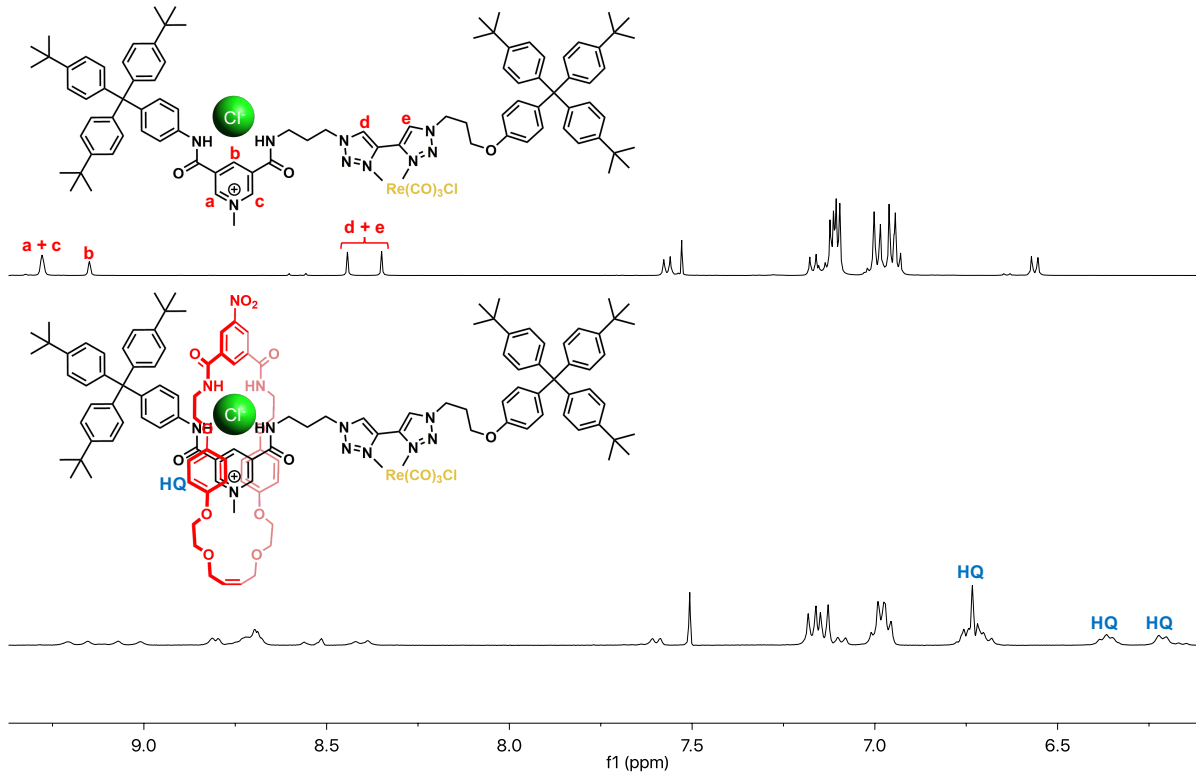


Figure 2.20 – Comparison of the ^{1}H NMR spectra of i) axle **36.Cl** and ii) rotaxane **38.Cl** (1:1 $CDCl_3/CD_3OD$, 400 MHz, 298 K).

Peak broadening persisted in spectra of rotaxane **38.Cl** recorded in 1:1 $CD_3CN/CDCl_3$ and DMSO-d_6. ESI mass spectrometry detected a single peak corresponding to the expected mass of rotaxane **38.Cl** (m/z = 2313.97, $[\mathbf{M}]^+$). Peaks corresponding to the masses of starting materials **37** and **36.Cl** were not observed. Due to the inability to characterise the rotaxane product by NMR, ^{1}H NMR anion binding titrations and UV-vis anion sensing studies were not undertaken.

2.5.5. Summary

Precursor bta rotaxane **33.Cl** was successfully synthesised, albeit in low yield, *via* a CuAAC mediated mono-stoppering rotaxanation with novel terphenyl stoppering component **31**. Due to the limited availability of the rotaxane, rhenium(I) complexation was not attempted. An alternative Grubbs' II catalysed RCM clipping synthetic strategy afforded the rhenium(I)-bta rotaxane **38.Cl** which unfortunately

could not be characterised with certainty. This precluded anion recognition and optical anion sensing studies from being conducted.

2.6. Towards Neutral Halogen Bonding Rhenium(I) Anion Sensors

2.6.1. Design of an acyclic chelating halogen bonding receptor

In a first step towards producing a neutral halogen bonding rhenium(I) rotaxane host system, the synthesis of a pyridine N-oxide appended rhenium(I) pyridine-triazole (pyta)[24] was investigated (**Figure 2.21**).

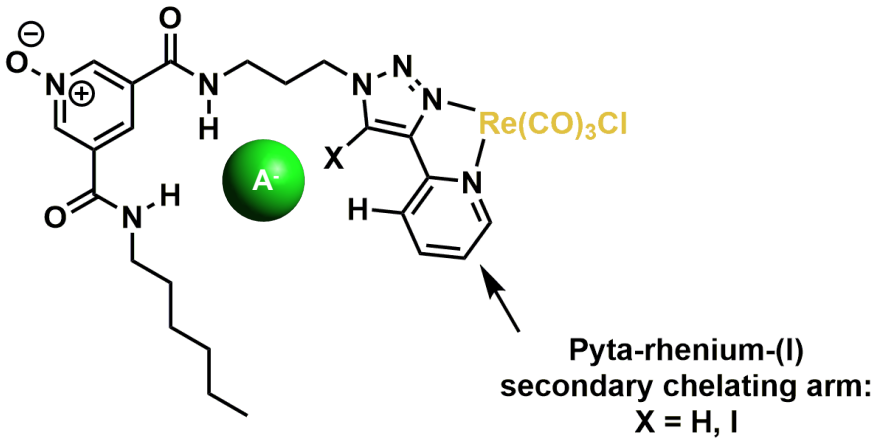
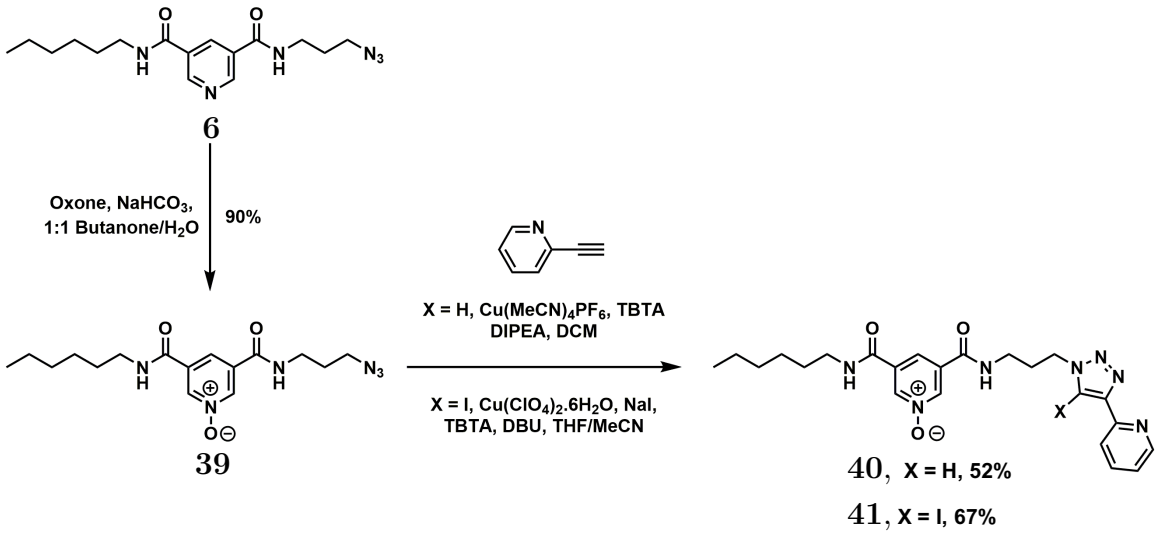


Figure 2.21 – Design of target halogen bonding (X = I) and hydrogen bonding (X = H) pyridine *N*-oxide pyta-rhenium(I) chelating anion receptors.

2.6.2. Receptor synthesis

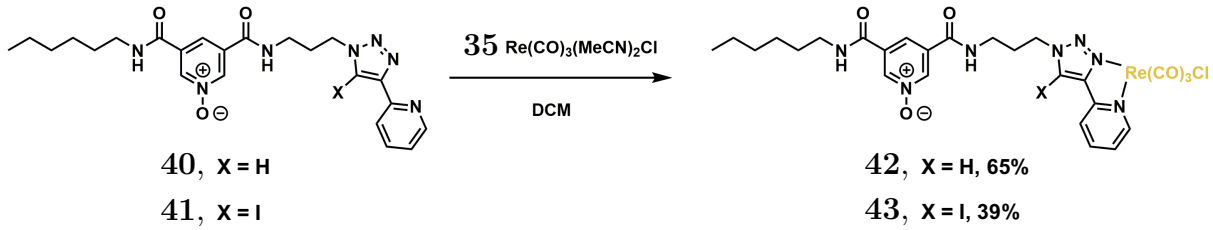
Hydrogen bonding (X = H) and halogen bonding (X = I) pyta motifs were appended to the pyridine *N*-oxide azide **39** *via* CuAAC 'click' reaction with commercially available 2-ethynylpyridine. Previously synthesized pyridine azide **6** was dissolved in butanone/H_2O and reacted with Oxone® in the presence of $NaHCO_3$ to give pyridine *N*-oxide **39** in a 90% yield. **39** was stirred in DCM with excess 2-ethynylpyridine, $Cu(MeCN)_4PF_6$, TBTA and a catalytic amount of DIPEA to afford pyridine *N*-oxide-pyta **40** in a 52% yield. Similarly, azide **39** was subjected to one-

pot iodotriazole CuAAC conditions[32] ($Cu(ClO_4)_2.6H_2O$, TBTA, NaI and DBU in THF/MeCN) to furnish pyridine *N*-oxide iodo-pyta **41** in a 67% yield (**Scheme 2.19**).



Scheme 2.19 – Synthesis of pyridine N-oxide/pyta receptor precursors **40** and **41**.

Activated $Re(CO)_3Cl(MeCN)_2$ complex **35** was added to MeCN solutions of **40** and **41** to afford the target rhenium(I) appended pyridine *N*-oxide receptors **42** and **43** in 65% and 39% yields respectively (**Scheme 2.20**).



Scheme 2.20 – Complexation of **40** and **41** to give rhenium(I)-containing receptors **42** and **43**.

Both rhenium(I) containing receptors **42** and **43** were characterized by ^1H NMR spectroscopy and ESI-HRMS (**Figure 2.22 and Figure 2.23**).

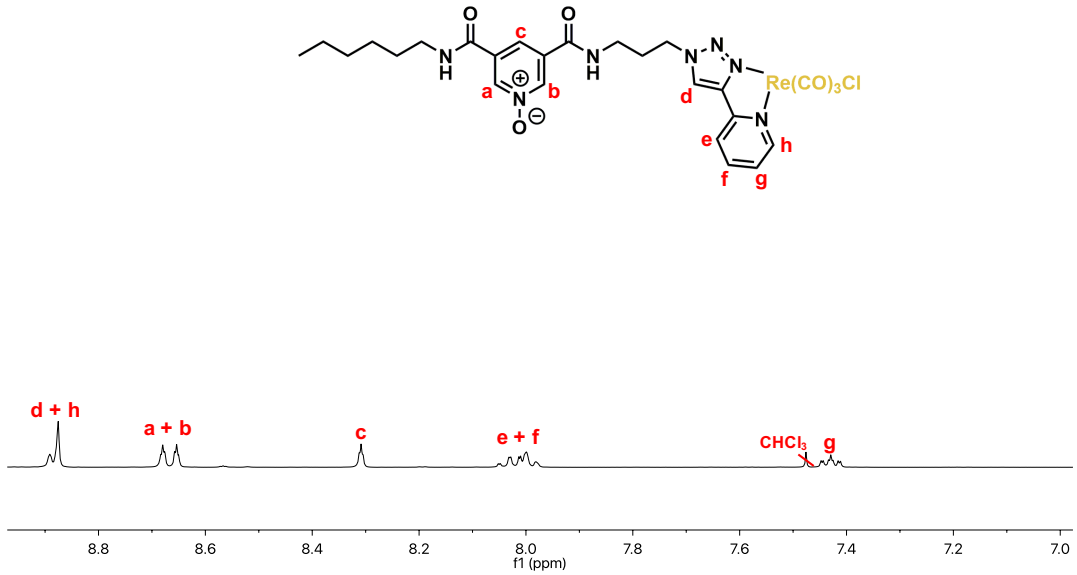


Figure 2.22 – Truncated ^{1}H NMR spectrum of rhenium(I)-containing pyridine *N*-oxide receptor **42** (1:1 $CDCl_3/CD_3OD$, 400 MHz, 298 K).

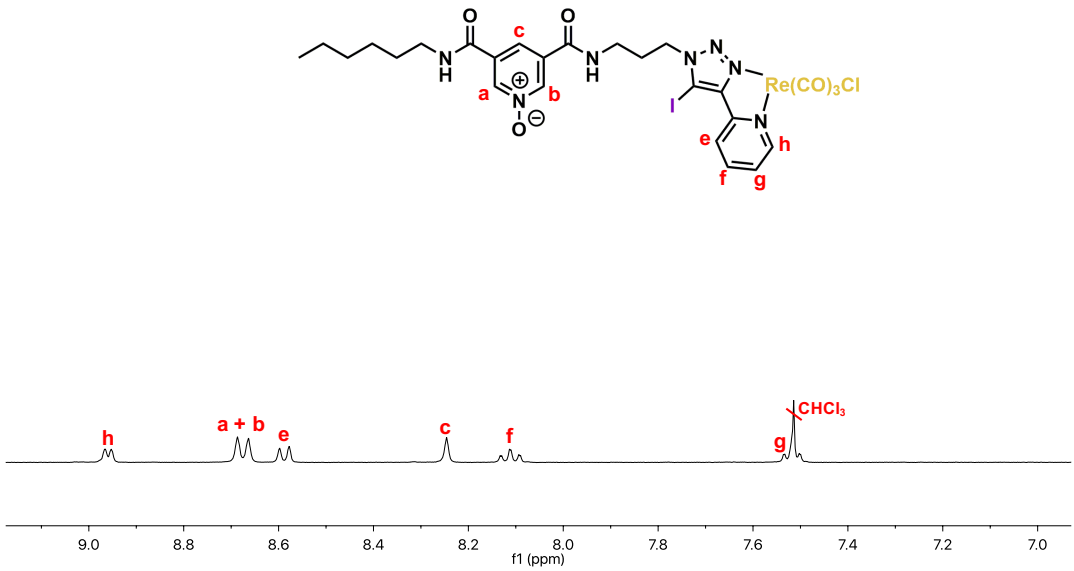


Figure 2.23 – Truncated ^{1}H NMR spectrum of rhenium(I)-containing pyridine *N*-oxide receptor **43** (1:1 $CDCl_3/CD_3OD$, 400 MHz, 298 K).

2.6.3 ^{1}H NMR anion binding studies

Benchmarking ^{1}H NMR titration studies with TBACl and rhenium(I) containing receptor **42** were conducted in acetone-d_6 to establish if the chelating mode of halide anion binding was evident with the neutral receptor. Upon addition of one equivalent of TBACl to **42**, large downfield shifts of pyridine *N*-oxide binding cleft protons **c** ($\Delta\delta$(ppm) = 1.41), amides **NH** ($\Delta\delta$(ppm) = 1.29 and 1.16), and pyta-triazole proton **d** ($\Delta\delta$(ppm) = 1.06) were observed, suggesting cooperative chelation of Cl^- (**Figure 2.24**). Small shifts were seen for protons exterior to the binding site such as pyridine *N*-oxide protons **a** and **b** ($\Delta\delta$(ppm) = -0.07) and pyta protons **h** ($\Delta\delta$(ppm) = -0.03), **e** ($\Delta\delta$(ppm) = 0.09) and **f** ($\Delta\delta$(ppm) = ~0.01), confirming anion chelation between the rhenium(I) complexed pyta motif and the pyridine N-oxide motif in the fashion depicted in **Figure 2.24**.

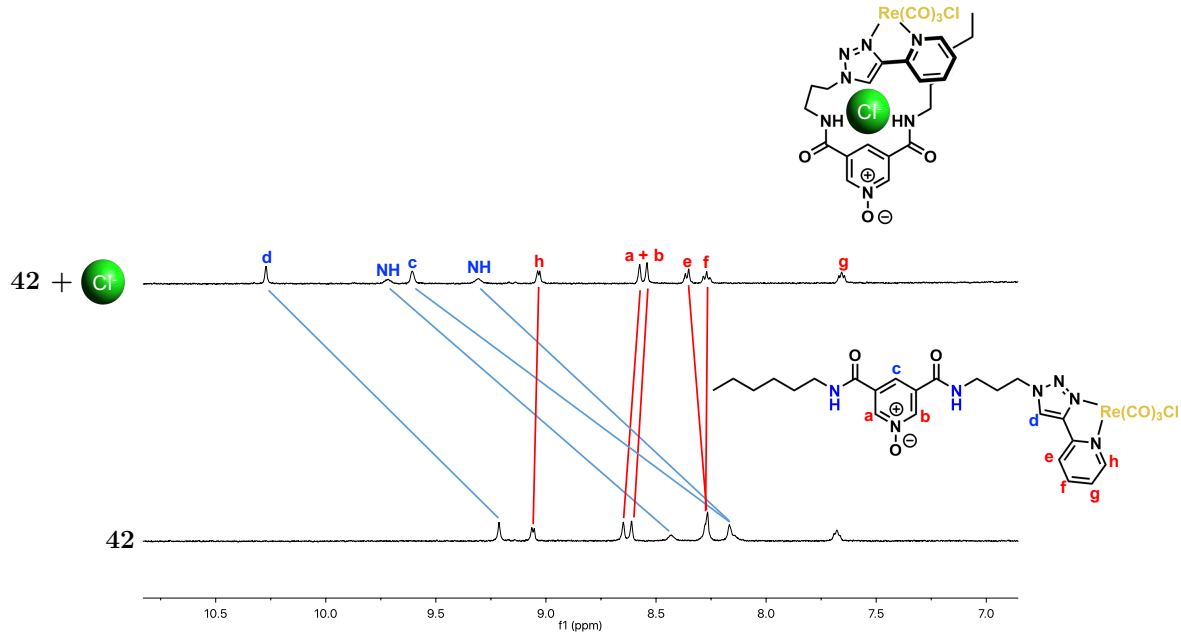


Figure 2.24 – ^{1}H NMR spectra of **42** before (bottom) and after (top) the addition of one equivalent of TBACl, binding site protons shown in blue (acetone-d_6, 500 MHz, 298 K).

Monitoring of the downfield shifts of pyridine *N*-oxide proton **c** upon the addition of further equivalents of TBACl gave titration data that upon WinEQNMR2[13]

analysis, indicated very strong binding of Cl^- ($K_A(Cl^-)$ = $>10^4$ M^{-1}). Analogous titrations of TBACl and TBABr halide salts with **42** and **43** were conducted in the more competitive solvent mixture of 9:1 $CDCl_3/CD_3OD$ (**Figure 2.25**).

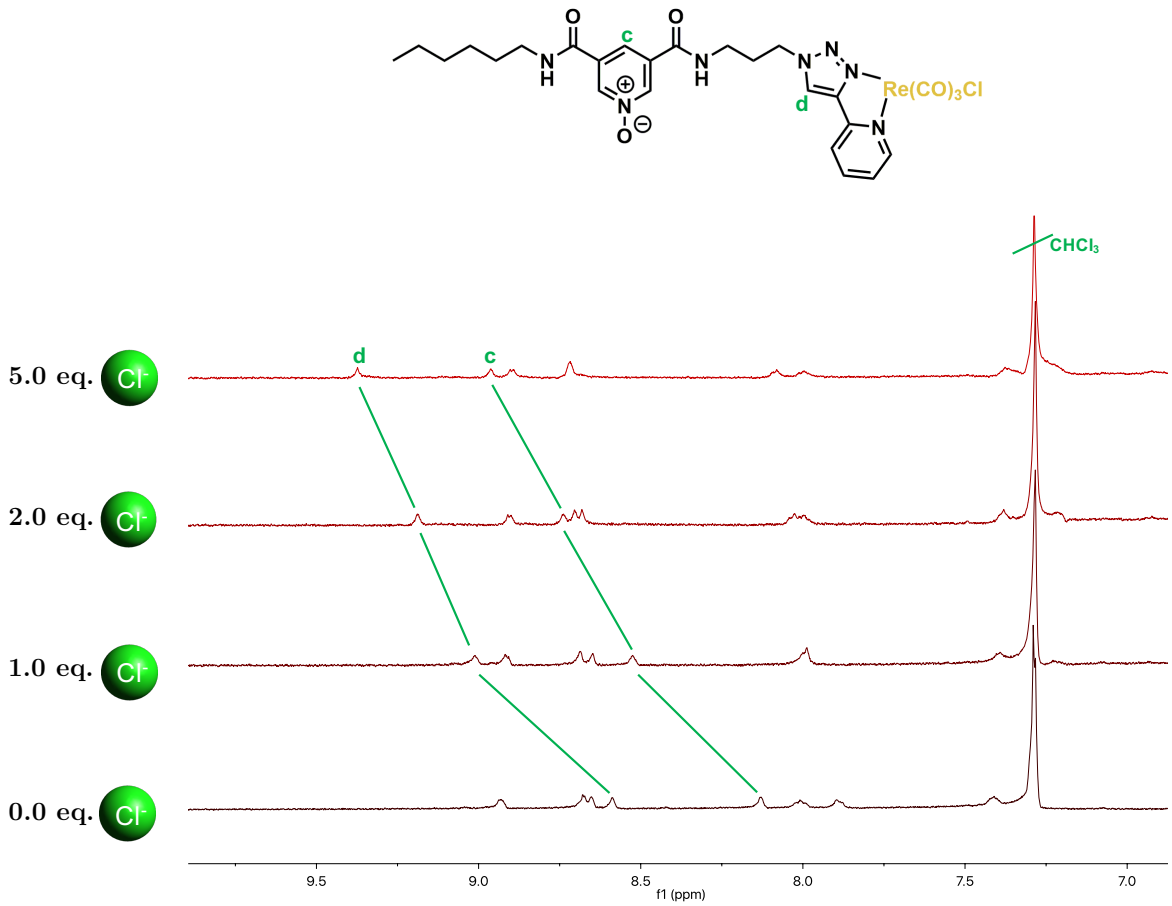


Figure 2.25 – Changes in the ^1H NMR spectrum upon the addition of increasing equivalents of TBACl to receptor **42** (9:1 $CDCl_3/CD_3OD$, 500 MHz, 298 K).

Significant perturbations were noted with hydrogen bonding receptor **42** with Cl^- and Br^-. However, upon the addition of TBACl to halogen bonding receptor **43**, although the downfield shifts of binding site pyridine *N*-oxide proton **c** were significant, shifts of the pyta protons **e**, **f**, **g** and **h** were very small in magnitude compared to receptor **42** (**Figure 2.26**). Identical behaviour was also observed upon addition of TBABr.

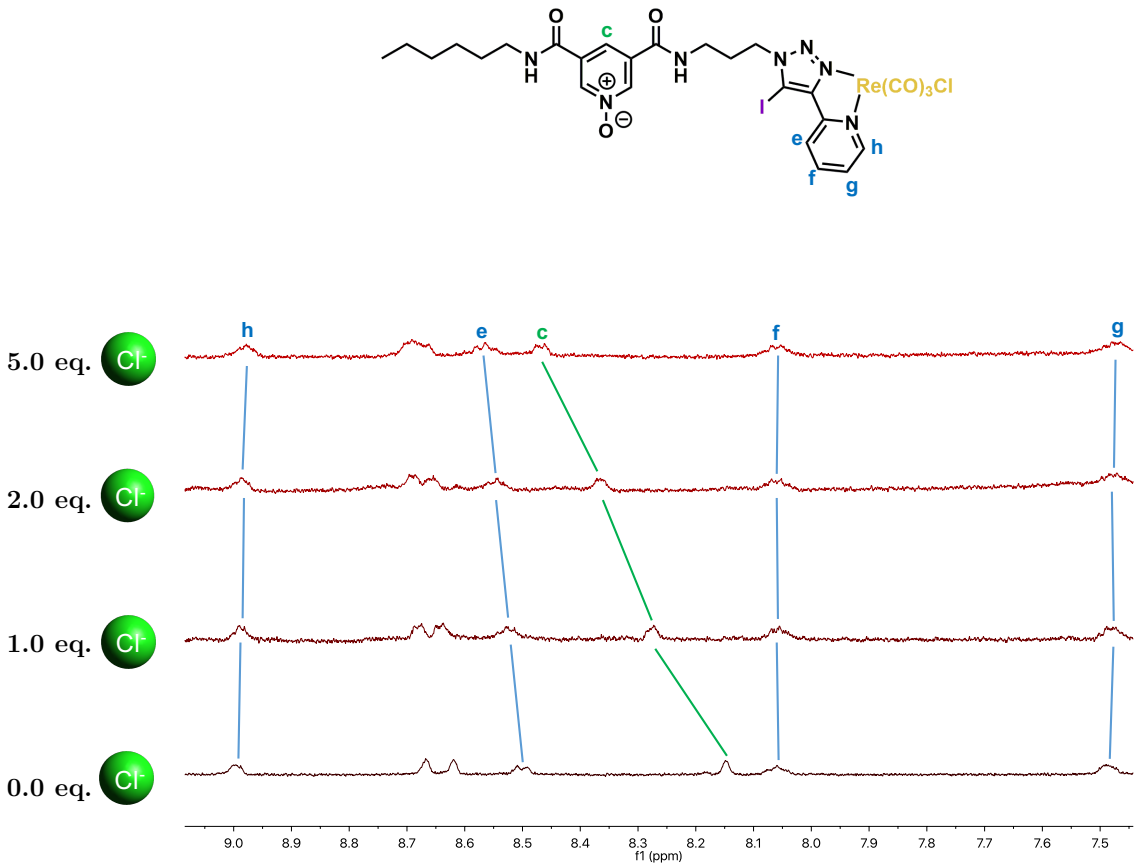


Figure 2.26 – Changes in the ^{1}H NMR spectrum upon the addition of increasing equivalents of TBACl to receptor **43** (9:1 $CDCl_3/CD_3OD$, 500 MHz, 298 K).

WinEQNMR2[13] analysis of the titration data monitoring pyridine *N*-oxide proton **c** in both receptors (**Figure 2.27**) determined 1:1 stoichiometric association constants, shown in **Table 2.3**.

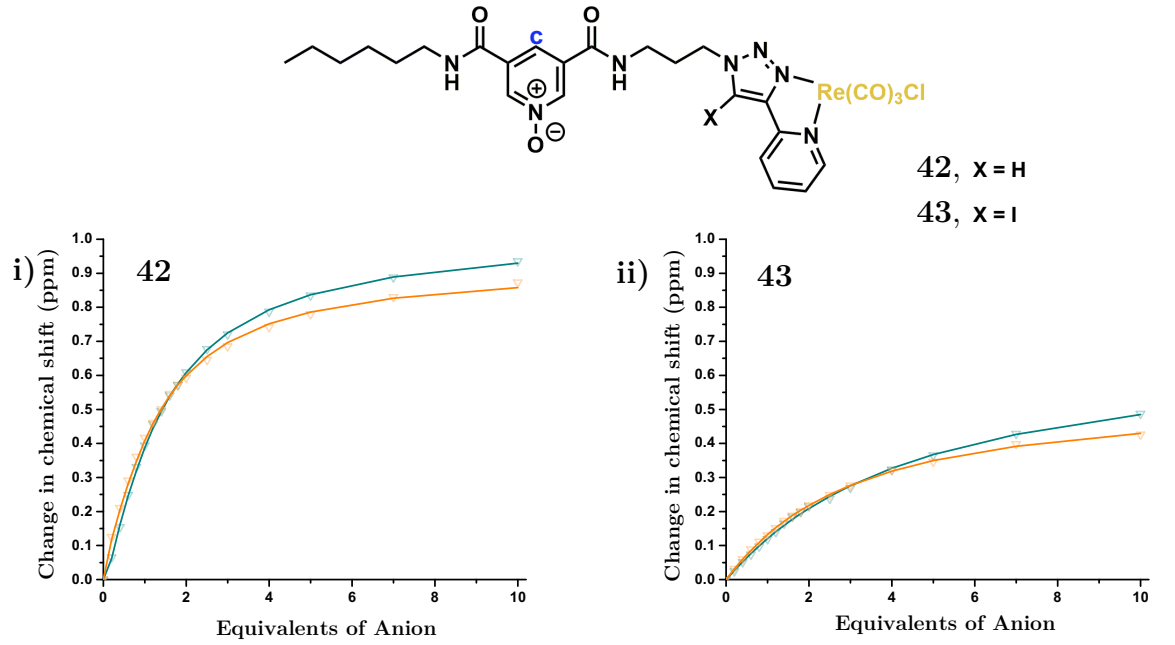


Figure 2.27 – Plots of change in chemical shift (ppm) against equivalents of anion added for i) **42** and ii) **43** (9:1 $CDCl_3/CD_3OD$, 298 K). Observed data (hollow triangles) and fitted isotherms (solid lines) are shown, monitoring internal pyridine *N*-oxide proton **c**.

Table 2.3 – Anion association constants for receptors **42** and **43** (9:1 $CDCl_3/CD_3OD$, 298 K).

(a) Anions added as their respective tetrabutylammonium (TBA) salts at 298K. (b) Anion association constants calculated using WinEQNMR2 using chemical shift data of internal binding site pyridine N-oxide proton ***c*** (**Figure 2.27**). ± *errors in parentheses.*

Anion[(a)]	**42** $K_a[M^{-1}]$[(b)]	**43** $K_a[M^{-1}]$[(b)]
Cl^-	738(67)	156(8)
Br^-	847(44)	263(8)

The hydrogen bonding receptor **42** binds both halides with similar strength and is a superior receptor to the halogen bonding analogue **43**. However, a modest preference for Br^- was observed with **43** which tentatively suggests a degree of halogen bonding contribution.

2.6.4. Summary

Synthesis of target hydrogen and halogen bonding neutral rhenium(I)-appended pyridine *N*-oxide receptors **42** and **43** was successful. Preliminary anion binding studies with Cl^- and Br^- revealed the halogen bonding receptor to be an inferior anion complexant to the hydrogen bonding analogue. Despite this fact, a modest degree of preference for Br^- was exhibited by halogen bonding receptor **43** in 9:1 $CDCl_3/CD_3OD$ solvent media.

2.7. Conclusion and Future Work

In the first part of this chapter, it was shown that the chelating mode of binding of the pyridinium-triazole anion recognition motif could be effectively exploited for anion recognition. Initial proof of principle established *via* the binding of Cl^- by both pyridinium and triazole moieties of acyclic receptor **9.PF$_6$** set the precedent for the chloride anion templated monostoppering synthesis of hydrogen bonding pyridinium-triazole axle containing rotaxane **10.PF$_6$** and halogen bonding homologue **11.PF$_6$**. Initial anion binding studies revealed that halides were bound strongly by both rotaxanes. In comparison to the hydrogen bonding rotaxane **10.PF$_6$**, a modest increase in the association constant value of Br^- was observed with halogen bonding rotaxane **11.PF$_6$**, which was attributed to a small but significant contribution of the halogen bond donor iodotriazole in binding the anion.

Efficient post-rotaxane methylation of the monocationic rotaxane hosts gave the corresponding dicationic triazolium/iodotriazolium containing rotaxanes **27.(PF$_6$)$_2$** and **28.(PF$_6$)$_2$**. The halogen bonding rotaxane demonstrated the strong influence of charge-assisted halogen bonding chelation, significantly enhancing the selective recognition of Br^- in competitive 45:45:10 $CDCl_3/CD_3OD/D_2O$ aqueous solvent media.

In attempts to synthesise an analogous rotaxane host system capable of sensing anions, chloride anion templated Grubbs' II catalysed ring closing metathesis was used to synthesise the rhenium(I) axle containing rotaxane **38.Cl**. The inability to verify the purity of the rotaxane precluded this anion host system from being studied further by ^{1}H NMR and UV-visible anion binding titrations.

In an initial step to synthesise a neutral halogen bonding rhenium(I) axle containing rotaxane host system, the synthesis of an acyclic hydrogen/halogen bonding pyridine N-oxide appended rhenium(I)-pyta receptor system was conducted. ^{1}H NMR anion binding studies in 9:1 $CDCl_3/CD_3OD$ solvent mixture revealed that hydrogen bonding receptor **42** was a superior receptor for Cl^- and Br^- in comparison to the halogen bonding counterpart **43**. However, a modest preference for Br^- over Cl^- was exhibited by halogen bonding receptor **43**, indicating charge assisted halogen bonding is required to enhance the anion binding capability of this receptor. This could be achieved in future work by the preparation of an analogous dicationic ruthenium(II) receptor.

In spite of these shortcomings, this chapter demonstrates the potent cooperation between the cationic pyridinium bis-amide motif and both hydrogen and halogen bonding triazolium groups especially in the strong recognition of halides *via* charge-assisted halogen bonding. Future exploitation of this unique chelating mode of anion recognition in the form of an all halogen bonding chelating anion host system is of continuing interest. Further attempts to incorporate optical reporter groups such as charged ruthenium(II) or iridium(III) bipyridyl derivatives to further explore charge assisted halogen bonding is justified. Finally, the addition of water solubilising groups such as permethylated β-cyclodextrin derivatives into rotaxane host systems as seen in **Figure 2.2-ii**[8] in order to construct chelating hosts for binding of anions in aqueous media would be worthy of study.

2.8. References for Chapter 2

(1) Cavallo, G.; Metrangolo, P.; Pilati, T.; Resnati, G.; Sansotera, M.; Terraneo, G. *Chem. Soc. Rev.* **2010**, *39* (10), 3772–3783.

(2) Erdélyi, M. *Chem. Soc. Rev.* **2012**, *41* (9), 3547–3557.

(3) Gilday, L. C.; Robinson, S. W.; Barendt, T. A.; Langton, M. J.; Mullaney, B. R.; Beer, P. D. *Chem. Rev.* **2015**, *115* (15), 7118–7195.

(4) Chudzinski, M. G.; McClary, C. A.; Taylor, M. S. *J. Am. Chem. Soc.* **2011**, *133* (27), 10559–10567.

(5) Chakraborty, S.; Dutta, R.; Ghosh, P. *Chem. Commun.* **2015**, *51* (79), 14793–14796.

(6) Kilah, N. L.; Wise, M. D.; Serpell, C. J.; Thompson, A. L.; White, N. G.; Christensen, K. E.; Beer, P. D. *J. Am. Chem. Soc.* **2010**, *132* (34), 11893–11895.

(7) Robinson, S. W.; Mustoe, C. L.; White, N. G.; Brown, A.; Thompson, A. L.; Kennepohl, P.; Beer, P. D. *J. Am. Chem. Soc.* **2015**, *137* (1), 499–507.

(8) Langton, M. J.; Robinson, S. W.; Marques, I.; Félix, V.; Beer, P. D. *Nat. Chem.* **2014**, *6* (12), 1039–1043.

(9) Spence, G. T.; Chan, C.; Szemes, F.; Beer, P. D. *Dalton Trans.* **2012**, *41* (43), 13474–13485.

(10) Hancock, L. M.; Beer, P. D. *Chem. Commun.* **2011**, *47* (21), 6012–6014.

(11) Joung, I. S.; Cheatham, Thomas E. *J. Phys. Chem. B* **2008**, *112* (30), 9020–9041.

(12) Norris, D. J.; Stewart, R. *Can. J. Chem.* **1977**, *55* (10), 1687–1695.

(13) Hynes, M. J. *J. Chem. Soc. Dalton Trans.* **1993**, No. 2, 311–312.

(14) Serpell, C. J.; Chall, R.; Thompson, A. L.; Beer, P. D. *Dalton Trans.* **2011**, *40* (45), 12052–12055.

(15) Gibson, H. W.; Lee, S. H.; Engen, P. T.; Lecavalier, P.; Sze, J.; Shen, Y. X.; Bheda, M. *J. Org. Chem.* **1993**, *58* (14), 3748–3756.

(16) Wisner, J. A.; Beer, P. D.; Drew, M. G. B. *Angew. Chem. Int. Ed.* **2001**, *40* (19), 3606–3609.

(17) Wang, Y.-M.; Zhou, C.-Q.; Chen, J.-X.; Lin, Y.-L.; Zeng, W.; Kuang, B.-C.; Fu, W.-L.; Chen, W.-H. *MedChemComm* **2013**, *4* (10), 1400–1404.

(18) Ng, K.-Y.; Felix, V.; Santos, S. M.; Rees, N. H.; Beer, P. D. *Chem. Commun.* **2008**, No. 11, 1281–1283.

(19) Collin, J.-P.; Frey, J.; Heitz, V.; Sauvage, J.-P.; Tock, C.; Allouche, L. *J. Am. Chem. Soc.* **2009**, *131* (15), 5609–5620.

(20) Mele, A.; Metrangolo, P.; Neukirch, H.; Pilati, T.; Resnati, G. *J. Am. Chem. Soc.* **2005**, *127* (43), 14972–14973.

(21) Cametti, M.; Raatikainen, K.; Metrangolo, P.; Pilati, T.; Terraneo, G.; Resnati, G. *Org. Biomol. Chem.* **2012**, *10* (7), 1329–1333.

(22) Tepper, R.; Schulze, B.; Görls, H.; Bellstedt, P.; Jäger, M.; Schubert, U. S. *Org. Lett.* **2015**, *17* (23), 5740–5743.
(23) Monkowius, U.; Ritter, S.; König, B.; Zabel, M.; Yersin, H. *Eur. J. Inorg. Chem.* **2007**, *2007* (29), 4597–4606.
(24) Struthers, H.; Mindt, T. L.; Schibli, R. *Dalton Trans.* **2009**, *39* (3), 675–696.
(25) Langton, M. J.; Xiong, Y.; Beer, P. D. *Chem. – Eur. J.* **2015**, *21* (52), 18910–18914.
(26) Müller, S.; Liepold, B.; Roth, G. J.; Bestmann, H. J. *Synlett* **1996**, *1996* (6), 521–522.
(27) Zheng, H.; Zhou, W.; Lv, J.; Yin, X.; Li, Y.; Liu, H.; Li, Y. *Chem. – Eur. J.* **2009**, *15* (47), 13253–13262.
(28) Jepsen, T. H.; Kristensen, J. L. *J. Org. Chem.* **2014**, *79* (19), 9423–9426.
(29) Doak, B. C.; Scanlon, M. J.; Simpson, J. S. *Org. Lett.* **2011**, *13* (3), 537–539.
(30) Zhao, H. C.; Mello, B.; Fu, B.-L.; Chowdhury, H.; Szalda, D. J.; Tsai, M.-K.; Grills, D. C.; Rochford, J. *Organometallics* **2013**, *32* (6), 1832–1841.
(31) Wisner, J. A.; Beer, P. D.; Drew, M. G. B.; Sambrook, M. R. *J. Am. Chem. Soc.* **2002**, *124* (42), 12469–12476.
(32) Brotherton, W. S.; Clark, R. J.; Zhu, L. *J. Org. Chem.* **2012**, *77* (15), 6443–6455.

CHAPTER 3

Halogen and Hydrogen Bonding Amide-Triazole Motifs for Anion Recognition

3.1. Introduction

3.1.1. Amide-triazole based anion receptors

As discussed in **Section 1.2.3.** of the introductory Chapter 1, receptors containing motifs such as ammonium groups[1–3], amides[4,5], ureas[6] and pyrroles[7] that utilise polarised N-H hydrogen bonds in the recognition of anions are considerably more common than those exploiting C-H hydrogen bonding interactions such as triazoles. This class of receptors distinctly often rely on preorganisation and the macrocyclic effect in order to function as effective anion binding host systems.[8,9] The recent emergence of the amide-triazole motif, with its ease of synthesis, has attracted interest in oxoanion binding applications. Li and co-workers constructed neutral amide-triazole based acyclic receptors[10] and helical foldamers[11] which are selective for sulphate over other oxoanions studied in DMSO/acetone and DCM respectively (**Figure 3.1**).

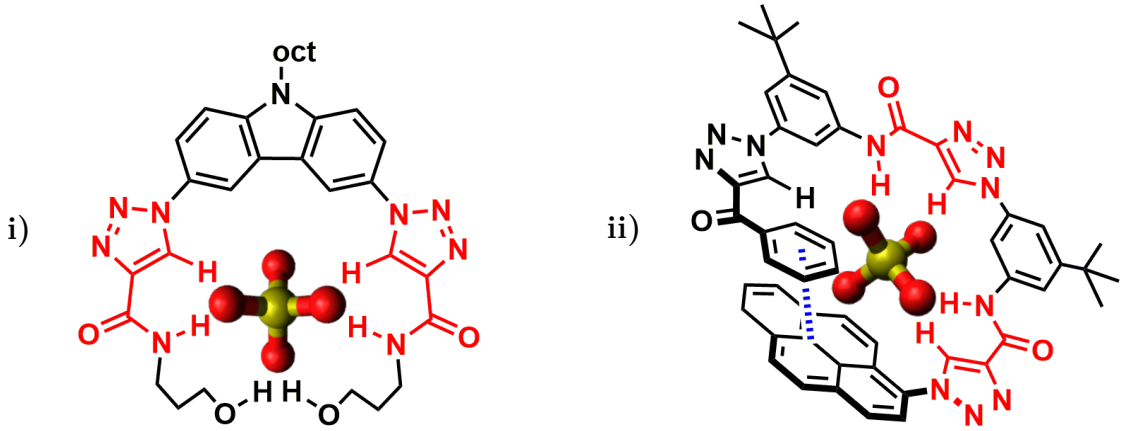


Figure 3.1 – Li's SO_4^{2-} binding i) bis-triazole-amide carbazole receptor and ii) amidetriazole-based helical foldamer.

3.1.2. Intramolecular hydrogen bonding: preorganisation

Intramolecular hydrogen bonds (IHBs) play an important role in the structure-property relationships of molecules in both biotic and synthetic systems. It has been shown that they strongly influence the solubility parameters of drug compounds[12],

the excited states of chromophores such as cyclovalone[13] and are key factors in the stabilization of the helical structures found in proteins[14] and biomimetic polymers.[15]

For the purposes of molecular recognition, they have been shown to be powerful preorganisational tools for enforcing favourable geometries of hosts to optimise interactions with a variety guests. Hamilton's ferrocene-diphenylacetylene single molecule switch exhibits a redox-switchable conformation mediated by an IHB (**Figure 3.2-i**).[16] Rarely observed amide NH-F IHBs have been shown to not only preorganise the structure of Li's helical foldamer but also instigate unusually strong hydrogen bonding between ammonium guests to the IHB-polarised fluorine atoms within the cavity of the foldamer in $CHCl_3$ (**Figure 3.2-ii**).[17] Five-membered IHB regimes involving other halogens, such as iodo-substituted aromatic amides, are relatively weak but have been observed in the solid state (**Figure 3.2-iii**).[18]

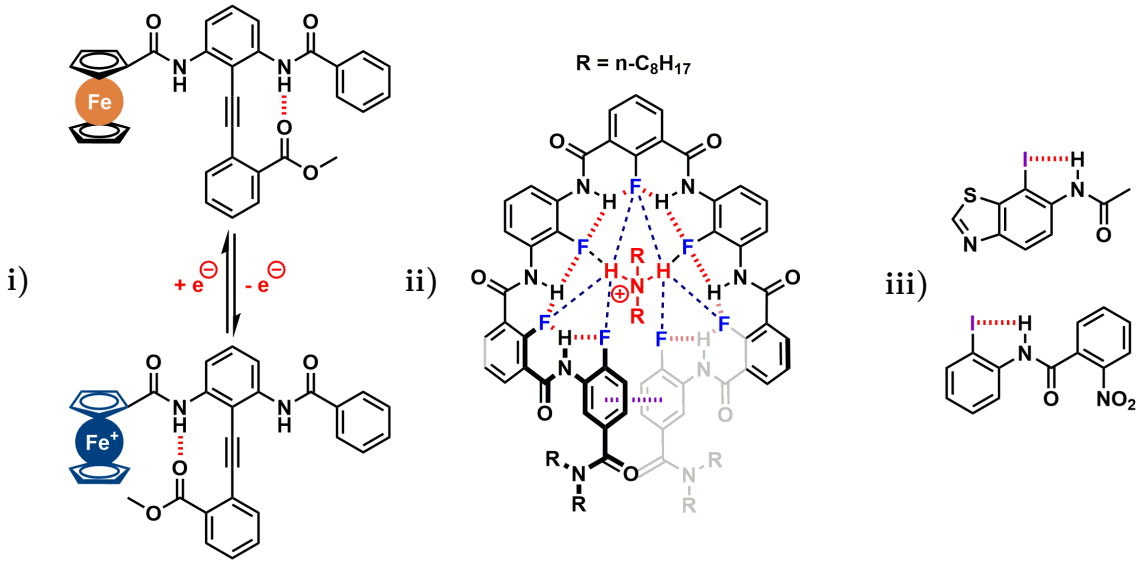


Figure 3.2 – i) Hamilton's redox switchable IHB; ii) Li's IHB foldamer binding an ammonium guest *via* multiple F-H interactions, iii) Examples of NH-iodine IHBs observed in the solid state.

3.2. Amide-iodotriazole and amide-triazole receptors for anion recognition

3.2.1. Receptor design

Firstly, this chapter describes the pursuit towards incorporating a novel halogen bonding amide-iodotriazole (**Figure 3.1**) and the analogous hydrogen bonding motif into a series of acyclic receptors. The precedent set for IHBs interacting with halogen atoms (**Figure 3.2-ii/iii**) inspired the synthesis of the amide-iodotriazole motif where importantly an IHB may offer a means to preorganise and thus enhance the anion recognition properties of the iodotriazole motif. It was envisioned that an amide functional group covalently linked to an iodotriazole motif would be in the correct position to form an intramolecular hydrogen bond with the electron rich so called 'equatorial belt' of the iodine atom, which arises due to the anisotropic distribution of electron density about the halogen atom when polarised by an electron withdrawing group (**Figure 3.3**).[19]

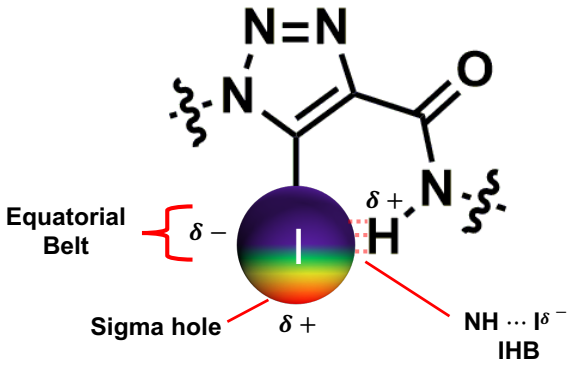


Figure 3.3 – Proposed intramolecular amide hydrogen bonding preorganisation of the iodine atom of an iodotriazole motif from a pendant amide functional group.

3.2.2. Chapter aims

It was envisioned that IHB interactions could be exploited in the structures of a series of neutral amide functionalised iodotriazole and charge assisted iodotriazolium halogen bonding acyclic, macrocyclic and interlocked anion host frameworks where intramolecular amide-halogen hydrogen bonding preorganisation may lead to enhanced halogen bonding anion recognition properties. Initially, a series of structural isomers based on the amide-(iodo)triazole motif will be synthesised to investigate the effect of IHBs on the anion recognition properties of this new class of receptor (**Figure 3.4**).

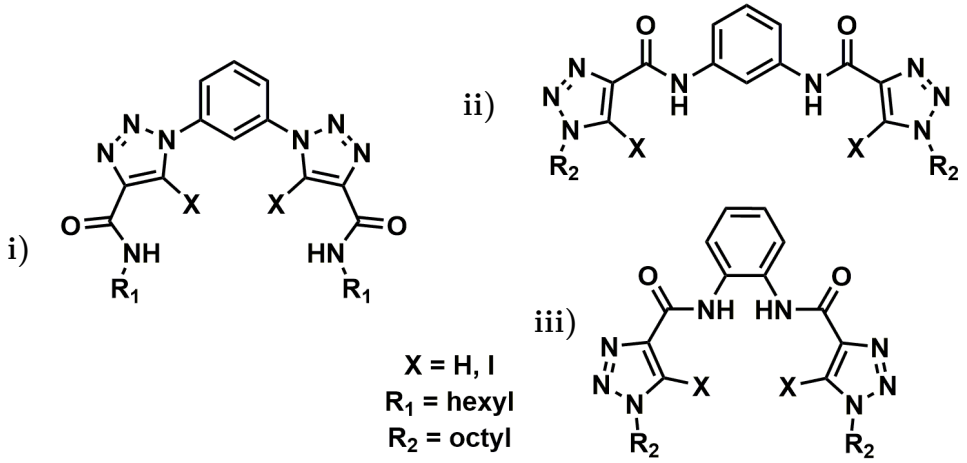
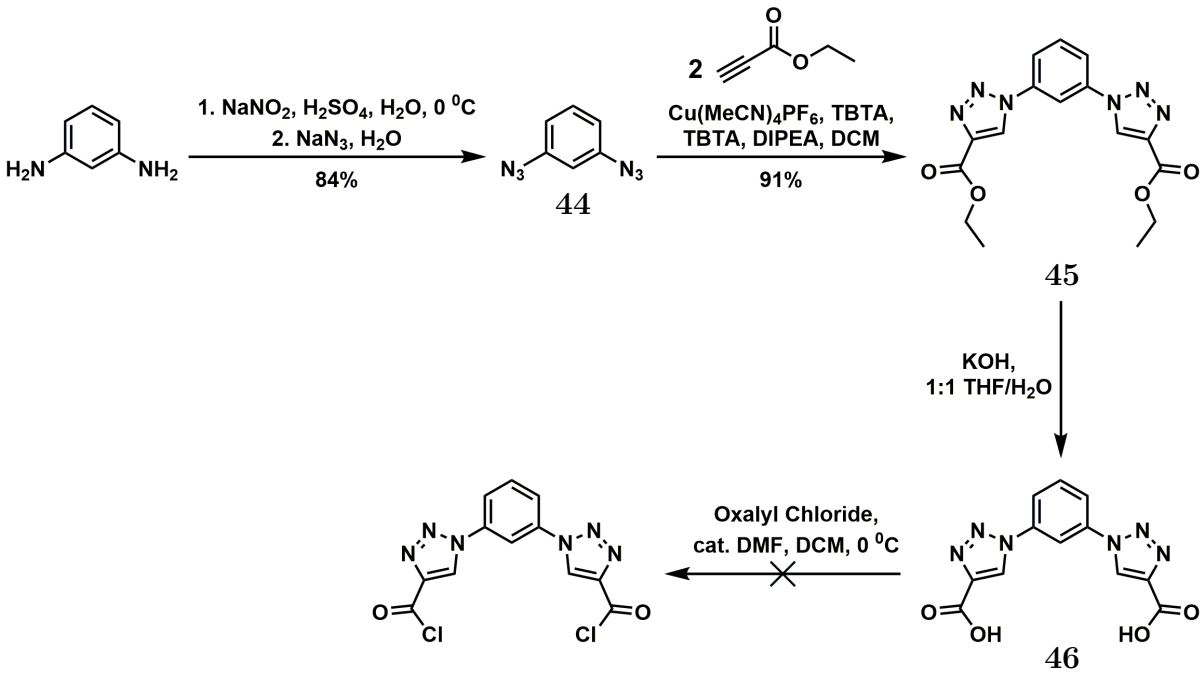


Figure 3.4 – The substitution of target acyclic amide-triazole (X = H) and amide-iodotriazole (X = I) anion receptors: i) 1,3-bis-triazole-amide ii) *N*,*N*'-(1,3-phenylene)diamidetriazole and iii) *N*,*N*'-(1,2-phenylene)diamidetriazole.

3.2.3. Synthesis of acyclic halogen and hydrogen bonding bis-triazole-amide receptors

The synthesis of target halogen and hydrogen bonding acyclic 1,3-bis-triazole-amide phenyl-based receptors (**Figure 3.4-i**) was approached initially *via* the synthetic route detailed in **Scheme 3.1**. Diazotization of commercially available *m*-phenylenediamine followed by reaction with NaN_3 afforded 1,3-diazidobenzene **44**[20] in an 84% yield. Two equivalents of commercially available ethyl propiolate and di-

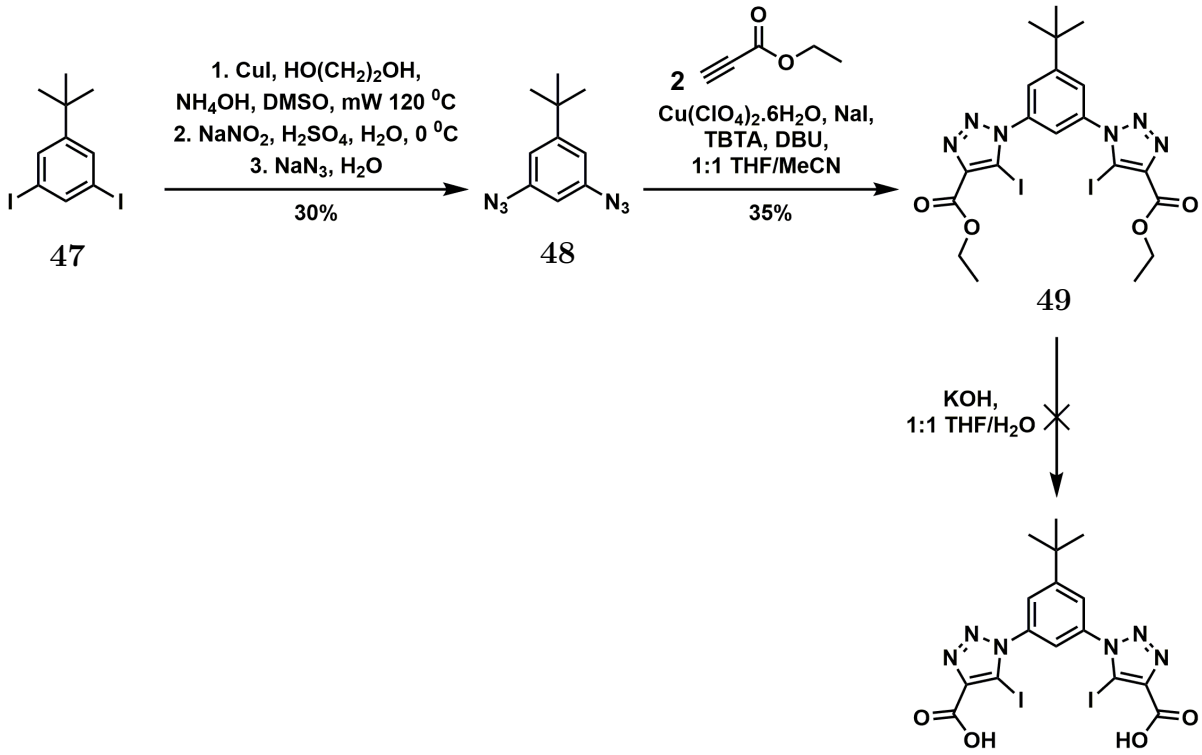
azide **44** were subjected to CuAAC 'click' conditions with $Cu(MeCN)_4PF_6$ as a catalyst to give the desired bis-triazole di-ethyl ester **45** in a 91% yield. Basic ester hydrolysis and acidic workup gave the bis-carboxylic acid **46** which was found to be sparingly soluble in common solvents. Attempts were made to convert **46** to the bis-acid chloride using oxalyl chloride and catalytic amount of DMF in DCM, however very little conversion was observed, likely due to the very low solubility of the starting material.



Scheme 3.1 – Synthesis of receptor precursor **46**.

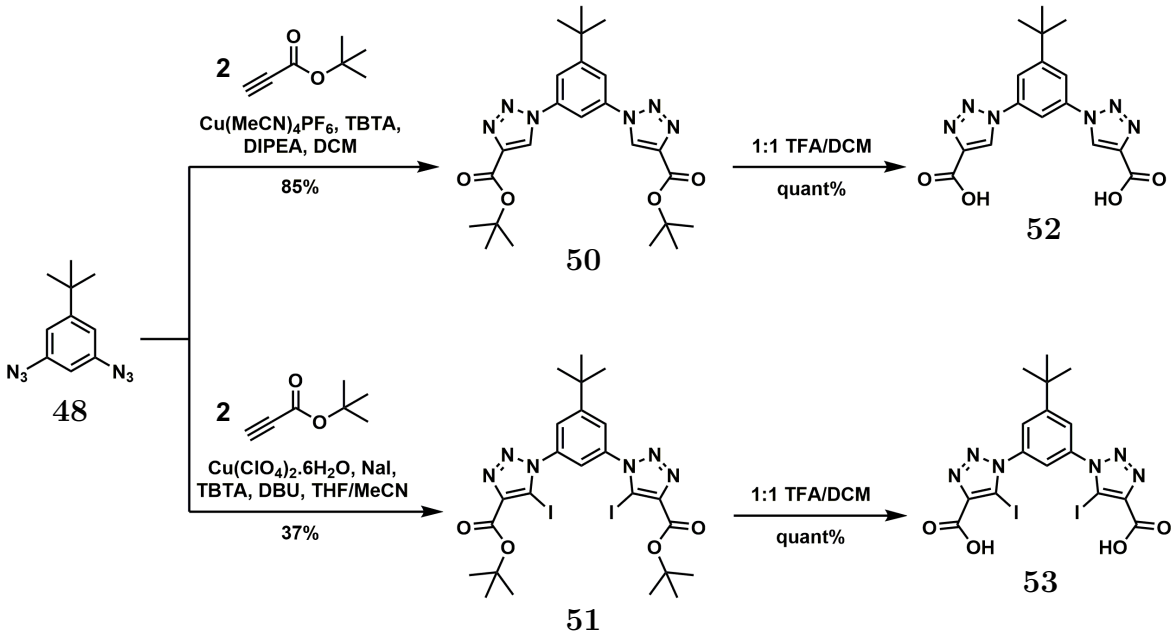
To overcome these solubility issues, the synthesis of a more soluble homologous *tert*-butyl group appended precursor bis-acid was sought. 5-*Tert*-butyl-1,3-diiodobenzene **47**[21], kindly donated by Dr. Nicholas White, was converted to the bis-amine intermediate *via* a modified Cu(I)-ethylene glycol Ullman protocol[22] in the presence of excess NH_4OH in DMSO. Subsequent diazotization followed by reaction with NaN_3 gave *tert*-butyl phenyl bis-azide **48** in an overall yield of 30%. Bis-azide **48** was reacted with two equivalents of ethyl propiolate under one-pot iodotriazole

CuACC conditions[23] to give *tert*-butyl phenyl bis-iodotriazole bis-ethyl ester **49** in a 35% yield. Unfortunately, upon exposure to basic conditions necessary for cleavage of the ester groups, rapid decomposition occurred (**Scheme 3.2**).



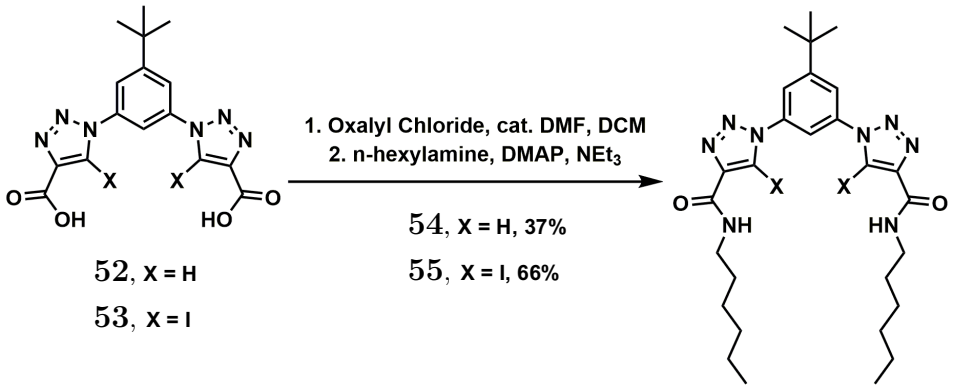
Scheme 3.2 – Attempted synthesis of bis-iodotriazole receptor precursor bis-acid.

Noting the instability of the bis-iodotriazole motif towards base, substitution of the bis-ethyl ester protecting groups for acid-labile *tert*-butyl ester groups was undertaken. Bis-azide **48** was reacted with two equivalents of commercially available *tert*-butyl propiolate under CuACC conditions to afford bis-triazole bis-*tert*-butyl ester **50** in an 85% yield. Bis-azide **48** was also subjected to identical one-pot iodotriazole CuAAC conditions as before (**Scheme 3.2**) and the desired bis-iodotriazole bis-*tert*-butyl ester **51** was obtained in a 37% yield. Both bis-esters **50** and **51** underwent acidic ester hydrolysis in 1:1 TFA/DCM solvent mixture to give bis-acids **52** and **53** (**Scheme 3.3**).



Scheme 3.3 – Synthesis of dicarboxylic acids **52** and **53**.

Reaction of bis-acids **52** and **53** with oxalyl chloride followed by amide condensation with excess n-hexyamine in DCM afforded bis-triazole-amide receptor **54** in a 37% yield and bis-iodotriazole-amide **55** in a 66% yield (**Scheme 3.4**).



Scheme 3.4 – Amide-coupling synthesis of triazole-amide receptors **54** and **55**.

Both receptors were characterised by ^{1}H NMR, ^{13}C NMR and ESI-HRMS. Tentative evidence for the presence of an IHB between amide proton **d** and the iodine of the iodotriazole motif in halogen bonding receptor **55** was suggested by the amide's downfield shift ($\Delta\delta$(ppm) = 0.1) in comparison with hydrogen bonding triazole-

amide receptor **54**; analogous observations have been made with similar amide-based IHB systems.[24,25] A large upfield shift of internal aromatic cleft proton **b** in **55** ($\Delta\delta$(ppm) = 0.49) was also observed in contrast to **54** (**Figure 3.5**).

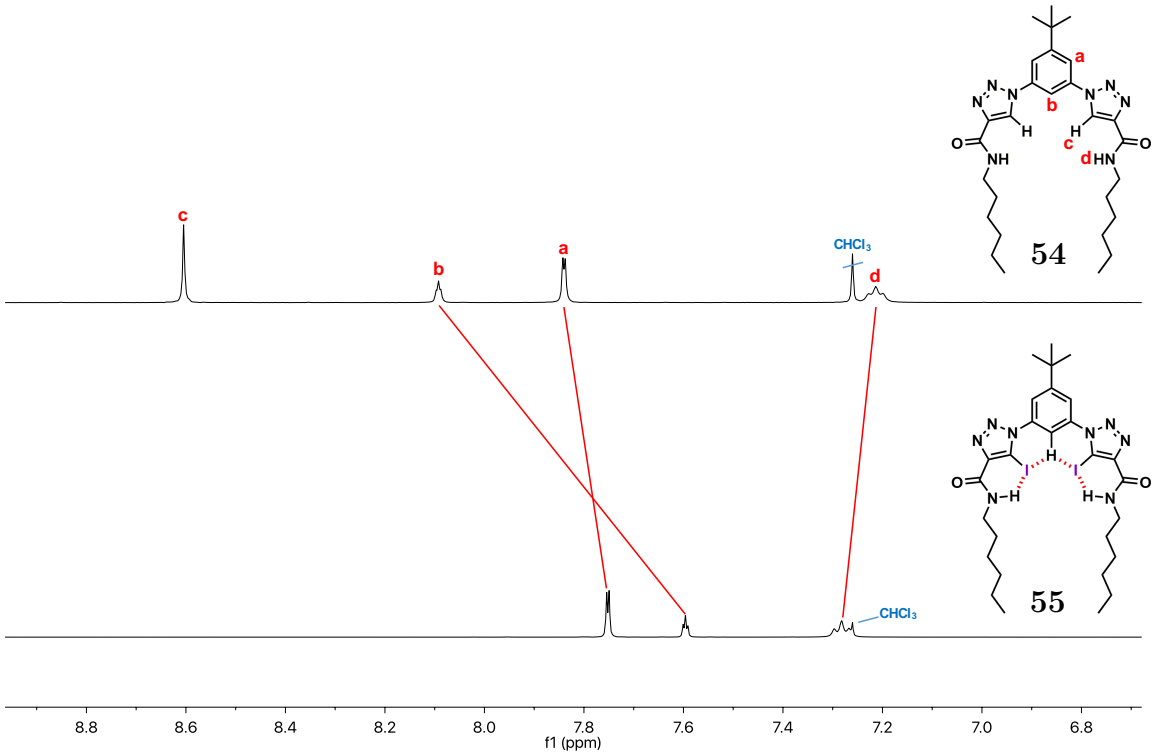
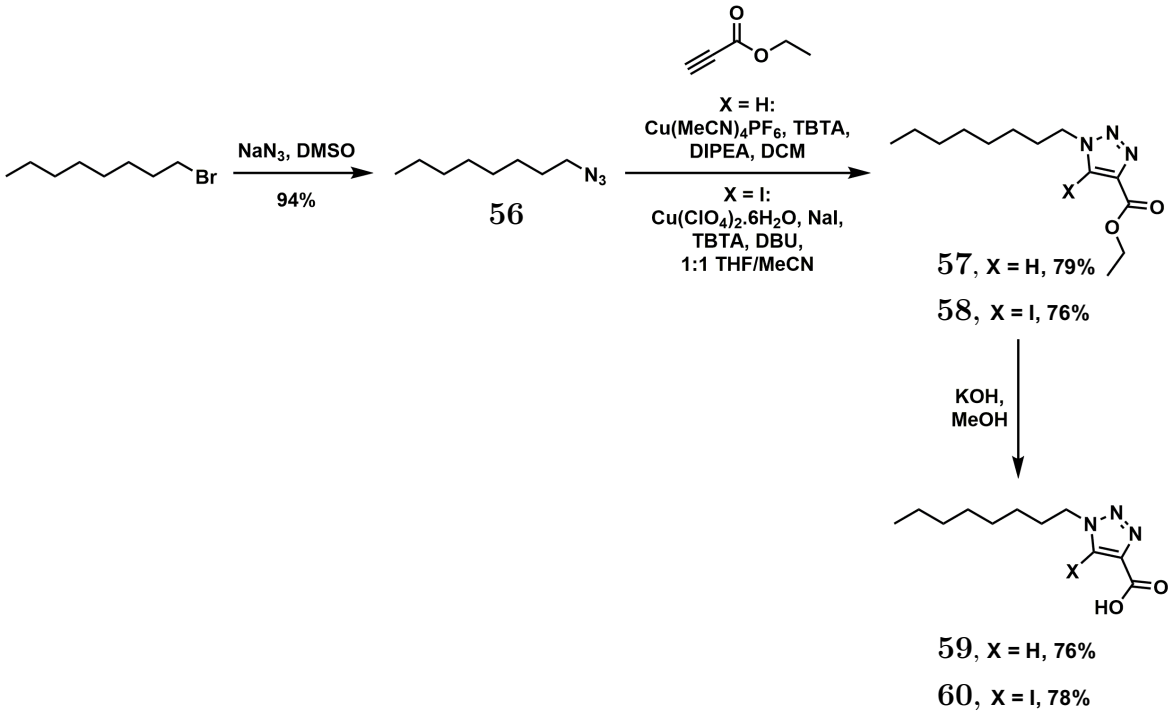


Figure 3.5 – Differences in observed chemical shifts for protons **a**, **b** and **d** for receptors **54** and **55** ($CDCl_3$, 400 MHz, 298 K).

3.2.4. Synthesis of isomeric halogen and hydrogen bonding bis-amide-triazole receptors

The synthesis of target *N*,*N*'-(1,3-phenylene)bis-amide-triazole and *N*,*N*'-(1,2-phenylene)bis-amide-triazole acyclic receptors was approached first by the preparation of triazole and iodotriazole carboxylic acid derivatives **59** and **60** (**Scheme 3.5**). These precursors would be appended *via* amide coupling methodology to the central aromatic spacer group, giving the target bis-amide-triazole and bis-amide-iodotriazole isomerically-related receptors depicted in **Figure 3.4-ii, iii**. 1-Bromooctane was converted to azide **56**[26] with NaN_3 in DMSO in a 94% yield. Azide **56** was subjected to CuAAC 'click' conditions with ethyl propiolate to

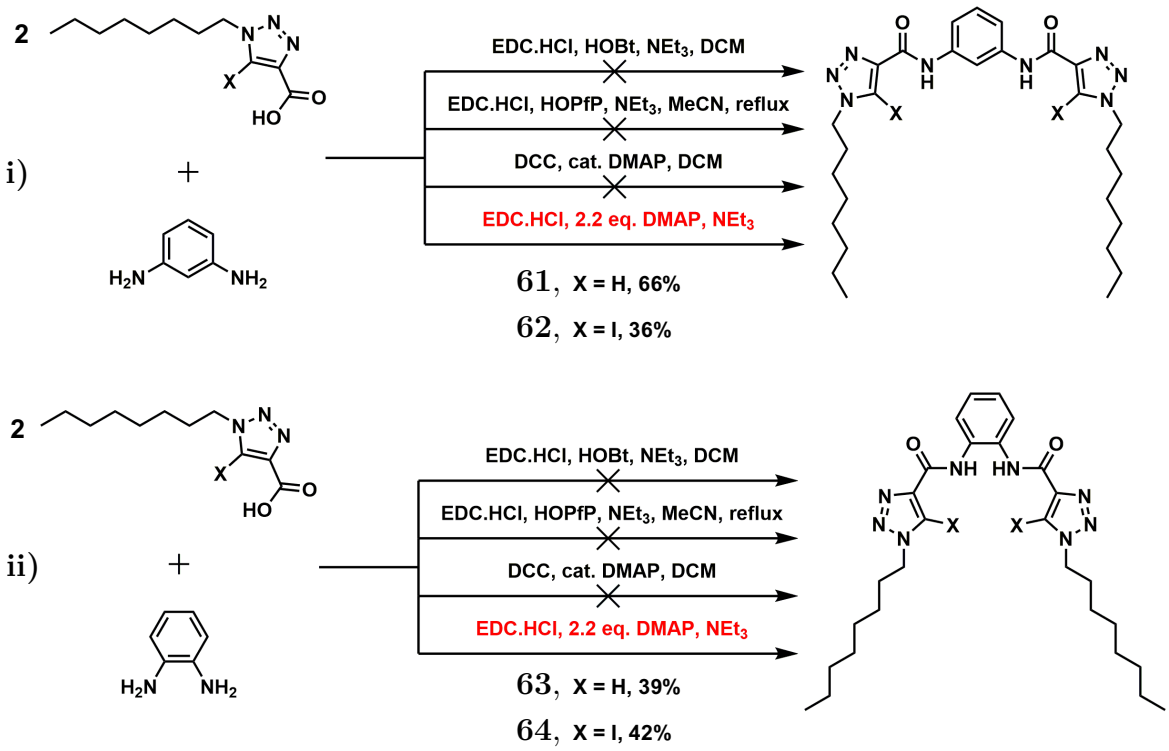
give triazole arm precursor ester **57**[27] in a 79% yield. Using iodotriazole formation CuAAC conditions, the corresponding iodotriazole homologue **58** was isolated in 76% yield. Basic ester hydrolysis with KOH in MeOH gave carboxylic acid derivatives **59** and **60** in 76% and 78% yields respectively (**Scheme 3.5**).



Scheme 3.5 – Synthesis of target triazole and iodotriazole carboxylic acid derivatives **59** and **60**.

Initially, EDC.HCl mediated amide coupling was undertaken with 2.2 equivalents of respective carboxylic acid and NEt_3 with respect to *meta*-phenylene diamine and *ortho*-phenylene diamine in DCM. Yields of desired 1,3- and 1,2-disubstituted amide-triazoles and amide-iodotriazoles were consistently low using these conditions, giving mono-amide-triazole species as the major products which proved to be unstable in all cases. Analogous reaction attempts using established alternative activated ester groups such as PFP[28], HOBt[29], and other carbodiimide amide coupling regents such as DCC also gave mono-amide-triazoles as the major product. These observations were ascribed to the reduced nucleophilicity of the second amine resulting from the formation of an electron withdrawing amide at the first position, which disfavours the second amide coupling reaction. Fortunately, the use of a

stoichiometric amount of amide coupling catalyst DMAP furnished the desired 1,3-substituted phenylene bis-amidetriazole **61** and bis-amideiodotriazole **62** in acceptable respective yields of 66% and 36% (**Scheme 3.6-i**). The 1,2-substituted phenylene counterparts were also obtained through this method; **63** and **64** were isolated in 39% and 42% yields respectively (**Scheme 3.6-ii**).



Scheme 3.6 – Failed and successful attempts to synthesise i) 1,3-disubstituted receptors **61** and **62**; ii) 1,2-disubstituted receptors **63** and **64**.

Receptors **61** – **64** were characterised by ^{1}H NMR, ^{13}C NMR and ESI-HRMS. Comparison of the ^{1}H NMR spectra of hydrogen bonding amide-triazole receptor **61** and halogen bonding amide-iodotriazole receptor **62** in $CDCl_3$ showed that **62** experiences a small downfield shift of amide resonance **d** ($\Delta\delta$(ppm) = 0.05) and other aromatic environments (**a**, **b** and **c**) (**Figure 3.6**).

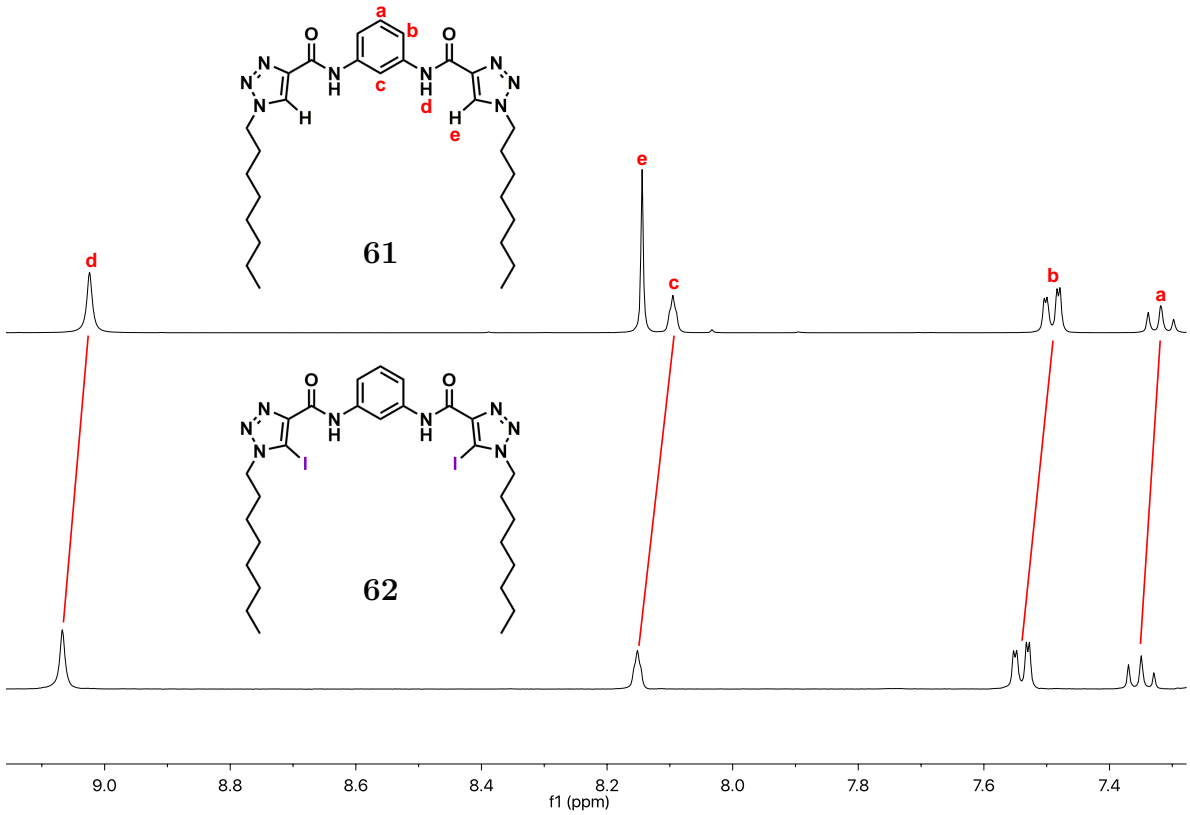


Figure 3.6 – Differences in observed chemical shifts for protons **a**, **b**, **c** and **d** for receptors **61** and **62** ($CDCl_3$, 400 MHz, 298 K).

Similarly, the halogen bonding receptor **64** exhibited a small downfield shift of amide resonance **c** ($\Delta\delta$(ppm) = 0.08) and phenylene protons **a** and **b** in comparison to hydrogen bonding receptor **63** (**Figure 3.7**).

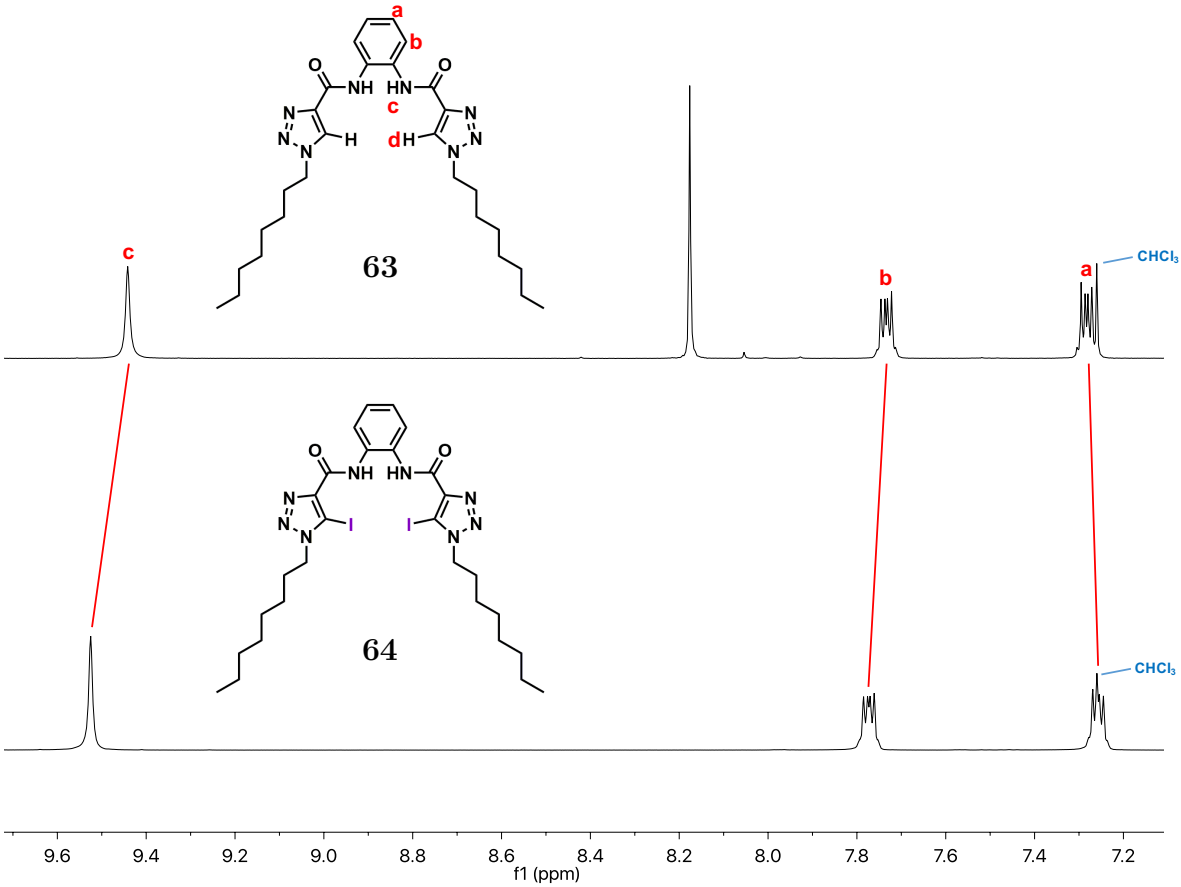


Figure 3.7 – Differences in observed chemical shifts for protons **a**, **b** and **c** for receptors **62** and **63** ($CDCl_3$, 400 MHz, 298 K).

The relatively modest downfield perturbations of the amide protons observed with all of the halogen bonding receptors in comparison to the hydrogen bonding receptors ($\Delta\delta$(ppm) $\leq$ 0.1) suggests the IHBs depicted in **Figure 3.8** are comparatively weak.

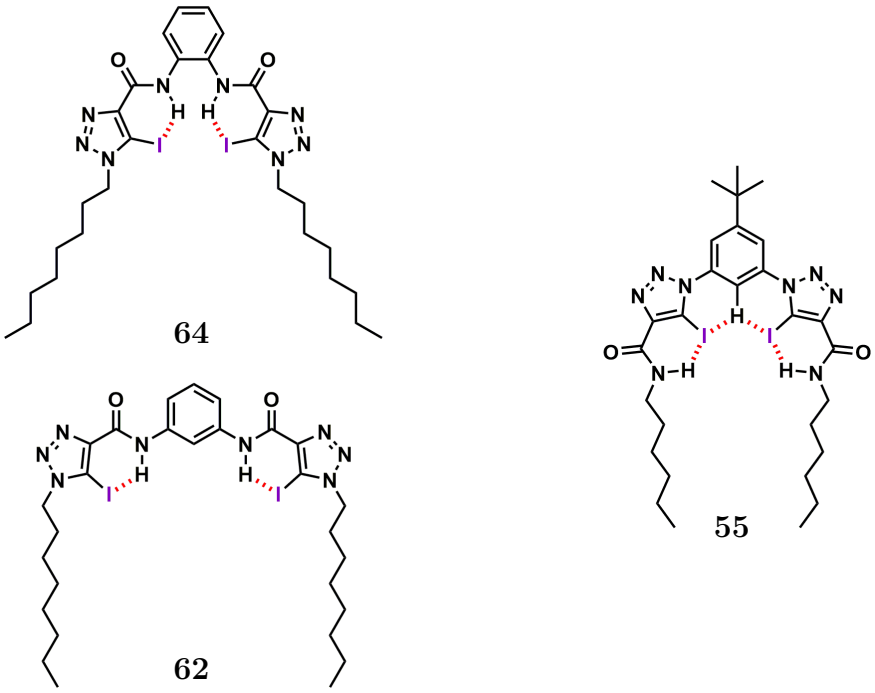


Figure 3.8 – Comparison of IHBs (shown in red) present in receptors **62**, **64** and **55**.

3.2.5. Anion binding studies

^{1}H NMR anion binding titrations were carried out in acetone-d_6 initially with **54** and **55** and the TBA salts of halides Cl^-, Br^- and I^-. *Tert*-butyl phenyl amide-triazole receptor **54** exhibited modest downfield shifts of internal phenyl proton **b** ($\Delta\delta$(ppm) = 0.02), triazole proton **c** ($\Delta\delta$(ppm) = 0.1) and amide proton **d** ($\Delta\delta$(ppm) = 0.06) upon addition of one equivalent of TBACl, indicating hydrogen bonding interactions to the halide anion (**Figure 3.9-i**). Halogen bonding receptor counterpart **55** exhibited larger magnitude shifts of proton **b** ($\Delta\delta$(ppm) = 0.06) and contrasting upfield shifts of amide proton **c** ($\Delta\delta$(ppm) = 0.1) (**Figure 3.9-ii**).

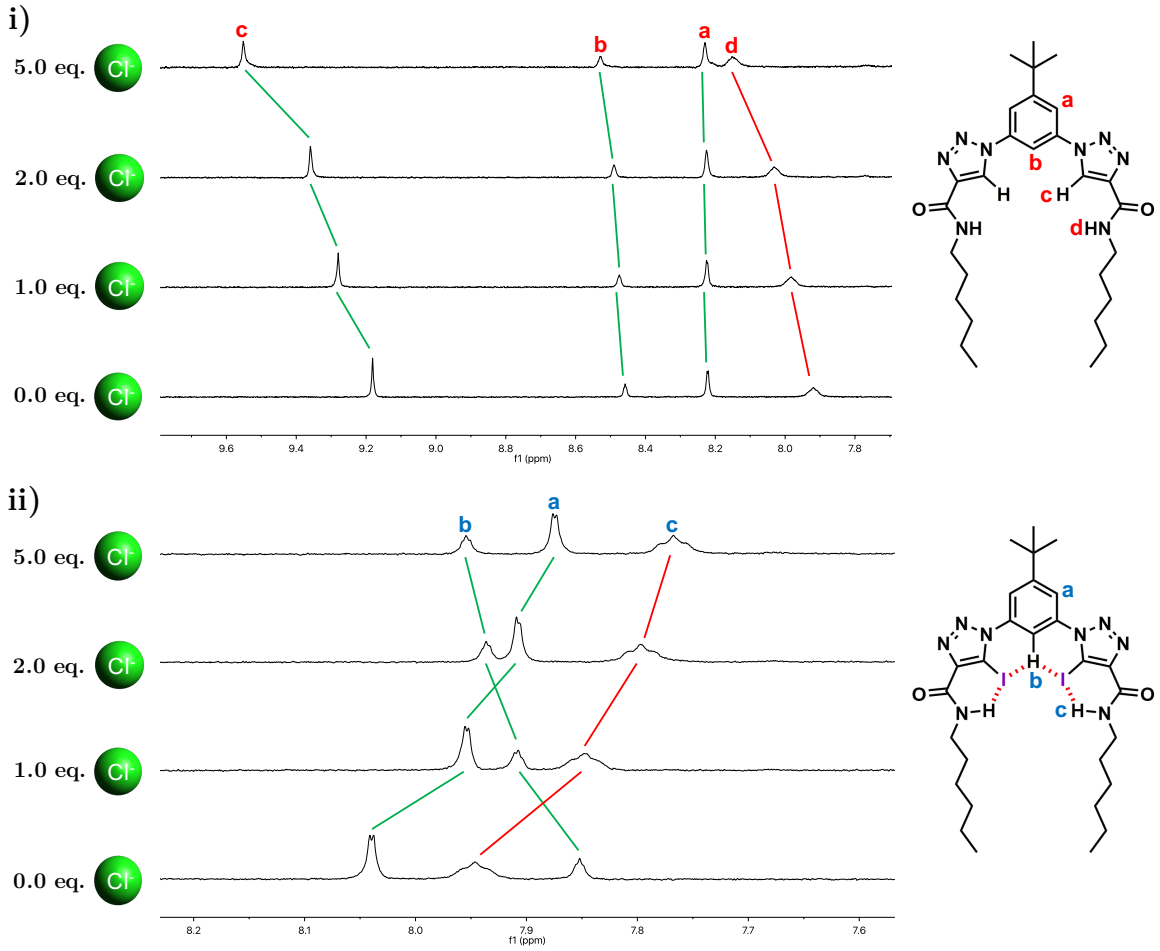


Figure 3.9 – Changes in the NMR spectrum of i) **54** and ii) **55** upon addition of increasing equivalents of TBACl ($CDCl_3$, 400 MHz, 298 K). Amide resonance shifts indicated by red lines.

Similar observations were noted with the additions of TBABr and TBAI to both receptors. Very small shifts of binding protons were seen upon titration with $TBANO_3$ to both receptors, indicative of weak binding. The addition of TBAOAc to hydrogen bonding receptor **54** lead to downfield shifts of **b**, **c** and **d**, followed by significant peak broadening during the course of the titration. The halogen bonding receptor **55** again exhibited upfield perturbations of amide proton **c**. WinEQNMR2[30] analysis of the titration data (**Figure 3.10**) monitoring the respective amide resonances of both receptors determined 1:1 stoichiometric association constants (**Table 3.1**).

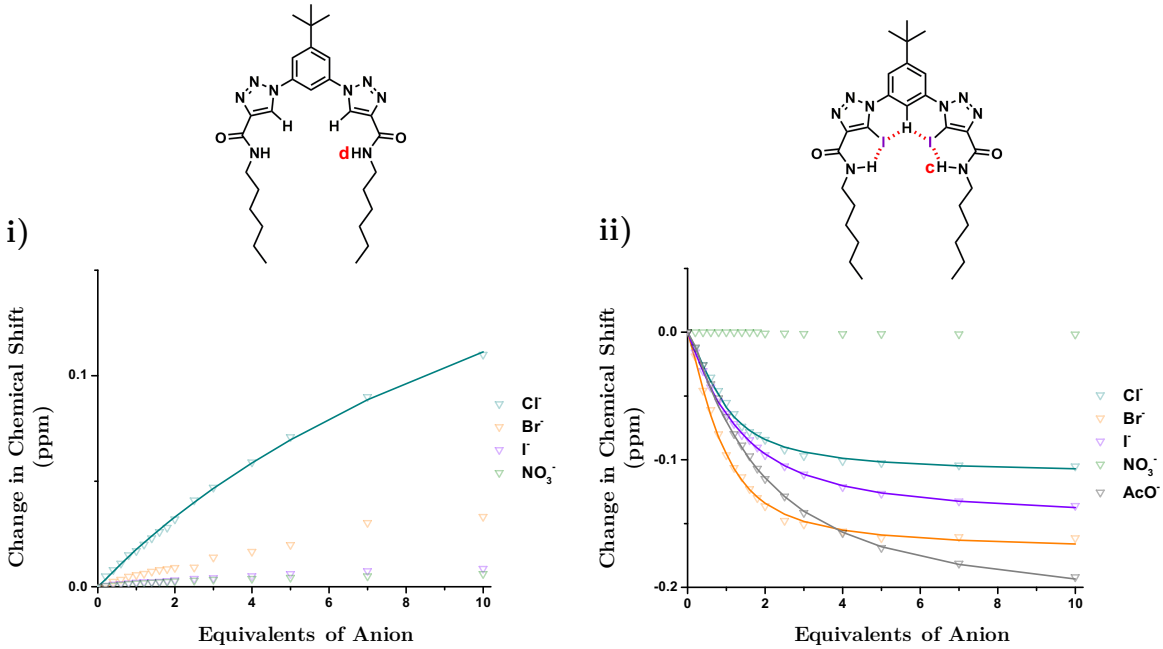


Figure 3.10 – Plots of changes in amide proton chemical shift (ppm) against equivalents of anion added for i) **54** and ii) **55** (acetone-d_6, 298 K). Observed data (hollow triangles) and fitted isotherms (lines) are shown, monitoring amide protons (**d** for **54** and **c** for **55**).

Table 3.1 – Anion association constants for receptors **54 and 55** (acetone-d_6, 298 K).

(a) *Anions added as their respective tetrabutylammonium (TBA) salts at 298K. Anion association constants calculated using WinEQNMR2* [30] *using chemical shift data of amide resonance* **d** (**Figure 3.10-i**, (b)) and amide resonance **c** (**Figure 3.10-ii**, (c)). ± *Errors in parentheses.* (d) *Binding strength too weak to be quantified.* (e) *Titration data could not be fitted.*

Anion[a]	**54**[b] K_a[M^{-1}]	**55**[c] K_a[M^{-1}]
Cl$^-$	33(4)	1675(177)
Br$^-$	-[d]	1995(178)
I$^-$	-[d]	884(24)
NO$_3^-$	-[d]	-[d]
AcO$^-$	-[e]	506(62)

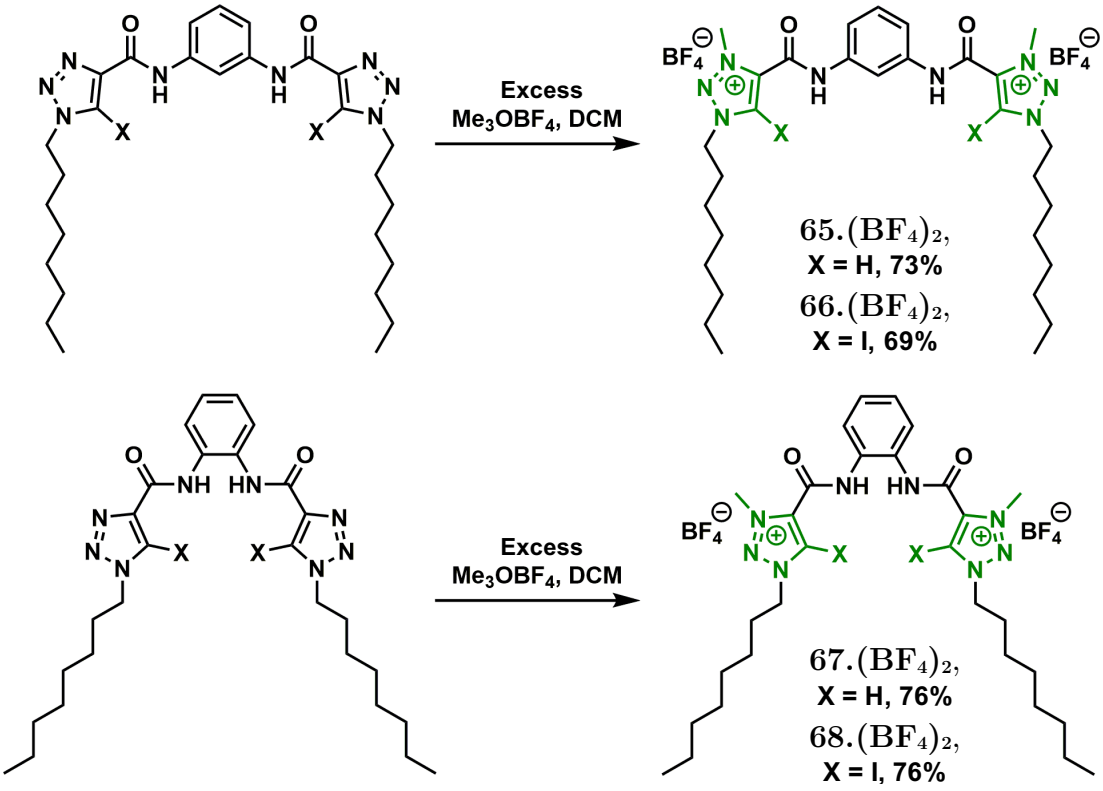
Halogen bonding receptor **55** exhibited remarkably enhanced binding of the halides in comparison to hydrogen bonding receptor **54**, with a particular preference for the

smaller halides Cl^- and Br^-, adopting the selectivity trend $Br^->Cl^->I^-$. Also, the halogen bonding receptor **55** displayed a bias for the more basic oxoanion AcO^- over NO_3^-. The amide proton perturbation titration data obtained for Br^-, I^- and NO_3^- with hydrogen bonding receptor **54** was of such small magnitude ($\Delta\delta$(ppm) $\leq$ 0.03) that the weak binding could not be quantified.

Preliminary Cl^- and Br^- halide binding studies were conducted with 1,2- and 1,3-disubstituted amide-triazole receptors **61** – **64** in acetone-d_6. All four receptors exhibited very small shifts of their respective amide resonances ($\Delta\delta$(ppm) $\leq$ 0.04) with both halides, indicating very weak association that could not be quantified.

3.2.6. Synthesis and anion binding studies of isomeric amide-triazolium and amide-iodotriazolium receptors

In an effort to augment the anion recognition properties of receptors **61** – **64**, methylation of the respective triazole motifs was undertaken. This was performed *via* reaction with an excess of trimethyloxonium tetrafluoroborate (Meerwein's salt) in DCM and the corresponding dicationic receptors **65.(BF$_4$)$_2$** – **68.(BF$_4$)$_2$** were isolated in good yields (**Scheme 3.7**).



Scheme 3.7 – Synthesis of 1,3-bis-amide-triazolium receptors **65.**$(BF_4)_2$ and **66.**$(BF_4)_2$ and 1,2-bis-amide-triazolium receptors **67.**$(BF_4)_2$ and **68.**$(BF_4)_2$.

The anion recognition properties of the receptors were investigated *via* ^{1}H NMR titration experiments in d_3-MeCN solvent. Addition of TBACl initially caused small downfield shifts of the respective amide and phenyl binding cleft protons in 1,3-disubstituted hydrogen bonding receptor **65.**$(BF_4)_2$ and halogen bonding receptor **66.**$(BF_4)_2$ followed by shifts of increased magnitude. Triazolium resonance **e** of **65.**$(BF_4)_2$ exhibited moderate perturbations ($\Delta\delta$(ppm) $\approx$ 0.1) upon each addition up to ten equivalents of Cl^-, inferring weak anion association. In contrast, with 1,2-disubstituted hydrogen bonding receptor **67.**$(BF_4)_2$, strong binding of Cl^- was implied by the large shifts of binding cleft triazolium proton **d** after just one equivalent of TBACl added (**Figure 3.10**).

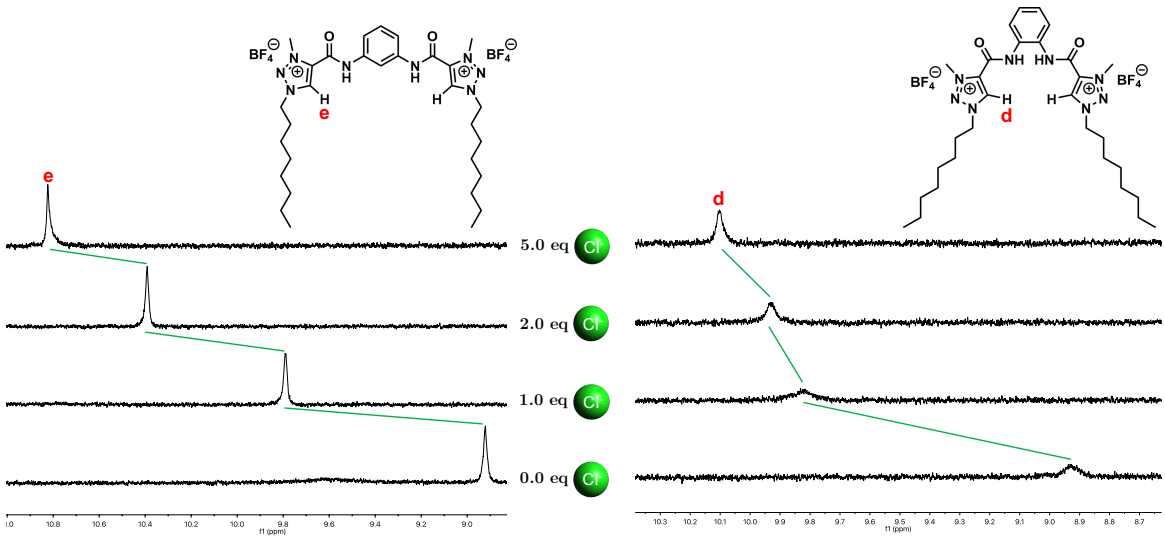


Figure 3.10 – The contrasting changes in the triazolium resonances in the ^{1}H NMR spectra of i) **65.(BF$_4$)$_2$** and ii) **67.(BF$_4$)$_2$** upon additions of TBACl (d_3-MeCN, 500 MHz, 298 K).

The 1,2-disubstituted halogen bonding receptor **68.(BF$_4$)$_2$** exhibited significant broadening of the amide resonance following addition of TBACl. The phenyl proton resonances were not significantly perturbed and as a consequence, association constants could not be determined. Analogous titrations conducted with TBABr and TBAI to both hydrogen bonding receptors **65.(BF$_4$)$_2$** and **67.(BF$_4$)$_2$** caused downfield shift magnitude changes akin to that seen before and after the addition of one equivalent of Cl^-. However in the case of halogen bonding receptor **66.(BF$_4$)$_2$**, precipitation was observed upon titration of two equivalents of Br^- and I^-.

65.(BF$_4$)$_2$ exhibited downfield shifts of triazolium proton **e** and upfield shifts of the phenyl binding cleft resonance upon additions of $TBANO_3$ and $TBAN_3$, indicating interaction of the linear and trigonal geometry of these anions within the wide binding cleft of this receptor configuration (**Figure 3.11**).

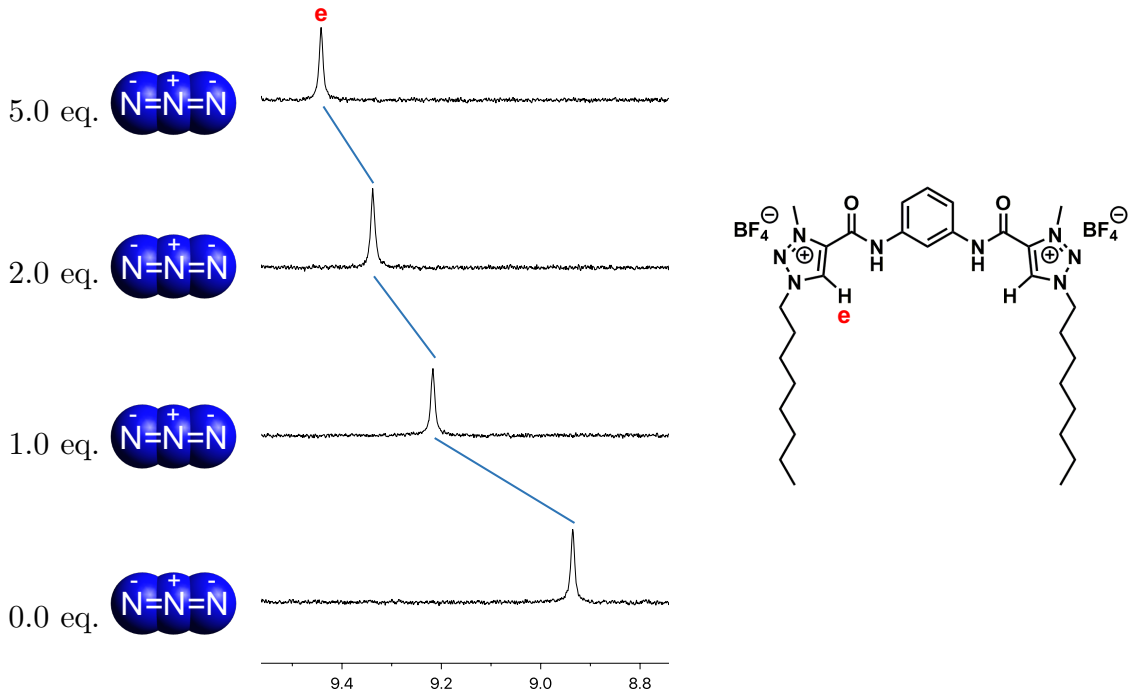


Figure 3.11 – Changes in the triazolium resonace **e** ^{1}H NMR spectrum of **65.(BF$_4$)$_2$** upon additions of TBAN$_3$ (d_3-MeCN, 500 MHz, 298 K).

Titrations conducted with AcO$^-$ caused peak broadening of the respective binding proton resonances of all four receptors. Attempts to fit the Cl$^-$ and Br$^-$ titration data obtained for **65.(BF$_4$)$_2$** (**Figure 3.12-i**) and **66.(BF$_4$)$_2$** (**Figure 3.12-ii**) to various 1:1, 1:2 and 2:1 stoichiometric host-guest binding models *via* WinEQNMR2[30] analysis were not successful. WinEQNMR2[30] analysis of the titration data for these halides with 1,2-disubstituted hydrogen bonding receptor **67.(BF$_4$)$_2$** (**Figure 3.12-iii**) indicated that the strength of binding was too strong to be quantified (K_A(Cl$^-$, Br$^-$) = >10^4 M^{-1}). Otherwise, 1:1 stoichiometric association constants were determined for all other anions with receptors **64.(BF$_4$)$_2$** and **65.(BF$_4$)$_2$** and with the exception of I$^-$ with **66.(BF$_4$)$_2$** (**Table 3.2**).

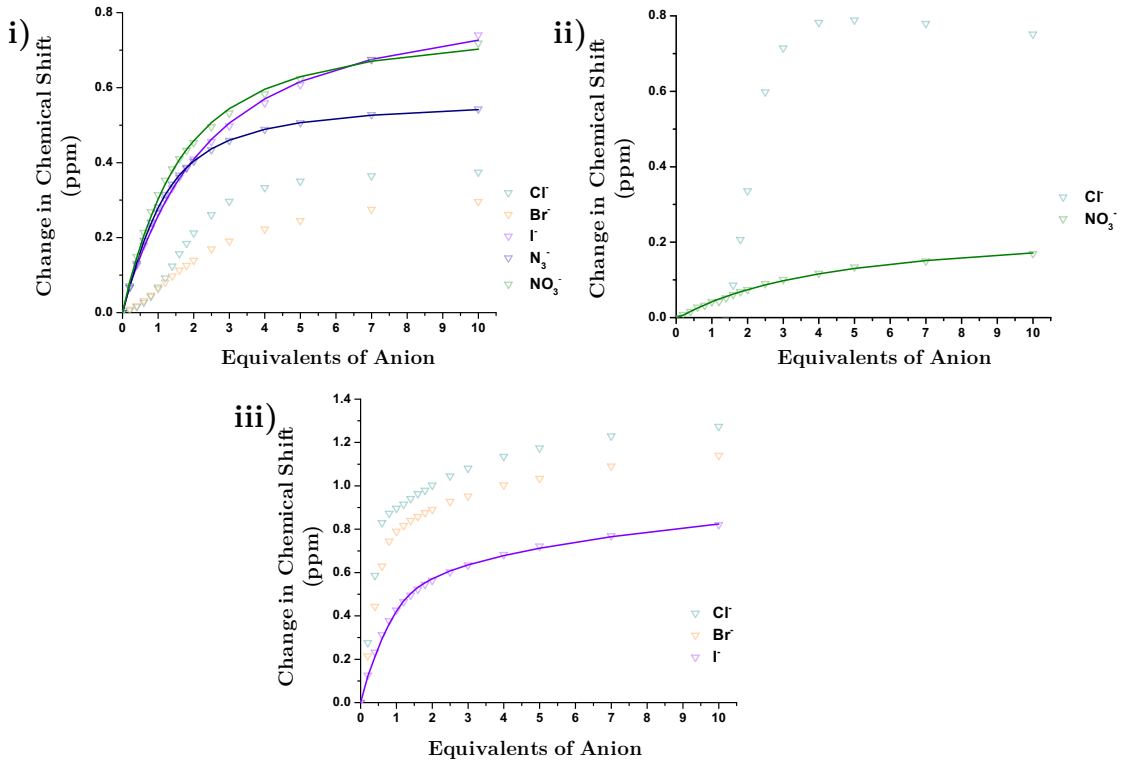


Figure 3.12 – Plots of the changes in chemical shift (ppm) *versus* equivalents of anion added for i) **65.$(BF_4)_2$** (monitoring proton **e**), ii) **66.$(BF_4)_2$** (monitoring amide resonance) and iii) **67.$(BF_4)_2$** (monitoring proton **d**) (d_3-MeCN, 298 K). Observed data (hollow triangles) and fitted isotherms (solid lines) are shown.

Table 3.2 – Association constants for receptors **65.$(BF_4)_2$**, **66.$(BF_4)_2$** and **67.$(BF_4)_2$** in d_3-MeCN. (a) *Anions added as their respective tetrabutylammonium (TBA) salts at 298K.* (b) *Anion association constants calculated using WinEQNMR2* [30] *using chemical shift data of triazolium proton resonances unless otherwise indicated,* ± *errors in parentheses.* (c) *Association constant obtained via monitoring of amide resonance* **c**. (d) *Titration data could not be fitted.* (e) *Precipitation occurred.* (f) *Decomposition occurred.*

Anion[a]	**65.$(BF_4)_2$**[b] K_a[M^{-1}]	**66.$(BF_4)_2$**[c] K_a[M^{-1}]	**67.$(BF_4)_2$**[b] K_a[M^{-1}]
Cl^-	-[d]	-[d]	$>10^4$
Br^-	-[d]	-[e]	$>10^4$
I^-	363(18)	-[e]	$k_1 = 4326(731)$ $k_2 = 40(30)$
NO_3^-	642(41)	351(9)	-[e]
N_3^-	1219(18)	-[f]	-[e]
AcO^-	-[d]	-[d]	-[d]

The weak anion association behaviour of **65.(BF$_4$)$_2$** and **66.(BF$_4$)$_2$** with the smaller anions Cl^- and Br^- indicates the receptors' 1,3-disubstituted phenyl binding cleft is not of a complementary size to favour binding; preferentially binding the larger I^- anion instead. By contrast, the corresponding 1,2-disubstituted hydrogen bonding receptor **67.(BF$_4$)$_2$** exhibited strong association with Cl^- and Br^- ($K_A(Cl^-, Br^-) > 10^4$ M^{-1}) within its smaller anion recognition cleft and relatively weaker complexation of I^-.

The strong association of linear N_3^- and trigonal planar NO_3^- with **65.(BF$_4$)$_2$** suggests the receptor's configuration is complementary to the geometry of these anions. The halogen bonding system **66.(BF$_4$)$_2$** exhibited weaker binding of NO_3^-, consistent with observed trends for oxoanion binding in analogous acyclic halogen bonding receptors.[31]

3.2.7. Summary

A series of six acyclic halogen and hydrogen bonding isomeric bis-amide-triazole receptors were successfully prepared. Halogen bonding bis-iodotriazole-amide receptor **55** exhibited a superior anion recognition profile in comparison to its hydrogen bonding counterpart **54**. In acetone-d_6, halides Cl^- and Br^- were bound almost two orders of magnitude more strongly by halogen bonding receptor **55** in comparison to the hydrogen bonding analogue **54**.

Despite the lack of anion recognition exhibited by neutral hydrogen and halogen bonding receptors **61** – **64**, conversion to their dicationic counterparts **65.(BF$_4$)$_2$** – **68.(BF$_4$)$_2$** enabled the effects of regioisomerism on the anion binding properties of this class of receptor to be examined. In particular, regioisomeric hydrogen bonding receptors **65.(BF$_4$)$_2$** and **67.(BF$_4$)$_2$** exhibited notable anion guest geometry and size preferences in anion recognition studies conducted in d_3-MeCN. Receptor **65.(BF$_4$)$_2$** preferentially bound trigonal planar NO_3^- and especially linear

N_3^-, whilst smaller spherical anions such as Cl^- and Br^- were bound strongly by receptor **67.$(BF_4)_2$**, which possesses a smaller, constrained anion binding cleft.

Unfortunately, halogen bonding receptors **66.$(BF_4)_2$** and **68.$(BF_4)_2$** were plagued by a combination of solubility issues in the former and lack of observable binding site protons in the latter, hindering the acquisition of a comprehensive set of titration data for the majority of anions studied.

3.3. Synthesis of halogen bonding macrocycles

3.3.1. Chloride anion templated synthesis of interlocked structures

A widely used methodology of anion templated interlocked structure synthesis is the chloride templated 'clipping' amide condensation. For example, the double amide condensation of bis-amine and bis-acid chloride macrocycle precursors can be conducted in the presence of a pyridinium-based axle component to form an [n]rotaxane (**Figure 3.10-i**)[32] or another pyridinium-based macrocycle to form an [n]catenane (**Figure 3.10-ii**).[33] Other bis-acid chlorides such as 4,4'-bis-(chlorocarbonyl)-2,2'-bipyridine can be used to install optical reporter groups for anion sensing such as that seen in Beer's permethylated β-cyclodextrin stoppered ruthenium(II)-bipyridyl appended halogen bonding [2]rotaxane receptor (**Figure 3.10-iii**).[34]

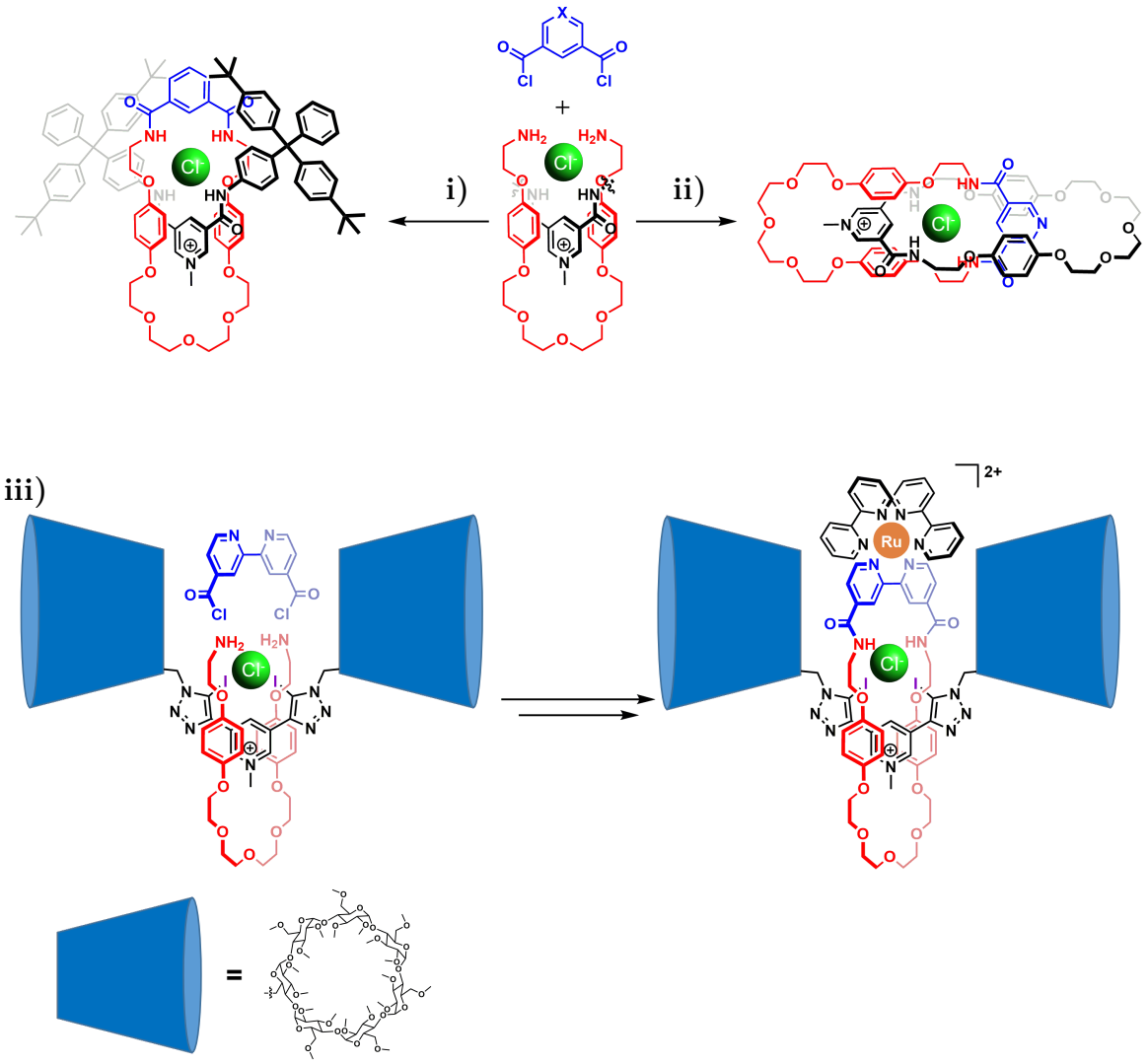


Figure 3.10 – Chloride anion templated acid chloride mediated clipping synthesis of Beer's i) [2]rotaxane, ii) [2]catenane and iii) β-cyclodextrin stoppered halogen bonding ruthenium(II) appended [2]rotaxane.

3.3.2. Chloride anion templated synthesis of halogen bonding macrocycles

It was envisoned that the previously prepared bis-carboxylic acid motifs **52** and **53** (**Scheme 3.4**) could ultimately be exploited in chloride anion templated 'clipping' synthesis of interlocked structures. Given the favourable anion recognition characteristics exhibited by halogen bonding receptor **55** (synthesized from bis carboxylic acid **53**), this methodology may permit the synthesis of interlocked structures containing this novel halogen bonding motif (**Figure 3.11**).

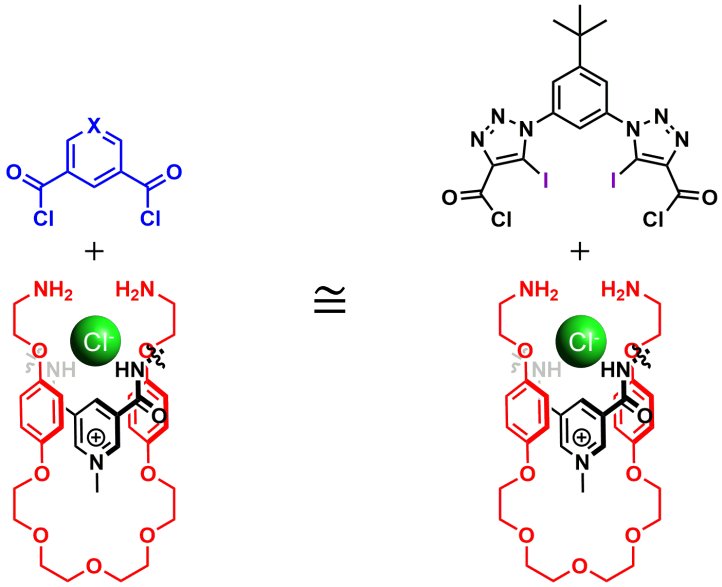
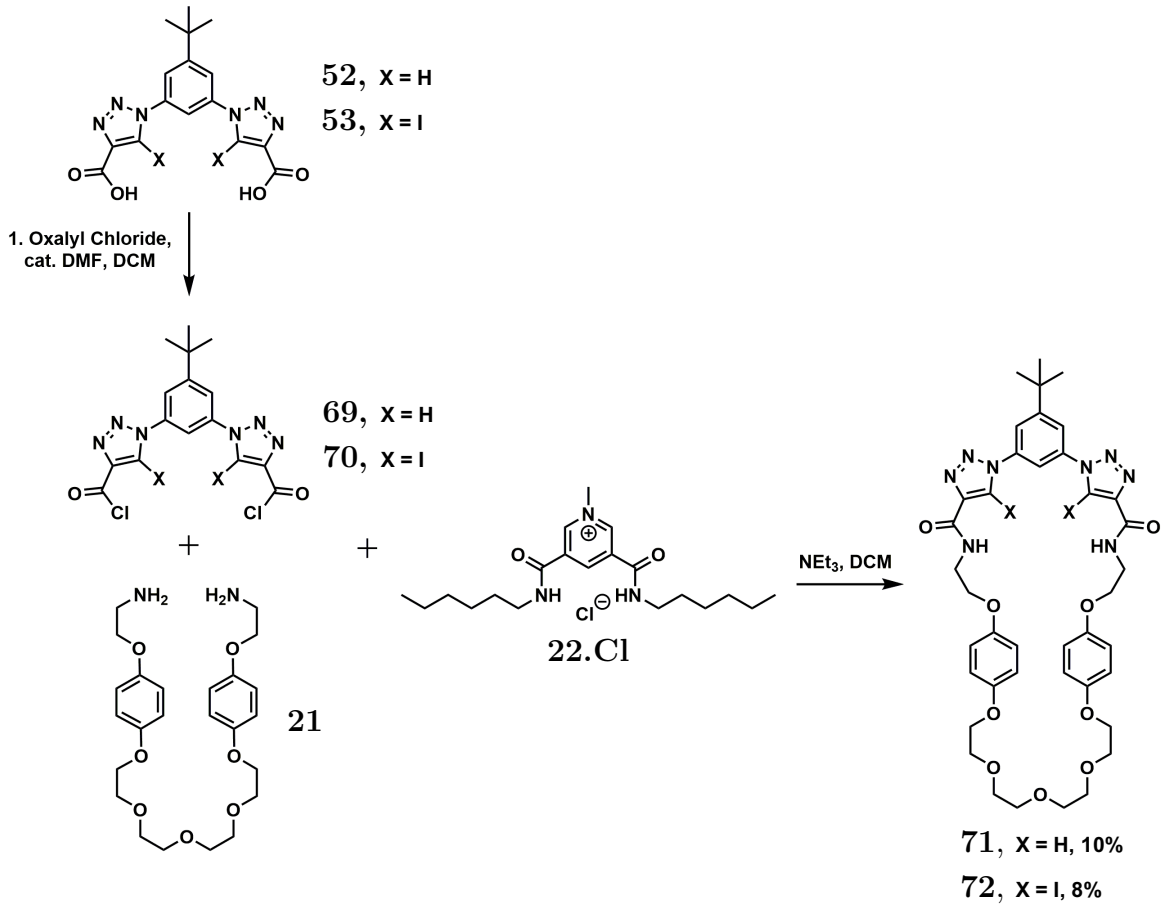


Figure 3.11 – Proposed adaptation of previously used chloride anion templated clipping protocols using the bis-acid chloride homologue of bis-iodotriazole bis-carboxylic acid **53**.

To explore this proposition, a preliminary chloride anion templated synthesis of a macrocycle homologous to halogen bonding receptor **55** was undertaken. Carboxylic acids **52** and **53** were reacted with oxalyl chloride and a catalytic amount of dry DMF in DCM to afford bis-acid chloride intermediates **69** and **70**. Adapting a literature procedure[32], **69** and **70** were immediately added to a DCM solution of macrocycle precursor bis-amine **21** in the presence of chloride template **22.Cl**, to afford hydrogen bonding macrocycle **71** and halogen bonding homologue **72** in isolated yields of 10% and 8% (**Scheme 3.8**). Macrocycles **71** and **72** were characterised by ^{1}H NMR, ^{13}C NMR and ESI-HRMS (**Figure 3.12** + **Figure 3.13**).



Scheme 3.8 – Synthesis of macrocycles **71** and **72**.

The yields obtained for both macrocycles were low when compared to reported yields of analogous macrocycles synthesised *via* this method, which are typically in the 30-50% range.[32] Repeating the macrocyclisation reactions using high dilution conditions in the absence of **22.Cl** template did not affect the isolated yields for both macrocycles.

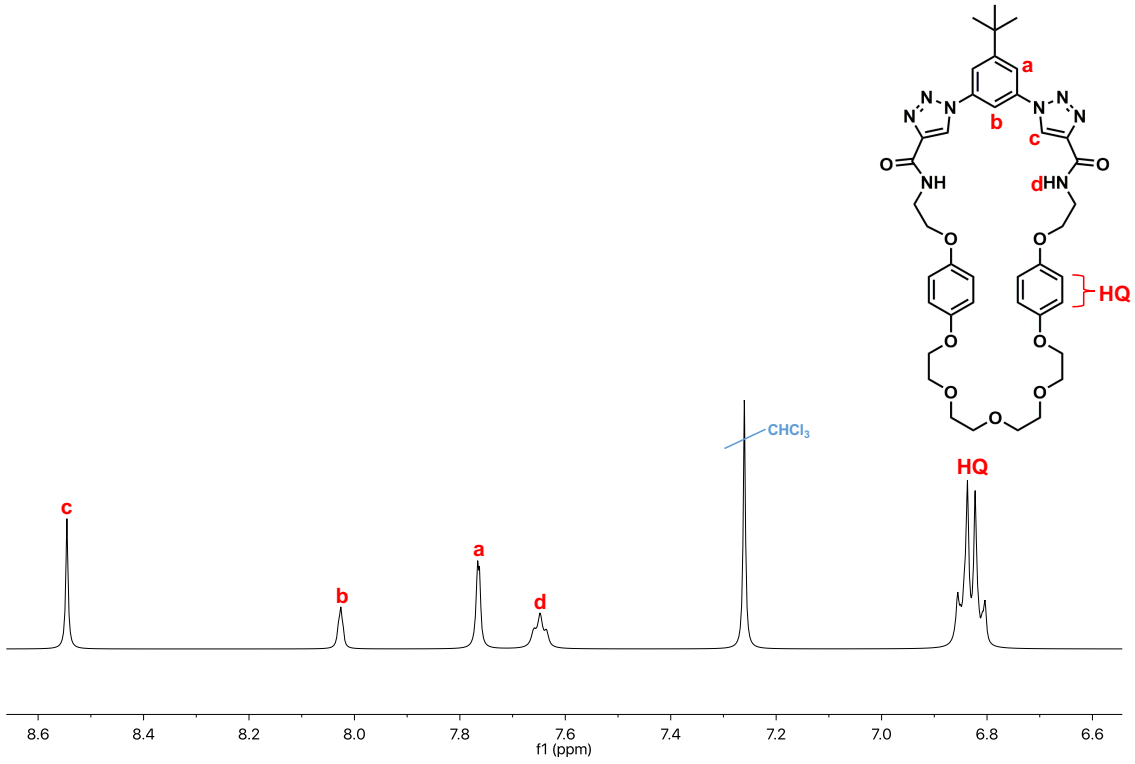


Figure 3.12 – Truncated ^{1}H NMR spectrum of macrocycle **71** ($CDCl_3$, 500 MHz, 298 K).

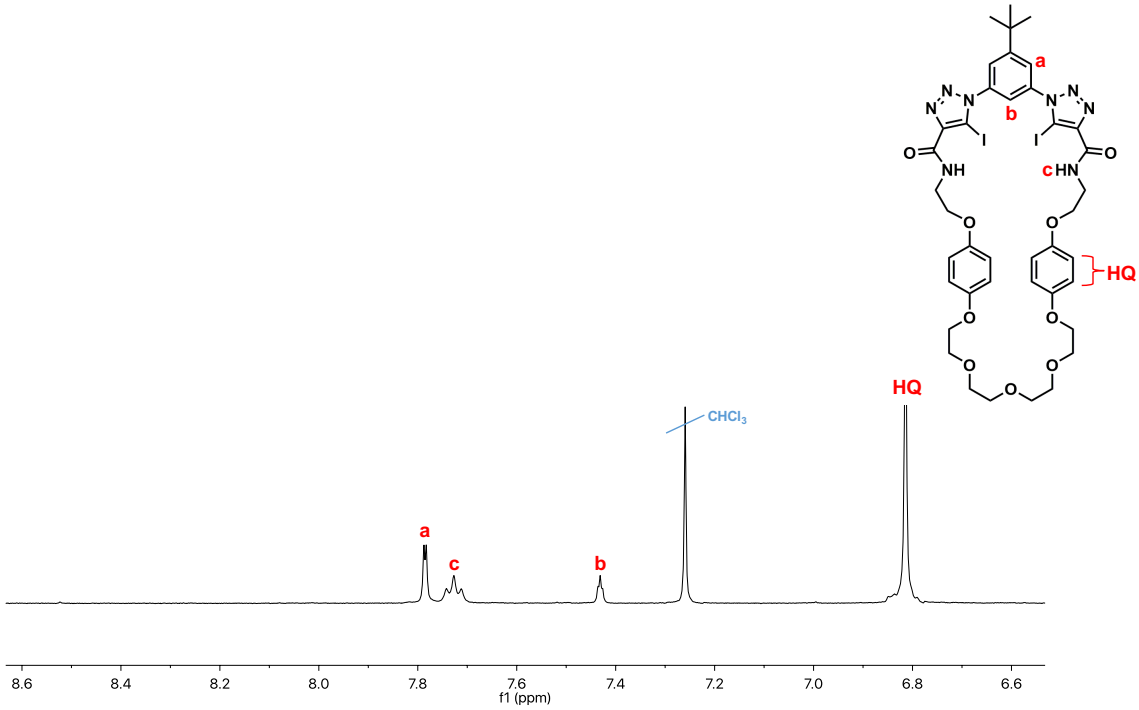
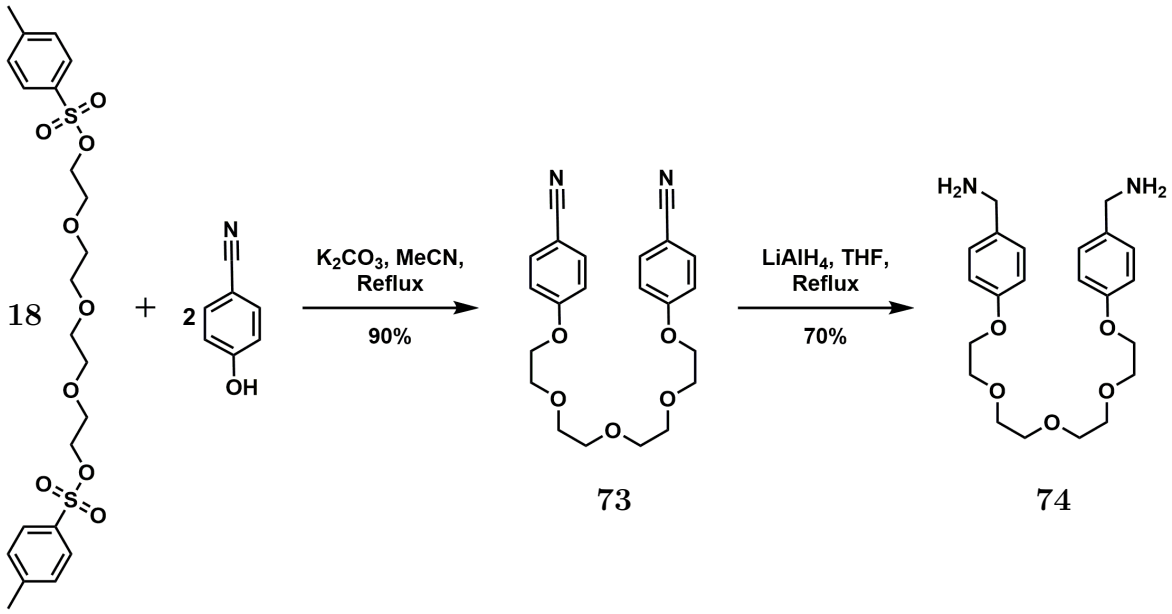


Figure 3.13 – Truncated ^{1}H NMR spectrum of macrocycle **72** ($CDCl_3$, 500 MHz, 298 K).

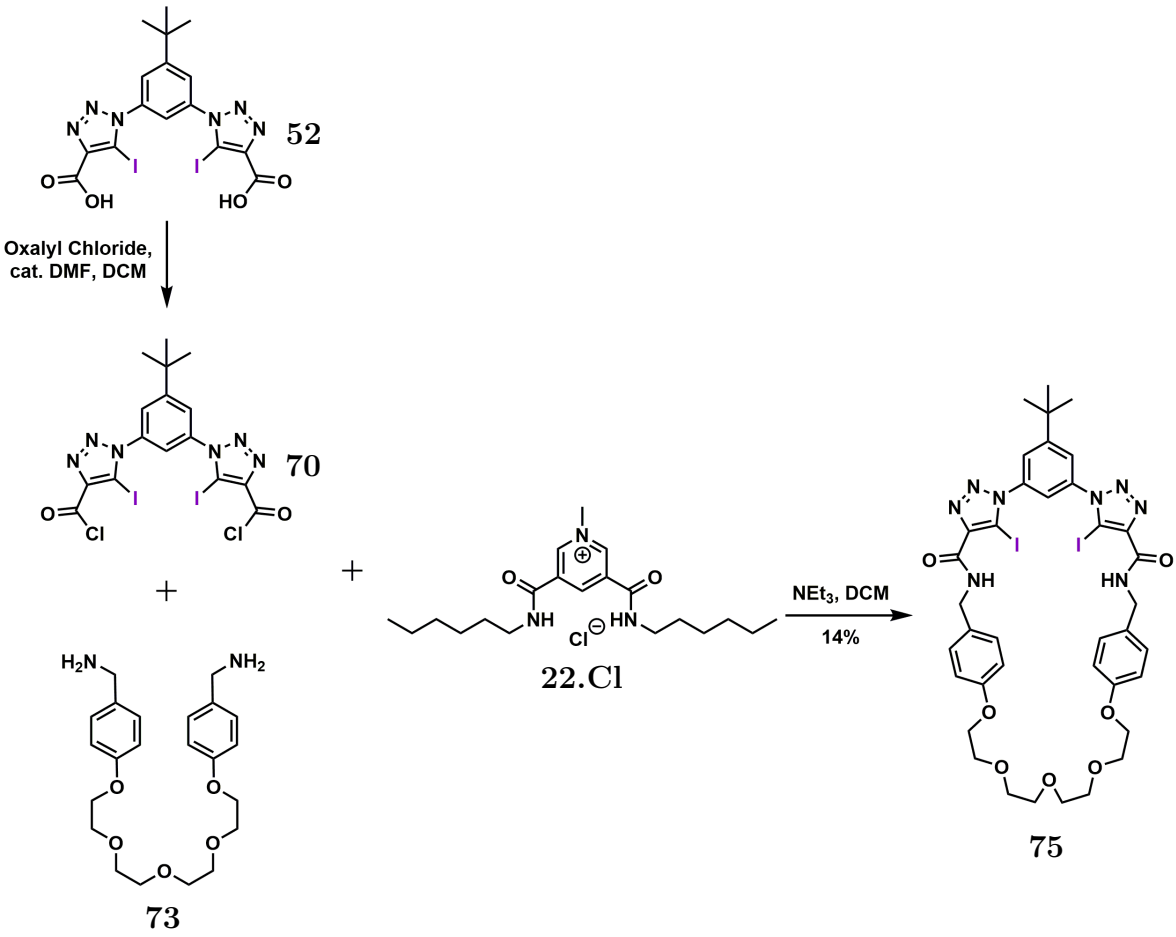
Given the larger annulus of macrocycles **71** and **72** in comparison to known isophthalamide/pyridine bis-amide based macrocycles (**Figure 3.10**), it was thought that the low yielding syntheses of the macrocycles could result from either i) entropic barriers to efficient cyclisation of the relatively large ring size macrocycles and/or ii) poor templation of the macrocycle precursors by **22.Cl**.

In efforts to combat the first possible factor, an analogous shorter macrocycle precursor bis-amine **74** was prepared (**Scheme 3.9**). Two equivalents of commercially available 4-cyanophenol was reacted with tetraethylene glycol di-tosylate **18** to afford bis-nitrile **73** in a 90% yield, which upon reduction with $LiAlH_4$ in THF gave bis-amine **74** in a 70% yield.



Scheme 3.9 – Synthesis of shorter bis-amine polyether macrocycle precursor **74**.

Bis-amine **74** was reacted with the bis-iodotriazole bis-acid chloride **70** in the presence of **22.Cl** template in DCM to give smaller macrocycle bis-iodotriazole-amide **75** in a slightly improved yield of 14% (**Scheme 3.10**). **75** was characterised by ^{1}H NMR, ^{13}C NMR and ESI-HRMS (**Figure 3.15**).



Scheme 3.10 – Synthesis of macrocycle **75**.

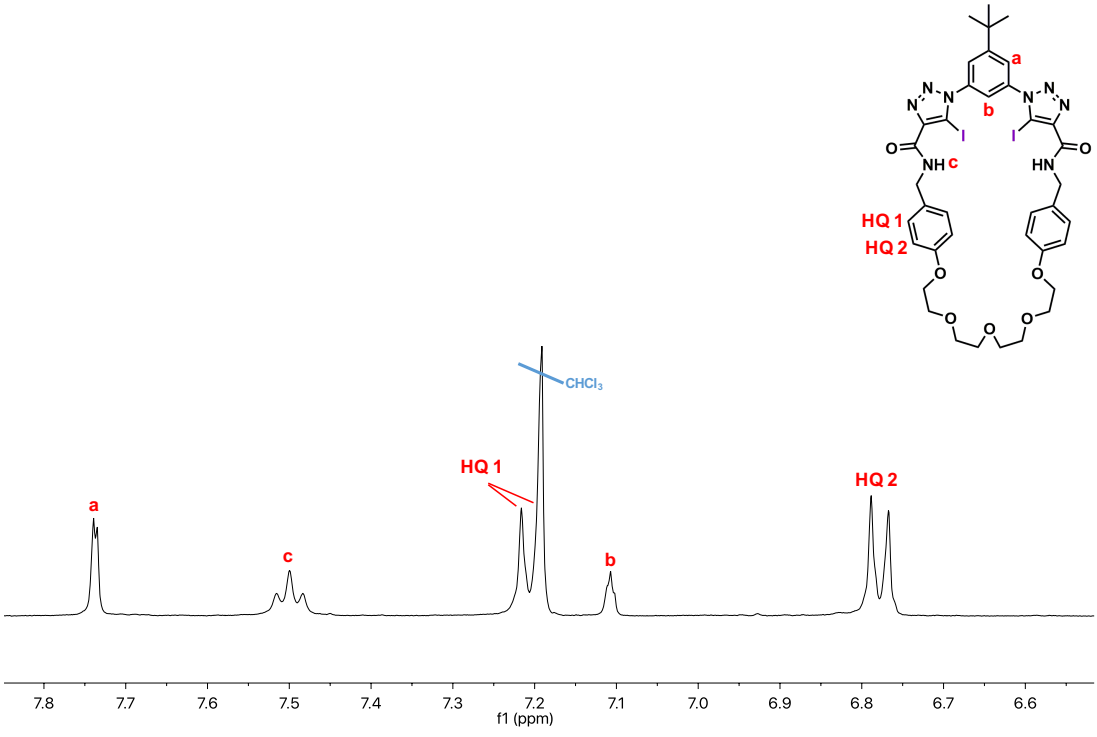


Figure 3.15 – Truncated ^{1}H NMR spectrum of macrocycle **75** ($CDCl_3$, 400 MHz, 298 K).

3.3.3. Pseudorotaxane studies

Qualitative ^{1}H NMR chloride anion templated threading studies were conducted to investigate the association between halogen bonding macrocycles **72** and **75** with templating agent **22.Cl**. Upon addition of one equivalent of **22.Cl** to a $CDCl_3$ solution of macrocycle **72,** no evidence of aromatic donor-acceptor interaction induced splitting of the hydroquinone resonance (**HQ**) was observed. Additionally, no shifts of macrocycle phenyl **b** or amide **c** protons were observed. Modest upfield shifts of thread protons 2 and 3 ($\Delta\delta$(ppm) = -0.02) were only seen between the macrocycle **72** and thread **22.Cl**, which may explain the poor macrocyclisation yields (**Figure 3.16**).

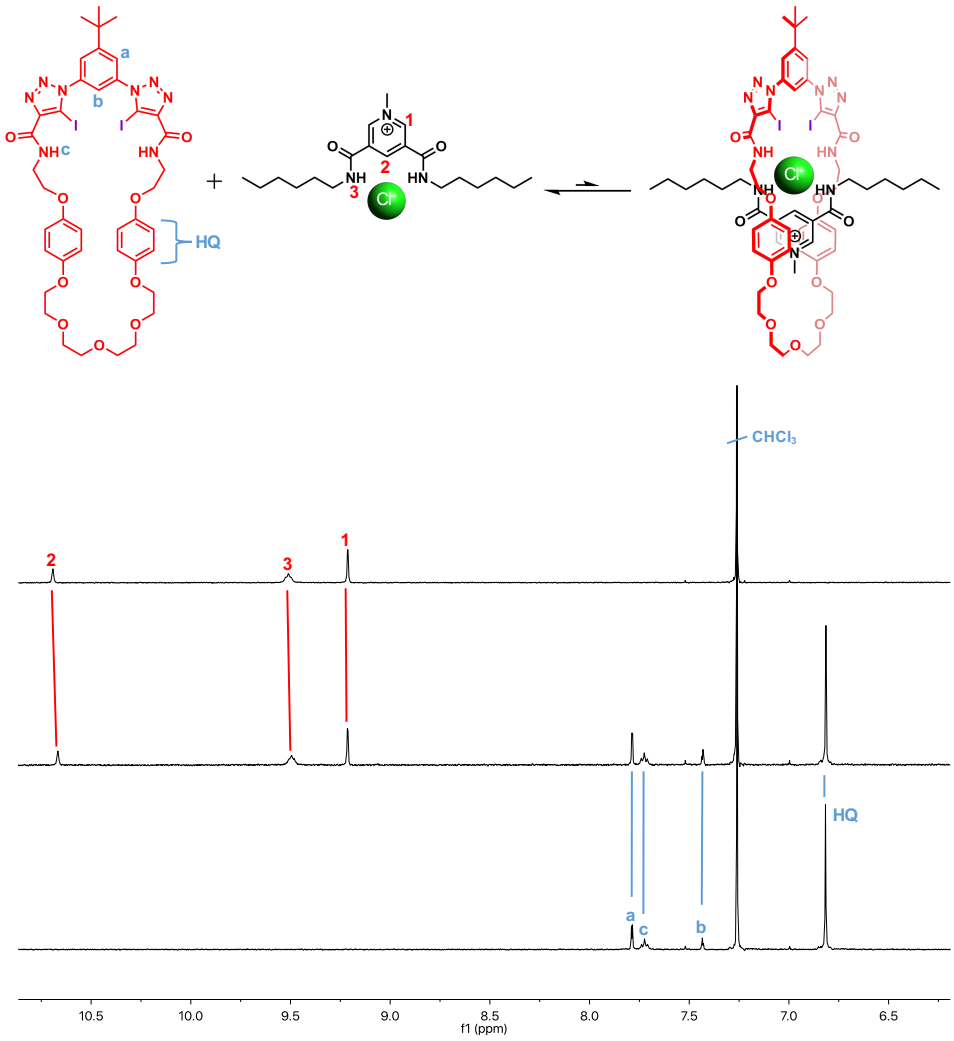


Figure 3.16 – Truncated ^{1}H NMR spectra of i) **22.Cl**, ii) 1:1 **22.Cl** and **72**, iii) **72** ($CDCl_3$, 400 MHz, 298 K).

An equimolar mixture of **22.Cl** and smaller macrocycle **75** led to slightly increased upfield shifts of thread protons 2 ($\Delta\delta$(ppm) = -0.12) and 3 ($\Delta\delta$(ppm) = -0.07), however, the hydroquinone environments were not perturbed, indicating that the smaller macrocycle **75** does not form a pseudorotaxane assembly with **22.Cl** (**Figure 3.17**).

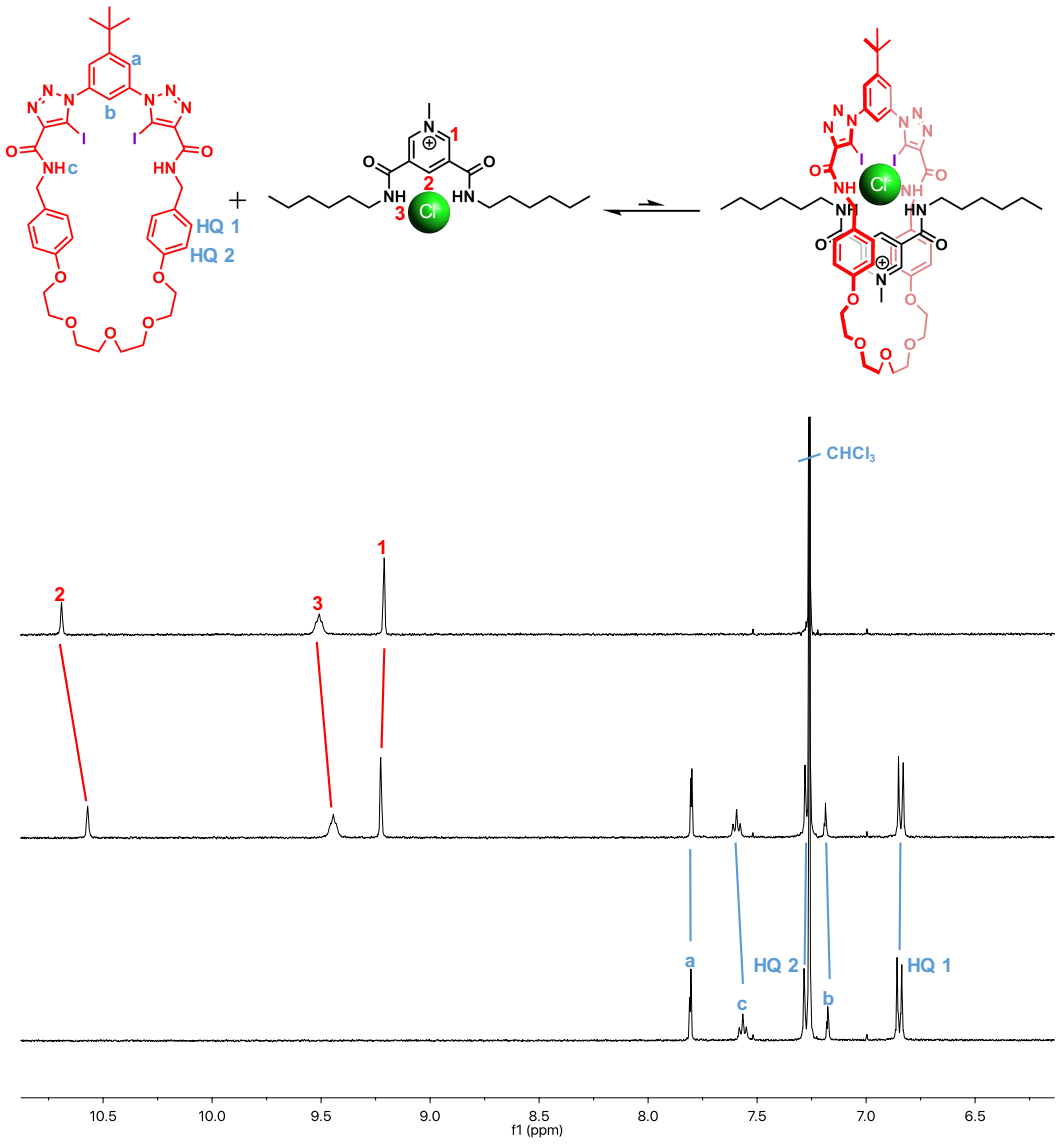


Figure 3.17 – Truncated ^{1}H NMR spectra of i) **22.Cl**, ii) 1:1 **22.Cl** and **75**, iii) **75** ($CDCl_3$, 400 MHz, 298 K).

3.3.4. Summary

Novel bis-triazole-amide and two halogen bonding bis-iodotriazole-amide macrocycles were isolated in modest yields from acid chloride amine condensation reactions. The low cyclisation yields can be attributed to the inability of the potential templating agent **22.Cl** to form a stable pseudorotaxane assembly with the halogen bonding macrocycles **72** and **75**, as evidenced by ^{1}H NMR studies. This suggests the pyridinium bis-amide chloride motif is not a suitable templating reagent for the synthesis of a bis-triazole-amide containing macrocyclic component of an interlocked structure.

3.4. Synthesis of a [3]Rotaxane Anion Host System

3.4.1. Higher order [3]rotaxane structures for anion recognition

Anion recognition within the unique three dimensional, two component cavity of interlocked structures such as [2]rotaxanes[35–38] and [2]catenanes[26,39–41] has been well documented with both halogen and hydrogen bonding regimes in competitive solvent media. However, the use of higher order interlocked structures such as [3]rotaxanes for anion recognition is relatively under-explored. Two examples of pyridinium bis-amide axle containing [3]rotaxanes, one possessing a redox active ferrocene spacer motif[42] and the other incorporating a naphthalene fluorophore[43], have demonstrated respective electrochemical and optical sensing of sulphate in aqueous media *via* the formation of 1:1 stoichiometric host-guest 'sandwich' complexes of the oxoanion between both pyridinium interlocked cavities (**Figure 3.18**).

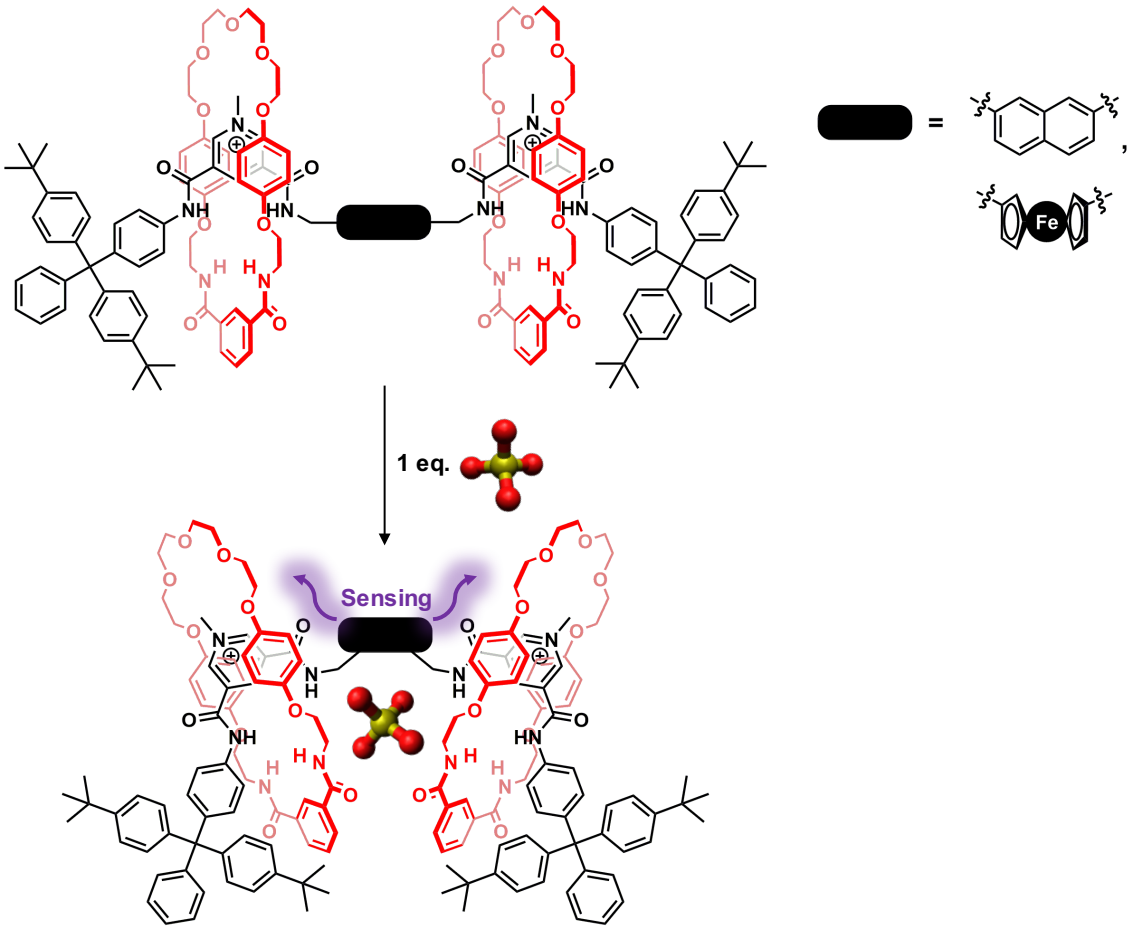


Figure 3.18 Beer's naphthalene and ferrocene containing [3]rotaxane anion sensors demonstrating the 1:1 host-guest "sandwich" recognition of sulphate between both pyridinium interlocked cavities.

3.4.2. [3]Rotaxane design

It was envisaged that a hydrogen or halogen bonding axle component based on the 1,3-bis-amide-triazolium and 1,3-bis-amide-iodotriazolium motifs (**Scheme 3.7**), would possibly be large enough to thread two macrocyclic components, to produce a novel [3]rotaxane host capable of displaying 'sandwich' anion recognition in competitive solvent mixtures.

The synthesis of the target [3]rotaxanes could be realised *via* initial preparation of a phenylene 1,3-bis-amide-triazolium containing axle component

stoppered at both ends by bulky terphenyl groups. A double chloride anion templated Grubbs' catalysed RCM synthetic strategy with two equivalents of bis-vinyl nitro-isophthalamide macrocycle precursor derivative would afford the desired hydrogen and halogen bonding [3]rotaxane structures depicted in **Figure 3.19**.

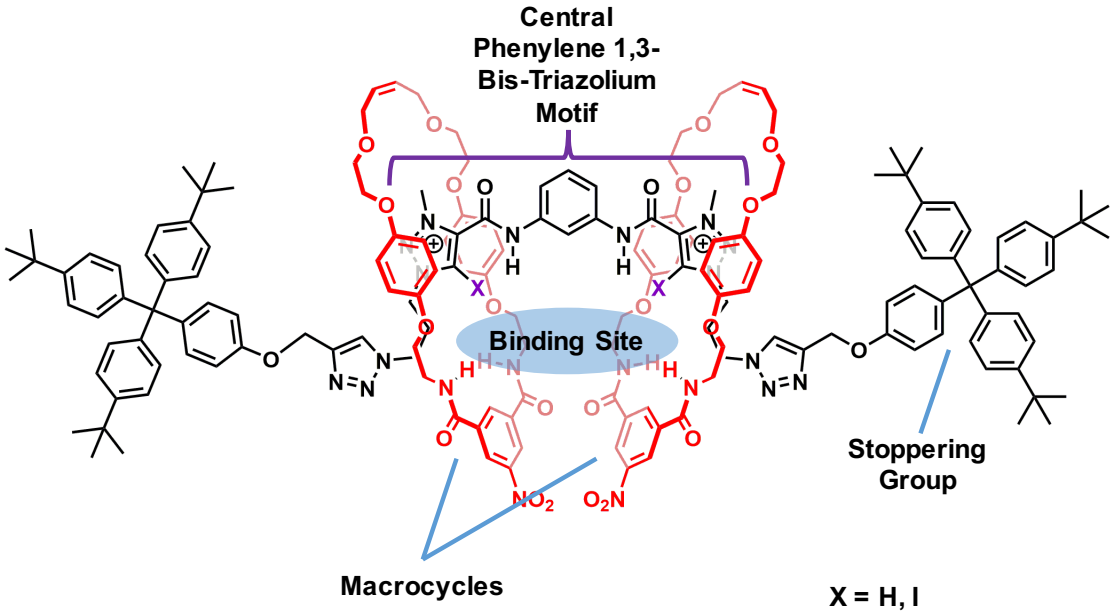


Figure 3.19 – Structures of the target hydrogen bonding (X = H) and halogen bonding (X = I) [3]rotaxanes.

3.4.3. Pseudorotaxane studies

To establish the feasibility of the synthesis of such an anion templated, higher order interlocked structure incorporating the phenylene 1,3-bis-triazolium motif, preliminary chloride anion templated pseudorotaxane threading studies were conducted with the hydrogen bonding thread **65.**$(BF_4)_2$, halogen bonding thread **66.**$(BF_4)_2$ and macrocycle **23** in acetone-d_6.

Addition of one equivalent of TBACl to an equimolar mixture of **65.**$(BF_4)_2$ and macrocycle **23** resulted in an upfield shift accompanied by splitting of the hydroquinone resonance (**HQ**) of macrocycle **23** ($\Delta\delta$(ppm) = -0.14), indicating aromatic donor-acceptor interactions between the macrocycle and the interpenetrated triazolium loci of $\mathbf{65}^{2+}$. Downfield shifts of amide proton **d** were also

observed in thread **65.(BF$_4$)$_2$**, indicative of hydrogen bonding to the Cl$^-$ template (**Figure 3.20**).

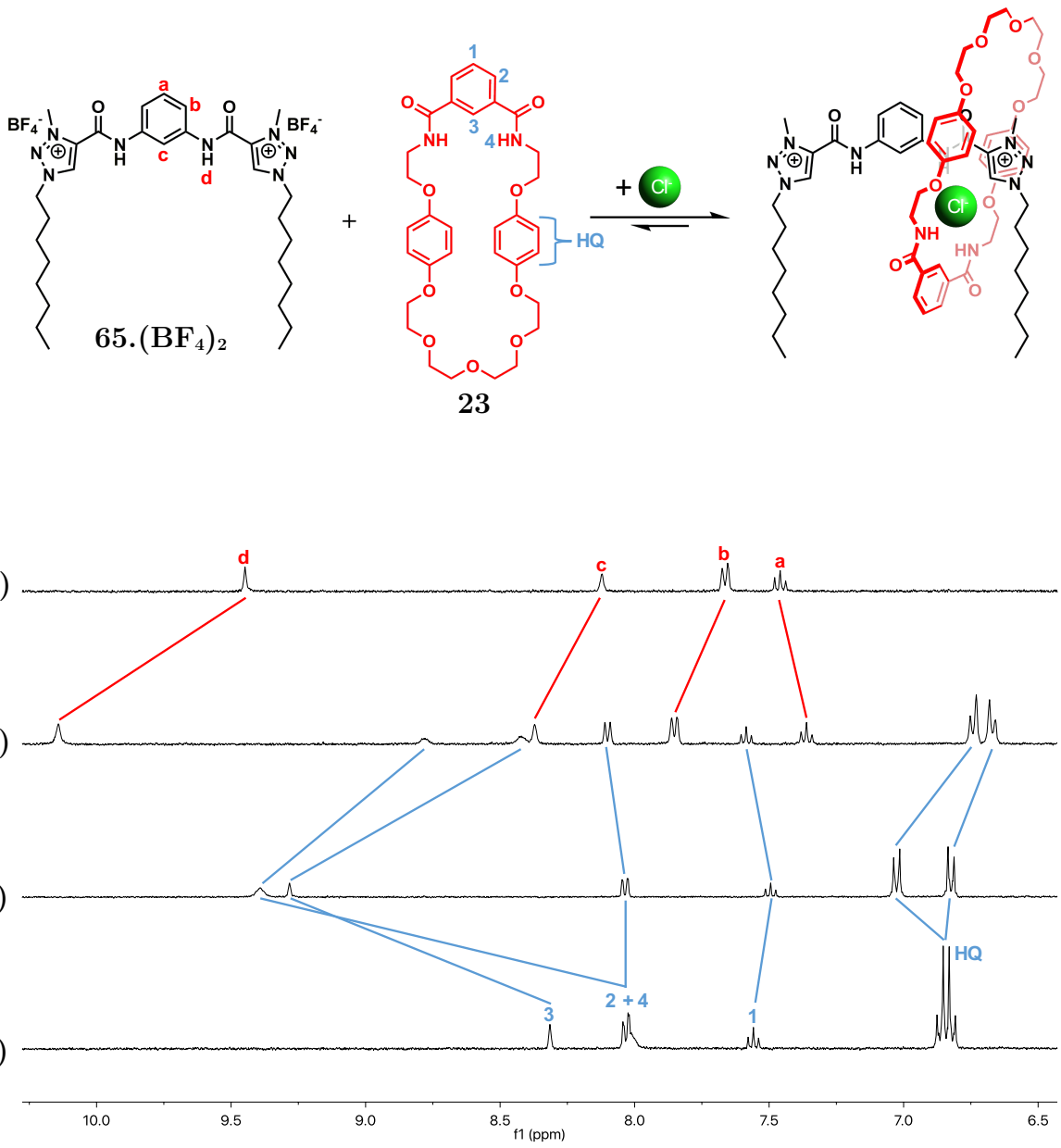


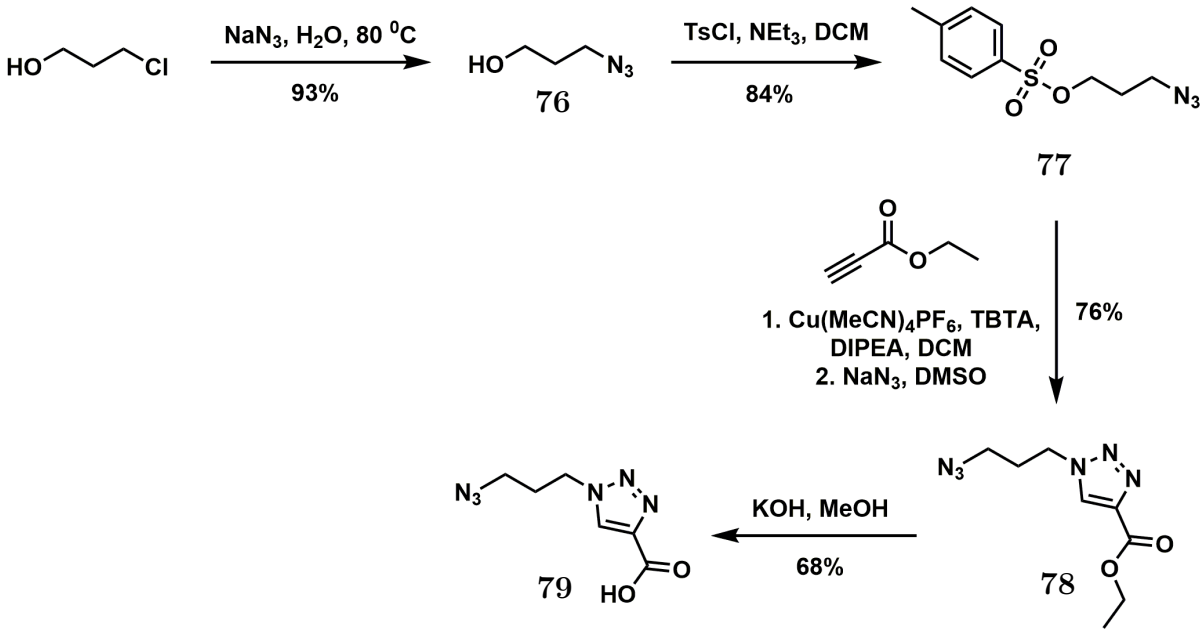
Figure 3.20 – Truncated ^{1}H NMR spectra of i) Thread **65.(BF$_4$)$_2$**, ii) **65.(BF$_4$)$_2$** + **23** + 1 eq. TBACl iii) **23** + 1 eq. TBACl, iv) **23** (acetone-d_6, 400 MHz, 298 K).

Analogous ^{1}H NMR threading studies conducted with halogen bonding counterpart **66.(BF$_4$)$_2$** were met with solubility issues. Upon addition of one equivalent of

TBACl to an equimolar mixture of **66.$(BF_4)_2$** and macrocycle **23** in acetone-d_6 and $CDCl_3$ ensued immediate precipitation.

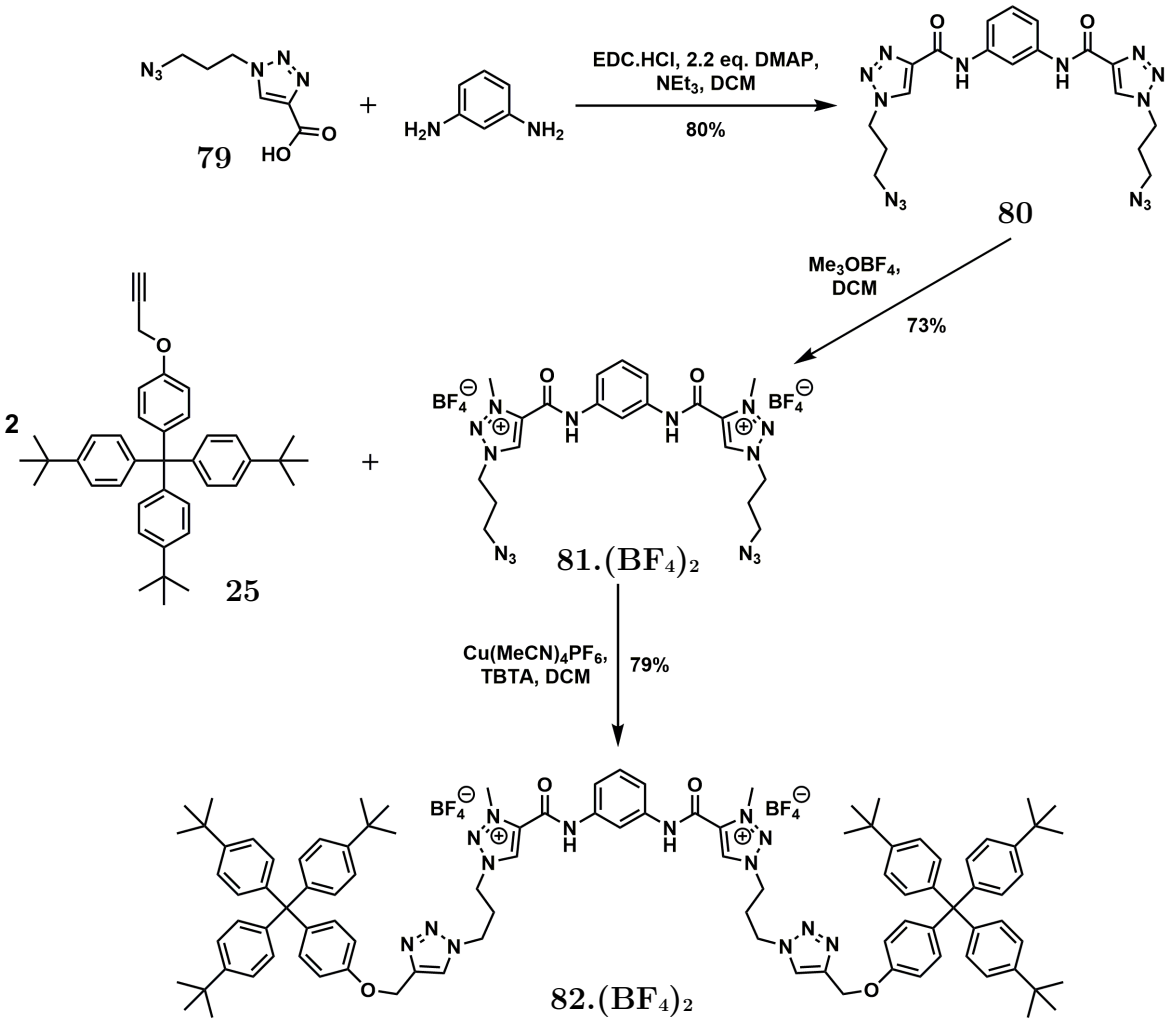
3.4.4 [3]Rotaxane synthesis

The promising chloride anion templated pseudorotaxane association observed between **65.$(BF_4)_2$** and macrocycle **23** prompted the synthesis of a bis-amide-triazolium axle component containing triazole linked terphenyl stopper groups. 3-Chloropropan-1-ol was converted to azide **76**[44] using NaN_3 in H_2O in a 93% yield and treated with TsCl in DCM in the presence of NEt_3 to give azidopropyl tosylate **77**[45] in a 84% yield. A CuAAC 'click' reaction between **77** and ethyl propiolate in the presence of $Cu(MeCN)_4PF_6$, TBTA and DIPEA afforded a tosyl-propyl triazole ethyl ester intermediate which was subsequently converted to ethyl ester azide **78** in a 76% overall yield. Basic hydrolysis in KOH/MeOH gave triazole carboxylic acid azide derivative **79** in a 68% yield (**Scheme 3.11**).



Scheme 3.11 – Synthesis of triazole carboxylic acid azide **79**.

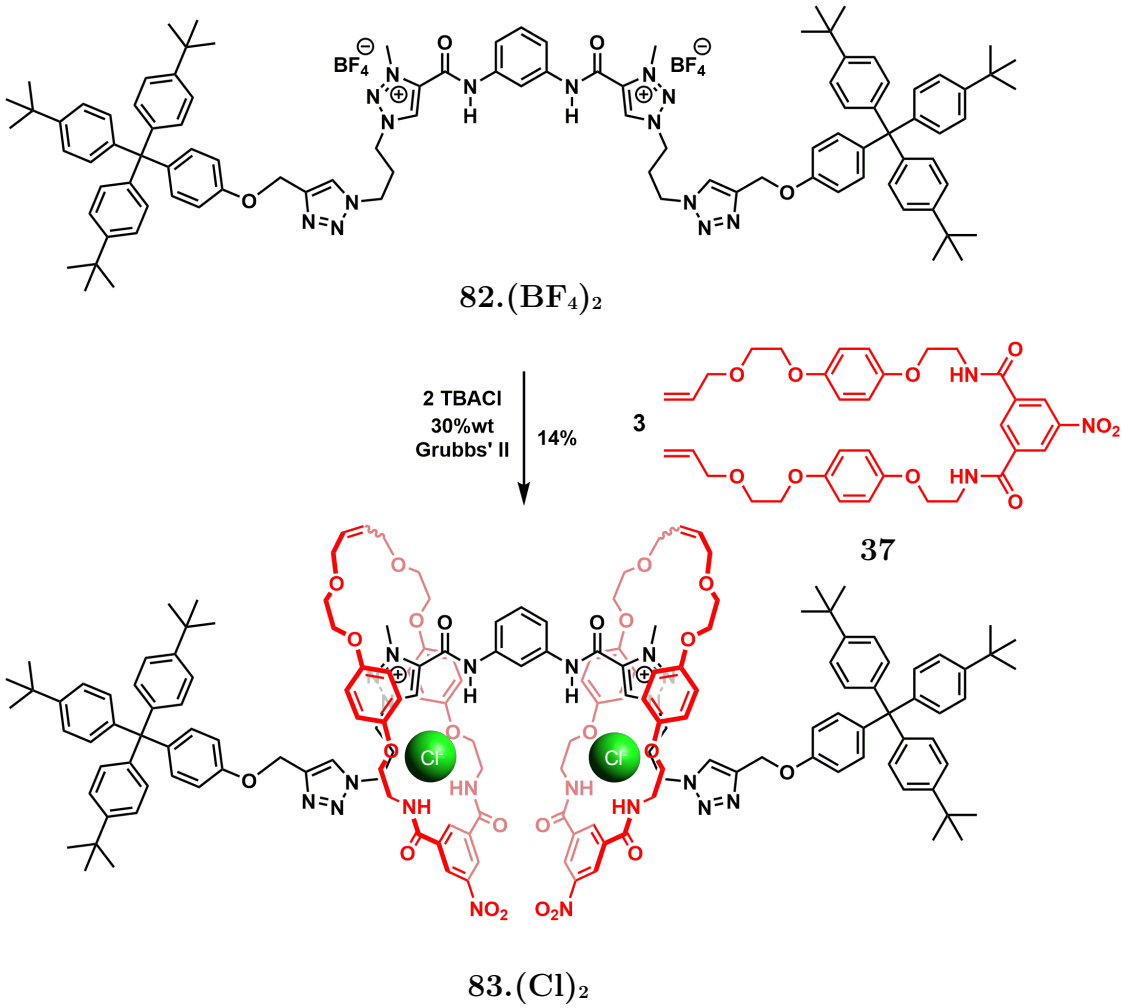
EDC.HCl-mediated amide condensation between 2.2 equivalents of **79** and *meta*-phenylene diamine in the presence of excess DMAP gave bis-amide-triazole bis-azide **80** in an 80% yield. Methylation with trimethyloxonium tetrafluoroborate afforded bis-triazolium bis-azide axle precursor **81.$(BF_4)_2$** in a 73% yield. Just over two equivalents of stopper alkyne **25** was reacted with bis-azide **81.$(BF_4)_2$** using CuAAC conditions in de-oxygenated DCM to afford axle component **82.$(BF_4)_2$** in a 79% yield (**Scheme 3.12**).



Scheme 3.12 – The synthesis of bis-amide-triazolium containing stoppered axle **82.$(BF_4)_2$**.

[3]Rotaxane synthesis was achieved *via* a double Grubbs' II catalysed (30%wt) RCM clipping reaction with three equivalents of bis-vinyl appended nitro-iosphthalamide

macrocycle precursor **37**[35], one equivalent of axle **82.(BF$_4$)$_2$** and two equivalents of TBACl (**Scheme 3.13**). Target hydrogen bonding [3]rotaxane **83.(Cl)$_2$** was obtained in a yield of 14% after purification *via* preparative TLC and characterised by ^{1}H NMR, ^{13}C NMR and ESI-HRMS.



Scheme 3.13 – Grubbs' 2nd generation catalysed, double ring closing metathesis clipping synthesis of [3]rotaxane **83.(Cl)$_2$**.

The product exhibited a peak by ESI-HRMS analysis, m/z = 1410.7051 ([**M**$^{2+}$]) corresponding to the doubly interlocked, dicationic structure. The ^{1}H NMR spectrum of **83.(Cl)$_2$** in 1:1 d_3-MeCN/$CDCl_3$ revealed several features diagnostic of a [3]rotaxane structure. Integration of the macrocycle hydroquinone resonances

(**HQ**) corresponded to an interlocked structure containing two macrocyclic components. These resonances were shifted upfield as a result of aromatic donor-acceptor interactions between the macrocycles and axle triazolium groups. Large downfield shifts were observed for axle triazolium and amide protons **d** and **e** and macrocycle protons 2 and 3, indicative of hydrogen bonding to the chloride anion templates (**Figure 3.21**).

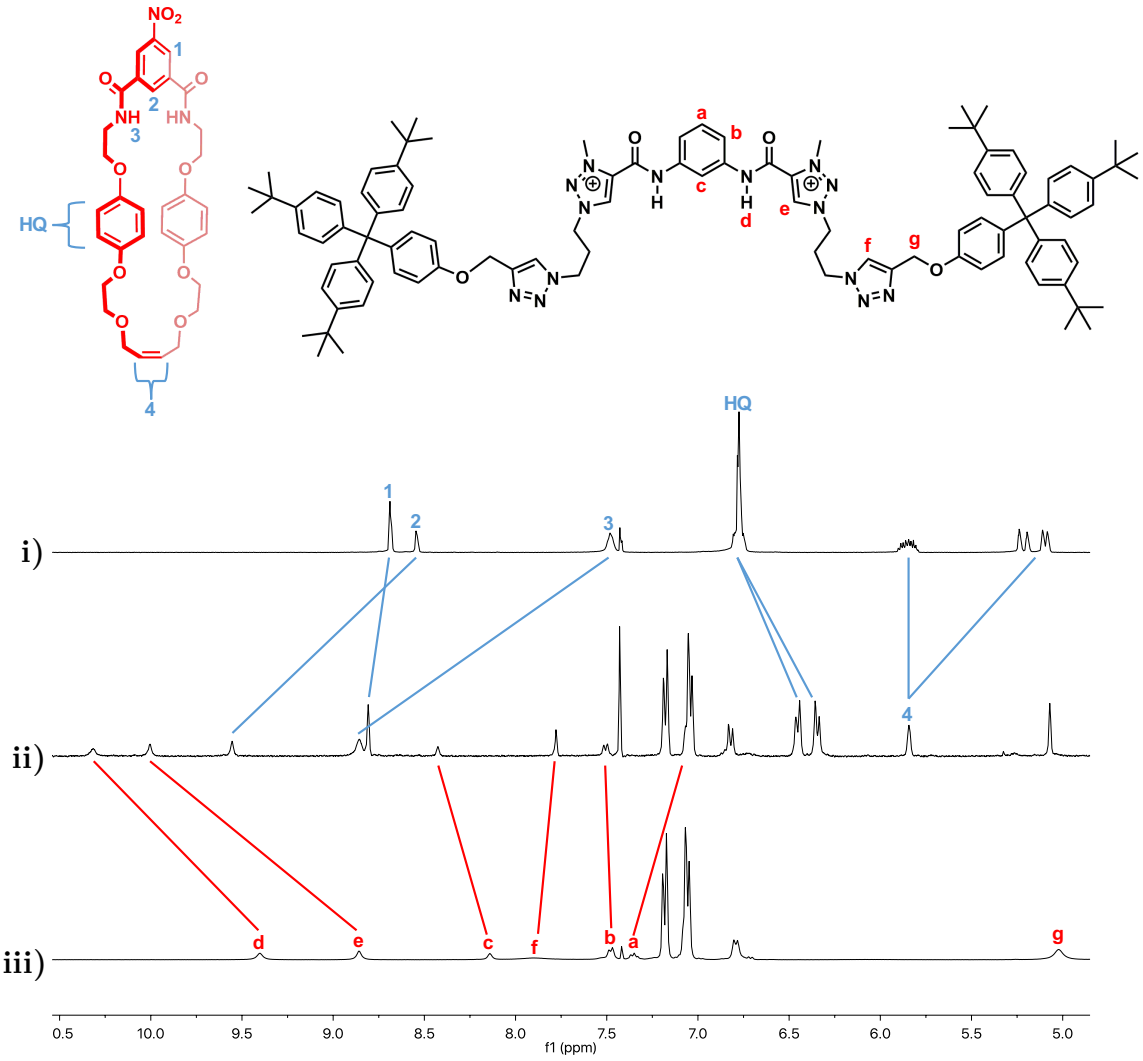


Figure 3.21 – Truncated ^{1}H NMR spectra i) bis-vinyl macrocycle precursor **37**, ii) [3]rotaxane **83.(Cl)$_2$** and iii) axle **82.(Cl)$_2$** (1:1 $CDCl_3$/CD_3CN, 400 MHz, 298 K).

Removal of the chloride anion templates from the interlocked cavities of the [3]rotaxane was achieved *via* anion exchange to non-coordinating PF_6^- by passing **83.(Cl)$_2$** down a Amberlite® column (PF_6^- form) in 45:45:10 $CHCl_3$/MeOH/H_2O

solvent mixture. The interlocked nature of [3]rotaxane **83.(PF$_6$)$_2$** was confirmed *via* a ^{1}H-^{1}H NMR ROESY spectrum. Crosspeaks were observed between the hydroquinone resonances (**HQ**) and axle protons **b**, **c**, **h**, **f** and **g** (**Figure 3.22**).

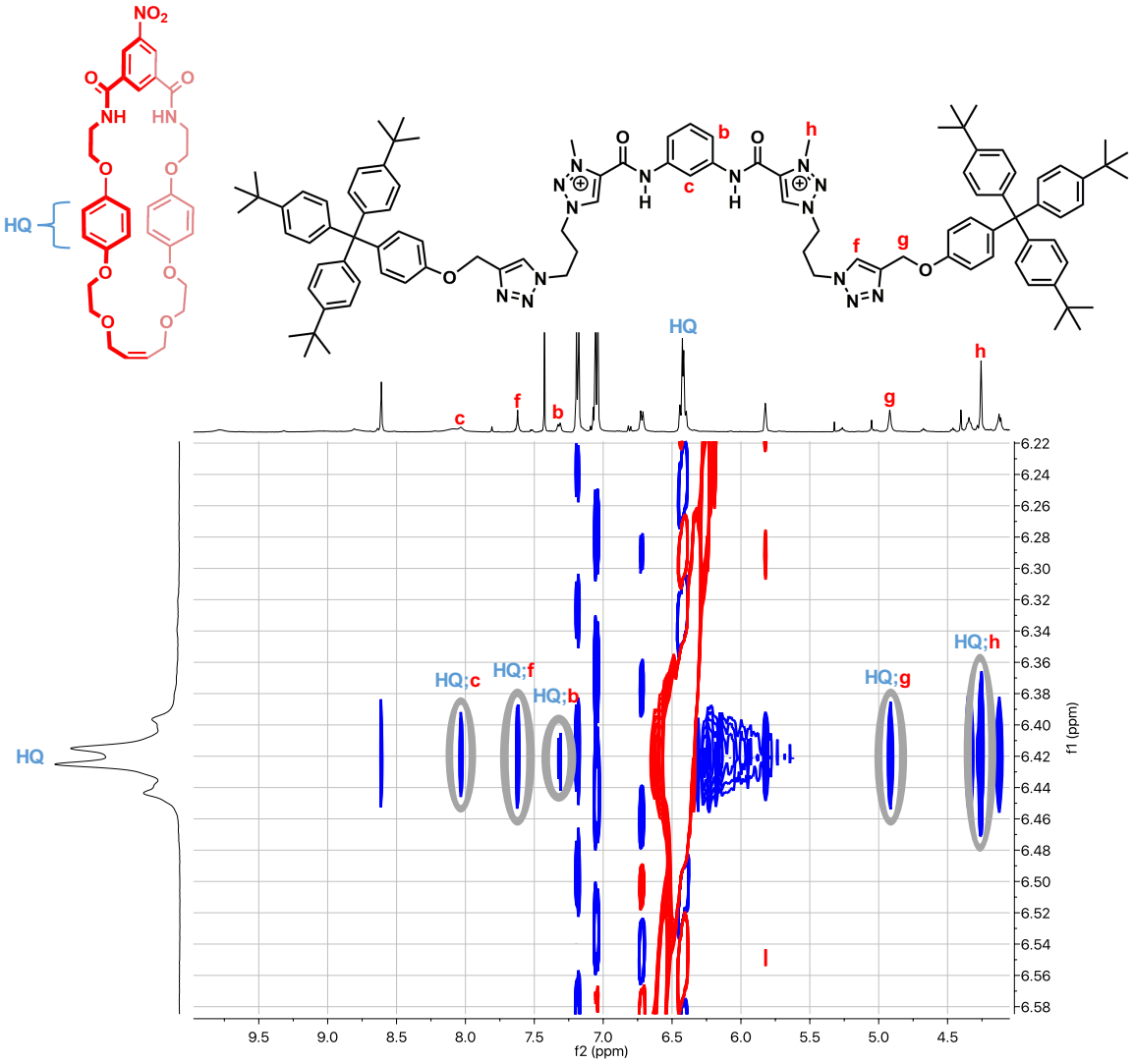


Figure 3.22 – Truncated ^{1}H NMR ROESY spectrum of [3]rotaxane **83.(PF$_6$)$_2$**, through-space proton-proton correlations between axle protons **b**, **c**, **f**, **g** and **h** and macrocyclic hydroquinone resonance **HQ**, indicated by grey ovals (1:1 $CDCl_3$/CD_3CN, 500 MHz, 298 K).

3.4.5 Anion binding studies

^{1}H NMR titration experiments with [3]rotaxane **83.(PF$_6$)$_2$** and a variety of anions were conducted in 1:1 $CDCl_3/CD_3OD$. The addition of TBACl to [3]rotaxane **83.(PF$_6$)$_2$** resulted in small downfield perturbations of the [3]rotaxane's internal macrocycle proton 2 and axle protons **a** and **e**, indicative of inclusion of a chloride anion within each of the amide-triazolium interlocked cavities (**Figure 3.23**).

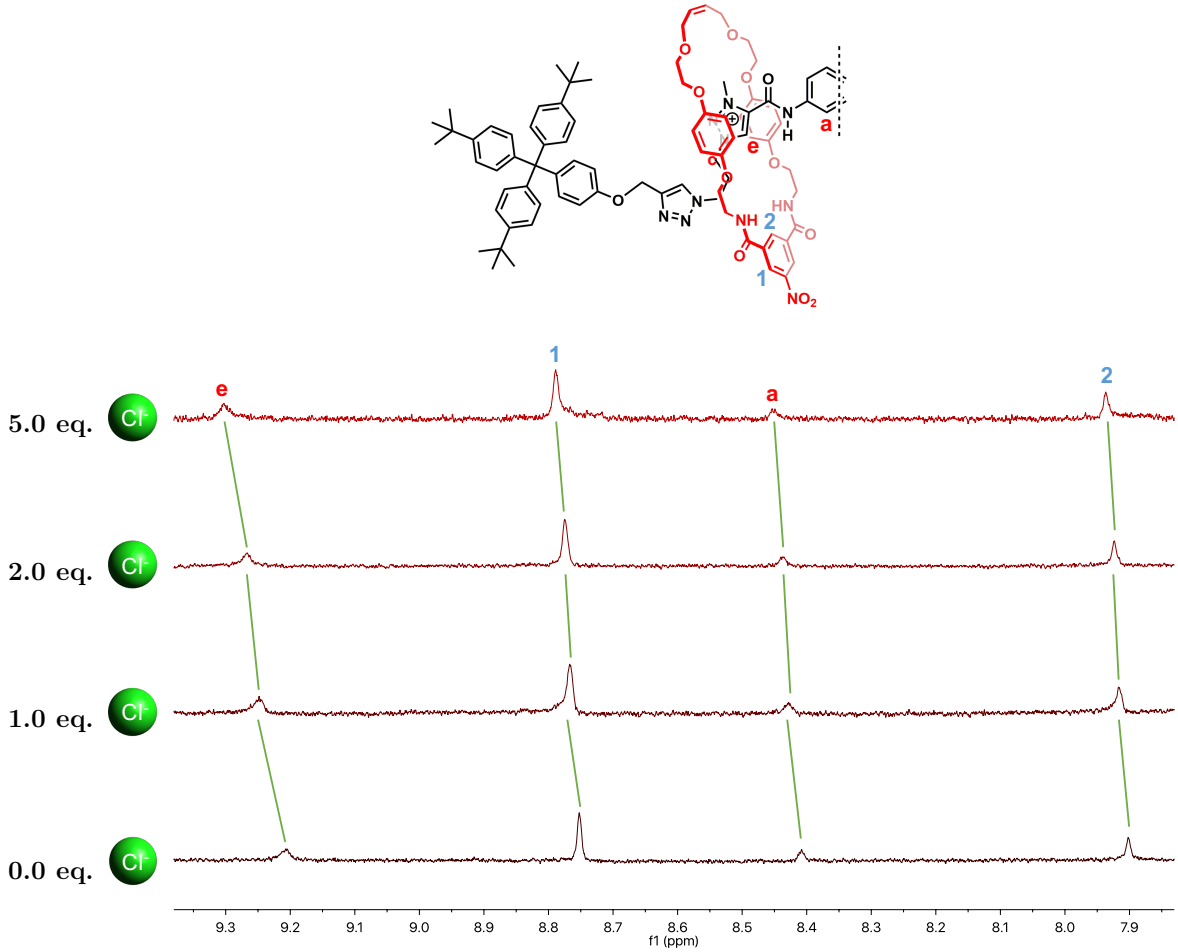


Figure 3.23 – Changes in the ^{1}H NMR spectrum with addition of increasing equivalents of TBACl to rotaxane **83.(PF$_6$)$_2$** (1:1 $CDCl_3/CD_3OD$, 500 MHz, 298 K).

In contrast, small upfield shifts ($\Delta\delta$(ppm) ≤ -0.05) of these resonances were observed upon addition of N_3^- and NO_3^- (**Figure 3.24**). Upon titration of one equivalent of $H_2PO_4^-$, large upfield shifts were observed for axle proton **a** ($\Delta\delta$(ppm) = -0.25) and internal macrocycle proton 2 ($\Delta\delta$(ppm) = -0.1), accompanied by a concomitant

downfield shift of triazolium proton **e** ($\Delta\delta$(ppm) = 0.08) (**Figure 3.24**). After the addition of two equivalents $H_2PO_4^-$, the shifts attenuated indicative of strong binding of the tetrahedral oxoanion.

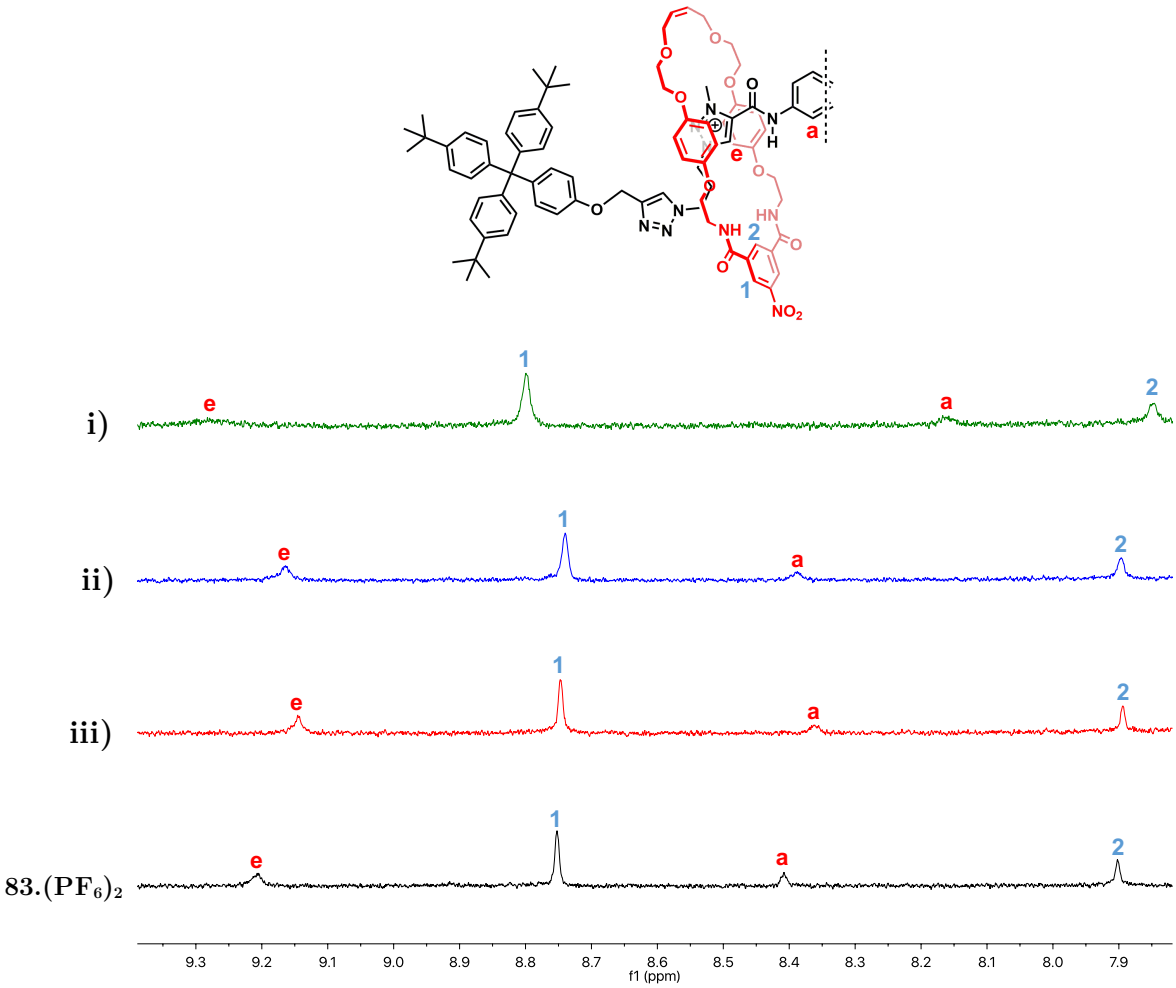


Figure 3.24 – Changes in the ^{1}H NMR spectrum of [3]rotaxane **83.$(PF_6)_2$** upon addition of one equivalent of i) $TBAH_2PO_4$, ii) $TBAN_3$ and iii) $TBANO_3$ (1:1 $CDCl_3/CD_3OD$, 500 MHz, 298 K).

Addition of $(TBA)_2SO_4$ initially induced upfield perturbations of axle triazolium proton **e** and macrocycle proton 2, followed by downfield shifts that attenuated in magnitude after two equivalents (**Figure 3.25-i**). This was attributed to initial binding of one equivalent of sulphate followed by considerable receptor reorganization to accommodate a second oxoanion within the [3]rotaxane structure

(**Figure 3.25-ii**). Analogous sulphate anion association behaviour was observed with the [3]rotaxanes shown in **Figure 3.18**.[43]

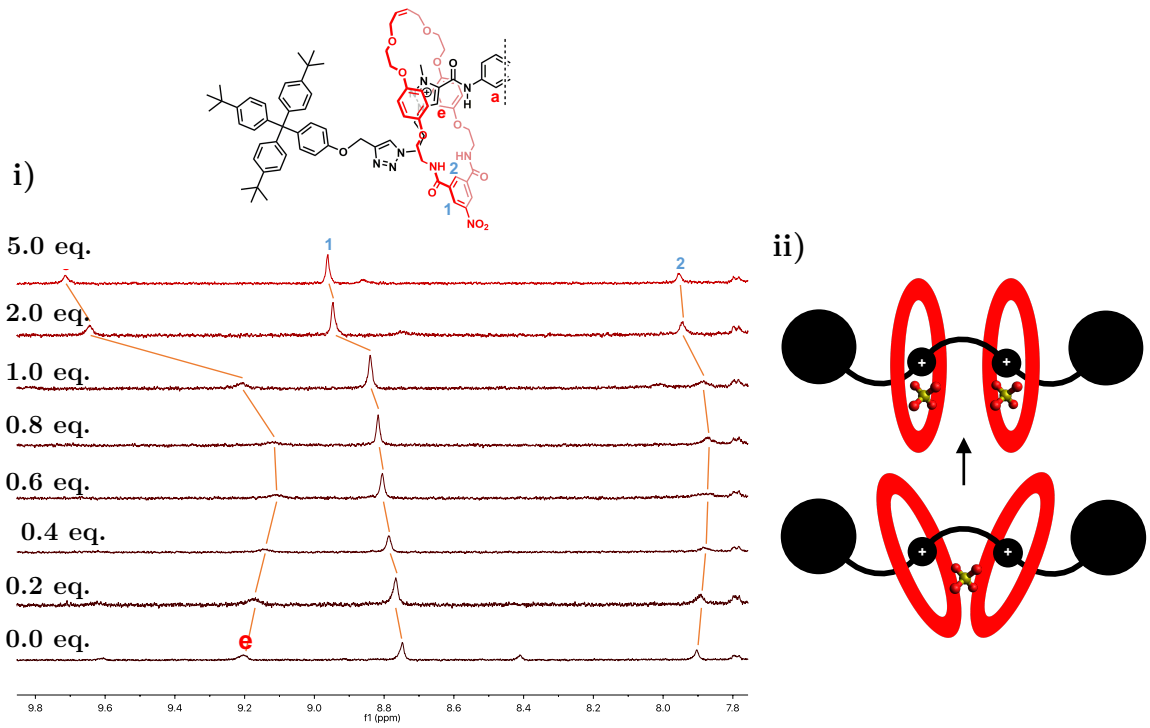


Figure 3.25 – i) Changes in the ^{1}H NMR spectrum of [3]rotaxane **83.$(PF_6)_2$** upon additions of sulpahte^{-} (1:1 $CDCl_3/CD_3OD$, 500 MHz, 298 K). ii) Schematic representation of the sequential binding of sulphate by [3]rotaxane **83.$(PF_6)_2$**,

WinEQNMR2[30] analysis of the titration data (**Figure 3.25**) monitoring internal macrocycle proton 2 determined 1:1 stoichiometric association constants shown in **Table 3.3**, which suggests 1:2 stoichiometric host-guest binding interactions were negligible. Due to the apparent strong association of sulphate, accurate fitting of the titration data for this dianion was not possible (**Figure 3.25**).

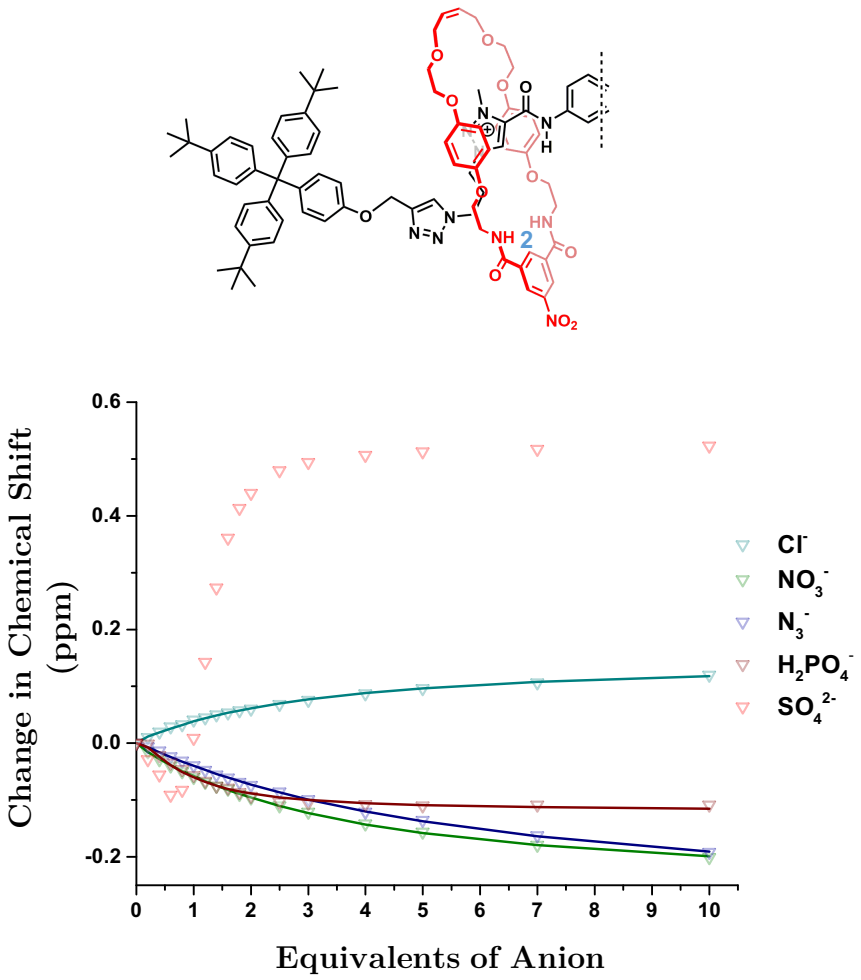


Figure 3.25 – Plots of the changes in chemical shift (ppm) against of equivalents of anion added for [3]rotaxane **83.$(PF_6)_2$**, monitoring internal macrocycle proton 2 (1:1 $CDCl_3$:CD_3OD, 298 K). Observed data (hollow triangles) and fitted isotherms (solid lines) are shown.

Table 3.3 – Anion association constants for [3]rotaxane **83.$(PF_6)_2$** (1:1 $CDCl_3$:CD_3OD, 298 K).

(a) *Anions added as their respective tetrabutylammonium (TBA) salts at 298K.* (b) *Anion association constants calculated using WinEQNMR2* [30] *using chemical shift data of macrocycle proton resonance* 2 (**Figure 3.25**). ± *errors in parentheses.* (c) *Titration data could not be fitted.*

Anion[(a)]	**83.$(PF_6)_2$**[(b)] K_a[M^{-1}]
Cl^-	257(18)
NO_3^-	218(9)
N_3^-	112(5)
$H_2PO_4^-$	1684(82)

The [3]rotaxane host forms the strongest association with $H_2PO_4^-$, followed by Cl^- >NO_3^->N_3^- indicating the selective 1:1 stoichiometric 'sandwich' recognition of tetrahedral oxoanion $H_2PO_4^-$ within the [3]rotaxane extended cavity in $CDCl_3/CD_3OD$ in preference to the other monoanion guest geometries.

3.4.6 Summary

Initial pseudorotaxane threading studies between macrocycle **23** and **65.$(BF_4)_2$** in the presence of Cl^- (**Figure 3.20**) confirmed the feasibility of the chloride anion templation of an interlocked architecture incorporating the novel hydrogen bonding 1,3-disubstituted amide-triazolium motif. It was found upon reaction of 1,3-disubstituted amide-triazolium containing axle component with an excess bis-vinyl macrocycle precursor and Grubbs' II catalyst it was possible to obtain a [3]rotaxane structure in an acceptable yield. Upon anion exchange of the chloride anion templates for non-coordinating PF_6^- counterions, it was discovered that the novel [3]rotaxane receptor **83.$(PF_6)_2$** selectively bound the tetrahedral anion $H_2PO_4^-$ over a geometrically diverse range of anions such as spherical Cl^-, trigonal planar NO_3^- and linear N_3^- in competitive protic solvent media, as evidenced by the strong 1:1 stoichiometric 'sandwich' complexation of $H_2PO_4^-$ by **82.$(PF_6)_2$**.

3.5 Conclusions and Future Work

Overall, this Chapter sought to evaluate the potential of the halogen bonding amide-iodotriazole motif and its homologous hydrogen bonding amide-triazole motif in anion recognition *via* its incorporation within a diverse range of receptor geometries.

In the first part of this chapter, the synthesis and anion recognition properties of a series of isomeric amide-triazole and amide-iodotriazole hosts were described. Enhanced halogen bonding halide anion recognition was observed in neutral receptor

55, in particular the strength of association of halides Cl^- and Br^- was markedly enhanced in comparison to its hydrogen bonding counterpart **54**.

The wider receptor geometry of 1,3-di-substituted hydrogen bonding receptor **65.$(BF_4)_2$** preferentially bound the complementary anions I^-, trigonal NO_3^- and linear N_3^-, whilst the more constrained binding cleft created by the 1,2-disubstituted geometry of **67.$(BF_4)_2$** preferred smaller spherical halides such as Cl^- and Br^- in d_3-MeCN. Unfortunately, solubility issues and inherent difficulties of studying the anion recognition properties of the halogen bonding analogues **66.$(BF_4)_2$** and **68.$(BF_4)_2$** prevented the full potential of these receptors from being realised.

Encouraged by the formation of a chloride anion templated pseudorotaxane between macrocycle **23** and thread **65.$(BF_4)_2$**, the synthesis of a novel bis-amide-triazolium axle containing [3]rotaxane was achieved *via* a double chloride templated Grubbs' catalysed RCM clipping methodology. The [3]rotaxane demonstrated selective 1:1 stoichiometric 'sandwich' recognition of tetrahedral anion $H_2PO_4^-$ over a geometrically diverse range of monoanion guests in competitive 1:1 $CDCl_3/CD_3OD$.

The incorporation of the halogen bonding amide-iodotriazole motif within a [3]rotaxane structure in future work is of ongoing interest. The exploitation of IHB-enhanced halogen bonding in neutral hosts as seen in **Section 3.2.4** could be expanded upon *via* incorporation into existing polarised aromatic motifs such as nitro-phenyl and fluorinated phenyl derivatives to enable anion recognition in more competitive solvent media.

3.6 References for Chapter 3

(1) Park, C. H.; Simmons, H. E. *J. Am. Chem. Soc.* **1968**, *90* (9), 2431–2432.

(2) Schmidtchen, F. P. *Angew. Chem. Int. Ed. Engl.* **1977**, *16* (10), 720–721.

(3) Worm, K.; Schmidtchen, F. P. *Angew. Chem. Int. Ed. Engl.* **1995**, *34* (1), 65–66.

(4) Kavallieratos, K.; de Gala, S. R.; Austin, D. J.; Crabtree, R. H. *J. Am. Chem. Soc.* **1997**, *119* (9), 2325–2326.

(5) Chmielewski, M. J.; Jurczak, J. *Chem. Weinh. Bergstr. Ger.* **2005**, *11* (20), 6080–6094.

(6) Brooks, S. J.; Gale, P. A.; Light, M. E. *Chem. Commun.* **2006**, No. 41, 4344–4346.

(7) Lee, C.-H.; Na, H.-K.; Yoon, D.-W.; Won, D.-H.; Cho, W.-S.; Lynch, V. M.; Shevchuk, S. V.; Sessler, J. L. *J. Am. Chem. Soc.* **2003**, *125* (24), 7301–7306.

(8) Li, Y.; Flood, A. H. *Angew. Chem. Int. Ed.* **2008**, *47* (14), 2649–2652.

(9) McDonald, K. P.; Ramabhadran, R. O.; Lee, S.; Raghavachari, K.; Flood, A. H. *Org. Lett.* **2011**, *13* (23), 6260–6263.

(10) Li, Y.-J.; Xu, L.; Yang, W.-L.; Liu, H.-B.; Lai, S.-W.; Che, C.-M.; Li, Y.-L. *Chem. – Eur. J.* **2012**, *18* (15), 4782–4790.

(11) Cao, L.; Jiang, R.; Zhu, Y.; Wang, X.; Li, Y.; Li, Y. *Eur. J. Org. Chem.* **2014**, *2014* (13), 2687–2693.

(12) Shalaeva, M.; Caron, G.; Abramov, Y. A.; O'Connell, T. N.; Plummer, M. S.; Yalamanchi, G.; Farley, K. A.; Goetz, G. H.; Philippe, L.; Shapiro, M. J. *J. Med. Chem.* **2013**, *56* (12), 4870–4879.

(13) Lamperti, M.; Maspero, A.; Tønnesen, H. H.; Bondani, M.; Nardo, L. *Molecules* **2014**, *19* (9), 13282–13304.

(14) Voet, D.; Voet, J. G. *Biochemistry*, 4th Edition edition.; John Wiley & Sons: Hoboken, NJ, 2011.

(15) Nomura, R.; Tabei, J.; Masuda, T. *J. Am. Chem. Soc.* **2001**, *123* (34), 8430–8431.

(16) Jones, I. M.; Knipe, P. C.; Michaelos, T.; Thompson, S.; Hamilton, A. D. *Molecules* **2014**, *19* (8), 11316–11332.

(17) Li, C.; Ren, S.-F.; Hou, J.-L.; Yi, H.-P.; Zhu, S.-Z.; Jiang, X.-K.; Li, Z.-T. *Angew. Chem.* **2005**, *117* (35), 5871–5875.

(18) Wang, D.; Wang, J.; Zhang, D.; Li, Z. *Sci. China Chem.* **2012**, *55* (10), 2018–2026.

(19) Clark, T.; Hennemann, M.; Murray, J. S.; Politzer, P. *J. Mol. Model.* **2006**, *13* (2), 291–296.

(20) Gallardo, H.; Bortoluzzi, A. J.; Santos, D. M. P. D. O. *Liq. Cryst.* **2008**, *35* (6), 719–725.

(21) Miura, Y.; Ushitani, Y.; Inui, K.; Teki, Y.; Takui, T.; Itoh, K. *Macromolecules* **1993**, *26* (14), 3698–3701.
(22) Kwong, F. Y.; Klapars, A.; Buchwald, S. L. *Org. Lett.* **2002**, *4* (4), 581–584.
(23) Brotherton, W. S.; Clark, R. J.; Zhu, L. *J. Org. Chem.* **2012**, *77* (15), 6443–6455.
(24) Somma, M. S.; Medforth, C. J.; Nelson, N. Y.; Olmstead, M. M.; Khoury, R. G.; Smith, K. M. *Chem. Commun.* **1999**, No. 13, 1221–1222.
(25) Haynes, C. J. E.; Busschaert, N.; Kirby, I. L.; Herniman, J.; Light, M. E.; Wells, N. J.; Marques, I.; Félix, V.; Gale, P. A. *Org Biomol Chem* **2014**, *12* (1), 62–72.
(26) Robinson, S. W.; Mustoe, C. L.; White, N. G.; Brown, A.; Thompson, A. L.; Kennepohl, P.; Beer, P. D. *J. Am. Chem. Soc.* **2015**, *137* (1), 499–507.
(27) Ozkal, E.; Llanes, P.; Bravo, F.; Ferrali, A.; Pericàs, M. A. *Adv. Synth. Catal.* **2014**, *356* (4), 857–869.
(28) Klausner, Y. S.; Bodansky, M. *Synthesis* **1972**, *1972* (9), 453–463.
(29) König, W.; Geiger, R. *Chem. Ber.* **1970**, *103* (3), 788–798.
(30) Hynes, M. J. *J. Chem. Soc. Dalton Trans.* **1993**, No. 2, 311–312.
(31) Chudzinski, M. G.; McClary, C. A.; Taylor, M. S. *J. Am. Chem. Soc.* **2011**, *133* (27), 10559–10567.
(32) Hancock, L. M.; Beer, P. D. *Chem. - Eur. J.* **2009**, *15* (1), 42–44.
(33) Hancock, L. M.; Gilday, L. C.; Kilah, N. L.; Serpell, C. J.; Beer, P. D. *Chem. Commun.* **2011**, *47* (6), 1725–1727.
(34) Langton, M. J.; Marques, I.; Robinson, S. W.; Félix, V.; Beer, P. D. *Chem. – Eur. J.* **2016**, *22* (1), 185–192.
(35) Wisner, J. A.; Beer, P. D.; Drew, M. G. B.; Sambrook, M. R. *J. Am. Chem. Soc.* **2002**, *124* (42), 12469–12476.
(36) White, N. G.; Beer, P. D. *Org. Biomol. Chem.* **2013**, *11* (8), 1326–1333.
(37) Mullaney, B. R.; Thompson, A. L.; Beer, P. D. *Angew. Chem. Int. Ed.* **2014**, *53* (43), 11458–11462.
(38) Langton, M. J.; Robinson, S. W.; Marques, I.; Félix, V.; Beer, P. D. *Nat. Chem.* **2014**, *6* (12), 1039–1043.
(39) Chae, M. K.; Suk, J.; Jeong, K.-S. *Tetrahedron Lett.* **2010**, *51* (32), 4240–4242.
(40) Evans, N. H.; Rahman, H.; Leontiev, A. V.; Greenham, N. D.; Orlowski, G. A.; Zeng, Q.; Jacobs, R. M. J.; Serpell, C. J.; Kilah, N. L.; Davis, J. J.; Beer, P. D. *Chem. Sci.* **2012**, *3* (4), 1080–1089.
(41) Caballero, A.; Zapata, F.; White, N. G.; Costa, P. J.; Félix, V.; Beer, P. D. *Angew. Chem. Int. Ed.* **2012**, *51* (8), 1876–1880.
(42) Evans, N. H.; Serpell, C. J.; Beer, P. D. *Chem. Commun.* **2011**, *47* (31), 8775–8777.

(43) Langton, M. J.; Beer, P. D. *Chem. – Eur. J.* **2012**, *18* (45), 14406–14412.
(44) Fall, A.; Seck, I.; Diouf, O.; Gaye, M.; Seck, M.; Gómez, G.; Fall, Y. *Tetrahedron Lett.* **2015**, *56* (36), 5128–5131.
(45) Steinhilber, D.; Rossow, T.; Wedepohl, S.; Paulus, F.; Seiffert, S.; Haag, R. *Angew. Chem. Int. Ed.* **2013**, *52* (51), 13538–13543.

CHAPTER 4

Luminescent Cucurbit[n]uril Host-Guest Systems: Towards Redox Switchable Output†

4.1. Introduction

4.1.1. Donor-acceptor ternary complexes of CB[8]

As previously discussed in **Section 1.4.3** of Chapter 1, the large hydrophobic cavity of cucurbit[8]uril macrocycle (**CB[8]**) exhibits the ability to form inclusion complexes with two guest molecules of appropriate size in aqueous media, as seen in the homoternary complex of **CB[8]** and two phenylphosphonic acid guests (**Figure 1.54-viii**).[1] This unique complexation behaviour has been further exploited in a growing number of *heteroternary* complexes. For example, *via* a combination of solvophobic effects, macrocyclic ion-dipole interactions originating from the carbonyl portals of **CB[8]** and complementary aromatic donor-acceptor interactions, the formation of a **CB[8]**-encapsulated dimeric heteroternary complex of 2,6-dihydroxynaphthalene (**DHN**) and methyl viologen ($\mathbf{MV^{2+}}$) was reported by Kim and co-workers (**Figure 4.1**).[2] The close proximal binding of these two species induces a charge transfer (CT) absorption band in the visible region that is diagnostic of this heteroternary inclusion phenomenon. This readily self-assembled system provides an attractive scaffold for functionalisation of ternary components to facilitate applications such as sensing, switching and self-assembly.[3–5]

† Some of the research described in this chapter was conducted in collaboration with the research groups of Prof. J. J. Davis and Prof. S. Faulkner and specific individual contributions will be indicated accordingly.

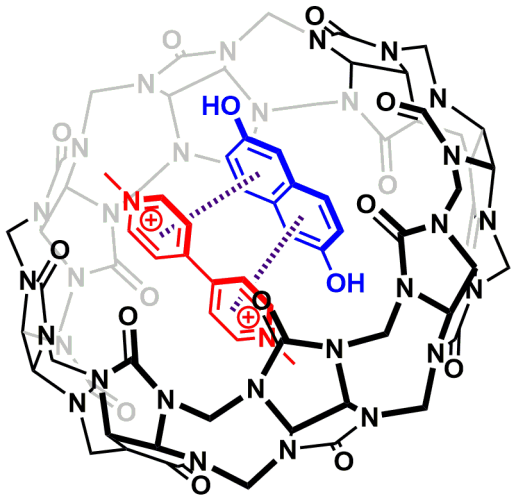


Figure 4.1 – Kim's prototypical heteroternary dimeric inclusion complex of electron-rich **DHN** (shown in blue) and electron-deficient $\mathbf{MV^{2+}}$ (shown in red) within **CB[8]**.

Bis-pyridinium 'viologen' type compounds are known for their ease of electrochemical reduction, the facile one-electron reduction of methyl viologen ($\mathbf{MV^{2+}}$) to the deep blue coloured monocation radical $\mathbf{MV^{\bullet+}}$ is well characterized (**Figure 4.2-i**).[6,7] The use of this redox behaviour and the observed formation of a stable homoternary complex of two reduced $\mathbf{MV^{\bullet+}}$ radical species within **CB[8]**-based ternary complexes has been exploited as a means of redox control of the bi-modal switching of the inclusion stoichiometry within **CB[8]** (**Figure 4.2-ii**).[8] More complex three-way supramolecular switches utilizing $\mathbf{MV^{2+}}$ in tandem with other redox active species such as tetrathiafulvalene (**TTF**) has also been demonstrated (**Figure 4.2-iii**).[9]

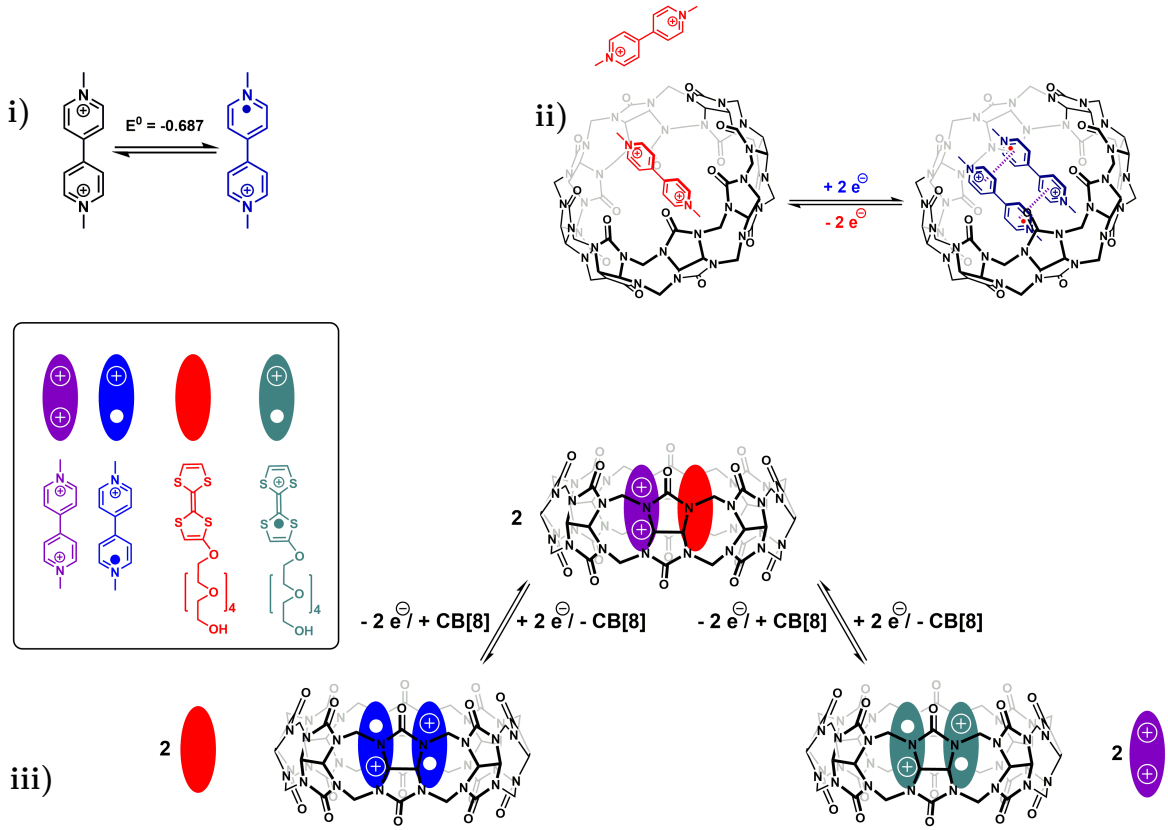


Figure 4.2 – i) The reduction potential of $\mathbf{MV^{2+}}$ to its mono-cationic radical counterpart $\mathbf{MV^{\bullet+}}$; ii) Kim's first demonstration of redox control over the inclusion stoichiometry of viologen species within **CB[8]** and iii) Kim's three-state supramolecular **CB[8]/MV^{2+}/TTF** switch.

4.1.2. Lanthanide luminescence: the antenna effect

Compared to commonly studied fluorescent organic probes, trivalent lanthanide ions possess distinctively sharp emission profiles and long lived luminescence in the range of micro- to milliseconds. Unfortunately, as a consequence of the Laporte forbidden nature of 4*f* electronic transitions, the generation of lanthanide luminescence *via* direct excitation is inefficient.[10] An effective approach to overcome this is to harness the absorption and subsequent energy transfer (ET) from a proximal chromophore 'antenna' to a lanthanide excited state.[11] This is typically achieved by utilising a species possessing a high absorption coefficient and efficient quantum yield of ET (Φ_{ET}) from a chromophore-localised triplet excited state to a lanthanide excited state (**Figure 4.3-i**). With the assistance of a Dieke diagram which depicts the

relative energies of the excited states of lanthanide ions (**Figure 4.3-ii)**, Φ_{ET} can be optimised by appropriate matching of the antenna triplet excited state to the lower lying lanthanide excited state of interest.

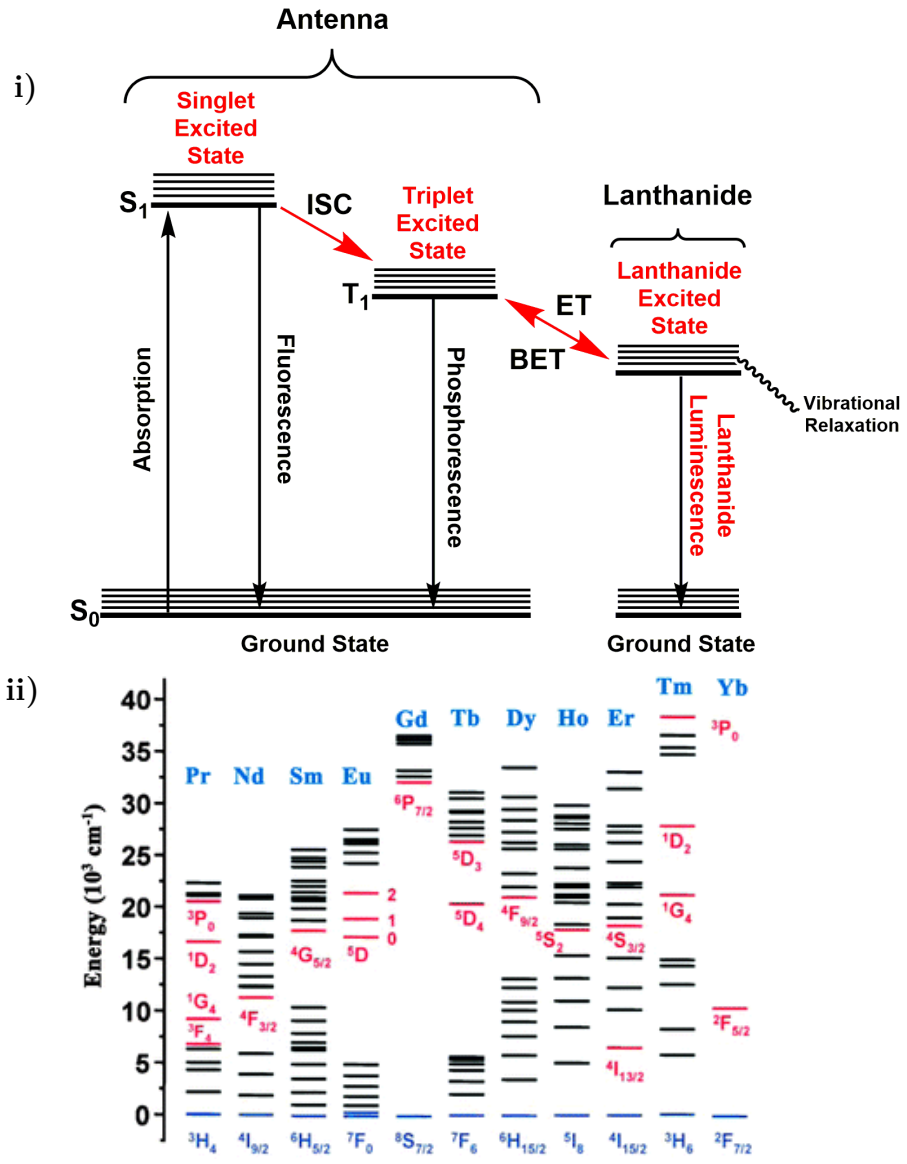


Figure 4.3 – i) Jablonski diagram depicting the photophysical processes possible upon excitation of an 'antenna' chromophore: singlet fluorescence, intersystem crossing (ISC), triplet phosphorescence and energy transfer (ET) or back energy transfer (BET) to/from a lanthanide excited state; ii) reproduced Dieke diagram[12] of the relative energies of lanthanide excited states (emissive states shown in red).

4.2. Towards a Redox Switchable Luminescent Ternary Complex Switch

4.2.1. Design of naphthalene-appended lanthanide complexes

Towards the generation of **CB[8]**-based ternary complexes with luminescent output, adaptation of the functional components of the prototypical **CB[8]** ternary complex (**Figure 4.1**) to include emissive lanthanide containing components was undertaken.

This could be realised *via* structural elaboration of the electron rich ternary guest species 2,6-dihydroxynapthalene (**DHN**), *via* its covalent attachment to the kinetically inert lanthanide complexing cyclen derivative known as DO3A, a tri-carboxylate homologue of the common tetra-carboxylate "DOTA"[13] (**Figure 4.4**). For ease of functionalization, the aromatic electron-rich mono-hydroxyl 2-napthol was chosen to act as a motif for ternary co-inclusion with a viologen derivative within the cavity of **CB[8]**. Additionally, it was thought that the substituted 2-naphthol group could act as an 'antenna' chromophore to sensitise lanthanide centred luminescence.

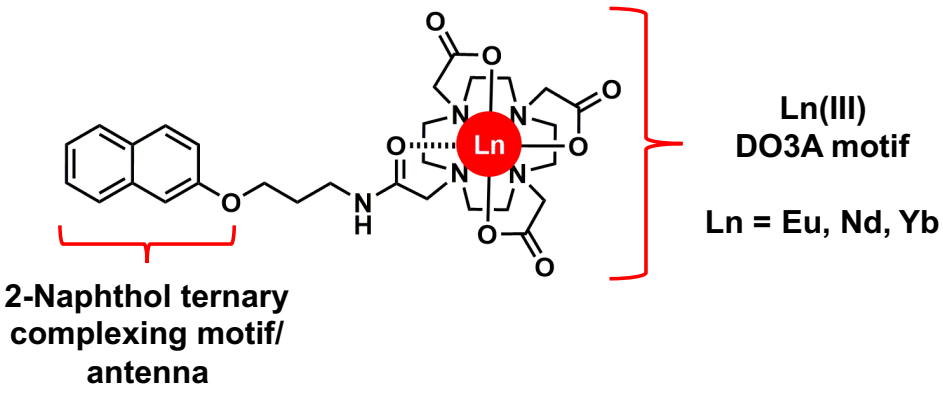


Figure 4.4 – Structural design of naphthyl DO3A lanthanide complexes.

4.2.2. Design of the ferrocene-viologen component

Monomeric lanthanide complexes containing a redox switchable ferrocene derivative have been shown to exploit the low lying excited state of the oxidised ferrocenium

species to quench the excited states of europium(III) and ytterbium(III).[14] Adoption of this switching behaviour was sought to enable redox switching of the lanthanide luminescence within a ternary complex. A ferrocene-functionalised viologen derivative **99**$^{2+}$ was accordingly devised (**Figure 4.5**). Asymmetric substitution of the **MV**$^{2+}$ species would enable preferential ternary co-inclusion of **99**$^{2+}$ at the viologen terminus whilst the ferrocene terminus would be situated at the exterior of the **CB[8]** internal cavity, available to electrochemically modulate the luminescence of a co-included luminescent lanthanide-functionalised component.

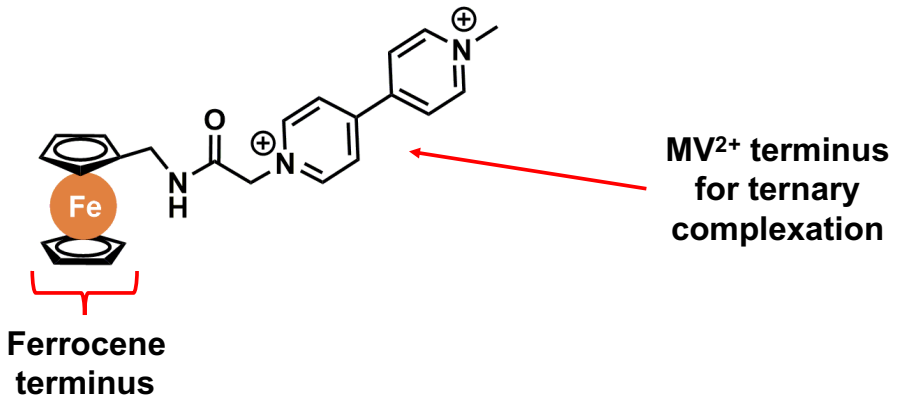


Figure 4.5 – Structural design of viologen derivative **99**$^{2+}$.

4.2.3. CB[8] ternary complex assembly design

Preparation of the model ternary complex of **MV**$^{2+}$ and the target lanthanide containing complexes depicted in **Figure 4.6-i)** would probe the luminescence properties of the system in the absence of the ferrocene viologen derivative. Next, it was envisioned that upon formation of the target ternary complex featuring **99**$^{2+}$ and a lanthanide complex, excitation of the naphthalene antenna would initiate ET from a naphthalene-centred triplet excited state to the excited state of the lanthanide ion, generating subsequent lanthanide luminescence. Oxidation to the ferrocenium species would induce luminescence quenching *via* ET from the lanthanide ion to a lower energy ferrocenium excited state of viologen derivative **99**$^{2+}$ (**Figure 4.6-ii**).

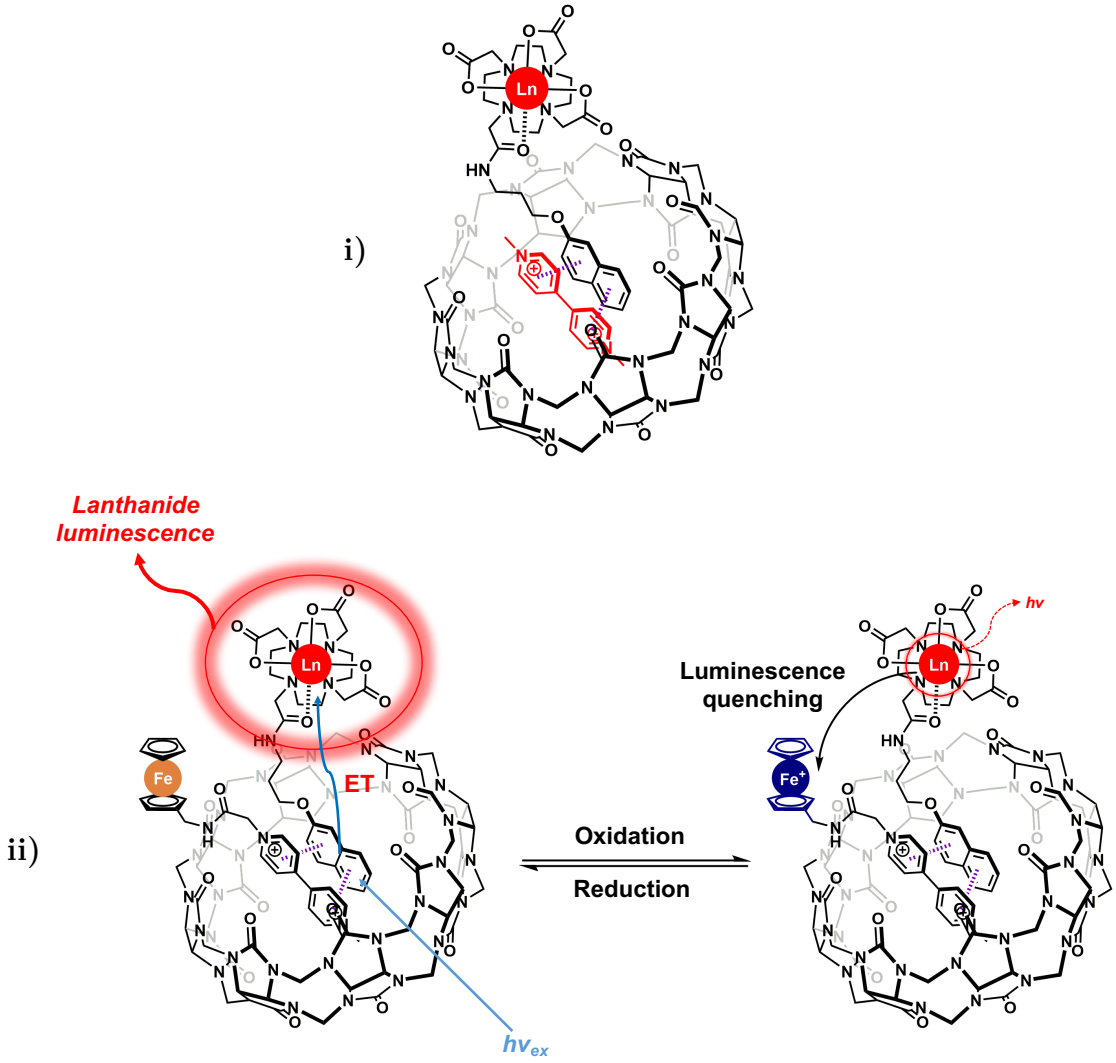


Figure 4.6 – i) Structure of lanthanide containing model ternary complexes (Ln = Eu(III), Nd(III), Yb(III)) ii) The proposed redox switching of lanthanide-centred luminescence *via* switching of the redox state of the co-included ferrocene-viologen derivative $\mathbf{99}^{2+}$ within the target ternary complex (Ln = Eu(III), Nd(III), Yb(III)).

4.2.4. Chapter aims

The work in this Chapter focuses on the preparation of potential redox tuneable heteroternary **CB[8]** complexes for the modulation of lanthanide luminescent output.

Firstly, the synthesis and characterisation of visible light and near infra-red (NIR) emitting naphthalene-functionalised DO3A complexes of europium(III), neodymium(III) and ytterbium(III) ternary partners for co-inclusion with viologen

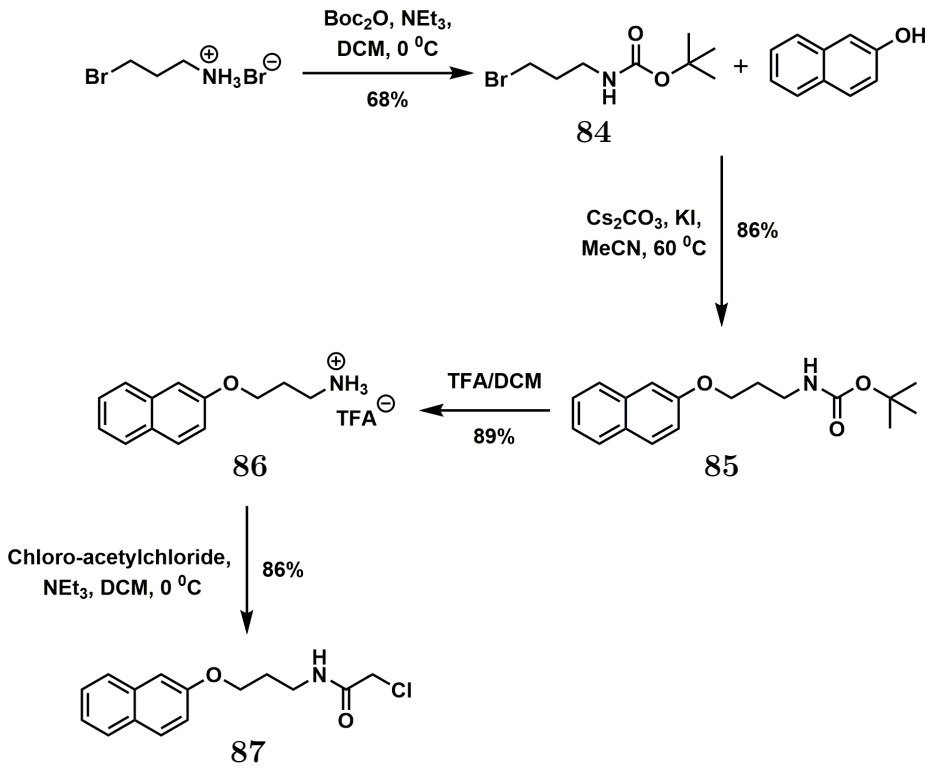
derivatives within **CB[8]** is described. The redox behaviour of the europium(III)-viologen ternary complex is then probed by UV-Vis, fluorescence and phosphorescence.

Secondly, the effect of the co-inclusion of the neodymium(III) and ytterbium(III) complexes with $\mathbf{MV^{2+}}$ within **CB[8]** on their NIR luminescent emission profiles are examined.

Finally, the synthesis and ternary complexation behaviour of a ferrocene appended viologen component is described, with the aim to enable redox modulation of luminescent output within the lanthanide functionalised ternary complexes.

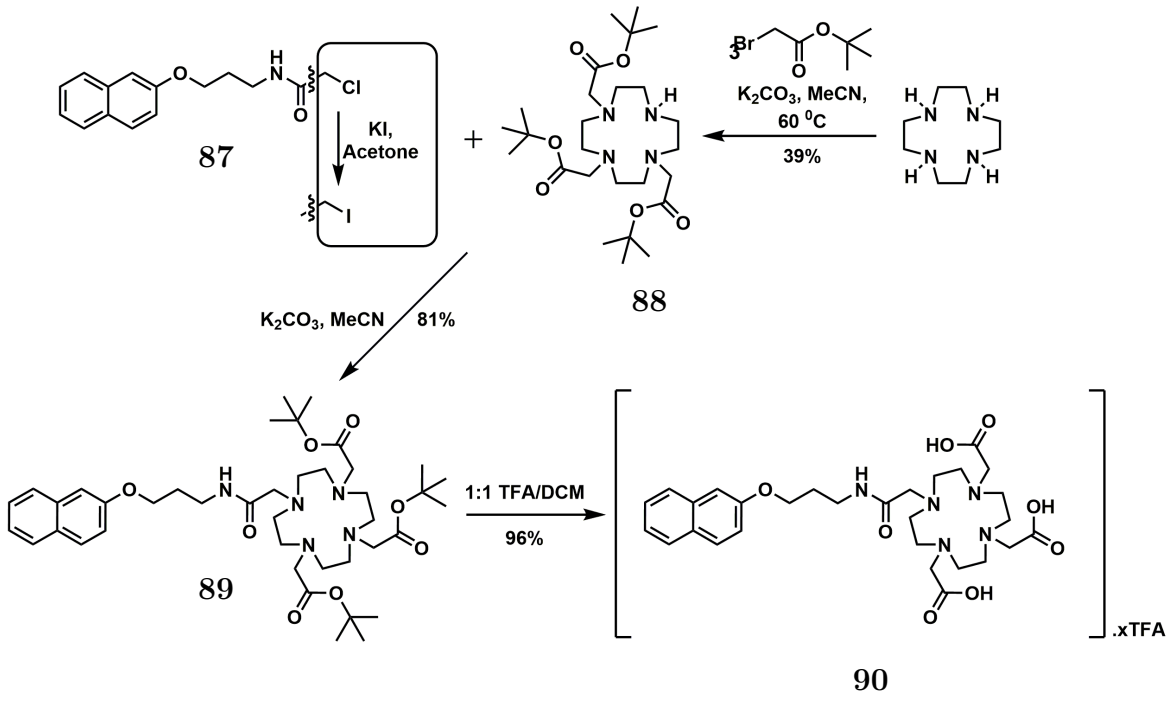
4.2.5. Synthesis of the lanthanide containing component

Synthesis of the target naphthalene-functionalised linker precursor to lanthanide DO3A complexes **91.Eu**, **92.Nd** and **93.Yb** is detailed in **Scheme 4.1**. Boc-protected amine bromide **84** was prepared according to a literature procedure *via* reaction of Boc_2O with bromo-propylamine hydrobromide and triethylamine in DCM in a 68% yield.[15] Reaction of 2-napthol with **84** under basic conditions afforded protected naphthyl amine **85** in 86% yield. Acid deprotection of the Boc group was undertaken in DCM with an excess of TFA to afford amine **86** as the protonated trifluoroacetate salt (89% yield). Subsequent reaction of **86** with excess chloro-acetylchloride in the presence of triethylamine gave *N*-acetylchloride linker **87** in 86% yield.



Scheme 4.1 – Synthesis of naphthyl *N*-acetylchloride linker **87**.

Synthesis of the tri-ester functionalised cyclen compound **88** was required, before reaction of the remaining secondary amine site of this derivative with naphthyl-*N*-acetylchloride linker **87** (**Scheme 4.2**). Statistical tri-alkylation of commercially available cyclen with three equivalents *tert*-butyl bromoacetate under basic conditions afforded tri-ester DO3A cyclen derivative **88**[16] in a 39% yield. Finkelstein halide exchange of **87** with KI in acetone followed by reaction with DO3A tri-ester **88** under basic conditions gave naphthyl-DO3A tri-*tert*-butyl-ester **89** in 81% isolated yield. Acidic ester hydrolysis in 1:1 TFA/DCM afforded naphthyl DO3A derivative **90** in 96% yield (**Scheme 4.2**) and was characterised by ^{1}H NMR and ESI-MS (**Figure 4.7**).



Scheme 4.2 – Synthesis of naphthyl DO3A derivative **90**.

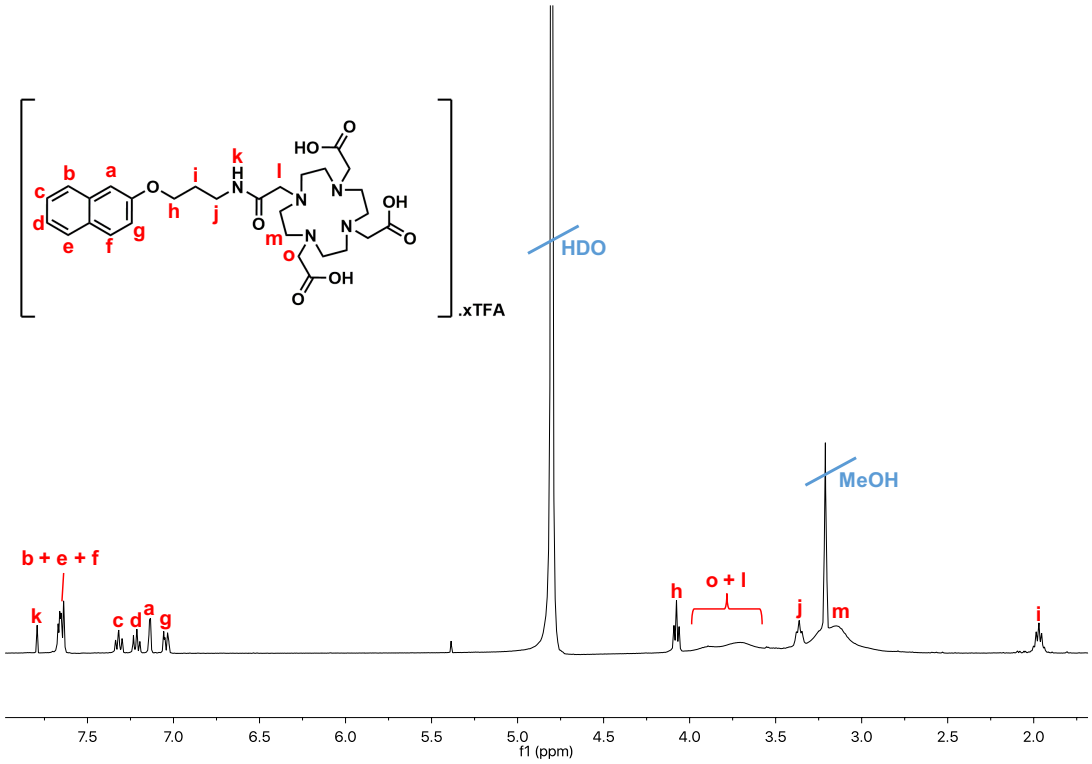
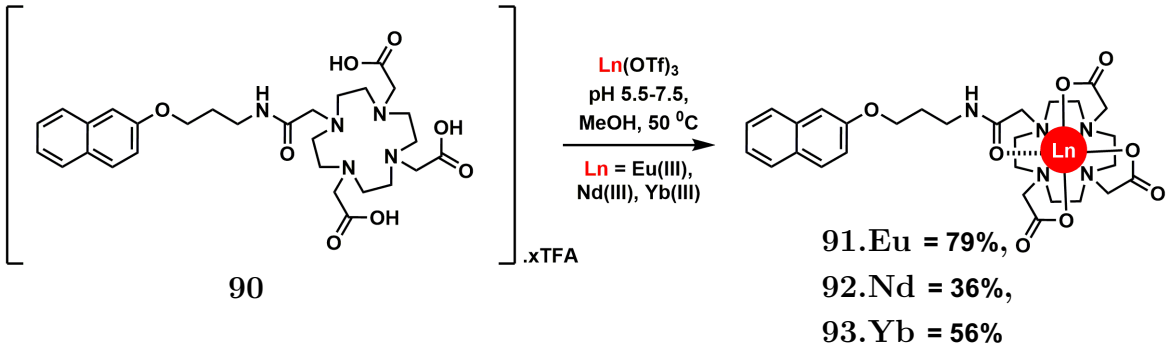


Figure 4.7 – Assigned ^{1}H NMR spectrum of tri-acid **90** (400 MHz, D_2O, 298 K).

90 was stirred with $Ln(OTf)_3$ (Ln = Eu(III), Nd(III), Yb(III)) in mildly acidic to neutral pH in MeOH followed by trituration in $MeOH/Et_2O$ to produce the target naphthalene-appended lanthanide complexes **91.Eu**, **92.Nd** and **93.Yb** (**Scheme 4.3**).



Scheme 4.3 – Synthesis of target naphtalene-appended lanthanide complexes **91.Eu**, **92.Nd** and **93.Yb**.

All three complexes were characterised by ^1H NMR and HRMS-ESI (**Figures 4.8 – 4.10**). The lanthanide containing complexes exhibited characteristic paramagnetically shifted ^1H NMR spectra. HRMS-ESI analysis in all cases gave one peak corresponding to complexes **91.Eu**, **92.Nd** and **93.Yb**.

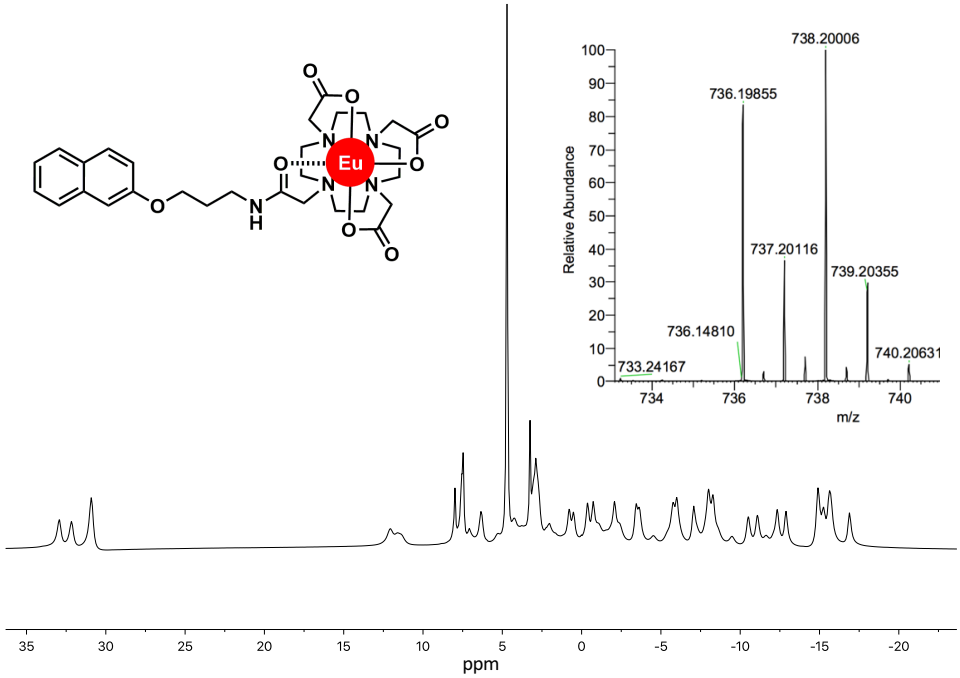


Figure 4.8 – Paramagnetically shifted ^{1}H NMR spectrum of **91.Eu** (400 MHz, D_2O, 298 K) and (inset) HRMS-ESI spectrum of **91.Eu**.

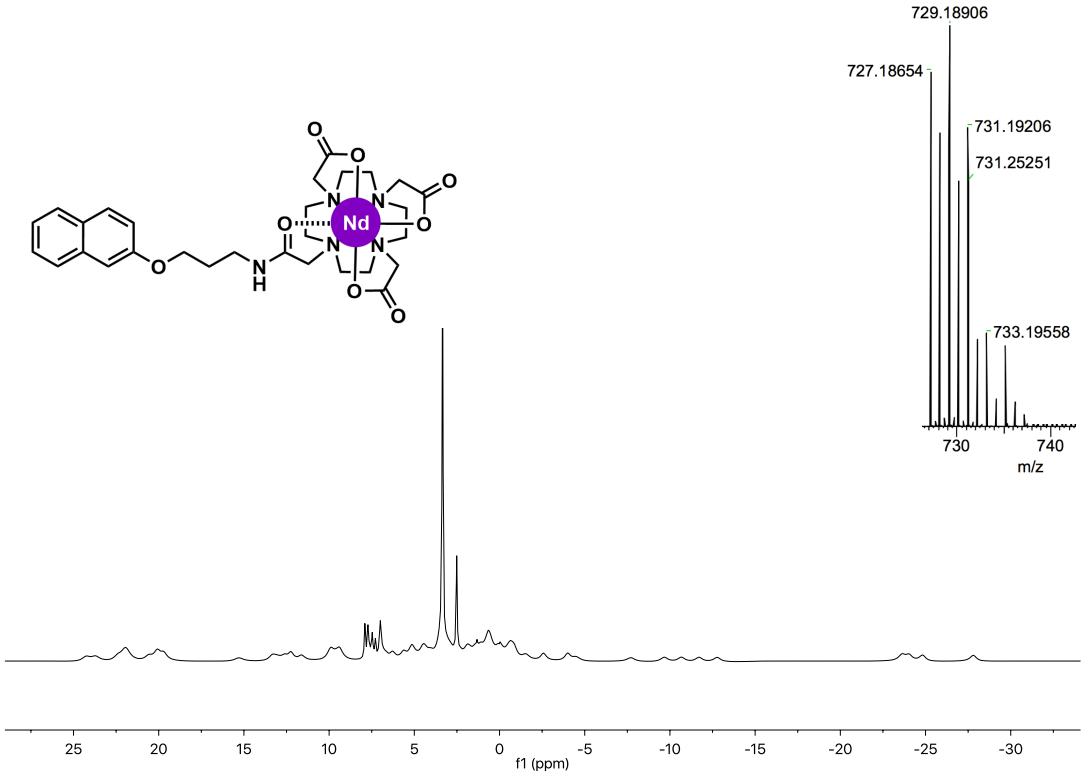


Figure 4.9 – Paramagnetically shifted ^{1}H NMR spectrum of **92.Nd** (d_6-DMSO, 400 MHz, 298 K) and (inset) HRMS-ESI spectrum of **92.Nd**.

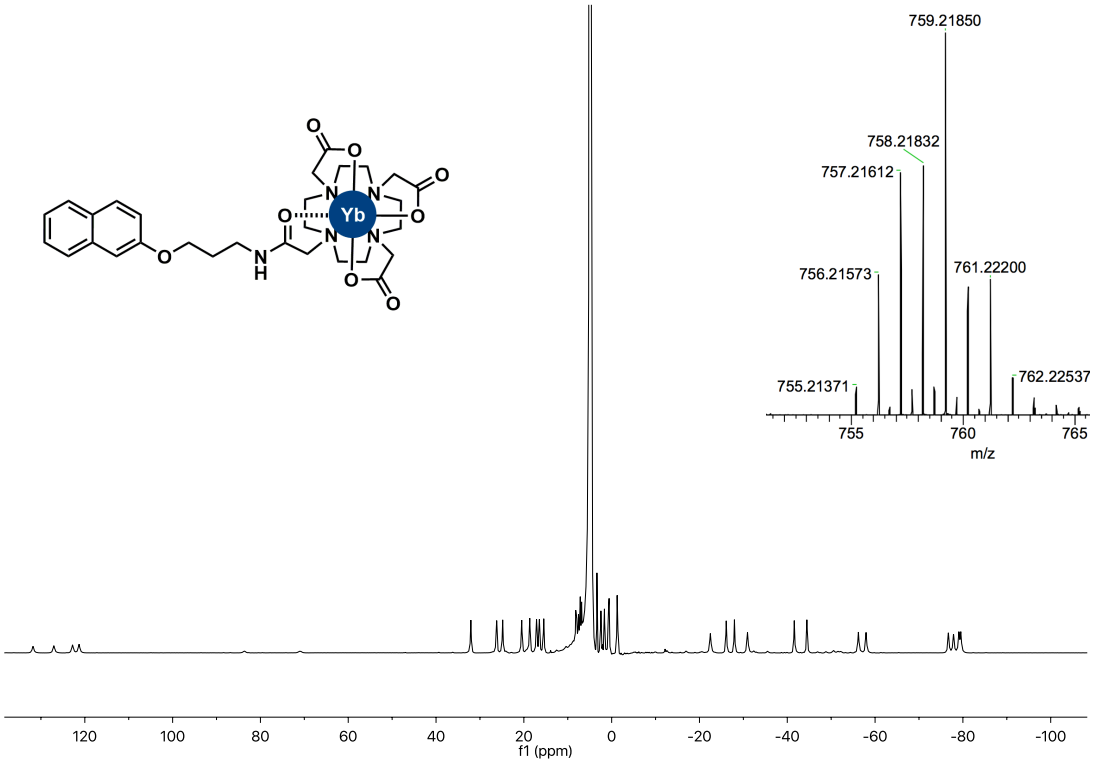


Figure 4.10 – Paramagnetically shifted ^{1}H NMR spectrum of **93.Yb** (D_2O, 400 MHz, 298 K) and (inset) HRMS-ESI spectrum of **93.Yb**.

4.2.6. Ternary complex studies

Ternary complexation studies with **91.Eu**, $\mathbf{MV^{2+}}$ and **CB[8]** were conducted in collaboration with A. Baxter (Part II student) and M. Cunningham of the Prof. J. J. Davis research group.

4.2.6.1. UV-Vis properties

Upon addition of an equimolar amount of **91.Eu** to an aqueous solution of pre-formed binary complex $\mathbf{MV^{2+}} \subset$ **CB[8]** (0.5 mM), the formation of a pale red solution was observed after a short sonication period. This was indicative of an interfacial aromatic donor-acceptor interaction between the naphthalene motif of **91.Eu** and the electron deficient $\mathbf{MV^{2+}}$ upon co-inclusion in the **CB[8]** cavity, as evidenced by the generation of a CT absorption band located between *ca.* 450 and

550 nm of the visible spectrum (**Figure 4.9**, red trace). By contrast, the CT absorption band observed in the model ternary complex (**DHN**, $\mathbf{MV^{2+}}$) ⊂ **CB[8]** (**Figure 4.9,** purple trace) was located between *ca.* 475 nm and 700 nm, generating a purple solution upon ternary complex formation. This was attributed to the differing electronic structure of the naphthyl motifs of **91.Eu** and **DHN**; the former possessing one electron-donating phenoxy ether substituent whilst the latter contains two electron-donating hydroxyl groups. This hypsochromic shift of the CT band going from **DHN** to **91.Eu** is in accordance with the Mulliken model of charge transfer electronics used to describe analogous changes in CT absorbance in similar systems.[17]

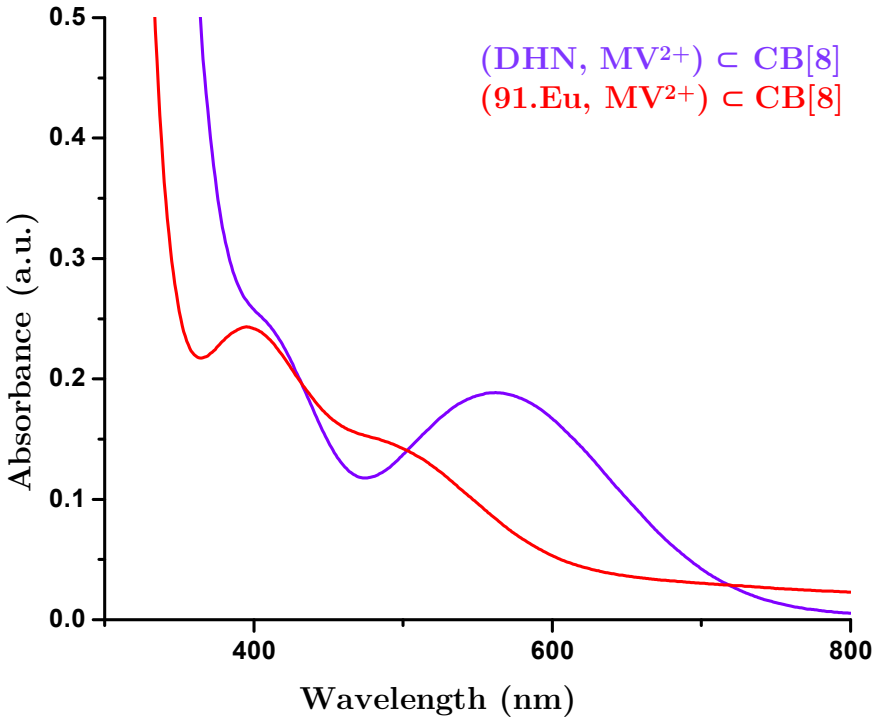


Figure 4.9 – UV-Vis spectra of ternary complexes i) 0.5 mM (**DHN**, $\mathbf{MV^{2+}}$) ⊂ **CB[8]** (purple trace) and 0.5 mM (**91.Eu**, $\mathbf{MV^{2+}}$) ⊂ **CB[8]** (red trace) (H_2O, 298 K).

4.2.6.2. Luminescence properties

Upon excitation of the pendant naphthalene chromophore antenna of **91.Eu** (λ_{ex} = 280 nm), naphthalene centered fluorescence was observed with a λ_{max} = 350

nm (**Figure 4.10**). Additionally, sensitisation of the europium(III) centred phosphorescent emission was observed, showing the characteristic emission spectrum of europium(III) (**Figure 4.11**). Minimal changes in these optical outputs were observed upon addition of one equivalent of **CB[8]**. An equimolar mixture of $\mathbf{MV^{2+}}$ and **91.Eu** did not exhibit any significant change in the europium(III) emission response, inferring that $\mathbf{MV^{2+}}$ alone was not an efficient quencher of europium(III) phosphorescence. However, upon ternary complex formation with **CB[8]**, (**91.Eu**, $\mathbf{MV^{2+}}$) ⊂ **CB[8]** fluorescence and phosphorescence output was significantly quenched. This indicates the formation of the ternary complex provides a quenching decay pathway for the triplet excited state of the naphthalene antenna. This alternative energy transfer pathway leads to less energy available for sensitisation and therefore the diminution of europium(III) phosphorescent emission from the $^7D_0$ excited state. Therefore, the formation of the CT complex could act as a switching mechanism for europium(III) luminescent output.

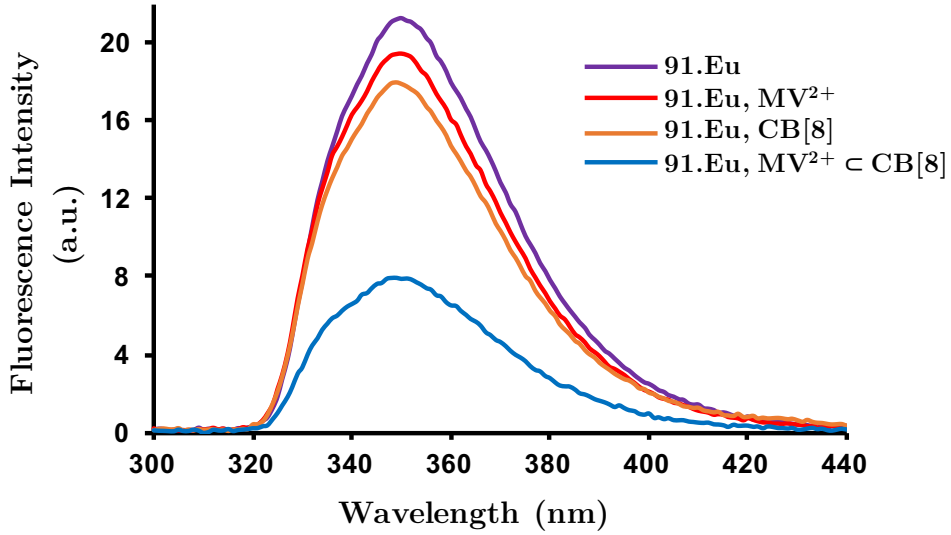


Figure 4.10 – Changes in fluorescent output of **91.Eu** upon addition one equivalent of $\mathbf{MV^{2+}}$ (red trace), one equivalent of **CB[8]** (orange trace) and ternary inclusion with $\mathbf{MV^{2+}}$ within **CB[8]** (blue trace). *All species were generated in H_2O solution at 298 K, and at a concentration of 0.5 mM. All spectra were recorded at 298 K upon excitation of the naphthalene chromophore (λ_{ex} = 280 nm). The fluorescent output from the naphthalene chromophore was acquired using excitation and emission slit widths of 5 nm and a PMT voltage of 500 V. All spectra provided are those acquired following averaging over 10 scans.*

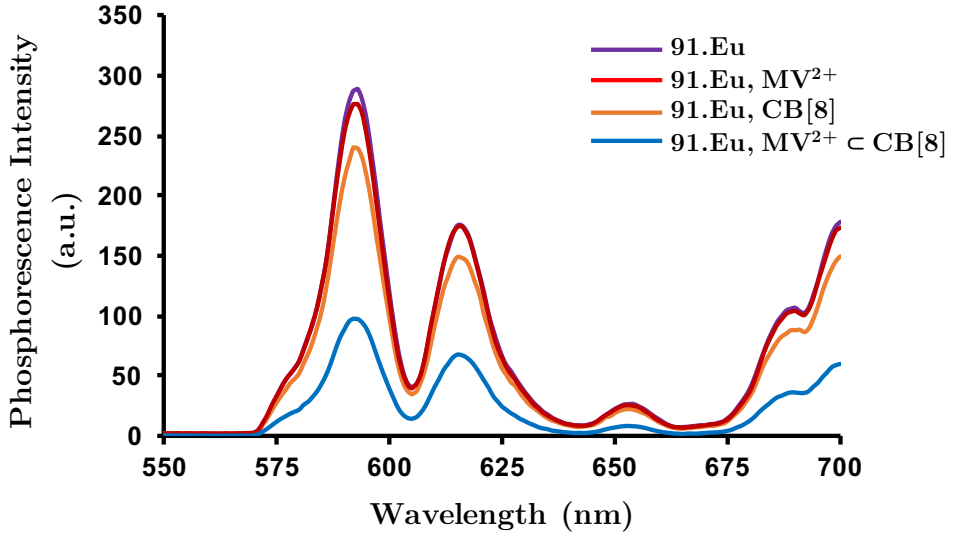


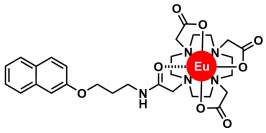
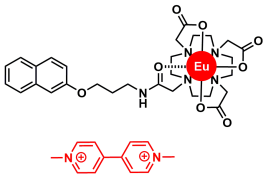
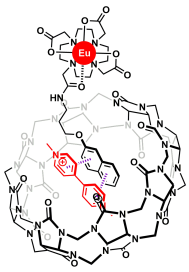
Figure 4.11 – Changes in phosphorescent output of **91.Eu** upon addition one equivalent of $\mathbf{MV^{2+}}$ (red trace), one equivalent of **CB[8]** (orange trace) and ternary inclusion with $\mathbf{MV^{2+}}$ within **CB[8]** (blue trace). *All species were generated in H_2O solution at 298 K, and at a concentration of 0.5 mM. All spectra were recorded at 298 K upon excitation of the naphthalene chromophore (λ_{ex} = 280 nm). The phosphorescent outputs from the europium(III) centre were acquired using excitation and emission slit widths of 10 nm, a PMT voltage of 1000 V, a total decay time of 0.020 s, a delay time of 0.20 s and a gate time of 0.50 s. All spectra provided are those acquired following averaging over 10 scans.*

4.2.6.3 Towards redox switching of optical output

Luminescence lifetime experiments with **91.Eu** were conducted with the assistance of Dr. M. Tropiano of the Prof. S. Faulkner research group.

It was found that the phosphorescent decay of ternary complex (**91.Eu**, $\mathbf{MV^{2+}}$) ⊂ **CB[8]** (monitoring emission at $\lambda_{em} = 616$ nm) was biexponential, implying the existence of two luminescent europium(III) species in equilibrium. This suggested a certain proportion of ternary component **91.Eu** remained free in solution. Luminescence lifetimes extracted from fitting of the biexponential decay curve gave a reduced emission lifetime of 0.1 ms and a second component emission lifetime of 0.6 ms, the latter measurement being identical to the lifetime measurement of free **91.Eu** and an equimolar mixture of **91.Eu** and $\mathbf{MV^{2+}}$ (**Table 4.1**).

Table 4.1 – The luminescence lifetimes of free **91.Eu**, **1:1 91.Eu/MV²⁺** and ternary complex (**91.Eu**, **MV²⁺**) ⊂ **CB[8]**. *All species were generated in H_2O solution at 298 K, and at a concentration of 0.5 mM. All lifetime measurements were recorded at 298 K (λ_{ex} = 280 nm, λ_{em} = 616 nm). The delay times, excitation/emission slit widths used were identical to those used previously. Lifetime measurement error = ±10%.*

Species	Structure	Lifetime (ms)
91.Eu		0.6
91.Eu + MV²⁺		0.6
(**91.Eu**, **MV²⁺**) ⊂ **CB[8]**		0.1 (88.3% complexed **91.Eu**) & 0.6 (11.7% free **91.Eu**) (*Biexponential*)

Further analysis confirmed that 88.3% of **91.Eu** was confined within the ternary complex and 11.7% was free in solution. Upon the addition of one equivalent of reducing agent $Na_2S_2O_4$, the percentage of free **91.Eu** increased to 36%. This was in accordance with the formation of the homoternary complex (**2MV⁺•**) ⊂ **CB[8]** upon reduction of the heteroternary complex (**91.Eu**, **MV²⁺**) ⊂ **CB[8]**, with concomitant loss of the ternary CT interaction and expulsion of the free **91.Eu** emissive species from the **CB[8]** cavity (**Figure 4.12**).

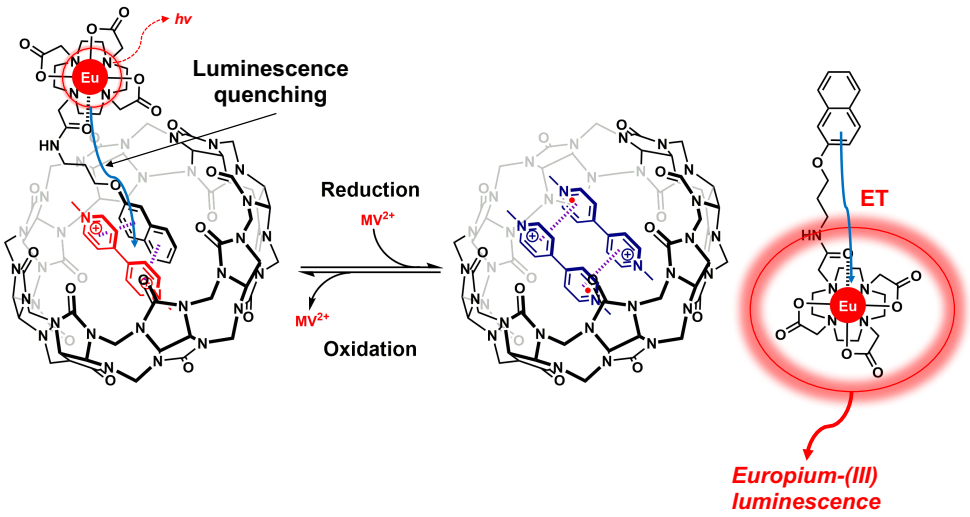


Figure 4.12 – Structural representation rationalising the redox mediated changes of **91.Eu** phosphorescent emission intensity and lifetime.

Upon reduction of ternary complex (**91.Eu**, $\mathbf{MV^{2+}}$) ⊂ **CB[8]**, the formation of the distinctive absorption band at *ca.* 540 nm corresponding to the diradical homoternary complex ($\mathbf{2MV^{+\bullet}}$) ⊂ **CB[8]** was observed in the UV-Vis absorption spectrum of the reduced species, identical to that observed upon the reduction of model ternary complex (**DHN**, $\mathbf{MV^{2+}}$) ⊂ **CB[8]** (**Figure 4.13**, purple trace). Reoxidation of the species was achieved under a stream of oxygen, causing the disappearance of the homoternary CT absorbance inferring the reformation of heteroternary complex (**91.Eu**, $\mathbf{MV^{2+}}$) ⊂ **CB[8]**. Over repeated reduction/oxidation cycles, spectral features consistent with the formation of free $\mathbf{MV^{+\bullet}}$ monomer (*ca.* 600 nm) were observed to increase in intensity (**Figure 4.13**, dotted purple trace). This decomplexation of $\mathbf{MV^{+\bullet}}$ is likely to result from competitive coordination of the carbonyl portals of **CB[8]** by Na^+ ions with the increasing amounts of reducing agent used and precipitation of the sparingly soluble **CB[8]**. It was presumed that without this effect, the full reversibility of optical switching could be achieved.

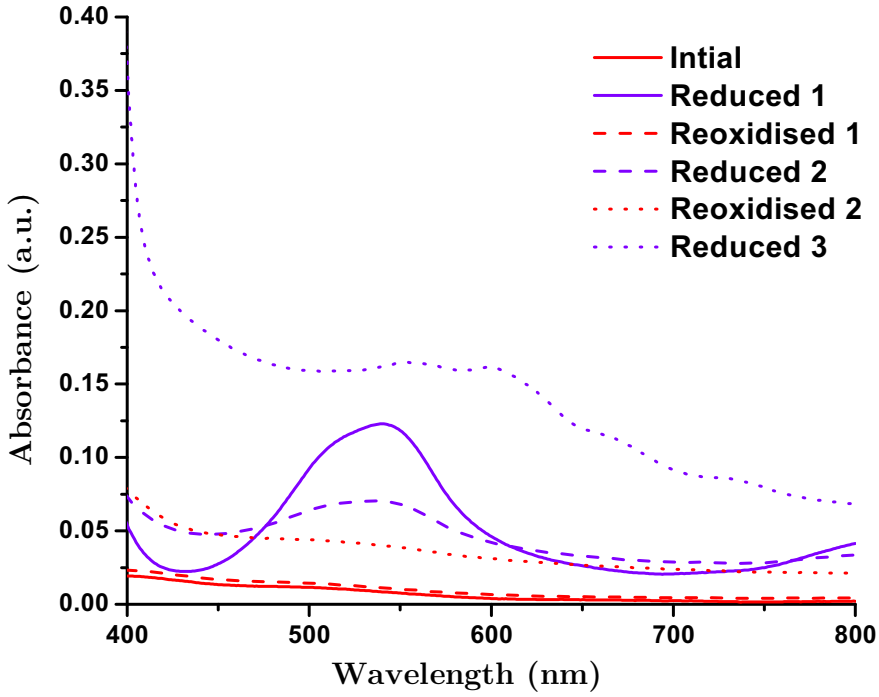


Figure 4.13 – UV-Vis spectra showing the pseudo-reversible switching of the absorption attributed to homoternary complex (**2MV**$^{+\bullet}$) ⊂ **CB[8]** (*ca.* 540 nm) enacted by oxidation/reduction cycles of ternary complex (**91.Eu**, **MV**$^{2+}$) ⊂ **CB[8]**, disrupted by competitive complexation of **CB[8]** by Na^+ cations.

4.2.7 Summary

The heteroternary complex of (**MV**$^{2+}$, **91.Eu**) ⊂ **CB[8]** was successfully generated and characterised. Unexpected ternary CT-mediated quenching of the sensitisation of the luminescent output of **91.Eu** was observed, mediated by the semi-reversible redox modulation of inter-guest CT interactions between **91.Eu** and the **MV**$^{2+}$ species within a **CB[8]** host macrocycle.

4.3 Towards Redox Switchable NIR Lanthanide Luminescence

4.3.1 Introduction

NIR emission in ytterbium(III) and neodymium(III) complexes has been shown to be efficiently sensitised by ligand-based CT features, notably in Faulkner *et al.*'s use of ET sensitisation from proximal transition metal complex MLCT (**Figure 4.14-**

i)[18] and Maury *et al.*'s use of variable energy ligand CT states to sensitise lanthanide luminescence within a series of 'push-pull' donor appended dipicolinate ligands (**Figure 4.14-ii**).[19]

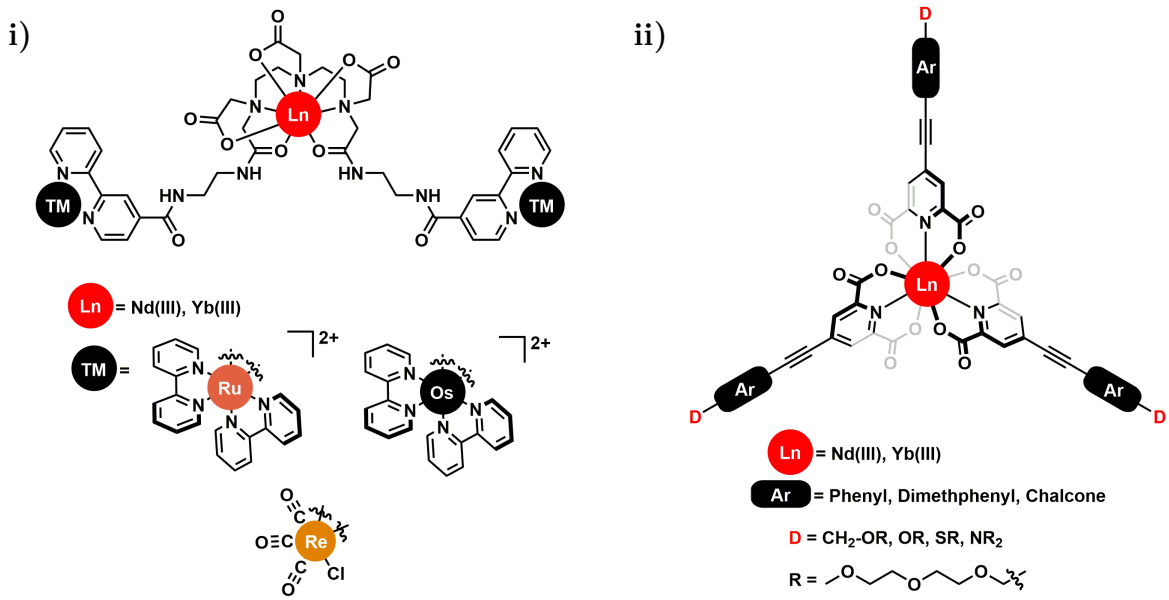


Figure 4.14 – Examples of sensitised NIR luminescence in neodymium(III) and ytterbium(III) complexes: i) Faulkner's transition metal antenna containing lanthanide ligand systems ii) Maury's 'push-pull' dipicolinate ligand antennae.

4.3.2 Design of NIR emitting heteroternary complexes

With the knowledge that the neodymium(III) $^4F_{3/2}$ and ytterbium(III) $^2F_{5/2}$ excited states are relatively lower in energy than the europium(III) $^5D_{0\text{-}2}$ excited states (**Figure 4.15**), it was envisaged that the lower in energy CT excited state of the aforementioned ternary complexes may be of the correct energy to *activate* NIR-emission of co-included **92.Nd** or **93.Yb**, in contrast to the observed *deactivation* of europium(III)-centred emission in the presence of CT in the case of ternary complex (**MV**$^{2+}$, **91.Eu**) ⊂ **CB[8]**.

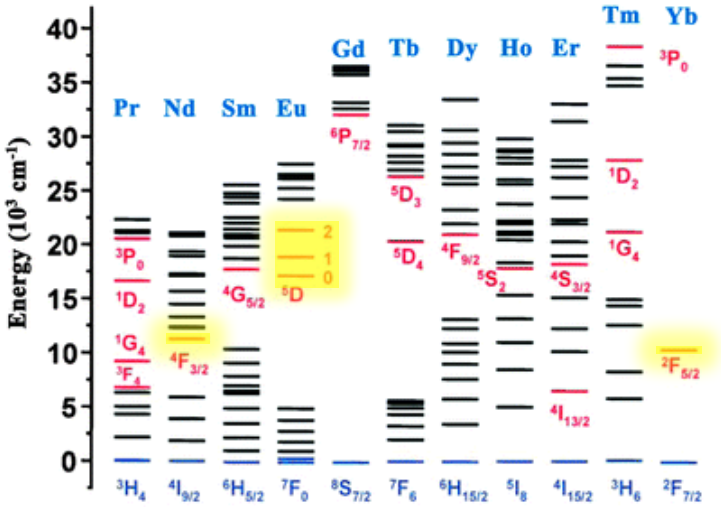


Figure 4.15 – Reproduced Dieke diagram[12], with the excited states of neodymium(III), europium(III) and ytterbium(III) highlighted.

Upon co-inclusion of target naphthalene complexes **92.Nd** or **93.Yb** with $\mathbf{MV^{2+}}$ and **CB[8]** (**Figure 4.16-i**), excitation of the manifested lower energy excited state of the ternary CT would initiate efficient ET (in the regime where Φ_B ET > Φ_A ET) to the respective low lying neodymium(III) $^4F_{3/2}$ and ytterbium(III) $^2F_{5/2}$ excited states of **92.Nd** and **93.Yb** (**Figure 4.16-ii**).

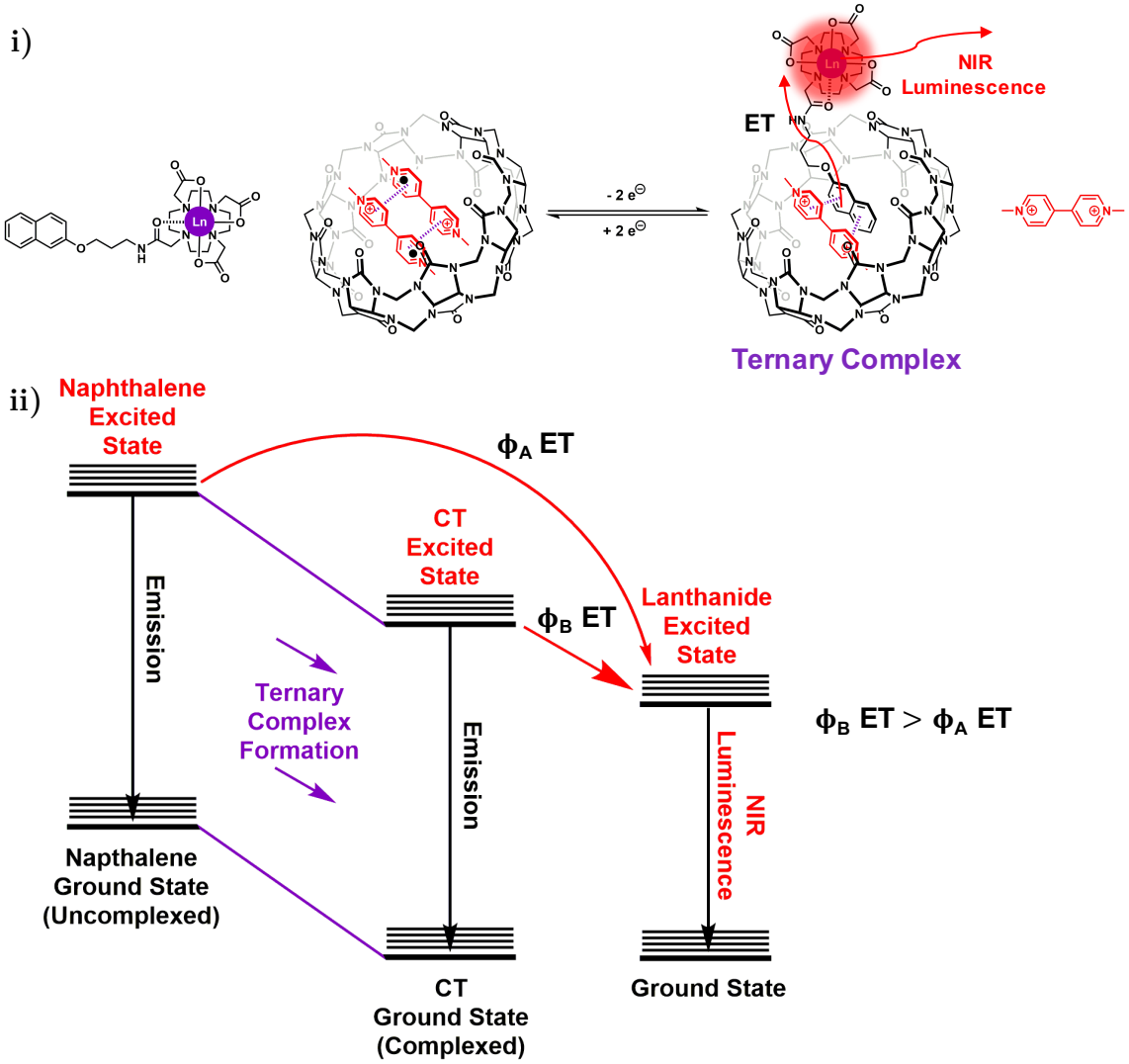


Figure 4.16 – i) Proposed ternary complex mediated redox switching of NIR lanthanide luminescence (Ln = ytterbium(III), neodymium(III)) and ii) the proposed photophysical mechanism for CT-sensitised NIR lanthanide luminescence.

4.3.3 Ternary complex studies

Ternary complexation studies with **92.Nd** and **93.Yb** were conducted with the assistance of M. Cunningham (Prof. J. J. Davis research group) and Dr. O. A. Blackburn (Prof. S. Faulkner research group).

4.3.3.1 Luminescence properties

Upon excitation of the naphthalene antenna at λ_{ex} = 280 nm, uncomplexed **92.Nd** and **93.Yb** exhibited naphthalene centred fluorescence with maxima at λ_{max} = 350 nm. The fluorescence intensity of **93.Yb** was lower in comparison to **92.Nd**, inferring a greater degree of ET between the naphthalene and the ytterbium(III) metal centre rather than the neodymium(III) metal centre. Upon co-inclusion with **CB[8]** and **MV²⁺**, extensive quenching of naphthalene fluorescence was observed in both ternary complexes (**92.Nd**, **MV²⁺**) ⊂ **CB[8]** and (**93.Yb**, **MV²⁺**) ⊂ **CB[8]**, attributed to the presence of the ternary complex CT interaction (**Figure 4.17**).

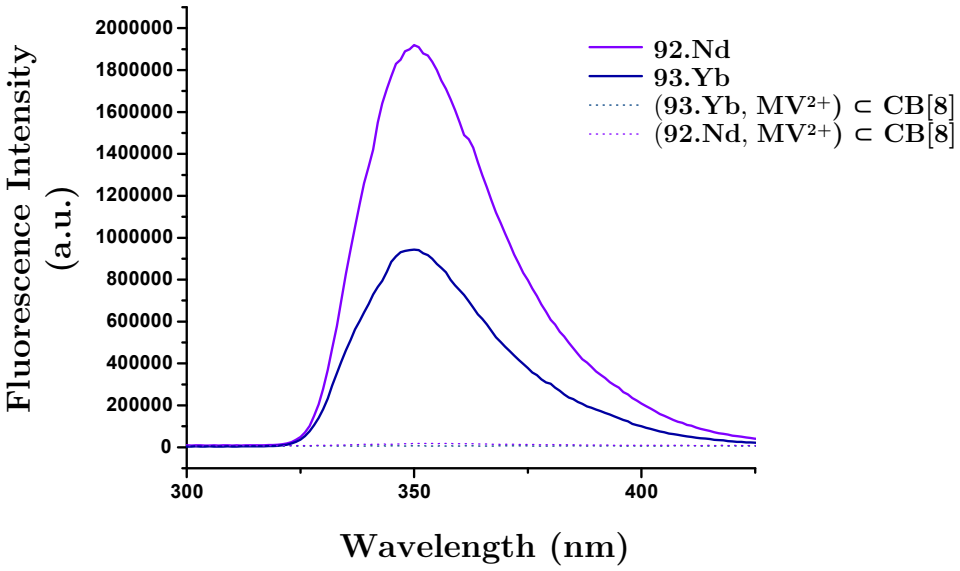


Figure 4.17 – Fluorescent outputs of uncomplexed **92.Nd**, **93.Yb** (solid lines) and ternary complexes (**92.Nd**, **MV²⁺**) ⊂ **CB[8]**, (**93.Yb**, **MV²⁺**) ⊂ **CB[8]** (dotted lines). *All complexes were generated in H_2O solution at 298 K, and at a concentration of 0.5 mM. All spectra were recorded at 298 K upon excitation of the naphthalene chromophore (λ_{ex} = 280 nm). The fluorescent output from the organic chromophore were acquired using excitation and emission slit widths of 14 nm, and all spectra provided are those acquired following averaging over 10 scans.*

Free **92.Nd** and **93.Yb** exhibited sensitised NIR phosphorescent emission upon excitation of the naphthalene antenna chromophore, with characteristic emission wavelengths of λ_{max} = 803 nm, 1058 nm in the case of **92.Nd** and λ_{max} = 1040 nm in the case of **93.Yb**. In a similar manner to the fluorescent emission, the

phosphorescent emission was extensively quenched upon ternary complex formation (**Figure 4.18-i, ii**).

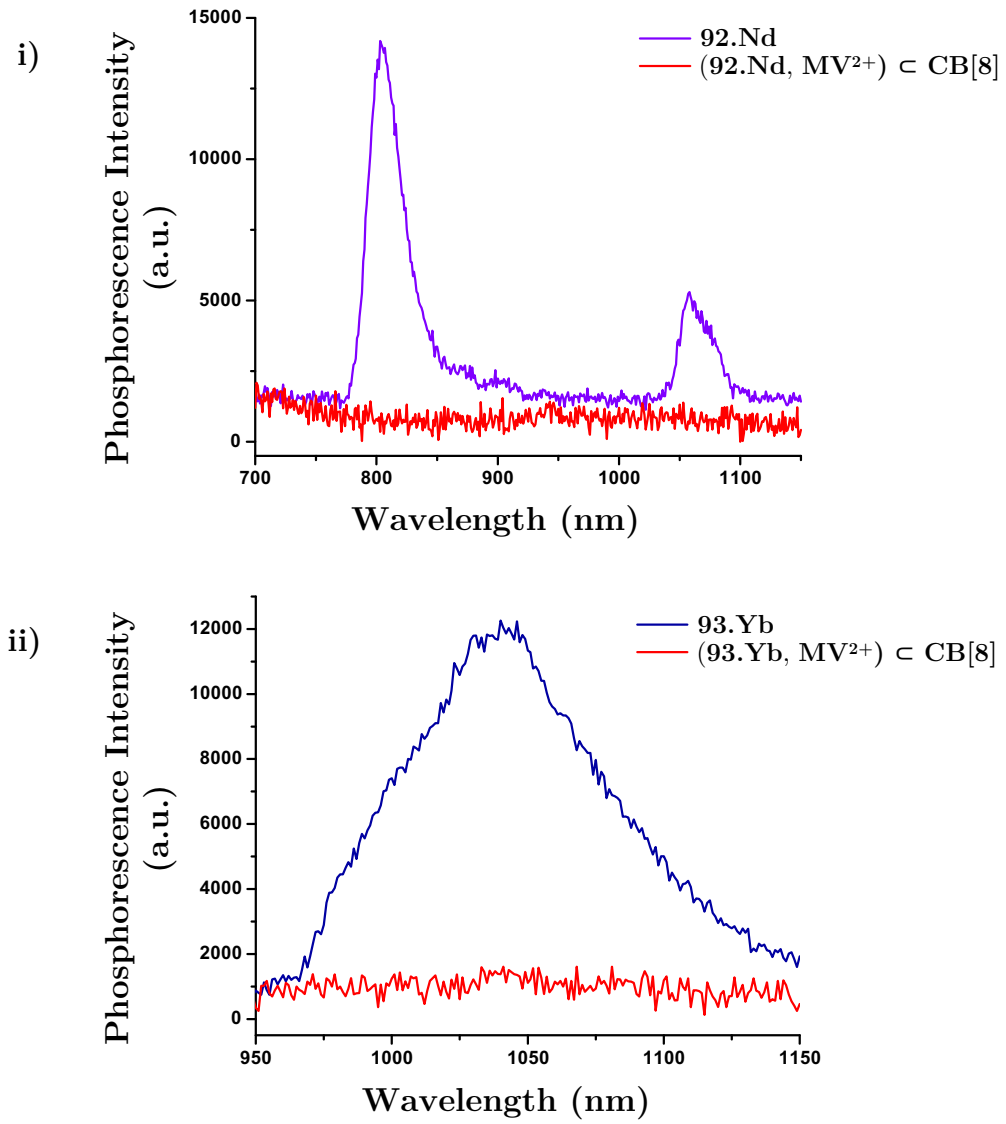


Figure 4.18 – Phosphorescent emission of i) uncomplexed **92.Nd** (purple trace) and ternary complex (**92.Nd**, $\mathbf{MV^{2+}}$) ⊂ **CB[8]** (red trace); ii) uncomplexed **93.Yb** (blue trace) and ternary complex (**93.Yb**, $\mathbf{MV^{2+}}$) ⊂ **CB[8]** (red trace). *All complexes were generated in H_2O solution at 298 K, and at a concentration of 0.5 mM. All spectra were recorded at a detector temperature of 195 K upon excitation of the naphthalene chromophore (λ_{ex} = 280 nm). The phosphorescent output from the lanthanide metal centres (ytterbium(III), neodymium(III)) were acquired using excitation and emission slit widths of 14 nm, and all spectra provided are those acquired following averaging over 10 scans.*

Attempts at excitation in the CT region (*ca.* 450 nm) of the ternary complexes of **92.Nd** and **93.Yb** similarly gave highly quenched NIR phosphorescent outputs. To confirm the quenching energetic pathway, the effect of oxygen on the luminescent

output was deduced *via* degassing of the solutions of free and complexed **92.Nd**. These experiments produced no changes to the phosphorescent emission features, suggesting that irrespective of ternary complex formation, ET from the naphthalene antenna to the respective lanthanide excited states is faster than any potential oxygen mediated triplet luminescence quenching processes (**Figure 4.19**).

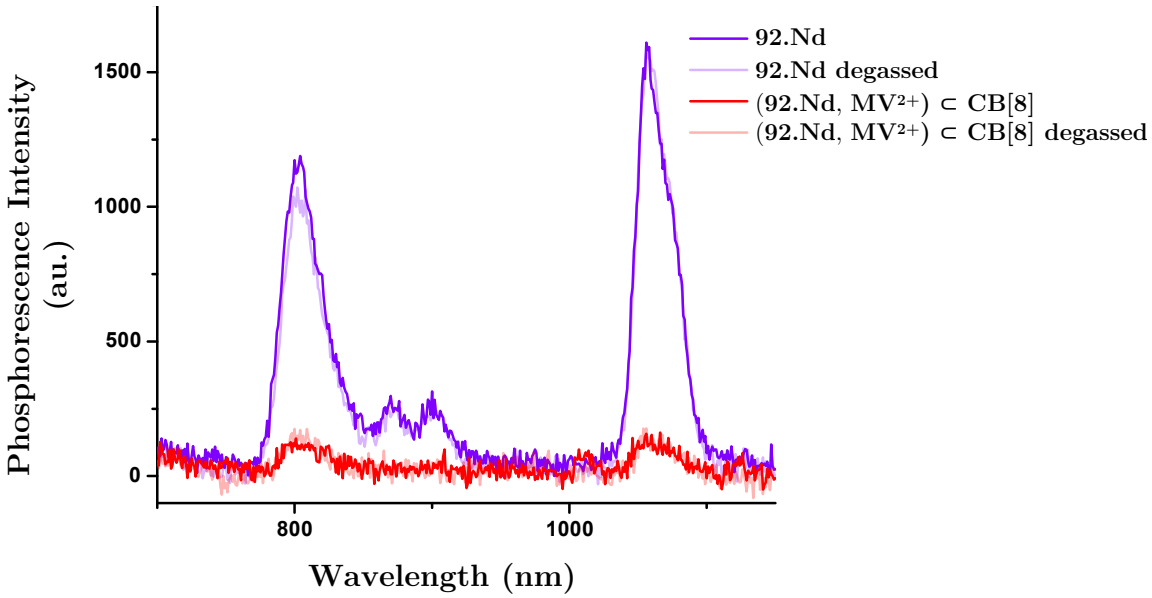


Figure 4.19 – NIR luminescent outputs of oxygenated and deoxygenated solutions of free **92.Nd** (purple traces) and (**92.Nd**, **MV²⁺**) ⊂ **CB[8]** (red traces). *All complexes were generated in H_2O at 298 K, and at a concentration of 0.5 mM. All spectra were recorded at a detector temperature of 195 K upon excitation of the naphthalene chromophore (λ_{ex} = 280 nm). The phosphorescent output from the neodymium(III) centre was acquired using excitation and emission slit widths of 14 nm, and all spectra provided are those acquired following averaging over 10 scans.*

4.3.4 Summary

It was found that sensitised NIR luminescent emission could be achieved through excitation of the proximal naphthalene antenna components of **92.Nd** and **93.Yb** much like the sensitised europium(III) luminescence of **91.Eu** (**Section 4.2**). The extent of fluorescent and NIR phosphorescent emission quenching by the presence of CT in ternary complexes (**92.Nd**, **MV²⁺**) ⊂ **CB[8]** and (**93.Yb**, **MV²⁺**) ⊂ **CB[8]** was significantly greater than that observed in the ternary complex (**91.Eu**, **MV²⁺**) ⊂ **CB[8]** and no evidence of CT sensitised NIR luminescent output was observed.

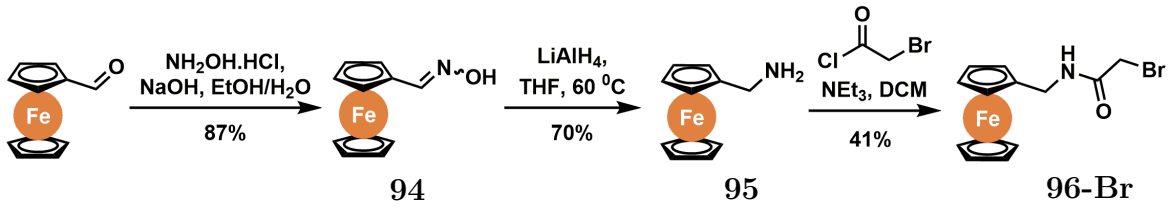
It was additionally found that the observed NIR luminescence quenching was not sensitive to the presence of oxygen, confirming the CT mediated NIR luminescence quenching phenomenon.

4.4 Towards a Ferrocene Containing Heteroternary Complex Featuring Redox Switchable Luminescent Output

4.4.1 Synthesis of ferrocene-viologen component

Given the promise exhibited by the redox switchable output of the heteroternary complexes in the previous section, the effects on the system upon inclusion of the redox active ferrocene-appended viologen derivative $\mathbf{99}^{2+}$ was explored.

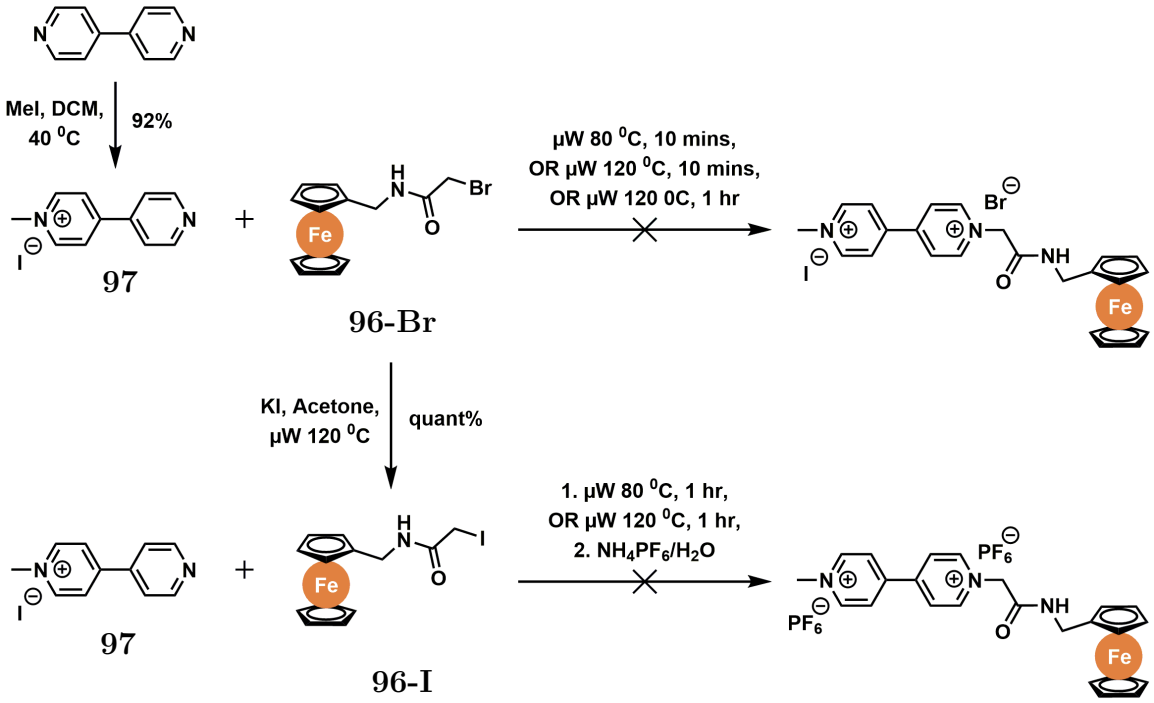
Firstly, an appropriately functionalised ferrocene end group motif was synthesised for attachment to a mono-substituted viologen motif. Reaction of commercially available ferrocene carboxaldehyde with hydroxylammonium hydrochloride in the presence of NaOH afforded ferrocene oxime **94**[20] in 87% yield. The oxime was reduced using $LiAlH_4$ in THF to give corresponding amine **95**[20] in 70% yield which upon condensation with excess bromoacetyl chloride in DCM/NEt_3 afforded ferrocene *N*-amidoacetyl bromide **96-Br** in 41% yield (**Scheme 4.4**).



Scheme 4.4 – Synthesis of ferrocene derivative **96-Br**.

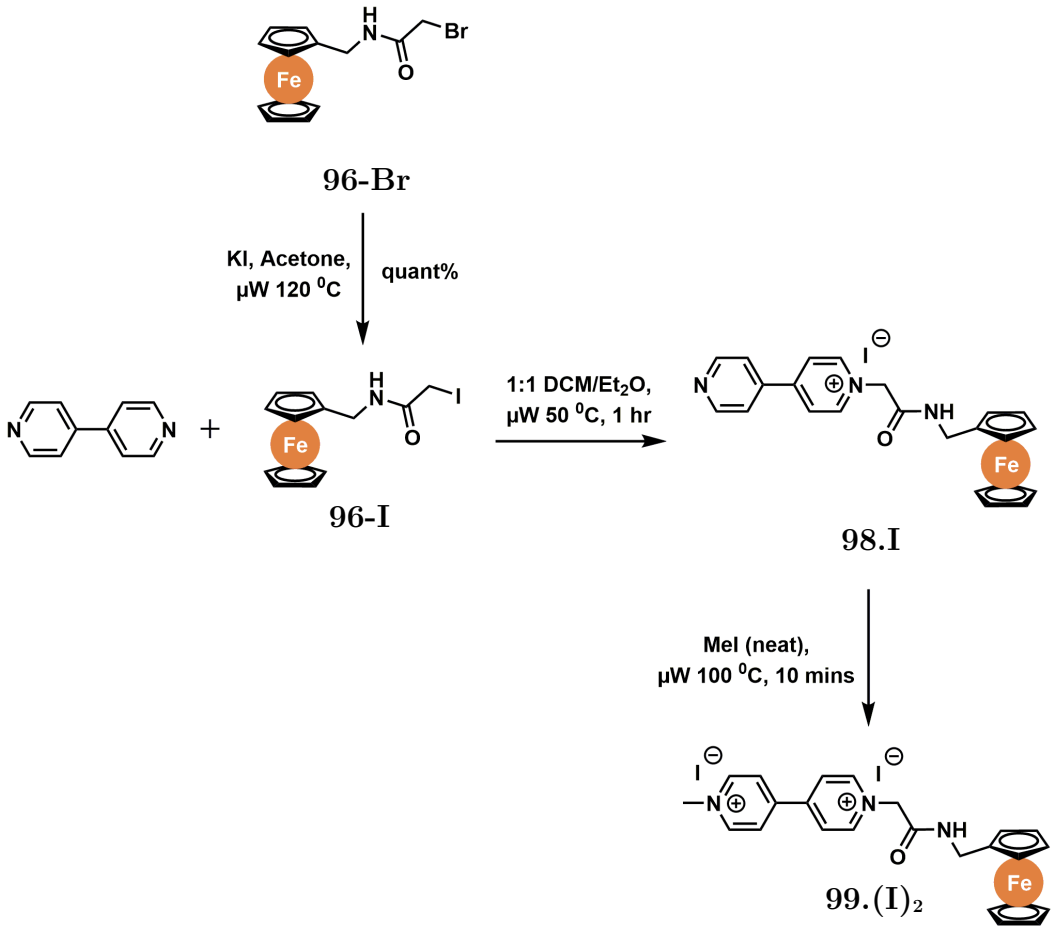
A sequential two-step alkylation strategy of 4,4'-bipyridine was devised to prepare the ferrocene-appended viologen derivative $\mathbf{99}^{2+}$. Firstly, 4,4'-bipyridine was mono-alkylated with MeI in DCM to give 1-methyl-4,4'-bipyridinium iodide **97** in 75% yield. Lamberto et. al.[21] described the use of microwave heating to facilitate the

second alkylation step in the preparation of a variety of asymmetric viologen derivatives. However, despite the use of a variety of reaction times, temperatures and addition of KI, the product $\mathbf{99}^{2+}$ could not be isolated in an acceptable yield (**Scheme 4.5**).



Scheme 4.5 – Attempted synthesis of ferrocene viologen derivative $\mathbf{99}^{2+}$.

Hence an alternative synthetic approach was undertaken. The intermediate monoalkylated ferrocene appended salt **98.I** was isolated in an acceptable yield of 41% after reaction of a three-fold excess of 4,4'-bipyridine with **96-I** in MeCN. Subsequent methylation with MeI afforded a crude product which decomposed during purification on silica preparative TLC. However, sequential washing with increasingly polar solvents afforded the desired product $\mathbf{99.(I)_2}$ in a yield of 44% (**Scheme 4.6**) and was characterised by ^{1}H NMR, ^{13}C NMR and ESI-HRMS (**Figure 4.20**).



Scheme 4.6 – Alternative synthetic route to ferrocene viologen derivative **99.(I)$_2$**.

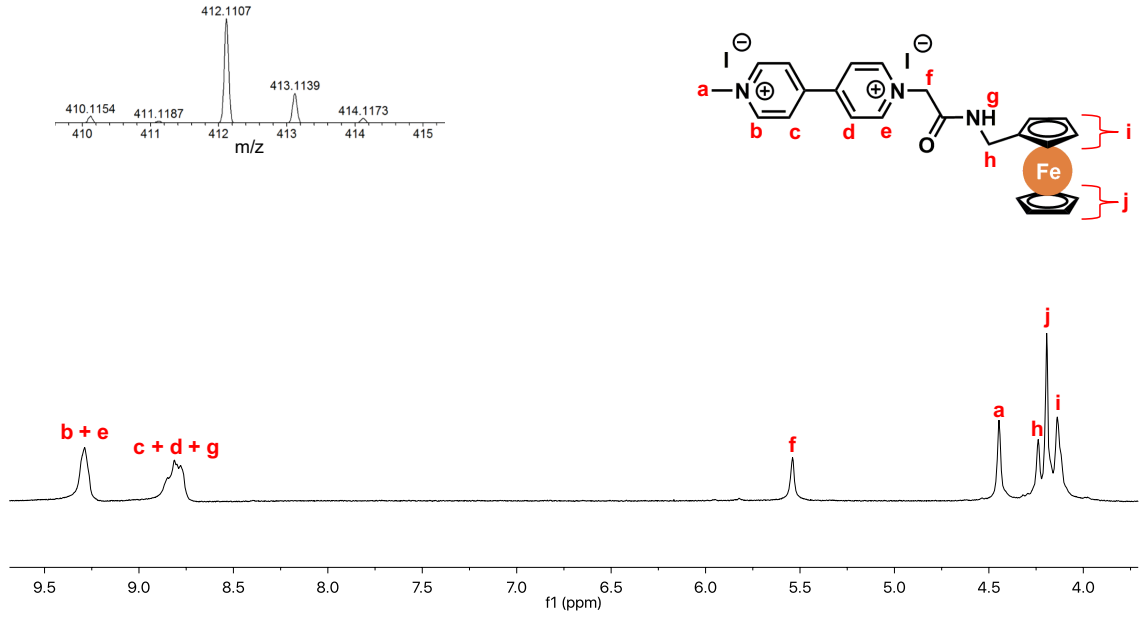


Figure 4.20 – Truncated ^{1}H NMR spectrum of **99.(I)$_2$** (400 MHz, DMSO-d_6) and (inset) ESI-HRMS of **99.(I)$_2$**.

4.4.2 Ternary complex studies

Initially it was found that **99.(I)$_2$** did not possess sufficient solubility in D_2O to conduct ^{1}H NMR complexation studies with **CB[8]** and **DHN**. The desired concentrations of 0.5 mM were achieved with the corresponding chloride salt **99.(Cl)$_2$**, which was acquired *via* anion exchange on Amberlite® resin (H_2O, Cl^- form). The ^{1}H NMR spectrum of an equimolar mixture of **99.(Cl)$_2$**, **CB[8]** and **DHN** exhibited distinctive upfield shifts of ferrocene proton resonances **i** and **j** ($\Delta\delta$(ppm) = -0.6), indicative of an equilibrium between binary complexation of the ferrocene terminus within the shielding cavity of **CB[8]** and ternary complexation of **DHN** and the viologen terminus of **99.(Cl)$_2$**. Further confirmation of this equilibrium process was seen in the broadening of **DHN** (proton resonances **1** – **3**) and viologen resonances of **99.(Cl)$_2$** (proton resonances **a** – **e**), in contrast to previous studies conducted on analogous systems (**Figure 4.21**).[2]

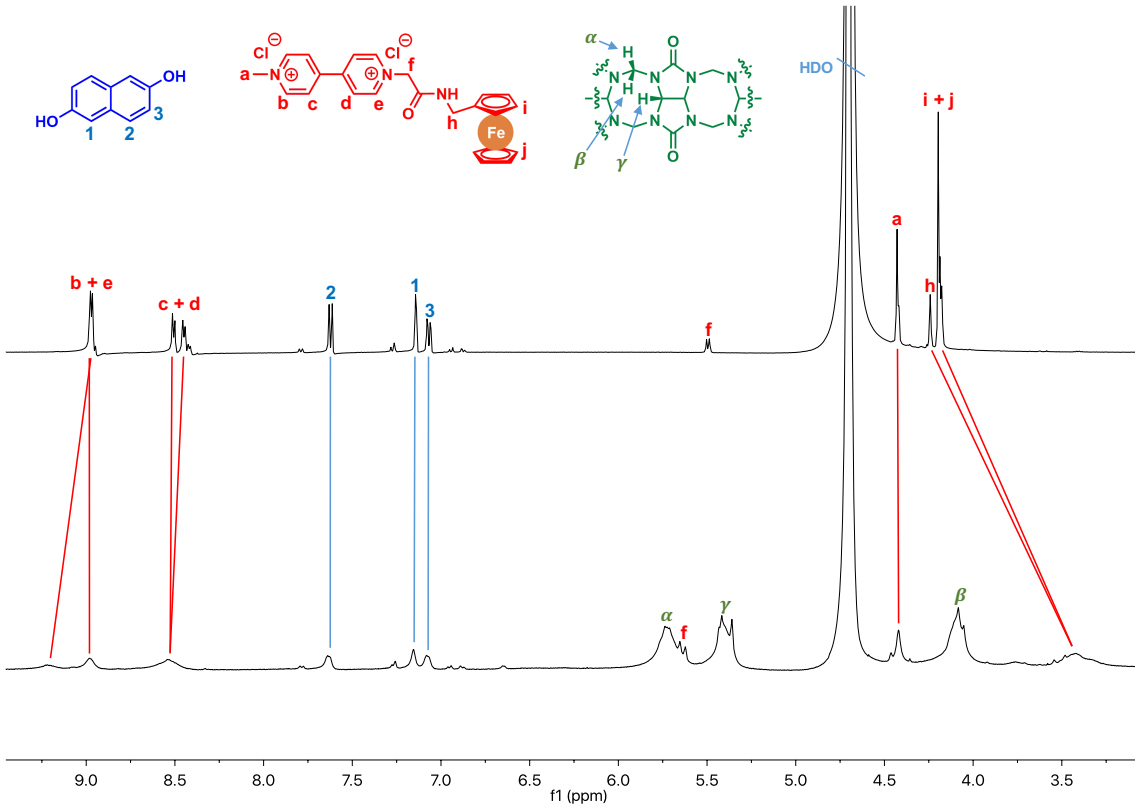


Figure 4.21 – Truncated ^{1}H NMR spectra of i) 1:1 **DHN/99.(Cl)$_2$** and ii) 1:1:1 **CB[8]/DHN/99.(Cl)$_2$** (D_2O, 500 MHz, 298 K).

During ternary complexation experiments between **99.(Cl)$_2$**, **DHN** and **CB[8]** in H_2O, ESI-MS analysis of the mixtures showed a distinctive peak at m/z = 585.87, corresponding to **99^{3+} ⊂ CB[8]** (**Figure 4.22-i**). This was attributed to oxidation of the dicationic ferrocenyl species **99^{2+}** to a tricationic ferrocenium species **99^{3+}**. Further ESI-MS analysis of the ternary complex solutions after one week revealed complete, irreversible decomposition of the **99.(Cl)$_2$** species (**Figure 4.22-ii**). A UV-Vis absorbance characteristic of ferrocenium species at *ca.* 625 nm was observed in many of the experiments conducted (**Figure 4.22-iii**). The absence of this absorption in the UV-Vis spectrum of **99.(Cl)$_2$** infers that the apparent oxidation is induced during the complexation event; *via* acid of crystallisation present in the commercially sourced **CB[8]** or the heating of the solutions induced by the prolonged sonication period used to form the complexes. This oxidation process is observable by the naked eye, solutions in many cases undergoing a colour change to a faint green. Attempts at reconverting the ferrocenium species **99^{3+}** to ferrocene species **99^{2+}** with reducing agents such as ascorbic acid failed. As a result, the formation of target ternary complexes (**91.Eu/92.Nd/93.Yb**, **99^{2+}**) ⊂ **CB[8]** (**Figure 4.6-ii**) was not attempted.

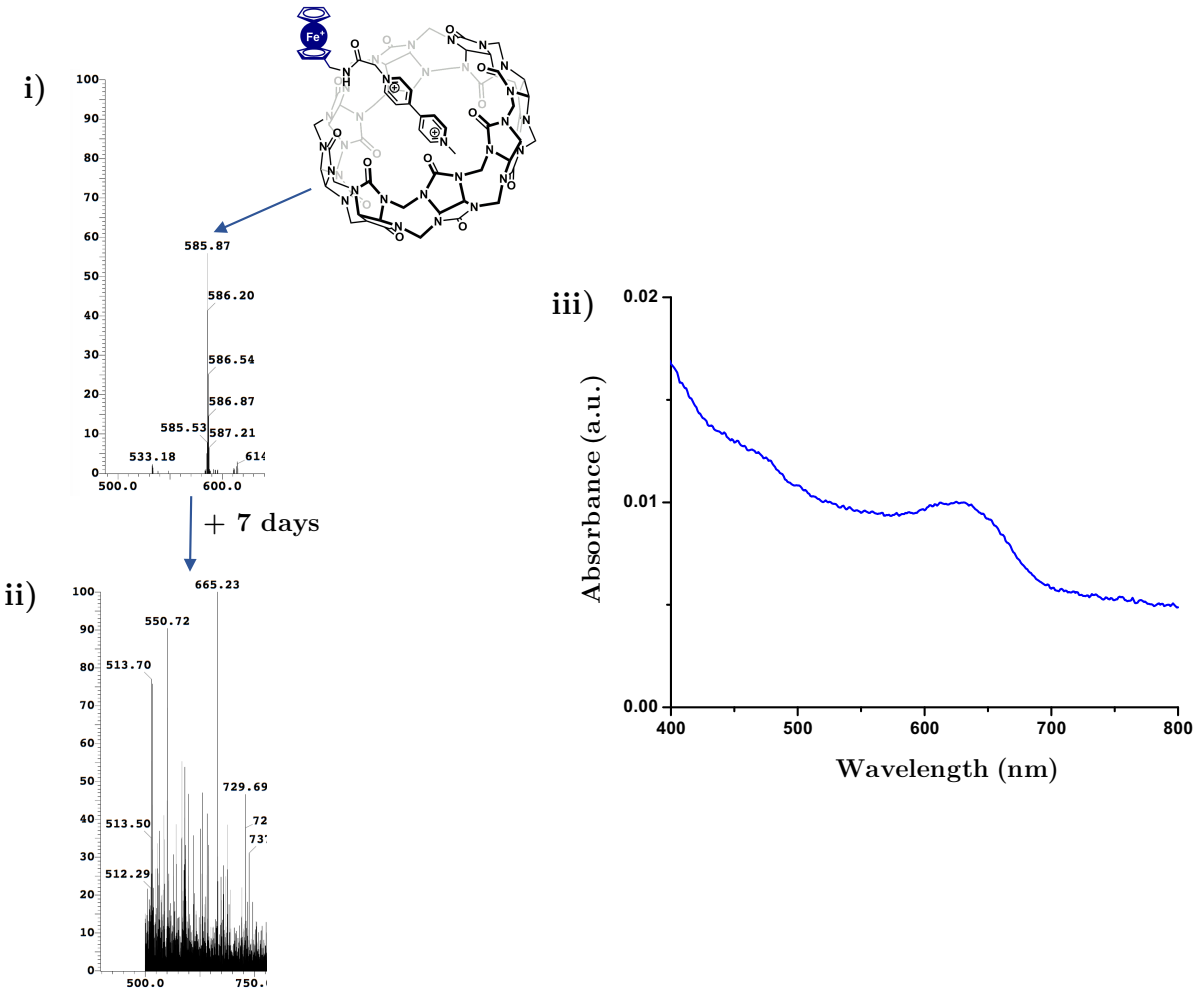


Figure 4.22 – Oxidation of $\mathbf{99}^{2+}$ to tricationic ferrocenium derivative $\mathbf{99}^{3+}$ upon addition of **CB[8]** evidenced by i) observation of molecular ion $[\mathbf{99} \subset \mathbf{CB[8]}]^{3+}$ by ESI-MS, followed by ii) complete decomposition of the complex and components; iii) the characteristic UV-Vis absorption of ferrocenium species *ca.* 625 nm in solutions of **CB[8]** and $\mathbf{99.(Cl)_2}$.

4.4.3 Summary

Discrete redox modulation of the luminescent output of ternary complex lanthanide luminescence *via* the ferrocene-functionalised viologen ternary component $\mathbf{99}^{2+}$ was unfortunately not realised due to a combination of stability issues and undesirable complexation phenomena of the ferrocene viologen with **CB[8]**, preventing the formation of the desired ternary complexes with **DHN** and lanthanide components.

4.5 Conclusions

The unprecedented potential of redox manipulation of supramolecular interactions within a ternary complex as method of modulating of lanthanide luminescence has been clearly demonstrated in the work described within this chapter.

In the first section, the application of the known redox tuneable inclusion stoichiometry within the **CB[8]** ternary complexes of viologen and electron rich aromatic components was successfully harnessed towards the reversible modulation of the luminescent output of novel europium(III)-containing component **91.Eu** *via* formation of a ternary complex stabilised CT.

In the second section, efforts were made to create a CT activated NIR-luminescent ternary complex. The synthesis of two novel NIR emitting ternary components **92.Nd** and **93.Yb** were realised and NIR luminescence in the uncomplexed state. The apparent lack of CT sensitised NIR luminescence by both (**92.Nd**, $\mathbf{MV^{2+}}$) $\subset$ **CB[8] and** (**93.Yb**, $\mathbf{MV^{2+}}$) $\subset$ **CB[8]** ternary complexes was attributed to either i) a poor match between the excited state of the ternary induced CT and neodymium(III)/ytterbium(III) excited states, ii) the existence of another lower energy quenching state in the ternary complex or iii) unusually high quantum yield of luminescence quenching of both lanthanide excited states and triplet naphthalene excited states in the presence of the ternary complex CT band.

In the third section the target ferrocene functionalised viologen component $\mathbf{99^{2+}}$ was synthesised. However, a combination of instability issues and unfavourable complexation characteristics precluded its use as a co-included motif to further augment the redox behaviour of lanthanide containing heteroternary complexes.

4.6 References for Chapter 4

(1) Chubarova, E. V.; Samsonenko, D. G.; Sokolov, M. N.; Gerasko, O. A.; Fedin, V. P.; Platas, J. G. *J. Incl. Phenom. Macrocycl. Chem.* **2004**, *48* (1–2), 31–35.

(2) Kim, H.-J.; Heo, J.; Jeon, W. S.; Lee, E.; Kim, J.; Sakamoto, S.; Yamaguchi, K.; Kim, K. *Angew. Chem. Int. Ed.* **2001**, *40* (8), 1526–1529.

(3) Ko, Y. H.; Kim, E.; Hwang, I.; Kim, K. *Chem. Commun.* **2007**, No. 13, 1305–1315.

(4) Biedermann, F.; Rauwald, U.; Cziferszky, M.; Williams, K. A.; Gann, L. D.; Guo, B. Y.; Urbach, A. R.; Bielawski, C. W.; Scherman, O. A. *Chem. – Eur. J.* **2010**, *16* (46), 13716–13722.

(5) Appel, E. A.; Barrio, J. del; Loh, X. J.; Scherman, O. A. *Chem. Soc. Rev.* **2012**, *41* (18), 6195–6214.

(6) Bird, C. L.; Kuhn, A. T. *Chem. Soc. Rev.* **1981**, *10* (1), 49–82.

(7) Bockman, T. M.; Kochi, J. K. *J. Org. Chem.* **1990**, *55* (13), 4127–4135.

(8) Jeon, W. S.; Kim, H.-J.; Lee, C.; Kim, K. *Chem. Commun.* **2002**, No. 17, 1828–1829.

(9) Hwang, I.; Ziganshina, A. Y.; Ko, Y. H.; Yun, G.; Kim, K. *Chem. Commun.* **2009**, No. 4, 416–418.

(10) Gschneidner, K. A. *Handbook on the Physics and Chemistry of Rare Earths*; Elsevier, 2005.

(11) Alpha, B.; Ballardini, R.; Balzani, V.; Lehn, J.-M.; Perathoner, S.; Sabbatini, N. *Photochem. Photobiol.* **1990**, *52* (2), 299–306.

(12) Liu, Y.; Tu, D.; Zhu, H.; Chen, X. *Chem. Soc. Rev.* **2013**, *42* (16), 6924–6958.

(13) Viola-Villegas, N.; Doyle, R. P. *Coord. Chem. Rev.* **2009**, *253* (13–14), 1906–1925.

(14) Tropiano, M.; Kilah, N. L.; Morten, M.; Rahman, H.; Davis, J. J.; Beer, P. D.; Faulkner, S. *J. Am. Chem. Soc.* **2011**, *133* (31), 11847–11849.

(15) Huang, A. Y.-T.; Tsai, C.-H.; Chen, H.-Y.; Chen, H.-T.; Lu, C.-Y.; Lin, Y.-T.; Kao, C.-L. *Chem. Commun.* **2013**, *49* (51), 5784–5786.

(16) Dadabhoy, A.; Faulkner, S.; Sammes, P. G. *J. Chem. Soc. Perkin Trans. 2* **2002**, No. 2, 348–357.

(17) Biedermann, F.; Scherman, O. A. *J. Phys. Chem. B* **2012**, *116* (9), 2842–2849.

(18) Gnoatto, S. C. B.; Dassonville-Klimpt, A.; Da Nascimento, S.; Galéra, P.; Boumediene, K.; Gosmann, G.; Sonnet, P.; Moslemi, S. *Eur. J. Med. Chem.* **2008**, *43* (9), 1865–1877.

(19) Lamberto, M.; Rastede, E. E.; Decker, J.; Raymo, F. M. *Tetrahedron Lett.* **2010**, *51* (42), 5618–5620.

(20) Pope, S. J. A.; Coe, B. J.; Faulkner, S.; Laye, R. H. *Dalton Trans.* **2005**, No. 8, 1482–1490.

(21) D'Aléo, A.; Picot, A.; Beeby, A.; Gareth Williams, J. A.; Le Guennic, B.; Andraud, C.; Maury, O. *Inorg. Chem.* **2008**, *47* (22), 10258–10268.

CHAPTER 5

Experimental

5.1. General Considerations

5.1.1. Solvents and reagents

All reagents and solvents were acquired from commercial sources and used without further purification. Where necessary, solvents were dried by passing through a MBraun MPSP-800 column and degassed with nitrogen. NEt_3 was distilled from and stored over KOH. Diethyl carbonate was distilled from CaH_2 and stored under nitrogen atmosphere. All TBA salts, $Cu(MeCN)_4PF_6$ and Grubb's II catalysts were stored in a vacuum desiccator prior to use. H_2O was de-ionised and microfiltered using a Milli-Q® Millipore machine. A Biotage Initiator 2.0 microwave was used to perform reactions where microwave heating was required. Column chromatography was carried out on Merck® brand silica gel 60 under a positive pressure provided by hand-held air bellows. Size exclusion chromatography was carried out using Biobeads SX-1 and $CHCl_3$ used as eluent. Where mixtures of solvents were used, they are reported summarily in v/v ratios. Amberlite® columns were prepared by washing the resin with 10% $NaOH_{(aq.)}$, H_2O, 1M NH_4X (where X is the anion required), H_2O and finally the solvent or solvent mixture to be used in the anion exchange.

5.1.2. Instrumental methods

5.1.2.1. NMR spectroscopy and other characterisation methods

Routine nuclear magnetic resonance spectroscopy (NMR) was carried out on Varian Mercury 300, Bruker AVIII 400, Bruker AVII 500 (with cryoprobe) or Bruker AVIII 500 at 298 K. All ^{1}H-^{1}H J coupling constants are reported as three bond couples (^3J) by default unless otherwise indicated. ^{13}C NMR spectra of paramagnetic lanthanide complexes were not obtained due to inherent peak broadening effects. Mass spectrometry was carried out on Waters Micromass LCT and Bruker µTOF spectrometers.

5.1.2.2. Absorption and luminescence spectroscopy

A Shimadzu UV-2401 PC UV-Vis recording spectrometer was used for UV-Vis absorption measurements. Luminescence spectra of lanthanide derivatives were measured on a Horiba Fluorolog 3. In the case of the neodymium(III) and ytterbium(III) complexes, the aqueous samples were excited using a pulsed nitrogen laser (PTI-3301-337nm) or using a dye laser (PTI-3302). All lanthanide luminescence spectra were collected in phosphorescence mode exciting at 270 nm

using a flash delay of 0.05 ms. Light emitted at right angles to the excitation beam was focused onto the slits of the monochromator (PTI120), which was used to select the desired wavelength. The growth and decay of the luminescence at selected wavelengths was detected using a germanium photodiode (Edinburgh Instruments, EI-P) and recorded using a digital oscilloscope (Tektronix TDS220) before being transferred to a computer for analysis. Luminescence lifetimes were obtained by iterative reconvolution of the detector response (obtained by using a scatter) with exponential tail fits used for the europium(III) species.

5.1.3. ^{1}H titration protocol

^{1}H NMR spectra were recorded on a Bruker AVIII 500 spectrometer at 298 K, unless otherwise stated. Initial sample volumes were made up to 0.5 ml, at a concentration of 1.5 mM of host. A solution of the anion as the tetrabutylammonium (TBA) salt was added in aliquots to the host solution and the chemical shift of the relevant protons were monitored for 17 data points. The spectra were referenced to the residual solvent peak. The values of the observed chemical shift and the guest concentration were entered into a WinEQNMR2[1] programme input file for every titration point and estimates for the binding constant and limiting chemical shifts were made. The parameters were refined using non-linear least squares analysis to obtain the best fit between the observed and calculated chemical shifts for a 1:1 or 2:1 binding stoichiometry as appropriate. The input parameters were varied until the best-fit values of the stability constants and their corresponding errors converged. Unfortunately, owing to the limiting 10-20 mg quantities of the host systems which were obtained, it was impractical to perform multiple repetitions of each titration experiment in order to demonstrate reproducibility. Each reported association constant value was therefore derived from a single titration experiment, and the reproducibility of the outcome within acceptable error was assumed. However, in cases where unexpected or outlying values were obtained the titration experiment was repeated in order to verify the result.

5.1.4. Ternary complexation protocol

CB[8].16H_2O (8.1 mg, 50 μmol) was added to an aqueous solution of the first guest partner (50 μmol) in H_2O (10 ml) and subjected to an extended sonication period of 2-3 hours, or until a homogenous solution of the binary complex (0.5 mM) was

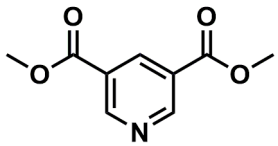
obtained. Addition of the second guest partner (50 μmol) yielded the complex after a short further sonication period of approximately 60 seconds.

5.1.5. General procedure for acid chloride synthesis

For the conversion of carboxylic acids to their corresponding acid chloride derivatives, the following general procedure was used: To a suspension of acid (1 mmol) in dry DCM (10 ml) oxalyl chloride (2 mmol) was added drop-wise under N_2 atmosphere. A drop of DMF (~0.01 ml, cat.) was added and the reaction stirred at 0^0C under N_2 until the solution became homogeneous. The solvent was removed *in vacuo* to leave a crude solid. This was immediately re-dissolved in dry DCM and reacted on as desired, the yield was assumed to be quantitative in all cases.

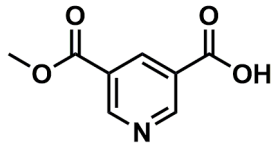
5.2. Synthesis of Compounds from Chapter 2

Dimethyl pyridine-3,5-dicarboxylate 2[2]



Pyridine-3,5-dicarboxylic acid (1.00 g, 5.98 mmol), suspended in MeOH (3.6 ml) and conc. H_2SO_4 (3.4 ml), was irradiated with microwaves at 120 ^{0}C for 1 hour. The solution was then cooled to room temperature and NH_4OH (10 ml) was added drop-wise. The product then was extracted with Et_2O (3 x 20 ml). The organic layers were combined and dried over $MgSO_4$, before the solvent was removed *in vacuo* to afford the product **2** as a white solid (1.08 g, 87%). **^{1}H NMR** (300 MHz, $CDCl_3$) **δ** (ppm): 9.37 (d, Pyr-H, ^4J = 2.1 Hz, 2H), 8.91 (t, Pyr-H, ^4J = 2.0 Hz, 1H), 4.00 (s, COOMe, 6H). **MS** (ESI +ve) m/z: 196.1 ($[M+H]^+$, $C_9H_{10}NO_4$ requires 196.1).

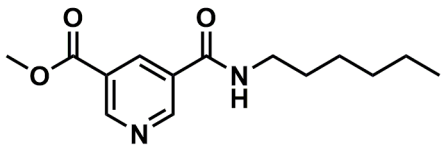
5-(Methoxycarbonyl)nicotinic acid 3[2]



Dimethyl pyridine-3,5-dicarboxylate **2** (2.98 g, 15.2 mmol) was dissolved in MeOH (100 ml) and KOH pellets (852 mg, 15.2 mmol) were added to the solution and the mixture was stirred for 16 hrs. The solvent was removed by rotary evaporation and redissolved in the minimum of H_2O (~10 ml) and acidified to pH 2-3 by careful drop-wise addition of aqueous 1M HCl, at which point large amounts of white precipitate

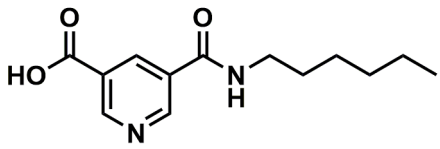
formed. The product **3** was isolated by vacuum filtration and rinsed with Et_2O (2 x 20 ml) and subsequently dried under a vacuum (2.545 g, 92%). **^{1}H NMR** (300 MHz, CD_3OD) δ (ppm): 9.29 (m, Pyr-H, 2H), 8.90 (s, Pyr-H, 1H), 3.98 (s, COOMe, 3H). **MS** (ESI +ve) m/z: 182.1 ($[M+H]^+$, $C_8H_8NO_4$, requires 182.2).

Methyl 5-(hexylcarbamoyl)nicotinate 4[3]



5-(Methoxycarbonyl)nicotinic acid **3** (500 mg, 2.76 mmol) was converted to the corresponding acid chloride using the general procedure, and dissolved in DCM (30 ml), before a solution of hexylamine (0.40 ml, 3.03 mmol), NEt_3 (.77 ml, 5.52 mmol) in DCM (30 ml) was added drop-wise at 0 ^{0}C. The reaction mixture was stirred at room temperature under N_2 atmosphere for 16 hrs and then washed with 10% $HCl_{(aq.)}$ (30 ml), 10% $NaOH_{(aq.)}$ (30 ml) and brine (50 ml). The organic layer was dried over $MgSO_4$ and solvent removed *in vacuo*. Purification by silica gel chromatography (9:1 DCM/EtOAc) afforded the product **4** as a white solid (401 mg, 55%). **^{1}H NMR** (300 MHz, $CDCl_3$) δ (ppm): 9.20 (d, Pyr-H, ^4J = 2.1 Hz, 1H), 8.62 (s, Pyr-H, 1H), 7.02 (bs, CON-H, 1H), 3.91 (s, COOMe, 3H), 3.42 (m, NH-CH_2, 2H), 1.83 – 1.26 (m, CH_2, 8H), 0.83 (t, J = 6.9 Hz, CH_3, 3H). **MS** (ESI +ve) m/z: 287.1 ($[M+Na]^+$, $C_{14}H_{20}N_2O_3Na$ requires 287.3).

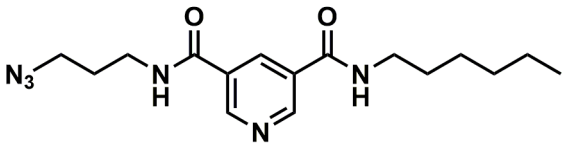
5-(Hexylcarbamoyl)nicotinic acid 5[3]



Methyl 5-(hexylcarbamoyl)nicotinate **4** (1 g, 3.49 mmol) was dissolved in MeOH (40 ml) and KOH pellets (410 mg, 7.31 mmol) were added to the solution and the mixture was stirred for 16 hrs. The solvent was removed by rotary evaporation and redissolved in the minimum of H_2O (~ 10 ml) and acidified to pH 2-3 by careful drop-wise addition of aqueous 1M HCl, at which point large amounts of white precipitate formed. This was isolated by vacuum filtration and rinsed with Et_2O (2 x 10 ml) and subsequently dried under a vacuum to give the product **5** (738 mg, 77 %). **^{1}H NMR** (300 MHz, DMSO-*d*$_6$) δ (ppm): 9.07 (d, Pyr-H, ^4J = 2.2 Hz, 1H), 9.03 (d, Pyr-H, ^4J = 2.2 Hz, 1H), 8.75 (s, CON-H, 1H), 8.58 (t, Pyr-H, ^4J = 2.1 Hz,

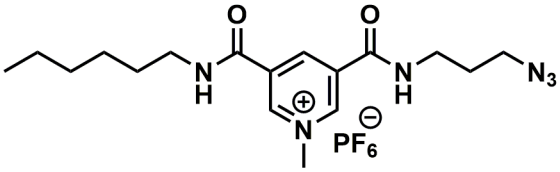
1H), 3.23 (q, NH-C$\underline{H}_2$, J = 6.7 Hz, 2H), 1.58 – 1.14 (m, C$\underline{H}_2$, 8H), 0.83 (t, C$\underline{H}_3$, J = 6.5 Hz, 3H). **MS** (ESI +ve) m/z: 251.1 ($[M+H]^+$, $C_{13}H_{19}N_2O_3$ requires 251.1).

Pyridine bis-amide azide 6



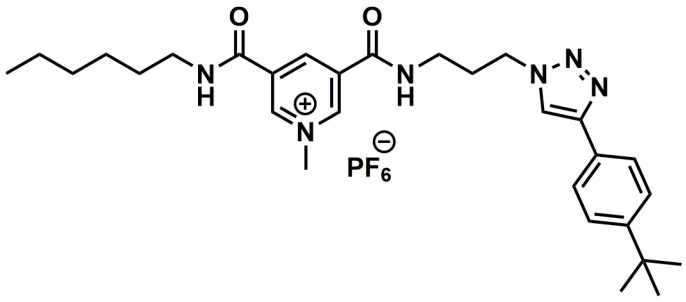
5-(hexylcarbamoyl)nicotinic acid **5** (1.141 g, 4.53 mmol) was converted to the corresponding acid chloride using the general procedure, and dissolved in DCM (20 ml). 3-Bromopropylamine hydrobromide (817 mg, 5.88 mmol) was suspended in dry DCM (50 ml) and stirred in an ice bath. NEt_3 (3.16 ml, 27.15 mmol) was slowly added under an atmosphere of N_2 and the mixture was stirred for 24 hours whilst allowing the reaction temperature to reach room temperature. The mixture was washed with 1M $HCl_{(aq.)}$ (2 x 30 ml), 1M $NaOH_{(aq.)}$ (2 x 30 ml), distilled H_2O (1 x 30 ml), dried over $MgSO_4$ and the solvent removed under reduced pressure to yield a crude yellowish oil. Without further purification, the crude bromide was dissolved in dry DMF (50 ml) and NaN_3 (2.95 g, 45.3 mmol) added to the solution under stirring. The mixture was placed under an atmosphere of N_2 and heated at 80 ^oC for 24 hours. The reaction mixture was then poured onto ice water (200 ml) and extracted with DCM (4 x 50 ml). The combined organic fractions were then washed with brine (2 x 50 ml), dried over $MgSO_4$ and the solvent removed *in vacuo* followed by high vacuum to remove residual amounts of DMF. The crude azide was then purified using flash column chromatography (0 » 3% MeOH/EtOAc) to obtain azide **6** as a white solid (647 mg, 43%). **^{1}H NMR** (400 MHz, $CDCl_3$) δ (ppm): 9.07 (s, Pyr-$\underline{H}$, 2H), 8.45 (s, Pyr-$\underline{H}$, 1H), 6.75 (s, CON-$\underline{H}$, 1H), 6.36 (s, CON-$\underline{H}$, 1H), 3.54 (t, J = 7.1 Hz, C$\underline{H}_2$-NH, 2H), 3.42 (2 x t, C$\underline{H}_2$-N_3 + C$\underline{H}_2$-NH, 4H), 1.88 (bs, $CH_2C\underline{H}_2CH_2$, 2H), 1.76 – 1.14 (m, $CH_2C\underline{H}_2CH_2$, 6H), 0.84 (t, C$\underline{H}_3$, J = 6.2 Hz, 3H). **^{13}C NMR** (76 MHz, CD_3OD) δ (ppm): 158.59, 146.56, 137.90, 110.03, 48.63, 39.85, 37.16, 31.18, 28.79, 28.08, 26.27, 22.15, 4 peaks missing; presumed overlapped. **MS** (ESI +ve) m/z: 333.2 ($[M+H]^+$, $C_{16}H_{25}N_6O_2$ requires 333.2). **HRMS** (ESI +ve) m/z: 355.1842 ($[M+Na]^+$, $C_{16}H_{24}N_6O_2Na$ requires 355.1853).

Pyridinium bis-amide azide 7.PF$_6$



6 (100 mg, 0.3 mmol) was dissolved in dry $CHCl_3$ (3 ml) and MeI (3 ml) was added drop-wise to the solution. The mixture was heated to 45 ^{O}C and placed under an atmosphere of N_2 and stirred for 16 hours. The solvent of the reaction mixture was removed *in vacuo* and redissolved in DCM (10 ml) and the organic phase washed with aqueous NH_4PF_6 (1 M, 8 x 10 ml). The combined aqueous washes were back extracted with DCM (2 x 10 ml) and the combined organic phases were washed with H_2O (2 x 15 ml) and dried over $MgSO_4$. The solvent was removed to give **7.PF$_6$** as a light yellow powder in near quantitative yield (141 mg, 97% yield). **^{1}H NMR** (300 MHz, CD_3OD) δ (ppm): 9.54 – 9.35 (m, Pyr-H, 3H), 4.05 (s, 6H), 3.54 (t, J = 6.9 Hz, 2H), 3.54 – 3.28 (m, 4H), 1.93 (p, J = 6.6 Hz, 2H), 1.64 (q, J = 7.7 Hz, 2H), 1.36 – 1.17 (m, 4H), 0.85 (t, J = 4.6 Hz, 3H). **^{13}C NMR** (101 MHz, CD_3OD) δ (ppm): 161.62, 161.39, 146.76, 140.98, 134.31, 134.16, 48.71, 48.43, 40.14, 37.39, 31.27, 28.82, 28.14, 26.38, 22.24, 12.99, 1 peak missing; presumed overlapped. **MS** (ESI +ve) m/z: 347.2 ([M-PF_6^-]$^+$, $C_{17}H_{27}N_6O_2^+$ requires 347.2). **HRMS** (ESI +ve) m/z: 347.2194 ([M-PF_6^-]$^+$, $C_{17}H_{27}N_6O_2^+$ requires 347.2190).

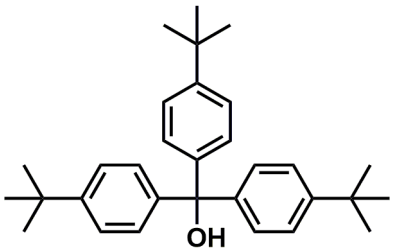
Pyridinium-triazole receptor 9.PF$_6$



Azide **7.PF$_6$** (27.7 mg, 0.056 mmol) was dissolved in dry, degassed DCM (5 ml). 4-*tert*-butyl phenyl acetylene (9.8 mg, 0.062 mmol), TBTA (5.93 mg, 0.011 mmol) and $Cu(MeCN)_4PF_6$ (6.29 mg, 0.017 mmol) were added sequentially and the reaction mixture was stirred under a N_2 atmosphere for 48 hours. The solution was then washed $NH_4OH_{(aq.)}$ (1M, 2 x 30 ml) and H_2O (2 × 30 ml). The organic layer was then dried over $MgSO_4$ and the solvent removed *in vacuo* and the crude product was purified using flash column chromatography (5% MeOH/DCM) to give pure product **9.PF$_6$** as a pale yellow solid (10.2 mg, 28% yield). **^{1}H NMR** (300 MHz, CD_3OD) δ (ppm): 9.39 – 9.31 (m, Pyr-H, 2H), 9.22 (s, Pyr-H, 1H), 8.31 (s, Triazole

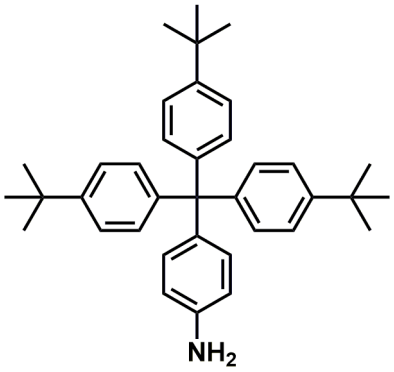
Ar-H, 1H), 7.67 (d, Ar-H, J = 8.2 Hz, 2H), 7.46 (d, Ar-H J = 8.2 Hz, 2H), 4.58 (t, CH_2-triazole, J = 6.7 Hz, 2H), 4.45 (s, Pyr-N^+Me, 3H), 3.56 (t, CON-H, J = 6.5 Hz, 2H), 3.44 (t, CON-H, J = 7.3 Hz, 3H), 2.35 (q, $CH_2CH_2CH_2$, J = 6.5 Hz, 2H), 1.65 (q, $CH_2CH_2CH_2$, J = 7.0 Hz, 3H), 1.47 – 1.10 (s + m, Ar-tBu + $CH_2CH_2CH_2$, 15H), 0.93 (t, CH_3, J = 6.9 Hz, 3H). **^{13}C NMR** (76 MHz, $CDCl_3$) δ (ppm): 161.11, 160.79, 151.67, 147.48, 146.01, 134.88, 134.48, 127.03, 125.80, 125.22, 49.05, 48.04, 40.93, 34.63, 31.38, 31.20, 29.70, 28.92, 26.57, 22.68, 22.49, 13.99, 2 peaks missing, presumed overlapped. **^{19}F NMR** (283 MHz, CD_3OD) δ (ppm): -74.45 (d, ^2J = 707.9 Hz). **MS** (ESI +ve) m/z: 505.3 ($[M^+\text{-}PF_6^-]^+$, $C_{29}H_{41}N_6O_2^+$ requires 505.3). **HRMS** (ESI +ve) m/z: 505.3272 ($[M^+\text{-}PF_6^-]^+$, $C_{29}H_{41}N_6O_2^+$ requires 505.3286).

Tris(4-(*tert*-butyl)phenyl)methanol 12[4]



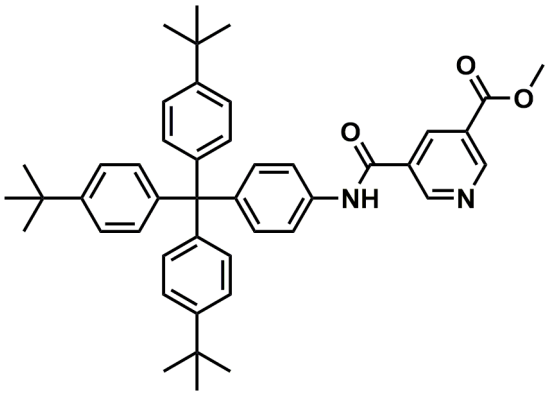
Magnesium turnings (1.5 g, 0.0618 mol) were suspended in dry THF (20 ml) before a few iodine crystals were added. 1-Bromo-4-*tert*-butyl benzene (7.55 g, 0.176 mol) was dissolved in dry THF (20 ml) and 2 ml of this solution was added to the magnesium suspension, under N_2, to initiate the reaction, with the remainder of the solution then left to add drop-wise at a rate to maintain a gentle reflux. Once addition was complete, the reaction mixture was refluxed for 1 hour under N_2. After this time, pre-distilled and dried diethyl carbonate (2.16 ml, 0.017 mmol) dissolved in dry THF (20 ml) was added drop-wise to the reaction mixture, which was then refluxed for 1 hour under N_2. The vessel was left to cool in an ice bath and a 10% $HCl_{(aq.)}$ (20 ml) was added carefully, whereupon a yellow suspension formed. The solids were filtered and the THF was then removed in vacuo and the resulting solution extracted into DCM (3 x 50 ml) and washed with 5% $NaHCO_{3(aq.)}$ (100 ml) and H_2O (100 ml). The organic phase was then dried over $MgSO_4$, filtered and the solvent removed to give the crude product, which was purified via recrystallisation from boiling cyclohexane to give **12** as an off-white solid (1.79 g, 23%). **^{1}H NMR** (400 MHz, $CDCl_3$) δ (ppm): 7.31 (d, Ar-H, J = 7.9 Hz, 6H), 7.19 (d, Ar-H, J = 8.1 Hz, 6H), 1.34 – 1.28 (m, Ar-tBu, 27H). **MS** (ESI +ve) m/z: 411.3 ($[M\text{-}OH]^+$, $C_{31}H_{39}^+$ requires 411.3).

Terphenyl amine 13[5]



Tris(4-(*tert*-butyl)phenyl)methanol **12** (1.79 g, 4.18 mmol) was suspended in acetyl chloride (40 ml) and heated for 16 hours at 60 ^{0}C. MeOH (40 ml) was added to the mixture and the solvents removed *in vacuo* to give a yellow solid which was immediately redissolved in aniline (20 ml, neat) and heated to 130 ^{0}C under an atmosphere of N_2 for 16 hours. The resulting deep purple solution was cooled to room temperature and quenched by pouring onto 10% $HCl_{(aq.)}$ (25 ml) and stirring for 20 minutes to give a purple precipitate. The residue was extracted with DCM (3 x 20 ml) and the combined extracts were washed with 5% $NaHCO_{3\,(aq.)}$ (1 x 20 ml), H_2O (1 x 20 ml) and the organic layer was dried over $MgSO_4$, filtered and dried *in vacuo* to give a faint purple residue that was purified via silica gel column chromatography (DCM, neat) to give product stopper amine **13** as a white solid (1.15 g, 55% yield). **^{1}H NMR** (400 MHz, $CDCl_3$) **δ** (ppm): 7.22 (d, Ar-H, J = 8.0 Hz, 6H), 7.09 (d, Ar-H, J = 8.2 Hz, 6H), 6.97 (d, Ar-H, J = 8.2 Hz, 2H), 6.60 (d, Ar-H, J = 8.1 Hz, 2H), 4.01 (bs, Ar-NH_2, 2H), 1.30 (s, Ar-tBu, 27H).

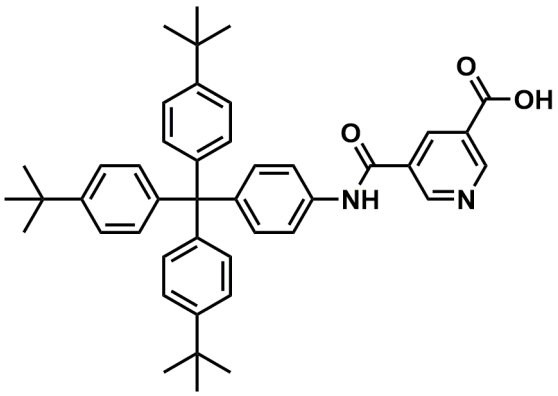
Mono-terphenyl mono-methyl nicotinic ester 14



5-(methoxycarbonyl)nicotinic acid **2** (543 mg, 3 mmol), terphenyl amine **13** (1.5 g, 3 mmol) and DMAP (cat.) was suspended in dry, degassed DCM (20 ml). EDC.HCl (690 mg, 3.6 mmol) was added to the suspension and the mixture was refluxed under

an atmosphere of N_2 for 16 hours. After cooling to room temperature, the mixture was washed with 1M $HCl_{(aq.)}$ (2 x 10 ml), 1M $NaOH_{(aq.)}$ (2 x 10 ml), distilled H_2O (1 x 10 ml), dried over $MgSO_4$ and the solvent removed under reduced pressure. The crude solid obtained was purified *via* flash column chromatography (gradient, 20 » 40% EtOAc/hexane) to give **14** as a white solid (1.171 g, 59% yield). **^{1}H NMR** (400 MHz, $CDCl_3$) δ (ppm): 9.26 (d, Pyr-H, ^4J = 1.9 Hz, 1H), 9.22 (d, Pyr-H, ^4J = 2.2 Hz, 1H) 8.67 (t, Pyr-H, ^4J = 2.2 Hz, 1H), 7.97 (bs, CON-H, 1H), 7.45 (d, Stopper-H, J = 8.4 Hz, 2H), 7.21 – 7.11 (m, Stopper-H, 8H), 7.07 – 6.96 (m, Stopper-H, 6H), 3.92 (s, CO_2Me 3H), 1.23 (s, Stopper t-Bu, 27H). **^{13}C NMR** (101 MHz, $CDCl_3$) δ (ppm): 165.00, 162.83, 152.98, 152.02, 148.47, 144.53, 143.73, 135.81, 134.94, 131.96, 130.69, 125.93, 124.19, 124.11, 119.25, 63.42, 52.82, 34.32, 31.39. **MS** (ESI +ve) *m/z*: 667.3 ($[M+H]^+$, $C_{45}H_{51}N_2O_3^+$ requires 667.4). **HRMS** (GCMS-EI +ve) m/z: 666.3807 ($[M]^+$, $C_{45}H_{50}N_2O_3^+$ requires 666.3816).

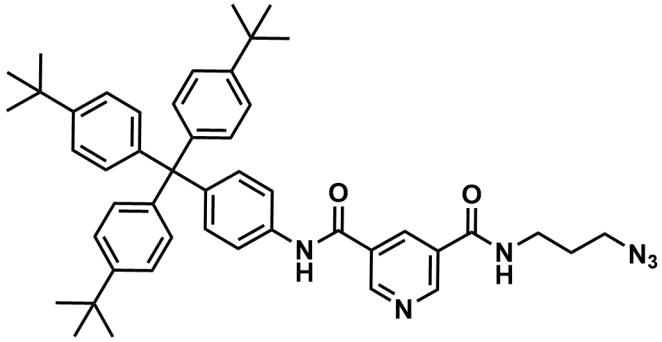
Mono-terphenyl nicotinic acid 15



Terphenyl-stoppered nicotinic ester **14** (1 g, 1.5 mmol) was dissolved in THF (5 ml) and stirred until the solution was homogenous. KOH (202 mg, 3 mmol) was dissolved in distilled H_2O (5 ml) and added drop-wise to the THF solution of **14** and stirred under an atmosphere of N_2 for 24 hours. The pH was adjusted to 7 using 10% Citric $Acid_{(aq.)}$ and DCM (30 ml) was added to partition the mixture. The mixture was further extracted with DCM (2 x 20 ml) and the combined organic fractions were dried over $MgSO_4$ and the solvent removed under reduced pressure. The crude solid obtained was recrystallized in boiling $CHCl_3$ and the solid was filtered and dried under high vacuum to give **15** as a white solid (806 mg, 82% yield). **^{1}H NMR** (400 MHz, DMSO-d_6) δ (ppm): 13.72 (s, COOH, 1H) 10.62 (s, CON-H, 1H), 9.28 (s, Pyr-H, 1H), 9.23 (s, Pyr-H, 1H), 8.75 (s, Pyr-H, 1H), 7.67 (d, Stopper-H, J = 8.5 Hz, 2H), 7.32 (m, Stopper-H, 6H), 7.14 (m, Stopper-H, 8H), 1.27

(s, Stopper t-Bu, 27H). **^{13}C NMR** (101 MHz, DMSO-d_6) δ (ppm): 166.21, 163.53, 152.84, 152.69, 148.22, 144.23, 143.10, 136.75, 136.41, 131.08, 130.92, 130.47, 126.87, 124.83, 120.03, 63.38, 34.49, 31.58. **MS** (ESI +ve) m/z: 653.4 ($[M+H]^+$, $C_{44}H_{49}N_2O_3^+$ requires 653.4). **HRMS** (ESI +ve) m/z: 653.3735 ($[M+H]^+$, $C_{44}H_{49}N_2O_3^+$requires 653.3737).

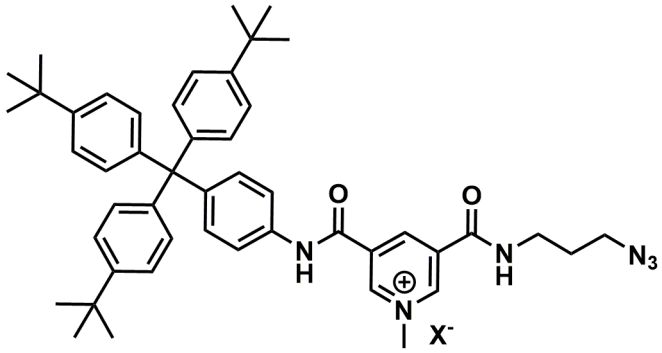
Mono-terphenyl pyridine azide 16



15 (600 mg, .92 mmol), 3-Bromopropylamine hydrobromide (240 mg, 1.1 mmol) and DMAP (cat.) were suspended in dry DCM (20 ml) and cooled in an ice bath. EDC.HCl (210 mg, 1.1 mmol) was added followed by NEt_3 (.26 ml, 1.84 mmol) under an atmosphere of N_2 and the mixture was stirred for 24 hours whilst allowing the reaction temperature to reach room temperature. The mixture was washed with 1M $HCl_{(aq.)}$ (2 x 10 ml), 1M $NaOH_{(aq.)}$ (2 x 10 ml), distilled H_2O (1 x 10 ml), dried over $MgSO_4$ and the solvent removed under reduced pressure to yield a crude yellowish solid. Without further purification, the crude bromide was dissolved in dry DMF (20 ml) and NaN_3 (600 mg, 9.2 mmol) added to the solution under stirring. The mixture was placed under an atmosphere of N_2 and heated at 80 ^{O}C for 24 hours. The reaction mixture was then poured onto ice water (200 ml) and extracted with DCM (4 x 50 ml). The combined organic fractions were then washed with brine (2 x 50 ml), dried over $MgSO_4$ and the solvent removed *in vacuo* followed by high vacuum to remove residual amounts of DMF. The crude azide was then purified using flash column chromatography (20% acetone/$CHCl_3$) to obtain **16** as a white solid (400 mg, 59% yield). **^{1}H NMR** (400 MHz, 1:1 v/v $CDCl_3$/CD_3OD) δ (ppm): 9.06 (s, Pyr-H, 1H), 8.98 (s, Pyr-H, 1H), 8.53 (t, Pyr-H, ^4J = 2.1 Hz, 1H), 7.51 (d, Stopper-H, 2H), 7.24 – 7.13 (m, Stopper-H, 8H), 7.14 – 7.04 (m, Stopper-H, 6H), 3.42 (t, CH_2-NH, J = 6.9 Hz, 2H), 3.33 (t, CH_2-N_3, J = 6.7 Hz, 2H), 1.81 (p, $CH_2CH_2CH_2$, J = 6.8 Hz, 2H), 1.21 (s, Stopper t-Bu, 27H). **^{13}C NMR** (101 MHz, 1:1 v/v $CDCl_3$/CD_3OD) δ (ppm): 163.82, 150.47, 150.24, 148.49, 144.15, 144.08,

135.56, 134.31, 131.33, 130.85, 130.37, 130.11, 124.28, 119.61, 63.40, 53.88, 53.60, 53.33, 53.06, 52.79, 49.57, 37.48, 34.11, 30.96, 28.49. **MS** (ESI +ve) m/z: 735.4 ($[M+H]^+$, $C_{47}H_{55}N_6O_2$ requires 735.4). **HRMS** (ESI +ve) m/z: 757.4196 ($[M+Na]^+$, $C_{47}H_{54}N_6O_2Na$ requires 757.4200).

Mono-terphenyl pyridinium azide axle precursor 17^+

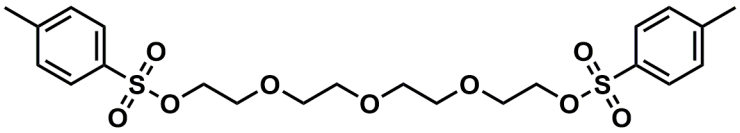


16 (400 mg, .544 mmol) was dissolved in dry $CHCl_3$ (3 ml) and MeI (3 ml) was added drop-wise to the solution. The mixture was heated to 45 ^{0}C and placed under an atmosphere of N_2 and stirred for 16 hours. The solvent of the reaction mixture was removed *in vacuo* to obtain the pure product **17.I** as golden yellow flakes (429 mg, 90% yield). **^{1}H NMR** (400 MHz, $CDCl_3$) δ (ppm): 10.05 (s, CON-H, 1H), 9.91 (s, Pyr-H, 1H), 9.24 (s, Pyr-H, 1H), 8.77 (t, CON-H, J = 5.8 Hz, 2H), 8.67 (s, Pyr-H, 1H), 7.79 – 7.71 (m, Stopper Ar-H, 2H), 7.25 – 7.14 (m, Stopper Ar-H, 8H), 7.10 (d, Stopper Ar-H, J = 8.6 Hz, 6H), 4.02 (s, Pyr-N$^+$Me, 3H), 3.46 (q, CH_2-NH, J = 6.4 Hz, 2H), 3.37 (t, CH_2-N_3, J = 6.7 Hz, 2H), 1.91 (p, $CH_2CH_2CH_2$, J = 6.7 Hz, 2H), 1.23 (s, Stopper t-Bu, 27H).

17.I (429 mg, .490 mmol) was dissolved in DCM (10 ml) and the organic phase washed with aqueous $NH_4Cl_{(aq.)}$ (1M, 8 x 10 ml). The combined aqueous washes were back extracted with DCM (2 x 10 ml) and the combined organic phases were washed with H_2O (2 x 15 ml) and dried over $MgSO_4$. The solvent was removed to give **17.Cl** as a pale yellow solid in a near quantitative yield (377 mg, 98% yield). **^{1}H NMR** (400 MHz, $CDCl_3$) δ (ppm): 10.57 (s, CON-H, 1H), 10.41 (s, Pyr-H, 1H), 9.32 (s + bs, Pyr-H + CON-H, 2H), 8.19 (s, Pyr-H, 1H), 7.68 (d, Stopper Ar-H, J = 8.6 Hz, 2H), 7.26 – 7.12 (m, Stopper Ar-H, 14H), 3.82 (s, Pyr-N$^+$Me, 3H), 3.45 (q + t, CH_2-NH + CH_2-N_3, 4H), 1.91 (p, $CH_2CH_2CH_2$, J = 6.7 Hz, 2H), 1.23 (s, Stopper t-Bu, 27H). **^{13}C NMR** (101 MHz, CD_3CN) δ (ppm): 161.24, 159.82, 149.20, 147.32, 145.25, 144.76, 141.83, 135.42, 131.76, 130.74, 125.17, 120.23, 117.85, 64.02, 54.77, 54.22, 49.58, 38.05, 34.55, 31.14, 28.65. **MS** (ESI +ve) m/z: 749.4 ($[M\text{-}Cl^-]^+$, $C_{48}H_{57}N_6O_2^+$

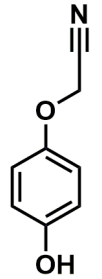
requires 749.5). **HRMS** (ESI +ve) m/z: 749.4540 ($[M\text{-}Cl^-]^+$, $C_{48}H_{57}N_6O_2^+$ requires 749.4538).

Tetraethylene glycol bis-tosylate 18[6]



Tetraethylene glycol (5 ml, 29 mmol) was dissolved in DCM (30 ml) and cooled to 0 ^{0}C with an ice bath. TsCl (11 g, 58 mmol) was added followed by a portion wise addition of KOH (13 g, 232 mmol) to the cooled solution. The reaction mixture was stirred at 0 ^{0}C for a further 3 hours before the solution was diluted with DCM (40 ml) and partitioned with ice water (150 ml). The organic layer was dried over $MgSO_4$, filtered and the solvent removed to obtain bis-tosylate **18** as a viscous clear oil (13.2 g, 91% yield). **^{1}H NMR** (400 MHz, $CDCl_3$) δ (ppm): 7.76 (d, Tosyl-Ar-H, J = 6.1 Hz, 4H), 7.32 (d, Tosyl-Ar-H, J = 7.9 Hz, 4H), 4.17 – 4.09 (t, Ts-O-CH_2-CH_2, J = 3.6 Hz, 4H), 3.65 (m, Tosyl-O-CH$_2$-CH_2, 4H), 3.53 (m, CH_2, 8H), 2.42 (s, Tosyl-CH_3, 6H).

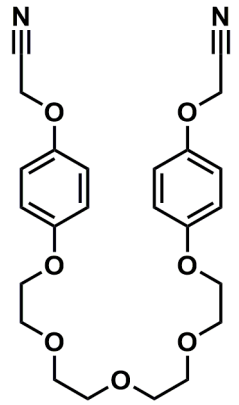
2-(4-Hydroxyphenoxy)acetonitrile 19[7]



Hydroquinone (5.51 g, 50 mmol) and NaOH (4 g, 100 mmol) were dissolved in 1:1 v/v dioxane/H_2O (170 ml) and degassed with N_2 *via* a needle. A degassed solution of bromoacetonitrile (8.72 g, 72.7 mmol) in dioxane (20 ml) was added while stirring under N_2. The solution was stirred for 1 hour whilst degassing. 1M $HCl_{(aq.)}$ was added and the reaction mixture was then extracted with DCM (3 × 50 ml). The combined organic extracts were dried over $MgSO_4$, filtered and the solvent removed *in vacuo* to obtain a crude brown oil. Purification by silica gel chromatography (2% MeOH/DCM) afforded the product as an unstable pale yellow oil that darkens on exposure to air (3.71 g, 44% yield). **^{1}H NMR** (400 MHz, $CDCl_3$) δ (ppm): 6.90 –

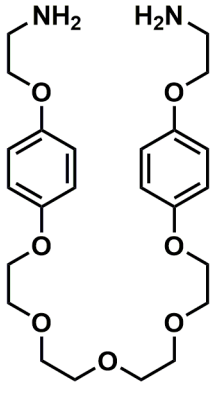
6.84 (m, Ar-H, 2H), 6.82 – 6.75 (m, Ar-H, 2H), 4.85 – 4.58 (m, Phenyl-O-CH$_2$-CN, 2H).

Bis-nitrile 5-oxygen polyether 20[7]



2-(4-hydroxyphenoxy)acetonitrile **19** (1.86 g, 12.44 mmol), tetraethylene glycol bis-tosylate **18** (3.12 g, 6.22 mmol) and Cs_2CO_3 (8.14 g, 25 mmol) were dissolved in dry MeCN (30 ml) and heated to reflux under an atmosphere of N_2 for 16 hours. The mixture was then cooled to room temperature and diluted with DCM (50 ml) and the solids filtered off and the solvent removed *in vacuo* to give bis-nitrile **20** as a light brown oil (1.44 g, 51% yield). **^{1}H NMR** (400 MHz, $CDCl_3$) δ (ppm): 6.99 – 6.80 (m, Ar-H, 8H), 4.69 (s, Phenyl-O-CH$_2$-CN, 4H), 4.07 (t, Phenyl-O-CH$_2$-CH$_2$, J = 4.8 Hz, 4H), 3.83 (t, Phenyl-O-CH$_2$-CH$_2$, J = 4.8 Hz, 4H), 3.69 (m, CH$_2$, 8H). **MS** (ESI +ve) m/z: 479.2 ([M+Na]$^+$, $C_{24}H_{28}N_2NaO_7^+$ requires 479.2).

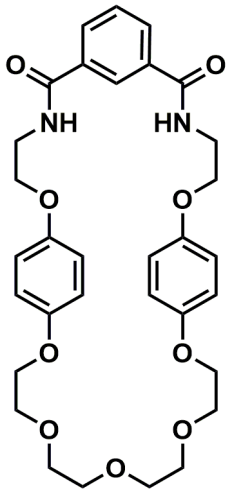
Bis-amine 5-oxygen polyether 21[7]



Bis-nitrile 5-oxygen polyether **20** (1.44 g, 3.15 mmol) was dissolved in dry THF (25 ml) and BH_3 (25 ml, 1M in THF) was added before the reaction was refluxed at 70 ^{0}C for 4 hours. The reaction was cooled to room temperature, MeOH (10 ml) and 10% $HCl_{(aq.)}$ (30 ml) were then added to quench the reaction. The solvent was removed *in vacuo* and the resulting solid redissolved in H_2O (10 ml) and $KOH_{(aq.)}$

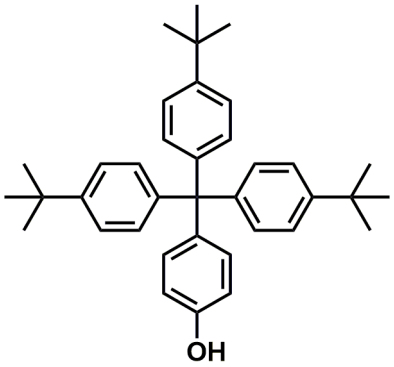
(20 ml, 2M) added. After 30 minutes of stirring, bis-amine **21** precipitated and was isolated by vacuum filtration and dried under high vacuum to give a white solid (854 mg, 58% yield). **^{1}H NMR** (400 MHz, CD_3OD) δ (ppm): 6.87 (s, Ar-H, 8H), 4.06 (t, Hydroquinone-O-CH_2, J = 4.2 Hz, 4H), 3.95 (t, Hydroquinone-O-CH_2, J = 5.3 Hz, 4H), 3.81 (t, CH_2, J = 4.7 Hz, 4H), 3.74 – 3.64 (m, CH_2, 8H), 2.97 (t, CH_2-NH_2, J = 5.3 Hz, 4H). **MS** (ESI +ve) m/z: 465.3 ($[M+H]^+$, $C_{24}H_{37}N_2O_7^+$ requires 465.3).

Isopthalamide 5-oxygen polyether macrocycle 23[8]



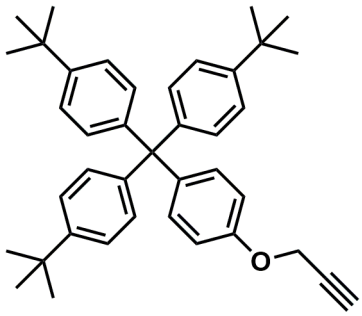
Bis-amine 5-oxygen polyether **21** (800 mg, 0.0017 mmol), pyridinium chloride template **22.Cl** (592 mg, 0.0017 mmol) and NEt_3 (4 ml, excess) were dissolved in DCM (150 ml) and cooled to 0 ^{0}C in an ice bath. Isophthaloyl dichloride (343 mg, 0.0017 mmol) was dissolved in DCM (50 ml) and added drop-wise to the cooled solution over a 30-minute period and gradually allowed to warm to room temperature. The reaction was allowed to stir for 24 hours under an atmosphere of N_2. The solution was then washed with 10% $HCl_{(aq.)}$ (20 ml) and H_2O (20 ml) and the organic layer was dried over $MgSO_4$, filtered and the solvent removed *in vacuo* to give a crude white solid which was subsequently recrystallized in hot MeOH to give product isopthalamide macrocycle **23** as vitreous prismatic crystals (416 mg, 41% yield). **^{1}H NMR** (400 MHz, 1:1 v/v $CDCl_3$/CD_3OD) δ (ppm): 8.07 (s, Phenyl Ar-H, 1H), 7.89 (d, Phenyl Ar-H, ^4J = 7.8 Hz, 2H), 7.47 (t, Phenyl Ar-H, ^4J = 7.8 Hz, 1H), 6.72 (m, Hydroquinone Ar-H, 8H), 4.02 (t, Hydroquinone-O-CH_2, J = 5.1 Hz, 4H), 3.93 (t, Hydroquinone-O-CH_2, J = 4.6 Hz, 4H), 3.75 – 3.70 (m, CH_2, 4H), 3.68 (t, CH_2-NH, J = 5.0 Hz, 5H), 3.64 – 3.56 (m, CH_2, 8H). **MS** (ESI +ve) m/z: 617.3 ($[M+Na]^+$, $C_{32}H_{38}N_2NaO_9^+$ requires 617.2).

Terphenyl alcohol 24[4]



Tris(4-(*tert*-butyl)phenyl)methanol **12** (1.79 g, 4.18 mmol) and phenol (20 g) were heated until a homogenous melt was achieved. Conc. 37% $HCl_{(aq.)}$ (0.2 ml) was carefully added and the mixture was heated for 16 hours at 120 ^{0}C under an atmosphere of N_2. The mixture was cooled to room temperature and saturated $KOH_{(aq.)}$ (30 ml) was added slowly and the mixture was filtered. The resulting pale yellow solid was washed with H_2O (50 ml), 20% $AcOH_{(aq.)}$ (100 ml) and then H_2O (50 ml) again. The off-white powder acquired was dissolved in DCM (200 ml), dried over $MgSO_4$, decolourised over activated charcoal, filtered and the solvent removed *in vacuo* to give crude product which was subsequently recrystallized in refluxing cyclohexane to give pure product stopper alcohol **24** as a white powder (1.83 g, 78% yield). **^{1}H NMR** (400 MHz, $CDCl_3$) δ (ppm): 7.34 – 7.22 (m, Ar-H, 6H), 7.09 (m, Ar-H, 8H), 6.76 – 6.68 (m, Ar-H, 2H), 1.33 (s, Ar-tBu, 27H).

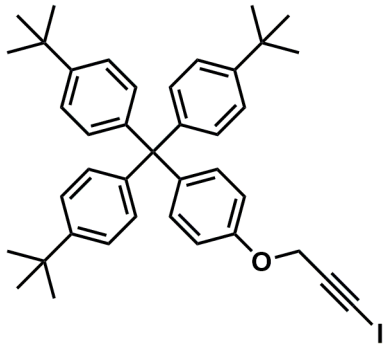
Stopper alkyne 25[9]



Stopper alcohol **24** (400 mg, 0.75 mmol) was dissolved in dry DMF (20 ml) and propargyl bromide (0.18 ml, 80% v/v toluene, 4.5 mmol), K_2CO_3 (500 mg, 3.6 mmol) were added and the reaction mixture was heated to 80 ^{0}C for 16 hours under a N_2 atmosphere. The mixture was concentrated and poured onto brine (100 ml) and extracted with EtOAc (30 ml x 3). The organic extracts were washed with brine (1 x 20 ml) and the solvent removed *in vacuo* to give crude product, which was subsequently recrystallized in hot 5% $CHCl_3$/MeCN to give pure product stopper

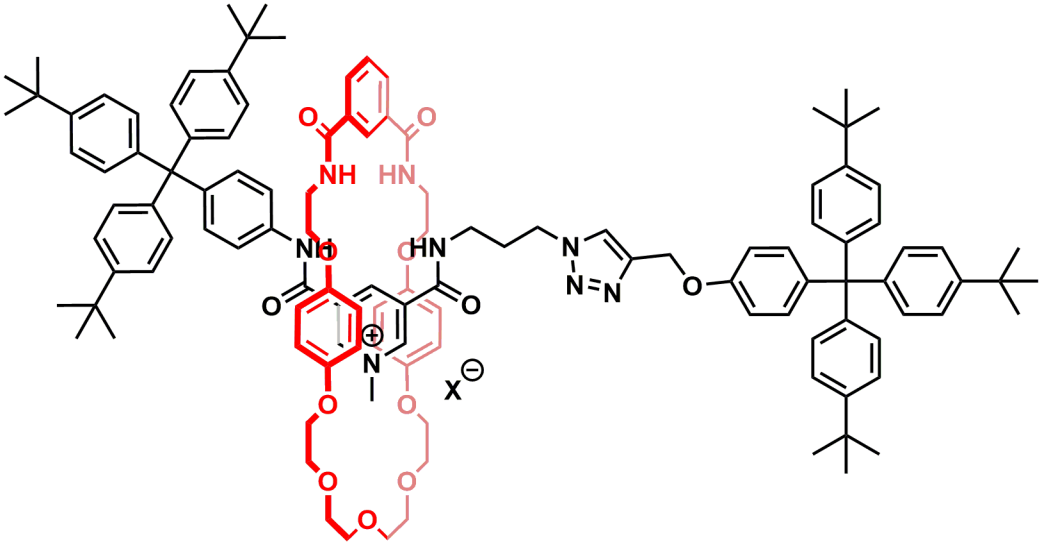
alkyne **25** in a near quantitative yield as a white solid (400 mg, 98%). **^{1}H NMR** (400 MHz, $CDCl_3$) δ (ppm): 7.25 – 7.20 (m, Ar-H, 6H), 7.13 – 7.04 (m, Ar-H, 8H), 6.88 – 6.81 (m, Ar-H, 2H), 4.66 (d, Phenyl-O-CH_2, $J = 2.4$ Hz, 2H), 2.51 (t, Alkyne-CH, $^4J = 2.4$ Hz, 1H), 1.30 (s, Ar-tBu, 27H).

Stopper iodo-alkyne 26[10]



Stopper alkyne **25** (100 mg, 0.184 mmol) was dissolved in dry THF (3 ml) followed by additions of N-iodomorpholine (125.5 mg, 0.368 mmol) and CuI (7 mg, 0.037 mmol) portion-wise. The reaction mixture was stirred in the dark under a N_2 atmosphere until the reaction was judged complete by TLC, then the solvent was removed *in vacuo*, redissolved in DCM (4 ml) and filtered through a plug of silica. The red filtrate was washed with saturated $Na_2S_2O_{3(aq.)}$, dried over $MgSO_4$, filtered and dried *in vacuo* to give the pure product iodo-alkyne **26** as off-white crystalline needles (119 mg, 97% yield). **^{1}H NMR** (500 MHz, $CDCl_3$) δ (ppm): 7.26 – 7.21 (m, Ar-H, 6H), 7.09 (m, Ar-H, 8H), 6.85 – 6.79 (m, Ar-H, 2H), 4.80 (s, Phenyl-O-CH_2, 2H), 1.30 (s, Ar-tBu, 27H).

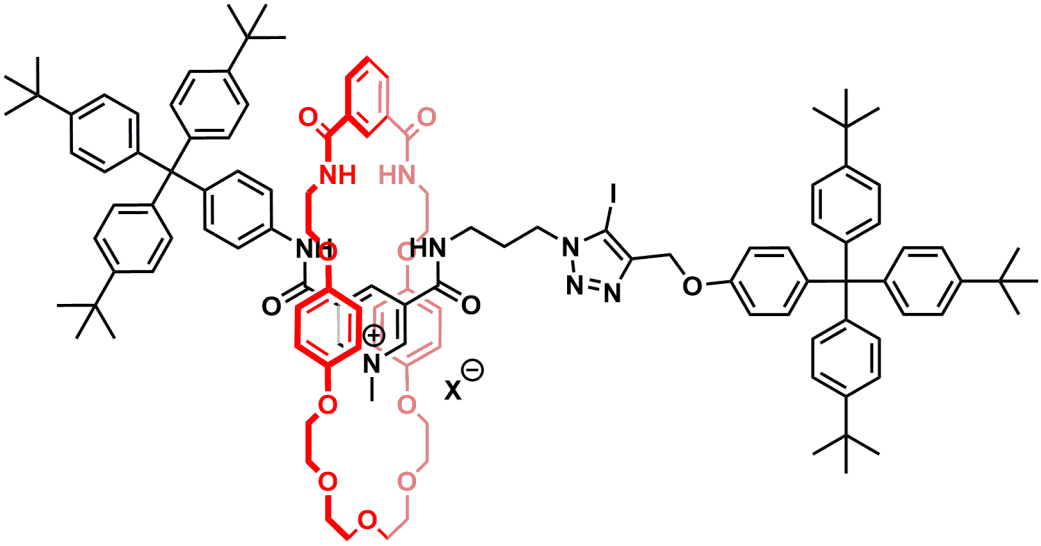
Pyridinium-triazole rotaxane 10^+



17.Cl (30 mg, .0382 mmol) and isophthalamide macrocycle **23** (34.11 mg, .0574 mmol) were dissolved in dry DCM (2 ml) and subject to sonication until the solution was homogenous. Stopper alkyne **25** (24.86 mg, .0458 mmol) was dissolved in dry DCM (.5 ml) and half of this solution was added to the stirring mixture of **17.Cl** and macrocycle **23** followed by $Cu(MeCN)_4PF_6$ (5.7 mg, .0153 mmol) and TBTA (8.12 mg, .0153 mmol). After 30 minutes, the remaining solution of stopper alkyne was added to the reaction mixture. The reaction vessel was sealed, placed under an atmosphere of N_2 and stirred for 24 hours. The solvent of the reaction mixture was removed and the crude solid was purified by preparative TLC (First run in 4% MeOH in DCM, followed by neat EtOAc). The product contaminated with free macrocycle and TBTA was dissolved in $CHCl_3$ and subject to size exclusion chromatography. The eluted fractions containing the rotaxane product were collected and the solvent removed to give pure rotaxane **10.Cl** as a pale yellow solid (17.9 mg, 24% yield). **^{1}H NMR** (500 MHz, 1:1 v/v $CDCl_3$/CD_3OD) δ (ppm): 9.10 (s, Pyr-H, 1H), 9.07 (s, Pyr-H, 1H), 8.93 (s, Pyr-H, 1H), 8.67 (s, Macrocycle Ar-H, 1H), 7.94 (d, Macrocycle Ar-H, J = 7.8 Hz, 2H), 7.86 (s, Triazole Ar-H, 1H), 7.71 – 7.66 (m, Stopper Ar-H, 2H), 7.37 (t, Macrocycle Ar-H, ^4J = 7.8 Hz, 1H), 7.21 – 7.09 (m, Stopper Ar-H, 14H), 7.04 – 6.93 (m, Stopper Ar-H, 14H), 6.78 – 6.73 (m, Stopper Ar-H, 2H), 6.41 – 6.35 (m, Hydroquinone Ar-H, 4H), 6.17 – 6.12 (m, Hydroquinone Ar-H, 4H), 5.05 (s, O-CH_2-triazole, 2H), 4.46 (s, Pyr-N$^+$Me, 3H), 4.19 (t, CH_2-triazole, J = 7.3 Hz, 2H), 4.11 (t, Macrocycle CH_2, J = 9.1 Hz, 2H), 3.92 (m, Macrocycle CH_2, 2H), 3.79 – 3.47 (m, Macrocycle CH_2, 20H), 3.25 (t, CH_2-NH, 2H), 1.97 (p, CH_2C$H_2$$CH_2$, J = 7.0 Hz, 2H), 1.21 (m, Stopper t-Bu, 54H).

10.Cl (17.9 mg, .00917 mmol) was dissolved in DCM (10 ml) and the organic phase washed with aqueous $NH_4PF_{6(aq.)}$ (1M, 8 x 10 ml). The combined aqueous washes were back extracted with DCM (2 x 10 ml) and the combined organic phases were washed with H_2O (2 x 15 ml) and dried over $MgSO_4$. The solvent was removed to give **10.PF$_6$** as a pale yellow solid in a near quantitative yield (18.5 mg, 99% yield). **^{1}H NMR** (500 MHz, 1:1 v/v $CDCl_3/CD_3OD$) δ (ppm): 9.01 (s, Pyr-H, 1H), 8.81 (s, Pyr-H, 1H), 8.77 (s, 1H), 8.44 (s, Macrocycle Ar-H, 1H), 7.94 (d, Macrocycle Ar-H, J = 7.8, 2H), 7.84 (s, Triazole Ar-H, 1H), 7.61 – 7.56 (m, Stopper Ar-H, 2H), 7.42 (t, Macrocycle Ar-H, ^4J = 7.8 Hz, 1H), 7.22 – 7.11 (m, Stopper Ar-H, 14H), 7.07 – 6.94 (m, Stopper Ar-H, 14H), 6.81 – 6.76 (m, Stopper Ar-H, 2H), 6.47 – 6.41 (m, Hydroquinone Ar-H, 4H), 6.24 – 6.18 (m, Hydroquinone Ar-H, 4H), 5.07 (s, O-CH_2-triazole, 2H), 4.32 (s, Pyr-N$^+$Me, 3H), 4.23 (t, CH_2-triazole, J = 7.1 Hz, 2H), 4.04 – 3.44 (m, Macrocycle CH_2, 24H), 3.25 (t, CH_2-NH, 2H), 2.00 (p, $CH_2CH_2CH_2$, J = 6.9 Hz, 2H), 1.21 (m, Stopper t-Bu, 54H). **^{13}C NMR** (126 MHz, 1:1 v/v $CDCl_3/CD_3OD$) δ (ppm): 167.96, 160.43, 158.81, 156.06, 153.09, 151.92, 148.52, 148.29, 145.91, 145.17, 144.10, 143.66, 140.30, 134.56, 134.11, 133.80, 132.86, 132.22, 131.92, 131.00, 129.09, 128.68, 125.13, 124.16, 123.96, 119.79, 115.05, 114.83, 113.16, 70.59, 70.01, 68.16, 67.90, 66.24, 63.43, 62.99, 61.33, 40.00, 38.71, 37.36, 34.13, 31.80, 31.69, 29.50, 29.45, 29.22, 29.03, 24.88, 22.52. **^{19}F NMR** (376 MHz, 1:1 v/v $CDCl_3/CD_3OD$) δ (ppm): -73.33 (d, ^2J = 710 Hz, PF_6^-). **MS** (ESI +ve) m/z: 1886.1 ($[M\text{-}PF_6^-]^+$, $C_{120}H_{141}N_8O_{12}^+$ requires 1886.1). **HRMS** (ESI +ve) m/z: 1886.0699 ($[M\text{-}PF_6^-]^+$, $C_{120}H_{141}N_8O_{12}^+$ requires 1886.0664).

Pyridinium-iodotriazole rotaxane 11$^+$

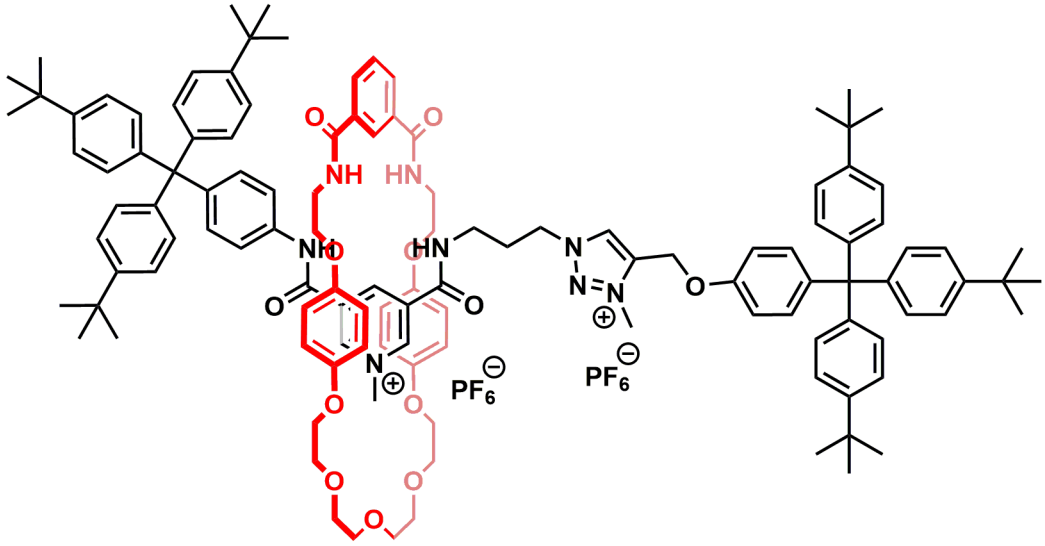


17.Cl (15 mg, .0191 mmol) and isophthalamide macrocycle **23** (17 mg, .0287 mmol) were dissolved in dry DCM (1 ml) and subject to sonication until the solution was homogenous. Stopper iodoalkyne **26** (16.2 mg, .0229 mmol) was dissolved in dry DCM (.5 ml) and half of this solution was added to the stirring mixture of **17.Cl** and macrocycle **23** followed by $Cu(MeCN)_4PF_6$ (2.85 mg, .0077 mmol) and TBTA (4.06 mg, .0077 mmol). After 30 minutes, the remaining solution of stopper iodoalkyne was added to the reaction mixture. The reaction vessel was sealed, placed under an atmosphere of N_2 and stirred for 24 hours in the dark. The solvent of the reaction mixture was removed and the crude solid was purified by preparative TLC (2.5% MeOH in DCM) to yield pure rotaxane **11.Cl** as a light orange solid (11.4 mg, 29% yield). **^{1}H NMR** (500 MHz, 1:1 v/v $CDCl_3/CD_3OD$) δ (ppm): 9.08 (s, Pyr-H, 1H), 9.01 (s, Pyr-H, 1H), 8.92 (s, Pyr-H, 1H), 8.57 (s, Macrocyle Ar-H, 1H), 8.03 (d, Macrocycle Ar-H, J = 7.8, 2H), 7.67 (d, Stopper Ar-H, J = 8.8 Hz, 2H), 7.48 (t, Macrocycle Ar-H, ^4J = 7.8 Hz, 1H), 7.29 – 7.18 (m, Stopper Ar-H, 14H), 7.14 – 7.04 (m, Stopper Ar-H, 14H), 6.93 – 6.84 (m, Stopper Ar-H, 2H), 6.60 – 6.49 (m, Hydroquinone Ar-H, 4H), 6.34 – 6.24 (m, Hydroquinone Ar-H, 4H), 5.06 (s, O-CH_2-triazole, 2H), 4.42 (s, Pyr-N$^+$Me, 3H), 4.37 (t, CH_2-triazole, J = 7.0 Hz, 2H), 4.15 – 3.98 (m, Macrocycle CH_2, 4H), 3.92 – 3.54 (m, Macrocycle CH_2, 20H), 3.40 (t, CH_2-NH, J = 6.9 Hz, 2H), 2.15 (p, $CH_2CH_2CH_2$, J = 7.0 Hz, 2H), 1.37 – 1.21 (m, Stopper t-Bu, 54H).

11.Cl (11.4 mg, .00556 mmol) was dissolved in DCM (10 ml) and the organic phase washed with aqueous $NH_4PF_{6(aq.)}$ (1M, 8 x 10 ml). The combined aqueous washes were back extracted with DCM (2 x 10 ml) and the combined organic phases were

washed with H_2O (2 x 15 ml) and dried over $MgSO_4$. The solvent was removed to give **11.PF$_6$** as a pale yellow/brown solid in a quantitative yield (11.9 mg). **^{1}H NMR** (500 MHz, 1:1 v/v $CDCl_3$/CD_3OD) δ (ppm): 8.96 (s, Pyr-H, 1H), 8.77 (s, Pyr-H, 1H), 8.73 (s, Pyr-H, 1H), 8.33 (s, Macrocycle Ar-H, 1H), 7.93 (d, Macrocycle Ar-H, J = 7.7, 2H), 7.57 – 7.49 (m, Stopper Ar-H, 2H), 7.42 (t, Macrocycle Ar-H, ^4J = 7.8 Hz, 1H), 7.23 – 7.11 (m, Stopper Ar-H, 14H), 7.06 – 6.96 (m, Stopper Ar-H, 14H), 6.81 (m, Stopper Ar-H, 2H), 6.48 (m, Hydroquinone Ar-H, 4H), 6.24 (m, Hydroquinone Ar-H, 4H), 4.98 (s, O-CH_2-triazole, 2H), 4.57 (s, Pyr-N$^+$Me, 3H), 4.31 (d, CH_2-triazole, J = 7.0 Hz, 2H), 4.25 (m, Macrocycle CH_2, 2H), 3.94 (m, Macrocycle CH_2, 2H), 3.75 – 3.49 (m, Macrocycle CH_2, 20H), 3.33 (t, CH_2-NH, J = 6.9 Hz, 2H), 2.09 (p, $CH_2CH_2CH_2$, J = 7.0 Hz, 2H), 1.28 – 1.13 (m, Stopper t-Bu, 54H). **^{13}C NMR** (126 MHz, 1:1 v/v $CDCl_3$/CD_3OD) δ (ppm): 168.05, 160.57, 158.85, 156.12, 153.05, 151.94, 148.51, 148.29, 145.78, 145.23, 144.07, 143.66, 140.97, 140.46, 134.50, 134.21, 133.89, 133.04, 132.19, 131.89, 130.88, 130.60, 130.56, 129.02, 124.15, 123.96, 119.86, 115.23, 114.85, 113.37, 70.61, 70.51, 70.01, 67.84, 66.50, 63.42, 63.01, 61.44, 48.97, 39.83, 37.43, 34.10, 34.05, 30.97, 29.50, 28.84, 3 peaks missing, presumed overlapped. **^{19}F NMR** (376 MHz, 1:1 v/v $CDCl_3$/CD_3OD) δ (ppm): -73.33 (d, ^2J = 710 Hz, PF_6^-). **MS** (ESI +ve) m/z: 2012.0 ([M-PF_6^-]$^+$, $C_{120}H_{140}IN_8O_{12}^+$ requires 2012.0). **HRMS** (ESI +ve) m/z: 2011.9660 ([M-PF_6^-]$^+$, $C_{120}H_{141}N_8O_{12}^+$ requires 2011.9630).

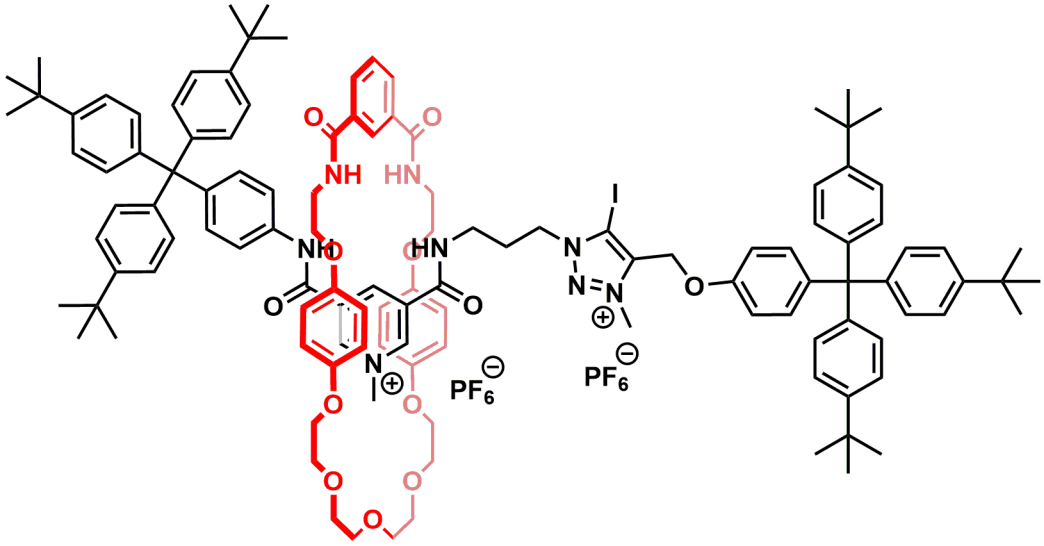
Pyridinium-triazolium rotaxane 27.(PF$_6$)$_2$



Rotaxane **10.PF$_6$** (20 mg, 0.0098 mmol) was dissolved in DCM (1 ml) and trimethyloxonium tetrafluorborate (1.8 mg, 0.012 mmol) was added in one portion.

The mixture was placed under an atmosphere of N_2 and stirred overnight. Upon completion by TLC, the reaction mixture was quenched with MeOH (2 ml) and the solvent was removed *in vacuo* to give dicationic rotaxane **27.(BF$_4$)$_2$**. The product was subsequently dissolved in DCM (10 ml) and the organic phase washed with aqueous $NH_4PF_{6(aq.)}$ (1M, 8 x 10 ml). The combined aqueous washes were back extracted with DCM (2 x 10 ml) and the combined organic phases were washed with H_2O (2 x 15 ml) and dried over $MgSO_4$. The solvent was removed to give **27.(PF$_6$)$_2$** as a pale yellow solid (16.32 mg, 76% overall). **^{1}H NMR** (500 MHz, 1:1 v/v $CDCl_3/CD_3OD$) δ (ppm): 9.13 (s, Pyr-H, 1H), 8.77 (t, Pyr-H, 1H), 8.67 (s, Pyr-H, 1H), 8.45 (s, Macrocycle Ar-H, 1H), 7.95 (d, Macrocycle Ar-H, $J = 7.8$, 2H), 7.61 – 7.56 (m, Stopper Ar-H, 2H), 7.46 (t, Macrocycle Ar-H, $^4J = 7.8$ Hz, 1H), 7.24 – 7.10 (m, Stopper Ar-H, 14H), 7.07 – 6.98 (m, Stopper Ar-H, 14H), 6.87 – 6.82 (m, Stopper Ar-H, 2H), 6.49 – 6.44 (m, Hydroquinone Ar-H, 4H), 6.27 – 6.21 (m, Hydroquinone Ar-H, 4H), 5.17 (s, O-CH_2-triazolium, 2H), 4.38 (s, Pyr-N$^+$Me, 3H), 4.31 (s + t, Triaz-N$^+$Me + CH_2-triazolium, 5H), 4.18 – 3.43 (m, Macrocyle CH_2, 24H), 3.27 (t, CH_2-NH, $J = 7.0$ Hz, 2H), 2.01 (p, $CH_2CH_2CH_2$, $J = 7.0$ Hz, 2H), 1.30 – 1.12 (m, Stopper t-Bu, 54H), triazolium C-H singlet missing due to hydrogen-deuterium exchange. **^{13}C NMR** (126 MHz, 1:1 v/v $CDCl_3/CD_3OD$) δ (ppm): 168.54, 161.24, 159.72, 155.64, 153.80, 152.73, 149.27, 149.19, 146.91, 145.87, 144.61, 144.45, 143.99, 142.80, 135.40, 134.91, 134.69, 133.29, 132.66, 131.85, 131.33, 130.05, 125.64, 124.89, 124.81, 120.48, 115.79, 115.61, 114.08, 92.33, 71.30, 70.72, 68.89, 68.60, 67.02, 64.19, 63.82, 59.44, 52.86, 40.76, 39.73, 39.46, 37.46, 34.85, 32.54, 31.72, 30.25; 3 peaks missing, presumed overlapped. **^{19}F NMR** (376 MHz, 1:1 v/v $CDCl_3/CD_3OD$) δ (ppm): -73.33 (d, $^2J = 711.2$ Hz). **MS** (ESI +ve) m/z: 950.6 ($[M\text{-}2PF_6^-]^{2+}$, $C_{121}H_{144}N_8O_{12}^{2+}$ requires 950.5). **HRMS** (ESI +ve) m/z: 950.5442 ($[M\text{-}2PF_6^-]^{2+}$, $C_{121}H_{144}N_8O_{12}^{2+}$ requires 950.5446).

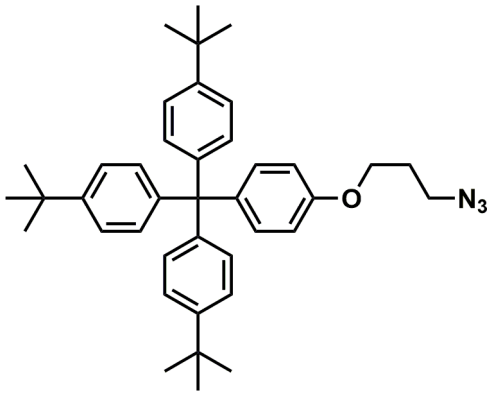
Pyridinium-iodotriazolium rotaxane 28.$(PF_6)_2$



Rotaxane **11.(PF_6)** (15 mg, 0.007 mmol) was dissolved in DCM (1 ml) and trimethyloxonium tetrafluoroborate (1.23 mg, 0.0083 mmol) was added in one portion. The mixture was placed under an atmosphere of N_2 and stirred overnight. Upon completion by TLC, the reaction mixture was quenched with MeOH (2 ml) and the solvent was removed *in vacuo* to give dicationic rotaxane **28.$(BF_4)_2$**. The product was subsequently dissolved in DCM (10 ml) and the organic phase washed with aqueous $NH_4PF_{6(aq.)}$ (1M, 8 x 10 ml). The combined aqueous washes were back extracted with DCM (2 x 10 ml) and the combined organic phases were washed with H_2O (2 x 15 ml) and dried over $MgSO_4$. The solvent was removed to give **28.$(PF_6)_2$** as a pale yellow solid (11.5 mg, 71% overall). **^{1}H NMR** (500 MHz, 1:1 v/v $CDCl_3/CD_3OD$) δ (ppm): 9.14 (s, Pyr-H, 1H), 8.79 (s, Pyr-H, 1H), 8.57 (s, Pyr-H, 1H), 8.41 (s, Macrocycle Ar-H, 1H), 7.96 (d, Macrocycle Ar-H, J = 7.8 Hz, 2H), 7.61 – 7.55 (m, Stopper Ar-H, 2H), 7.47 (t, Macrocycle Ar-H, ^4J = 7.9 Hz, 1H), 7.25 – 6.96 (m, Stopper Ar-H, 28H), 6.86 – 6.80 (m, Stopper Ar-H, 2H), 6.48 – 6.42 (m, Hydroquinone Ar-H, 4H), 6.26 – 6.20 (m, Hydroquinone Ar-H, 4H), 5.24 (s, O-CH_2-triazolium, 2H), 4.39 (t, CH_2-triazolium, J = 7.5 Hz, 2H), 4.36 (s, Pyr-N^+Me, 3H), 4.26 (s, Triaz-N^+Me, 3H), 4.16 – 3.41 (m, Macrocyle CH_2, 24H), 3.22 (t, CH_2-NH, J = 6.6 Hz, 2H), 1.98 (p, $CH_2CH_2CH_2$, J = 7.0 Hz, 2H), 1.28 – 1.13 (m, Stopper t-Bu, 54H). **^{13}C NMR** (126 MHz, 1:1 v/v $CDCl_3/CD_3OD$) δ (ppm): 168.63, 161.32, 159.83, 155.63, 153.76, 152.67, 149.27, 146.91, 145.85, 144.62, 144.45, 142.55, 140.60, 135.41, 134.96, 134.71, 133.25, 132.67, 131.83, 131.29, 129.94, 129.42, 125.60, 124.89, 120.47, 116.28, 115.80, 115.61, 114.43, 113.90, 71.33, 71.15, 70.74, 70.44, 68.50, 67.04, 64.19, 63.79, 58.50, 51.99, 40.72, 40.33, 39.46, 39.00, 37.22, 34.85, 34.81, 32.53, 31.73, 31.70.

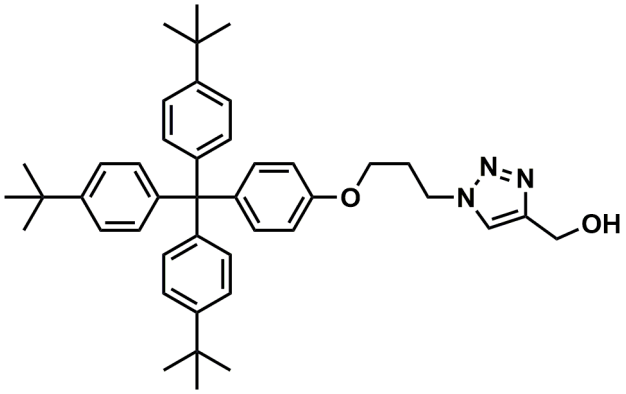
^{19}F NMR (376 MHz, 1:1 v/v $CDCl_3/CD_3OD$) δ (ppm): -73.45 (d, ^2J = 711.1 Hz). **MS** (ESI +ve) m/z: 1013.6 ($[M\text{-}2PF_6^-]^{2+}$, $C_{121}H_{143}IN_8O_{12}^{2+}$ requires 1013.5). **HRMS** (ESI +ve) m/z: 1013.4925 ($[M\text{-}2PF_6^-]^{2+}$, $C_{121}H_{143}IN_8O_{12}^{2+}$ requires 1013.4929).

Stopper azide 29[11]



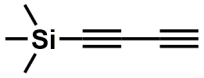
Terphenyl alcohol **24** (660 mg, 1.307 mmol) and 1,3-dibromopropane (0.4 ml, 3.92 mmol) was dissolved in dry MeCN (27 ml). To the stirring solution, K_2CO_3 (542 mg, 3.92 mmol) was added in one portion and the reaction mixture was placed under an N_2 atmosphere and heated to 80 ^{0}C for 48 hours. The reaction mixture was then diluted with DCM (40 ml) and the solids filtered and the filtrate dried over $MgSO_4$. The solvent was removed *in vacuo* and the crude product purified using silica gel column chromatography (2:1 petroleum ether/DCM) to give stopper bromide as a white solid that matched previous characterization (678 mg, 83% yield). Stopper bromide (375 mg, 0.6 mmol) was immediately taken up in dry DMF (20 ml) and NaN_3 (117 mg, 1.8 mmol) was added to the solution. The mixture was heated to 80 ^{0}C for 24 hours. The reaction mixture was poured onto ice water (150 ml) and extracted with DCM (3 x 40 ml) and washed with brine (2 x 40 ml) before the solvent of the organic layer removed *in vacuo*. The crude material was purified by recrystallization using in boiling of $CHCl_3$/MeOH mixture (1:9) and the pure product stopper azide **29** was isolated by vacuum filtration as a white solid (200 mg, 57% yield). **^{1}H NMR** (400 MHz, $CDCl_3$) δ (ppm): 7.21 – 7.05 (m, Ar-H, 6H), 7.07 – 6.94 (m, Ar-H, 8H), 6.73 – 6.63 (m, Ar-H, 2H), 3.94 (t, Phenyl-O-CH_2, J = 5.9 Hz, 2H), 3.42 (t, CH_2-N_3, J = 6.7 Hz, 2H), 1.96 (q, $CH_2CH_2CH_2$, J = 6.3 Hz, 2H), 1.22 (s, Ar-tBu, 27H).

Stopper triazole alcohol 30



Stopper azide **29** (200 mg, .340 mmol), propargyl alcohol (0.0197 ml, .340 ml), $Cu(MeCN)_4PF_6$ (50.68 mg, 0.136 mmol) and TBTA (cat.) were dissolved in dry, degassed DCM (10 ml). NEt_3 was added by syringe (0.1 ml, 0.68 mmol) and the yellow mixture was left to stir under a N_2 atmosphere for 48 hours. The reaction mixture was washed with EDTA/$NH_4OH_{(aq.)}$ (.1M EDTA in 1M NH_4OH, 2 x 20 ml) and brine (1 x 20 ml) and the organic layer was dried over $MgSO_4$ and the solvent removed *in vacuo*. The crude white solid was recrystallized using a boiling of $CHCl_3$/MeOH mixture (1:9) and the pure product triazole **30** was isolated by vacuum filtration as a white solid (185 mg, 84% yield). **^{1}H NMR** (400 MHz, 1:1 v/v $CDCl_3$/DMSO-d_6) δ (ppm): 7.89 (s, Triazole Ar-H, 1H), 7.19 (d, Stopper Ar-H, J = 8.1 Hz, 6H), 6.99 (m, Stopper Ar-H, 8H), 6.73 (d, Stopper Ar-H, J = 8.4 Hz, 2H), 5.05 (t, Triazole-CH_2-OH, J = 5.7 Hz, 2H), 4.51 – 4.40 (t, Triazole-CH_2, J = 7.9 Hz, 2H), 3.87 (t, Phenyl-O-CH_2, J = 5.9 Hz, 2H), 2.22 (p, $CH_2CH_2CH_2$, J = 6.6 Hz, 2H), 1.21 (s, Stopper tBu, 27H). **^{13}C NMR** (101 MHz, 1:1 v/v $CDCl_3$/DMSO-d_6) δ (ppm): 148.11, 144.34, 139.58, 131.93, 130.49, 124.56, 123.06, 113.66, 64.64, 62.99, 55.60, 48.24, 46.85, 34.44, 31.57, 30.10, 1 peak missing, presumed overlapped. **MS** (ESI +ve) m/z: 644.3 ($[M+H]^+$, $C_{43}H_{54}N_3O_2^+$ requires 644.4). **HRMS** (ESI +ve) m/z: 644.4208 ($[M+H]^+$, $C_{43}H_{54}N_3O_2^+$ requires 644.4210).

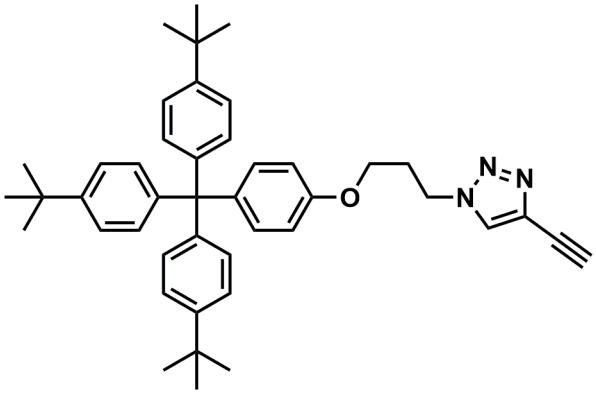
Mono-TMS butadiyne 32[12]



1,4-Bis(trimethylsilyl)butadiyne (4 g, 20 mmol) was placed in an oven-dried Schlenk flask equipped with a stirrer bar which was placed under a vacuum and backfilled with an atmosphere of N_2. Dry Et_2O (40 ml) was added to the dissolve the solid and the solution was cooled to 0 ^{0}C before MeLi (1.6M in Et_2O, 20.6 ml, 24 mmol) was added drop-wise over 20 minutes *via* syringe. After the addition was complete, the

reaction mixture was left to stir for 16 hours. The mixture was cooled to -78 ^{0}C and saturated $NH_4Cl_{(aq.)}$ (20 ml) was added slowly to quench the reaction. After slowly warming to room temperature, the reaction mixture was extracted with Et_2O (3 x 30 ml), dried over $MgSO_4$ and gently concentrated with no heating (product volatile) to give an ethereal solution of Mono-TMS butadiyne **32** (0.6:1 **32**:Et_2O molar ratio, 1.01 g of **32**, 41% yield). **^{1}H NMR** (400 MHz, $CDCl_3$) δ (ppm): 2.10 (s, Alkyne-H, 1H), 0.18 (s, Si-Me_3, 9H).

Stopper triazole alkyne 31

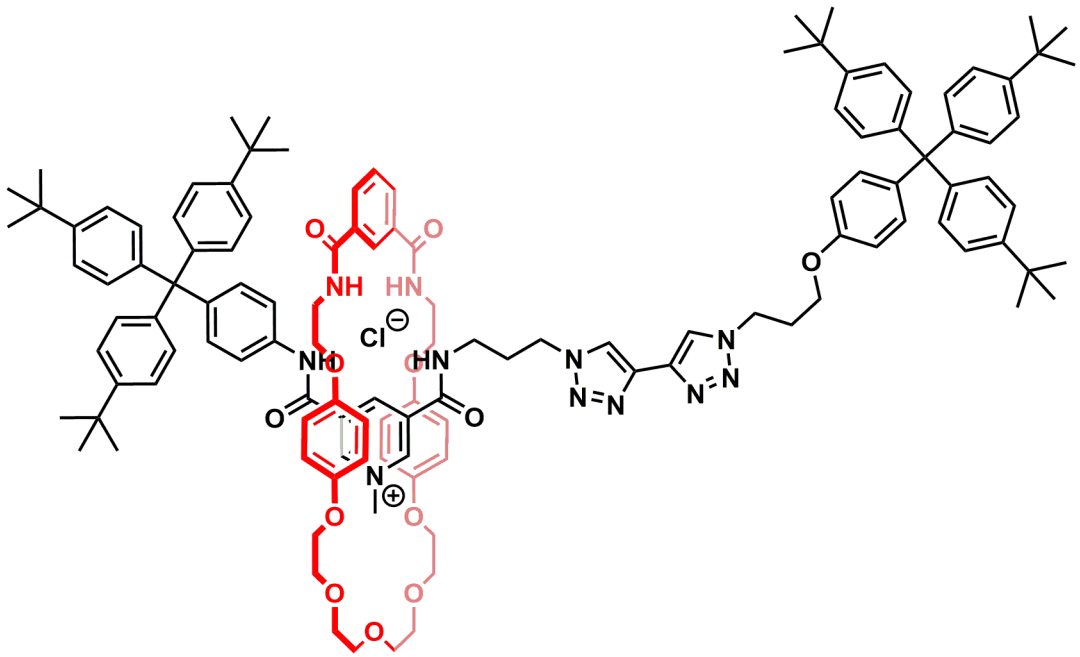


Method 1 (Swern oxidation/Bestmann-Ohira Homolgation): Dry THF (5 ml) was cooled to -78 ^{0}C under an atmosphere of N_2. DMSO (.251 ml, 3.54 mmol, dried over molecular sieves) was added drop-wise via syringe and oxalyl chloride (.15 ml, 1.77 mmol) was added drop-wise slowly to the solution and left to stir under cooling for 15 minutes. Stopper triazole alcohol **30** (228 mg, 0.354 mmol) was added slowly and the reaction mixture was allowed to stir for 1 hour at room temperature. NEt_3 (0.74 ml, 5.31 mmol) was added drop-wise and the reaction mixture was stirred for a further hour. The reaction was quenched by the addition of $HCl_{(aq.)}$ (20 ml) and the mixture was extracted with DCM (3 x 30 ml) and the organic layer dried over $MgSO_4$. The solvent was removed to give intermediate triazole aldehyde which was dried under high vacuum and subsequently redissolved in THF/ MeOH (1:1 v/v) and several molecular sieves were added. Dimethyl-(diazomethyl)phosphate (Bestmann-Ohira reagent, 68 mg, 0.354 mmol) was added to the solution and the reaction was stirred for 24 hours. The solvent was removed *in vacuo* and the yellow-green residue subjected to silica gel column chromatography (Neat DCM) to give the product triazole alkyne **31** as a translucent pale white solid (31.2 mg, 14% yield).
Method 2 (CuACC): Mono-TMS butadiyne (34 mg of 0.6:1 molar ration **32**:Et_2O solution, 0.102 mmol) and stopper azide **29** (50 mg, 0.085 mmol) were dissolved in

dry DCM (2 ml) and subjected to 3 freeze-thaw-pump degassing cycles. $Cu(MeCN)_4PF_6$ (16 mg, 0.042 mmol) was added to the solution and the reaction mixture was placed under an N_2 atmosphere, sealed and left to stir for 72 hours. The yellow-orange solution was washed with EDTA/$NH_4OH_{(aq.)}$ (.1M EDTA in 1M NH_4OH, 2 x 10 ml) and brine (1 x 10 ml) and the organic layer was dried over $MgSO_4$ and the solvent removed *in vacuo*. The crude yellow film was subjected to silica gel column chromatography (Neat DCM) to give the product triazole alkyne **31** as a translucent pale white solid (18.5 mg, 54% yield, the TMS group is removed in the workup stage).

^{1}H NMR (400 MHz, $CDCl_3$) δ (ppm): 7.60 (s, Triazole Ar-H, 1H), 7.23 – 7.09 (m, Stopper Ar-H, 6H), 7.07 – 6.94 (m, Stopper Ar-H, 8H), 6.75 – 6.57 (m, Stopper Ar-H, 2H), 4.51 (t, Triazole-CH_2, J = 6.8 Hz, 2H), 3.86 (t, Phenyl-O-CH_2, J = 5.6 Hz, 2H), 3.14 (s, Alkyne-H, 1H), 2.30 (p, $CH_2CH_2CH_2$, J = 6.3 Hz, 2H), 1.22 (s, Stopper-tBu, 27H). **^{13}C NMR** (101 MHz, $CDCl_3$) δ (ppm): 156.11, 148.37, 144.04, 140.28, 132.39, 130.71, 129.92, 127.13, 124.07, 112.93, 81.06, 73.09, 63.65, 63.07, 47.36, 34.31, 31.40, 29.85. **MS** (ESI +ve) m/z: 638.4 ($[M+H]^+$, $C_{44}H_{52}N_3O^+$ requires 638.4). **HRMS** (ESI +ve) m/z: 638.4104 ($[M+H]^+$, $C_{44}H_{52}N_3O^+$ requires 638.4104).

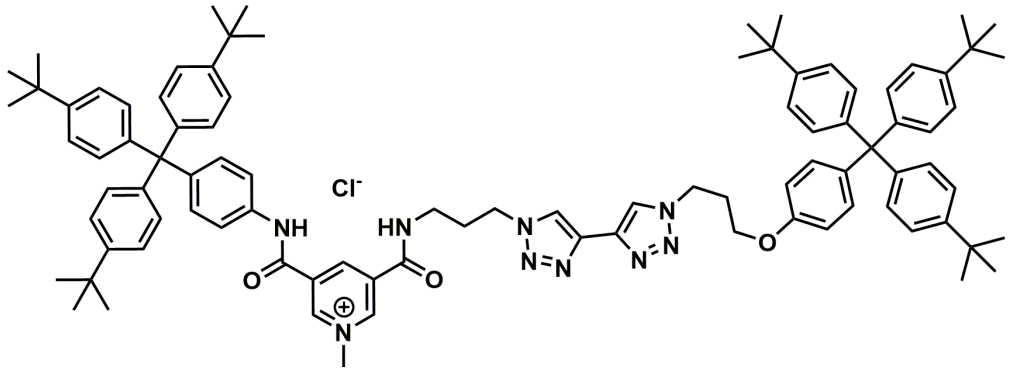
Pyridinium-bta rotaxane 33.Cl



17.Cl (15 mg, .0191 mmol) and isophthalamide macrocycle **23** (17 mg, .0287 mmol) were dissolved in dry DCM (1 ml) and subject to sonication until the solution was homogenous. Stopper triazole alkyne **31** (14.6 mg, .0229 mmol) was dissolved in dry

DCM (.5 ml) and half of this solution was added to the stirring mixture of **17.Cl** and macrocycle **23** followed by $Cu(MeCN)_4PF_6$ (2.85 mg, .0077 mmol) and TBTA (4.06 mg, .0077 mmol). After 30 minutes, the remaining solution of stopper triazole alkyne was added to the reaction mixture. The reaction vessel was sealed, placed under an atmosphere of N_2 and stirred for 24 hours in the dark. The solvent of the reaction mixture was removed and the crude solid was purified by preparative TLC (4% MeOH in DCM) to yield pure rotaxane **33.Cl** as a light yellow solid (5.1 mg, 11% yield). **^{1}H NMR** (400 MHz, 1:1 v/v $CDCl_3/CD_3OD$) δ (ppm): 9.32 (s, Pyr-H, 1H), 9.08 (s, Pyr-H, 1H), 9.00 (s, Pyr-H, 1H), 8.86 (s, Macrocyle Ar-H, 1H), 8.22 – 8.11 (2 x s, 2 x Triazole Ar-H, 2H), 7.98 (d, Macrocyle Ar-H, J = 7.7 Hz, 2H), 7.76 (d, Stopper Ar-H, J = 8.6 Hz, 2H), 7.39 (t, Macrocyle Ar-H, J = 7.8 Hz, 1H), 7.24 – 7.08 (m, Stopper Ar-H, 14H), 7.07 – 6.93 (m, Stopper Ar-H, 14H), 6.69 (d, Stopper Ar-H, J = 8.7 Hz, 2H), 6.36 (d, Hydroquinone Ar-H, J = 8.9 Hz, 4H), 6.11 (d, Hydroquinone Ar-H, J = 8.8 Hz, 4H), 4.67 – 4.47 (2 x t, 2 x Triazole-CH_2, J = 6.9 Hz, 2H), 4.31 – 4.15 (2 x t, Phenyl-O-CH_2 + CH_2-NH, 4H), 4.05 – 3.47 (m, Macrocycle-CH_2, 24H) 3.25 (s, Pyr-N$^+$-Me, 3H), 2.36 (p, $CH_2CH_2CH_2$, J = 6.0 Hz, 2H), 2.02 (p, $CH_2CH_2CH_2$, J = 6.9 Hz, 2H), 1.31 – 1.12 (m, Stopper tBu, 54H). **^{13}C NMR** (126 MHz, 1:1 v/v $CDCl_3/CD_3OD$) δ (ppm): 167.64, 160.49, 158.44, 156.30, 153.27, 152.00, 148.40, 146.19, 145.68, 144.89, 144.12, 143.75, 139.99, 134.71, 133.52, 133.08, 132.67, 132.14, 131.75, 130.60, 130.57, 129.11, 125.04, 124.13, 123.92, 119.92, 114.66, 112.93, 70.59, 70.46, 69.89, 68.16, 65.22, 63.93, 63.41, 62.97, 49.24, 47.48, 40.78, 37.04, 34.10, 34.04, 31.78, 31.00, 30.98, 29.81, 29.71, 29.51, 29.34, 29.20, 26.9861, 22.5060, 13.6244. **MS** (ESI +ve) m/z: 1981.7 ($[M\text{-}Cl^-]^+$, $C_{124}H_{146}N_{11}O_{12}^+$ requires 1981.1). **HRMS** (ESI +ve) m/z: 1981.1106 ($[M\text{-}Cl^-]^+$, $C_{124}H_{146}N_{11}O_{12}^+$ requires 1981.1157).

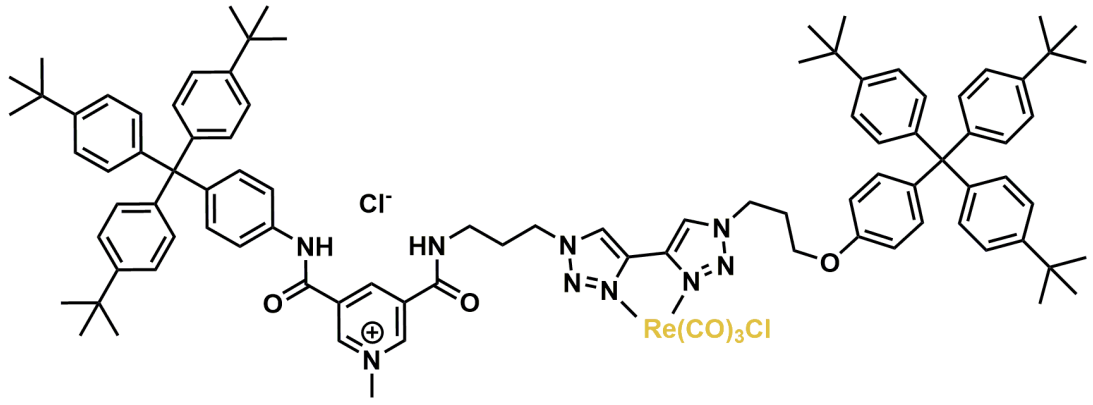
Pyridinium-bta axle 34.Cl



Pyridinium azide **34.Cl** (43.28 mg, 0.0055 mmol) and stopper triazole alkyne **31**

(33.5 mg, 0.0525 mmol) were dissolved in dry DCM (5 ml) and subject to 3 freeze-thaw-pump degassing cycles. $Cu(MeCN)_4PF_6$ (7.82 mg, 0.021 mmol), TBTA (11.15 mg, 0.021 mmol) was added to the solution and the reaction mixture was placed under an N_2 atmosphere, sealed and left to stir for 48 hours. The yellow-orange solution was washed with $EDTA/NH_4OH_{(aq.)}$ (.1M EDTA in 1M NH_4OH, 2 x 10 ml) and brine (1 x 10 ml) and the organic layer was dried over $MgSO_4$ and the solvent removed *in vacuo*. The crude yellow solid was redissolved in DCM (2 ml) and MeOH (10 ml) was slowly added drop-wise to precipitate the product bis-triazole axle **34.Cl** as a pale yellow solid (55 mg, 73% yield). **^{1}H NMR** (400 MHz, 1:1 v/v $CDCl_3/CD_3OD$) δ (ppm): 9.50 (d, Pyr-H, ^4J = 1.8 Hz, 1H), 9.41 (s, Pyr-H, 1H), 9.37 (s, Pyr-H, 1H), 8.23 (s, Triazole Ar-H, 1H), 8.06 (s, Triazole Ar-H, 1H), 7.62 (d, Stopper Ar-H, J = 8.8 Hz, 2H), 7.20 – 7.06 (m, Stopper Ar-H, 14H), 7.05 – 6.91 (m, Stopper Ar-H, 14H), 6.60 (d, Stopper Ar-H, J = 8.8 Hz, 2H), 4.54 – 4.41 (1 x s + 2 x t, Pyr-N^+-Me + 2 x Triazole-CH_2, 7H), 3.84 (t, Phenyl-O-CH_2, J = 5.7 Hz, 2H), 3.51 (t, CH_2-NH, J = 6.3 Hz, 2H), 2.36 – 2.21 (m, 2 x $CH_2CH_2CH_2$, 4H), 1.19 (s, Stopper tBu, 54H). **^{13}C NMR** (101 MHz, 1:1 v/v $CDCl_3/CD_3OD$) δ (ppm): 161.11, 159.15, 156.23, 148.39, 148.20, 146.86, 146.72, 144.81, 144.11, 143.74, 141.19, 140.00, 139.01, 135.06, 134.72, 133.94, 132.17, 131.67, 130.61, 130.59, 124.07, 123.92, 122.08, 121.66, 119.47, 112.89, 63.99, 63.38, 62.97, 47.52, 37.74, 34.06, 34.03, 30.98, 29.77, 28.85, 3 peaks missing, presumed overlapped. **MS** (ESI +ve) m/z: 1386.9 ($[M\text{-}Cl^-]^+$, $C_{92}H_{108}N_9O_3^+$ requires 1386.9). **HRMS** (ESI +ve) m/z: 1386.8567 ($[M\text{-}Cl^-]^+$, $C_{92}H_{108}N_9O_3^+$ requires 1386.8569).

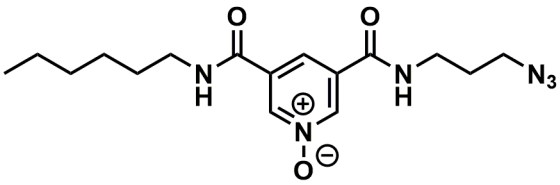
Bta-rhenium(I) axle 36.Cl



$Re(CO)_5Cl$ (9.15 mg, 0.0236 mmol) was dissolved in MeCN (5 ml) and refluxed under N_2 for 2 hours and the solvent removed *in vacuo* to yield the reactive intermediate di-acetonitrile complex $Re(CO)_3(MeCN)_2Cl$ **35** (assuming quantitative

conversion). Bis-triazole axle **34.Cl** (28 mg, 0.0197 mmol) was dissolved in DCM (2 ml) and **35** was added to the stirring solution. The reaction mixture was placed under a N_2 atmosphere and stirred at room temperature for 48 hours. The solvent was removed *in vacuo* and the crude product purified by silica gel column chromatography (2 » 6% MeOH/DCM, gradient elution) to give the product rhenium(I) complex as a pale yellow solid (17.1 mg, 50% yield). **^{1}H NMR** (500 MHz, 1:1 v/v $CDCl_3/CD_3OD$) δ (ppm): 9.28 (s, Pyr-H, 2H), 9.15 (s, Pyr-H, 1H), 8.44 (s, Triazole Ar-H, 1H), 8.35 (s, Triazole Ar-H, 1H), 7.61 – 7.55 (m, Stopper Ar-H, 2H), 7.20 – 7.05 (m, Stopper Ar-H, 14H), 7.04 – 6.89 (m, Stopper Ar-H, 14H), 6.60 – 6.53 (m, Stopper Ar-H, 2H), 4.64 – 4.47 (m, 2 x Triazole-CH_2, 4H), 4.35 (s, Pyr-N^+-Me, 3H), 3.84 (t, Phenyl-O-CH_2, J = 5.7 Hz, 2H), 3.68 – 3.41 (m, CH_2-NH, 2H), 2.46 – 2.21 (m, 2 x $CH_2CH_2CH_2$, 4H), 1.25 – 1.13 (m, Stopper-tBu, 54H). **^{13}C NMR** (126 MHz, 1:1 v/v $CDCl_3/CD_3OD$) δ (ppm): 195.62, 195.28, 188.45, 161.30, 159.15, 156.13, 148.43, 148.23, 148.19, 146.57, 146.54, 144.92, 144.11, 143.77, 143.74, 141.63, 140.12, 140.00, 134.94, 134.88, 133.99, 132.21, 131.74, 130.62, 130.58, 124.10, 123.91, 122.77, 122.24, 119.53, 112.92, 64.01, 63.39, 62.98, 50.50, 49.34, 37.95, 34.04, 31.77, 30.94, 29.47, 28.51, 22.48. **MS** (ESI +ve) m/z: 1690.6 ($[M\text{-}Cl^-]^+$, $C_{95}H_{108}ClN_9O_6Re^+$ requires 1690.8). **HRMS** (ESI +ve) m/z: 1691.7672 ($[M\text{-}Cl^-]^+$, $C_{95}H_{108}ClN_9O_6Re^+$ requires 1691.7668).

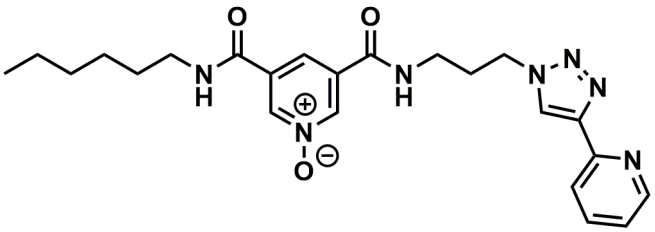
Pyridine *N*-oxide bis-amide azide 39



Pyridine bis-amide azide **6** (96.5 mg, 0.29 mmol) was dissolved in butanone (15 ml) and $NaHCO_3$ (73 mg, 0.87 mmol) was suspended in the vigorously stirring mixture. Oxone® (268 mg, 0.87 mmol) was dissolved and added dropwise in distilled H_2O (15 ml) to the mixture that was allowed to stir overnight. NaCl (1 g, 17.4 mmol) was added in one portion and the mixture extracted with $CHCl_3$ (3 x 40 ml) and washed with H_2O (1 x 40 ml) and the organic extracts were dried over $MgSO_4$, filtered, dried *in vacuo* to give *N*-oxide azide **39** as a tacky white solid (90.6 mg, 90% yield). **^{1}H NMR** (400 MHz, 1:1 v/v $CDCl_3/CD_3OD$) δ (ppm): 9.02 – 7.99 (m, N-oxide Pyr-H, 3H), 3.57 – 3.17 (m, 2 x CH_2-NH + CH_2-N_3, 6H), 1.83 (p, $CH_2CH_2CH_2$, J = 6.5 Hz, 2H), 1.54 (p, $CH_2CH_2CH_2$, J = 6.9 Hz, 2H), 1.44 – 1.07 (m, CH_2, 6H), 0.80 (t, CH_3,

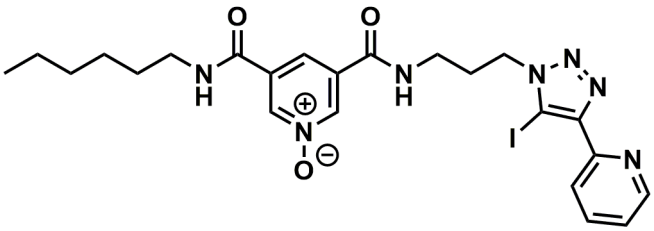
J = 6.7 Hz, 3H). **^{13}C NMR** (101 MHz, 1:1 v/v $CDCl_3/CD_3OD$) δ (ppm): 163.00, 162.65, 140.88, 133.68, 126.82, 40.34, 37.58, 31.36, 29.07, 28.94, 28.41, 28.27, 26.52, 22.39, 13.52, 1 peak missing, presumed overlapped. **MS** (ESI -ve) m/z: 383.1 ($[M+Cl]^-$, $C_{16}H_{24}ClN_6O_3^-$ requires 383.2). **HRMS** (ESI -ve) m/z: 383.1600 ($[M+Cl]^-$, $C_{16}H_{24}ClN_6O_3^-$ requires 383.1603).

Pyridine *N*-oxide bis-amide pyta 40



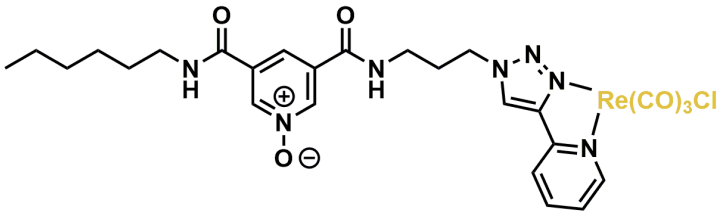
N-oxide azide **39** (30 mg, 0.086 mmol) was dissolved in dry, degassed DCM (5 ml). 2-ethynylpyridine (8.88 mg, 0.086 mmol), $Cu(MeCN)_4PF_6$ (6.3 mg, 0.017 mmol), TBTA (9 mg, 0.017 mmol) and finally DIPEA (0.01 ml, cat.) were added sequentially and the reaction mixture was stirred under a N_2 atmosphere for 48 hours. The solution was then washed $NH_4OH_{(aq.)}$ (1M, 2 x 30 ml) and H_2O (2 × 30 ml). The organic layer was then dried over $MgSO_4$ and the solvent removed *in vacuo* and the crude product was purified using flash column chromatography (7% MeOH/DCM) to give pure product **40** as a white solid (20.3 mg, 52% yield). **^{1}H NMR** (400 MHz, 1:1 v/v $CDCl_3/CD_3OD$) δ (ppm): 8.65 (2 x t, *N*-oxide Pyr-H, 2H), 8.46 (s, Pyr-H, 1H), 8.29 (s, Triazole Ar-H, 1H), 8.23 (s, *N*-oxide Pyr-H, 1H), 7.99 (d, Pyr-H, J = 7.9 Hz, 1H), 7.78 (td, Pyr-H, J = 7.8, 1.8 Hz, 1H), 7.25 (dd, Pyr-H, J = 7.5, 4.9 Hz, 1H), 4.49 (t, CH_2-triazole, 2H), 3.42 (t, CH_2-NH, J = 6.6 Hz, 2H), 3.31 (t, CH_2-NH, J = 7.3 Hz, 2H), 2.25 (q, $CH_2CH_2CH_2$, J = 6.7 Hz, 2H), 1.53 (q, $CH_2CH_2CH_2$, J = 7.3 Hz, 2H), 1.36 – 1.15 (m, CH_2, 6H), 0.79 (t, CH_3, J = 6.8 Hz, 1H). **^{13}C NMR** (101 MHz, 1:1 v/v $CDCl_3/CD_3OD$) δ (ppm): 162.91, 162.51, 149.45, 149.00, 147.49, 139.93, 137.65, 134.32, 133.76, 125.65, 123.29, 122.93, 120.49, 48.17, 40.37, 37.28, 31.38, 29.53, 29.13, 29.00, 26.54, 22.41, 13.61. **MS** (ESI -ve) m/z: 383.1 ($[M+Cl]^-$, $C_{16}H_{24}ClN_6O_3^-$ requires 383.2). **HRMS** (ESI -ve) m/z: 383.1600 ($[M+Cl]^-$, $C_{16}H_{24}ClN_6O_3^-$ requires 383.1603).

Pyridine *N*-oxide bis-amide iodo-pyta 41



N-oxide azide **39** (69 mg, 0.198 mmol) was dissolved in dry, degassed THF (2 ml) and NaI (79.5 mg, 0.530 mmol) was added, followed by $Cu(ClO_4)_2.6H_2O$ (98.26 mg, 0.265 mmol). The mixture was stirred for 5 minutes at room temperature after which TBTA (cat.) and an MeCN (2 ml) solution of DBU (20.18 mg, 0.132 mmol) were added, followed by 2-ethynylpyridine (13.67 mg, 0.1326 mmol). The reaction mixture was sealed and left to stir at room temperature overnight in the dark. After the reaction was complete, the mixture was diluted with DCM (20 ml) before being washed with $NH_4OH_{(aq.)}$ (20 ml) and $NaCl_{(sat.\ aq.)}$ (2 × 10 ml). The organics were collected dried over $MgSO_4$, filtered and the solvent removed *in vacuo*. The crude solid was purified by silica gel column chromatography using (5% MeOH/DCM) to elute the product **41** as a white solid (76 mg, 67% yield). **^{1}H NMR** (400 MHz, DMSO-d_6) δ (ppm): 8.75 – 8.61 (2s + d, 2 x *N*-oxide Pyr-H + Pyr-H, 3H), 8.13 (s, *N*-oxide Pyr-H, 1H), 8.02 (d, Pyr-H, J = 7.9 Hz, 1H), 7.91 (td, Pyr-H, J = 7.7, 1.8 Hz, 1H), 7.40 (dd, Pyr-H, J = 7.5, 4.9 Hz, 1H), 4.56 (t, CH_2-triazole, J = 7.1 Hz, 2H), 3.37 (t, CH_2-NH, J = 6.8 Hz, 2H), 3.25 (t, CH_2-NH, J = 7.1 Hz, 2H), 2.18 (p, $CH_2CH_2CH_2$, J = 7.0 Hz, 2H), 1.52 (p, $CH_2CH_2CH_2$, J = 6.9 Hz, 2H), 1.40 – 1.20 (m, CH_2, 6H), 0.87 (t, CH_3, J = 5.9 Hz, 3H). **^{13}C NMR** (101 MHz, DMSO-d_6) δ (ppm): 162.55, 162.28, 162.20, 150.25, 149.46, 147.90, 139.63, 137.43, 133.90, 133.64, 123.57, 123.18, 121.67, 82.53, 48.61, 37.15, 31.42, 29.37, 29.14, 26.55, 22.50, 14.38, 1 peak missing, presumed overlapped. **MS** (ESI +ve) m/z: 578.1 ($[M+H]^+$, $C_{23}H_{29}IN_7O_3^+$ requires 578.1). **HRMS** (ESI +ve) m/z: 383.1363 ($[M+H]^+$, $C_{23}H_{29}IN_7O_3^+$ requires 578.1377).

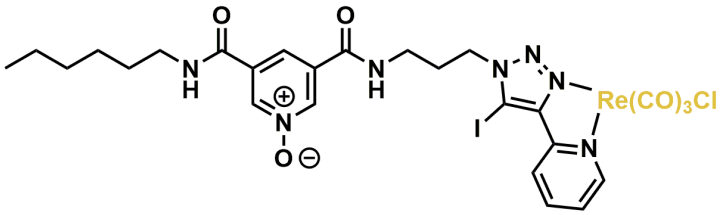
Pyridine *N*-oxide pyta-rhenium(I) complex 42



$Re(CO)_5Cl$ (20 mg, 0.054 mmol) was dissolved in MeCN (5 ml) and refluxed under

N_2 for 2 hours and the solvent removed in vacuo to yield the reactive intermediate di-acetonitrile complex $Re(CO)_3(MeCN)_2Cl$ **35** (assuming quantitative conversion). Pyridine *N*-oxide **40** (20.3 mg, 0.045 mmol) was dissolved in DCM (5 ml) and **35** was added to the stirring solution. The reaction mixture was placed under a N_2 atmosphere and stirred at room temperature for 24 hours. The solvent was removed *in vacuo* and the crude product purified by silica gel column chromatography (10% MeOH/DCM) to give the product rhenium(I) complex **42** as a pale yellow solid (22 mg, 65% yield). **^{1}H NMR** (400 MHz, 1:1 v/v $CDCl_3/CD_3OD$) δ (ppm): 8.91 – 8.86 (s + d, Triazole Ar-H + Pyr-H, 2H), 8.68 (d, *N*-oxide Pyr-H, ^4J = 1.6 Hz, 1H), 8.65 (d, *N*-oxide Pyr-H, ^4J = 1.6 Hz, 1H), 8.31 (t, *N*-oxide Pyr-H, ^4J = 1.5 Hz, 1H), 8.08 – 7.95 (m, Pyr-H, 2H), 7.43 (ddd, Pyr-H, J = 7.3, 5.6, 1.8 Hz, 1H), 4.59 (t, CH_2-triazole, J = 6.9 Hz, 2H), 3.45 (t, CH_2-NH, J = 6.4 Hz, 2H), 3.31 (t, CH_2-triazole, J = 7.3 Hz, 2H), 2.31 (p, $CH_2CH_2CH_2$, J = 6.9 Hz, 2H), 1.55 (p, $CH_2CH_2CH_2$, J = 7.2 Hz, 2H), 1.38 – 1.15 (m, CH_2, 6H), 0.81 (t, CH_3, J = 6.5 Hz, 2H). **^{13}C NMR** (101 MHz, 1:1 v/v $CDCl_3/CD_3OD$) δ (ppm): 196.88, 195.29, 188.72, 163.19, 162.50, 152.98, 149.36, 148.77, 140.07, 139.98, 139.84, 134.25, 133.62, 125.89, 125.63, 125.02, 122.29, 49.77, 40.38, 36.95, 31.37, 29.28, 28.97, 26.53, 22.40, 13.59. **MS** (ESI +ve) m/z: 756.1 ($[M+H]^+$, $C_{26}H_{30}ClN_7O_6Re^+$ requires 756.1). **HRMS** (ESI +ve) m/z: 758.1491 ($[M+H]^+$, $C_{26}H_{30}ClN_7O_6Re^+$ requires 758.1498).

Pyridine *N*-oxide pyta-rhenium(I) complex 43

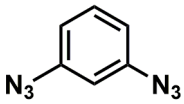


$Re(CO)_5Cl$ (7.78 mg, 0.021 mmol) was dissolved in MeCN (5 ml) and refluxed under N_2 for 2 hours and the solvent removed in vacuo to yield the reactive intermediate di-acetonitrile complex $Re(CO)_3(MeCN)_2Cl$ **35** (assuming quantitative conversion). Pyridine *N*-oxide **41** (10 mg, 0.017 mmol) was dissolved in DCM (2 ml) and **35** was added to the stirring solution. The reaction mixture was placed under a N_2 atmosphere and stirred at room temperature for 24 hours. The solvent was removed *in vacuo* and the crude product purified by silica gel column chromatography (10% MeOH/DCM) to give the product rhenium(I) complex **43** as a pale yellow solid (5.8 mg, 39% yield). **^{1}H NMR** (400 MHz, 1:1 v/v $CDCl_3/CD_3OD$) δ (ppm): 8.96 (d, J = 5.1 Hz, Pyr-H, 1H), 8.68 (2 x s, *N*-oxide Pyr-H, 2H), 8.59 (dt, Pyr-H, J = 8.1, 1.1

Hz, 1H), 8.25 (t, Pyr-H, J = 1.4 Hz, 1H), 8.11 (td, Pyr-H, J = 7.9, 1.6 Hz, 1H), 7.55 – 7.48 (t, Pyr-H, 1H), 4.62 (t, CH_2-triazole, J = 7.4 Hz, 2H), 3.49 (t, CH_2-NH, J = 6.7 Hz, 2H), 3.31 (t, CH_2-NH, J = 7.3 Hz, 2H), 2.33 (p, $CH_2CH_2CH_2$, J = 7.0 Hz, 2H), 1.54 (p, $CH_2CH_2CH_2$, J = 7.4 Hz, 2H), 1.36 – 1.12 (m, CH_2, 6H), 0.81 (t, CH_3, J = 7.4 Hz, 3H). **MS** (ESI +ve) m/z: 882.0 ($[M+H]^+$, $C_{26}H_{29}ClIN_7O_6Re^+$ requires 882.1). **HRMS** (ESI +ve) m/z: 882.0444 ($[M+H]^+$, $C_{26}H_{29}ClIN_7O_6Re^+$ requires 882.0436).

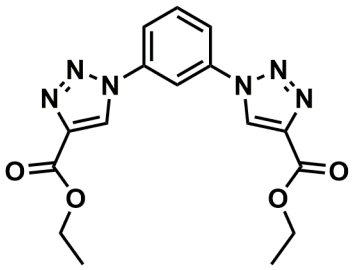
5.3. Synthesis of Compounds from Chapter 3

1,3-Diazidobenzene 44[13]



m-phenylenediamine (1 g, 9.24 mmol) was dissolved in glacial AcOH (10 ml) and cooled to 0 ^{0}C with an ice bath before concentrated H_2SO_4 (3 ml) was added dropwise under a N_2 atmosphere. $NaNO_2$ (7.4 g, 107.2 mmol) was added in distilled H_2O (15 ml) over a 15-minute period and the temperature was maintained at 0 ^{0}C for 2 hours. NaN_3 (6 g, 92.4 mmol) was added in distilled H_2O (23 ml) was added over a 1 hour period and the reaction was allowed to gradually warm to room temperature over a further hour of stirring. The resulting mixture was extracted with Et_2O (3 x 30 ml) and washed with saturated $NaHCO_{3(aq.)}$ (10 ml), H_2O (2 x 10 ml), dried over $MgSO_4$, filtered and the solvent removed cautiously under a stream of N_2 to give a crude reddish oil that was purified by silica gel column chromatography (hexane) to give a 1,3-diazidobenzene **44** as a pale yellow oil (1.25 g, 84% yield.) **^{1}H NMR** (400 MHz, $CDCl_3$) δ (ppm): 7.32 (t, Ar-H, J = 8.0 Hz, 1H), 6.82 (d, Ar-H, J = 8.1 Hz, 2H), 6.65 (t, Ar-H, ^4J = 2.1 Hz, 1H).

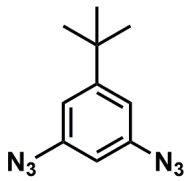
1,3-Bis-triazole bis-ethyl ester 45



1,3-diazidobenzene **44** (150 mg, 0.936 mmol) and ethyl propiolate (192 mg, 1.96 mmol) were dissolved in dry, degassed DCM (10 ml) and $Cu(MeCN)_4PF_6$ (140 mg,

0.374 mmol), TBTA (24 mg, 0.047 mmol) and DIPEA (0.35 ml, 1.87 mmol) were sequentially added before the reaction mixture was placed under an N_2 atmosphere for 16 hours. The yellow solution was washed with EDTA/$NH_4OH_{(aq.)}$ (.1M EDTA in 1M $N3H_4OH$, 2 x 20 ml) and brine (1 x 20 ml) and the organic layer was dried over $MgSO_4$, filtered and the solvent removed *in vacuo*. The crude white solid was recrystallized in hot MeOH to give the product bis-triazole bis-ester **45** as a white solid (302.6 mg, 91% yield). **^{1}H NMR** (400 MHz, DMSO-d_6) δ 9.61 (s, Triazole Ar-H, 2H), 8.63 (t, Phenyl Ar-H, ^4J = 2.1 Hz, 1H), 8.17 (d, Phenyl Ar-H, J = 8.2 Hz, 2H), 7.84 (t, Phenyl Ar-H, J = 8.2 Hz, 1H), 4.39 (q, 2 x COO-CH_2-CH_3, J = 7.1 Hz, 4H), 1.37 (t, 2 x COO-CH_2-CH_3, J = 7.1 Hz, 6H). **^{13}C NMR** (101 MHz, DMSO-d_6) δ (ppm): 160.41, 140.42, 137.39, 132.10, 127.82, 120.93, 112.56, 61.33, 14.65. **MS** (ESI +ve) m/z: 357.2 ($[M+H]^+$, $C_{16}H_{17}N_6O_4^+$ requires 357.1). **HRMS** (ESI +ve) m/z: 357.1305 ($[M+H]^+$, $C_{16}H_{17}N_6O_4^+$ requires 357.1305).

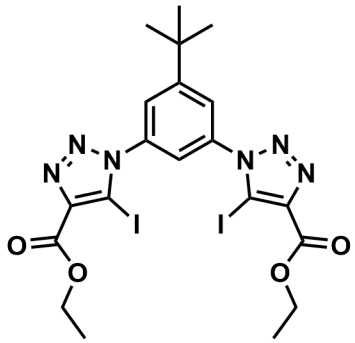
1,3-Diazido-5-(*tert*-butyl)benzene 48[14]



5-(*tert*-butyl)-1,3-diiodobenzene **47**[15] (1.39 g, 3.6 mmol) CuI (685 mg, 3.6 mmol), ethylene glycol (2.23 g, 36 mmol) and $NH_4OH_{(aq.)}$(1 ml, 37%) were dissolved in dry DMSO (10 ml) and heated in a microwave reactor for 1 hour at 150 ^{0}C. The mixture was extracted with Et_2O (3 x 30 ml), washed with brine (2 x 30 ml) and the organic layer was dried over $MgSO_4$. The solvent was removed *in vacuo* to give intermediate bis-amine as a dark brown oil which was immediately used without further purification. Intermediate bis-amine was redissolved in H_2O (15 ml) cooled in an ice bath and concentrated $H_2SO_{4(aq.)}$ (1.5 ml) was added drop-wise under an atmosphere of N_2. $NaNO_2$ (2.9 g, 42 mmol) was added in distilled H_2O (15 ml) over a 15-minute period and the temperature was maintained at 0 ^{0}C for 2 hours. NaN_3 (2.34 g, 36 mmol) was added in distilled H_2O (23 ml) was added over a 1-hour period and the reaction was allowed to gradually warm to room temperature for a further hour. The resulting mixture was extracted with Et_2O (3 x 30 ml) and washed with saturated $NaHCO_{3(aq.)}$ (10 ml), H_2O (2 x 10 ml), dried over $MgSO_4$, filtered and the solvent was removed under a stream of N_2 to give a crude red oil that was purified by silica gel column chromatography (10% DCM/petroleum ether) to give product

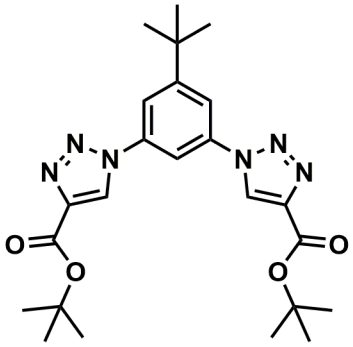
diazide **48** as a pale yellow oil (226 mg, 30% overall yield). **^{1}H NMR** (400 MHz, $CDCl_3$) δ (ppm): 6.73 (d, Ar-H, ^4J = 2.0 Hz, 2H), 6.44 (t, Ar-H, ^4J = 2.0 Hz, 1H), 1.23 (s, Ar-tBu, 9H). **MS** (ESI +ve) m/z: 217.1 ($[M+H]^+$, $C_{10}H_{13}N_6^+$ requires 217.1).

1,3-Bis-iodotriazole bis-ethyl ester 49



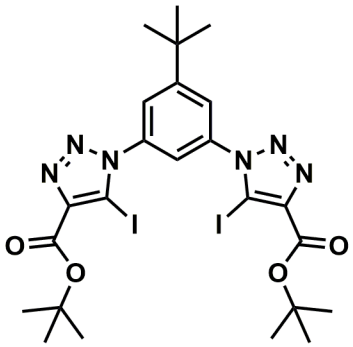
1,3-diazido-5-(*tert*-butyl)benzene **48** (100 mg, 0.462 mmol) was dissolved in dry, degassed THF (3 ml) and NaI (553 mg, 3.69 mmol) was added, followed by $Cu(ClO_4)_2.6H_2O$ (684.7 mg, 1.848 mmol). The mixture was stirred for 5 minutes at room temperature after which TBTA (cat.) and an MeCN (1 ml) solution of DBU (140.3 mg, 0.922 mmol) were added, followed by ethyl propiolate (113.4 mg, 1.156 mmol). The reaction mixture was sealed and left to stir at room temperature overnight in the dark. After the reaction was complete, the mixture was diluted with DCM (20 ml) before being washed with $EDTA/NH_4OH_{(aq.)}$ (.1M EDTA in 1M NH_4OH, 2 x 20 ml) and brine (1 x 20 ml). The organics were collected and dried over $MgSO_4$, filtered and the solvent removed *in vacuo*. The crude solid was purified by silica gel column chromatography using (5 » 10% EtOAc/DCM) to elute the product bis-iodotriazole bis-ester **49** as a white solid (107.6 mg, 35% yield). **^{1}H NMR** (400 MHz, $CDCl_3$) δ (ppm): 7.70 (d, Ar-H, ^4J = 1.9 Hz, 2H), 7.54 (t, Ar-H, ^4J = 1.9 Hz, 1H), 4.44 (q, 2 x COO-CH_2-CH_3, J = 7.1 Hz, 4H), 1.45 – 1.34 (m, 2 x COO-CH_2-CH_3 + Ar-tBu, 15H). **^{13}C NMR** (101 MHz, $CDCl_3$) δ (ppm): 160.01, 155.15, 142.62, 136.74, 125.85, 121.52, 85.71, 61.86, 35.66, 31.00, 14.30. **MS** (ESI +ve) m/z: 665.0 ($[M+H]^+$, $C_{20}H_{23}I_2N_6O_4^+$ requires 665.0).

1,3-Bis-triazole bis-tBu ester 50



1,3-diazido-5-(*tert*-butyl)benzene **48** (100 mg, 0.46 mmol) and *tert*-butyl propiolate (122 mg, 0.97 mmol) were dissolved in dry, degassed DCM (10 ml) and $Cu(MeCN)_4PF_6$ (34 mg, 0.092 mmol), TBTA (cat.) and DIPEA (0.16 ml, 0.92 mmol) were sequentially added before the reaction mixture was placed under an N_2 atmosphere for 16 hours. The yellow solution was washed with $EDTA/NH_4OH_{(aq.)}$ (.1M EDTA in 1M NH_4OH, 2 x 20 ml) and brine (1 x 20 ml) and the organic layer was dried over $MgSO_4$ and the solvent removed *in vacuo*. The crude white solid was recrystallized in hot $MeOH/H_2O$ (7:3) to give the product bis-triazole bis-tBu-ester **50** as a white solid (183 mg, 85% yield). **^{1}H NMR** (400 MHz, $CDCl_3$) δ (ppm): 8.48 (s, Triazole Ar-H, 2H), 7.96 (s, Phenyl Ar-H, 1H), 7.82 (s, Phenyl Ar-H, 2H), 1.57 (s, 2 x COO-tBu, 18H), 1.37 (s, Ar-tBu, 9H). **^{13}C NMR** (101 MHz, $CDCl_3$) δ (ppm): 159.49, 156.29, 142.38, 137.42, 125.34, 110.52, 82.84, 35.67, 31.19, 31.09, 28.24. **MS** (ESI +ve) m/z: 469.3 ($[M+H]^+$, $C_{24}H_{33}N_6O_4^+$ requires 469.3). **HRMS** (ESI +ve) m/z: 469.2558 ($[M+H]^+$, $C_{24}H_{33}N_6O_4^+$ requires 469.2557).

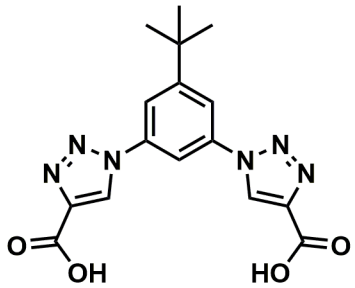
1,3-Bis-iodotriazole bis-tBu ester 51



1,3-diazido-5-(*tert*-butyl)benzene **48** (228 mg, 1.504 mmol) was dissolved in dry, degassed THF (4 ml) and NaI (1.263 g, 8.432 mmol) followed by $Cu(ClO_4)_2.6H_2O$ (1.562 g, 4.216 mmol). The mixture was stirred for 5 minutes at room temperature after which TBTA (cat.) and an MeCN (3 ml) solution of DBU (320.92 mg, 2.108

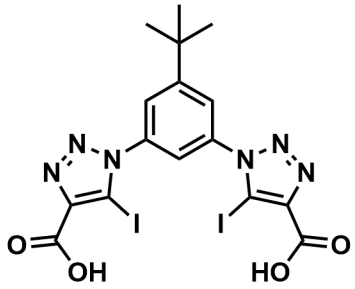
mmol) were added, followed by *tert*-butyl propiolate (332 mg, 2.635 mmol). The reaction mixture was sealed and left to stir at room temperature overnight in the dark. After the reaction was complete, the mixture was diluted with DCM (20 ml) before being washed with EDTA/$NH_4OH_{(aq.)}$ (.1M EDTA in 1M NH_4OH, 2 x 20 ml) and brine (1 x 20 ml) and the organic layer was dried over $MgSO_4$, filtered and the solvent removed *in vacuo*. The crude white solid was purified by silica gel column chromatography using (5% EtOAc/DCM) to elute the product bis-iodotriazole bis-tBu ester **51** as a white solid (280 mg, 37% yield). **^{1}H NMR** (400 MHz, $CDCl_3$) δ (ppm): 7.72 (d, Ar-H, J = 2.0 Hz, 2H), 7.55 (t, Ar-H, J = 1.9 Hz, 1H), 1.66 (s, 2 x COO-tBu, 18H), 1.42 (s, Ar-tBu, 9H). **^{13}C NMR** (101 MHz, $CDCl_3$) δ (ppm): 159.07, 154.97, 143.64, 136.84, 125.80, 121.55, 85.04, 83.41, 35.60, 30.99, 28.27. **MS** (ESI +ve) m/z: 721.1 ($[M+H]^+$, $C_{24}H_{31}I_2N_6O_4^+$ requires 721.0). **HRMS** (ESI +ve) m/z: 743.0302 ($[M+Na]^+$, $C_{24}H_{30}I_2N_6NaO_4^+$ requires 743.0310).

1,3-Bis-triazole bis-acid 52



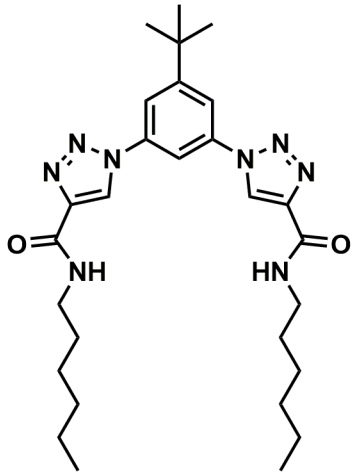
1,3-bis-triazolephenyl bis-tBu ester **50** (160 mg, 0.34 mmol) was dissolved in DCM/TFA (1:1) at 0 ^{0}C under a N_2 atmosphere, allowed to gradually warm to room temperature and left to stir for 24 hours or until the starting material was determined to be completely consumed by TLC. The solvent was removed *in vacuo* and redissolved in MeOH (5 ml) and dried three times to remove any residual TFA to give bis-acid **52** in a quantitative yield as a white solid (121 mg). **^{1}H NMR** (400 MHz, 1:1 v/v $CDCl_3$/CD_3OD) δ (ppm): 9.13 (s, Triazole Ar-H, 2H), 8.24 (s, Phenyl-Ar-H, 1H), 8.04 (s, Phenyl-Ar-H, 2H), 1.44 (s, Ar-tBu, 9H). **^{13}C NMR** (101 MHz, 1:1 v/v $CDCl_3$/CD_3OD) δ (ppm): 156.27, 137.77, 126.55, 118.47, 117.97, 110.41, 35.48, 30.56, 28.70. **MS** (ESI +ve) m/z: 379.2 ($[M+Na]^+$, $C_{16}H_{16}N_6NaO_4^+$ requires 379.1). **HRMS** (ESI +ve) m/z: 379.1124 ($[M+Na]^+$, $C_{16}H_{16}N_6NaO_4^+$ requires 379.1125).

1,3-Bis-iodotriazole bis-acid 53



1,3-diiodotriazolephenyl bis-tBu ester **51** (50 mg, 0.07 mmol) was dissolved in a 1:1 DCM/TFA solvent mixture (4 ml) at 0 ^{0}C and allowed to gradually warm to room temperature whilst stirring. Once the reaction was judged as complete by TLC (16 hours), the solvent was removed *in vacuo* and repeatedly re-dissolved in MeOH and eavpourated to dryness to remove any excess TFA (3 times). The pure product bis-acid **53** was isolated without further purification as a white solid in a quantitative yield (42.5 mg). **^{1}H NMR** (400 MHz, CD_3OD) δ (ppm): 7.93 (d, Ar-H, ^4J = 1.9 Hz, 2H), 7.76 (t, Ar-H, ^4J = 1.9 Hz, 1H), 1.48 (s, Ar-tBu, 9H). **^{13}C NMR** (101 MHz, CD_3OD) δ (ppm): 161.45, 154.95, 142.85, 137.18, 126.02, 122.10, 88.66, 35.23, 30.05. **MS** (ESI +ve) m/z: 609.0 ($[M+H]^+$, $C_{16}H_{15}I_2N_6O_4^+$ requires 608.9). **HRMS** (ESI +ve) m/z: 608.9237 ($[M+H]^+$, $C_{16}H_{15}I_2N_6O_4^+$ requires 608.9238).

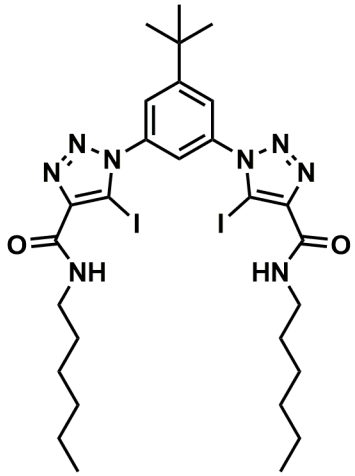
Bis-triazole amide receptor 54



Bis-acid **52** was converted to the corresponding bis acid chloride according to the standard procedure. Bis-acid chloride (31.6 mg, 0.08 mmol) was dissolved in DCM (10 ml), before n-hexylamine (0.023 ml, 0.17 mmol) followed by NEt_3 (0.024 ml, 0.17 mmol) was added drop-wise at 0 °C. The reaction mixture was stirred at room temperature under an N_2 atmosphere for 16 hours and then washed with 10% $HCl_{(aq.)}$ (10 ml), 10% $NaOH_{(aq.)}$ (10 ml) and brine (10 ml). The organic layer was dried over

$MgSO_4$, filtered and the solvent removed *in vacuo*. The crude white solid was recrystallized in hot MeOH to give the product bis-triazole amide receptor **54** as a white solid (15.3 mg, 37% yield). **^{1}H NMR** (400 MHz, $CDCl_3$) δ (ppm): 8.60 (s, Triazole Ar-H, 2H), 8.09 (t, Phenyl Ar-H, ^4J = 2.0 Hz, 1H), 7.84 (d, Phenyl Ar-H, ^4J = 2.0 Hz, 2H), 7.21 (t, CON-H, J = 6.0 Hz, 2H), 3.50 (q, CH_2-NH, J = 6.8 Hz, 4H), 1.72 – 1.61 (m, CH_2, 4H), 1.44 (s, Ar-tBu, 9H), 1.48 – 1.28 (m, CH_2, 12H), 0.90 (t, CH_3, J = 6.9 Hz, 6H). **^{13}C NMR** (101 MHz, $CDCl_3$) δ (ppm): 159.43, 156.30, 144.39, 137.56, 123.43, 118.25, 110.51, 39.34, 35.67, 31.48, 31.09, 29.57, 26.61, 22.56, 14.03. **MS** (ESI +ve) m/z: 545.4 ($[M+Na]^+$, $C_{28}H_{42}N_8NaO_2^+$ requires 545.3). **HRMS** (ESI +ve) m/z: 545.3323 ($[M+Na]^+$, $C_{28}H_{42}N_8NaO_2^+$ requires 545.3322).

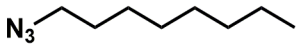
Bis-iodotriazole amide receptor 55



Bis-acid **53** was converted to the corresponding bis acid chloride according to the standard procedure. Bis-acid chloride (45.15 mg, 0.07 mmol) was dissolved in DCM (30 ml), before n-hexylamine (0.0193 ml, 0.147 mmol) followed by NEt_3 (0.02 ml, 0.147 mmol) was added drop-wise at 0 °C. The reaction mixture was stirred at room temperature under an N_2 atmosphere for 16 hours and then washed with 10% $HCl_{(aq.)}$ (10 ml), 10% $NaOH_{(aq.)}$ (10 ml) and brine (10 ml). The organic layer was dried over $MgSO_4$, filtered and the solvent removed *in vacuo*. Purification by silica gel chromatography (2% MeOH/DCM) afforded the product **55** as a white solid (35.6 mg, 66% yield). **^{1}H NMR** (400 MHz, $CDCl_3$) δ (ppm): 7.75 (d, Phenyl Ar-H, ^4J = 1.9 Hz, 2H), 7.60 (t, Phenyl Ar-H, ^4J = 1.9 Hz, 1H), 7.28 (t, CON-H, J = 6.1 Hz, 2H), 3.47 (q, CH_2-NH, J = 7.0 Hz, 4H), 1.64 (p, CH_2, J = 7.4 Hz, 4H), 1.43 (s, Ar-tBu, 9H), 1.42 – 1.21 (m, CH_2, 12H), 0.88 (t, CH_3, J = 7.0 Hz, 6H). **^{13}C NMR** (101 MHz, $CDCl_3$) δ 159.06, 154.96, 143.55, 136.70, 125.65, 121.38, 81.88, 39.34, 35.64, 31.47, 31.01, 29.56, 26.63, 22.56, 14.03. **MS** (ESI +ve) m/z: 797.2 ($[M+Na]^+$,

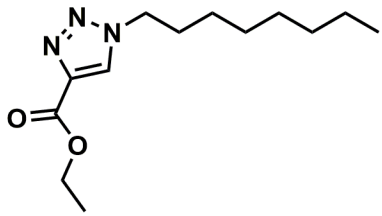
$C_{28}H_{40}I_2N_8NaO_2^+$ requires 797.1). **HRMS** (ESI +ve) m/z: 797.1252 ($[M+Na]^+$, $C_{28}H_{40}I_2N_8NaO_2^+$ requires 797.1255).

Octyl azide 56[16]



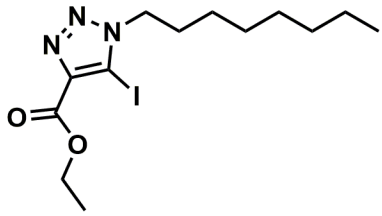
Octyl bromide (1.8 ml, 10.4 mmol) and NaN_3 (800 mg, 12.48 mmol) were dissolved in DMSO (30 ml) and stirred at room temperature under an atmosphere of N_2 for 24 hours. The reaction mixture was then poured onto brine (60 ml) and extracted with Et_2O (3 x 40 ml). The combined organic extracts were washed with brine (1 x 20 ml), dried over $MgSO_4$, filtered and dried *in vacuo* with no heating to give octyl azide **56** as a pale yellow-green liquid (1.45 g, 94% yield). **^{1}H NMR** (400 MHz, $CDCl_3$) δ (ppm): 3.25 (t, C$\underline{H_2}$-N_3, J = 7.1 Hz, 2H), 1.67 – 1.51 (m, C$\underline{H_2}$, 2H), 1.43 – 1.18 (m, C$\underline{H_2}$, 10H), 0.88 (t, C$\underline{H_3}$, J = 7 Hz, 3H).

Octyl triazole ethyl ester 57[17]



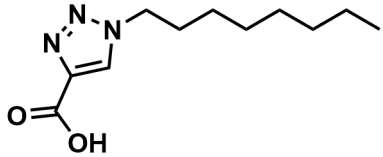
Octyl azide **56** (512 mg, 3.3 mmol) and ethyl propiolate (294.3 mg, 3 mmol) were dissolved in dry, degassed DCM (40 ml) and $Cu(MeCN)_4PF_6$ (224 mg, 0.6 mmol), TBTA (cat.) and DIPEA (1 ml, 6 mmol) were sequentially added before the reaction mixture was placed under an N_2 atmosphere for 16 hours. The yellow solution was washed with EDTA/$NH_4OH_{(aq.)}$ (.1M EDTA in 1M NH_4OH, 2 x 20 ml) and brine (1 x 20 ml) and the organic layer was dried over $MgSO_4$, filtered and the solvent removed *in vacuo*. The crude white solid was recrystallized in warm hexane to give the product octyl triazole ester **57** as a white powder (600 mg, 79% yield). **^{1}H NMR** (400 MHz, $CDCl_3$) δ (ppm): 8.06 (s, Triazole Ar-$\underline{H}$, 1H), 4.51 – 4.30 (m, Triazole-C$\underline{H_2}$ + COO-C$\underline{H_2}$-CH_3, 4H), 1.91 (q, CH_2-C$\underline{H_2}$-CH_2, J = 7.1 Hz, 2H), 1.57 – 1.10 (m, C$\underline{H_2}$ + COO-CH_2-C$\underline{H_3}$, 13H), 0.85 (t, C$\underline{H_3}$, J = 6.7 Hz, 3H). **^{13}C NMR** (101 MHz, $CDCl_3$) δ (ppm): 160.86, 140.20, 127.21, 61.27, 50.70, 31.64, 30.14, 28.97, 28.86, 26.33, 22.55, 14.29, 14.01. **MS** (ESI +ve) m/z: 254.2 ($[M+H]^+$, $C_{13}H_{24}N_3O_2^+$ requires 254.2).

Octyl iodotriazole ethyl ester 58



Octyl azide **56** (250 mg, 1.07 mmol) was dissolved in dry, degassed THF (8 ml) and NaI (641 mg, 4.28 mmol) was added, followed by $Cu(ClO_4)_2.6H_2O$ (793 mg, 2.14 mmol). The mixture was stirred for 5 minutes at room temperature after which TBTA (cat.) and an MeCN (4 ml) solution of DBU (162.8 mg, 1.07 mmol) were added, followed by ethyl propiolate (332 mg, 2.635 mmol). The reaction mixture was sealed and left to stir at room temperature overnight in the dark. After the reaction was complete, the mixture was diluted with DCM (20 ml) before being washed with $EDTA/NH_4OH_{(aq.)}$ (.1M EDTA in 1M NH_4OH, 2 x 20 ml) and brine (1 x 20 ml) and the organic layer was dried over $MgSO_4$, filtered and the solvent removed *in vacuo*. The crude white solid was purified by silica gel column chromatography using (10% hexane/DCM) to elute the product iodotriazole ester **58** as a white solid (307 mg, 76% yield). **^{1}H NMR** (400 MHz, $CDCl_3$) δ (ppm): 4.48 – 4.38 (m, Triazole-C$\underline{H}_2$ + COO-C$\underline{H}_2$-CH_3, 4H), 1.90 (p, CH_2-C$\underline{H}_2$-CH_2, J = 7.6 Hz, 2H), 1.42 (t, COO-CH_2-C$\underline{H}_3$, J = 7.2 Hz, 3H), 1.35 – 1.18 (m, C$\underline{H}_2$, 10H), 0.85 (t, C$\underline{H}_3$, J = 7.2 Hz, 3H). **^{13}C NMR** (101 MHz, $CDCl_3$) δ (ppm): 160.36, 141.69, 84.23, 61.51, 51.11, 31.66, 29.76, 28.99, 28.89, 26.27, 22.57, 14.25, 14.04. **MS** (ESI +ve) m/z: 402.0 ($[M+Na]^+$, $C_{13}H_{22}IN_3NaO_2^+$ requires 402.1). **HRMS** (ESI +ve) m/z: 402.0649 ($[M+Na]^+$, $C_{13}H_{22}IN_3NaO_2^+$ requires 402.0648).

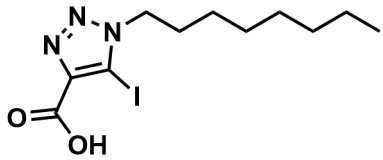
Octyl triazole acid 59



Octyl triazole ethyl ester **57** (572 mg, 2.26 mmol) was dissolved in MeOH (10 ml) and KOH pellets (254 mg, 4.52 mmol) were added to the solution and the mixture was stirred for 16 hrs. The solvent was removed by rotary evaporation, redissolved in the minimum of H_2O (~ 5 ml) and acidified to pH 1 by drop-wise addition of aqueous 1M HCl, at which point large amounts of white precipitate formed. This was isolated by vacuum filtration and rinsed with H_2O (1 x 10 ml), Et_2O (2 x 10

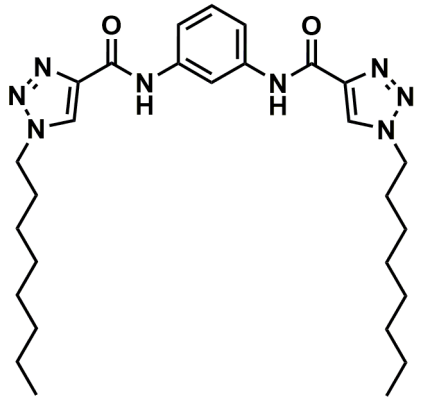
ml) and subsequently dried under a vacuum to give triazole carboxylic acid **59** as a white powder (386 mg, 76 %). **^{1}H NMR** (400 MHz, DMSO-d_6) δ (ppm): 13.06 (bs, COO-H, 1H), 8.68 (s, Triazole Ar-H, 1H), 4.38 (t, Triazole-CH_2, J = 7.1 Hz, 2H), 1.82 (p, CH_2-CH_2-CH_2, J = 7.1 Hz, 2H), 1.33 – 1.12 (m, CH_2, 10H), 0.84 (t, CH_3, J = 6.8 Hz, 3H). **^{13}C NMR** (101 MHz, DMSO-d_6) δ (ppm): 162.22, 140.11, 129.17, 50.07, 31.60, 29.91, 28.93, 28.73, 26.17, 22.50, 14.37. **MS** (ESI +ve) m/z: 248.1 ([M+Na]$^+$, $C_{11}H_{19}N_3NaO_2^+$ requires 248.1). **HRMS** (ESI +ve) m/z: 248.1371 ([M+Na]$^+$, $C_{11}H_{19}N_3NaO_2^+$ requires 248.1369).

Octyl iodotriazole ethyl ester 60



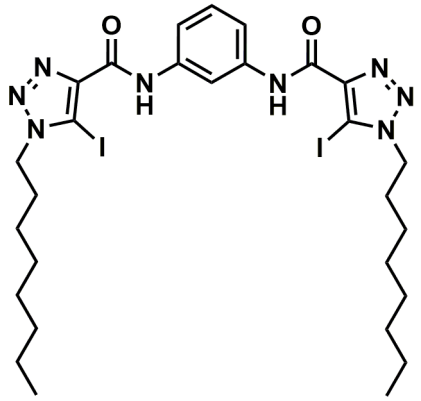
Octyl triazole ethyl ester **58** (225 mg, 0.594 mmol) was dissolved in MeOH (10 ml) and KOH pellets (67 mg, 1.187 mmol) were added to the solution and the mixture was stirred for 16 hrs. The solvent was removed by rotary evaporation, redissolved in the minimum of H_2O (~ 10 ml) and acidified to pH 1 by drop-wise addition of aqueous 1M HCl, at which point large amounts of white precipitate formed. This was isolated by vacuum filtration and rinsed with H_2O (1 x 10 ml), Et_2O (2 x 10 ml) and subsequently dried under a vacuum to give iodotriazole carboxylic acid **60** as a white powder (164 mg, 78 %). **^{1}H NMR** (400 MHz, DMSO-d_6) δ (ppm): 13.22 (s, COO-H, 1H), 4.41 (t, Triazole-CH_2, J = 7.1 Hz, 2H), 1.82 (p, CH_2-CH_2-CH_2, J = 7.0 Hz, 2H), 1.32 – 1.20 (m, CH_2, 10H), 0.84 (t, J = 6.6 Hz, CH_3, 3H). **^{13}C NMR** (101 MHz, DMSO-d_6) δ (ppm): 161.90, 142.40, 89.84, 50.74, 31.59, 29.55, 28.91, 28.72, 26.10, 22.50, 14.40. **MS** (ESI +ve) m/z: 352.1 ([M+H]$^+$, $C_{11}H_{19}IN_3O_2^+$ requires 352.1). **HRMS** (ESI +ve) m/z: 374.0335 ([M+Na]$^+$, $C_{11}H_{18}IN_3NaO_2^+$ requires 374.0335).

1,3-Bis-amidetriazole receptor 61



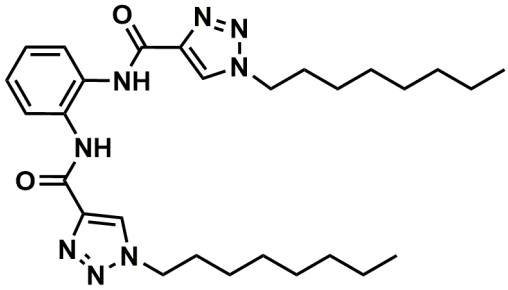
Octyl triazole acid **59** (50 mg, 0.222 mmol) and EDC.HCl (43 mg, 0.222 mmol) were dissolved in dry DCM (5 ml) and stirred for 30 minutes at 0 ^{0}C until the solution was homogenous. *m*-phenylenediamine (10.8 mg, 0.1 mmol) was then added, followed by DMAP (13.21 mg, 0.222 mmol) and NEt_3 (0.032 ml, 0.222 mmol) and the mixture placed under a N_2 atmosphere and stirred for 48 hours. The reaction mixture was then washed with 1M $HCl_{(aq.)}$ (20 ml), 1M $NaOH_{(aq.)}$ (20 ml) and brine (10 ml). The organic layer was dried over $MgSO_4$, filtered and the solvent removed *in vacuo* to give a crude white solid which was purified *via* silica gel column chromatography (10% EtOAc/DCM) to give bis-amidetriazole **61** as a white solid (34.5 mg, 66% yield). **^{1}H NMR** (400 MHz, $CDCl_3$) δ (ppm): 9.02 (s, CON-H, 2H), 8.14 (s, Triazole Ar-H, 2H), 8.10 (t, Phenyl Ar-H, ^{4}J = 2.1 Hz, 1H), 7.49 (d, Phenyl Ar-H, J = 8.2 Hz, 2H), 7.32 (t, Phenyl Ar-H, J = 8.1 Hz, 1H), 4.39 (t, Triazole-CH_2, J = 7.2 Hz, 4H), 1.90 (p, CH_2-CH_2-CH_2, J = 7.0 Hz, 4H), 1.34 – 1.15 (m, CH_2, 20H), 0.83 (t, CH_3, J = 6.8 Hz, 6H). **^{13}C NMR** (101 MHz, $CDCl_3$) δ (ppm): 158.01, 143.27, 138.18, 129.67, 125.67, 115.75, 111.13, 50.83, 31.63, 30.12, 28.97, 28.85, 26.34, 22.53, 14.00. **MS** (ESI +ve) m/z: 523.4 ($[M+H]^+$, $C_{28}H_{43}N_8O_2^+$ requires 523.4). **HRMS** (ESI +ve) m/z: 523.3506 ($[M+H]^+$, $C_{28}H_{43}N_8O_2^+$ requires 523.3503).

1,3-Bis-amideiodotriazole receptor 62



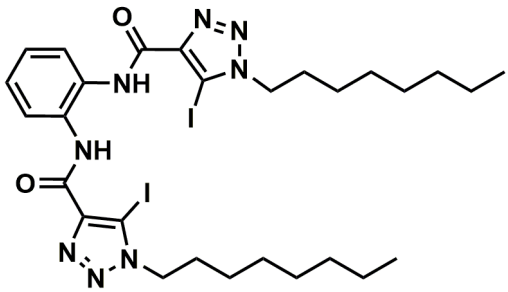
Octyl iodotriazole acid **60** (30 mg, 0.085 mmol) and EDC.HCl (16.3 mg, 0.085 mmol) were dissolved in dry DCM (5 ml) and stirred for 30 minutes at 0 ^{0}C until the solution was homogenous. *m*-phenylenediamine (4.4 mg, 0.041 mmol) was then added, followed by DMAP (5.06 mg, 0.085 mmol) and NEt_3 (0.012 ml, 0.085 mmol) and the mixture placed under a N_2 atmosphere and stirred for 48 hours. The reaction mixture was then washed with 1M $HCl_{(aq.)}$ (20 ml), 1M $NaOH_{(aq.)}$ (20 ml) and brine (10 ml). The organic layer was dried over $MgSO_4$, filtered and the solvent removed *in vacuo* to give a crude white solid which was purified *via* silica gel column chromatography (3% EtOAc/DCM) to give bis-amideiodotriazole **62** as a white solid (11.3 mg, 36% yield). **^{1}H NMR** (400 MHz, $CDCl_3$) δ (ppm): 9.07 (s, CON-H, 2H), 8.15 (t, Phenyl Ar-H, ^{4}J = 2.1 Hz, 1H), 7.54 (d, Phenyl Ar-H, J = 8.1 Hz, 2H), 7.26 (s, Phenyl Ar-H, 1H), 4.45 (t, Triazole-CH_2, J = 7.4 Hz, 4H), 1.94 (p, CH_2-CH_2-CH_2, J = 7.1 Hz, 4H), 1.40 – 1.22 (m, CH_2, 20H), 0.89 (t, CH_3, J = 7.0 Hz, 6H). **^{13}C NMR** (101 MHz, $CDCl_3$) δ (ppm): 157.55, 142.55, 138.14, 129.75, 115.72, 110.99, 81.28, 50.99, 31.69, 29.78, 29.02, 28.92, 26.33, 22.60, 14.06. **MS** (ESI +ve) m/z: 775.2 ($[M+H]^+$, $C_{28}H_{41}I_2N_8O_2^+$ requires 775.1). **HRMS** (ESI +ve) m/z: 797.1252 ($[M+Na]^+$, $C_{28}H_{40}I_2N_8NaO_2^+$ requires 797.1255).

1,2-Bis-amidetriazole receptor 63



Octyl triazole acid **59** (43 mg, 0.190 mmol) and EDC.HCl (36.42 mg, 0.190 mmol) were dissolved in dry DCM (5 ml) and stirred for 30 minutes at 0 ^{0}C until the solution was homogenous. *o*-phenylenediamine (9.8 mg, 0.090 mmol) was then added, followed by DMAP (11.3 mg, 0.190 mmol) and NEt_3 (0.027 ml, 0.190 mmol) and the mixture placed under a N_2 atmosphere and stirred for 48 hours. The reaction mixture was then washed with 1M $HCl_{(aq.)}$ (20 ml), 1M $NaOH_{(aq.)}$ (20 ml) and brine (10 ml). The organic layer was dried over $MgSO_4$, filtered and the solvent removed *in vacuo* to give a crude white solid which was purified *via* silica gel column chromatography (10% EtOAc/DCM) to give bis-amidetriazole **63** as a white solid (18.4 mg, 39% yield). **^{1}H NMR** (400 MHz, $CDCl_3$) δ (ppm): 9.44 (s, CON-H, 2H), 8.18 (s, Triazole Ar-H, 2H), 7.73 (dd, Phenyl Ar-H, J = 6.0, 3.6 Hz, 2H), 7.28 (dd, Phenyl Ar-H, J = 6.1, 3.5 Hz, 2H), 4.38 (t, Triazole-CH_2, J = 7.2 Hz, 4H), 1.91 (p, CH_2-CH_2-CH_2, J = 7.4 Hz, 4H), 1.37 – 1.20 (m, CH_2, 20H), 0.87 (t, CH_3, 6H). **^{13}C NMR** (126 MHz, $CDCl_3$) δ (ppm): 158.88, 143.02, 129.94, 126.44, 125.94, 125.25, 50.81, 31.69, 30.13, 29.00, 28.90, 26.40, 22.58, 14.05. **MS** (ESI +ve) m/z: 523.4 ($[M+H]^+$, $C_{28}H_{43}N_8O_2^+$ requires 523.4). **HRMS** (ESI +ve) m/z: 523.3499 ($[M+H]^+$, $C_{28}H_{43}N_8O_2^+$ requires 523.3503).

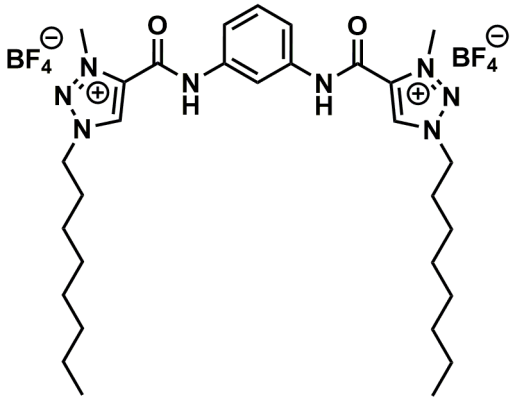
1,2-Bis-amideiodotriazole receptor 64



Octyl iodotriazole acid **60** (250 mg, 0.712 mmol) and EDC.HCl (136 mg, 0.712 mmol) were dissolved in dry DCM (10 ml) and stirred for 30 minutes at 0 ^{0}C until the solution was homogenous. *o*-phenylenediamine (36.67 mg, 0.339 mmol) was then added, followed by DMAP (87 mg, 0.712 mmol) and NEt_3 (0.1 ml, 0.712 mmol) and

the mixture placed under a N_2 atmosphere and stirred for 48 hours. The reaction mixture was then washed with 1M $HCl_{(aq.)}$ (20 ml), 1M $NaOH_{(aq.)}$ (20 ml) and brine (10 ml). The organic layer was dried over $MgSO_4$, filtered and the solvent removed *in vacuo* to give a crude white solid which was purified *via* silica gel column chromatography (3% EtOAc/DCM) to give bis-amideiodotriazole **64** as a white solid (111.9 mg, 42%). **^{1}H NMR** (400 MHz, $CDCl_3$) δ (ppm): 9.56 (s, CON-H, 2H), 7.77 (dd, Phenyl Ar-H, J = 6.0, 3.5 Hz, 2H), 7.25 (dd, Phenyl Ar-H, J = 5.1, 2.6 Hz, 2H), 4.37 (t, Triazole-CH_2, J = 7.4 Hz, 4H), 1.88 (p, CH_2-CH_2-CH_2, J = 7.3, 6.8 Hz, 4H), 1.38 – 1.19 (m, CH_2, 20H), 0.86 (t, CH_3, J = 7.1 Hz, 6H). **^{13}C NMR** (101 MHz, $CDCl_3$) δ (ppm): 158.27, 142.51, 129.83, 126.20, 125.25, 81.83, 50.92, 31.71, 29.70, 29.02, 28.92, 26.34, 22.60, 14.09. **MS** (ESI +ve) m/z: 775.2 ($[M+H]^+$, $C_{28}H_{41}I_2N_8O_2^+$ requires 775.1). **HRMS** (ESI +ve) m/z: 797.1248 ($[M+Na]^+$, $C_{28}H_{40}I_2N_8NaO_2^+$ requires 797.1255).

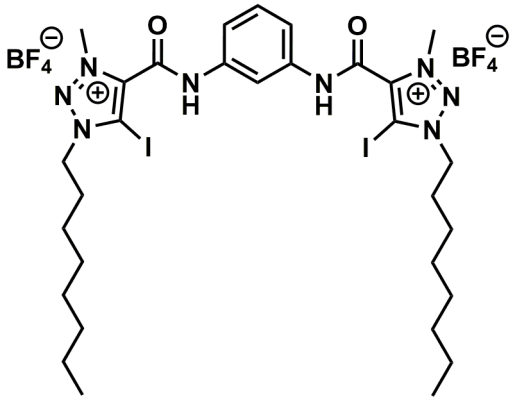
1,3-Bis-amidetriazolium receptor 65.$(BF_4)_2$



1,3-bis-amidetriazole **61** (31.3 mg, 0.059 mmol) was dissolved in DCM (2 ml) and trimethyloxonium tetrafluorborate (44 mg, 0.3 mmol) was added in one portion. The mixture was placed under an atmosphere of N_2 and stirred until the starting material and any mono-methylated side-product was consumed by TLC (72 hours). The reaction mixture was quenched with MeOH (2 ml) and the solvent was removed *in vacuo* and purified *via* silica gel column chromatography (10% MeOH/DCM) to give dicationic bis-triazolium receptor **65.$(BF_4)_2$** as a white solid (31.3 mg, 73% yield). **^{1}H NMR** (400 MHz, 1:1 v/v $CDCl_3$/CD_3OD) δ (ppm): 8.03 (s, Phenyl Ar-H, 1H), 7.41 (d, Phenyl Ar-H, J = 8.1 Hz, 2H), 7.27 (t, Phenyl Ar-H, J = 8.1 Hz, 1H), 4.55 (t, Triazolium-CH_2, J = 6.5 Hz, 4H), 4.46 (s, Triaz-N^+Me, 6H), 1.97 (p, CH_2-CH_2-CH_2, J = 7.3 Hz, 4H), 1.41 – 1.13 (m, CH_2, 20H), 0.80 (t, CH_3, J = 6.4 Hz, 6H). **^{13}C NMR** (101 MHz, 1:1 v/v $CDCl_3$/CD_3OD) δ (ppm): 152.70, 137.53, 135.37,

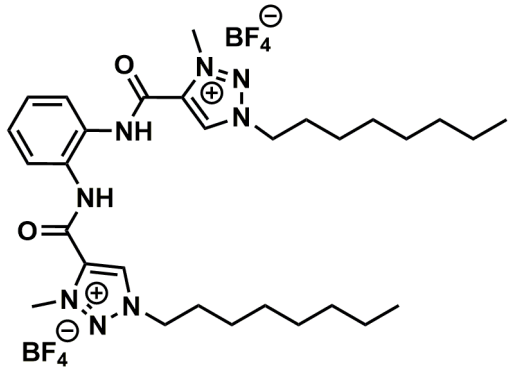
129.51, 117.91, 113.24, 54.45, 40.33, 31.57, 28.89, 28.83, 28.69, 25.94, 22.40, 13.56, 1 peak missing; presumed overlapped. **^{19}F NMR** (376 MHz, 1:1 v/v $CDCl_3/CD_3OD$) δ (ppm): -152.97 (s, $B\underline{F}_4^-$). **MS** (ESI +ve) m/z: 638.4 ($[M^{2+}+BF_4^-]^+$, $C_{30}H_{48}BF_4N_8O_2^+$ requires 638.4). **HRMS** (ESI +ve) m/z: 638.3959 ($[M^{2+}+BF_4^-]^+$, $C_{30}H_{48}BF_4N_8O_2^+$ requires 638.3960).

1,3-Bis-amideiodotriazolium receptor 66.$(BF_4)_2$



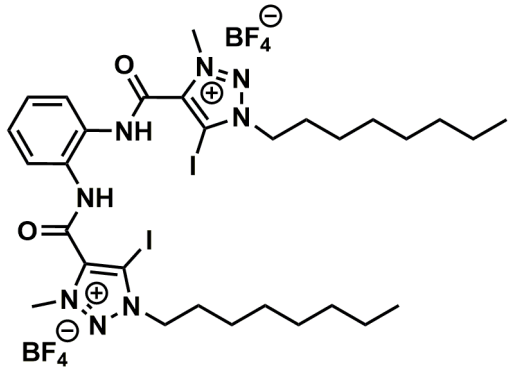
1,3-bis-amideiodotriazole **62** (40.1 mg, 0.051 mmol) was dissolved in DCM (2 ml) and trimethyloxonium tetrafluoroborate (38.3 mg, 0.258 mmol) was added in one portion. The mixture was placed under an atmosphere of N_2 and stirred until the starting material and any mono-methylated side-product was consumed by TLC (48 hours). The reaction mixture was quenched with MeOH (2 ml) and the solvent was removed *in vacuo* and purified *via* silica gel column chromatography (10% MeOH/DCM) to give dicationic bis-iodotriazolium receptor **66.$(BF_4)_2$** as a light brown solid (34.3 mg, 69% yield). **^{1}H NMR** (400 MHz, CD_3CN) δ (ppm): 9.53 (bs, CON-H, 2H), 8.18 (s, Phenyl Ar-H, 1H), 7.60 – 7.47 (m, Phenyl Ar-H, 3H), 4.59 (t, Triazolium-$C\underline{H}_2$, J = 7.3 Hz, 4H), 4.38 (s, Triaz-$N^+\underline{Me}$, 6H), 2.03 – 1.88 (m, $C\underline{H}_2$, 4H), 1.50 – 1.21 (m, $C\underline{H}_2$, 20H), 0.90 (t, $C\underline{H}_3$, J = 6.6 Hz, 7H). **^{13}C NMR** (101 MHz, CD_3CN) δ (ppm): 153.62, 142.04, 138.37, 131.07, 118.83, 118.26, 113.45, 91.08, 55.90, 41.09, 32.36, 29.61, 29.41, 26.43, 23.25, 14.30. **^{19}F NMR** (376 MHz, 1:1 v/v $CDCl_3/CD_3OD$) δ (ppm): -152.97 (s, $B\underline{F}_4^-$). **MS** (ESI +ve) m/z: 402.1 ($[M]^{2+}$, $C_{30}H_{46}I_2N_8O_2^{2+}$ requires 402.1). **HRMS** (ESI +ve) m/z: 402.0914 ($[M]^{2+}$, $C_{30}H_{46}I_2N_8O_2^{2+}$ requires 402.0911).

1,2-Bis-amidetriazolium receptor 67.$(BF_4)_2$



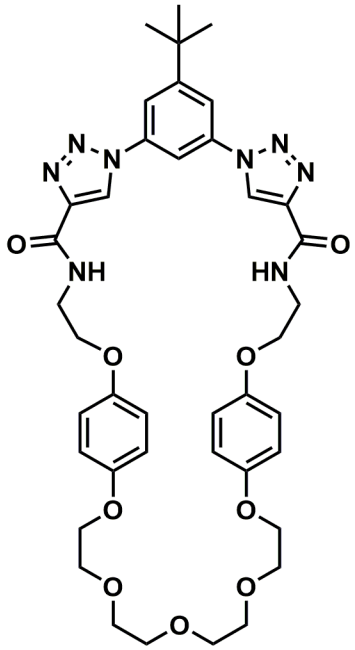
1,2-bis-amidetriazole **63** (17 mg, 0.032 mmol) was dissolved in DCM (2 ml) and trimethyloxonium tetrafluoroborate (24 mg, 0.163 mmol) was added in one portion. The mixture was placed under an atmosphere of N_2 and stirred until the starting material and any mono-methylated side-product was consumed by TLC (72 hours). The reaction mixture was quenched with MeOH (2 ml) and the solvent was removed *in vacuo* and purified *via* silica gel column chromatography (10% MeOH/DCM) to give dicationic bis-triazolium receptor **67.$(BF_4)_2$** as a white solid (17.6 mg, 76% yield). **^{1}H NMR** (400 MHz, 1:1 v/v $CDCl_3/CD_3OD$) δ (ppm): 7.64 (dd, Phenyl Ar-H, J = 6.0, 3.5 Hz, 2H), 7.25 (dd, Phenyl Ar-H, J = 6.1, 3.5 Hz, 2H), 4.50 (t, Triazolium-CH_2, J = 7.5 Hz, 4H), 4.43 (s, Triaz-N^+Me, 6H), 1.96 (p, CH_2-CH_2-CH_2, J = 7.3 Hz, 4H), 1.43 – 1.10 (m, CH_2, 20H), 0.80 (t, CH_3, J = 6.9 Hz, 6H). **^{13}C NMR** (101 MHz, 1:1 v/v $CDCl_3/CD_3OD$) δ (ppm): 153.62, 135.68, 130.17, 126.86, 125.55, 54.29, 40.13, 31.57, 28.82, 28.76, 28.69, 25.95, 22.40, 13.55, 1 peak missing; presumed overlapped. **^{19}F NMR** (376 MHz, 1:1 v/v $CDCl_3/CD_3OD$) δ (ppm): 152.90 (s, BF_4^-). **MS** (ESI +ve) m/z: 638.4 ($[M^{2+}+BF_4^-]^+$, $C_{30}H_{48}BF_4N_8O_2^+$ requires 638.4). **HRMS** (ESI +ve) m/z: 638.3958 ($[M^{2+}+BF_4^-]^+$, $C_{30}H_{48}BF_4N_8O_2^+$ requires 638.3960).

1,2-Bis-amideiodotriazolium receptor 68.$(BF_4)_2$



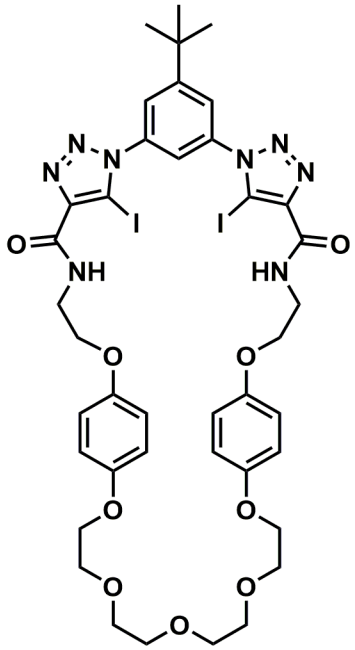
1,2-bis-amideiodotriazole **64** (112 mg, 0.144 mmol) was dissolved in DCM (4 ml) and trimethyloxonium tetrafluoroborate (107 mg, 0.723 mmol) was added in one portion. The mixture was placed under an atmosphere of N_2 and stirred until the starting material and any mono-methylated side-product was consumed by TLC (72 hours). The reaction mixture was quenched with MeOH (3 ml) and the solvent was removed *in vacuo* and purified *via* silica gel column chromatography (10% MeOH/DCM) to give dicationic bis-iodotriazolium receptor **68.$(BF_4)_2$** as a light brown solid (102.8 mg, 73% yield). **^{1}H NMR** (400 MHz, CD_3CN) δ (ppm): 9.46 (bs, CON-H, 2H), 7.84 (dd, Phenyl Ar-H, J = 6.1, 3.6 Hz, 2H), 7.29 (dd, Phenyl Ar-H, J = 6.1, 3.5 Hz, 2H), 4.48 (t, Triazolium-CH_2, J = 7.3 Hz, 4H), 4.37 (s, Triaz-N^+Me, 6H), 1.94 – 1.86 (m, CH_2, 4H), 1.41 – 1.23 (m, CH_2, 20H), 0.89 (t, CH_3, J = 6.6 Hz, 6H). **^{13}C NMR** (101 MHz, CD_3CN) δ (ppm): 154.68, 141.69, 131.77, 127.50, 125.75, 118.26, 92.81, 55.81, 55.27, 49.88, 41.52, 32.42, 29.68, 29.51, 29.41, 26.52, 23.30, 14.36. **^{19}F NMR** (376 MHz, 1:1 v/v $CDCl_3$/CD_3OD) δ (ppm): -152.97 (s, BF_4^-). **MS** (ESI +ve) m/z: 402.1 ($[M]^{2+}$, $C_{30}H_{46}I_2N_8O_2^{2+}$ requires 402.1). **HRMS** (ESI +ve) m/z: 402.0901 ($[M]^{2+}$, $C_{30}H_{46}I_2N_8O_2^{2+}$ requires 402.0911).

Bis-amidetriazole macrocycle 71



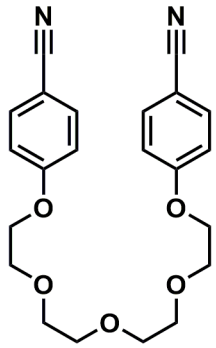
1,3-ditriazolephenyl bis-acid chloride **69** was prepared from 1,3-ditriazolephenyl bis-acid **52** according to the standard procedure. Bis-amine 5-oxygen polyether **21** (70 mg, 0.152 mmol), pyridinium chloride template **22.Cl** (53.17 mg, 0.152 mmol) and NEt_3 (0.8 ml, excess) were dissolved in DCM (30 ml) and cooled to 0 ^{0}C in an ice bath. 1,3-bis-triazolephenyl bis-acid chloride **69** (60 mg, 0.152 mmol) was dissolved in DCM (10 ml) and added drop-wise to the cooled solution over a 30 minute period and gradually allowed to warm to room temperature. The reaction was allowed to stir for 24 hours under an atmosphere of N_2. The solution was then washed with 10% $HCl_{(aq.)}$ (20 ml) and H_2O (20 ml) and the organic layer was dried over $MgSO_4$, filtered and the solvent removed *in vacuo* to give a crude white solid which was subsequently purified by preparative TLC (3% MeOH in DCM) to yield pure bis-amidetriazole macrocycle **71** as a white solid (11.9 mg, 10% yield). **^{1}H NMR** (500 MHz, $CDCl_3$) δ (ppm): 8.55 (s, Triazole Ar-H, 2H), 8.03 (t, Phenyl Ar-H, ^4J = 2.0 Hz, 1H), 7.76 (d, Phenyl Ar-H, ^4J = 2.1 Hz, 2H), 7.65 (t, CON-H, J = 6.1 Hz, 2H), 6.89 – 6.77 (m, Hydroquinone-Ar-H, 8H), 4.12 (t, Hydroquinone-O-CH_2, J = 4.9 Hz, 4H), 4.06 (t, Hydroquinone-O-CH_2, J = 5.0 Hz, 4H), 3.87 (q, CH_2-NH, J = 5.2 Hz, 4H), 3.78 (t, CH_2, J = 5.0 Hz, 4H), 3.71 – 3.60 (m, 8H), 1.44 (s, Phenyl-tBu, 9H). **^{13}C NMR** (126 MHz, $CDCl_3$) δ (ppm): 159.77, 156.29, 153.27, 153.05, 144.03, 137.58, 123.84, 118.45, 115.74, 112.61, 70.76, 70.68, 69.71, 68.02, 67.55, 39.03, 35.67, 31.10, 29.71. **MS** (ESI +ve) m/z: 785.5 ($[M+H]^+$, $C_{40}H_{49}N_8O_9^+$ requires 785.4). **HRMS** (ESI +ve) m/z: 785.3613 ($[M+H]^+$, $C_{40}H_{49}N_8O_9^+$ requires 785.3617).

Bis-amideiodotriazole macrocycle 72



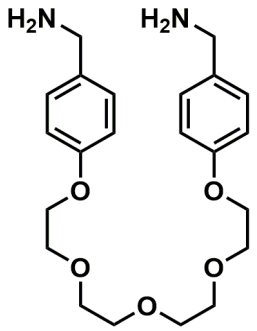
1,3-diiodotriazolephenyl bis-acid chloride **70** was prepared from 1,3-bis-iodotriazolephenyl bis-acid **53** according to the standard procedure. Bis-amine 5-oxygen polyether **21** (46.05 mg, 0.1 mmol), pyridinium chloride template **22.Cl** (34.85 mg, 0.1 mmol) and NEt_3 (0.5 ml, excess) were dissolved in DCM (27 ml) and cooled to 0 ^{0}C with an ice bath. 1,3-diiodotriazolephenyl bis-acid chloride **70** (60 mg, 0.1 mmol) was dissolved in DCM (5 ml) and added drop-wise to the cooled solution over a 30-minute period and gradually allowed to warm to room temperature. The reaction was allowed to stir for 24 hours under an atmosphere of N_2. The solution was then washed with 10% $HCl_{(aq.)}$ (10 ml) and H_2O (10 ml) and the organic layer was dried over $MgSO_4$, filtered and the solvent removed *in vacuo* to give a crude white solid which was subsequently purified by preparative TLC (30% EtOAc/DCM) to yield pure bis-amideiodotriazole macrocycle **72** as a white solid (7.8 mg, 8% yield). **^{1}H NMR** (400 MHz, $CDCl_3$) δ (ppm): 7.79 (d, Phenyl Ar-H, ^4J = 1.9 Hz, 2H), 7.72 (t, CON-H, J = 6.1 Hz, 2H), 7.43 (t, Phenyl Ar-H, ^4J = 1.9 Hz, 1H), 6.82 (m, Hydroquinone-Ar-H, 8H), 4.07 (m, Hydroquinone-O-CH_2, 8H), 3.87 (q, CH_2-NH, J = 5.3 Hz, 4H), 3.79 (t, CH_2, J = 4.9 Hz, 4H), 3.68 (m, CH_2, 8H), 1.46 (s, Phenyl-tBu, 9H). **^{13}C NMR** (126 MHz, $CDCl_3$) δ (ppm): 158.24, 153.78, 152.18, 151.88, 142.34, 135.78, 124.43, 121.25, 114.62, 114.41, 81.16, 69.79, 69.70, 68.71, 66.98, 66.42, 37.86, 34.65, 30.00. **MS** (ESI +ve) m/z: 1037.3 ($[M+H]^+$, $C_{40}H_{47}I_2N_8O_9^+$ requires 1037.2). **HRMS** (ESI +ve) m/z: 1037.1521 ($[M+H]^+$, $C_{40}H_{47}I_2N_8O_9^+$ requires 1037.1549).

Bis-nitrile 5-oxygen polyether 73[18]



4-cyanophenol (597 mg, 5.01 mmol), tetraethylene glycol bis-tosylate **18** (1.26 g, 2.51 mmol) and K_2CO_3 (1.4 g, 10.1 mmol) were dissolved in dry MeCN (50 ml) and heated to reflux under an atmosphere of N_2 for 16 hours. The mixture was then cooled to room temperature, diluted with DCM (50 ml), the solids filtered off and the solvent removed *in vacuo* to give a crude oil that was purified by silica gel column chromatography (10% EtOAc/DCM) to give bis-nitrile **73** as a light yellow oil (1.78 g, 90% yield). **^{1}H NMR** (400 MHz, $CDCl_3$) **δ** (ppm): 7.61 – 7.52 (m, Ar-H, 4H), 7.00 – 6.91 (m, Ar-H, 4H), 4.16 (dd, Phenol-CH_2, J = 5.6, 3.9 Hz, 4H), 3.89 – 3.82 (m, CH_2, 4H), 3.75 – 3.63 (m, CH_2, 8H).

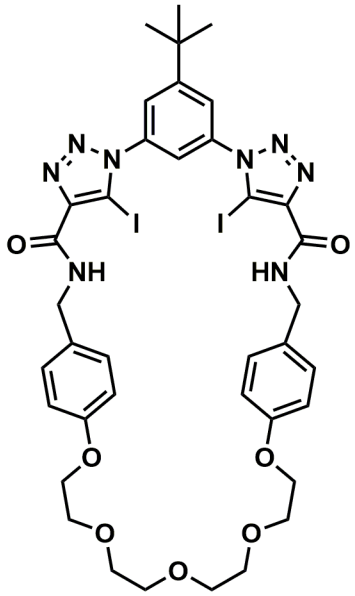
Bis-amine 5-oxygen polyether 74[18]



$LiAlH_4$ (150 mg, 3.88 mmol) was suspended in dry THF (25 ml) and bis-nitrile 5-oxygen polyether **73** was dissolved in THF (25 ml) and added slowly *via* a dropping funnel to the stirring $LiAlH_4$ suspension under a N_2 atmosphere. Once the addition was complete, the mixture was heated to 60 ^{0}C for 16 hours. The reaction mixture was cooled to 0 ^{0}C and quenched with cautious additions of H_2O, at which point a large amount of light grey precipitate formed. The solids were filtered and washed with H_2O (30 ml) and DCM (50 ml) and all collected filtrates were combined in a separating funnel and the organic layer separated, washed with 1M $KOH_{(aq.)}$ (30 ml), dried over $MgSO_4$, filtered and the solvent removed *in vacuo* to give free-base bis-amine **74** as a colourless solid (366 mg, 70% yield). **^{1}H NMR** (400 MHz, $CDCl_3$) **δ**

(ppm): 7.24 – 7.15 (m, Ar-H, 4H), 6.94 – 6.82 (m, Ar-H, 4H), 4.09 (dd, Phenol-CH$_2$, J = 5.7, 4.1 Hz, 4H), 3.83 (dd, CH$_2$, J = 5.8, 4.0 Hz, 4H), 3.78 (s, CH$_2$-NH, 4H), 3.76 – 3.63 (m, CH$_2$, 8H).

Bis-amideiodotriazole macrocycle 75



1,3-diiodotriazolephenyl bis-acid chloride **70** was prepared from 1,3-bis-iodotriazolephenyl bis-acid **53** according to the standard procedure. Short bis-amine 5-oxygen polyether **74** (20.22 mg, 0.05 mmol), pyridinium chloride template **22.Cl** (17.42 mg, 0.05 mmol) and NEt_3 (0.18 ml, 0.125 mmol) were dissolved in DCM (20 ml) and cooled to 0 ^{0}C with an ice bath. 1,3-diiodotriazolephenyl bis-acid chloride **X** (30 mg, 0.05 mmol) was dissolved in DCM (15 ml) and added drop-wise to the cooled solution over a 30-minute period and gradually allowed to warm to room temperature. The reaction was allowed to stir for 24 hours under an atmosphere of N_2. The solution was then washed with 10% $HCl_{(aq.)}$ (20 ml), H_2O (20 ml), the organic layer was dried over $MgSO_4$, filtered and the solvent removed *in vacuo* to give a crude white solid which was subsequently purified by preparative TLC (3% MeOH in DCM) to yield pure bis-amideiodotriazole macrocycle **75** as a white solid (6.7 mg, 14% yield). **^{1}H NMR** (400 MHz, $CDCl_3$) δ (ppm): 7.81 (d, Phenyl Ar-H, ^4J = 1.9 Hz, 2H), 7.57 (t, CON-H, J = 6.5 Hz, 2H), 7.27 (m, Benzyl Ar-H, 4H), 7.18 (t, Phenyl Ar-H, ^4J = 1.9 Hz, 1H), 6.88 – 6.80 (m, Benzyl Ar-H, 4H), 4.57 (d, Benzyl-CH$_2$-NH, J = 6.5 Hz, 4H), 4.11 (t, CH$_2$, J = 5.1 Hz, 4H), 3.79 (t, CH$_2$, J = 5.1 Hz, 4H), 3.74 – 3.59 (m, CH$_2$, 8H), 1.47 (s, Phenyl-tBu, 9H). **^{13}C NMR** (126 MHz, $CDCl_3$) δ (ppm): 158.80, 158.14, 155.35, 143.50, 136.74, 131.00, 129.37, 125.39,

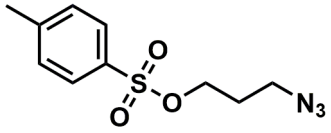
123.52, 114.87, 82.81, 70.72, 70.69, 69.50, 67.29, 42.50, 35.71, 31.08. **MS** (ESI +ve) m/z: 977.0 ($[M+H]^+$, $C_{38}H_{43}I_2N_8O_7^+$ requires 977.1). **HRMS** (ESI +ve) m/z: 977.1310 ($[M+H]^+$, $C_{38}H_{43}I_2N_8O_7^+$ requires 977.1338).

3-Azidopropan-1-ol 76[19]



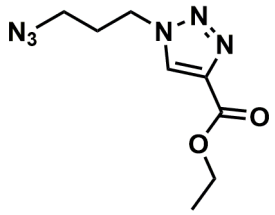
3-chloropropan-1-ol (5 ml, 46 mmol) and NaN_3 (6.11 g, 94 mmol) were dissolved in H_2O (70 ml) and heated to 80 ^{0}C under an atmosphere of N_2 for 16 hours. The reaction mixture was then extracted with DCM (3 x 40 ml) and the combined organic extracts were washed with brine (20 ml), dried over $MgSO_4$, filtered and dried *in vacuo* with no heating to give 3-azidopropan-1-ol **76** as a pale yellow oil (4.33 g, 93% yield). **^{1}H NMR** (400 MHz, $CDCl_3$) δ (ppm): 3.73 (q, C$\underline{H_2}$-OH, J = 5.3 Hz, 2H), 3.43 (t, C$\underline{H_2}$-N_3, J = 6.6 Hz, 2H), 1.82 (p, CH_2-C$\underline{H_2}$-CH_2, J = 6.3 Hz, 2H).

Azido-propyl tosylate 77[20]



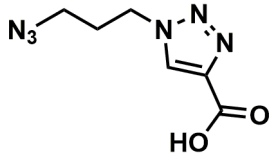
3-azidopropan-1-ol **76** (3 g, 29.67 mmol) and NEt_3 (8.351 ml, 59.34 mmol) were dissolved in DCM (275 ml) and cooled to 0 ^{0}C with an ice bath. TsCl (5.957 g, 31.3 mmol) was added portion-wise over a 10-minute period to the cooled solution. The reaction mixture was allowed to warm to room temperature and stirred for a further 18 hours under a N_2 atmosphere. The solution was washed with H_2O (3 x 50 ml), the organic layer was dried over $MgSO_4$, filtered and the solvent removed to obtain a crude semi-crystalline oily solid that was purified by silica gel chromatography (3:1 Hexane/EtOAc) to yield azido-propyl tosylate **77** as a yellow liquid (6.36 g, 84% yield). **^{1}H NMR** (400 MHz, $CDCl_3$) δ (ppm): 7.79 (d, Tosyl Ar-$\underline{H}$, J = 8.2 Hz, 2H), 7.36 (d, Tosyl Ar-$\underline{H}$, J = 8.0 Hz, 2H), 4.10 (t, C$\underline{H_2}$-OTs, J = 6.0 Hz, 2H), 3.37 (t, C$\underline{H_2}$-N_3, J = 6.5 Hz, 2H), 2.45 (s, Tosyl-C$\underline{H_3}$, 3H), 1.89 (p, CH_2-C$\underline{H_2}$-CH_2, J = 6.2 Hz, 2H). **MS** (ESI +ve) m/z: 278.0 ($[M+H]^+$, $C_{10}H_{13}N_3NaO_3S^+$ requires 278.1).

Azido-propyl triazole ethyl ester 78



Azido-propyl tosylate **77** (843 mg, 3.3 mmol) and ethyl propiolate (294 mg, 3 mmol) were dissolved in dry, degassed DCM (60 ml) to which $Cu(MeCN)_4PF_6$ (223 mg, 0.6 mmol), TBTA (cat.) and DIPEA (1.05 ml, 6 mmol) were sequentially added before the reaction mixture was placed under an N_2 atmosphere for 16 hours. The yellow solution was washed with $EDTA/NH_4OH_{(aq.)}$ (.1M EDTA in 1M NH_4OH, 2 x 20 ml), brine (1 x 20 ml) and the organic layer was dried over $MgSO_4$, filtered and the solvent removed *in vacuo*. The crude white solid was recrystallized in warm MeOH to give the intermediate tosyl-propyl triazole ester **78** as shiny white crystals that were immediately used for the next step. The pure tosylate (780 mg, 2.207 mmol) was redissolved in DMSO (10 ml) and NaN_3 (430 mg, 6.62 mmol) was added to the stirring mixture. The reaction was heated to 60 ^{0}C for 16 hours, cooled, poured onto brine (50 ml) and extracted with EtOAc (3 x 40 ml). The organic extracts were then washed with brine (2 x 20 ml), dried over $MgSO_4$, filtered and the solvent removed *in vacuo* to yield azido-propyl triazole ethyl ester **78** as a white solid (495 mg, 76% yield overall) **^{1}H NMR** (400 MHz, $CDCl_3$) δ (ppm): 8.10 (s, Triazole Ar-H, 1H), 4.51 (t, Triazole-CH_2, $J = 6.8$ Hz, 2H), 4.39 (q, COO-CH_2-CH_3, $J = 7.2$ Hz, 2H), 3.36 (t, CH_2-N_3, $J = 6.3$ Hz, 2H), 2.19 (p, CH_2-CH_2-CH_2, $J = 6.6$ Hz, 2H), 1.38 (t, COO-CH_2-CH_3, $J = 7.1$ Hz, 3H). **^{13}C NMR** (101 MHz, $CDCl_3$) δ (ppm): 160.62, 140.32, 127.77, 61.32, 47.85, 47.53, 29.34, 14.29. **MS** (ESI +ve) m/z: 225.1 ($[M+H]^+$, $C_8H_{13}N_6O_2^+$ requires 225.1). **HRMS** (ESI +ve) m/z: 225.1092 ($[M+H]^+$, $C_8H_{13}N_6O_2^+$ requires 225.1094).

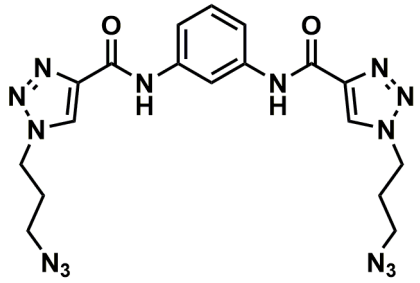
Azido-propyl triazole acid 79



Azido-propyl triazole ester **78** (448 mg, 2 mmol) was dissolved in MeOH (15 ml) to which KOH pellets (224 mg, 4 mmol) were added to the solution and the mixture was stirred for 16 hrs. The solvent was removed by rotary evaporation and redissolved in the minimum of H_2O (~ 3 ml), acidified to pH 1 by drop-wise addition

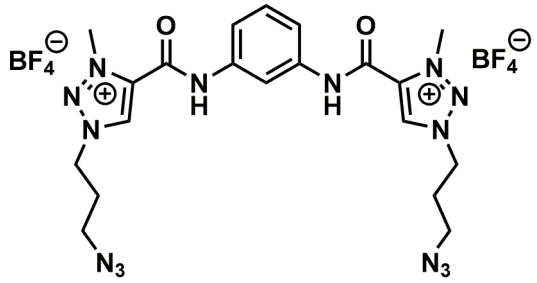
of aqueous 1M HCl and placed in the freezer at -32 ^{0}C. After 1 hour, large amounts of white crystals formed that were isolated by vacuum filtration and rinsed with H_2O (1 x 5 ml) and subsequently dried under a vacuum to give azido-propyl triazole acid **79** as a white powder (265 mg, 68%). **^{1}H NMR** (400 MHz, DMSO-d_6) δ (ppm): 13.06 (s, COO-H, 1H), 8.71 (s, Triazole Ar-H, 1H), 4.48 (t, Triazole-CH$_2$, J = 6.9 Hz, 2H), 3.38 (t, CH$_2$-N$_3$, J = 6.6 Hz, 2H), 2.10 (p, CH$_2$-CH$_2$-CH$_2$, J = 6.8 Hz, 2H). **^{13}C NMR** (101 MHz, DMSO-d_6) δ (ppm): 161.71, 139.71, 129.01, 47.79, 39.52, 28.7981. **MS** (ESI +ve) m/z: 219.1 ([M+Na]$^+$, $C_6H_8N_6NaO_2^+$ requires 219.1). **HRMS** (ESI +ve) m/z: 219.0600 ([M+Na]$^+$, $C_6H_8N_6NaO_2^+$ requires 219.0600).

1,3-Bis-amidetriazole bis-azide 80



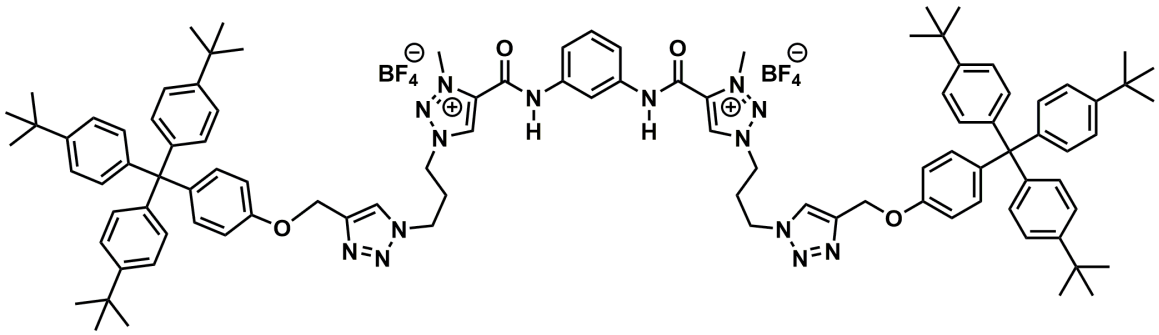
Azido-propyl triazole acid **79** (200 mg, 1.02 mmol) and EDC.HCl (195 mg, 1.02 mmol) were dissolved in dry DCM (6 ml) and stirred for 30 minutes at 0 ^{0}C until the solution was homogenous. *m*-phenylenediamine (52 mg, 0.485 mmol) was then added followed by DMAP (124 mg, 1.02 mmol) and NEt_3 (0.143 ml, 1.02 mmol) and the mixture placed under a N_2 atmosphere and stirred for 48 hours. The reaction mixture was then diluted with DCM (10 ml), washed with 1M $HCl_{(aq.)}$ (20 ml), 1M $NaOH_{(aq.)}$ (20 ml) and brine (10 ml). The organic layer was dried over $MgSO_4$, filtered and the solvent removed *in vacuo* to give a crude white solid which was purified *via* silica gel column chromatography (3% MeOH/DCM) to give bis-amidetriazole bis-azide **80** as a white solid (180 mg, 80% yield). **^{1}H NMR** (400 MHz, DMSO-d_6) δ (ppm): 10.41 (s, CON-H, 2H), 8.77 (s, Triazole Ar-H, 2H), 8.34 (s, Phenyl Ar-H, 1H), 7.52 (d, Phenyl Ar-H, J = 8.1 Hz, 2H), 7.29 (t, Phenyl Ar-H, J = 8.1 Hz, 1H), 4.53 (t, Triazole-CH$_2$, J = 6.9 Hz, 4H), 3.41 (t, CH$_2$-N$_3$, J = 6.6 Hz, 4H), 2.14 (p, CH$_2$-CH$_2$-CH$_2$, J = 6.8 Hz, 4H). **^{13}C NMR** (101 MHz, DMSO-d_6) δ (ppm): 158.32, 142.88, 138.58, 128.55, 127.37, 116.35, 113.16, 47.79, 47.28, 28.85. **MS** (ESI +ve) m/z: 465.2 ([M+H]$^+$, $C_{18}H_{21}N_{14}O_2^+$ requires 465.2). **HRMS** (ESI +ve) m/z: 465.1963 ([M+H]$^+$, $C_{18}H_{21}N_{14}O_2^+$ requires 465.1966).

Bis-amidetriazolium bis-azide 81.$(BF_4)_2$



1,3-bis-amidetriazole bis-azide **80** (80 mg, 0.172 mmol) was dissolved in DCM (10 ml) and trimethyloxonium tetrafluoroborate (77 mg, 0.517 mmol) was added in one portion. The mixture was placed under an atmosphere of N_2 and stirred until the starting material and any mono-methylated side-product was consumed by TLC (48 hours). The reaction mixture was quenched with MeOH (5 ml) and the solvent was removed *in vacuo* and purified *via* silica gel column chromatography (10% MeOH/DCM) to give bis-amidetriazolium bis-azide **81.$(BF_4)_2$** (102.8 mg, 73% yield). **^{1}H NMR** (400 MHz, CD_3CN) δ (ppm): 9.59 (s, CON-H, 2H), 8.90 (s, Triazolium Ar-H, 2H), 8.34 (s, Phenyl Ar-H, 1H), 7.58 – 7.49 (m, Phenyl Ar-H, 3H), 4.74 (t, Triazolium-CH_2, J = 6.9 Hz, 4H), 4.49 (s, Triaz-N$^+$Me, 6H), 3.53 (t, CH_2-N_3, J = 6.5 Hz, 4H), 2.32 – 2.22 (m, CH_2-CH_2-CH_2, 4H). **^{13}C NMR** (101 MHz, CD_3CN) δ (ppm): 153.33, 138.24, 136.10, 130.84, 130.51, 118.25, 113.21, 52.34, 47.98, 41.09, 28.71. **^{19}F NMR** (376 MHz, CD_3CN) δ (ppm): -151.26 (s, BF_4^-). **MS** (ESI +ve) m/z: 580.2 ($[M^{2+}+BF_4^-]^+$, $C_{20}H_{26}BF_4N_{14}O_2^+$ requires 580.2).

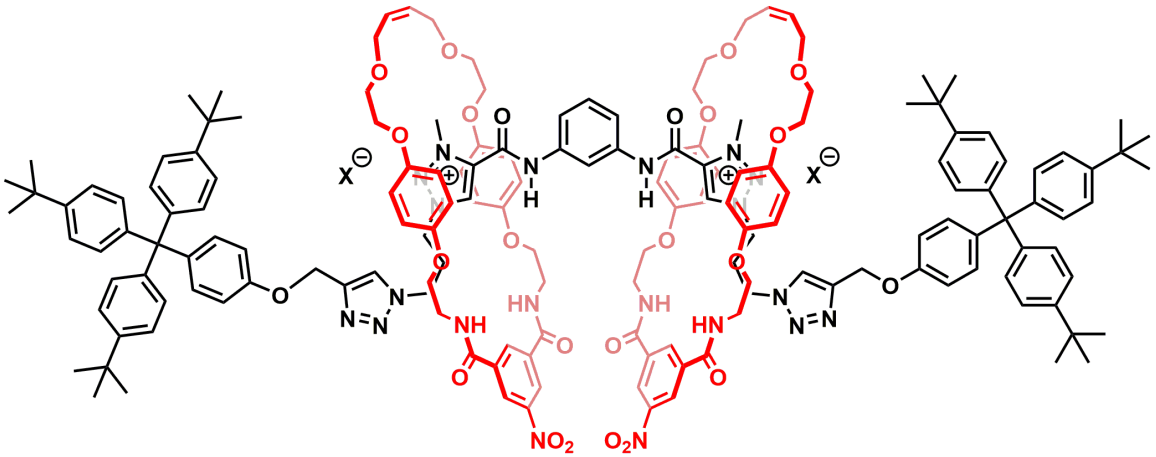
Bis-amidetriazolium axle 82$(BF_4)_2$



Bis-amidotriazolium azide **81.$(BF_4)_2$** (28 mg, 0.041 mmol) and stopper alkyne **25** (47.22 mg, 0.087 mmol) were dissolved in dry DCM/MeCN solvent mixture (1:1, 4 ml) and subjected to 3 freeze-thaw-pump degassing cycles. $Cu(MeCN)_4PF_6$ (6 mg, 0.016 mmol) and TBTA (21 mg, 0.016 mmol) was added to the solution and the reaction mixture was placed under an N_2 atmosphere, sealed and left to stir for 72

hours. The yellow solution was washed with EDTA/$NH_4OH_{(aq.)}$ (.1M EDTA in 1M NH_4OH, 2 x 10 ml), brine (1 x 10 ml), the organic layer was dried over $MgSO_4$ and the solvent removed *in vacuo*. The crude yellow-white solid was recrystallized in the minimum of warm MeOH to give the product bis-amidetriazolium axle **82.$(BF_4)_2$** as a white solid (57.4 mg, 79% yield). **^{1}H NMR** (400 MHz, 1:1 v/v $CDCl_3/CD_3CN$) δ (ppm): 9.40 (s, CON-H, 2H), 8.86 (s, Triazolium-Ar-H, 2H), 8.14 (s, Phenyl Ar-H, 1H), 7.90 (bs, Triazole-Ar-H, 2H), 7.48 (d, Phenyl Ar-H, J = 8.1 Hz, 2H), 7.35 (t, Phenyl Ar-H, J = 7.7 Hz, 1H), 7.23 – 7.13 (m, Stopper Ar-H, 12H), 7.13 – 6.99 (m, Stopper Ar-H, 16H), 6.86 – 6.70 (m, Stopper Ar-H, 4H), 5.02 (s, O-CH_2-triazole, 4H), 4.73 – 4.60 (m, Triazolium-CH_2, 4H), 4.53 – 4.42 (m, Triazole-CH_2, 4H), 4.39 (s, Triaz-N^+Me, 6H), 2.68 – 2.50 (m, CH_2-CH_2-CH_2, 4H), 1.21 (s, Stopper-tBu, 54H). **^{13}C NMR** (101 MHz, 1:1 v/v $CDCl_3/CD_3CN$) δ (ppm): 156.24, 152.46, 148.35, 144.36, 140.19, 137.49, 135.51, 131.97, 131.88, 130.41, 129.93, 129.48, 124.35, 117.86, 113.46, 63.06, 51.83, 46.54, 40.79, 34.16, 31.06, 29.20, 3 peaks missing; presumed overlapped. **^{19}F NMR** (376 MHz, 1:1 v/v $CDCl_3/CD_3CN$) δ (ppm): -151.10 (s, BF_4^-). **MS** (ESI +ve) m/z: 789.4 ($[M]^{2+}$, $C_{100}H_{118}N_{14}O_4^{2+}$ requires 789.5). **HRMS** (ESI +ve) m/z: 789.4722 ($[M]^{2+}$, $C_{100}H_{118}N_{14}O_4^{2+}$ requires 789.4724).

Bis-amidetriazolium [3]rotaxane 83$(BF_4)_2$



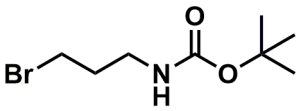
Axle **82$(BF_4)_2$** (28.7 mg, 0.0163 mmol), TBACl (9.1 mg, 0.0327 mmol) and bis-vinyl macrocycle precursor **37** (31.84 mg, 0.049 mmol) were dissolved in DCM (10.9 ml) and stirred at room temperature for 1 hour. To the homogenous solution, Grubbs' II catalyst (6.36 mg, 20 wt% with respect to bis-alkene **37**) was added and the reaction mixture was stirred for 48 hours. An additional portion of Grubbs' 2nd generation catalyst (3.18 mg, 10 wt% with respect to bis-alkene **37**) was added to consume any un-clipped macrocycle precursor **37** remaining and stirred for an

additional 24 hours. The solvent was removed *in vacuo* and the crude mixture was purified using 3 rounds of preparative TLC (1. Neat EtOAc, 2. 7% MeOH/DCM 3. 6% MeOH/DCM) to isolate [3]rotaxane **83(BF$_4$)$_2$** as a white solid (7 mg, 14% yield). **Cl$^-$ salt** (X = Cl): **^{1}H NMR** (400 MHz, 1:1 v/v $CDCl_3/CD_3OD$) δ (ppm): 9.46 (s, Triazolium Ar-H, 2H), 9.06 (s, Macrocycle Ar-H, 2H), 8.64 (s, Macrocycle Ar-H, 4H), 8.31 (s, Phenyl Ar-H, 1H), 7.82 (s, Triazole-Ar-H, 2H), 7.42 (d, Phenyl Ar-H, J = 8.1 Hz, 2H), 7.14 (d, Stopper Ar-H, J = 8.3 Hz, 12H), 7.10 – 7.01 (m, Phenyl Ar-H + Stopper Ar-H, 4H), 6.98 (d, Stopper Ar-H, J = 8.3 Hz, 12H), 6.78 (d, Stopper Ar-H, J = 8.6 Hz, 4H), 6.42 (d, Hydroquinone-Ar-H, J = 8.7 Hz, 8H), 6.32 (d, Hydroquinone-Ar-H, J = 8.7 Hz, 8H), 5.87 (s, Alkene C-H, 4H), 5.06 (s, Stopper-O-CH_2, 4H), 4.38 (s, Triaz-N$^+$-Me, 6H) 4.36 – 3.54 (m, Triazolium-CH_2 + Triazole-CH_2 + Macrocycle CH_2, 52H), 2.26 (m, CH_2-CH_2-CH_2, 4H), 1.19 (m, Stopper Ar-tBu, 54H). **^{13}C NMR** (126 MHz, 1:1 v/v $CDCl_3/CD_3CN$) δ (ppm): 164.19, 156.20, 152.70, 152.45, 151.98, 148.71, 148.33, 144.36, 143.95, 140.15, 137.01, 135.81, 133.86, 131.94, 130.38, 129.49, 128.76, 125.63, 124.35, 124.18, 119.08, 114.76, 114.23, 113.44, 70.55, 69.14, 67.74, 65.75, 63.04, 61.99, 61.41, 51.01, 46.25, 40.71, 39.63, 38.73, 34.1614, 33.8032, 33.4318, 31.8185. **MS** (ESI +ve) m/z: 1410.7 ($[M]^{2+}$, $C_{164}H_{188}N_{20}O_{24}^{2+}$ requires 1410.7). **HRMS** (ESI +ve) m/z: 1410.7051 ($[M]^{2+}$, $C_{164}H_{188}N_{20}O_{24}^{2+}$ requires 1410.7047).

PF$_6^-$ salt (X = PF_6): **^{1}H NMR** (400 MHz, 1:1 v/v $CDCl_3/CD_3OD$) δ (ppm): 9.60 (s, Triazolium Ar-H, 2H), 9.21 (s, Macrocycle Ar-H, 2H), 8.89 (s, Macrocycle CON-H, 2H), 8.69 (s, Macrocycle Ar-H, 4H), 8.37 (s, Phenyl Ar-H, 1H), 7.87 (s, Triazole Ar-H, 2H), 7.45 (d, Phenyl Ar-H, J = 9.1 Hz, 2H), 7.14 (d, Stopper Ar-H, J = 8.2 Hz, 12H), 7.00 (m, Stopper Ar-H + Phenyl Ar-H, 17H), 6.78 (d, Stopper Ar-H, J = 8.7 Hz, 4H), 6.44 (d, Hydroquinone-Ar-H, J = 8.6 Hz, 9H), 6.32 (d, Hydroquinone-Ar-H, J = 8.6 Hz, 8H), 5.87 (s, Alkene C-H, 4H), 5.08 (s, Stopper-O-CH_2, 4H), 4.37 (s, Triaz-N$^+$-Me, 6H), 4.35 – 3.53 (m, Triazolium-CH_2 + Triazole-CH_2 + Macrocycle CH_2, 52H), 2.39 – 2.16 (m, CH_2-CH_2-CH_2, 4H), 1.19 (m, Stopper Ar-tBu, 54H). **^{19}F NMR** (376 MHz, 1:1 v/v $CDCl_3/CD_3CN$) δ (ppm): -73.15 (d, PF_6^-, ^2J = 708.2 Hz).

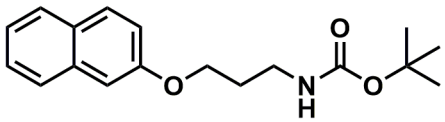
5.4. Synthesis of Compounds from Chapter 4

Bromopropylamine-Boc 84[22]



3-Bromopropylamine hydrobromide (1 g, 7.19 mmol) was suspended in dry DCM (40 ml) and di-*tert*-butyl dicarbonate (1.88 g, 8.63 mmol) was added to the stirring suspension. NEt_3 (3.3 ml, 28.78 mmol) was added drop-wise to the stirring suspension which became homogenous once the addition was complete. The reaction mixture was placed under an atmosphere of N_2 and stirred at room temperature for 16 hours. The reaction mixture was then washed with 1M $HCl_{(aq.)}$ (20 ml), 1M $NaOH_{(aq.)}$ (20 ml) and brine (10 ml). The organic layer was dried over $MgSO_4$, filtered and the solvent removed *in vacuo* to give a crude white solid which was purified *via* silica gel column chromatography (20% EtOAc/hexane) to give bromopropylamine-Boc **84** as a light yellow oil (1.17 g, 68%). **^{1}H NMR** (400 MHz, $CDCl_3$) δ (ppm): 4.65 (bs, Carbamate N-H, 1H), 3.44 (t, CH_2-Br, J = 6.5 Hz, 2H), 3.26 (m, J = 7.9 Hz, 2H), 2.05 (p, CH_2-CH_2-CH_2, J = 6.5 Hz, 2H), 1.44 (s, Boc-tBu, 9H).

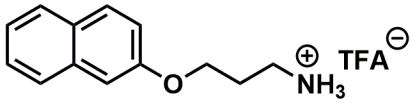
Boc-protected naphthyl amine 85



2-naphthol (1.4 mg, 9.69 mmol) and bromopropylamine-Boc (3 g, 12.6 mmol) in were dissolved in acetone (50 ml), to which Cs_2CO_3 (4.73 g, 14.8 mmol) and NaI (1.89 g, 12.6 mmol) were added. The reaction mixture was placed under an atmosphere of N_2 and heated at 60 °C overnight with stirring. The reaction mixture was diluted with DCM (50 ml), washed with brine (2 x 30 ml), dried over $MgSO_4$, filtered and dried *in vacuo* to give crude product which was purified by silica gel column chromatography (20% ethyl acetate in hexane) to yield the Boc-protected naphthyl amine **85** as a white solid (2.5 g, 86%). **^{1}H NMR** (400 MHz, CD_3OD) δ(ppm): 7.74 (m, Ar-H, 3H), 7.40 (m, Ar-H, 1H), 7.30 (m, Ar-H, 1H), 7.21 (d, Ar-H, J = 2.3 Hz, 1H), 7.12 (dd, Ar-H, J = 9 Hz, 2 Hz, 1H), 4.13 (t, Napthol-CH_2, J = 6.2 Hz, 2H), 3.28 (t, CH_2-NH, J = 6.9 Hz,), 2.00 (p, $CH_2CH_2CH_2$, J = 6.5 Hz, 2H), 1.43 (s, Boc-tBu, 9H). **^{13}C NMR** (125 MHz, $CDCl_3$) δ(ppm): 156.70, 156.02, 134.51, 129.40, 128.98, 127.62, 126.71, 126.37, 123.63, 118.82, 106.62, 79.24, 65.77,

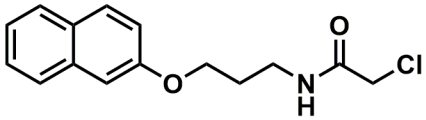
38.06, 29.52, 28.40. **MS** (ESI +ve) m/z: 324.2 ([M+Na]$^+$, $C_{18}H_{23}NO_3^+$ requires 324.2). **HRMS** (ESI +ve) m/z: 324.1578 ([M]$^{2+}$, $C_{18}H_{23}NO_3^+$ requires 324.1570).

Napthyl amine salt 86



Boc-protected napthyl amine **85** (316 mg, 1.05 mmol) was dissolved in dry DCM (20 ml), cooled to 0 ^{0}C and placed under an atmosphere of N_2. TFA (0.80 ml, 10.5 mmol) was added drop-wise to the stirring solution, the reaction mixture was allowed to gradually warm to room temperature and left to stir for 48 hours. The solvent was removed *in vacuo* and redissolved in MeOH (5 ml) and dried again three times to remove any residual TFA to give deprotected napthyl amine (trifluoroacetate salt) **86** as a brown solid (293 mg, 89% yield). **^{1}H NMR** (400 MHz, CD_3OD) δ(ppm): 7.77 (m, Ar-H, 3H), 7.43 (m, Ar-H, 1H), 7.33 (m, Ar-H, 1H), 7.26 (d, J = 2.6 Hz, Ar-H, 1H), 7.16 (dd, J = 9 Hz, 2.6 Hz, Ar-H, 1H), 4.25 (t, J = 5.7 Hz, Napthol-CH$_2$, 2H), 3.21 (t, J = 7.3 Hz, CH$_2$-NH$_3^+$, 2H), 2.21 (p, CH$_2$-CH$_2$-CH$_2$, J = 6.5 Hz, 2H). **^{13}C NMR** (125 MHz, CD_3OD) δ (ppm): 156.40, 134.67, 129.26, 129.06, 127.20, 126.45, 126.03, 123.43, 118.19, 106.43, 64.79, 37.28, 26.97. **MS** (ESI +ve) m/z: 202.1 ([M+H]$^+$, $C_{13}H_{16}NO^+$ requires 202.1). **HRMS** (ESI +ve) m/z: 202.1226 ([M+H]$^+$, $C_{13}H_{16}NO^+$ requires 202.1226).

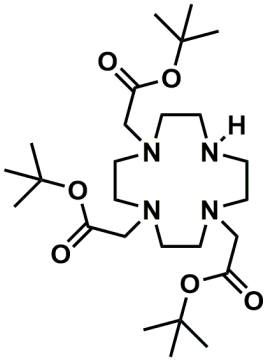
Naphthyl *N*-acetylchloride linker 87



Naphthyl amine **86** (292 mg, 0.93 mmol) was dissolved in DCM (10 ml) and placed under an atmosphere of N_2. NEt_3 (0.6 ml, 4.65 mmol) was added and the reaction mixture was cooled to 0 °C with an ice bath, at which point chloroacetyl chloride (0.22 ml, 2.78 mmol) was added drop-wise to the solution. The reaction mixture was allowed to warm to room temperature and left stirring for 48 hours. The reaction mixture was then washed with H_2O (20 ml), 1M $HCl_{(aq.)}$ (2 x 20 ml) and brine (2 x 20 ml). The solvent was removed *in vacuo* and the crude product was purified by silica gel column chromatography (gradient, 20 » 80% EtOAc/hexane) to give the product naphthyl *N*-acetylchloride **87** as an off-white solid (222 mg, 86%). **^{1}H NMR** (400 MHz, $CDCl_3$) δ (ppm): 7.76 (m, Ar-H, 3H), 7.46 (m, Ar-H, J = 7 Hz, 1H), 7.36

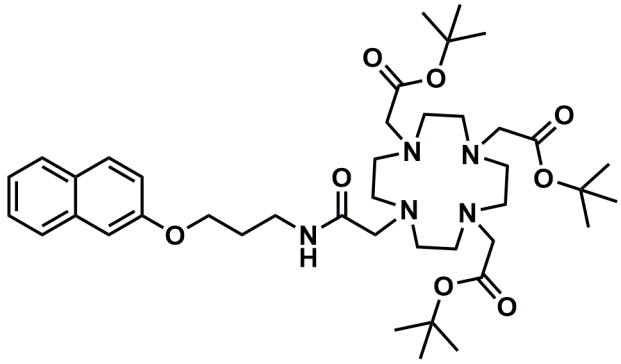
(m, Ar-H, 1H), 7.17 (m, Ar-H, 2H), 4.22 (t, Napthol-CH_2, J = 5.7 Hz, 2H), 4.09 (s, NHCO-CH_2-Cl, 2H), 3.61 (t, CH_2-NH, J = 7.3 Hz, 2H), 2.14 (p, CH_2-CH_2-CH_2, J = 6 Hz, 2H). **^{13}C NMR** (125 MHz, $CDCl_3$) δ (ppm): 165.94, 156.43, 134.46, 129.55, 129.12, 127.66, 126.76, 126.47, 123.81, 118.64, 106.64, 66.68, 42.71, 38.32, 28.60. **MS** (ESI +ve) m/z: 278.1 ($[M+H]^+$, $C_{15}H_{17}ClNO_2^+$ requires 278.1). **HRMS** (ESI +ve) m/z: 300.0759 ($[M+Na]^+$, $C_{15}H_{16}ClNaNO_2^+$ requires 300.0762).

DO3A tri-*tert*-butyl ester 88[23]



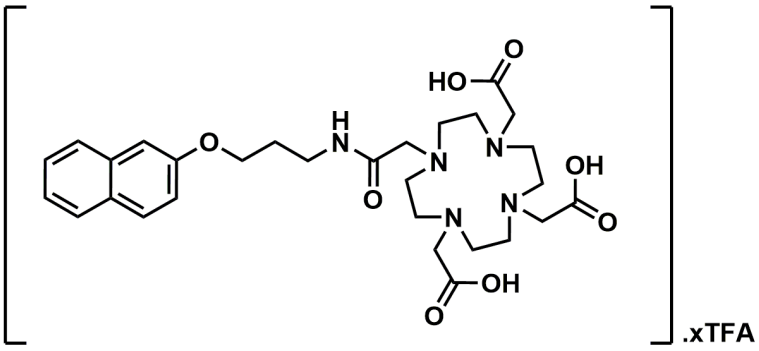
Cyclen (1.78 g, 10 mmol) and $NaHCO_3$ (2.78 g, 31 mmol) were suspended in dry MeCN (50 ml) and stirred under a N_2 atmosphere and cooled to 0 ^{0}C with an ice bath. *Tert*-butyl bromoacetate (4.89 ml, 31 mmol) was dissolved in dry MeCN (10 ml) and added drop-wise over a 30-minute period and left to stir for 48 hours at room temperature. The reaction mixture was diluted with DCM (50 ml), filtered and dried *in vacuo* to give a crude beige solid that was redissolved in the minimum of refluxing toluene (~10 ml) and left to stand in a freezer at -27 ^{0}C for several hours, at which point the product precipitated. The precipitate was isolated *via* vacuum filtration and rinsed with cold Et_2O (10 ml) and dried under high-vacuum to give pure DO3A tri-*tert*-butyl ester **88** as a fluffy white solid (1.98 g, 39% yield). **^{1}H NMR** (400 MHz, $CDCl_3$) δ (ppm): 10.06 (bs, N-H, 1H), 3.54 – 2.75 (m, Cyclen arm CH_2 + Cyclen ring CH_2, 22H), 1.46 (s, COO-tBu, 27H). **MS** (ESI +ve) m/z: 515.4 ($[M+H]^+$, $C_{26}H_{51}N_4O_6^+$ requires 515.4).

Naphthyl DO3A tri-tBu ester 89



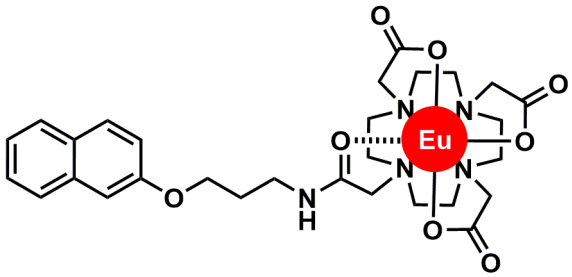
Naphthyl N-acetylchloride linker **87** (1.03 g, 3.74 mmol) and KI (1.128 g, 6.8 mmol) were dissolved in acetone (50 ml) and halogen exchange was conducted under an atmosphere of N_2 at room temperature for 16 hours. K_2CO_3 (1.41 g, 10.2 mmol) and DO3A tri-*tert*-butyl ester **88** were added and the reaction mixture stirred under an atmosphere of N_2 at room temperature for a further 72 hours until mass spectrometry showed no starting material **88** remaining. The solvent was removed *in vacuo* and the crude product purified by column chromatography (silica, 5% MeOH/$CHCl_3$) to yield the product naphthyl DO3A tri-tBu ester **89** as a viscous yellow oil (2.28 g, 81% yield). **^{1}H NMR** (400 MHz, $CDCl_3$) δ (ppm): 7.87 (t, J = 5.6 Hz, CON-H), 7.72 (dd, J = 8.1 Hz, 3.7 Hz, Ar-H, 2H), 7.68 (d, J = 8.9 Hz, Ar-H, 1H), 7.39 (m, Ar-H, 1H), 7.30 (d, Ar-H, J = 7.7 Hz, 1H), 7.18 (d, Ar-H, J = 2.1 Hz, 1H), 7.10 (dd, Ar-H, J = 8.9 Hz, 2.4 Hz, 1H), 4.15 (t, Napthol-CH_2, J = 5.9 Hz, 2H), 3.44 (m, CH_2-NH, 2H), 3.37 (s, NHCO-CH_2- cyclen), 2.14 (p, CH_2-CH_2-CH_2, J = 6.3 Hz, 2H), 3.30 – 1.72 (m, Cyclen arm CH_2 + Cyclen ring CH_2, 22H), 1.45 – 1.40 (m, COO-tBu, 27H). **^{13}C NMR** (125 MHz, $CDCl_3$) δ (ppm): 172.34, 172.08, 171.69, 156.85, 134.55, 129.03, 128.74, 127.38, 126.80, 126.10, 123.31, 118.90, 106.76, 81.73, 66.18, 56.31, 55.62, 55.46, 53.5- 47.5 (broad region due cyclen ring inversion, 4 resonances expected), 36.35, 28.93, 27.91, 27.84. **MS** (ESI +ve) m/z: 756.4 ($[M+H]^+$, $C_{41}H_{66}N_5O_8^+$ requires 756.5); also found: 700.4 $[M-tBu+H]^+$, 644.3 $[M-2tBu+H]^+$, 588.3 $[M-3tBu+H]^+$ fragments. **HRMS** (ESI +ve) m/z: 756.4890 ($[M+H]^+$, $C_{41}H_{66}N_5O_8^+$ requires 756.4906).

Naphthyl DO3A tri-acid 90



Naphthyl DO3A tri-tBu ester **89** (48 mg, 0.06 mmol) was dissolved in a 1:1 DCM/TFA solvent mixture (4 ml) at 0 ^{0}C that was allowed to gradually warm to room temperature whilst stirring. Once the reaction was judged to be complete by TLC (36 hours), the solvent was removed *in vacuo* and repeatedly re-dissolved in MeOH and evapourated to dryness to remove any excess TFA (3 times). The pure product naphthyl DO3A tri-acid **90** was isolated without further purification as a viscous yellow oil (41 mg, 96%). **^{1}H NMR** (400 MHz, CD_3OD) δ (ppm): 7.89 (bs, CON-H, 1H), 7.76 (m, Ar-H, 3H), 7.42 (m, Ar-H, J = 7.6 Hz, 1H), 7.31 (m, ArH, 1H), 7.24 (d, Ar-H, ^{3}J = 2.2 Hz, 1H), 7.14 (m, Ar-H, 1H), 4.18 (t, Napthol-CH_2, J = 5.9 Hz, 2H), 3.46 (t, CH_2-NH, J = 6.4 Hz, 2H), 4.22 – 2.51 (m, Cyclen arm CH_2 + Cyclen ring CH_2, 24H), 2.07 (p, CH_2-CH_2-CH_2, J = 6.3 Hz, 2H). **^{13}C NMR** (125 MHz, CD_3OD) δ (ppm): 175.17, 174.68, 162.83 (q, ^{1}J = 35 Hz, $^{-}$OOC-CF_3), 158.38, 136.27, 130.61, 130.56, 128.74, 127.98, 127.56, 124.81, 120.04, 118.21 (q, ^{2}J = 290 Hz, $^{-}$OOC-CF_3), 107.97, 66.83, 57-50 (broad region, 7 resonances expected), 38.03, 30.11. **MS** (ESI +ve) m/z: 588.3 ($[M+H]^+$, $C_{29}H_{42}N_5O_8^+$ requires 588.3). **HRMS** (ESI +ve) m/z: 588.3022 ($[M+H]^+$, $C_{29}H_{42}N_5O_8^+$ requires 588.3030).

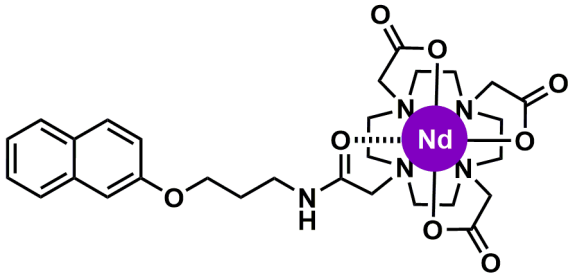
Naphthyl DO3A Eu(III) complex 91.Eu



Naphthyl DO3A tri-acid **90** (18.1 mg, 0.031 mmol) was dissolved in MeOH (4 ml), and the pH of the solution adjusted by drop-wise addition of 1M $NaOH_{(aq.)}$ to 5.5-7.5. $Eu(OTf)_3$ (57.52 mg, 0.096 mmol) was added and the reaction mixture stirred

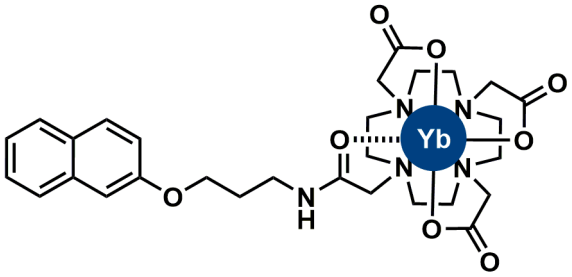
under an atmosphere of N_2 at 50 ^{0}C for 48 hours. The crude product was triturated from MeOH using Et_2O to yield the product naphthyl DO3A complex **91.Eu** as an off-white solid (15.0 mg, 79%). **^{1}H NMR** (400 MHz, D_2O) δ (ppm): 33.01, 32.23, 30.99, 12.13, 11.67, 8.04, 7.61, 7.52, 7.12, 6.40, 3.30, 2.94, 2.08, 0.84, 0.57, 0.32, -0.63, -0.99, -2.02, -2.32, -3.39, -3.57, -4.45, -5.72, -5.94, -7.95, -8.23, -9.43, -10.46, -11.03, - 11.58, -12.28, -12.83, -14.86, -15.20, -15.58, -16.84. **MS** (ESI +ve) m/z: 736.2 ($[M+H]^+$, $C_{29}H_{39}EuN_5O_8^+$ requires 736.2). **HRMS** (ESI +ve) m/z: 736.1986 ($[M+H]^+$, $C_{29}H_{39}EuN_5O_8^+$ requires 736.1992).

Naphthyl DO3A Nd(III) complex 92.Nd



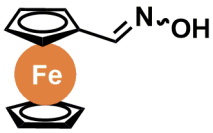
Naphthyl DO3A tri-acid **90** (72 mg, 0.122 mmol) was dissolved in MeOH (10 ml), and the pH of the solution adjusted by drop-wise addition of 1M $NaOH_{(aq.)}$ to 5.5-7.5. $Nd(OTf)_3$ (76.24 mg, 0.129 mmol) was added and the reaction mixture stirred under an atmosphere of N_2 at 50 ^{0}C for 48 hours. The crude product was triturated from MeOH using Et_2O to yield the product naphthyl DO3A complex **92.Nd** as a white solid (34 mg, xx% yield). **^{1}H NMR** (400 MHz, DMSO-d_6) δ (ppm): 24.45, 22.45, 22.02, 20.67, 20.13, 15.54, 13.47, 13.43, 12.66, 12.31, 11.69, 9.99, 9.52, 7.92, 7.73, 7.47, 7.29, 7.00, 6.66, 6.31, 5.67, 5.19, 4.53, 3.34, 2.50, 1.82, 1.31, 1.08, 0.54, 0.06, -0.08, -0.68, -0.92, -1.65, -2.68, -4.08, -4.64, -7.91, -9.83, -10.83, -11.87, -12.99, -24.13, -25.03, -28.07. **MS** (ESI +ve) m/z: 727.1 ($[M+H]^+$, $C_{29}H_{39}NdN_5O_8^+$ requires 727.2). **HRMS** (ESI +ve) m/z: 727.1865 ($[M+H]^+$, $C_{29}H_{39}NdN_5O_8^+$ requires 727.1870).

Naphthyl DO3A Yb(III) complex 93.Yb



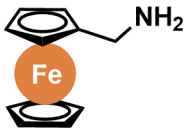
Naphthyl DO3A tri-acid **90** (72 mg, 0.122 mmol) was dissolved in MeOH (10 ml), and the pH of the solution adjusted by drop-wise addition of 1M $NaOH_{(aq.)}$ to 5.5-7.5. $Yb(OTf)_3$ (80 mg, 0.129 mmol) was added and the reaction mixture stirred under an atmosphere of N_2 at 50 ^{0}C for 48 hours. The crude product was triturated from MeOH using Et_2O to yield the product naphthyl Yb(III) DO3A complex as an off-white solid (53.8 mg, xx% yield). **^{1}H NMR** (400 MHz, D_2O) δ (ppm): 131.85, 127.09, 122.83, 121.34, 83.70, 71.07, 32.07, 26.19, 24.82, 20.48, 19.41, 18.65, 17.10, 16.46, 15.77, 15.46, 8.18, 7.94, 7.55, 7.15, 6.84, 4.83, 3.34, 2.44, 2.09, 1.64, 0.70, 0.56, -1.23, -1.35, -12.16, -22.50, -26.11, -27.97, -30.95, -41.60, -44.47, -56.22, -57.97, -76.72, -77.89, -79.11, -79.55. **MS** (ESI +ve) m/z: 755.1 ($[M+H]^+$, $C_{29}H_{39}YbN_5O_8^+$ requires 755.2). **HRMS** (ESI +ve) m/z: 755.2137 ($[M+H]^+$, $C_{29}H_{39}YbN_5O_8^+$ requires 755.2140).

Ferrocene oxime 94[21]



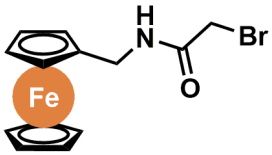
An aqueous solution of $NH_2OH.HCl$ (930 mg, 13.4 mmol) in H_2O (5 ml) was added to a solution of ferrocene carboxaldehyde (2 g, 9.3 mmol) dissolved in EtOH (20 ml). NaOH pellets (900 mg, 22.6 mmol) were added slowly to the reaction mixture with stirring. The mixture was heated to 70 ^{0}C for 4 hours under an atmosphere of N_2, cooled to room temperature and concentrated *in vacuo* (CAUTION – Dry $NH_2OH.HCl$ is potentially shock sensitive). H_2O (30 ml) was added and the organic product extracted with Et_2O (3 x 40 mL). The combined organic layers were dried over $MgSO_4$, filtered and the solvent removed *in vacuo* to yield the product as a deep orange solid (1.84 g, 87%). **^{1}H NMR** (400 MHz, CD_3OD) δ (ppm): 7.92 (s, C<u>H</u>=NOH, 1H), 7.16 (s, CH=NO<u>H</u>, 1H), 4.53 – 4.35 (m, Ferrocene Ar-<u>H</u>, 4H), 4.20 (s, Ferrocene Ar-<u>H</u>, 5H). **MS** (ESI +ve) m/z: 230.1 ($[M+H]^+$, $C_{11}H_{12}FeNO^+$ requires 230.0).

Ferrocene amine 95[21]



$LiAlH_4$ (1.4 g, 37 mmol) was suspended in dry THF (30 ml) and ferrocene carboxaldehyde oxime **94** (1.84 g, 8 mmol) was dissolved in THF (30 ml) and added slowly *via* a dropping funnel to the stirring suspension under a N_2 atmosphere. Once the addition was complete, the mixture was heated to 60 ^{0}C for 16 hours. The reaction mixture was cooled to 0 ^{0}C with an ice bath and H_2O added cautiously to quench the $LiAlH_4$, at which point a large amount of light grey precipitate formed. The solids were filtered and washed with H_2O (50 ml) and DCM (100 ml) and all collected filtrates were combined in a separating funnel and the organic layer separated, dried over $MgSO_4$, filtered and the solvent removed *in vacuo*. The obtained crude product was purified by column chromatography (10% $NH_4OH_{(aq.)}$ (1M)/MeOH) to give ferrocene amine product **95** as an unstable yellow oil (1.21 g, 70% yield). **^{1}H NMR** (400 MHz, CD_3OD) δ (ppm): 4.22 (m, Ferrocene Ar-H, 2H), 4.15 (s, Ferrocene Ar-H, 5H), 4.13 (m, Ferrocene Ar-H, 2H), 3.54 (s, CH_2-NH_2, 2H). **MS** (ESI +ve) m/z: 238.0 ($[M+Na]^+$, $C_{11}H_{13}FeNNa^+$ requires 238.0).

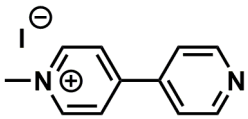
Ferrocene *N*-acetylbromide 96-Br



Ferrocene amine **95** (50 mg, 0.23 mmol) and NEt_3 (0.01 ml, 0.69 mmol) were dissolved in dry DCM (10 ml) and cooled to 0 ^{0}C using an ice bath. Bromoacetyl chloride (0.06 ml, 0.68 mmol) was added drop-wise and the reaction mixture was placed under a N_2 atmosphere, allowed to warm to room temperature and stirred for 16 hours. The reaction mixture was then washed with 1M $HCl_{(aq.)}$ (20 ml), 1M $NaOH_{(aq.)}$ (20 ml) and brine (10 ml). The organic layer was dried over $MgSO_4$, filtered and the solvent removed *in vacuo* to give a crude yellow/brown oil that was purified *via* silica gel column chromatography (gradient, 50 » 100% EtOAc/hexane) to give the mixed ferrocene *N*-acetylbromide **96-Br** (trace amount of *N*-acetylchloride byproduct present) as a yellow solid (31 mg, 41% yield). **^{1}H NMR** (400 MHz, CD_3OD) δ (ppm): 4.23 (bs, Ferrocene Ar-H, 2H), 4.19 (s, Ferrocene Ar-H, 5H), 4.14 (s, Ferrocene Ar-H, 2H), 4.12 (bs, CH_2COCH_2Br/Cl, 2H), 4.04 - 3.83

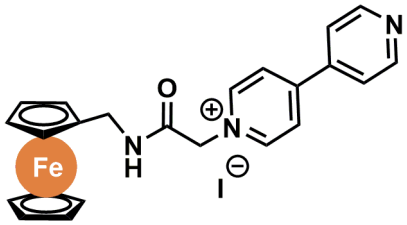
(2 x s, CH_2COCH_2Br/Cl, 2H). **^{13}C NMR** (125 MHz, CD_3OD) δ (ppm): 167.28, 167.11, 68.43, 68.08, 68.00, 67.87, 41.87, 38.87, 38.66, 27.55. **MS** (ESI +ve) m/z: 358.1 ($[M+Na]^+$, $C_{11}H_{14}BrFeNNaO^+$ requires 358.0). **HRMS** (ESI): m/z: 357.9508 ($[M+Na]^+$, $C_{11}H_{14}BrFeNNaO^+$ requires 357.9502).

Monomethylated 4,4'bipyridine iodide 97.I[24]



4,4'-bipyridine (2 g, 12.8 mmol) was dissolved in DCM/MeI (1:1 v/v, 10 ml) was refluxed for 1 hour whereupon a yellow precipitate formed. The precipitate was isolated *via* vacuum filtration and washed with EtOAc (2 x 10 ml) to remove unreacted starting material, followed by Et_2O (2 x 10 ml). The solid was dried *in vacuo* to give monomethylated 4,4'bipyridine iodide **97.I** as a golden yellow powder (3.5 g, 92% yield). **^{1}H NMR** (400 MHz, CD_3OD) δ (ppm): 9.04 (d, Pyr^+ Ar-H, J = 6.6 Hz, 2H), 8.83 (m, Pyr^+ Ar-H, 2H), 8.51 (d, Pyr Ar-H, J = 6.6 Hz, 2H) 7.99 (m, Pyr Ar-H, 2H), 4.47 (s, $PyrN^+$-Me, 3H). **MS** (ESI +ve) m/z: 171.1 ($[M-I]^+$, $C_{11}H_{11}N_2^+$ requires 171.1).

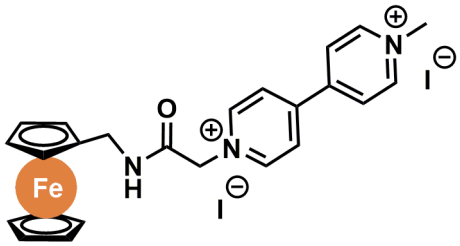
Monoalkylated ferrocene-bipyridinium iodide 98.I



Ferrocene *N*-acetylbromide **96-Br** (200 mg, 0.58 mmol) and KI (480 mg, 2.89 mmol) were placed in a microwave vial and dissolved in MeCN (10 ml). The mixture was heated to 120 ^{0}C for 20 minutes in the microwave with stirring to facilitate halogen exchange to ferrocene *N*-acetyliodide, confirmed by TLC and mass spectrometric analysis. 4,4'-bipyridine (181 mg, 1.16 mmol) was added and the reaction mixture heated to 50 ^{0}C in the microwave for 1 hour with stirring. The reaction vessel was cooled in an ice bath mix to encourage precipitation of the product, and the crude product filtered and washed with Et_2O (2 x 20 ml). The solvent was reduced *in vacuo* and the filtrate subjected to further reaction cycles until all starting material had been consumed. The monoalkylated ferrocene bipyridinium iodide **98.I** was obtained as a red-brown solid (128 mg, 41% yield). **^{1}H NMR** (400 MHz, CD_3OD)

δ (ppm): 9.02 (d, Pyr$^+$ Ar-H, J = 6.5 Hz, 2H), 8.85 (d, Pyr$^+$ Ar-H, J = 5.3 Hz, 2H), 8.55 (d, Pyr Ar-H, J = 6.4 Hz, 2H) 8.01 (d, Pyr Ar-H, J = 5.3 Hz, 2H), 5.47 (s, Pyr-N$^+$-CH$_2$CONH, 2H), 4.25 – 4.15 (m, Ferrocene Ar-H, 11H). **^{13}C NMR** (125 MHz, D_2O) δ (ppm): 163.99, 154.53, 150.27, 146.38, 142.25, 125.50, 122.38, 70.2-66.8 (broad, 4 resonances expected), 61.32, 39.14. **MS** (ESI +ve) m/z: 412.1 ([M-I]$^+$, $C_{23}H_{22}FeN_3O^+$ requires 412.1). **HRMS** (ESI +ve) m/z: 412.1104 ([M-I]$^+$, $C_{23}H_{22}FeN_3O^+$ requires 412.1107).

Ferrocene viologen component 99.(I)$_2$



Monoalkylated ferrocene-bipyridinium iodide **98.I** (127 mg, 0.08 mmol) was placed in a microwave vial, to which MeI (2 ml, excess) was added. The reaction mixture was heated in a microwave to 100 ^{0}C for 10 minutes with stirring. Upon cooling, diethyl ether (5 ml) was added to encourage precipitation of product. The precipitate was removed by filtration; the filtrate was dried *in vacuo*, then subjected to further reaction cycles until no starting material was visible by TLC or mass spectrometry. The combined batches were washed firstly with DCM (10 ml), Et_2O (20 ml), MeCN (20 ml) and MeOH (30 ml) to remove any impurities. The product ferrocene viologen component **99.(I)$_2$** was isolated as an orange-brown solid (70 mg, 44%). **^{1}H NMR** (400 MHz, DMSO-*d*$_6$) δ (ppm): 9.28 (m, Pyr$^+$ Ar-H, 4H), 8.84 (bs, CON-H, 1H), 8.80 (d, Pyr$^+$ Ar-H, J = 5.9 Hz, 2H), 8.77 (d, Pyr$^+$ Ar-H, J = 4.9 Hz, 2H), 5.54 (s, Pyr-N$^+$-CH$_2$CONH, 2H), 4.45 (s, PyrN$^+$-Me, 3H), 4.24 – 4.14 (m, Ferrocene Ar-H, 11H). **^{13}C NMR** (125 MHz, DMSO-*d*$_6$) δ (ppm): 163.51, 149.11, 148.18, 147.22, 146.80, 126.21, 125.95, 84.67, 68.46, 68.11, 67.59, 61.45, 48.06, 38.50. **MS** (ESI +ve) m/z: 213.6 ([M-2I]$^{2+}$, $C_{24}H_{25}FeN_3O^{2+}$ requires 213.6). **HRMS** (ESI +ve) m/z: 213.5667 ([M-2I]$^{2+}$, $C_{24}H_{25}FeN_3O^{2+}$ requires 213.5668).

5.5. References for Chapter 5

(1) Hynes, M. J. *J. Chem. Soc. Dalton Trans.* **1993**, No. 2, 311–312.

(2) Hancock, L. M.; Beer, P. D. *Chem. Commun.* **2011**, *47* (21), 6012–6014.

(3) Joung, I. S.; Cheatham, Thomas E. *J. Phys. Chem. B* **2008**, *112* (30), 9020–9041.

(4) Gibson, H. W.; Lee, S. H.; Engen, P. T.; Lecavalier, P.; Sze, J.; Shen, Y. X.; Bheda, M. *J. Org. Chem.* **1993**, *58* (14), 3748–3756.

(5) Serpell, C. J.; Chall, R.; Thompson, A. L.; Beer, P. D. *Dalton Trans.* **2011**, *40* (45), 12052–12055.

(6) Wang, Y.-M.; Zhou, C.-Q.; Chen, J.-X.; Lin, Y.-L.; Zeng, W.; Kuang, B.-C.; Fu, W.-L.; Chen, W.-H. *MedChemComm* **2013**, *4* (10), 1400–1404.

(7) Ng, K.-Y.; Felix, V.; Santos, S. M.; Rees, N. H.; Beer, P. D. *Chem. Commun.* **2008**, No. 11, 1281–1283.

(8) Wisner, J. A.; Beer, P. D.; Drew, M. G. B. *Angew. Chem. Int. Ed.* **2001**, *40* (19), 3606–3609.

(9) Collin, J.-P.; Frey, J.; Heitz, V.; Sauvage, J.-P.; Tock, C.; Allouche, L. *J. Am. Chem. Soc.* **2009**, *131* (15), 5609–5620.

(10) Kilah, N. L.; Wise, M. D.; Serpell, C. J.; Thompson, A. L.; White, N. G.; Christensen, K. E.; Beer, P. D. *J. Am. Chem. Soc.* **2010**, *132* (34), 11893–11895.

(11) Zheng, H.; Zhou, W.; Lv, J.; Yin, X.; Li, Y.; Liu, H.; Li, Y. *Chem. – Eur. J.* **2009**, *15* (47), 13253–13262.

(12) Doak, B. C.; Scanlon, M. J.; Simpson, J. S. *Org. Lett.* **2011**, *13* (3), 537–539.

(13) Gallardo, H.; Bortoluzzi, A. J.; Santos, D. M. P. D. O. *Liq. Cryst.* **2008**, *35* (6), 719–725.

(14) Li, Y.; Flood, A. H. *Angew. Chem. Int. Ed.* **2008**, *47* (14), 2649–2652.

(15) Miura, Y.; Ushitani, Y.; Inui, K.; Teki, Y.; Takui, T.; Itoh, K. *Macromolecules* **1993**, *26* (14), 3698–3701.

(16) Robinson, S. W.; Mustoe, C. L.; White, N. G.; Brown, A.; Thompson, A. L.; Kennepohl, P.; Beer, P. D. *J. Am. Chem. Soc.* **2015**, *137* (1), 499–507.

(17) Ozkal, E.; Llanes, P.; Bravo, F.; Ferrali, A.; Pericàs, M. A. *Adv. Synth. Catal.* **2014**, *356* (4), 857–869.

(18) Barrell, M. J.; Leigh, D. A.; Lusby, P. J.; Slawin, A. M. Z. *Angew. Chem. Int. Ed.* **2008**, *47* (42), 8036–8039.

(19) Fall, A.; Seck, I.; Diouf, O.; Gaye, M.; Seck, M.; Gómez, G.; Fall, Y. *Tetrahedron Lett.* **2015**, *56* (36), 5128–5131.

(20) Steinhilber, D.; Rossow, T.; Wedepohl, S.; Paulus, F.; Seiffert, S.; Haag, R. *Angew. Chem. Int. Ed.* **2013**, *52* (51), 13538–13543.

(21) Gnoatto, S. C. B.; Dassonville-Klimpt, A.; Da Nascimento, S.; Galéra, P.; Boumediene, K.; Gosmann, G.; Sonnet, P.; Moslemi, S. *Eur. J. Med. Chem.* **2008**, *43* (9), 1865–1877.

(22) Ryabchun, A.; Bobrovsky, A.; Chun, S.-H.; Shibaev, V. *J. Polym. Sci. Part Polym. Chem.* **2013**, *51* (19), 4031–4041.

(23) Dadabhoy, A.; Faulkner, S.; Sammes, P. G. *J. Chem. Soc. Perkin Trans. 2* **2002**, No. 2, 348–357.

(24) Grenier, M. C.; Davis, R. W.; Wilson-Henjum, K. L.; LaDow, J. E.; Black, J. W.; Caran, K. L.; Seifert, K.; Minbiole, K. P. C. *Bioorg. Med. Chem. Lett.* **2012**, *22* (12), 4055–4058.

CHAPTER 6

Conclusions

Conclusions

The objective of thesis was to demonstrate that, *via* meticulous receptor design and consideration of supramolecular effects described in Chapter 1, a wide variety of favourable anion recognition properties can be obtained. Additionally, the unprecedented supramolecular modulation of lanthanide luminescence was exhibited, opening an avenue of research towards applying this unique approach in future work towards luminescent devices that exploit supramolecular interactions.

Chapter 2 described the synthesis of a series of chelating pyridinium-triazole acyclic and interlocked anion hosts. *Via* exploitation of this unique mode of anion recognition, the hydrogen bonding monocationic pyridinium-triazole and halogen bonding pyridinium-iodotriazole axle containing [2]rotaxanes bound halides strongly in competitive aqueous media. Additionally, the synthesis of the dicationic pyridinium-triazolium and pyridinium-iodotriazolium [2]rotaxane counterparts was undertaken. The halogen bonding [2]rotaxane demonstrated charge-assisted halogen bonding chelation of halides, significantly enhancing the selective recognition of Br^- in comparison to the hydrogen bonding analogue (**Figure 6.1**).

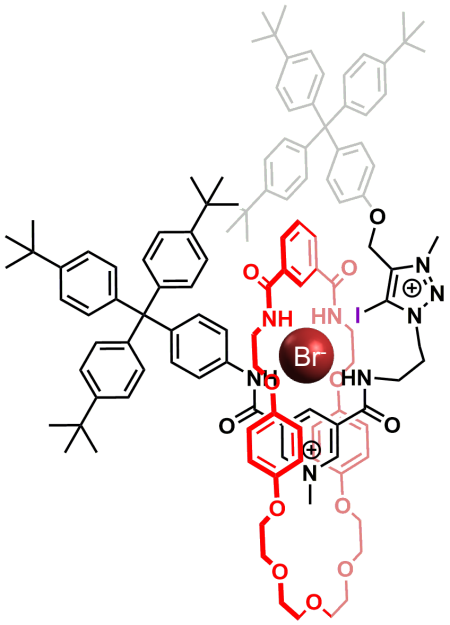


Figure 6.1 – The proposed chelating recognition of Br^- pyridinium-iodotriazolium axle containing [2]rotaxane **28.**$(PF_6)_2$.

Chapter 3 initially explored the anion recognition properties of a series of novel hydrogen and halogen bonding amide-triazole and amide-iodotriazole receptors. Unprecedented large enhancements in the halide binding strength observed in the neutral halogen bonding 1,3-bis-iodotriazole receptor configuration (X = I, **Figure 6.2-i**) in comparison to the isostructural hydrogen bonding configuration. It was found that the anion binding selectivity trends of the dicationic 1,3- and 1,2-disubstituted hydrogen bonding amide-triazolium receptors were dictated by regioisomerism; the more constrained 1,2-substituted receptor geometry selectively bound the smaller halides such as Cl^- and Br^- (X = H, **Figure 6.2-ii**) whilst the more open 1,3-substituted receptor geometry displayed preferences towards binding the complementary trigonal NO_3^- and linear N_3^- anions (X = H, **Figure 6.2-iii**).

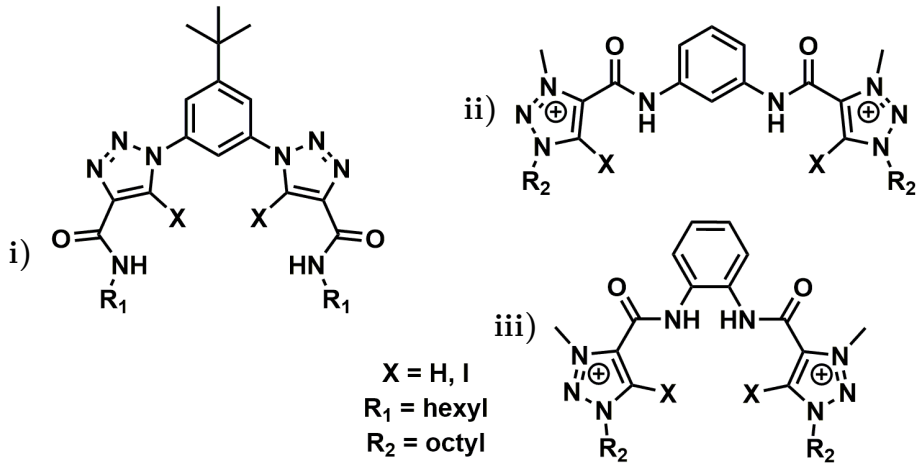


Figure 6.2 – The substitution of acyclic amide-triazole (X = H) and amide-iodotriazole (X = I) anion receptors: i) 1,3-bis-(iodo)triazole-amide ii) 1,3-bis-amide(iodo)triazolium and iii) 1,2-bis-amideiodotriazolium.

This 1,3- receptor substitution was further exploited in the synthesis of a novel bis-amide-triazolium axle containing [3]rotaxane (**Figure 6.3**). Selective 1:1 stoichiometric 'sandwich' binding of the tetrahedral anion $H_2PO_4^-$ was observed over a diverse range of monoanions, confirming the intrinsic bias of this receptor structure towards binding tetrahedral anionic guest geometries.

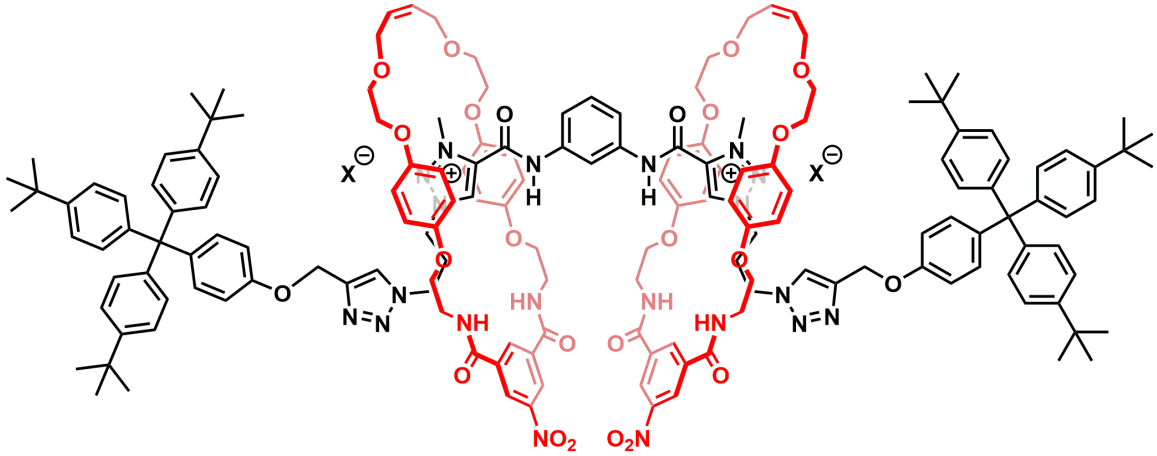


Figure 6.3 – Structure of [3]rotaxane $\mathbf{83}^{2+}$.

Chapter 4 described the CB[8] ternary complex mediated supramolecular modulation of lanthanide luminescence output in aqueous solvent media (**Figure 6.4**). Upon the formation of the ternary complex stabilised CT optical feature, the fluorescent and phosphorescent outputs of the europium(III) containing ternary complex was significantly quenched. Preliminary redox switching studies of the europium(III) functionalised CB[8] ternary complex indicated that this host-guest system could be applied as a supramolecular switch of europium(III) luminescence. Additionally, it was found that the NIR phosphorescence of the neodymium(III) and ytterbium(III) containing CB[8] ternary complexes was extensively quenched in the presence of CT, displaying potential as an effective means to 'switch off' NIR luminescence.

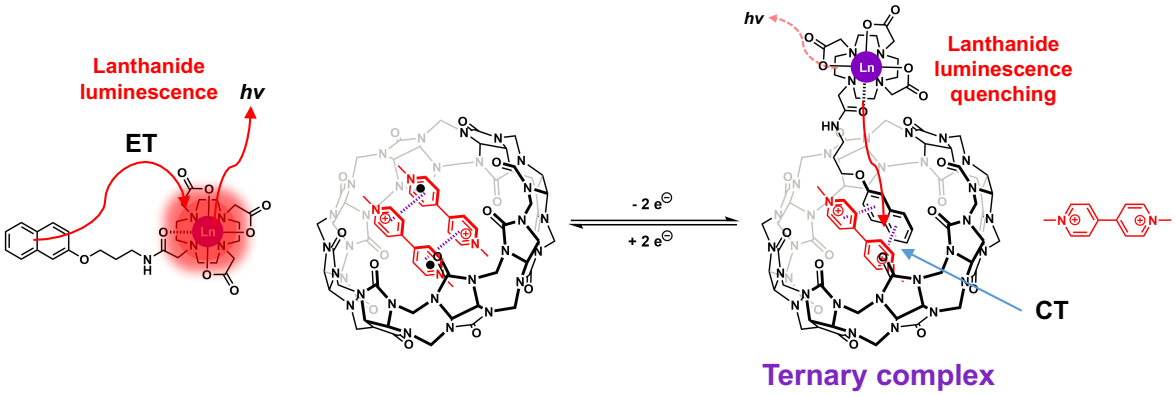


Figure 6.4 – Structural representation rationalising the redox modulation of lanthanide phosphorescent output *via* ternary complex CT.

To overcome solubility issues, future work will focus on the preparation of CB[8] based SAMs functionalised to electrochemically active surfaces such as gold in order to recruit the necessary viologen and lanthanide containing components and enable electrochemically mediated switching of lanthanide luminescent output.

7. Appendix

7.1. Excitation Spectra

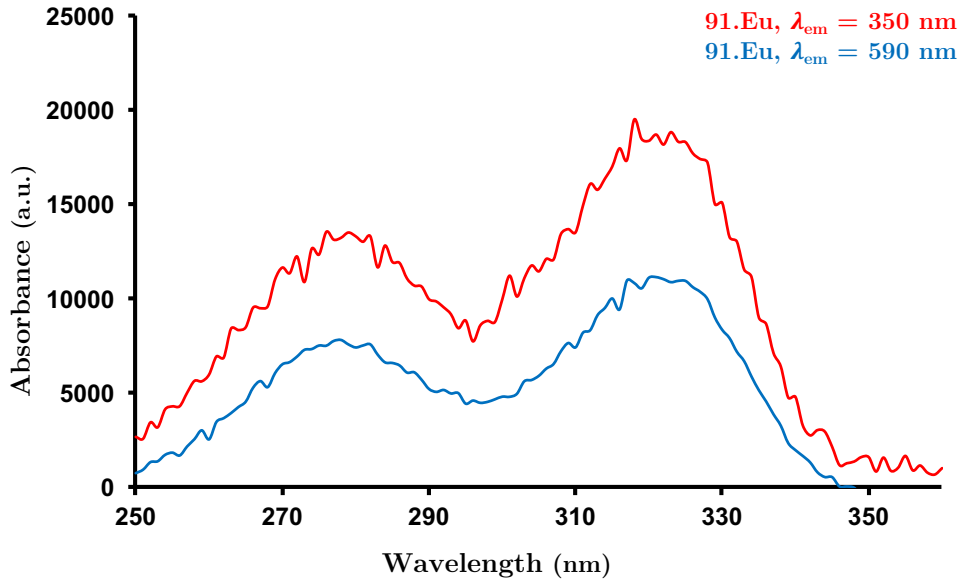


Figure 7.1 – Excitation spectra of **91.Eu** (H_2O, 298 K).

7.2. Europium(III) Luminescence Lifetime Experiment Methodology

Luminescence spectra and lifetimes were recorded on a Horiba Fluorolog 3 at 298 K. The experimental emission decay curves of the europium(III) phosphorescence at λ_{em} = 616 nm were obtained *via* decay by delay in phosphorimeter mode and fitted to either a monoexponential (**Equation 1**) or biexponential (**Equation 2**) decay function to acquire the luminescence lifetime(s) of the relevant emissive species:

$$\textbf{Equation 1: } F(t) = A + B_1 e^{\frac{-t}{\tau_1}}$$

$$\textbf{Equation 2: } F(t) = A + B_1 e^{\frac{-t}{\tau_1}} + B_2 e^{\frac{-t}{\tau_2}}$$

where t = time, A = empirical background noise factor, B_1/B_2 = empirical amplitude scaling factor for the emissive species (1 and/or 2) and τ_1/τ_2 = luminescence lifetime(s) of species (1 and/or 2).

The percentages of complexed/uncomplexed **91.Eu** prior to and following addition of reducing agent $Na_2S_2O_4$ was estimated by comparing the relative concentrations of each component present (**91.Eu** [species 1], (**91.Eu**, $\mathbf{MV^{2+}}$) ⊂ **CB[8]**, ternary complex, [species 2]) and assuming that each component possesses the identical quantum yield of phosphorescence (Φ_{phos}, normally dependent upon both concentration and brightness).[1]

Prior to addition of $Na_2S_2O_4$: $\left[\frac{B_1}{B_2}\right] = \Phi_{phos}(1)/\,\Phi_{phos}(2)$

B_1: 1.65 x 10^5 a.u., $\tau_{\mathbf{91.Eu}}$: 0.6 ms, B_2: 1.24 x 10^6 a.u., $\tau_{\text{Ternary Complex}}$: 0.1 ms, $B_1 + B_2$: 1.41 x 10^6 a.u.

Percentage of uncomplexed **91.Eu**: ((1.65 x 10^5)/(1.41 x 10^6)) x 100 = <u>11.7%</u>

Percentage of **91.Eu** *in ternary complex:* ((1.24 x 10^6)/(1.41 x 10^6)) x 100 = <u>88.3%</u>

Following addition of $Na_2S_2O_4$: $\left[\frac{B_1}{B_2}\right]' = \Phi_{phos}(1)'/\,\Phi_{phos}(2)'$

B_1: 1.24 x 10^5 a.u., $\tau_{\mathbf{91.Eu}}$: 0.6 ms, B_2: 2.20 x 10^5 a.u., $\tau_{\text{Ternary Complex}}$: 0.1 ms, $B_1 + B_2$: 3.44 x 10^5 a.u.

Percentage of uncomplexed **91.Eu**: ((1.24 x 10^5)/(3.44 x 10^5)) x 100 = <u>36%</u>

Percentage of **91.Eu** *in ternary complex:* ((2.20 x 10^5)/(3.44 x 10^5)) x 100 = <u>64%</u>

References for Appendix

(1) Blackman, M. J.; Corrie, J. E. T.; Croney, J. C.; Kelly, G.; Eccleston, J. F.; Jameson, D. M. *Biochemistry (Mosc.)* **2002**, *41* (40), 12244–12252.